EIGHTH EUROPEAN CONFERENCE ON CONTROLLED FUSION AND PLASMA PHYSICS

Volume I

Contributed Papers

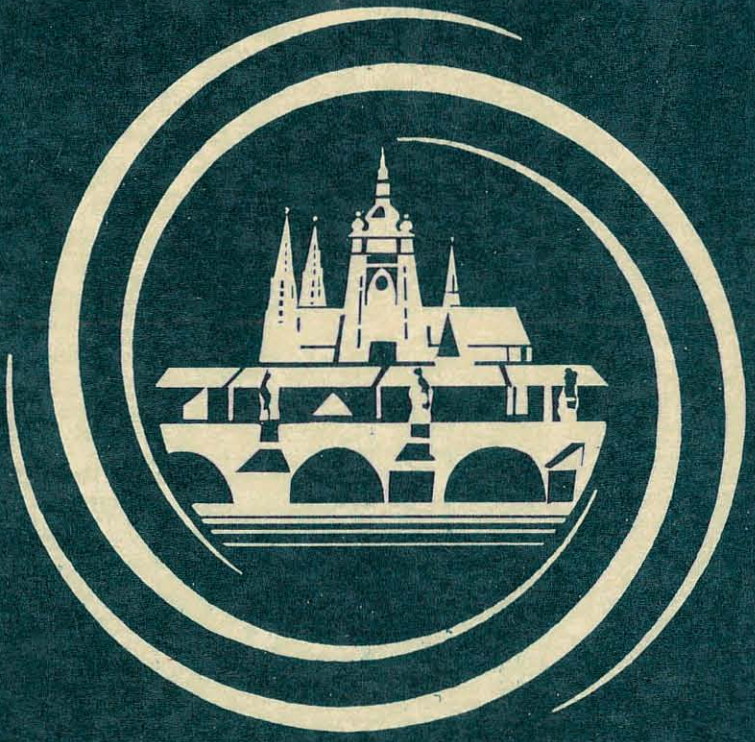

VIII FUSION PRAGUE 1977

C O N T E N T S

P R E F A C E

This volume contains the Contributed Papers of the Eighth European Conference on Controlled Fusion and Plasma Physics, to be held in Prague, Czechoslovakia, 19-23 September, 1977. Previous conferences in this series were held in Munich (1965), Stockholm (1967), Utrecht (1969), Rome (1970), Grenoble (1972), Moscow (1973) and Lausanne (1975).

The Conference is organized by the Institute of Plasma Physics, Czechoslovak Academy of Sciences, the Czechoslovak Scientific and Technical Society and the Czech Technical University, under the auspices of the Plasma Physics Division of the European Physical Society (EPS).

The papers contained in this book have been selected for presentation by the Paper Selection and Programme Committee. The responsibility for the contents is exclusively that of the authors. Some minor editorial work was carried out where the presentation was really not adequate for the reproduction by photographic processes.

Invited and Supplementary Papers will be published after the Conference, in Vol. II of the Proceedings.

The Organizing Committee

ORGANIZING COMMITTEE

V. Kopecký, chairman
academician B. Kvasil, honorary vice-chairman
J. Váňa, vice-chairman
J. Kracík, vice-chairman
R. Klíma, scientific secretary

K. Jakubka
Mrs P. Jarošová
K. Jungwirth
Š. Körbel
J. Maloch
Mrs V. Nováková
P. Pasternak
K. Šobra
P. Šunka

PAPER SELECTION AND PROGRAMME COMMITTEE

C. Bobeldijk, Rijnhuizen, Jutphaas, the Netherlands
O.N. Krokhin, Moscow, U.S.S.R.
A.M. Messiaen, Brussels, Belgium
K.A. Razumova, Moscow, U.S.S.R.
P. Šunka, Prague, Czechoslovakia
D.R. Sweetman, Culham, England

FINANCIAL SUPPORT

The Organizations listed below have contributed financially to the Conference. Their support is gratefully acknowledged:

CZECHOSLOVAK ATOMIC ENERGY COMMISSION

CZECH TECHNICAL UNIVERSITY

CONFINEMENT OF HIGH ENERGY ELECTRONS IN T.F.R.

T.F.R. Group (Presented by M. Chatelier)

ASSOCIATION EURATOM-CEA SUR LA FUSION
Département de Physique du Plasma et de la Fusion Contrôlée
Centre d'Etudes Nucléaires
Boite Postale n° 6. 92260 FONTENAY-AUX-ROSES (FRANCE)

Experiments done on the TFR device have shown that the behaviour of runaway electrons depends on the gross properties of the dicharge [1], [2]. Depending on the density regime, the plasma can be

1) either highly unstable and runaways rapidly lost in the anti-loss cones of the toroidal field ($\bar{n}_e \lesssim 10^{13}$ cm^{-3}, type A and B discharges) ;
2) or mildly unstable (10^{13} cm$^{-3} \lesssim \bar{n}_e \lesssim 2\ 10^{13}$ cm^{-3} type C discharges)
3) or weakly unstable ($\bar{n}_e \gtrsim 2\ 10^{13}$ cm^{-3}, type D discharges). We investigate here the high density type D discharges where high energy electrons (in the 10 MeV range) can be stably confined.

The main experimental features characterizing the discharge are the following

(i) the hard X ray flux due to runaway electrons hitting the limiter is weak throughout the discharge and is concentrated at the end when the current drops.

(ii) the spectrum emitted by the plasma around the electron cyclotron frequency indicates that the gross distribution function of electrons is maxwellian. In addition a peak at the central electron plasma frequency is observed early in the discharge and decays away with a time constant ~ 100 ms, the integrated power in the peak being correlated with the runaway creation rate calculated from the measured n_e and T_e [2].

(iii) early measurements showed that the limiter is the main neutron source [3]. Neutron spectra were recorded near the limiter by using a proton recoil proportional counter [4]. These measurements indicated that a photonuclear process related to the hard X-rays shower in the molybdenum limiter, itself created by the impact of runaway electrons, is responsible for the neutron production. As a fact the shape of the spectrum shown on figure 1 is typical of photonuclear reactions induced by a bremsstrahlung distribution of photons in a thick target. The maximum energy of the spectrum ~ 3 MeV indicates that electrons with an energy $\gtrsim$ 10 MeV are present into the discharge (since the minimum threshold of photoneutron reactions is close to 7 MeV in molybdenum).

In order to make sure about the process and also to gain more information on runaway dynamics, two further experiments have been carried out [5].

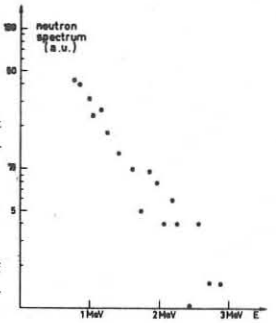

Fig.1

Taking advantage of the replacement of the molybdenum limiter by a carbon limiter and of the subsequent reduction of the hard X rays and photoneutrons fluxes, we successively inserted targets of different materials at the edge of the plasma. These targets were located in the outer region of the equatorial plane where runaways are expected to be lost. Three targets have been used : carbon (z = 6, A = 12), molybdenum (Z = 42, A ≃ 96), and tungsten (Z = 74, A ≃ 184). We checked that the NZ/A relationship between the target composition and the reaction rate which is expected for photonuclear processes [6] holds in TFR as can be seen on figure 2. It must be noted that in the case of carbon, 10 MeV electrons or photons have a penetration depth which is larger than the actual target thickness, so that photoneutrons were probably produced in the stainless steel support. Figure 3 shows the thresholds for photoneutron production in the different targets (stainless steel, molybdenum and tungsten as a function of the neutron flux starting time. One can see that the heavier the target, the earlier the start up of the neutron signal. On the same figure is plotted the straight line corresponding to the free acceleration of electrons under the experimental loop voltage ~ 2.76 volts/turn (free fall slope). The free fall law corresponds to an increase of 13.5 MeV/ 100 ms while the actual increase is only 8.4 MeV/ 100 ms. This result is similar to Ormak [7] and PLT results [8],

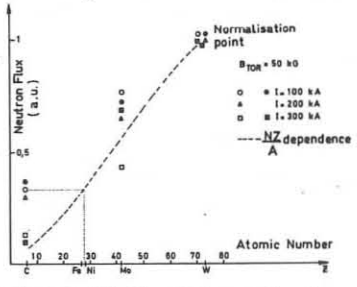

Fig.2 *Verification of the NZ/A dependence of the neutron flux.*

it seems to indicate that the confinement of high energy electron is anomalous.

Figure 3 shows that within the 400 ms of the discharge runaway electrons could reach an energy as high as 35 MeV. (The plasma current, 300 kA, allows the confinement of such electrons).

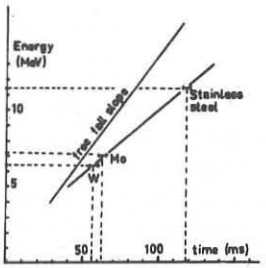

Fig.3

As a matter of fact an analysis of the radioisotopes created in the molybdenum limiter seems to indicate the presence of electrons with an energy as high as ∿ 20 MeV. The activity was chiefly concentrated just where the surface of the limiter melted that is in that part which intersects the equatorial plane in the outer region of the plasma. The activity was 3 mrem/h a few days after removal from the machine. A γ spectrum recorded with a Ge (Li) diode showed 27 peaks belonging to 9 radionucleïdes. $_{39}Y^{88}$, $_{40}Zr^{88}$, $_{41}Nb^{91m, 92m, 95, 95m, 96}$, $_{42}Mo^{99}$, $_{43}Tc^{99m}$.

The different nuclear reactions and decay schemes leading from the limiter nucleï to the observed radionucleïdes are shown on figure 4. Most of the observed radionucleïdes cannot be obtained but through photo nuclear processes (γ,n), (γ, p) and (γ, α). It must be also noticed that the presence of $_{41}Nb^{92m}$ seems to indicate that electrons of energy larger than the corresponding (γ, pn) threshold (17.3 MeV) are present.

We conclude that in the high density discharges in TFR, the neutron production arising in the limiter is due to photonuclear reactions induced by the hard X ray shower caused by the impact of high energy runaway electrons. As a consequence incident electrons must have energies at least in the 10 MeV range. There is an indication that some electrons reach an energy as high as 17.3 MeV. Finally, the rate at which electrons gain energy is significantly lower than the free fall rate.

REFERENCES.-

[1] TFR Group, Nucl. Fus. 16, (1976) 473.

[2] P. BROSSIER, A.E. COSTLEY, D.S. KOMM, G. RAMPONI, S. TAMOR, in 6th Int. Conf. on Plasma Phys. and Cont. Nuc. Fus. Research, Berchtesgaden FRG, Oct. 1976 IAEA-CN-35/A13-2

[3] TFR Group, Lausanne, Vol. 1, p. 2

[4] E. Korthaus, Report KFK 1994 (1974) Kernforschungszentrum, Karlsruhe

[5] TFR Group Phys. Letters 60 A, 1977 (219).

[6] W.C. BARBER and W.D. GEORGE, Phys. Rev. 116 (1959) 1551.

[7] H. KNOEPFEL, D.A. SPONG, S.J. ZWEBEN, in "7th Eur. Conf. on Controlled Fus. and Plasma Phys." Vol. 1, p. 3, (1975).

[8] J.D. STRACHAN, E.B. MESERVEY, W. STODIEK, R.A. NAUMANN, F. GIRSHICK, Nuclear Fusion 17, (1977), 140.

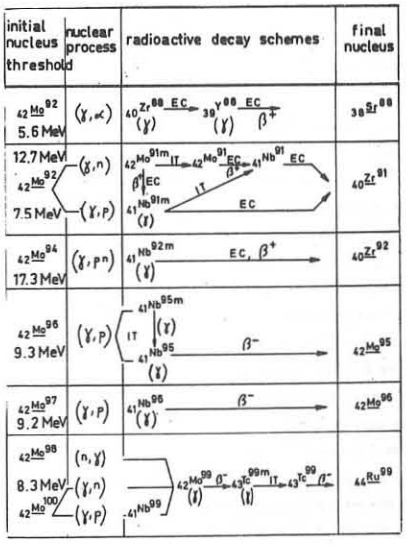

Fig.4 Decay schemes observed by means of gamma spectrometry. m:metastable; (γ)gamma emission observed; EC:electron capture; IT:isomeric transition; underlined elements are stable.

DENSITY FLUCTUATIONS IN THE T.F.R. TOKAMAK PLASMA

T.F.R. Group (presented by F.Koechlin)

ASSOCIATION EURATOM-CEA SUR LA FUSION
Département de Physique du Plasma et de la Fusion Contrôlée
Centre d'Etudes Nucléaires
Boite Postale n° 6. 92260 FONTENAY-AUX-ROSES (FRANCE)

ABSTRACT : Low frequency ($\omega \ll \omega_{ci}$) density fluctuations have been measured in the T.F.R. tokamak plasma by microwave scattering techniques. The frequency and wave vector spectra are compared with those predicted by the theory for drift waves. An estimation of the turbulence-induced electron heat transfer is given, using the measured fluctuation level and the model of dissipative trapped electron drift modes.

An anomalous electron heat transfer, transverse to the magnetic confinement field, is indicated by energy balance considerations in tokamak devices (K_e experimental $\simeq 50$ -100 K_e neoclassical) /1,2,3/. Turbulent diffusion schemes based on electrostatic drift modes, energized by circulating or by trapped electrons have been proposed /4,5/ . In order to investigate these modes, electron density fluctuations in the T.F.R. tokamak plasma have been measured with a 2mm microwave scattering system (fig.1) /6/. Their azimuthal and radial wave vector spectra can be measured from 5 to 15cm^{-1} with a zero toroidal component of $\vec{k}$. Calculations of the microwave beam propagation in a refractive plasma have been performed, giving the effective scattering angles and scattering volume for any plasma density ($0.15 \leqslant \omega_p^2/\omega^2 \leqslant 0.40$ at the plasma center). A heterodyne receiver, frequency locked to the emitter, allows measurement of the fluctuations frequency spectra (20 kHz to 300 MHz). In the microwave scattering technique, the scattered power is proportional to the Fourier transform $S(\vec{k},\omega)$ of the space and time autocorrelation function of the fluctuating density $\tilde{n}$, i.e. $P_{scatt} \propto \langle \tilde{n} \rangle^2$.

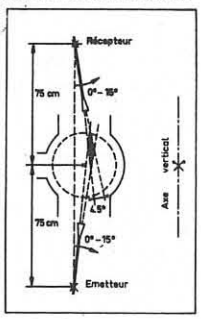

Fig.1-Apparatus for microwave scattering

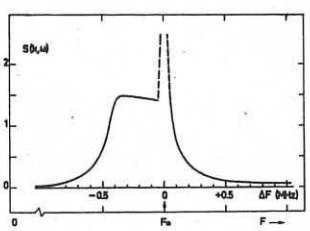

Fig.2- Frequency spectrum of the density fluctuations ($k_{//} \leqslant 1.5.cm^{-1}$, $k_\theta \simeq 10\ cm^{-1}$, $k_r \simeq 3\ cm^{-1}$, $r \sim 15$ cm; F_o = source frequency).

Figure 2 shows the frequency spectrum of the power scattered by the density fluctuations, in the region $r/a \sim 0.7$, during the quasi-stationnary state of a 300 kA, 50 kG, T.F.R. discharge. The spectrum is independent of the toroidal magnetic field; its width and level increase marginally with the discharge current (i.e. the energy content of the plasma) . Its strong dissymmetry with respect to the source frequency reveals that most of the density fluctuations propagate in a well defined sense with respect to the wave vector $\vec{k}_\perp \sim \vec{k}_\theta$; this has been verified to be the electron diamagnetic drift direction. On the contrary, when $\vec{k}_\perp \sim \vec{k}_r$, the spectrum is symmetrical, showing that no preferential radial direction of propagation exists. Figure 3 shows the main data of a 200 kA, 40 kG deuterium plasma and the radial variation of the amplitude of the fluctuations at constant wave vector and frequency. As the radial resolution was $\sim a/3$, this indicates that the amplitude is a maximum in the region $r/a \geqslant 0.7$. Figure 4 shows the azimuthal and radial wave vector spectra measured in the plasma of fig.3 , with a resolution $\Delta k \sim 3 cm^{-1}$. The k_θ -spectra were measured close to the vertical of the magnetic axis, keeping r/a 0.7, and the k_r- spectra measured in the equatorial plane, close to the plasma center.

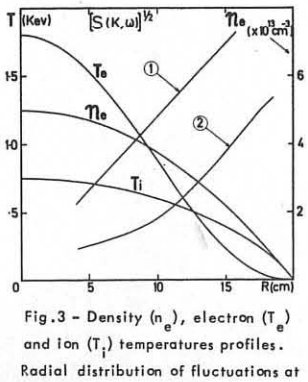

Fig.3 - Density (n_e), electron (T_e) and ion (T_i) temperatures profiles. Radial distribution of fluctuations at ① f =0.3 MHz ② f =0.6 MHz, signal x 3

At the center of the frequency spectrum (f =300 kHz), the maximum of the k_θ spectrum occurs at $k_\theta \simeq 8\ cm^{-1}$, $k_r \simeq 1.5\ cm^{-1}$ and $r \sim 15$cm. Comparing the transverse wave vector of the fluctuations $k_\perp$ with the ion gyroradius $\rho_i = (T_i M)^{1/2}/eB$ gives $k_\perp \rho_i \sim 0.6$ (at f = 600 kHz, $k_\perp \rho_i \sim 0.7$). Such a value of $k_\perp \rho_i$ is expected to give an appreciable growth rate to drift waves. This result, together with the frequency range of the fluctuations ($f \ll \omega_{ci}/2\pi$ = 30 MHz), suggests that these are indeed drift waves. We can also compare the mean azimuthal phase velocity of the detected waves (2.4×10^5cm/s) to the phase velocity deduced from the dispersion relation (0.3×10^5cm/s), taking into account finite Larmor radii and temperature gradient effects (fig.3). This large difference can be explained by an ExB plasma rotation due to a negative electrostatic plasma potential, as was indeed measured in the S.T. tokamak /7/ . The required rotationnal velocity (at $r/a \sim 0.7$) is of the order of the ion diamagnetic velocity ($v_{di} \simeq 1.5 \times 10^5$cm/s) and would cancel the plasma angular momentum around axis.

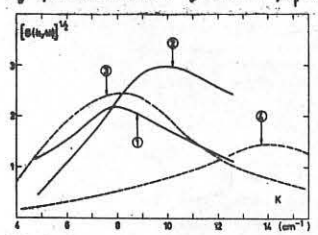

Fig.4- Transverse wave number spectra of density fluctuations. ① k_θ spectrum. $k_r \ll k_\theta$, $r \sim 15$cm, f = 0.3 MHz . ② f =0.6 MHz, signal x 3 . ③ k_r spectrum $k_\theta \ll k_r$, $0 < r \leqslant 5$cm, f = 0.3 Mhz. ④ f = 0.6 MHz, signal x 3.

Using the value of the fluctuating electrostatic potential $\tilde{\varphi}$ deduced from the measurements, the turbulent heat transfer coefficient can be calculated, assuming the dissipative trapped electron drift wave model (D.T.E.M.) to be valid. The spectral density $S(\vec{k},\omega)$ is first deduced from the microwave scattering measurements ; then, the RMS fluctuating density is obtained by $\langle |\tilde{n}(r,t)|^2 \rangle = n_e \int d\omega\, d^3\vec{k}\, S(\vec{k},\omega)$ integrated over the measured spectra. This yields $|\tilde{n}| \simeq 3\text{-}7 \times 10^{21}\ cm^{-6}$ at $r/a \sim 0.7$ - 0.8 in the 200 kA plasma ($1\text{-}2 \times 10^{22}$ at 300 kA) , so that $\tilde{n}/n_e \sim 3\text{-}4 \times 10^{-3} \sim e\tilde{\varphi}/T_e$. The momentum exchange between the waves and the trapped electrons can be calculated by simple quasi-linear theory of the D.T.E.M., giving the radial heat diffusion by these particles : $\tilde{K}_e = A (e\tilde{\varphi}/T_e)^2 (k_\theta \rho_e)^2 v_e^2 \nu_{eff}^{-1} (2\ r/R)^{1/2}$ where $A \sim 6$. This yields typical values of $\tilde{K}_e \simeq 50\ cm^2/s$ at $r/a \sim 0.7$ and a maximum $\sim 500\ cm^2/s$ at $r/a \sim 0.5$, due to the strong temperature dependence of $\tilde{K}_e$. The question of why these heat conduction coefficients (measured at the vertical of the magnetic axis) are lower than those required for the electron power balance, (3000 cm^2/s at r/a = 0.5 and 4000 cm^2/s at r/a = 0.7) /2/ still remains to be answered. A strong ballooning of the D.T.E.M. in the weak field region could reduce this difference; this will be studied in the future.

REFERENCES

/1/ L.A.Artsimovich et al. Plasma Physics and Controlled Nuclear Fusion Research (Proc. 2nd Int.Conf. Novosobirsk, 1968) 1 , 17 (I.A.E.A Vienna 1969).

/2/ T.F.R. Group. Plasma Physics and Controlled Nuclear Fusion Research (Proc. 6 th Int. Conf. Berchtesgaden, 1976) 1 , 35 (I.A.E.A. Vienna 1977) .

/3/ J.D.Callen and G.L. Jahns : Phys.Rev. Letters 38 , 491 (1977)

/4/ B.B.Kadomtsev and O.Pogutse. Doklady Akad. Nauk 186 , 553 (1969)

/5/ W.Horton et al. Plasma Physics and Controlled Nuclear Fusion Research (Proc. 5th. Int.Conf. Tokyo, 1974) 1 , 541 (I.A.E.A. Vienna 1975).

/6/ F.Koechlin, V.Glaude, J.How. EUR-CEA Report FC-871 (Fontenay-aux-Roses, 1977) .

/7/ J.C.Hosea, F.C.Robes, R.L.Hickock, A.N.Dellis. Phys.Rev.Letters 30 , 839 (1973) .

INFLUENCE OF A RESONANT HELICAL OCTOPOLE FIELD ON THE PULSATOR TOKAMAK PLASMA

F. Karger, W. Feneberg, D. Meisel, H. Murmann, J. Gernhardt, O. Klüber, K. Lackner

Abstract: A plateau in the temperature profile on the q = 2 surface and a damping of the m = 2 mode is observed when a helical m = 4, n = 2 ocotopole field is applied. In addition, a correlation is found between the threshold values for the induced disruption and the ergodization of magnetic field lines.

Experimental setup: In Pulsator the helical windings which are resonant to the q = 2 surface can generate an m = 2, n = 1 helical quadrupole field /1/ or they can be connected so that the currents in all helical windings flow in the same sense, thus producing an m = 4, n = 2 octopole field. (Fig.1)

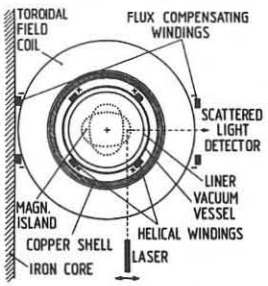

Fig.1 Experimental setup

Islands on the q = 2 surface: The m = 4, n = 2 field in conjunction with the plasma current forms four islands on the q =2 surface, the opposite ones being connected in pairs (Fig.2a). The octopole field decreases faster towards the centre than the quadrupole field. In addition, since the return conductors are not helical they do not contribute to island formation as they do in the quadrupole case. Hence, a much stronger current is required in the helical conductors for the case m=4, n=2 (Fig.2a) in order to achieve the same island width as in the case m=2, n=1 (Fig. 2b). In the case m=4, n=2 with the same island width roughly one half of the number of trips around the major circumference are required to get from the inner to the outer side of the island on one field line. The enhanced transport along these field lines should therefore result in a pronounced temperature plateau across the island.

This prediction about the temperature profile in Pulsator was tested by means of Thomson scattering, the test points being located across an island (Fig.1). The result is shown in Fig.3a. The step in the profile can clearly be discerned. This plateau is located around the q=2 surface as can be seen from Fig.3b which was calculated from Fig3a assuming $j \propto T_e^{3/2}$. Such a current profile should have a stabilizing effect on the m=2, n=1 tearing mode /2//3/. Strong damping of the m=2 MHD mode is in fact observed experimentally when the m = 4, n=2 field is switched on (Fig.4). The damping is generally stronger than that observed for the m=2, n=1 field /1//4/.

Even without the helical field switched on, it is possible to observe flattening of the temperature profile at the q=2 surface, this apparently being due to the strong m=2 MHD mode (see /5/).

Ergodization of field lines: Besides the islands on the q=2 surface, islands of higher mode numbers are also formed on the corresponding surfaces owing to the toroidal curvature /1/. In the case of the octopole field m=4, n=2, the higher harmonics are particularly well represented since the field increases strongly towards the outside /6/. If the current in the helical windings is strong enough, the q=2, q=2.5 and q=3 islands may overlap, i.e. the field lines are ergodized and transport may be brought about along field lines from the inner side of the q=2 island to the limiter. Magnetic limiting of the plasma is thus possible /6/. The remaining plasma, however, has too low a q value at the boundary to be stable.

Experimentally, one does in fact observe the onset of disruption at a certain critical current in the helical windings, this threshold being about one order of magnitude higher than in the quadrupole case because of the island width. For the octopole field one can distinguish two cases: For the case when the helical currents flow parallel to the plasma current the critical current threshold is higher than in the anti-parallel case. The same trend appears in the calculations of the ergodization /6/. In the parallel case the ergodization appears at higher helical current than in the anti-parallel case since the relative positions of the primary islands and the harmonics are different in the two cases. The windings available in Pulsator thus seem to allow indirect demonstration of plasma limitation by ergodization. With m=3, n=1 or m=4, n=1 windings, however, it ought to be possible to demonstrate directly stable magnetic limiting and diverting of the plasma /7/.

References:

/1/ F. Karger et al., Plasma Phys.Contr.Nucl.Fus.Res., Proc. 5th Int.Conf., Tokyo (1974), IAEA,Vienna(1975) 2o7

/2/ A.H. Glasser et al., Phys.Rev.Letters 38 (1977) 234

/3/ K. Lackner and F. Karger, this conference

/4/ F. Karger et al., Plasma Phys.Contr.Nucl.Fus.Res.,Proc. 6th Int.Conf.Berchtesgaden (1976) 1, IAEA, Vienna(1977) 267

/5/ S.v.Goeler, Proc.7th Europ.Conf., Lausanne,(1975) 2 , 71

/6/ W. Peneberg, this conference

/7/ F. Karger, K. Lackner, Resonant Helical Divertor, to be published in Physics Letters A

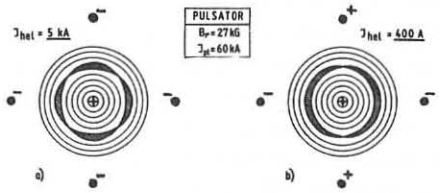

Fig.2: Production of islands with comparable width on the q = 2 surface by an a) m = 4, n = 2 octopole field, b) m = 2, n = 1 quadrupole field (calculations without toroidal curvature)

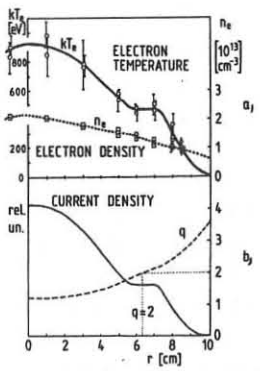

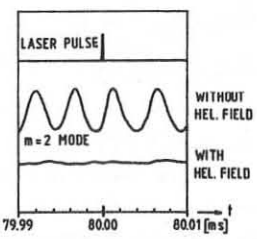

Fig.3: a) Temperature and density profiles with externally applied m = 4, n = 2 field measured at 80 ms (B_v=27 kG, J_p= 60 kA). b) Derived current and q profiles

Fig.4: Damping of the m = 2 mode by the m = 4, n = 2 field at the time of the laser pulse

THE USE OF EXTERNAL HELICAL WINDINGS FOR THE PRODUCTION OF A SCREENING LAYER IN ASDEX AND A TOKAMAK WITH MATERIAL LIMITER.

W. Feneberg

Max-Planck-Institut für Plasmaphysik

D-8046 Garching, Fed.Rep.of Germany

Abstract: The paper presents a solution of the magnetic differential equation for investigating the coupling between an external resonant helical field and the toroidal curvature. The properties of a boundary layer created by ergodization of the magnetic surfaces are discussed.

It is known that a purely helical perturbation (m, n) externally superposed on an axisymmetric tokamak equilibrium produces on all magnetic surfaces primary islands whose rotational transform agrees with the harmonics ($m \pm N$, n; $N = 1, 2, \ldots$ etc.) of the basic mode (where m denotes the meridional and n the azimuthal mode number). The magnetic surfaces of the primary islands are thereby destroyed by secondary resonances, starting from the separatrix, and a more or less large part of the volume is ergodically filled with field lines. This effect was investigated in /1/ and /2/ and applied to the tearing mode ($m = 2$, $n = 1$), only the first harmonic ($m \pm 1$, $n = 1$) being taken into account.

This destruction of the magnetic surfaces can be used for producing a magnetic limiter: an external helical field with high mode number m, n generates a magnetic field $\delta B_r \sim r^{m-1}$ concentrated on the boundary region, while the interior is only perturbed by small islands.

To calculate the size of the primary islands, the magnetic differential equation ($\vec{B}\nabla\Psi = 0$, Ψ = const are the magnetic surfaces) was solved by expanding in terms of the aspect ratio. A helical perturbation (m, n) was thereby superposed on an unperturbed magnetic field with circular magnetic surfaces which is free of divergence and whose shear can be freely chosen. The result for the diameter δ of the islands in the individual orders of the aspect ratio is as follows:

(R = major radius, r = distance from torus axis, B = main magnetic field, δB_r = radial component of the perturbing magnetic field)

$$\delta_{m,n} = A \qquad A = 4\sqrt{\frac{Rq}{nq'}\frac{\delta B_r}{B}}$$

$$\delta_{m\pm1,n} = A\left(\frac{r}{2R}\left(m+1\pm1\right)\right)^{1/2}$$

$$\delta_{m\pm2,n} = A\left(\frac{r^2}{8R^2}\left((m+2)^2 \pm (m+2)\right)\right)^{1/2}$$

$$\vdots$$

$$\delta_{m+N,n} = A\left(\left(\frac{r}{R}\right)^N \frac{(m+N)^N}{N!\,2^N} + O\left((m+N)^{N-2}\right)\right)^{1/2}$$

In ASDEX ergodization is due to overlapping of an infinite succession of islands between the excited basic mode $q = \frac{m}{n}$ and the separatrix ($q_s = \infty$), while in the limiter tokamak the magnetic surfaces break up because the resonant surfaces located inside the limiter overlap with those located outside the limiter.

Figure 1 shows a case in which the topology of a perturbed ASDEX equilibrium is investigated by means of the Gourdon program. Here the thickness of the ergodized layer is about $\Delta = 5$ cm.

Like the scrape-off layer of an axisymmetric divertor, the line density of the plasma in the boundary layer can be estimated by means of the confinement time $\tau = \frac{L}{v_i}$ in the layer to be $n\Delta = \frac{\bar{n}\, a\, \tau}{2\tau_p}$. (L = mean length of the field lines to the limiter of divertor, v_i = ion sound velocity, $\bar{n}$ = mean particle density, a = plasma radius, τ_p = particle confinement time).

The ionization of neutral hydrogen in the boundary layer is thereby neglected. The strength of the external helical field can be chosen such that the boundary layer absorbs the heavy impurities. A shielding effect occurs if the impurity ions from the ergodic layer that impinge on the wall stick there /3/. As the temperature in the layer is reduced by heat conduction along the field lines, it can be assumed that secondary sputtering can be neglected. The impurity density is then $n_z \sim \tau$ and hence is small.

In Pulsator it was attempted to investigate a magnetic limiter by means of an $m = 4$, $n = 2$ configuration /4/. In Fig.2 it is shown that in the anti-parallel case (direction of helical current opposite to that of plasma current) the magnetic surfaces for the same current in the helix are much more strongly ergodized than in the parallel case (Fig.3). It might be concluded from this that the earlier onset of disruptive instability experimentally observed in the anti-parallel case represents the sudden appearance of a magnetic limiter which limits the plasma at $q = 2$.

References:

/1/ J.M.Finn, MATT-1137, 1975

/2/ J.A.B.Rechester and H.Stix, MATT-1168, 1976

/3/ H.Vernickel, B.Scherzer, J.Bohdanski, R.Behrisch, Int. Symp.on Plasma-Wall Interaction, Jülich 1976.

/4/ F.Karger et al., this Conference.

Fig. 1

Asdex
with $l = 3$
$I_{Hel} = 4$ kA
$r_{Hel} = 68$ cm
$I_P = 500$ kA
$\Delta \approx 5$ cm

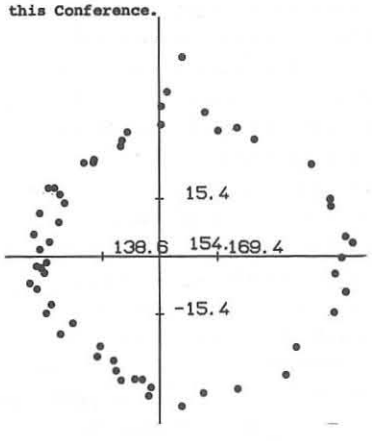

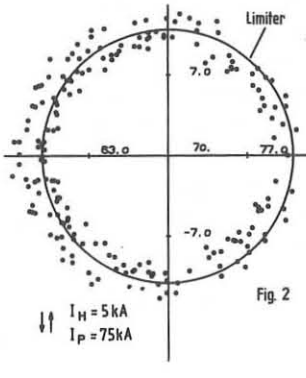

Fig. 2

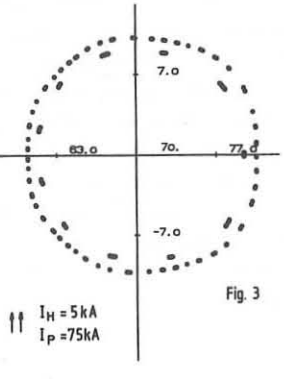

Fig. 3

MODELS FOR THE INFLUENCE OF RESONANT HELICAL WINDINGS ON TOKAMAK DISCHARGES AND FOR THE CURRENT DECAY FOLLOWING THE DISRUPTIVE INSTABILITY

K.Lackner,and F.Karger, Max-Planck-Institut für Plasmaphysik, D-8046 Garching, Federal Republic of Germany

1. Stabilization of disruptive instability by resonant helical windings

Application of external resonant l = 2 windings has been shown experimentally to lead for a certain regime of external winding currents I_{hel} to a quenching of the m = 2 oscillations and a retardation in the onset of the disruptive instability /1/,/2/. We suggest that this effect is due to the local enhancement of radial heat conduction due to the magnetic islands produced by the resonant helical windings. The increased heat conduction leads to a flattening of the temperature and current profile around the q = 2 surface with a stabilizing effect on the m = 2, n = 1 mode /3/.

Quantitative examinations are carried out by first fitting a heat conduction coefficient profile $\hat{D}(r)$ to the measured unperturbed temperature distributions. This coefficient is then enhanced over a region corresponding to the size of the magnetic islands by

$$D(r) = \hat{D}(r)\ (1+\alpha \exp - ((q(r)-2)/\delta)^2)$$

and used to compute a modified temperature profile. The resulting current distribution, obtained by assuming $j \sim T_e^{3/2}$ is then tested for stability against the m = 2/n = 1 tearing mode, using the familiar model of Glasser et al. /3/.

Typical unperturbed temperature distributions in Pulsator can be described by $T_e = T_{eo}\ (1 - (r/a)^2)^2$ (a being the limiter radius), corresponding to a current distribution as shown in Fig. 1 (dashed line). For this current distribution and an assumed $q_a = 3.65$, the m =2/n = 1 mode is tearing unstable: a very small plateau in the current distribution is, however, sufficient for its stabilization. The solid line shows the current distribution corresponding to the marginally stable state, which according to the above model can be produced by $\alpha = 5$, $\delta = 0.12$. Stabilization of the m = 2/n =1 mode becomes more difficult if one tries to simulate the action of the sawtooth oscillations by a central flattening of the T_e profile, eliminating the q<1 region in Fig.1. For α =5 one then requires δ = .22 to result in marginal stability (Fig. 2).

For both cases, however, the required island sizes (also for smaller values of α) are well within the range that can be produced by helical currents I_{hel} in the observed stabilizing regime. For values of I_{hel} in excess of a critical value, the region of increased heat conduction will extend out to the limiter (either by direct contact with the m = 2/n = 1 islands, or because of overlapping of the secondary resonances and ergodization of field lines), leading not any more to a local plateau, but to the shrinking of the discharge and an induced disruption.

The crucial point of this model is that it interprets the observed influence of applied m = 2/n = 1 fields on the m = 2/n=1 tearing mode not by some form of direct resonant interaction, but by the modification of the m = 0/n = 0 temperature and current distribution. Further support for this explanation is given by recent experiments using m = 4/n = 2 helical windings (also in resonance with the unperturbed field at the q = 2 surface), which were shown to have a qualitatively similar effect on the m = 2/n = 1 modes at the m = 2/n = 1 windings /4/.

2. Current decay following disruptive instability

The characteristic time for the current decay $\tau_{c.d.}$ following the negative voltage spike in Pulsator has been found consistent with the assumption of a resistive decay following the observed loss of thermal energy /2/. Comparison between published current decay times for other copper-shell tokamaks also shows a surprisingly clear dependence $\tau_{c.d.} \sim a^2$, in spite of the uncertainties in the value of $\langle\sigma\rangle$ after the voltage spike.

Recent results of tokamaks without a copper shell (PLT, Wega) have shown,however, a much faster current decay, with $\tau_{c.d.}$ up to a factor 20 smaller than expected from the above scaling.

Our model for the current decay phase starts from the fact that the observed T_e reduction corresponds to both a resistivity increase and a β_{pol} decay resulting in a loss of equilibrium. In a copper-shell tokamak the plasma immediately finds a secondary equilibrium position in which it then decays resistively. In the absence of a copper shell, such a secondary equilibrium position exists only for the penetration time of vertical fields through the vacuum vessel (unless one has a sufficiently fast feedback system): with this characteristic time the plasma will drift inward and decay. This qualitative model explaining the observed differences in $\tau_{c.d.}$ is supported by calculations combining the equations governing the drift of a plasma in a thin casing /5/ with the circuit equations for the plasma loop - OH system.

References

/1/ F. Karger et al., 5th Conf.on Plasma Phys. and Contr.Nucl. Fusion Research, Tokyo, IAEA-CN-33/PD2

/2/ F. Karger et al., 6th Conf.on Plasma Phys. and Contr.Nucl. Fusion Research, Berchtesgaden 1976, IAEA-CN-35/A-7

/3/ A.H.Glasser, H.P. Furth and P.H.Rutherford, Phys.Rev. Letters 38 (1977) 234

/4/ F. Karger et al., this conference

/5/ V.S.Mukhovatov, V.D.Shafranov, Nucl. Fusion 11 (1971) 605

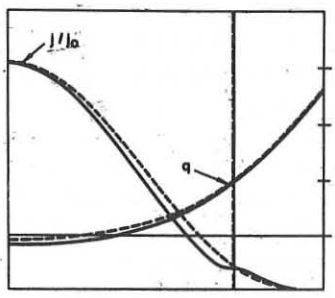

FIG. 1

Stabilization of m = 2/n = 1 tearing mode by current plateau formation for $q_o < 1$ (α =5, δ = 0.12, q_a = 3.65)

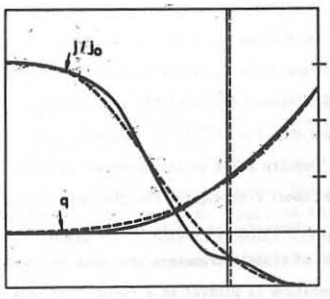

FIG. 2

Stabilization of m = 2/n = 1 tearing mode by current plateau formation for $q_o \geq 1$ (α = 5, δ = 0.22, q_a = 3.65)

TOKAMAK EXPERIMENTS ON JIPP T-II DEVICE

J. Fujita, Y. Hamada*, S. Itoh, K. Kadota, K. Kawahata, Y. Kawasumi, T. Kuroda, K. Matsuoka, K. Matsuura, A. Miyahara, K. Miyamoto, N. Noda, K. Ohkubo, S. Tanahashi, Y. Terashima and K. Toi

Institute of Plasma Physics, Nagoya University, Nagoya 464, JAPAN

Abstract A low $\bar{Z}_{eff}$ ($= \bar{\sigma}_{Spitzer}/\bar{\sigma}_{exp} \simeq 2.5 - 3.2$) tokamak plasma of T_{eo} = 1.1 keV, T_{io} = 570 eV and $I_{pm} \simeq 160$ kA is obtained in JIPP T-II by the feedback control of plasma position and clean vacuum system. The optimization of feedback control also allows tokamak discharge at low safety factor without abrupt current disruption.

Device and Diagnostics JIPP T-II is a hybrid device of tokamak and stellarator with resistive shell [1].

The diagnostic instruments are: Thomson scattering, fast neutral atom energy analyzer, 4mm microwave interferometer, visible light spectrometer, hard X-ray detector and magnetic probes. The image of H_α light at limiter section is always monitored by high speed scanning TV camera through the tangential port. The internal structure of MHD oscillations are examined by an array of five PIN diodes.

Feedback Control Experiment of Plasma Position In tokamak without conducting shell, the feedback control of plasma position is required to reduce the plasma-limiter interaction and to improve the MHD stability which is regarded to have connection with disruptive instabilities. The feedback system has been analyzed and the optimum gain is fixed for the discharge of $I_{pm} \simeq 90$ kA and $B_t = 21.7$ kG. With this loop gain, good tokamak plasmas are obtained for different discharges. As for the plasma position, however, a considerable deviation has been found depending on the time-varying plasma current. This shift is explained by the existence of the effective reference input of feedback control system being used [2]. This is due to the difference between stationary vertical field (B_{VD}) and the one required for equilibration without shell ($B_{\perp o}$).

Figure 1 shows the time behavior of typical plasma parameters for the following three cases. When the plasma position is maintained around the optimum position (case I), the plasma current and loop voltage varies smoothly with time and the MHD oscillation of m = 2 and n = 1 is suppressed. No oscillation is observed on the signals of PIN diodes. When the plasma is shifted outward (case II) by about 3 cm from the optimum position at time of current peak, the safety factor q(a) decreases due to a scraping of plasma minor radius and the oscillation of large amplitude with m = 2 and n = 1 appears from t ≃ 50 to 110 ms. If the plasma is still shifted outward till q(a) becomes less than 2, the discharge tends to be disruptive accompanied with negative voltage spikes (Fig.2). The signals of PIN diodes of chord radii 0, 8 and 15 cm show remarkable relaxation oscillations. In the discharge of inward shift (case III), the oscillation of large amplitude with m = 2 and n = 1 grows up because of significant narrowing of current channel ($\ell_i \gtrsim 1.8$)rather than the decrease of q(a). In contrast to case II, weak relaxation oscillations are observed in the signal of PIN diodes.

The device has been constructed carefully to realize a good vacuum condition; Base pressure of 1.2×10^{-9} Torr. The mean effective ionic charge ($\bar{Z}_{eff}$) derived from the ratio of the Spitzer's conductivity to the measured one remains at about 2 throughout the discharge in the optimum case. For case II, $\bar{Z}_{eff}$ increases from 2 to 4 and $\bar{Z}_{eff} \simeq 3.5$ for case III.

The time variation of plasma parameters are shown in Fig.3. In Fig.4 the peak electron temperature is plotted as a function of peak plasma current. The scaling of ion temperature is also shown together with data of the T-4 tokamak.

Conclusion A realization of good vacuum condition and an optimization of feedback control of plasma position are found to be important to obtain a low $\bar{Z}_{eff}$ and disruption-free tokamak plasma at low q-value.

Acknowledgements Technical assistance by S. Kato and T. Tabata is gratefully acknowledged.

References

[1] J. Fujita et al., 6th IAEA Conf. on Plasma Physics and Controlled Nuclear Fusion Research (Berchtesgaden, 1976), IAEA CN-35/D3.

[2] K. Matsuura, S. Itoh and K. Toi, submitted to Japan J. appl.Phys.

[3] E. P. Gorbunov et al., 6th European Conf. on Controlled Fusion and Plasma Phys., (1973) paper 1.1.

* Present address:
Faculty of Science, Kyoto University, Kyoto, Japan.

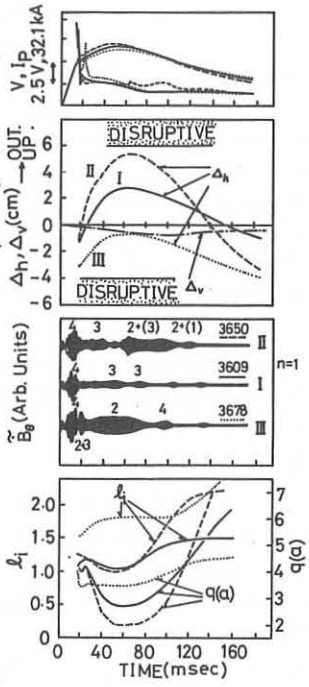

Fig.1 Time variation of typical plasma parameters for three cases; case I: optimum (——), case II: outward shifted discharge (-----), case III: inward shifted one (.....). The numbers on $\tilde{B}_\theta$ are mode numbers (m). $B_t = 21.7$ kG, $I_{pm} \simeq 90$ kA, $p_f = 4.0 \times 10^{-4}$ Torr H_2, $T_{eo} \simeq 0.8$ keV and $n_e \simeq 1.2 \times 10^{13}$ cm^{-3} (t = 80 ms).

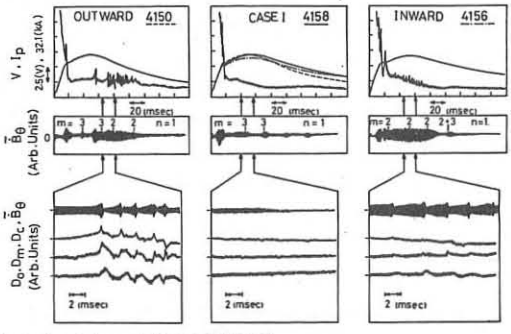

Fig.2 Comparison of three different discharges. D_c, D_m and D_o are the signals of PIN diodes at chord radii 0, 8 and 15 cm, respectively.

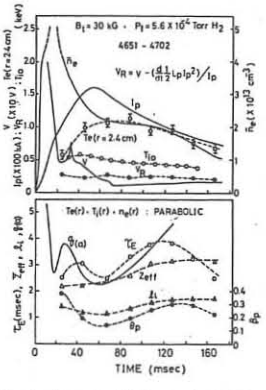

Fig.3 Time variations of plasma parameters.

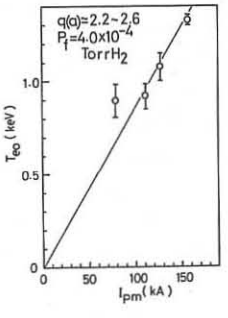

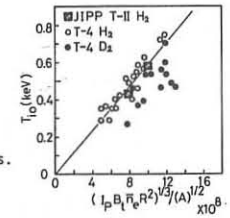

Fig.4 Scalings of plasma temperatures.

SKIN HEATING AND CONFINEMENT IN A TOKAMAK PLASMA

H. de Kluiver, C.J. Barth, H.J.B.M. Brocken, J.J.L. Caarls, B. de Groot, H.W. Kalfsbeek, H.W. Piekaar, W.R. Rutgers, B. de Stigter, H.W.H. Van Andel* and H.W. van der Ven
Association Euratom-FOM, FOM-Instituut voor Plasmafysica, Rijnhuizen, Jutphaas, The Netherlands

(* On leave from Dépt. de Physique, Université de Montréal, Montréal, Canada)

Abstract. Results on plasma confinement, heating and suprathermal radiation during current-driven turbulence in the toroidal device "TORTUR" are reported.

Introduction. TORTUR has been built to investigate turbulent skin heating of a tokamak. The description of the experiment is given in Ref.1. During the turbulent skin heating toroidal electric fields of up to 7 kV/m are generated in the plasma for a few microseconds. Most of the data are obtained for the following conditions: plasma current $I_p = 100 - 180$ kA, toroidal magnetic field 0.8 - 1.6 T, plasma density $\approx 10^{20}$ m^{-3}. Figure 1 shows the time development of the radial current profile. The skin character is still identifiable at some 5 μs after the start of the heating current, changing into a nearly uniform current profile after the heating period is ended by crowbarring (see also Fig. 5.B).

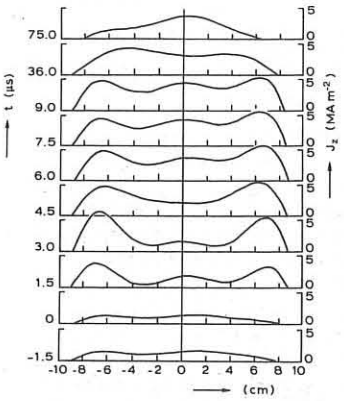

Fig. 1. Toroidal current density as a function of radius and time.

Heating. Due to the anomalous dissipation in the skin the energy density increases in a few microseconds from typically 0.6 kJ m^{-3} up to at least 8 kJ m^{-3}. Comparison with $\int i^2 R dt$ indicates no appreciable loss of energy during turbulent heating. The electron temperature is on the average 1 keV in the skin with a local and temporary peak value near 2.5 keV, as deduced from X-ray emission. This electron temperature is in good agreement with the expected value for turbulent heating $T_e + T_i = \mu_o I_{sk}^2 / 12\pi^2 a^2 n_e e$, where I_{sk} denotes the skin current and a the plasma radius. Some 15 microseconds after current skin collapse, electron temperatures up to 120 eV are measured near the axis with Thomson scattering (Fig. 2). During the skin phase local q-values can be as low as 0.75 during 1 microsecond. To obtain higher temperatures multiple pulsing may have to be considered.

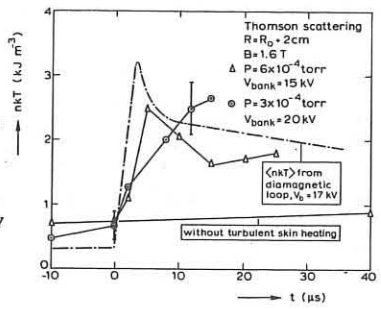

Fig. 2. Energy content at r = + 2 cm vs time as measured by Thomson scattering.

Numerical calculations. A one-dimensional two-fluid MHD-code to follow the development of the skin during the first microseconds of the turbulent heating pulse has been developed[2]. Various anomalous effective collision frequencies have been used and compared. It turns out that the level to which the collision frequency during the saturated state of the ion-acoustic instability can increase has no significant influence on the final results. The ratio of drift velocity and ion sound velocity is found to be constant and equal to ≈ 6 in the turbulent plasma, leading to T_e/T_i-values around 5. Figure 3 shows numerically computed values of resistance and energy density.

Microwave radiation. Suprathermal electromagnetic radiation is emitted during the first microseconds of the heating pulse, at frequencies near f_{pi}, but also at higher frequencies up to f_{ce}.

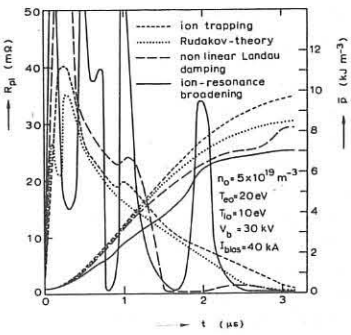

Fig.3. Resistance (the peaked curves) and energy-density values as computed from the one-dimensional code.

Time-resolved measurements of the radiation, covering the band 8-40 GHz**, have been performed with a ten-channel microwave spectrometer. The emitted microwave spectrum averaged over 2 microseconds of the heating pulse, for various values of the magnetic field, is shown in Fig. 4. The spectrum may be interpreted as being the result of a beam-plasma Cerenkov mode, caused by the interaction of freely accelerated electrons with the bulk of the plasma distribution[3]. The latter is limited to drift speeds of the order of the ion-acoustic speed by the ion-acoustic instability.

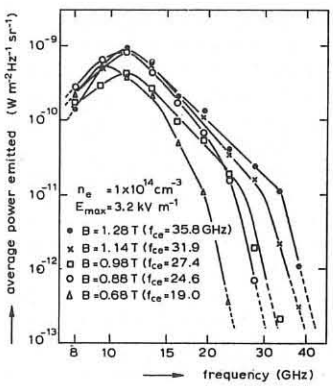

Fig.4. Spectra of average microwave emission during the current pulse rise for various values of the toroidal field B.

Containment. Although plasma temperatures in the keV-range are obtained only a modest plasma confinement (approx. 40 μsec) is achieved after crowbarring the heating bank. The reason for this is the steepening-up of the current profile during the passive current decay which provokes a strong increase in the plasma self-inductance. It is proposed that the rapid current decay is caused by a strong skin cooling due to influxing neutral gas adsorbed on the quartz vessel wall (surface covering up to 2×10^{16} cm^{-2} has been reported[4]). This is demonstrated in Figs. 5A, B, C. The plasma confinement is expected to be considerably improved when a bakable - closed - stainless-steel liner is used instead of the quartz discharge vessel. This proposal has been worked out and looks very promising[5].

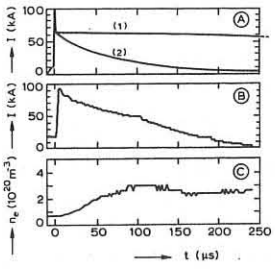

Fig. 5.
A. Plasma currents vs time from computer simulation.
(1) Without influx of neutral gas the current is zero at 1000 μs.
(2) The effect on the plasma current of a five-fold increase in density while the plasma radius decreases in 200 μs from 8.5 cm down to 1 cm.
B. Plasma current vs time in the experiment. Bias current at the start of heating pulse 20 kA.
C. The corresponding average plasma density vs time from CO_2-laser interferometry.

Acknowledgement. This work was performed under the Euratom-FOM association agreement with financial support from ZWO and Euratom.

References

(1) H. de Kluiver et al., submitted to Physics Letters; H.W. Kalfsbeek et al., 7th Eur. Conf. on Contr. Fusion and Plasma Phys., Lausanne, I (1975) 163.
(2) H.W. Kalfsbeek, to be published as a Rijnhuizen Report.
(3) H.W.H. Van Andel, submitted to Physical Review Letters.
(4) W. Köppendörfer et al., 6th Int. Conf. on Plasma Phys. and Contr. Nucl. Fusion Res., Berchtesgaden (1976) E13-1.
(5) H.W. Piekaar, Rijnhuizen Report RR 77-102 (1977).

** This device was put at our disposal by courtesy of Drs. Hamberger and Sharp, UKAEA, Culham.

POLOIDAL BETA LIMITS IN HIGH-DENSITY TOKAMAKS DUE TO NEOCLASSICAL ION HEAT CONDUCTION

F.C. Schüller and D.C. Schram*
Association Euratom-FOM, FOM-Instituut voor Plasmafysica,
Rijnhuizen, Jutphaas, The Netherlands
(* Technical University, Eindhoven)

Abstract. It will be shown that the dominating energy loss mechanism in the centre of high-density tokamak discharges is neoclassical ion heat conduction. This leads to a maximal beta poloidal value which can be reached with ohmic heating at a given density and magnetic field.

Introduction. Gas injection in tokamak discharges have made it possible to raise the electron density n_e to values well above 10^{20} m^{-3} (Refs.1,2). The most important phenomenon is that the energy confinement, τ_E, and poloidal beta, β_θ, increase roughly proportional with the density, which indicates a change in the prevailing energy loss mechanisms. Rather than considering only the changes in τ_E or using elaborate numerical codes, a simple method is introduced[3] to evaluate the confinement. This method is based on the assumption that the experimental profiles can be approximated by gaussians.

The profiles of various plasma quantities. Here only the assumptions on which the evaluation method is based will be outlined: 1) The experimental current-density and electron pressure profiles can be approximated by gaussians: $j(r)/j_o = \exp(-r^2/\Lambda_c^2)$ (1a) and $p_e(r)/p_{eo} = \exp(-r^2/\Lambda_p^2)$ (1b)

2) The T_e-profiles - and consequently also $n_e(r)$ and $n_i(r) = Z_i n_e(r)$ - are taken to be gaussians with $j \propto T_e^{3/2}$.

3) The quantities n_{eo}, T_{eo}, Λ_c, Λ_p are calculated from Thomson-scattering measurements. If no complete profiles are available, Λ_c is calculated from the assumption $q_o \simeq 1$ and Λ_p is taken equal to Λ_c (uncertainty $\leq$ 10%).

4) The shape of the T_i-profile is taken to be equal to the T_e-profile ($T_i(r)=T_{io}T_e(r)/T_{eo}$). The ratio T_{io}/T_{eo} is calculated under the assumption that all ohmic dissipation is transferred to the ions by Coulomb collisions. With these assumptions all quantities of interest can be calculated.

The energy balance. The ohmic input power is the only source causing an energy flow $Q^{eff}(r)$. In a stationary situation ($\partial nkT/\partial t \ll \eta j^2$):

$$Q^{eff}(r) = \frac{1}{r}\int_0^r \eta j^2 r'dr' = 1.3\ 10^{-8} Z_{eff}\Lambda_c j_o^2 \hat{T}_{eo}^{-3/2}\{(1-\exp[-r^2/\Lambda_c^2])\Lambda_c/r\} Wm^{-2}, \quad (2)$$

in which $\hat{T}_{eo}$ is the electron temperature in keV on axis.

This energy flow must consist of contributions due to conduction, convection, radiation and charge-exchange losses. The heat flow due to ion-heat conduction, $Q_i^{cond}(r)$ can be calculated following the notation of Rutherford[4]:

$$Q_i^{cond} = -\kappa_i\ \partial T_i/\partial r = -C_{22}^i(r)\ \sqrt{2}\ n_i k T_i (m_i\omega_{ci}^2\tau_{ii})^{-1}\ \partial kT_i/\partial r, \quad (3)$$

in which $C_{22}^i(r)$ is a coefficient depending on geometry and regime. For a linear geometry: $C_{22}^i = \sqrt{2}$. For a toroidal geometry C_{22}^i is dependent on the collisionalities ν^* and ν^{**}: $\nu_i = (R/r)^{1.5}\nu^* = (R/r)^{1.5}\ qR/v_{thi}\tau_{ii}$.

The following expressions for C_{22}^i are used:

Banana + plateau ($\nu^{**} < 1$): $C_{22}^i = 2q^2(R/r)^{1.5}\ 0.48(1+0.36\nu_i^*)^{-1}$ (4a)

Pfirsch-Schlüter ($\nu^{**} > 1$): $C_{22}^i = 2.26\ q^2$. (4b)

For the high density discharges in Alcator the central core ($r < \Lambda_c$) is in the plateau regime, the outside in the Pfirsch-Schlüter regime. The expression of Hazeltine and Hinton[5] covers all three regimes:

$$C_{22}^i = 2q^2\ 0.47\ (1+0.43\nu_i^{**})(1+1.03(\nu_i^*)^{0.5}+0.18\nu_i^*)^{-1}\ (R/r)^{1.5}\ . \quad (4c)$$

The contribution of ion heat conduction to the total energy flow, given by the ratio Q_i^{cond}/Q^{eff} is shown in Fig. 1 for a typical high density discharge in Alcator, described by Apgar et al.[1]. From this figure the following conclusions can be drawn: 1) In the centre the calculated value of Q_i^{cond} is even larger than Q^{eff}. This must be due to the approximation by a gaussian for $T_i(r)$. Anyhow, the result leaves no space for other loss mechanisms than ion heat conduction. 2) At the outside region other loss mechanisms are more important than Pfirsch-Schlüter ion heat conduction, such as radiation and charge-exchange.

The sensitivity for the choice of Λ_c is tested by redoing the complete calculations with Λ_c enlarged, or diminished by 10% (Fig. 2). The case $\Lambda_c = 0.9\Lambda_p$ gives a somewhat better description especially at the outside, but this does not change the validity of the conclusions.

The scaling of the maximal β_θ. The ratio Q^{cond}/Q^{eff} for the plateau regime in the centre is given by:

$$Q_i^{cond}/Q^{eff} = 3\times10^6\ \frac{A_i^{1/2}}{Z_{eff}Z_i^3}\left(\frac{T_{io}}{T_{eo}}\right)^{5/2}\frac{\beta_{\theta e}^4 B^4}{\hat{n}_{eo}^3 q_o^5}\frac{\Lambda_c^{14}}{\Lambda_p^8 R^7}\left\{\frac{r^4}{\Lambda_c^4}\frac{\exp[-r^2(\frac{1}{\Lambda_p^2}+\frac{1}{\Lambda_c^2})]}{(1-\exp[-r^2/\Lambda_c^2])}\right\}, \quad (5)$$

in which A_i is the ion mass number and $\hat{n}_{eo}$ the electron density in 10^{20} m^{-3}. As $Q_i^{cond} \leq Q^{eff}$, this means that $\beta_{\theta e}$ must be limited to:

$$\beta_{\theta e} \leq 2.4\times10^{-2} Z_i A_i^{-1/8}(T_{eo}/T_{io})^{5/8}\hat{n}_{eo}^{3/4} q_o^{5/4} B^{-1} a^{1/4}(R/a)^{7/4}(\Lambda_p/\Lambda_c)^2(a/\Lambda_c)^{3/2}. \quad (6)$$

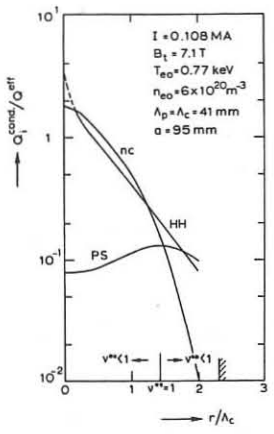

Fig. 1. The ratio Q^{cond}/Q^{eff} for neoclassical (nc), Pfirsch-Schlüter (PS), and Hazeltine-Hinton (HH) ion heat conduction for a typical high-density discharge in Alcator.

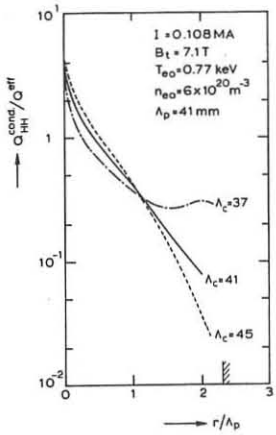

Fig. 2. The ratio Q_{HH}^{cond}/Q^{eff} recalculated for the same discharge as in Fig. 1 with all quantities unchanged except $\Lambda_c = 0.9\ \Lambda_p$ and $\Lambda_c = 1.1\ \Lambda_p$ respectively.

In Fig. 3 the experimental values of the product $\beta_{\theta e}$*B for high-density discharges in Alcator are plotted against n_{eo}. Two curves describing the $\beta_{\theta e}$-limit are plotted for a fixed set of ratios: $T_{eo}/T_{io} = 1.1$; $\Lambda_p = \Lambda_c$; $a/\Lambda_c = 2.3$; one curve is for $Q^{cond}/Q^{eff} = 1$ and the other for $Q^{cond}/Q^{eff} = 2$ (as a possible correction for approximation errors). The values plotted are for hydrogen. One point (encircled) indicates a high density discharge in helium in the ST-device[6] with $Z_{eff} = 2$, scaled with Z_i and geometry.

Conclusions. 1) At high density ($n_{eo} > 3\times10^{20}$ m^{-3}) the experimental $\beta_{\theta e}$ corresponds to the limit set by neoclassical ion heat conduction in the core. 2) At lower density the $\beta_{\theta e}$-values tend to be lower, which indicates the influence of other loss mechanisms. 3) It would be interesting to verify the Z_i-dependence of $\beta_{\theta e}$ by gathering more data of high-density discharges in helium. 4) When during the density increase of a gas-injected tokamak discharge the limiting $\beta_{\theta e}$ is reached, further increase in the density must lead to a lowering of $T_{eo} \propto n_{eo}^{-1/4}$ or to a further peaking of the current-density profile. Consequently, $\tau_E \propto \beta_{\theta e} T_e^{1.5} \Lambda_c^2$ levels off after the initial increase with increasing density at fixed B.

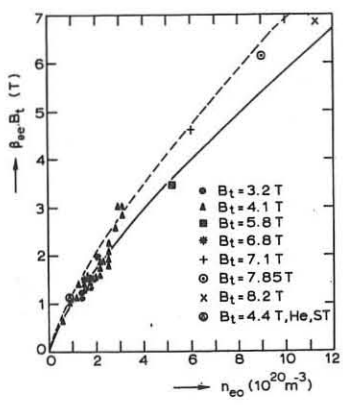

Fig. 3.
The product $\beta_{\theta e}$*B_t as a function of n_{eo} for Alcator discharges in H_2 at various discharge currents and magnetic fields as indicated. Ⓐ indicates an ST-discharge in He, scaled with Z_i and geometry.
— : the maximal $\beta_{\theta e}$-value as given by Eq. (6) for $Q^{cond}/Q^{eff} = 1$; $\Lambda_c = \Lambda_p$; $T_{io} = 0.9\ T_{eo}$; $a/\Lambda_c = 2.3$; $R/a = 5.7$; $q_o = 1$.
-- : the same with $Q^{cond}/Q^{eff} = 2$.

Acknowledgements. The authors thank the Alcator-team for the pleasant cooperation during several periods; they are indebted to Profs. B. Coppi, R.R. Parker and Dr. L.Th.M. Ornstein for stimulating discussions.
This work was performed under the Euratom-FOM association agreement with financial support from ZWO and Euratom, and under the US-ERDA contract at MIT;

References.

1. E. Apgar et al., Proc. 6th Int. Conf. on Plasma Phys. and Contr. Nucl. Fusion Res., Berchtesgaden 1976, Vol. 1, 247.
2. D. Meisel et al., ibid., Vol. 1, 259.
3. D.C. Schram, F.C. Schüller, Rijnhuizen Report 77-104.
4. P.H. Rutherford et al., Int. Symp. on Plasma Wall Interaction, Jülich 1976.
5. R.D. Hazeltine, F.L. Hinton, Phys. Fluids 16 (1973) 1883.
6. D. Dimock et al., Proc. 4th Int. Conf. on Plasma Phys. and Contr. Nucl. Fusion Res., Madison 1971, Vol. 1, 451.

TOKOMAK DISCHARGES IN PETULA WITH ALUMINA CHAMBER

R. BARDET, M. BERNARD, G. BRIFFOD, M. CLEMENT, A. GAUTHIER, M. GREGOIRE, P. GRELOT, M. HESSE, F. PARLANGE, D. PINET, E. PORROT, G. REY, B. TAQUET, J. WEISSE

ASSOCIATION EURATOM-CEA
Département de Physique du Plasma et de la Fusion Contrôlée
Service IGn - Centre d'Etudes Nucléaires
85 X - 38041 GRENOBLE CEDEX

ABSTRACT : Standard Tokomak operation with alumina chamber has been achieved on the PETULA Tokomak. Recycling from the wall is shown to be smaller than in case of the previous metallic liner . Average density up to 5.5 $10^{13}cm^{-3}$ has been obtained by use of fast pulsed valve. According to wall conditioning , Z_{eff} ranges within 1.5 to 4 whereas energy confinement time remains of the order of 4 msec.

INTRODUCTION : For the purpose of R.F. heating experiments, the PETULA Tokomak has been reassembled with a new vacuum vessel which is mainly made of alumina. Technical characteristics and outgassing properties of this vessel have been reported in ref. 1. In the present experimental conditions, the limiter and 80% of the wall facing the plasma are alumina . The radii of the limiter and of the chamber are respectively 14,5 and 16,5 cm. Pumping is provided by turbomolecular and cryogenic pumps. After baking at a moderate temperature (140°C) the base pressure is 2 10^{-8} torr . The filling gas is hydrogen and the magnetic field 16 kGauss. Before Tokomak operation, 15 minutes discharge cleaning at 1.5 kGauss, 25 KA, 0.3 sec repetition rate are performed.

EXPERIMENTAL RESULTS : Compared to those obtained with the previous stainless steel liner /2,3/, the discharges show two major differences. The loop voltage is lower and the electron density decreases continuously during the shot. The second point means that the wall material has a low recycling rate so that electron density must be sustained by gas injection during the discharge, the loop voltage then remaining low. For well conditionned chamber, electron density can be so varied within a large range. On Fig.1, curve 'c' corresponds to full aperture of the valve which has a conductance of 2.5 Torr-liter per second and must be compared to curve 'a' which is typical of a shot without injection. For case 'b,' the valve aperture was reduced after 30 ms. In all cases the filling pressure is 4 .10^{-4} torr before opening the fast valve. Comparison of H_β line emission measured in the vicinity of the gas valve and 60° apart in toroïdal azimuth shows that ionization of the injected gas occurs locally. Maximum value of 5.5 $10^{13}cm^{-3}$ average electron density has been reached, being apparently limited by the conductance of the gas fast valve and the poloïdal field duration.

The concentration of light impurities has been measured in those clean wall conditions for the following discharge characteristics : plasma current = 55 kAmp., B_t = 1.6 Tesla, $\bar{n}_e$ = 2.2 $10^{13}cm^{-3}$. Oxygen density deduced from O_{VI} line (1032 Å) intensity amounts to 3.$10^{11}cm^{-3}$ and aluminium could not be quantitatively measured. This low impurity rate is supported by the 1.8 Volt loop voltage and the electron temperature which shows a rather peaked radial profile with 620 eV axis value.

More detailed measurements have been performed immediately after a major opening. The wall recycling rate remains low in this experiment but a much larger hydrogen flow is required to get the same electron density. The electron density, electron and ion temperature profiles are shown in Fig. 2 and 3. for typical 60 kAmp. discharges the characteristics of which are shown in Fig.4a. Z effective is thus of the order of 4 while it was about 1.5 with the previous clean wall conditions. This increase in Z effective is in agreement with the 10-15 times higher emission level for the oxygen lines. The energy confinement time remains in the range of 4 ms for both conditions.

The time evolution of T_i from charge exchange neutral measurements is plotted on Fig. 4b for various radii as well as the temperature deduced from O_{VII} line (1623 Å) Doppler broadening. It shows that the O_{VII} emission can be located about r = 12cm. Fig.4c shows that ions follow the $(nI)^{1/3}$ Artsimovich dependance only after the plasma current reaches its maximum value.

In turns out from these results that clean wall conditions can be obtained with alumina. Oxygen concentration remains the dominant parameter for the obtention of low Z and high density discharges.

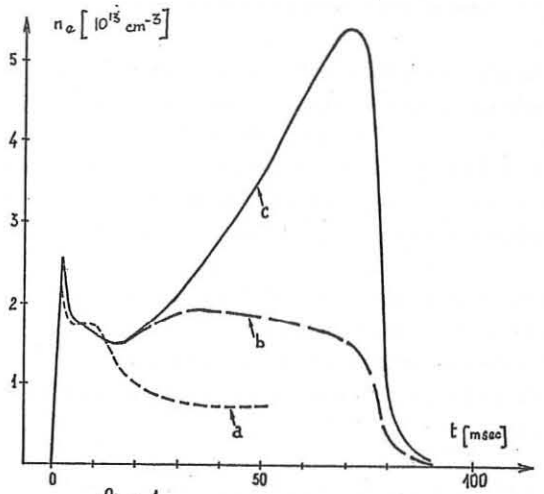

fig: 1

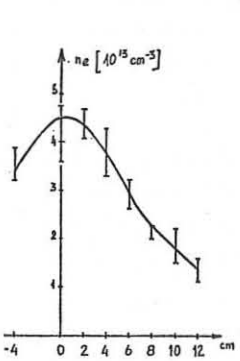

fig: 2

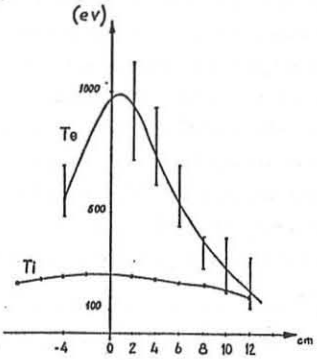

fig: 3

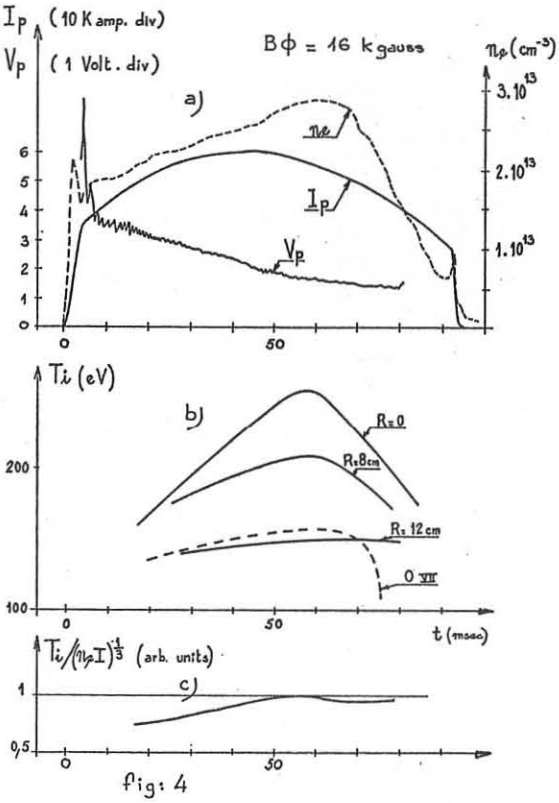

fig: 4

REFERENCES :

/1/ - PETULA GROUP, Int.Symp.on Plasma Wall Interaction, Jülich (1976)

/2/ - R. BARDET et al., Nuclear Fusion 16 4 (1976).

/3/ - PETULA GROUP, VIth Conf. on Plasma Physics and Controlled Nuclear Fusion Research, Berchtesgaden, 6 - 13 October 1976.

CURRENT DENSITY PROFILE OF NONCIRCULAR TOKAMAK

H. Toyama, T. Dodo*, A. Iwahashi, H. Kaneko, K. Makishima,
Y. Nagayama, O. Okada*, I. Ochiai, K. Sakuma, S. Shinohara,
and S. Yoshikawa**

Department of Physics, Faculty of Science, University of Tokyo, Tokyo, Japan
* Central Research Laboratory, Hitachi Ltd., Kokubunji, Tokyo, Japan
** Plasma Physics Laboratory, Princeton University, Princeton, N.J., U.S.A.

Abstract Direct measurements of the current density profile of the noncircular tokamak TNT are presented. In a low current operation (I_p = 8 kA), the elongation ratio has been 1.8 near the time of the current peak. The peaking of the current profile and the decreasing of the elongation with time have been observed.

Introduction A device named TNT (Tokyo Noncircular Tokamak) has been constructed to investigate what type of cross section makes the best use of the advantages of noncircular cross sections. In the first report[1] it has been shown that a D-shaped, elongated plasma can be obtained with a maximum plasma current of 50 kA corresponding to q_a = 2.4 by means of active field shaping. MHD properties, such as kinklike modes and disruptive instabilities, have been investigated. In noncircular tokamaks, a current profile is very important to improve the plasma confinement[2], as emphasized by the concept of FCT (Flux Conserving Tokamak)[3]. Here we present direct measurements of the current density profile of TNT by magnetic probes.

Device Figure 1 is a cross-sectional view of TNT[4]. The major radius is 40 cm. The vacuum chamber has a rectangular cross section (60 cm high and 24 cm wide). The plasma cross section is limited by the molybdenum limiter

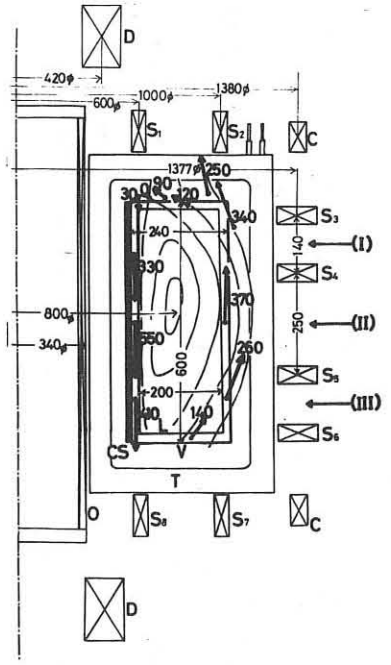

Fig. 1
Cross-sectional view of TNT.
T: toroidal coil
O: ohmic heating coil
S_1-S_8: shaping coils
C: ohmic-canceling coil
D: shaping decoupling coil
V: vacuum chamber
L: molybdenum limiter
CS: copper shell.
B_t = 2.2 kG
I_p = 50 kA.

with a rectangular aperture of 2a = 20 cm and 2b = 56 cm. The 24 toroidal coils supply a maximum toroidal magnetic field of 4.4 kG. The plasma current is driven by an air-core transformer of fifty turns, powered by a 25-kJ capacitor bank. The external shaping field is provided by 8 shaping coils. A 10 mm thick copper shell with gaps is placed as an open shell to restrict the magnetic surface. The vacuum chamber acts as a resistive shell with about 1.6 ms skin time. Hydrogen gas is fed pulsively through two fast-acting valves up to filling gas pressure of $0.7 \sim 7.0 \times 10^{-4}$ Torr, and is preionized with a 10-kW rf (800 kHz) oscillator and an electron gun. The 6-mm microwave interferometer has shown the electron density $\geq 2 \times 10^{13}$ cm^{-3}.

Measurement of Current Density Profile We have measured the poloidal field in the plasma directly, using magnetic probes in a low current operation (I_p = 8 kA). The magnetic probes are 2 mm long and 1.4 mm in diameter with the area-turn of 7×10^{-4} m^2, which give the signal of 140 μV corresponding to 50 G integrated with RC circuit of 26 ms time constant. The magnetic field is measured along the semi-axes of the apparatus; the radial component B_r at the 15 points along r = R_0 (R_0: major radius) and vertical component B_z at the 8 points along z = 0 (on midplane). The behaviors of the plasma current and the loop voltage have been little affected by the insertion of the probes. The procedure to get the current density profile of a noncircular tokamak is more complicated than that for a circular one[5]. The measured poloidal magnetic field $B_r(R_0, Z)$ and $B_z(R, 0)$ are fitted with 5-th order polinomials of z and r, respectively, by the least square method. The magnetic flux function ψ along the measured points is determined by integration of the magnetic field represented by the polynomial. Assuming the magnetic surfaces have elliptic cross sections and the same geometrical center, ψ in the plasma can be evaluated. The unmeasured term in the equation of the current density $j_\phi = \frac{1}{\mu_0}\left(\partial B_r/\partial z - \partial B_z/\partial r\right)$ can be determined from this ψ. A typical example of the current density profile at the current rising stage (t = 500 μs) and at the current peak (700 μs) is shown in Fig. 2. The up-to-down asymmetry observed at the current rising stage has almost vanished at the current peak. The elongation ratio has decreased with time due to the current peaking. The elongation ratio of 1.8 at 700 μs agrees with the data of B_p coils located poloidally on the limiter. In conclusion, these direct measurements have confirmed that the elongated

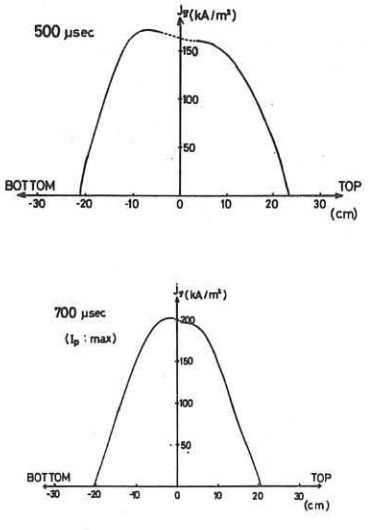

Fig. 2
Typical example of the current density profile, $j_\phi(R_0, Z)$.
B_t = 2 kG,
$I_{p\,max}$ = 8 kA (t = 700μs).

equilibrium can be actively controlled by shaping coils. These measurements also indicate that the current peaking leads to the decrease of the elongation.

References

(1) H. Toyama et al., Phys. Rev. Lett. 37, 18 (1976).
(2) R. L. Freeman et al., 6-th Conf. on Plasma Physics and Controlled Nuclear Fusion Research (Berchtesgaden, 1976) IAEA-CN-35/A10-3.
(3) J. D. Callen et al., ibid, IAEA-CN-35/B10.
(4) H. Toyama et al., ibid., IAEA-CN-35/A10-4.
(5) K.Makishima et al., Phys. Rev. Lett. 36, 142 (1976).

TOROIDAL PLASMA ROTATION IN TOKAMAK LT-3

M. G. Bell

Department of Engineering Physics
Research School of Physical Sciences
The Australian National University
Canberra, A.C.T., 2600, Australia

Abstract. Toroidal flow velocities up to 6 x 10^3 ms^{-1} have been measured in stable discharges in LT-3. The persistence of these velocities indicates the existence of significant non-ambipolar electron diffusion from the plasma.

Experiments. The toroidal flow of the plasma in tokamak LT-3 (R = 0.4m, a = 0.1m) has been deduced from the Doppler shift of the oxygen impurity line OV 2781 Å, the profile of which was analysed with a seven channel polychromator [1]. Light from a line of sight tangential to the minor axis was reflected into the analyser by a small mirror mounted just inside the vacuum vessel. The mirror could be rotated to view the plasma either parallel or anti-parallel to the discharge current. By comparing the results from the two directions, the absolute shift of the line could be determined. Figure 1 shows the radial profile of OV emission in a stable discharge at the time of peak current (t = 2.2ms, I_ϕ = 10kA, B_ϕ = 0.5T) together with a histogram indicating the relative contribution of each annular region to the total emission seen along the experimental line of sight. Although the contribution of the central region, r < 25mm, dominates, it was found in the analysis that there were small but detectable differences between the apparent shifts of the wings and the centre of the line profile. The line wings, which are dominated by emission from the hottest central region of the plasma, yielded velocities up to 50% greater than the line centre. As a result of the low ion temperature in LT-3, $T_i \lesssim 30$eV, rotation velocities as low as 1kms^{-1} could be detected. In figure 2, we show for two successive shots, the toroidal velocity and also the longitudinal ion temperature deduced from the line width during the interval 1.5 - 4.5ms when OV emission is strong. The results indicate fairly rapid flow of the OV ion component in the direction of the toroidal current. As a result of collisions with electrons, the OV ions with charge Z = 4 will tend to lag behind protons travelling parallel to the current by a velocity which may be as high as 1kms^{-1} in these conditions so that the bulk flow velocity may actually be somewhat higher than that shown.

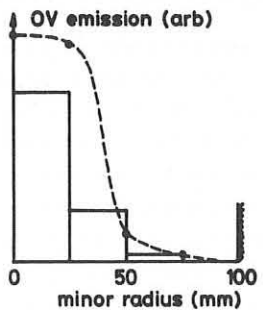

Figure 1

Discussion. In all collisionality regimes, neoclassical transport theory predicts a toroidal flow driven by radial gradients of temperature, density and the electrostatic potential [2]. Such rotation has previously been observed in ORMAK in the collisionless regime [3]. However, it has also been shown [4] that in the plateau and collisional regimes, which apply in LT-3, the flow should decay to zero as non-ambipolar ion diffusion, associated with charge exchange or magnetic ripples, readjusts the electrostatic potential. Since the charge exchange time in LT-3 is of order 200μs, we would not expect the observed rotation to persist through a discharge unless a mechanism exists to maintain the potential above the expected zero velocity level of about -100V. It may be calculated that an extra potential of order +10V is required to account for the observed velocities. The required mechanism may actually be provided by the neutral population in the plasma. Electron impacts with neutrals, which are relatively probable in LT-3 conditions, will cause a non-ambipolar drag on the electron component which is drifting with considerable velocity relative to the ions.

Acknowledgements. I wish to thank Dr. A. H. Morton and Dr. L. F. Peterson for help with some of the experiments, Dr. R. L. Dewar for helpful discussions and Professor B. S. Liley for his continuing interest in this work.

References.

[1] M. G. Bell: to appear in Plasma Physics.

[2] R. D. Hazeltine: Phys. Fluids 17 (1974) 961.

[3] D. J. Sigmar, J. F. Clarke, R. V. Neidigh, K. L. Vander Sluis: Phys. Rev. Lett. 33 (1974) 1376.

[4] K. T. Tsang, E. A. Frieman: Phys. Fluids 19 (1976) 747.

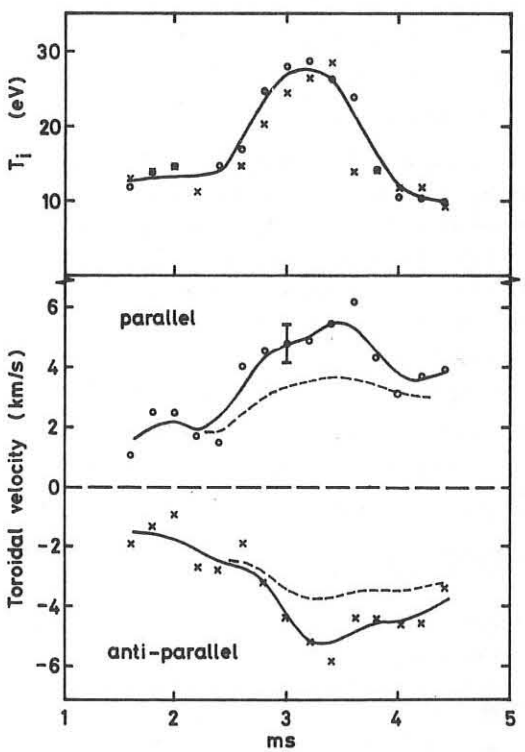

Figure 2. Toroidal rotation velocity and longitudinal ion temperature from measurements parallel and anti-parallel to the plasma current. The experimental points and full curves relate to the wings of the line profile, the dashed curves to the line centre.

Saturation of Kink Instability and Helical Equilibrium of Cylindrical Tokamak

Sanae Inoue*, Kimitaka Itoh* and Shoichi Yoshikawa+

* Department of Physics, Faculty of Science, University of Tokyo, Tokyo, Japan

+ Plasma Physics Laboratory, Princeton University, Princeton, N.J., U.S.A.

Abstract Nonlinear saturation levels of kink modes are obtained by use of the neighbouring equilibrium method for various current profile cases.

Generally we observe the kink modes in their nonlinearly saturated state in which they no longer grow (in MHD time); the plasma is in an equilibrium governed by the equation $\vec{J} \times \vec{B} = \nabla p$ with helical symmetry. This fact implies that the plasma moves from a cylindrical equilibrium to a helical one. The helical equilibria in linear theory dictates the bifurcation points of the cylindrical and helical equilibria. Here we evaluate the saturation levels of kink modes by finding helical equilibria with finite amplitude deformation.

In the large aspect ratio limit ($R/a \gg 1$), a tokamak plasma is approximated as a current carrying plasma cylinder (radius a) immersed in a strong magnetic field. We use helical coordinates, r, $\phi = m\theta + k_z z$ and $\chi = (mz - k_z r^2\theta)/(m^2 + k_z r^2)$ (r, θ and z are the ordinary cylindrical coordinates with $r=0$ at the axis of the cylinder, m and $k_z R$ correspond to mode numbers). The plasma column has the helical symmetry. We define ψ and B_ϕ as $\psi = k_z r A_\theta - m A_z$ and $B_\phi = k_z r B_\theta - m B_z$. The plasma equilibrium equation with χ independence gives

$$\left(k_z^2 + \frac{m^2}{r^2}\right)\frac{\partial^2\psi}{\partial\phi^2} + r\frac{\partial}{\partial r}\frac{1}{r}\frac{\partial\psi}{\partial r} + \frac{2m^2}{r[m^2+(k_z r)^2]}\frac{\partial\psi}{\partial r} + \frac{2mk_z B_\phi}{m^2+(k_z r)^2}$$

$$= -\,d(B_\phi^2/2)/d\psi - \mu_0[m^2+(k_z r)^2]\,dp/d\psi \quad , \qquad (1)$$

$B_\phi = B_\phi(\psi)$ and $p = p(\psi)$.

B_ϕ^2 is also expressed as $B_\phi^2 = B_\theta^2 + 2\mu_0\int[(mJ_z - k_z r J_\theta)d\psi - (k_z^2 r^2 + m^2)dp]$. In low β limit, B_ϕ in the left hand side of Eq.(1) is replaced by B_0 unless the case of $q < k_z^2 r^2 \ll 1$. We expand ψ as $\psi = \psi_0(r) + \alpha\psi_1(r)\cos\phi + \alpha^2\psi_2 + \cdots$ (both in the plasma and in the vacuum) and $J_z = J_0(r) + \alpha J_1(r)\cos\phi + \alpha^2 J_2(r) + \cdots$. The constant ψ surface is also deformed as $r(\psi,\phi) = r_0 + \delta_1\cos\phi + \delta_2 + \cdots$ where δ_1 and δ_2 are given like

$$\delta_1 = -\alpha\psi_1/\psi_0' \quad , \qquad (2\text{-}1)$$

$$\delta_2 = -\alpha^2(\psi_2/\psi_0' - \psi_1\psi_1'/2\psi_0'^2 + \psi_0''\psi_1/4\psi_0'^2) \quad . \qquad (2\text{-}2)$$

From now on, we analyze this problem noting the safety factor q and the current con entration ratio $\kappa = q(a)/q(0)$. Both are

$$q = q^*\left[1+\left(1-\frac{q^*}{m}\right)\left(\frac{\delta_1}{2r_0}\frac{d\delta_1}{dr} + \frac{\delta_2}{r} + \frac{d\delta_2}{dr}\right)\alpha^2\right] \equiv q^*[1+(1-\tfrac{q^*}{m})\sigma\alpha^2], \qquad (3\text{-}1)$$

$$\kappa = \kappa\left[1 + \frac{J_2\int_0^a J_0 r dr - J_0\int_0^a J_2 r dr}{J_0\int_0^a J_0 r dr}\alpha^2\right] \equiv \kappa_0 + \nu\alpha^2 \quad . \qquad (3\text{-}2)$$

We expand Eq.(1) and retain terms up to the 2nd order of α. To the lowest order of $(k_z r)^2$ we obtain

$$\frac{1}{r}\frac{d}{dr}\,r\,\frac{d\psi_0}{dr} - 2k_z B_0 = m\mu_0 J_0(r) \quad , \qquad (4\text{-}1)$$

$$\frac{1}{r}\frac{d}{dr}\,r\,\frac{d\psi_1}{dr} - \frac{m^2}{r^2}\psi_1 = m\mu_0\frac{J_0'}{\psi_0'}\psi_1 \quad , \qquad (4\text{-}2)$$

$$\frac{1}{r}\frac{d}{dr}\,r\,\frac{d\psi_2}{dr} = m\mu_0 J_2(r) \quad . \qquad (4\text{-}3)$$

The boundary condition is that $B_r = 0$ at the wall (radius b) and the continuity of $B_\perp$ to the plasma surface. This gives the condition which determines the critical q value q^* as

$$\psi_1'(a)/\psi_1(a) = -m[1+(a/b)^{2m}]/[1-(a/b)^{2m}] \quad , \qquad (5)$$

at which the plasma is in a helical equilibrium with infinitesimal deformation. From the 2nd order equation, we get the nontrivial solution of α in terms of q and κ. The plasma transport equation governs the time evolution of $\alpha(t)$ closely coupled with $\kappa(t)$ and $q(t)$. Here we do not simulate the history of $\alpha(t)$, we take a simple constraint that the current density profile does not change. Equation (3-1) gives $\alpha = \sqrt{(q-q^*)/\sigma}$ [2], the measurable quantity $\tilde{B}_r(a)/B_\theta(a)$ is given by

$$\left(\frac{\psi_1(a)}{k_z B_0 a^2}\frac{m^2}{\sqrt{\sigma}}\sqrt{\frac{mq^*}{m-q^*}}\right)\cdot\sqrt{q-q^*} \quad ,$$

where $|q-q^*| < 1$. The saturation amplitude given above indicates the linear growth rate, that is, $|\tilde{B}_r/B_\theta| \propto \gamma_L$ since γ_L^2 is approximately proportional to $q-q^*$.

Fig.1

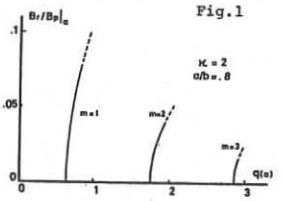

We show some examples of $\tilde{B}_r/B_\theta$. The current density is $J_0(r) = J_0[1-A(r/a)^2+(A-1)(r/a)^4]$. [3] Figure 1 shows the case of $\kappa=2$ and $a/b=.8$ for $m=1,2,3$ modes. For each case, the $q<m$ side (kink) branch is shown. In spite of the tendency of the linear growth rate, the saturation amplitude does not vanish at $q=m$ and will connect to the internal and/or the tearing mode. Figure 2 shows the dependence on the current profile for $m=2$ mode ($a/b=.8$). In Fig.3 we see that $\tilde{B}_r/B_p$ strongly depends on a/b. This tells that the shell (or shaping coils) must be placed as close as possible to the plasma surface.

In this paper we use the constraint $J_0(r) = J_2(r)$ from the following reason; real tokamak plasmas have the finite resistivity and the anomalous skin effect so that the flux conservation condition is not always a good approximation, the experimental observation shows us that the current profile changes much slower than MHD activities [3]. By means of the flux conservation condition which implies $\sigma(r) = 0$, ψ_2 can be solved from Eqs.(2) and (3-1). Using Eqs. (2-2) and (4-3), α as a function of κ is determined. It will be interesting to compare our results to the case of $\sigma = 0$.

Fig.2

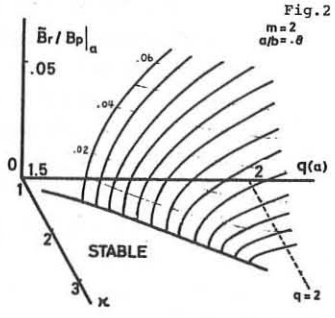

References

1] S.Inoue, K.Itoh and S.Yoshikawa, Phys. Letters 53A (1975) 342.

2] K.Itoh, S.Inoue and S.Yoshikawa, J. Phys.Soc.Japan 41 (1976) 725.

3] K.Makishima, T.Tominaga, H.Toyama and S.Yoshikawa, Phys.Rev.Letters 36 (1976) 142.

Fig.3

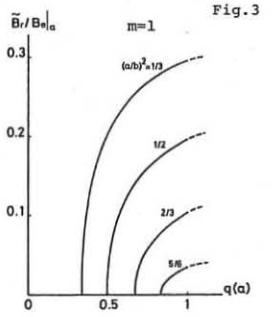

STATIONARY AXISYMMETRIC STATES WITH DIFFUSION AND HEATING OF TOKAMAK CONFIGURATIONS

C. Mercier

ASSOCIATION EURATOM-CEA SUR LA FUSION
Département de Physique du Plasma et de la Fusion Contrôlée
Centre d'Etudes Nucléaires
Boîte Postale n° 6. 92260 FONTENAY-AUX-ROSES (FRANCE)

ABSTRACT : A set of integro-differential equations describing the M.H.D equilibrium of a plasma in axisymmetry, including the transport coefficients and Ohmic and non-Ohmic heating, is established. These equations have been solved numerically.

The physical phenomena which occur in the equilibrium and evolution of Tokamak discharges are numerous and very complex and can only really be accounted for by means of numerical codes, such as the MAKOKOT code at Fontenay [1]. However, it is useful to study analytically these equilibria under more schematic conditions in order to gain a better insight into the results found both experimentally and by the numerical codes. In particular, the influence of the functional forms of the transport coefficients and of different forms of heating may be better understood. A good analytical description is also necessary to study the stability of the equilibria and to predict the behaviour of Tokamaks under various conditions.

In axisymmetry, the equilibrium is given by [2]

$$(1)\quad \mathcal{L}F = -\frac{1}{2}\frac{df^2}{dF} - X^2\frac{dP}{dF} = A(F) + (X_0^2 - X^2)\frac{dP}{dF}$$

upon defining $X_0(F)$ to be (2) $X_0 = \langle X^2 \rangle^{1/2}$

where $\langle M \rangle = \oint \frac{Mdl}{X|\text{grad } F|} \left(\oint \frac{dl}{X|\text{grad } F|}\right)^{-1}$, the integration being taken along a cross-section boundary of a magnetic surface F = const. We put $E_\varphi = \frac{\varepsilon_0}{X} = \frac{\eta_0}{T_e^{3/2}} j_\varphi$ where ε_0 = const.

As a simplification we will use, instead of the diffusion equation, the relation $n = \xi T_e^{\omega}$ which is very well satisfied in the actual Tokamaks. ω is generally close to 1/2 and we shall take this value as an example. We finally obtain :

$$(3)\quad \mathcal{L}F = A(F) + (X_0^2 - X^2)\frac{\xi}{\varepsilon_0}\frac{\eta_0}{}\frac{dA}{dF}$$

$$A = \frac{\varepsilon_0}{\eta_0} \langle T_e^{3/2} \rangle .$$

Determination of A(F). We write the heat transport equation in the form $\nabla Q = E_\varphi \gamma_\varphi + s$ where $E_\varphi \gamma_\varphi$ represents the ohmic heating and s the heat losses together with any other form of heating. Suppose that $Q = -\frac{H(F)}{X^2}\nabla F$ we obtain

$$H + \varepsilon_0 = \frac{1}{2\pi}\frac{\iiint s dv}{I(F)}$$

where I is the plasma current across the cross-section of the surface F = const. In order to account for the rapid transmission of the heat along the magnetic lines only the mean $\overline{s}(F)$ must enter into the problem and so we have

$$H = -\varepsilon_0 (1 + m\frac{J_{boundary}}{J(F)}) \quad \text{where}$$

$$(4)\ J(F) = \int_0^{S_r}\frac{A}{X_0} dS_r \Big/ \int_0^{S_r}\overline{s} X_0 dS_r \quad \text{and} \quad (5)\ S_r = \iint \frac{X_0}{X} dS \neq S .$$

We now choose the heat transport coefficient $K \sim F^{\overline{\alpha}} q^\beta n^\gamma \sim \overline{T}^{\alpha} q^\beta$. Then $Q = -\frac{K_0}{X^2}\overline{T}^{\alpha} q^\beta \nabla\overline{T}$ where (6) $q = \frac{f}{2\pi X_0}\frac{dS_r}{dF}$ is the safety factor and $\overline{T} = \langle T^{3/2} \rangle^{2/3}$.

We consequently find :

$$(7)\ A = \frac{\varepsilon_0}{\eta_0}\left[\frac{\varepsilon_0(\alpha+1)}{K_0}\int_{S_r}^{S_{r0}}(1 + m\frac{J_b}{J}) q^{-(1+\beta)}\frac{f}{2\pi X_0} dS_r\right]^N .$$

$N = \frac{3}{2(\alpha+1)}$. $\overline{s}(F)$ and $f = X B_\varphi$ being given, the set of equations (2)— (7) defines the problem posed.

The boundary condition will be taken to be F = o on the plasma boundary.

These equations have been solved numerically by Le Fol and Tooris under contract with the C.I.S.I.

Special cases - To illustrate the results, we will choose several special cases.

1) In the cylindrical case, the equations reduce to differential equations which have already been studied in particular in [3]. The principal result was the following:in the case of Ohmic heating alone there exists one and only one solution if $0 < N < \frac{2}{\beta}$ or $< +\infty$ if $\beta \leq 0$.

Otherwise , there is no equilibrium solution and the numerical code shows that the plasma temperature becomes progressively more and more peaked Fig.2

2) Ohmic heating alone (m = o)

As an example, let us choose $\beta = -1$ and f/X_0 = const. In this case, the equation becomes :

$$\mathcal{L}F = \lambda\left[(1 - S_r)^N - \frac{X_0^2 - X^2}{X_0^2}\frac{3\mu_0}{8\pi}(1 - S_r)^{N-1}\frac{dS_r}{dF}\left(\frac{dS_r}{dF}\right)^{-1}_{axis}\right]$$

where λ will be determined by the boundary conditions and $\frac{1}{\mu_0}$ is the ratio between the real transport coefficient taken on the magnetic axis and a reference coefficient $K_r = n\eta$ which is always close to the experimental value. The calculations have been performed for different values of N and μ_0 — N = 6 being close to actuality — and for elliptic, racetrack and D-shaped cross-sections. The domain of possible equilibria does not seem to be very dependent upon the type of cross-section. With Ohmic heating alone, the equilibrium β values are of the order of a few percent. With a more evenly distributed additional heating, one would expect β-values conderably higher.
In Figs. (3) and (4) are represented the magnetic surfaces, the temperature T_e and the current density for a D-shaped plasma. It is a limiting case with $\beta = 0.04$.

REFERENCES.-

[1] Code MAKOKOT, Rapport mixte C.E.A.-C.I.S.I. EUR-CEA 832.

[2] Lectures in Plasma Physics - EUR 5127e - Luxembourg, Sept. 1974.

[3] C. MERCIER, SOUBBARAMAYER, 7th European Conference on Cont. Fus. and Plasma Phys. 1975 - Vol.II - Supplem. papers-
C. MERCIER - Rapport EUR-CEA-FC-812, Février 1976.

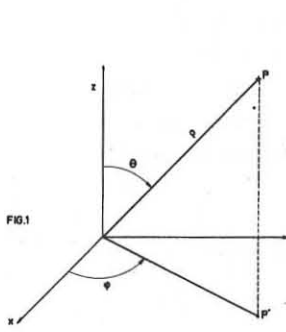

FIG.1

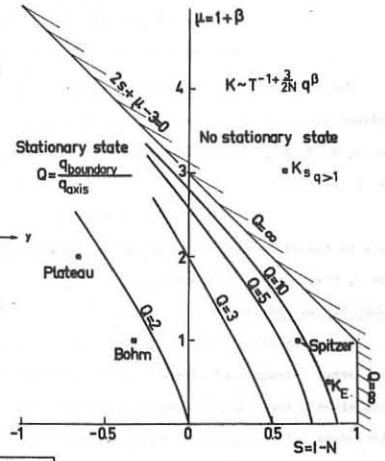

FIG 2

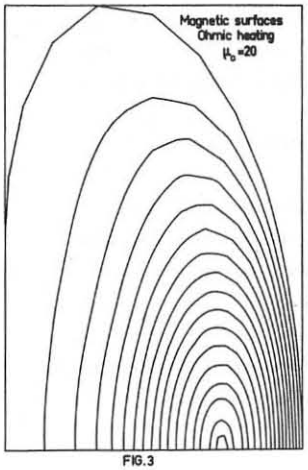

FIG.3

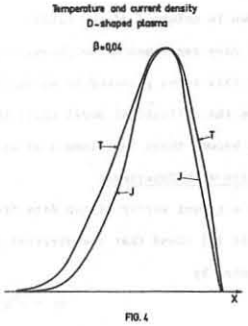

FIG. 4

SCALING LAWS FOR PLASMA CONFINEMENT

J.W. Connor and J.B. Taylor

Culham Laboratory, Abingdon, Oxon, OX14 3DB, UK
(Euratom-UKAEA Association)

Scaling laws must be invariant under any transformation which leaves the basic plasma equations invariant. The constraints which this imposes on the scaling law are derived for several plasma models and found to conflict with empirical scaling laws.

The 'scaling law' is the relation between energy confinement time τ and the main experimental parameters such as radius a, magnetic field B, plasma density n and temperature T.

The present discussion is based on the observation that if the basic equations of plasma behaviour are invariant under some group of transformations, then any scaling law derived from them must be invariant under the same transformations. This property severely circumscribes what scaling laws are compatible with any given plasma model.

Collisionless, low-β Vlasov model

The simplest case is that of a collisionless, low-β plasma described by the Vlasov equation

$$\frac{\partial f_i}{\partial t} + (\underset{\sim}{v} \cdot \nabla) f_i + \frac{e_i}{m_i}(\underset{\sim}{E} + \underset{\sim}{v} \times \underset{\sim}{B}) \frac{\partial f_i}{\partial \underset{\sim}{v}} = 0$$

where the electric field is determined by charge neutrality and the magnetic field is prescribed. There are three independent linear transformations which leave this model invariant. They are

$$A_1: \quad f \to \alpha f$$

$$A_2: \quad v \to \beta v, \; B \to \beta B, \; t \to \beta^{-1} t, \; E \to \beta^2 E$$

$$A_3: \quad x \to \gamma x, \; B \to \gamma^{-1} B, \; t \to \gamma t, \; E \to \gamma^{-1} E$$

One can show, (by considering the heat flux Q which is directly defined in terms of f and v), that an energy confinement time depending on n, B, T, a will be invariant under these transformations only if it is of the form

$$B\tau = F(T/a^2B^2)$$

This is therefore the only scaling law compatible with the collisionless, low-β, Vlasov model of plasma.

Other Plasma Models

In a similar way one can determine what scaling laws are compatible with other conventional plasma models. We have investigated (i) The collisional, low-β model - described by the Boltzman transport equation (including collisions) plus charge neutrality and prescribed magnetic field. (ii) The collisionless, high-β model - described by Vlasov's equation, charge neutrality and the Maxwell equations $\nabla \times B = 4\pi j$, $\nabla \times E = \partial B/\partial t$. (iii) The collisional, high-β model, described by the Boltzman equation, the Maxwell equations and charge neutrality.

The results, together with those for ideal and resistive fluid models, are shown in column 2 of the table.

In many experiments the plasma is heated by ohmic dissipation. If we take this to be governed by an ohm's law (not necessarily classical) based on the collisional model (iii) the scaling laws for ohmic heated plasmas become those in column 3 of the table.

Comparison with Experiment

In a recent survey of the data from Tokamak experiments, Hugill and Sheffield [1] found that the observed confinement times can be well represented by

$$B\tau = n^x B^y a^z$$

with $x = 0.61 \pm .08$, $y = 1.89 \pm .13$, $z = 1.57 \pm .17$. Unfortunately this

Plasma Model	Scaling Law for $B\tau$ (General)	Scaling Law for $B\tau$ (Ohmic Heating)
Collisionless low-β	$B\tau = F(T/a^2B^2)$	$B\tau = F(na^7B^4)$
Collisionless low-β	$B\tau = F\left(\frac{T}{a^2B^2}, \frac{na^2}{B^4a^3}\right)$	$B\tau = F(na^2, a^3B^4)$
Collisionless high-β	$B\tau = F\left(na^2, \frac{T}{a^2B^2}\right)$	$B\tau = F(na^2, a^3B^4)$
Collisionless high-β	$B\tau = F(na^2, Ta^{\frac{1}{2}}, Ba^{3/4})$	$B\tau = F(na^2, a^3B^4)$
Ideal MHD	$B\tau = (na^2)^{\frac{1}{2}} F(nT/B^2)$	$B\tau = n^{\frac{1}{2}}a\, F\left(\frac{n^2a^4}{a^3B^4}\right)$
Resistive MHD	$B\tau = (na^2)^{\frac{1}{2}} F(nT/B^2, Ta^{\frac{1}{2}})$	$B\tau = n^{\frac{1}{2}}a\, F\left(\frac{n^2a^4}{a^3B^4}\right)$

empirical law is not compatible with any of the models considered, as may be verified from the table.

A possible cause of this discrepancy may be radiation from impurities. This can be incorporated into the resistive fluid model through an effective charge Z introduced into ohm's law and the addition of a radiation energy-loss $P_{rad} \sim n^k T^\ell Z^m$. The invariance properties of the model then require the scaling law to be of the form

$$B\tau \sim n^{\frac{1}{2}} A^{\frac{1}{2}} a\, F\left(\frac{nT}{B^2}, \frac{Ta^{\frac{1}{2}}}{A^{\frac{1}{2}}}, Ba^b Z^c A^d\right)$$

where A is atomic mass and the indices b, c, d are related to the indices of the radiation energy-loss formula.

Conclusions

Each of the conventional plasma models imposes characteristic constraints on any scaling law which can be derived from it. In the extreme example of a collisionless low-β model $B\tau$ can depend only on the ratio $T/a^2B = B/N$. (Incidentally the only local transport coefficient possible in this regime scales like Bohm diffusion!) In the collisionless high-β regime $B\tau$ can depend only on β and the line density N. For ohmically heated plasmas all models require $B\tau$ to be a function of N and $(Ba^{5/4})$ and the temperature to be given by $T \sim a^{-\frac{1}{2}} F(N, Ba^{5/4})$.

These results reduce the number of adjustable parameters which have to be determined empirically - provided the appropriate model is known. Alternatively one could use the data to determine which models are appropriate.

Unfortunately the empirical laws which have so far been proposed appear incompatible with the conventional plasma models. This may be because radiation from impurities is important and the effect of this in the resistive fluid model has been determined.

Finally, we note that similar scaling laws apply to particle confinement times.

We thank Drs Hugill and Sheffield for many helpful discussions.

[1] Hugill, J and Sheffield J. "Empirical Tokamak Scaling", To be published. Also in R S Pease, Contemporary Physics 18 (1977) 113.

BALLOONING MODES IN TOKAMAKS WITH FINITE SHEAR

J. M. Greene, M. S. Chance, A. H. Glasser, and E. A. Frieman
Princeton University, Plasma Physics Laboratory
Princeton, New Jersey 08540 USA

D. R. Dobrott
General Atomic, San Diego, California 92112 USA

D. B. Nelson
Oak Ridge National Laboratory, Oak Ridge, Tennessee 37831 USA

ABSTRACT

Ballooning modes are calculated from two different approximations to ideal MHD theory. The first approximates the full set of equations numerically; the second utilizes an expansion in large toroidal mode number to reduce the problem to a series of differential equations along lines of force. Excellent agreement is found, and the importance of the modes is assessed.

Application of the Princeton Equilibrium, Stability, and Transport Code (PEST)[1] has shown that in many configurations a stability limit on achievable plasma pressure is determined by fully developed ballooning modes.[2] These are driven by force associated with the pressure gradient and have the character of interchanges, but are concentrated in regions where field line curvature is unfavorable. The interchange vortices penetrate to the core of the plasma, and exist even when the plasma surface is constrained to be stationary. Thus, they cannot be stabilized from outside the plasma, and could strongly affect the containment properties of high pressure systems.

In addition to the numerical work, we are also carrying out a more analytic approach to the understanding of these modes.[3] The method is to consider high toroidal mode numbers. This provides a complementary localization to that utilized in the usual interchange stability criterion, where localization in the vicinity of a magnetic surface is assumed.

The calculations have been done for systems with finite shear that satisfy the usual interchange stability criterion. PEST results have shown that marginal ballooning modes in these systems satisfy periodicity requirements by being fully modulated around the minor cross section. That is, the amplitude of the mode at some azimuth vanishes in the limit of large toroidal mode number n.

When these ideas are included, the energy principle for ideal MHD reduces to a set of ordinary differential equations for each magnetic surface, with the boundary condition that the solutions vanish ar $\theta = \pm \pi$, i.e., on the inside of the torus where the local curvature is most stabilizing.

A simple computer program has been written that integrates this differential equation along field lines for numerically determined equilibria. The results of this program are then compared with those from PEST for the same configuration. Excellent agreement is found.

The context of this agreement involves several considerations. The PEST code cannot accurately treat modes with really large values of n because the mode has fine scale structure and is hard to resolve in this limit. Typically, comparison is made with $n = 3$. Even so, care must be taken to ensure that a sufficiently fine mesh has been taken that the PEST results are meaningful. On the other hand, it is found experimentally that with proper numerical care, $n = 3$ agrees remarkably well with large n predictions. The implication is that higher order corrections in powers of $1/n$ are relatively small.

Further, the treatment for large mode numbers does not account for terms that drive free boundary instabilities. Thus, agreement between the two approaches is successful primarily when the perturbation is required to vanish at the plasma boundary.

To conclude, several features indicate that these fully developed ballooning modes should be taken seriously. They can occur for relatively small values of the toroidal mode number n, where MHD theory is most nearly valid. They can occur at significant values of plasma pressure, even under the conservative assumption that the plasma boundary is held fixed. Finally, the mode structure of vortices extending right into the center of the plasma could be quite damaging.

ACKNOWLEDGMENTS

The authors would like to thank many people for their aid and advice. The assistance of the PEST Group including Drs. R. C. Grimm, J. Manickam, Y. Y. Hsieh, and J. L. Johnson, has been essential in helping us visualize the nature of the instabilities. Finally, we would like to thank Drs. A. M. M. Todd, F. J. Helton, and M. Okabayashi for sharing their computational results with us.

Work supported by U. S. Energy Research and Development Administration Contract E(11-1)-3073.

REFERENCES

[1] R. C. Grimm, J. M. Greene, and J. L. Johnson, Methods in Computational Physics, J. Killeen, editor (Academic Press, New York, 1976) Vol. 16, p. 253.

[2] A. M. M. Todd, et al., Phys. Rev. Letters 38, 826 (1977).
G. Bateman and Y-K. M. Peng, Phys. Rev. Letters 38, 829 (1977).

[3] D. R. Dobrott et al., to be published.

QUASI-LINEAR PROCESSES IN THE SLIDE-AWAY REGIME OF A TOROIDAL PLASMA

A. Airoldi Crescentini, A. Orefice and R. Pozzoli

Laboratorio di Fisica del Plasma - Associazione CNR-EURATOM
Istituto di Fisica - Via Celoria 16, 20133 Milano (Italy)

ABSTRACT. The quasi-linear evolution of a current carrying plasma, in the presence of magnetically confined electrons, is considered. Under resonant conditions ($Re(\omega)=\underline{k}\cdot\underline{v}_i=k_\parallel v_{\parallel e}$) a considerable energy transfer is possible to the ion population.

In the so-called slide-away regime of a toroidal plasma /1,2/ a strong distortion is observed in the electron distribution function, in correlation with a considerable increase of transverse ion temperature and with a radiofrequency emission between ω_{pi} and $5\div10\,\omega_{pi}$. The parallel energy, imparted by the toroidal electric field to the circulating electrons, is partially transferred, through a Landau interaction, to the electrostatic modes characterizing the slide-away situation /2,3/, and drives some of them unstable. Another Landau mechanism provides a certain amount of (transverse) energy transfer from the waves to the ions. The relevant e.s. modes are induced by the current carrying electron population, and their growth rate is maximum for parallel propagation, while ion Landau damping is most efficient for quasi-trasversal propagation ($k_\perp \gg k_\parallel$) where the waves are basically of the ion-acoustic type. In the present paper we analyze the quasi-linear plasma evolution, in order to evaluate the energy transfer to the ions. We label by 'c', 't' and 'i' the quantities referring to circulating electrons, trapped electrons and ions respectively. In our model, the magnetically trapped electron population is simulated by a standing maxwellian F_t. Indeed, a more satisfying treatment would require the introduction of a space coordinate, while our plasma is taken to be uniform. The full dispersion relation was analyzed in ref. /3/. For computational simplicity, we consider here the limit

$$|x_i|\equiv\left|\frac{\omega}{k v_i}\right|\gg 1\ ;\ |x_t|\equiv\left|\frac{\omega}{k_\parallel v_t}\right|\gg 1\ ;\ |x_c|\equiv\left|\frac{\omega-k_\parallel u}{k_\parallel v_c}\right|\ll 1$$

where v_i, v_t, v_c are the thermal velocities, and u is the circulating electron drift. Moreover, we consider the limit $\gamma/\omega_R \ll 1$ (with $\omega=\omega_R+i\gamma$) so that $\gamma=-\epsilon_I/\epsilon'_R$, with $\epsilon(\omega,\underline{k})=\epsilon_R+i\epsilon_I$; $\epsilon'_R=\partial\epsilon/\partial\omega|_{\omega=\omega_R}$.

We obtain:

$$\epsilon_R(\omega_R,\underline{k})\cong 1-\frac{1}{k^2\lambda_{Di}^2}\left(\frac{1}{2x_i^2}+\frac{3}{4x_i^4}\right)-\frac{1}{k^2\lambda_{Dt}^2}\left(\frac{1}{2x_t^2}+\frac{3}{4x_t^4}\right)+\frac{1}{k^2\lambda_{Dc}^2} \qquad (1)$$

$$\epsilon'_R\simeq 2\,\frac{\omega_{pi}^2}{\omega_R^3}\left(1+\frac{n_t}{n}\frac{M}{m}\mu^2\right) \qquad (2)$$

with $\mu=k_\parallel/k$.

Assuming that the electrons are strongly magnetized, the quasi-linear electron diffusion process in velocity space is basically longitudinal. As far as the ions are concerned, they are assumed, in the present simple treatment, to be unmagnetized and maxwellian. In this scheme, we get the system:

$$\frac{\partial F_c}{\partial t}-\frac{eE}{m}\frac{\partial F_c}{\partial v_\parallel}=\frac{\partial}{\partial v_\parallel}\left(D_c\frac{\partial F_c}{\partial v_\parallel}+S_c F_c\right) \qquad (3)$$

$$D_c(v_\parallel,t)=\frac{16\pi^3e^2}{m^2|v_\parallel|}\int_0^\infty \kappa\,d\kappa\int_{-1}^{1}\mu^2 d\mu\,\frac{W_{\underline{k}}}{\omega_R\epsilon'_R}\,\delta\left(\mu-\frac{\omega_R}{k v_\parallel}\right) \qquad (4)$$

$$S_c(v_\parallel,t)=\frac{16\pi^3e^2}{m|v_\parallel|}\int_0^\infty d\kappa\int_{-1}^{1}d\mu\,\frac{\mu}{\epsilon'_R}\,\delta\left(\mu-\frac{\omega_R}{k v_\parallel}\right) \qquad (5)$$

$$\frac{\partial W_{\underline{k}}}{\partial t}=\left(\frac{\partial W_{\underline{k}}}{\partial t}\right)_e+\left(\frac{\partial W_{\underline{k}}}{\partial t}\right)_i= \qquad (6)$$

$$=\frac{2\pi}{\epsilon'_R}\left(\frac{\omega_{pe}}{k}\right)^2\kappa_\parallel\int dv_\parallel\,\delta\left(\omega_R-\underline{k}\cdot\underline{v}\right)\left(W_{\underline{k}}\,\underline{k}\cdot\frac{\partial F_e}{\partial v_\parallel}+\frac{m\omega_R}{\kappa_\parallel}F_e\right)+$$

$$+\frac{2\pi}{\epsilon'_R}\left(\frac{\omega_{pi}}{k}\right)^2\int d\underline{v}\,\delta\left(\omega_R-\underline{k}\cdot\underline{v}\right)\left(W_{\underline{k}}\,\underline{k}\cdot\frac{\partial f_i}{\partial\underline{v}}+M\omega_R f_i\right)$$

where E is the external, longitudinal electric field, which is taken to be $\gtrsim E_R$ (runaway Dreicer field);

$$F_{c,t}(v_\parallel,t)=\int dv_\perp\ f_{c,t}(\underline{v},t)\ ;\ F_e(v_\parallel,t)=\frac{n_c}{n}F_c(v_\parallel,t)+\frac{n_t}{n}F_t(v_\parallel)$$

ω_R is the solution of eq. (1), and $W_{\underline{k}}$ is the spectral energy of the oscillations:

$$W_{\underline{k}}=\omega_R\,\epsilon'_R\,\mathcal{E}_{\underline{k}}\quad,\quad \text{with}\ \left\langle\frac{E_{turb}^2}{8\pi}\right\rangle=\int d\underline{k}\,\mathcal{E}_{\underline{k}}.$$

Spontaneous emission terms /4/ are included in eqs. (3), (5) and (6), and play an important role when the plasma is close to thermal equilibrium. Indeed, when E=0 the equilibrium solution of the system is given by maxwellian f_i, F_e with equal temperature T, and by a Rayleigh-Jeans spectrum $W_{\underline{k}}=T$. A collision term and an equation for ion evolution shall be included in a further extension of the work.

From the numerical integration of the system (3)-(6) we obtain the evolution of such quantities as $F_e(v_\parallel,t)$, $W_{\underline{k}}(t)$,

$$W(t)=\int d\underline{k}\ W_{\underline{k}}(t),\quad W_i=\int_0^t dt\int d\underline{k}\ \left(\frac{\partial W_{\underline{k}}}{\partial t}\right)_i.$$

The last quantity, in particular, gives an estimate of the energy transfer to the ions.

References

/1/ B. Coppi, M. Oomens, R. Parker, L. Pieroni, C. Schüller, S. Segre, R. Taylor: M.I.T. Report PRR-7417 (1974).

/2/ B. Coppi, F. Pegoraro, R. Pozzoli, G. Rewoldt: Nuclear Fusion 16, 309 (1976).

/3/ A. Orefice, R. Pozzoli: Proc. Third Symposium on Plasma Heating in Toroidal Devices, Varenna 1976, pg. 240.

/4/ V.N. Tsytovich: Non-linear Effects in Plasma, Chap. VI - Plenum Press, New York (1970).

RECENT RESULTS IN THE LOWER-HYBRID HEATING OF THE WEGA DEVICE

J.-G.WEGROWE°- P. BLANC+- M. DURVAUX§ - C. GORMEZANO+- W.HESS+
G.ICHTCHENKO+- P. LALLIA+- R. MAGNE+- T.-K. NGUYEN+ - W.OHLENDORF°
G.W.PACHER°- H.D. PACHER°- G.TONON+

°MAX-PLANCK-INSTITUT FÜR PLASMAPHYSIK
GARCHING, Fed.Rep.of Germany

+ ASSOCIATION EURATOM-CEA
Département de Physique du Plasma et de la Fusion Contrôlée
Service IGn- Centre d'Etudes Nucléaires
85X-38041 GRENOBLE CEDEX

§ ECOLE ROYALE MILITAIRE
Laboratoire de Physique des Plasmas
Association " EURATOM- ETAT BELGE "
Avenue de la Renaissance,30
1040 BRUXELLES

ABSTRACT : HF Power near the Lower-Hybrid Frequency at a level comparable to the Ohmic Heating Power is fed to the WEGA-Tokamak. In the experiments presented here, the HF Heating is accompanied by a marked density increase. A comparison is made between the results obtained with HF, and without HF using a programmed gas-puffing that produces the same density evolution. The gas influx accounts but for a minor fraction of the heating observed.

INTRODUCTION : In previous experiments /1,2,3,4/, HF power at levels up to 90kW has been fed to the plasma in WEGA. The available power of the 500MHz amplifier system has now been raised to 200kW. In the present experiments, 165kW have been actually coupled. The antenna system consists in two small loops oriented in the equatorial plane, placed azimuthally about a quarter of the free-space wavelength apart, and fed out of phase in order to fulfill accessibility for the major part of the excited wave-spectrum /4/. The electron density as measured by Langmuir probes near the loops is of the order of $10^{11}cm^{-3}$, well above the cut-off density, just before and after the HF pulses. The density of the deuterium plasma is adjusted so that the lower hybrid frequency equals the applied frequency near the plasma center. By applying 90kW during 10ms, an increase of 90eV (60%) of the ion perpendicular temperature as measured by charge exchange was observed, which decayed slowly after switching off the HF.

The HF heating is often, but not always /1/, accompanied by an increase in density. In particular, in the series at high HF power presented here, the density increased regularly with the total coupled HF energy. The increase in ion temperature due to this density increase alone, if due solely to enhanced electron-ion exchange is expected to be much lower than the ion heating observed during the HF pulse. In this paper, an experimental comparison made between HF heating and gas puffing confirms this point.

EXPERIMENTAL RESULTS : Fig. 2 shows the evolution of the electron density (peak density assuming parabolic profile and using the plasma radius deduced from position measurements) during the HF pulse (full line). The density in the absence of HF as simulated by an additional programmed puff of cold deuterium into the discharge is shown by broken line, the dotted line pertains to the case without HF nor gas puffing.
Fig. 1 gives the perpendicular peak ion temperature as deduced from neutral energy analysis. During the HF pulse, a high-energy tail exists. The values during HF are obtained as described previously /5/ by subtracting the Maxwellian tail, extrapolated to low energies from the data, and thus are subject to doubt while not confirmed by another temperature measurement. Due to the rapid decay of the tail, (≈ 100µs), however, the value obtained 600µs after switch-off is reliable. At that time, a temperature of 220eV is deduced, as compared with a) the initial temperature of 120eV, b) the value of 150 eV obtained at the same time with gas-puffing.
Fig. 3 represents the product of loop voltage and current (the current remains practically constant in both HF and gas pulses) ; Fig. 5 shows the electron temperature by soft X-rays, and Fig. 4, the value of the impurity concentration as deduced from density and from the soft X-rays signals assuming the dominant impurity is oxygen. (The concentration assuming the dominant impurity to be iron has not been represented as it corresponds to values of Z_{eff} which are in much poorer agreement with those deduced from the resistivity during the entire discharge).

DISCUSSION : The total increase in T_i obtained under comparable experimental conditions /4/ for lower peak power was 90eV.
For higher peak power, but the same coupled energy, the difference between the end temperatures obtained in the present experiments with HF and gas puffing is 70eV and decays with a time constant of 3ms.

The HF power coupled to the ions is the difference between the rate of change of ion energy just before and just after the HF is turned off (in100µs), assuming that energy exchange between species and losses do not change during this time interval. The rate of change of ion energy just after the HF is deduced from the measured change of ion temperature and density. Before the HF, maximum and minimum values for this rate of change are obtained by assuming either that the ion temperature no longer varies at the end of the HF pulse or that the ion temperature rises linearly to its final value. The value of the total ion energy is determined using the impurity concentrations found above. As a result, 25 to 50 kW of HF energy are found to be coupled to the ions, i.e. 15% to 30% of the input power.
In contrast with the previous results at lower HF power, a large increase in the loop-voltage is presently observed. This does not seem to be related to an increase in the impurity concentration as deduced from the soft X-rays measurements.

CONCLUSIONS : In the experiments presented here, a programmed inlet of deuterium was used to simulate the density increase observed usually during the HF pulses. It is shown that the major part of the observed increase in the measured perpendicular ion temperature is not due to the increase in the deuteron density ; on the other hand, the evaluation of the impurities by soft X-rays make it appear likely that the dominant impurity is a light element whose concentration does not increase during the HF.
A relative increase of the order of 70% in T_i decaying slowly after the pulse is observed with HF as compared to the gas puffing case.

Aknowledgements The authors wish to aknowledge their debt to the entire WEGA staff, and in particular to Mme MOULIN and M. J.-J.CAPITAIN, for their many efforts.

References :

/1/ P.BLANC et al.,3rd Int. Meeting on Theoretical and Experimental Aspects of Heating of Toroidal Plasmas,Grenoble (1976) p.251,vol.II.
/2/ P.BLANC et al.,6th Int.Conference on Plasma Physics and Controlled Nuclear Fusion Research, Berchtesgaden(1976) paper IAEA CN-35/G9.
/3/ P.BLANC et al.,Bull.Am.Phys.Soc. 21 (1976) 5D-2.
W.HESS et al.,Bull. Am.Phys.Soc. 21 (1976) 5D-3.
/4/ P. BLANC et al., to be published in " Journal de Physique " (1977)
/5/ P. LALLIA, G.W.PACHER, H.D.PACHER, Int.Symposium on Plasma Heating Varenna (1976).

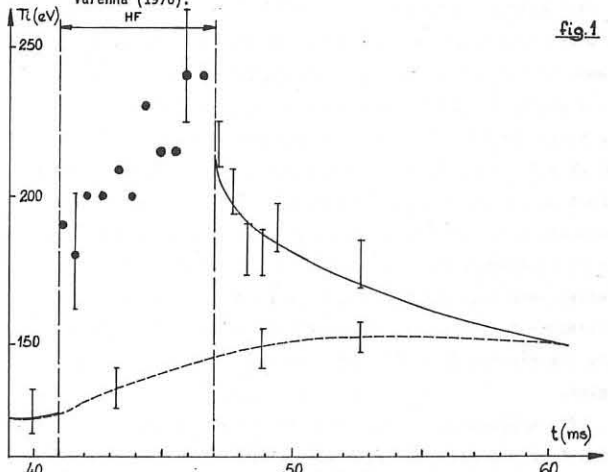

fig.1

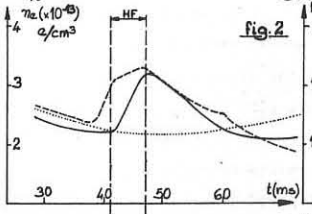

fig.2

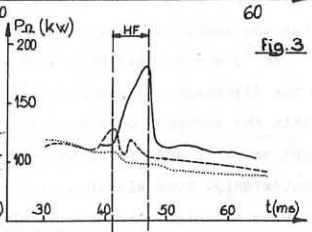

fig.3

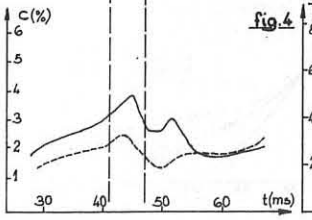

fig.4

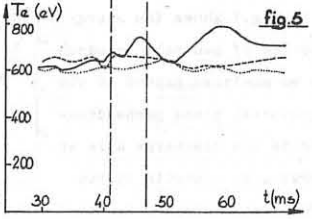

fig.5

FAST ION PRODUCTION IN A TOKAMAK PLASMA IN THE LOWER HYBRID HEATING EXPERIMENTS

.P.Gladkovsky, V.E.Golant, V.V.Djachenko, T.P.Evtushenko,
V.I.Ivanov, M.M.Larionov, L.S.Levin, A.D.Lebedev,
G.A.Serebreny, A.I.Tokunov, O.N.Shcherbinin
A.F.Ioffe Physical-Technical Institute, Leningrad, USSR

tract: Some experiments on HF plasma heating in the lower rid frequency range were carried out at the Tokamak FT-I h a slowing structure. It was found that the efficiency of t ion production by HF power increased sharply when the LHR ditions were met.

High efficiency of lower hybrid heating of Tokamak plas- has been not achieved yet. But in many experiments the ge- ation of fast ions was registered by charge exchange neu- l analyzers [1-4]. These iors are suggested usually to ori- ate at the plasma periphery by parametric decays of HF wa- .

In the reported experiments at the FT-I Tokamak the lower rid waves were excited by a passive slowing structure [5,6] unted in one quarter of the torus. It consisted of 22 rings aced in the shadow of the main limiters. The HF power was l by a flat coaxial line formed by a central plate inserted one of the ports of the Tokamak. The slowing factor was ex- ted to be 1.6-2.0 depending on plasma parameters.

The effect of HF pulse on plasma parameters was studied. changed the toroidal magnetic field from 5 up to 10 kG and rage hydrogen plasma density from 4.10^{12} up to 10^{13} cm^{-3}. these conditions the discharge remained MHD stable with sma current 27 kA and its duration 40 msec. Ohmic heating er was up to 70 kW. Laser scattering gave T_e=200-350 ev at axis. The 400 MHz generator was used with power up to kW and pulse duration 1 msec. The level of input power was sed up to 90% by external tuners . The character of wave pagation in the plasma was quite different in various regi- of discharge. At B = 5-6 kG the LHR condition was not sa- fied, and only the thin layer near the chamber wall was essible for waves. At B ≈10 kG the waves could penetrate to the central part of the plasma and reach the lower hybrid gion.

The application of the HF pulse did not change the cur- nt, loop voltage and equilibrium of the discharge. After the se the small increase of plasma density was observed ($\Delta n \approx 12$ cm^{-3}) which could point out at the particle injection in- the discharge. No change in plasma diamagnetism was found thin the accuracy of measurements (10^{14} ev.cm^{-3}). The total ght emission and intensity of spectral lines did not rise nsiderably. Some electron temperature increase was observed laser technique in the central part of the discharge.

Fig.1 shows the energy ectra of neutrals measured an analyzer placed in the natorial plane perpendicu- r to the discharge axis at rus side opposite to the antenna. One can see the high energy tail of the neutral flux during the HF pulse. Fig.2 and Fig.3 show the dependencies of the 1 kev neutral flux on plasma density and magnetic field. It turned out that

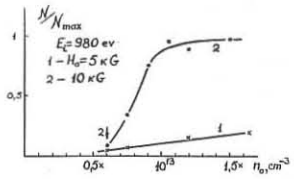

Fig. 2.

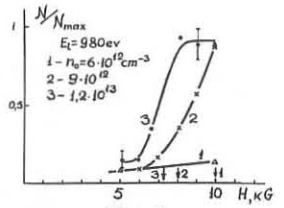

Fig. 3.

the flux of fast neutrals increased sharply when the LHR conditions were met. (They are marked by arrows.) It leads to a conclusion that the fast ion production occurs mainly in the inner part of the plasma in the LHR region.

Fig.4 represents the decrease of the neutral flux after the HF pulse. The flux drops rapidly with $\tau \approx$ 100 μsec corresponding to ion bouncing time along the banana orbits. Ions trapped on the "thick banana" orbits seem to be responsible for the registered flux. In our condition their life cannot be long since the current is not high enough. But it is clearly seen that there is a group of ions which do exist much longer. Even at 0.5 msec after the HF pulse the neutral flux is 10 times greater than before the pulse. It can be related to collisional scattering of passing ions. Curve 2 shows the calculated collisional damping rate of fast ions.

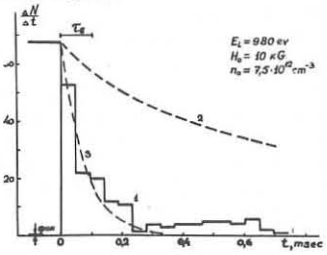

Fig. 4.

The energy sprctra (Fig.1) can be accounted for by the two temperature ion distribution. For B = 10 kG one can calculate T_{i1} = 40 ev, T_{i2} = 500 ev and $n_{i2}/n_{i1} \approx 10^{-2}$. If this ratio is valid through the whole plasma volume it is easy to estimate the HF power spent for the fast ion production. Taking 100 μsec as a life time one obtains $P_{i2} \approx 9$ kW, or 15% of the input power. Although being preliminary, this estimation is rather promising for future Tokamaks.

The authors are thankful the american physicists R.W.Motley, A.C.England and R.J.La Haye, who took part at the first stage of the experiments.

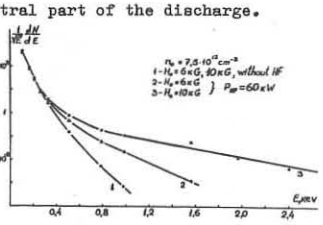

Fig. 1.

REFERENCES

1. I.P.Gladkovsky, V.E.Golant et al. Contr.papers of the V ECCFPP, Grenoble, 1972, p.109.
2. V.V.Alikaev, Yu.I.Arsenyev et al. Contr. papers of the VI ECCFPP, Moscow, 1973, p.63.
3. P.Blanc, W.Hess, G.Ichtchenko et al. III Int.Meeting on To roidal Plasma Heating, Grenoble, 1976, v.II, p.251.
4. F.W.Perkins, ibid.
5. Yu.F.Baranov, O.N.Shcherbinin, ibid v.I, p.131.
6. V.V.Djachenko, O.N.Shcherbinin. Jorn.Techn.Phys., 46, 2043, 1976.

ION-ION HYBRID RESONANCE AND ALFVEN WAVES IN TOKAMAK TM-1-HF

Vdovin V.L., Shapotkovsky N.V., Chesnokov A.V.
I.V.Kurchatov Institute of Atomic Energy, Moscow, USSR

In TM-1-HF tokamak the strong absorption of fast wave in deuterium plasma at the second harmonic of ion cyclotron frequency $\omega = 2\omega_{Bi}$ have been uncovered. The absorption is caused by minority protons for which $\omega = \omega_{Bi}^{H}$. The protons efficiently absorb the energy and the energetic "tail" of distribution function of protons is created [1], that may be essentially used in two-component tokamak [2].

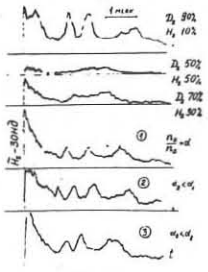

Fig.1

Here the possibility mechanisms of the strong absorption are considered and the coupling system for plasma with two sorts of ions is calculated. The main results of heating at alfven wave, when $\omega = \frac{1}{3}\omega_{Bi}$ and cyclotron absorption is eliminated, are reported.

1. The theory of minority protons [2,3] predicts that maximum of absorption occurs approximatly at 1% density of minority. But experimental value of wave quality is significantly lower and continue to diminish with increasing of protons density (fig.1 magnetic probe signals), therefore consideration must be given to ion-ion hybrid resonance (IIHR) also [4].

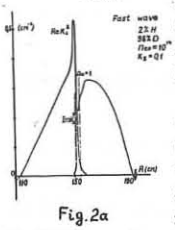

Fig.2a

The dispersive equation for two-ion mixture (fig.2), is calculated numerically considering cyclotron absorption in toroidal magnetic field in the model of two coaxial cylinders with parabolic density profile for parameters of T-10; $n_{e0}=10^{14}\,cm^{-3}$, $T_e=1$keV, $T_i=600$eV, $a=40$cm, $R_0=150$cm. It can be seen from fig.2a,b, that even for significant percent of protons: a) fast wave is not coupled at all with slow mode and IIHR is eliminated; b) $\max\left(\mathrm{Im}\,K_\perp/\mathrm{Re}\,K_\perp\right) \sim 1$ – corresponding to very strong absorbtion; c) maximum of absorbtion is placed not in point of CR $\omega = \omega_{Bi}^{H}$, but is removed to the surface $\varepsilon_1 = N_\parallel^2$ in the direction of greater magnetic field.

With increasing of minority ($K_\parallel = 0{,}2\,cm^{-1}$, p16,5%), fig.3, the transformation in slow mode is occured. One may obtain the relation between density of minority and $K_\parallel$ from equation

$$a N^4 + (\beta_r + i\beta_i) N^2 + c = 0$$

In the vicinity of critical layer $\varepsilon_1 = N_\parallel^2$ $\beta_r = 0$. If $\beta_i^2 \gg 4|ac|$ i.e. $\eta > K_\parallel |\bar{\varepsilon}_2|/\bar{\varepsilon}_3^{1/2}$ then the approximation $N_\perp^2 = -c\,(\beta_r + i\beta_i)^{-1} = \left[(\varepsilon_1 - N_\parallel^2)^2 - \varepsilon_2^2\right]/(\varepsilon_1 - N_\parallel^2)$ is always valid ($\varepsilon_1 = \bar{\varepsilon}_1 + i\eta$, $\varepsilon_2 = \bar{\varepsilon}_2 + i\eta$, ε_3 – components of tensor [3]).

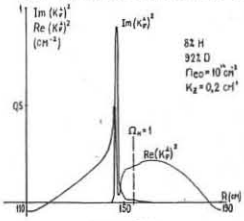

Fig.2b

The results obtained are connected with maximum of left-handed component of electric field of wave in the layer $\varepsilon_1 = N_\parallel^2$. In [2,3] the value of left-handed component was taken at point CR $\omega = \omega_{Bi}^{H}$ and then the variation with density was performed.

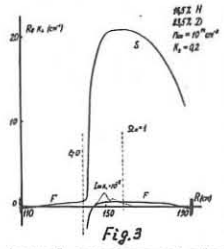

Fig.3

2. ABSORPTION AT THE ION-ION HYBRID RESONANCE. Now there are the vacuum layer by thick a_1 between plasma and external conducting cylinder, external boundary of plasma coincides with x=0, and along surface x=-S in direction "y" the current $J_0 \hat{y}\, e^{-i\omega t}$ flows. The band of current layer is 2d. Equation for fast wave ($K_y = 0$) is

$$\frac{d^2 E_y}{d\bar{x}^2} + \frac{(\varepsilon_1 - N_\parallel^2)^2 - \varepsilon_2^2}{\varepsilon_1 - N_\parallel^2} E_y = 0 \qquad \left(\bar{x} = x\frac{\omega}{c}\right)$$

Here the coefficient n^2 by E_y has the pole $\varepsilon_1 = N_\parallel^2$, three zeroes $\varepsilon_1 \pm |\varepsilon_2| = N_\parallel^2$ and now the cyclotron absorption is ignored. The W.K.B. solution in the vicinity external boundary of the plasma is

$$E_y = A\left[W_1(\zeta) e^{-i\psi_0} + R\, W_2(\zeta) e^{i\psi_0}\right] \qquad (*)$$

where $W_{1,2} = u \pm iv$ – Airy functions, $R = v^{-1}\left[1 - e^{-\delta}(1 + v e^{-2i\psi})\right]$ reflection coefficient, $\zeta = \gamma^{1/3}(\bar{x}_{10} - \bar{x})$

$$\delta = -2i\int_{\bar{x}_{20}}^{\bar{x}_{00}} n\, d\bar{x}\,, \qquad \psi = \int_{\bar{x}_{00}}^{\bar{x}_{30}} n\, d\bar{x}\,, \qquad \psi_0 = \int_{\bar{x}_{10}}^{\bar{x}_{20}} n\, d\bar{x} + i\frac{\pi}{4}\,,$$

$$v = \frac{\Gamma(1-i\nu)}{\Gamma(1+i\nu)} \exp\left[2i\nu(\ln\nu + 1)\right] \to \begin{cases} -i & |\nu| \gg 1 \\ 1 & |\nu| \ll 1 \end{cases}$$

$\Gamma(s)$ – standart gamma function, $\nu = \delta/2\pi$, $\bar{x}_{k0}$ and $\bar{x}_{\infty}$ – zeroes and pole n. The toroidal eigenmodes are obtained under the condition $E_y(x = a_1) = 0$ (for simplicity also $a_1 = 0$) in (*) resulting in absorption ($\omega = 2\omega_{Bi}^{D}$ in center, $\delta \ll 1$, $K_\parallel = m/R_0$)

$$\mathrm{Im}\,K_\parallel \cdot 2\pi R_0 \approx \frac{\pi\sqrt{3}}{20m}\,\frac{R_0}{a}\left(\frac{\omega_{pH} R_0}{c}\right)^2\left(1 - \frac{2K_\parallel^2 c^2}{\omega_{pD}^2}\right)$$

For TM-1-HF ($R_0 = 40$cm, $a = 10$cm, $n_D = 10^{13}\,cm^{-3}$, $n_H = 10^{11}\,cm^{-3}$) one obtains $\mathrm{Im}\,K_\parallel \cdot 2\pi R_0 \approx 1/m$, that is in agreement with experimental values $Q \lesssim 10$ [1]. For a large tokamaks (i.e. T-10, PLT) the damping is greater and toroidal eigenmodes are not exist, if $n_H/n_D \gtrsim 10^{-2}$.

3. LOADING RESISTANCE can be find using a Fourier series E_y and j in the z-direction ($2L = 2\pi R_0$). The power coupled to the plasma is evaluated as

$$P_c = \mathrm{Re}\left[-\frac{1}{2}\int_{-L}^{L} E_y(s, z, \omega) j^* H\, dz\right] = -\frac{1}{2} L H \sum_{n=1}^{\infty} j_n E_{yn}$$

where j_n and E_{yn} are Fourier-harmonics of the driving current and of the electrical field in the current layer X=-S:

$$E_{yn} = -\frac{4\pi i \omega j_n}{c^2}(a_1 - S)\left[1 - \varkappa_\perp(a_1 - S)\frac{1 + \rho_n \varkappa_\perp S}{\varkappa_\perp S + \rho_n}\right]$$

where parameters of plasma are given by surface impedance

$$\rho_n = -\frac{f(0)\varkappa_\perp}{f'(0)} = \frac{\varkappa_\perp}{\gamma^{1/3} K_0}\cdot\frac{W_1(\zeta_n^0) + R e^{2i\psi} W_2(\zeta_n^0)}{W_1'(\zeta_n^0) + R e^{2i\psi} W_2'(\zeta_n^0)}$$

where $K_0 = \omega/c$, $\varkappa_\perp = (K_\parallel^2 - K_0^2)^{1/2}$, $\gamma = \frac{6\omega_{pD}^2(0)}{a c^2 K_0^3}$, $\zeta_n^0 = \gamma^{1/3}\bar{x}_0^{(n)}$

Loading resistance

$$R_{0h} = \mathrm{Re}\sum_{n=1}^{\infty}\left\{i\,\frac{8\pi\omega L(a_1 - S)H}{c^2\pi^2 n^2 d^2}\,\sin^2\!\left(\frac{\pi n d}{L}\right)\left[1 - \varkappa_\perp(a_1 - S)\frac{1 + \rho_n\varkappa_\perp S}{\varkappa_\perp S + \rho_n}\right]\right.$$

For parameters of T-10 and $\omega = 2\omega_{Bi}^{D} = \pi\cdot 10^8\,sec^{-1}$, $a_1 = 2$cm, H=100cm. (H-height of HF current) $R_0 = 150$cm, S=0 it is obtained $R_{0h} = 0{,}499$ ohm, i.e. low impedance coupling system is required.

4. ALFVEN WAVE HEATING was performed at $\omega = \frac{1}{3}\omega_{Bi}$ (f=6,9 MHz, hydrogen, $P_\sim \lesssim 100$kW, asymmetrical loops [1]). The increasing of diamagnetism of plasma is $\Delta(nT) = \Delta n(T_e + T_i) \approx 10^{15}\,ev/cm^3$ (density $n_e \approx 10^{13}\,cm^{-3}$), i.e. $\Delta(T_e + T_i) \approx 100$eV. Consequently approximatly the same values are obtained as in ICR heating experiments ($\omega = \omega_{Bi}$) [1]. It was possible to increase $\Delta(nT)$ by the factor 1,5 by performing of equility $v_{Te} = v_A$ on the axis of plasma ($v_{Te}^2 = 2T_e/m_e$, $v_A^2 = B^2/4\pi nM$) Loop voltage is diminished during the HF pulse (Fig.4), that may be caused by the heating of electrons. The analysis of neutral detector spectrum (Fig.5 for comparison also are given dates at $\omega = \omega_{Bi}$) confirms this point of view (increasing of $\Delta T_i \approx 30$eV, $T_{i0} = 35$eV). The "tail" of distribution function also exists, but much less pronounced.

It is needed to point out the more high stability of the plasma in compare with one for heating at ICR. This probably is caused by much less bombardment of the chamber by uncontained particles (though there are ICR for CV ions).

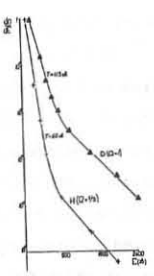

Fig.5

REFERENCES

1. Vdovin V.L. et al., 3-d Symp. on Plasma Heating (Grenoble). v.II, 349 (1976), JETP Lett., 24 (1976) 410.
2. T.Stix, Nucl.Fusion., 15 737 (1975).
3. Klima R. et al. Zh.Tehn. Fiz. 46, 704 (1976).
4. Klima R. et al., Nucl. Fusion 15, 1157 (1975).

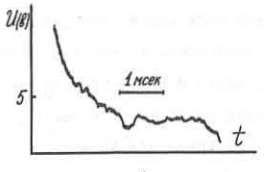

Fig.4

TOKAMAK PLASMA HEATING BY APPLICATION OF STRONG POLOIDALLY INDUCED ELECTRIC FIELD

M. Ichimura, N. Inoue, H. Nihei, K. Yamazaki, K. Hoshino, M. Kikuchi, Y. Ogawa and T. Uchida

Department of Nuclear Engineering, Faculty of Engineering, University of Tokyo, Hongo, Bunkyo-ku, Tokyo, Japan

Abstract: Ion heating of a tokamak plasma by the high-voltage theta-pinch technique is studied experimentally. Ions with larger mass number and higher charge number are accelerated more efficiently by the pulsed magnetic field. The efficiency of ion acceleration also depends on the bias magnetic field for a given amplitude of the pulsed field. The region of the bias field where ion acceleration occurs expands as the pulse amplitude increases.

For the purpose of quick heating of the tokamak plasma we have assembled the high-voltage theta-pinch into the tokamak with the major radius of 25 cm and the minor radius (limiter radius) of 8 cm.[1)-4)] Production of energetic ions has been confirmed by the spectroscopic measurement and the energy analysis of charge-exchange atoms emitted from the plasma. Superposition of the intense pulsed field on the steady toroidal field has not induced the violent changes of the toroidal plasma current and the loop voltage even if the pulse amplitude is larger than the toroidal field.

In this paper we report recent experimental results on ion heating. Two kinds of experiments have been carried out; one is for studying the dependence of heating efficiency on mass and charge number of ion species, and the other for seeking the effective region of the bias magnetic field (here the toroidal field B_t) to produce energetic ions for the given pulsed field amplitude. In both cases the pulsed field at its first half cycle is antiparallel to the bias magnetic field. Typically the conductivity temperature of the initial tokamak plasma is 15 eV and the electron density is $2.5 \sim 5 \times 10^{13}\,cm^{-3}$.

Figure 1 shows time variations of the pulsed field $\tilde{B}$ and the temperature of impurity ions measured by the doppler broadening of spectral lines. Emission of soft X-rays with the energy smaller than 6 keV was also observed with a solid state detector.

The dependence of maximum temperature on the product of mass number A and charge number Z of ion species is shown in Fig. 2. Spectral lines of carbon, nitrogen and oxygen are from the hydrogen plasma and helium line is from the helium plasma. The high-voltage theta-pinch generates the radially propagating magnetic sheath which is accompanied with the induced electric field.[5)] In our experimental conditions the sheath thickness is nearly as large as the plasma radius. If ions are accelerated as a result of reflection from the moving magnetic piston, they earn the kinetic energy proportional to their mass number and independent of the charge number. While, if ions acquire the kinetic energy from the radial electric potential during its life time, their final energy will proportional to Z^2/A. The results of Fig. 2 do not agree with any one of these simple acceleration models. Present results suggest the existence of several acceleration mechanisms. The similar results have been obtained by the turbulent heating experiment.[6)]

Bursts of charge-exchange hydrogen atoms emitted in the radial direction during about 2 μs were detected around the increasing phase (the second and the third quarter cycles) of the pulsed field. Figure 3 shows the region of the bias field for the occurrence of the burst emission as a function of the amplitude of the pulsed field. This result was obtained in such a case that the high-voltage theta-pinch was applied at 1/8 section of full torus and the charge-exchange atoms were detected at the opposite side of the theta-pinch coil. Operation of the tokamak with the higher toroidal field requires the more intense pulsed magnetic field. The energy of the emitted atoms is lower than 1 keV. Emission of atoms with the energy lower than several hundred eV continues about 150 μs after the burst.

Acknowledgment

Authors are indebted to Mr. A. Ozaki for his assistance in the experiment.

References

[1] Inoue, N., et al.; Third Topical Conf. on Pulsed High-Beta Plasmas (Culham, 1975) A3.5.

[2] Inoue, N., et al.; Rev. Sci. Instrum. 47 6 (1976) 735.

[3] Inoue, N., et al.; Sixth Conf. on Plasma Physics and Controlled Nuclear Fusion Research (Berchtesgaden, 1976) G5-1.

[4] Yamazaki, K., et al.; Symposium on Plasma Wall Interaction (Jülich, 1976).

[5] Krall, N. A., et al.; Plasma Physics and Controlled Nuclear Fusion Research (Tokyo, 1974) Vol.III, p.373.

[6] Adati, K., et al.; Seventh European Conf. on Controlled Fusion and Plasma Physics (Lausanne, 1975) Vol.I, p.166.

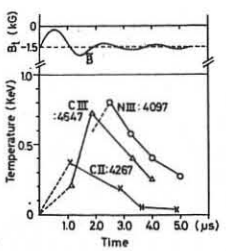

Fig. 1 Time variations of pulsed magnetic field (upper) and doppler ion temperatures (lower).

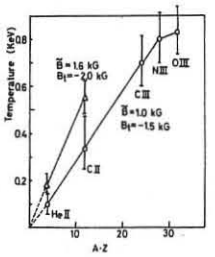

Fig. 2 Maximum ion temperature vs. product of mass number A and charge number Z.

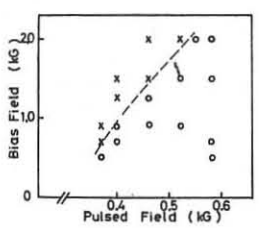

Fig. 3 Dependence of the emission of 400 eV hydrogen atom burst on the toroidal field as a function of the amplitude of pulsed magnetic field; o - emission observed, × - no emission.

COMPRESSION EXPERIMENTS ON A TOKAMAK PLASMA

D C Robinson and A J Wootton

Culham Laboratory, Abingdon, Oxon., UK
(Euratom/U.K.A.E.A. Fusion Association)

Abstract. Results of minor radius compression experiments on a tokamak plasma show that flux is conserved. Compensated toroidal flux loops show increases in β_I greater than those for an adiabatic compression. Measurements of poloidal field structure, accredited to tearing modes, are interpreted to show increases in the edge electron temperature.

Introduction. A small air cored tokamak, TOSCA(R=30, a ⩽ 10 cm) is used to study compressional heating. Previously reported results [1] have shown both line of sight and edge density changes. Increases in β_I were inferred from plasma displacement measurements. In this paper flux conservation, increases in β_I and changes in magnetic field structure caused by tearing modes are reported.

Device. The toroidal field B_ϕ has a rise time of 2.5 ms; the compression is achieved by increasing B_ϕ by a factor ⩽ 1.5 in times ∿ 150 μs. The vacuum vessel has a penetration time to B_ϕ ∿ 60 μs. Equilibrium is maintained by currents in conductors, with no shell.

Typical parameters of a pre-compressed plasma, lasting ∿ 2 ms, are: plasma current I_p ∿ 10 kA, line of sight average density ∿ 2 x 10^{13} cm^{-3}, peak electron temperature ∿ 100 eV (from laser light scattering), β_I ∿ 0.35.

Flux conservation. The timing of a minor radius compression can be chosen so that the uncompressed plasma has a time independent current, maintaining vertical field, and major radial position. The compression results in a plasma current reduction ΔI_p: with certain timings the major radial position remains unchanged, ($L_p I_p$ constant). Figure 1 shows the resultant $\Delta I_p/I_p$ against the compression ratio C, B_ϕ^f/B_ϕ^i. For the conditions described, poloidal and toroidal flux conservation result in the theoretical dependence shown by the solid line. The agreement with the experimental observations demonstrates that flux is conserved. Under these conditions the gain in β_I which keeps the plasma major radius constant is greater than adiabatic. Initial decompression results show increases in current, and a reduction in β_I is deduced.

Toroidal flux measurements. Compensated toroidal flux loops both inside and outside the vacuum vessel are used to deduce β_I before compression. Reversing the plasma current direction, and assuming the plasma pressure is unchanged, allows the misaligned internal loops to be used during the compression period. Figure 2 shows the plasma current, toroidal field and deduced β_I both with (broken line) and without (solid line) a compression with C = 1.3. The plasma current reduction is shown. The measured gain in β_I due to the compression is 1.4, compared to that expected for an adiabatic change of $C^{2/3}$ = 1.2. The uncompressed plasma energy confinement time of ⩽ 100 μs increases to ⩽ 140 μs with compression.

Assuming flux conservation and an internal inductance ℓi = 0.5, a gain in β_I of 1.4 is required to account for the constant radial position. The value of ℓi is compatible with the measured current distribution, using a magnetic probe. Thus the measured gain in β_I and that deduced from the motion are equivalent: the gain is greater than adiabatic [2]. Computational studies [3] using neoclassical transport coefficients, except for enhanced electron thermal conductivity, predict gains in β_I of $C^{1.2}$ (i.e. ∿ 1.35 for the case illustrated). This rise is attributed to detachment of the plasma from the material walls, as previously observed with a Langmuir probe.

Tearing mode studies. Oscillations of the poloidal field both inside and outside the plasma current carrying region are observed (Mirnov oscillations), with $b_r/\hat{B}_\theta$ ⩽ 1%. The magnetic probe can be inserted within 4 cm of the axis before it changes fluctuations at the vacuum vessel. The b_r signal does not change sign at the singular surface: the modes appear with q limiter ⩾ m/ℓ where m and ℓ are the poloidal and toroidal mode numbers. These measurements imply that the structure is a tearing mode, rotating in the electron diamagnetic drift direction. The oscillations (m = 3, ℓ = 1) increase in frequency with compression, and the amplitude is reduced. Figure 3 shows the rotation period T plotted against C for several experiments. The frequency increases by ∿ 1.3 for a compression of 1.3: initial decompression measurements show a reduction. Interpreting the increase as a change in the diamagnetic drift frequency [4] and assuming flux conservation, then $T \alpha T_e^{-1}$. The scatter in the points with C = 1 is attributed to slightly different initial toroidal fields. The frequency of the uncompressed case corresponds to an edge temperature ∿30 eV (approximately the conductivity temperature), and the final frequency to ∿40 eV.

The reduction in amplitude is accredited to increased stability, possibly associated with the changed plasma current distribution Experiments using the magnetic probe inside the plasma show that the reduction cannot be explained by relative motion.

Conclusions. Measurements of plasma current and position demonstrate flux conservation at the compression peak. Toroidal flux loops inside the vacuum vessel show gains in β_I greater than adiabatic: these gains are also deduced from the plasma major radial motion. Poloidal field perturbations are accredited to tearing modes whose rotational frequency increases with compression, consistent with a change in the edge electron temperature.

References

[1] G Cima et al. 7th European Conference on Controlled Fusion and Plasma Physics, Laussane 1 p.6 (1975).

[2] M G Kaganskii et al. 6th IAEA Conference on Plasma Physics and Controlled Nuclear Fusion Research, Berchtesgaden, paper CN-35/A12(1976).

[3] D C Robinson. 3rd Symposium on Plasma Heating in Toroidal Devices, p.168, Varenna (1976).

[4] J C Hosea et al. Phys. Rev. Letts. 30 p.839 (1973).

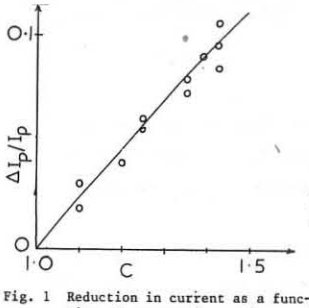

Fig. 1 Reduction in current as a function of compression ratio.

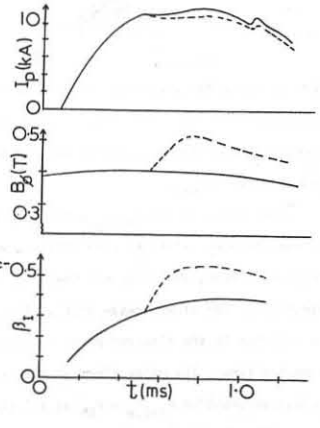

Fig. 2 Plasma current, toroidal field and β_I with (broken line) and without (solid line) compression.

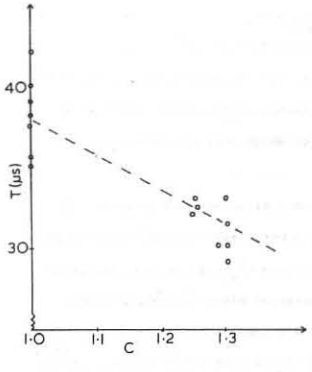

Fig. 3 Period of rotation T of an m = 3, ℓ = 1 perturbation as a function of compression ratio C.

ELECTRON HEATING BY NEUTRAL BEAM INJECTION IN ORMAK*

M. Murakami, J. F. Lyon, R. C. Isler, L. A. Berry, C. E. Bush, J. L. Dunlap, G. R. Dyer, P. H. Edmonds, P. W. King, D. H. McNeill, G. H. Nelson, and W. R. Wing

Oak Ridge National Laboratory, Oak Ridge, Tennessee, U.S.A.

Abstract: Substantial electron heating by energetic neutral beam injection is observed in ORMAK for different plasma densities, currents, and toroidal field values. The scaling of average electron temperature and electron power loss with total power input to electrons (ohmic + injection) suggests the equivalence of ohmic and injection power for electrons.

Introduction: While large increases in ion temperature with injection have been observed in ORMAK [1], TFR, and other tokamaks, little electron heating has been reported. In previous experiments the injection power delivered to electrons ($P_{inj,e}$) did not sufficiently compensate for reduced ohmic heating power (P_{OH}) and increased electron power losses during injection. The expected increases of electron temperature (T_e) were within the experimental uncertainties.

Demonstration of Electron Heating: We have optimized the experiment for electron heating by (1) use of high coinjection power (340 kW), (2) operation at low plasma current (70 kA) so $P_{OH} < P_{inj,e}$, and (3) operation at lower impurity levels ($Z_{eff} \sim 3$) to minimize radiation losses. Figure 1 shows the behavior of the basic plasma parameters for this discharge ($\bar{n}_e$ is the line-averaged electron density). Since about half of P_{inj} should go to electrons, and the loop voltage (and thus P_{OH}) decreases during injection, $P_{inj,e}$ (≈160 kW) significantly exceeds P_{OH} (≈100 kW) at 75 ms. Figure 2 shows the results of Thomson scattering measurements of $T_e(r,t)$ indicating

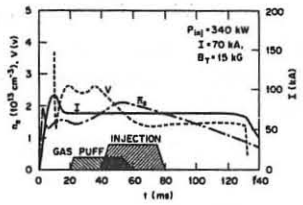

Figure 1

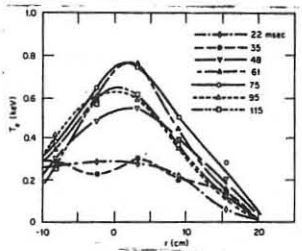

Figure 2

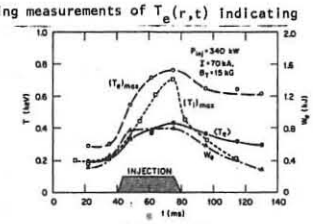

Figure 3

that T_e increases substantially at all radii as a result of injection. Figure 3 shows the time history of the peak $(T_e)_{max}$ and density-averaged $\langle T_e \rangle$ electron temperatures, the electron thermal energy W_e, and the peak ion temperature $(T_I)_{max}$.

The slow rise in $(T_e)_{max}$ and $\langle T_e \rangle$ is due to a concurrent density increase since W_e saturates after ≈15 ms, a time consistent with the 10-ms fast-ion slowing down time and the 5-ms gross energy confinement time for electrons. The slower decay of W_e, $(T_e)_{max}$, and $\langle T_e \rangle$ after injection is due to a change in the electron power loss mechanisms since $(T_I)_{max}$ decays in the expected time. The major electron energy loss mechanisms are (1) impurity radiation (≈50% of $P_{inj,e} + P_{OH}$ at all times), which falls rapidly after injection stops [2], and (2) heat conduction which does not increase during injection.

Other Electron Heating Cases: The base case discussed above was at low current, low density, and high injection power. Varying the injection power with other discharge conditions fixed produced $\langle T_e \rangle$ values that decreased with decreasing injection power. The observed electron heating is not limited to low current discharges. Figure 4 shows a high current case (I = 175 kA) where $T_e(0)$ = 0.85 → 1.3 keV and $\langle T_e \rangle$ = 0.55 → 0.7 keV (B_T = 26 kG, $\bar{n}_e = 2.2 \times 10^{13}$ cm^{-3}, P_{OH} = 480 kW, and $P_{inj,e}$ = 120 kW).

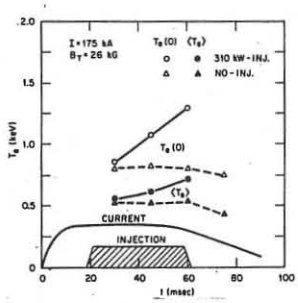

Figure 4

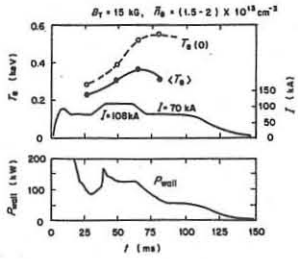

Figure 5

Equivalence of Ohmic Heating and Injection Powers: Correlation of the results described above with those of several other experiments indicates a general equivalence of injection and ohmic heating powers. When the beam heating is simulated by a 40-ms ohmic heating pulse (I = 70 → 110 → 70 kA) as shown in Fig. 5, we observe an electron temperature behavior similar to that with injection. T_e is left higher after the pulse, again primarily due to the fast decay of P_{rad}. As in the injection case, P_{rad} is ≈50% of the total electron power input at all times, similar to that observed in constant current discharges over a wide range of conditions. The increased radiative loss observed during injection therefore appears to be due to the increased power input, and is not specifically related to injection.

Losses through heat conduction (characterized by τ'_{Ee}) also demonstrate the general equivalence of discharges with and without injection. For ohmic heated discharges τ'_{Ee} increases with density, and the same trend is noted with injection. The specific experiment discussed here is injection at the highest power into a 70 kA discharge, but at a higher density ($\bar{n}_e$ = 3.3 × 10^{13} cm^{-3} vs 1.7 × 10^{13} cm^{-3}). The confinement time, τ'_{Ee}, is higher (≈15 ms), and as a result the observed increase of $\langle T_e \rangle$ is only slightly less than that at the lower density.

Finally, Fig. 6 shows $\langle T_e \rangle$ as a function of total power input into electrons ($P_{OH} + P_{inj,e}$) for a variety of discharges at different currents, densities, and toroidal fields. The scaling of $\langle T_e \rangle$ with total input power appears to be the same for plasmas with ohmic heating alone as for those with injection. Again we note the apparent absence of losses specific to injection.

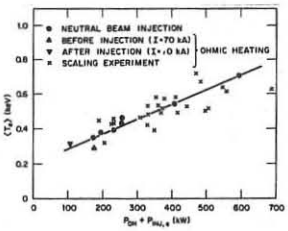

Figure 6

Summary: We have observed electron heating by neutral beam injection and have observed that $\langle T_e \rangle$ increases with total power ($P_{OH} + P_{inj,e}$). To first order, there are no power losses specific to injection. This study, combined with the significant ion heating previously demonstrated, increases our confidence in the use of neutral beam injection for supplementing ohmic heating in tokamak plasmas.

Acknowledgment: The work presented here is the result of the efforts of the entire ORMAK group in cooperation with the Plasma Heating and Fueling Section of the Fusion Energy Division.

References:

*Research sponsored by the Energy Research and Development Administration under contract with the Union Carbide Corporation.

[1] L. A. Berry et al., Proc. 6th Intl. Conf. on Plasma Physics and Controlled Nuclear Fusion Research, IAEA Berchtesgaden Conf. Paper CN-35/A4-1 (1976).

[2] J. F. Lyon, R. C. Isler et al., this conference.

RELATION OF NEUTRAL BEAM INJECTION TO IMPURITY BEHAVIOR AND EXTENSION OF PLASMA PARAMETERS IN ORMAK*

J. F. Lyon, R. C. Isler, M. Murakami, C. E. Bush, J. L. Dunlap, H. C. Howe, G. L. Jahns, H. E. Ketterer, J. T. Mihalczo, R. V. Neidigh, V. K. Paré, and J. B. Wilgen

Oak Ridge National Laboratory, Oak Ridge, Tennessee, U.S.A.

Abstract: Neutral beam injection extends the plasma parameter range (n_e, β_T, q, T_i) in ORMAK over that obtainable with ohmic heating alone. Impurity radiation also increases due to the added power, especially with counterinjection. Impurity trapping of injected beam neutrals is observed, but the large toroidal rotation velocities expected for unidirectional injection do not occur.

Introduction: In addition to heating future tokamak plasmas, massive neutral beam injection power may also permit attainment of higher plasma densities and higher toroidal beta β_T. Possible problems could be (1) large beam-induced toroidal rotation velocities or (2) increased impurity influx that leads to additional radiation losses and prevents beam penetration of the plasma.

Extension of Plasma Density Limit: As shown in Fig. 1, the density limits for ohmically heated plasmas in ORMAK (gas puffing limit ≈1.6 times steady filling limit) and in other tokamaks are proportional to B_T/R_o [1], which is a measure of the central current density since q(0) ≈ 1. This suggests that the maximum density is proportional to ohmic heating power. On this basis, we might expect the combination of neutral beam injection (as an auxiliary power input) and gas puffing (to provide an adequate particle source) to increase the attainable density. In fact, this does occur, as shown in Fig. 1.

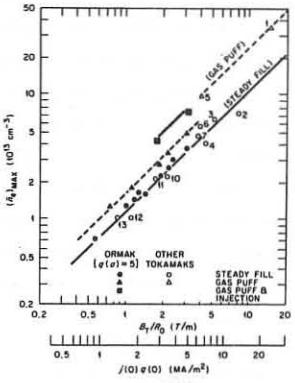

Figure 1

Extension of β_T and q with Injection: For the highest density reached in ORMAK ($\bar{n}_e = 6 \times 10^{13}$ cm^{-3}) with gas puffing and 240 kW injection [q(a) = 5 at B_T = 25 kG], we obtain τ_E = 15 ms, $\beta_T(0)$ = 1.2%, and $\bar{\beta}_T$ = 0.4%. Similar values for β_T can be obtained at lower q(a) with injection. Injection of 340 kW permits grossly stable and reproducible discharges with broad $T_e(r)$ profiles and normal internal MHD activity at q(a) down to 2.6 (B_T = 10.4 kG), which is not possible without injection. For this case $\bar{n}_e = 1.8 \times 10^{13}$ cm^{-3}, $\beta_T(0)$ = 1.4%, and $\bar{\beta}_T$ = 0.4%. Calculations and equilibrium measurements indicate that the stored fast-ion energy approximately equals the bulk plasma energy. Thus we estimate the total (beam + plasma) β_T values to be ≈3% peak and ≈1% average.

Effect of Injection on Impurities: Impurity radiation is increased by coinjection, but only to the degree expected for ohmically heated discharges with the same total power input to electrons [2]. The radiation loss is ≈50% of the total electron power input both with and without injection. Figure 2 illustrates the increased radiation due to added coinjection power for the base electron heating case described in our companion paper [2]. The signals are representative of the behavior of O^{6+} (21.6 Å), a segment of continuum thought to be due to closely spaced lines of tungsten (20.1 Å), and the total radiated power (P_{wall}).

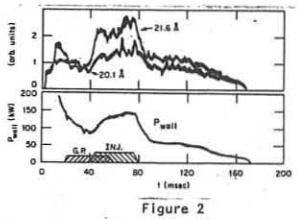

Figure 2

Counterinjection produces a larger increase in impurity radiation than does the same amount of coinjection power. This aspect is indicated in Fig. 3 for a line of Fe XVI (360.8 Å). Figure 4 shows the $T_e(r)$ profiles obtained for this case. The depression of the central electron temperature with counterinjection is thought to be related to tungsten impurity radiation cooling.

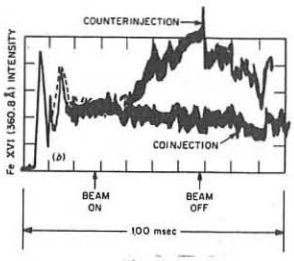

Figure 3

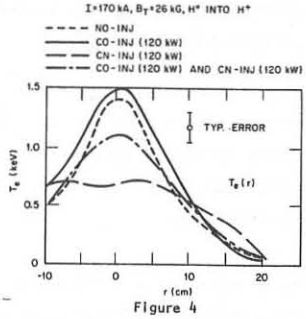

Figure 4

Absence of Beam-Induced Toroidal Rotation: Despite the deleterious effects associated with counterinjection, there has been a supposed need for counter-injected beams to balance the toroidal momentum input expected from coinjected neutral beams. The ion toroidal flow velocity calculated from a toroidal momentum balance equation has been compared with that estimated from the Doppler shift of the H_α line profile and from comparison of the parallel and perpendicular charge-exchange energy distributions ($\Delta V_{\parallel} \sim 2 \times 10^6$ cm/s). Agreement occurs only if the toroidal momentum damping time in the plasma interior is ~100 μs, much faster than any calculated interaction time (e.g. charge-exchange time ~50 ms).

Effect of Impurities on Injection: The role of neutral beam trapping by charge transfer to impurities can be significant, as shown by the measurements at ORNL by Phaneuf and co-workers of the cross sections for charge exchange between H^0 and various light (C,O) and heavy (Fe) ionized impurities present in tokamaks, and by calculations and beam trapping measurements on TFR by Moriette. Direct spectroscopic evidence for the charge transfer reaction $H^0 + O^{8+} \rightarrow H^+ + (O^{7+})^*$ is observed during ORMAK injection experiments. The intensity of the Balmer-α line of O VIII (102 Å) increases a factor of 4 within 4 ms after beam turn on, whereas the intensities of the Lyman-α, -β, and -γ lines of O VIII and the Balmer-β line of O VIII increase less than 20% in this interval, indicating a direct interaction between the neutral beam and the plasma.

When impurity charge exchange is included in calculations of the beam power deposition, the peak of the power deposition curve for the highest density case shifts from r = 0 to r = 15.5 cm (limiter radius a = 23 cm) and the injection power density exceeds the ohmic power density for r > 14 cm. This additional power input in the plasma may permit attainment of the higher plasma density before disruption occurs by heating the plasma edge and thus forestalling shrinkage of the current channel.

Summary: Addition of neutral beam injection power permits attainment of higher density and β_T and of stable operation at lower q than without injection. The impurity radiation also increases, but only in proportion to the added power.

Acknowledgment: The work presented here is the result of the efforts of the entire ORMAK group in cooperation with the Plasma Heating and Fueling Section of the Fusion Energy Division.

References:

*Research sponsored by the Energy Research and Development Administration under contract with the Union Carbide Corporation.

[1] M. Murakami, J. D. Callen, and L. A. Berry, Nucl. Fusion 16, 347 (1976).

[2] M. Murakami, J. F. Lyon et al., this conference.

INVESTIGATION OF THE FAST NEUTRAL PARTICLE CORONA SURROUNDING THE PULSATOR PLASMA

F. Wagner, H.M. Mayer
Max-Planck-Institut für Plasmaphysik, D-8046 Garching, F R G

Abstract: Non-Maxwellian tails have been observed in the distribution of fast atoms emitted from the plasma edge. It is demonstrated that backscattering from the liner may lead to such distributions.

The measurement of the temperature of the neutral particles at the plasma edge requires a low ripple of the toroidal field. Otherwise, details are washed out by the gross effects produced by the drift of locally trapped particles (1).On the Pulsator tokamak the toroidal field ripple is< 0.3% so that trapped particle effects do not play a major role.

The neutral particle flux is measured by a five-channel-analyzer. The line of sight of the analyzer can be swept in a poloidal plane across the plasma diameter from r= +11cm, which is the limiter radius,to r= -9cm. Within the range from -9 to -11 cm the line of sight of the analyzer is terminated by the tube connecting the plasma vessel and analyzer. These geometrical details are of importance in analyzing the experimental data.

The measurements of particle flux and temperature are carried out for: I_p= 60kA; B_{tor}= 27kG, peak electron density between $2x10^{13}$ and $1.5x10^{14}cm^{-3}$. The density is increased by gas puffing starting at 40 msec.

Fig.1 shows a series of ion temperature profiles obtained be - tween 45 and 70 msec. Due to the gas input the central ion temperature increases on account of the enhanced heat transfer between electrons and ions. The measured edge temperature also increases. From the shape of the flux spectrum one can deduce that the measured temperature does not represent the actual ion temperature at the plasma edge. At low energies (E<400eV) the slope of the flux spectrum increases defining a temperature of about 60eV. This rise indicates that the emitted particle flux has two components, a low energy branch originating in the cold ions at the edge and a high energy tail.

The question arises as to what process is responsible for the high energy tail in the flux spectrum. The most probable seems to be backscattering at the liner of hydrogen atoms born in the plasma centre. This conjecture is supported by the results of measurements of the particle flux and temperature in the range between r= -9 and -11cm. In this range the analyzer can only detect particles which are scattered from the wall. Sweeping the analyzer across the transition region, there is no discontinuity in flux or temperature. Fig.1 suggests that the particles at r= + 11cm are wall-reflected too. This experimental result implies that the plasma is surrounded by a corona of energetic atoms which do not totally loose their energy on scattering from the wall.

Calculations and measurements (2) give a backscattering coefficient from stainless-steel targets exposed to monoenergetic hydrogen atoms in the lower keV-range of about 20-30 %. The shape of the spectra of backscattered hydrogen atoms corresponds roughly to insert 1 in Fig.2 for low energies (E_o= 100V) and to insert 3 for E_o= 5keV (3). For the 3 cases of f(E) shown in Fig.2 the backscattered spectrum has been calculated assuming a Maxwellian distribution of incident particles. Fig.2 shows the calculated results of the temperature of the backscattered particles T_{edge} versus the temperature of the incident particles T_{centre} for the three spectra f(E). The data points are taken from Fig.1 The relatively good agreement with all three curves seems to indicate that the detected high energy flux at the plasma edge is the wall reflected flux emerging directly from the plasma. However, the assumptions of the calculation are too crude to conclude that the spectrum shown in insert 3 represents best the backscattering between 0.4 and 1.2 keV.

Fig. 3 demonstrates the effect of wall-reflection of neutral particles on the atomic density profile. The curves are the result of transport calculations which were fitted to experimental plasma profiles and normalized to the observed emission of neutral flux along the central chord of energies between .2 and 4 keV. The observed energy distribution was in full agreement with the calculation over this range of energies. Wall-reflection was taken into account using the reflection coefficients of Ref. 2. It is seen that wall reflection barely influences the shape of the interior profile. However, it facilitates the penetration of neutrals through the region close to the plasma surface and thereby roughly doubles the neutral density on axis for a peak electron density of $1.5x10^{14}cm^{-3}$. This experimental result may contribute to the understanding of the production of high central densities obtained by gas puffing.

Acknowledgement. Thanks are due to D.Düchs for making available his code to calculate the atomic density profile.

References:

/1/ M.P.Petrov, Proc.5thInt.Conf.on Plasma Phys.and Contr.Nucl. Fus.Res., Tokyo 1974, IAEA, Vienna 1975, Vol.I, 43
/2/ R.Behrisch, Journal de Physique, to be published 1977
/3/ O.S.Oen, M.T.Robinson, Nucl.Instr.Methods 132(1976) 647.

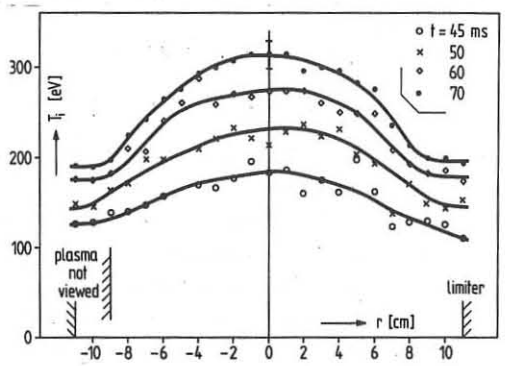

Fig.1: Profiles of the ion temperature for a high density discharge.

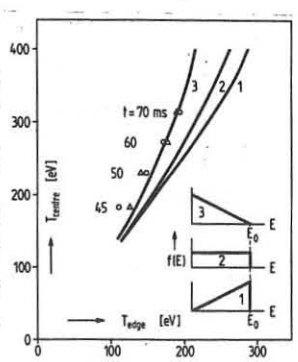

Fig.2: Calculated and measured temperature of the reflected particles.

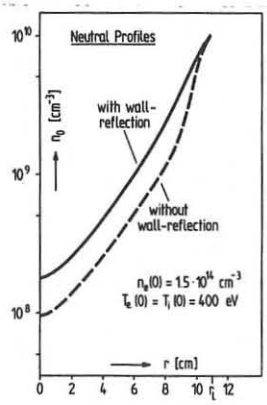

Fig.3: Neutral gas density with and without wall-reflection

ELECTROSTATIC POTENTIAL IN THE DIVERTOR SCRAPE-OFF LAYER

U. Daybelge and M. A. Mamedow†

Institut für Theoretische Physik, Ruhr-Universität Bochum,

4630 Bochum, F. R. Germany

†University of Baku, Azerb. Soviet Socialist Republic

Abstract: In a tokamak plasma bounded by a limiter or a divertor various transport mechanisms concerning plasma and impurity particles depend on the variation of the electric potential inside the scrape-off layer. An analysis is given for the detailed variation of the potential inside the scrape-off layer .

Radial Transport equations for plasma and impurity particles in a tokamak represent a boundary value problem to be complemented by the conditions imposed by the existing limiter(s) or divertor. In some cases, the interaction of plasma and the solid material boundaries causes large potential variations which have striking effect on the ion orbits [1,2]. Hinton and Hazeltine [3] have shown that if the T_e/T_i ratio is small, what is to be expected in a future divertor plasma, the electric dirfts effects can be neglected. For finite values of the temperature ratio, as is the case with a limiter plasma, however, radial as well as poloidal field effects play an important role in the formulation of the boundary conditions on the interior transport.

For definiteness, we consider the poloidal divertor geometry, which has the axial symmetry. For this geometry the conservation of the canonical angular momentum $p_\phi = (mv_\phi + eA_\phi)R$ permits an exact analysis for the boundary value problem of the collisionless plasma in contact with the divertor plates. Instead of expanding this invariant for small potential variation [1-3], we shall consider the full expression, since we expect that the strong potential variations can take place. In the weakly collisional regime the charged particles reaching the divertor plates are absorbed giving rise to the concept of a "loss cone". Neglecting magnetic shear effects the non-dimensional form of the p_ϕ for ions is

$$J = r + \sigma\delta h\left[E - \frac{\mu}{h} - \eta\phi(r,\theta)\right]^{1/2} = \text{Const.} \qquad (1)$$

where the length and velocities are normalized by the radius of the separatrix a, and the thermal speed, respectively. Further, $\sigma = \pm 1$, $\delta = \rho_{pi}/a$ where ρ_{pi} is the ion gyroradius in the poloidal field and $h = 1 + \varepsilon r\cos\theta$ where ε is the inverse aspect ratio, $\eta = e\phi_R/kT_i$, $E = \hat{E}/kT_i$ and $\mu = \hat{\mu}B_0/kT_i$. Under fairly general assumptions about the potential landscape over the (r,θ) plane, Eqn.(1) can be used to determine orbits passing through a point (r,θ) and reaching another point on the axis $(r_0, \theta_0 = \pm\pi/2)$. Two cylindric divertor plates are located over this axis at $r_0 > 1$. Loss regions in the velocity space (σ,E,μ) at the given point (r,θ) correspond to orbits leading to these plates. To distinguish the transiting orbits from the ones intercepted by the plates, we assume that over the axis for $r_0 < 1$ the plasma potential is constant and zero. Let us also assume that the plate potential is strongly negative. This is consistent with the results of the Ref.[3] where a monotonous potential in both r and θ was found.

We first consider the case for $\sigma = 1$, where $J > 0$ is an increasing function of r_0 with a positive jump at $r_0 = 1$. Hence, the intercepted orbits satisfy the following inequality:

$$J = r + h(E - \tfrac{\mu}{h} - \eta\phi)^{\frac{1}{2}} > 1 + \delta(E - \mu)^{\frac{1}{2}} \qquad (2)$$

In addition, for real velocities we have the constraints

$$E - \frac{\mu}{h} - \eta\phi \geq 0 \quad \text{and} \quad \mu \geq 0 \qquad (3)$$

Boundaries of the loss region defined by (2) is a skew parabola which has a maximum for μ, i.e.,

$$u^2\mu^2 + 2\mu\left[(2+\varepsilon u)t^2 - u^2(h+1)E + uh^2\frac{\eta}{\varepsilon}\phi\right] + \{[\varepsilon^2 t^2 - 4E$$
$$-2\varepsilon u(h+1)E + 2h^2\eta\phi]t^2 + u^2(h+1)^2E^2 + h^4\frac{\eta^2}{\varepsilon^2}\phi^2 - 2u(h+1)Eh^2\frac{\eta}{\varepsilon}\phi\} = 0. \qquad (4)$$

where $t = (r-1)/\varepsilon\delta$, $u = \cos\theta$. The loss region is the inside or outside of this parabola, depending whether $t > 0$ or $t < 0$, respectively.

If $\sigma = -1$, $J(r_0)$ is a sectionally increasing function which suffers a large drop at $r_0 = 1$. To distinguish the transiting particles we require

$$J = r - \delta h(E - \tfrac{\mu}{h} - \eta\phi)^{\frac{1}{2}} > \delta(E - \mu)^{\frac{1}{2}} \qquad (5)$$

The border of the loss region is found from (5) as another skew parabola:

$$\varepsilon^2\delta^2u^2\mu^2 + 2\mu\left[(2+\varepsilon u)r^2 + \varepsilon\delta^2uh^2\eta\phi - \varepsilon^2\delta^2u^2(h+1)E\right]$$
$$+ \frac{r^4}{\delta^2} + \varepsilon^2\delta^2u^2[(h+1)E - \frac{h^2}{u}\frac{\eta}{\varepsilon}\phi]^2 + 2r^2\{h^2\eta\phi - [2+\varepsilon u(h+1)]E\} = 0. \qquad (6)$$

where $r = 1+\varepsilon\delta t$. In either case of $t \gtrless 0$, the loss region is the inside of the parabola given in (6). Clearly, the interplay of the parameters ε, δ and η determine various regimes.

The ion distribution function is a function of the constants of the motion . In the non-diverted regions it can be written as $f_i = n_a \exp(-E)$. Due to the strongly negative plate potential the electrons can not easily reach the plates. Therefore, their distribution function has no loss-cone structure. The electron density is given by $n_e = n_a \exp(e\phi/kT_e)$. Imposing the condition of quasineutrality we obtain a transcendental equation for the potential. We note that the parameter T_e/T_i influences the solution strongly, since $n_e = n_a \exp(\eta\phi T_i/T_e)$. We can numerically solve

$$\exp(\eta\phi T_i/T_e) = \sum_\sigma \int_{D_\sigma} \exp(-E)\,\frac{d\mu\,dE}{2\sqrt{\mu}h(E - \frac{\mu}{h} - \eta\phi)^{1/2}}\,, \qquad (7)$$

where the integration is over non-vanishing regions, and determine the self consistent electrostatic potential.

This work was supported by the SFB 162 "Plasmaphysik Bochum/Jülich".

[1] H.P. Furth and M.N. Rosenbluth, in Plasma Physics and Controlled Nuclear Fusion Research (IAEA, Vienna),Vol.I, p.821(1969).

[2] H. L. Berk and A.A. Galeev, Phys. Fluids 10, 441(1967).

[3] F. L. Hinton and R. D. Hazeltine, Phys. Fluids, 12, 2236 (1974).

TRANSPORT CODE CALCULATIONS CONCERNING THE PLASMA PARAMETERS IN THE SCRAPE OFF LAYER OF A POLOIDAL LIMITER IN A TOKAMAK

A. Nicolai and G. Fuchs

Institut für Plasmaphysik der Kernforschungsanlage Jülich GmbH
Ass. EURATOM-KFA

Abstract: Using a diffusion model, and including special particle and energy loss mechanisms in the scrape off layer of a limiter, the plasma parameters are calculated. It turns out, that secondary electron emission from the limiter influences the electron temperature, the sheath voltage in front of the limiter, and as a consequence the energy flux. Some special results are discussed.

1. Introduction: To calculate the plasma parameters in the scrape off layer consistently to those in the central core, we introduce special source and sink terms into Düchs' code /1/, which describe the particle and energy fluxes parallel to the magnetic field thereby hitting the limiter. We assume anomalous transport perpendicular to the magnetic field according to the 6-regime model /1/ throughout the plasma. As the plasma density is very low in the scape off layer (10^{11} - 10^{10})/cm^3 we neglect the friction forces and the elastic collisions with the neutral gas background. The electrons and the ions then stream with their thermal velocity along the field lines and are completely absorbed by the limiter.

2. Diffusion model: In the scrape off layer (Fig. 1) the equation of continuity is

$$\partial\hat{n}(r,z)/\partial t = (\partial(rD\partial\hat{n}(r,z))/\partial r)/r - \partial/\partial z\,\hat{\Gamma}(z,r) + S$$

The source terms S take care of particle production and loss due to ionization and recombination. $\hat{\Gamma}(z,r)$ is the particle flux density parallel to the magnetic field. By integrating equation (2.1) from z = 0 to z = L and considering the equation for the plasma core, we get an equation that holds throughout the plasma

$$\partial n(r)/\partial t = (\partial(rD\partial n(r)/\partial r)/\partial r)/r + S + S'\Theta\,(r-r_{lm})$$

n(r) is the plasma density average with respect to z. This mean value is assumed to be very close to $\hat{n}(r,z)$ because of the assumptions made in the introduction. Θ is the heaviside-step-function and $S' = \hat{\Gamma}(z=L,r)/L$ represents the desired sink term, which is affected by the sheath potential and the secondary electron emission and in detail given below. As the convective part of the heat flow parallel the magnetic field is much greater than the conductive part, we argue along the same line as before and get for the temperatures T_e and T_i

$$1.5\;\partial(nkT_e)/\partial t = (\partial(rq_e)/\partial r)/r + P_e + P_e'\Theta(r-r_{lm})$$
$$1.5\;\partial(nkT_i)/\partial t = (\partial(rq_i)/\partial r)/r + P_i + P_i'\Theta(r-r_{lm})$$

where P_e and P_i stand for the energy gain or loss from ionization, recombination, radiation and charge exchange, $q_{i,e}$ are the heat flux densities perpendicular to the magnetic field. P_e' and P_i' are the loss terms due to the limiter given by the energy flux densities at z = L divided by L. These are dominated by the sheath potential and the secondary emission and are also given in detail below.

3. Sheath Potential and Secondary Emission: The voltage U between the limiter and the plasma is determined by the requirement of zero electric flux

$$nv_i\varphi_i + (\sigma_e nv_e\varphi_e + \sigma_i nv_i\varphi_i)\varphi_s = n_e v_e \varphi_e$$

where the Boltzmann factors $\varphi_{i,e,s}$ for the ions, electrons and secondaries are given by

$$\varphi_i = \Theta(U)\exp(-eU/kT_i) + \Theta(-U)$$
$$\varphi_e = \Theta(-U)\exp(eU/kT_e) + \Theta(U)$$
$$\varphi_s = \Theta(U)\exp(-eU/kT_s) + \Theta(-U)$$

$v_{i,e} = \sqrt{2kT_{i,e}/m_{i,e}}$ are the thermal velocities of the ions and electrons. The energy distribution of the secondaries is not quite maxwellian, we nevertheless used a temperature T_s = 5 eV. $\sigma_e(T_e)$, the secondary emission coefficient, was obtained by folding the function $\sigma_e'(E)$ given in /2/ with a maxwellian distribution. The secondary emission coefficient because of ion impact, σ_i, was set equal to 0.1 throughout. Depending on the sign of U, the secondary electrons can be accelerated in the sheath. This will cause a nonmaxwellian distribution function right in front of the sheath; fig. 2 gives a qualitative sketch. This type of distribution function is however unstable with respect to the two stream instabilitites, which will destroy the double humbed distribution over a distance of several ten to hundred Debeye lengths /3/. This is very short as compared to L and it is therefore justified to assume the incoming electrons as maxwellian. Considering the particle and energy flux densitites of the incoming electrons and ions and the outcoming secondaries we get

$$S' = \alpha\varphi_i nv_i/L;\quad P_e' = \alpha n(1.5\,kT_e v_e\varphi_e - 1.5(kT_e - eU\Theta(U))\,(\sigma_e v_e\varphi_e + \sigma_i v_i\varphi_i)\varphi_s + v_i\varphi_i e\,U\,\Theta(-U))/L$$
$$P_i' = \alpha n(1.5\,kT_i v_i\varphi_i + v_e\varphi_e eU\Theta(U))/L$$

The factor α = 0.564 arises from the maxwellian distribution function of the incoming particles. The terms containing the Θ-function account for electron energy loss because of ion acceleration in the sheath in case U<0, and vice versa, ion and secondary electron energy loss due to the electron acceleration in case U>0.

4. Results: Fig. 3 shows the profiles of the parameters characterizing the scrape off layer. The plasma parameters of the central core are typical for the TEXTOR-Tokamak /4/ (n = 1,5.10^{13}/cm^3, R = 175 cm, a = 50 cm, B_t = 20 kG, I_t = 476 kA) in the flat top phase. ($T_i \approx T_e \approx$ 800 eV). We used the secondary emission coefficient of tungsten. To account for oblique incidence we multiplied this by a factor 1.5. T_i turns out to be much greater than T_e. The physical reasons are that the electrons are efficiently cooled by accelerating the ions and by adding cold secondaries. For the example given in fig. 3 both processes are comparable. The voltage U is ion accelerating and varies between -140 V and -80 V. This is about one third of the value that would be obtained for $\sigma_i = \sigma_e = 0$. The maximum density is about 3 % of the mean density of the central core. The limiter loading P_{lm} falls rapidly and has the maximum value 1.1 kW/cm^2. The electron current density j_e is to a large fraction balanced by the secondary emission current density j_s. At the limiter edge the ion current density j_e contributes only 20 % to the balance.

References

/1/ D.M. Meade et. al. Proc. 5th Int. Conf. Japan, paper CN-33/1 14-4 (1974)

/2/ D.J. Gibson, Article in Handbook of Vacuum Physics V2 e.d. A.H. Beck, Pergamon Press, Oxford 1966

/3/ H. Amemiya, G. Fuchs, J. Wick, Computer Simulation unpublished

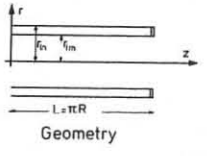

Geometry

Fig. 1

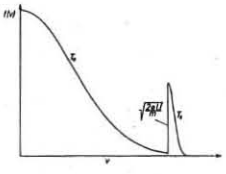

Fig. 2 Double Humbed Distribution Function

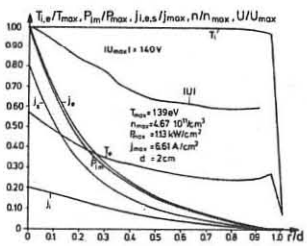

Fig. 3 Plasma Parameters in the Scrape off Region

PROBE MEASUREMENTS IN A SHEARLESS HIGH-BETA PLASMA SURROUNDED BY A GAS BLANKET

J.R. Drake and T. Hellsten
ROYAL INSTITUTE OF TECHNOLOGY, S-100 44 STOCKHOLM 70, SWEDEN

Abstract. The boundary layer between a fully ionized rotating plasma and the pressure profile inside the boundary layer were experimentally studied with probes.

1. Introduction. The Spherator with a purely poloidal magnetic field has been suggested as a device to confine a thermonuclear plasma [1]. Such a system has neither shear nor minimum-average-B properties. To study the stability against magneto-hydrodynamical perturbations for such a system we used an axi-symmetric open-ended device in which a high density plasma was generated by an ExB discharge. The strong centrifugal force due to the plasma rotation, which is assumed to be analogous to a large thermal pressure, apparently affected the plasma stability. Also, the boundary layer between the fully ionized plasma and the surrounding neutral gas blanket was changed by changing the geometry of the limiter.

2. Experimental Arrangement. The experiments were performed on the FI device shown in Fig.1. The vessel was filled with a hydrogen density of 2.0×10^{21} atoms/m^{-3}. Two condensor banks were discharged between the anode and the cathode, the first at t=0 and second at t=200 μs, thus generating a rotating plasma. The total magnetic flux between the cathode and the anode was 0.037 Vs and the potential drop was typically 2kV. The plasma and the surrounding neutral gas were separated by a partially ionized boundary layer. The cathode also acted as a limiter, and the geometry of the cathode and the plasma collisionality in the boundary layer defined the boundary conditions. We used two cathode geometries to study the boundary layer, a 2-mm thick ring and a plate of the type shown in Fig.1.

3. Probe measurements. The electric field was obtained by measuring the floating potential and the electron temperature T_e was obtained from probe current-voltage curves. We assumed that the rotation velocity was $V_\phi = \underline{E}\times\underline{B}/B^2$, and that $T_e = T_i$ for this dense plasma. It was then possible to estimate the density. However, probes (or any insulator surface) violently disrupted the plasma if inserted to a point where the rotation velocity exceeds Alfvén's critical velocity, V_c [2]. However, since V_ϕ/r was approximately constant along the field lines, it was possible to probe deeper into the plasmas with the probe which enters from the upper lid (see Fig.1).

3.1. The Boundary Region in the Midplane. The equivalent β value, obtained from the expansion of the field lines due to centrifugal force and pressure gradient [3], was 0.2. Earlier probe measurements of the plasma in the midplane demonstrated that the main plasma body, limited by the "cathode field lines", was surrounded by a partially ionized boundary region with a density of about 30% of that in the interior when a cathode plate was used as a limiter [4]. This dense, thick b.r. was assumed to be caused by Simon diffusion. The plasma diffusion perpendicular to B was dominated by collisions with neutrals and thus the ion diffusion coefficient greatly exceed that for electrons. Normally an ambipolar electric field would retard the cross-field ion transport, but the cathode plate short-circuited the field lines in this region. This effect and the drain of electrons to the cathode plate produced a flat negative potential distribution at the equatorial plane. This relatively high density outside the cathode field lines was reduced by replacing the cathode plate by a thinner ring, so that the ambipolar electric field was not short-circuited. Fig.2 shows the ion-retarding ambipolar electric field in the midplane for the cathode-ring case compared to the cathode plate case. The comparatively sharp density boundary at the cathode-ring field line is shown in Fig.3 and compared with the broad dense boundary seen with the cathode plate. Density measurements with the cathode plate as limiter are discussed in Ref.4.

3.2. The Upper Region. It was possible to make probe measurements of T_e, V_ϕ and the ion saturation current J_o, using the probe in the upper region where the rotation velocity was lower. These measurements were used to estimate the density distribution at the midplane. Assuming a constant angular rotation velocity Ω and T_e along a field line, the ratio of the density along the line to the density at the midplane is a function of major radius r and is given by $n/n_o = \exp(m\Omega^2(r^2-r_o^2)/4kT)$. However, because of the exponential dependence, extrapolations of the probe-measured profile to the midplane were very sensitive to small errors or deviations from isorotation. However, the density at the midplane during rotation was estimated by utilizing the J_o-profile observed immediately after the rotation was stopped and by assuming fast parallel transport and negligible cross-field transport during a brief period immediately after the centrifugal force of rotation was removed. Profiles of J_o just before and after the rotation was stopped are shown in Fig.4. Profiles of T_e and V_ϕ during rotation are shown in Fig.5. The density profile at the midplane derived from this second technique, which is just based on conservation of particles in a flux tube, indicated that the Ω for field lines in the interior region of the plasma was 40% higher at the midplane than at the point of the probe measurements above the midplane. This is favourable for rotating mirror devices since the angular velocity is limited by critical velocity phenomena at the mirror ends.

4. Stability Against Interchange Modes. Due to the strong centrifugal force the plasma is mainly concentrated into an almost straight cylinder. We have found that there is a region inside the cathode field lines where the density, temperature and velocity decrease outwards. Equilibrium between the outward directed centrifugal and pressure gradient forces is provided by an induced azimuthal plasma current. Thus stability can be obtained by compressional effects from rotation in the region inside the "cathode field lines" for this geometry where the flux tube volume increases outwards. The conclusion is that a pressure distribution decreasing when $q=\oint dl/B$ increases can be obtained for a Spherator configuration without minimum-average-B or shear stabilization.

Acknowledgements. We thank Prof. Bo Lehnert and the fusion research group of the Royal Institute of Technology. One of the authors (JRD) was supported by a U.S. Nat.Sci. Foundation Grant. This work has been supported by the European Communities under an association contract between Euratom and Sweden.

[1] B. Lehnert, Nature 181, 331(1958).
[2] H. Alfvén, On the Origin of the Solar System, Clarendon Press, Oxford (1954).
[3] B. Lehnert, T. Hellsten and R. Raggi, Phys. Scripta 9, 53(1974).
[4] T. Hellsten and R. Raggi, Nucl. Instruments and Methods, 124, 11(1975).

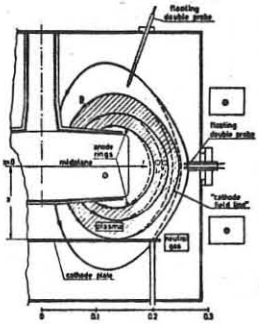

Fig.1

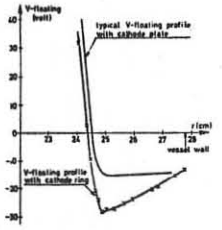

Fig.2

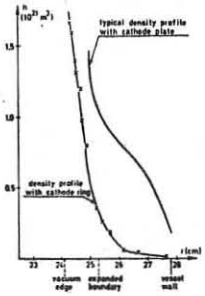

Fig.3

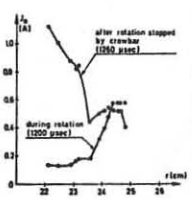

Fig.4

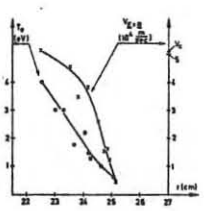
Fig.5

VELOCITY SPACE SELECTION PROPERTIES OF MAGNETIC DIVERTOR CONFIGURATIONS

G. Casati,* E. Lazzaro,† C. Perini,* G. Realini,‡

*Universita degli Studi di Milano - Italy.

†Laboratorio di Fisica del Plasma, C.N.R. - Milan

‡C.C.R. EURATOM-Ispra.

Abstract: The efficiency of divertors with one and two stagnation points is evaluated and compared for the case of containment of α particles produced in fusion reactions.

Fusion oriented tokamaks fitted with magnetic divertor systems have a complicated two dimensional magnetic structure. The use of zero dimensional models in which only particle balance at the plasma edge is considered,[1] or one dimensional transport codes, for the evaluation of particle and energy fluxes to the wall, require, when applied to divertor scheme, a knowledge of divertor efficiency. In this work, a systematical analysis of single particle behavior in realistic axisymmetric single and double null divertors is reported, which allows to define, evaluate, and compare the efficiency μ for energetic α particles which are generated by D-T reactions in the bulk of the plasma, well within the separatrix, by a monoenergetic source, at an energy[2] $W_{\alpha o} = \frac{m_\alpha \bar{v}_{\alpha o}^2}{2} \gg \overline{W} = \left[\frac{3\sqrt{\pi}}{4}\left(\frac{m_\alpha}{m_i}\right)\right]^{\frac{2}{3}}\left(\frac{m_\alpha}{m_e}\right)^{1/3} T_e$ and which are slowed down to ion thermal speed on a time scale of the order $\tau = \frac{1}{\nu_{\alpha e}} \ln\left[\frac{W_{\alpha o}}{\overline{W}}\right]^{1/2}$. The population of α which has energy larger than 3/2 T_i has a temperature $T_a \simeq (2/3)(W_{\alpha o}/\ln W_{\alpha o})$ and diffuses across the separatrix with a flux.[2] $\Gamma_\alpha(\psi_s) = D\frac{dN_\alpha}{dr} \approx \sqrt{\frac{R}{r}}\frac{q^2\nu_{\alpha\beta}}{\Omega_\alpha^2}\frac{T_\alpha}{m_\alpha}\frac{dN_\alpha}{dr}$ with the usual meaning of symbols.

The basic assumption of Ref. 2, perfect containment of the α, from which follows the isotropy of the α distribution function f_α^o does not hold in the region of the separatrix, since there are loss regions in velocity space, where f_α^o must vanish. From the data of a prototype reactor (FINTOR R = 10 m, a = 2 m, B = 50 kG, T_e = 25 keV, T_i = 21 keV, q = 2, n = 2,4 · $10^{13}cm^{-3}$) it appears that near the separatrix $1/\Omega_\alpha << \tau_{\alpha\parallel} << 1/\nu_{\alpha e}$ and $\rho_{\alpha p}/a_p << 1$ and $T_\alpha \sim 2.5$ MeV where Ω is the α gyrofrequency, $\tau_{\parallel\alpha} = 2(\pi qR/v_\alpha)$ the α flight time parallel to B, $\nu_{\alpha e}$ the electron - α collision frequency, ρ_p the poloidal Larmor radius. Therefore we may apply drift orbit theory to the suprathermal α which are essentially collisionless. On the bounce line scale orbits are completely identified by the constants of motion $\varepsilon = (m/2)(v_\parallel^2 + v_\perp^2)$, $\mu = (m/2)(v_\perp^2/B)$ and $P_\varphi = \frac{Ze}{c}A_\varphi + mrv_\varphi$ A_ϕ is the φ component of the magnetic vector potential computed numerically in axisymmetric geometry from the poloidal field coils and plasma data. Since $B_p/B << 1$, the orbits may be conveniently labeled by the approximate expression.

$$P_\varphi^* = \frac{Ze}{c} r A_\varphi(r,z) + \sigma v\left[r(r - r_o\sin^2\vartheta_o)\right]^{1/2}$$

where $\sigma = \mathrm{sign}(\underline{v}\cdot\underline{I})$, $\sin^2\vartheta_o = \frac{v_\perp^2}{v^2}$ and conservation of ε and μ is used. The analysis of the divertor operation is performed through a careful examination of the typology of single particle orbits and by performing a mapping on to velocity space, of the orbits which have special properties. Fixing two points of an orbit namely an initial point r_o, Z_o and a final point r_f, Z_f and equating the corresponding orbit labels $P_\varphi(r_o,z_o) = P_\varphi(r_f,z_f)$ an equation of a locus in $v_\parallel, v_\perp$ space is obtained, $v(\vartheta_o) = K(r_o,z_o,r_f,z_f)/\left[r_o|\cos\vartheta_o| - (r_f(r_f - r_o\sin^2\vartheta_o))^{1/2}\right]$

where $K(r_f,a_f,z_o z_o) = Ze/c[r_o A_\phi(r_o z_o) - r_j A_\phi(r_j r_j)]$ contains the magnetic information. The cases considered refer to initial points $r_s - \Delta_s < r_o < r_s + \Delta_a$ $z_o = 0$ where r_s is the mean separatrix radius and Δ_s the scrape of thickness, and as final points, points on the wall chamber and collector throat are selected. In velocity space we thus obtain the boundaries of regions which map the classes of (1) passing particles contained or lost, (2) coinjected ($\underline{v}\cdot\underline{J} > 0$) trapped particles, contained, (3) counterinjected ($\underline{v}\cdot\underline{J} < 0$) trapped particles, lost, (4) particles collected in the throat divertor throat. In this way, from a knowledge of the loss and capture regions in velocity space, of the magnetic divertor it is possible to evaluate the fraction

$$\mu_s = \frac{\int_s d\underline{v}\, f_\alpha^o(v_\perp^2, v_\parallel)}{\int_{all} d\underline{v}\, f_\alpha^o(v_\perp^2, v_\parallel)}$$

of particles which have any significant property, and μ_s can be taken as a measure of the configuration efficiency. Detailed description is given in (3). Fig. 1 and 2 show the two divertor configurations studied, with sample orbits of counterinjected particles, with approximately the same parameters. In the single null divertor the particle hits the wall, and is lost; in the double null divertor it is collected in the throat. This difference of behavior qualitatively explains the different efficiency. In Fig. 3, the velocity space region for an α at initial position r_o = 10 m, z_o = 1 m in the single wall divertor is shown, for multiples of T_α = 2.5 MeV. Region 1: α circulating and contained, Region 2,8: circulating and lost, Region 3: trapped and contained, Region 4: trapped and lost, Region 5,6: counterinjected particles, contained and lost, Region 7: circulating particles collected in the throat. Figure 4 shows the situation for the double null divertor, with the same throat width (200 cm). In region c: particles are contained, region ℓ: lost, Region d: diverted. The overall fractions of lost and diverted particles are for the double null divertor μ_D = 0.162 μ_ℓ = 0.034; for the single null divertor μ_D = 0.045 μ_ℓ = 0.056. In the single null divertor the largest contribution to losses is due to counterinjected particles which execute large banana orbits opening on the outer side of the plasma. In the double null divertor the topology of magnetic field prevents the occurence of these large banana orbits.

[1] R. Behrisch, B. B. Kadomtsev, IAEA-CH33[52 p. 229 (1974).

[2] F. Engelman, Nocentini, Nucl. Fus. 359 (1975).

[3] G. Casati, E. Lazzaro, C. Perini, C.C.R. ISPI Rep. (1977).

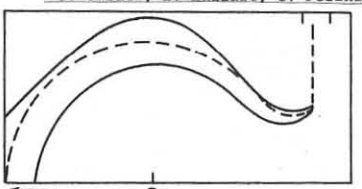

Fig. 1

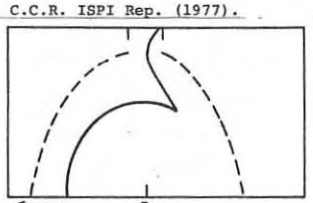

Fig. 2

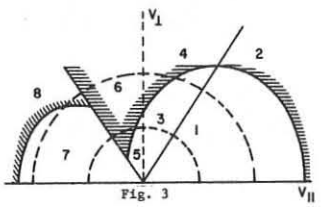

Fig. 3

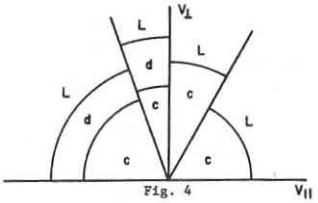

Fig. 4

X-RAY SPECTRA AND IMPURITY CONCENTRATION IN THE T-10 TOKAMAK

A.B. Berlizov, G.A. Bobrovskii, G.E. Notkin, V.A.Rantsev-Kartinov, K.A. Razumova, M.M. Stepanenko, D.A. Shcheglov
I.V. Kurchatov Institute of Atomic Energy, Moscow, USSR

In /1/ the radial distribution of Z_{eff} has been determined in a stationary stage of the T-10 discharge from the analysis of the X-ray spectra and Thomson scattering. The X-ray detector (a gas proportional counter) registrated radiation along the minor diameter and along the chords 8; 16 and 24 cm outwards. Typical spectra are shown in Fig.1. They are measured along the diameter in 4 successive time intervals. The value of $Z_{eff}(0)$ was equal to 1.3 for a 400 kA, 35 kOe regime.

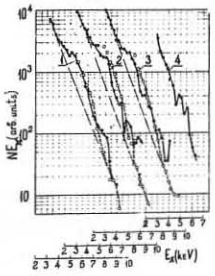

Fig. 1

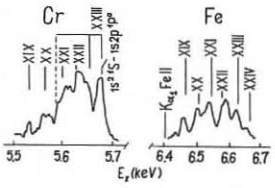

Fig. 2

Johann spectrometer was also used in the T-10 to cover simultaneously the energy range E_x=5...6.9 keV. A LiF crystal was out for reflection from 2 0 0 planes, with a radius of curvature of 30 cm. The spectral resolution E_x/E_x of the spectrometer is equal approximately to 3.10^{-3} for E_x- 6 keV. Photographic films were exposed by series of 80 shots, most of them being similar to those described in /1/. A typical spectrum is shown in Fig. 2. One can see X-radiation from the optical and inner shell transitions in highly ionized Fe- and Cr- atoms. The spectrum of Fe is rather similar to that obtained in the ST Tokamak /2/ and to a certain variant of computer spectra in /3, Fig. 9/.

K-lines of Fe and Cr are registrated by the proportional counter, too (see Fig. 1), but with a poor energy resolution ($\Delta E_x/E_x \simeq 0.17$). The ratio of the K-line intensity to the continuum intensity is shown in Fig. 3 for various chords. One can see that line radiation is emitted by a narrow central region. To evaluate Fe concentration in the center of the plasma column we use absolute intensity measurements of Fe K, taking into account the energy resolution of the counter. The results of /3/ concerning total radiation rate of Fe-impurity atoms in the (1s - 2p) - spectral region were used. The value of $n_{Fe}(0)$ appeared to be $\lesssim 1.10^{10}cm^{-3}$. Then one can evaluate the total concentration of Cr-, Fe- and Ni- impurity proceeding from the chemical composition of the vacuum chamber material and taking into account the spectra in Fig.1 and Fig. 2. This concentration appeared to be in a good accordance with the enhancement factor measurements in the centre of the plasma column.

We shall characterize the slope of the thermal X-ray spectra by "temperature" T_x. This value corresponds to

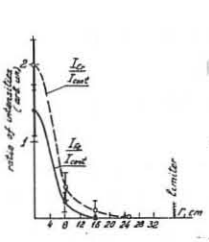

Fig. 3

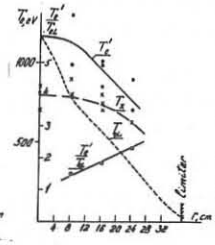

Fig. 4

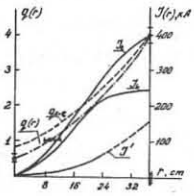

Fig. 5

the profile of T_e measured by laser, $T_{eL}(r)$, when observed along the diameter. The spectra registrated along other chords give higher values of T_e in comparison with T_{eL} as one can see in Fig. 4. The values of T_x and the radial profile of T_{eL} are given in this Figure. In the former case r means the distance from the center to the chord of observation. To describe the discrepancy we assumed the electron energy distribution function f_e to be bimaxwellian in the real plasma, the "cold" component has $T_e = T_{eL}$, the hotter one has $T_e = T'_e$. The T'_e values shown in Fig. 4 were given by the slope of spectra which were the difference between the registrated spectra and the ones calculated for the plasma with $T_e(r) = T_{eL}(r)$ and Z_{eff}= 1.3 including recombination. The part of the hotter component appeared to be ~10% of n_e in the central region of the column (r 16 cm) and to increase to ~30% at r=24 cm under assumption proposed.

The hot electron component is to increase markedly the electrical conductivity of the plasma column even without longitudinal anisotropy. In Fig. 5 radial profiles of the currents, which have to transport by both components, and of the total current $I_t = I_L + I'$ are given. In this Figure I(r) means the current flowing inside the radius r. The current profiles were calculated under assumption $Z_{eff}(r)$= const. In such a case the conductivity profile leads to the profile of the safety factor, q(r), represented in Fig. 5 as "$q_{z=c}$" curve. But the experimental data allow us to conclude that the current profile is more steep than the one shown in Fig. 5. Those data are: a) the q value is equal to 1 at r=8...12 cm as existance of the internal mode m=1 shows; b) $Z_{eff}(0)$= 1.3 from the enhancement factor measurements; c) q= 4 at the limiter. A certain variant of q profile which is in accordance with these data is given in Fig. 5 as "q(r)" curve. Such a distribution one can obtain only assuming Z_{eff} value increase when r is increased. Possibly this effect can be explained in part by the anomalous resistance.

REFERENCES

1 A.B. Berlizov et al., 6th Int. Conf. on Plasma Phys.and Contr.Nucl. Fusion Res., Berchtesgaden,1976,paper CN-35/A-1

2 N. Bretz, D. Dimock et al., Plasma Phys. and Contr. Nucl. Fusion Res. 1974, IAEA Vienna, 1975, v.1, p.55

3 A.L. Merts, R.D. Cowan, N.H. Magee, Jr. Report LA-6220-MS, Los-Alamos Scientific Lab., Los-Alamos.

IMPURITY BEHAVIOUR IN THE T-4 TOKAMAK

V.A. Abramov, A.B. Berlizov, V.V.Buzankin, A.H. Vertiporokh,
V.A. Vershkov, V.A. Krupin, G.E. Notkin
I.V. Kurchatov Institute of Atomic Energy, Moscow, USSR

The X-ray spectrometer with a plane crystal /1/ was used to the investigations of the impurity behaviour with scanning of a plasma column shot by shot. Gas proportional counter used as a detector provides secondary monochromatization. The 13...20Å spectrum obtained with KAP-crystal (2d=26.63Å) is shown in Fig. 1.

The O^{+7} ion diffusion was investigated by the method described in /2/, in a regime H_z=30kOe, I_p=80kA, $T_e(0) \simeq$ 0.7keV, $\pi_e \simeq 3.10^{13}$ cm^{-3} with the tungsten limiter (a_L=17cm). A diffusive flux j_7 of O^{+7} ion was determined from a balance equation for this ion.

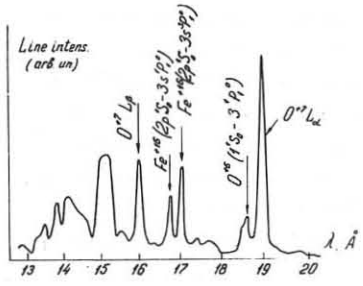

Fig. 1

$$div j_7 - n_N \alpha_N n_e = -\frac{dn_7}{dt} - n_7 n_e (S_7 + \alpha_7) + n_6 n_e S_6 .$$

Here n_6, n_7, n_N - the number density of O^{+6}, O^{+7} ions and of nuclei, S_6, S_7 and α_7, α_N - rate coefficients of ionization and recombination, respectively. The value of $(n_N \cdot \alpha_N \cdot n_e)$ was estimated from the balence equation for nuclei number density under 3 different assumptions: a) the life-time of nuclei in a plasma τ_N=0; b) τ_N=∞; c) inward diffusion of nuclei in Pfirsch-Schlüter (PS) regime. The terms in right hand part of the equation were determined from measured intensity profiles of the lines of the O^{+7} ion (19.0Å) and of the O^{+6} ion (21.6Å) (see Fig. 2a). The knowledge of the spectrometer relative efficiency at above mentioned wave lengths appears to be enough to determine the sign of the flux j_7.

The efficiency was experimentally measured. The electron temperature profile was obtained inside r=6cm by foil absorption technique. The T_e value was evaluated in the periphery from intensity profile of C^{+4} line. The T_e profile is shown in Fig. 2b. One can see that the outward diffusion of O^{+7} ions exists even at τ_N=0 while the inward diffusion depends on assumptions made.

The Ar ions in the maximum ionization stage were investigated in a T-4 regime which is characterized by oscillograms shown in Fig. 3. In the regime with $T_e(0) \simeq$ 1keV the Ar^{+16} ions serve as nuclei (the Ar^{+17} radiation at λ =3.733Å is praxtically absent). The absolutely calibrated X-ray spectrometer with NaCl-crystal (2d=5.64Å) was used. The Thomson scattering and λ =2mm interferometer were used for $T_e(0)$ and $\bar{n}_e$ measurements. To study the dynamics of impurity diffusion the pulse valve usually was opened for 10ms in the steady state of the discharge. The time delay of Ar^{+16} radiation after the injection is 7ms in the centre. This time delay enable us to estimate mean velocity of inward diffusion of Ar ions $\bar{v}_d \simeq 2.10^3$ cm.sec^{-1}. The total ionization time for Ar ions does not exceed 4ms at T_e=1keV. The time behaviour of Ar^{+1} radiation both near to the limiter (point of injection) and on opposite side is shown in Fig.3e. The constancy of the intensity points to a recycling without appreciable losses. The bolometer registrates the radiation power losses which do not change 20ms after the injection up to the end of the discharge (the power is by factor 1.5 higher than the initial one). Because these losses is to be due to a line radiation of highly ionized Ar atoms one can suppose the constant influx of these in Ar^{+16}. However one can see in Fig. 3h the fast rise of Ar^{+16} ion density in the center ($r \lesssim 1.5$cm) is changed by the slow one caused mainly by the sharpening of the intensity profile (see Fig. 3i). The noticeable growth of Ar^{+16} radiation is absent near to the axis during 50ms if Ar atoms are injected at the initial stage of a discharge rather than at the steady stage. These results enable us to conclude that there is outward diffusion of Ar^{+16} ions from the area near to the axis with the characteristic time $\tau_d(Ar^{+16}) \simeq$ 30-35ms. One can suppose that Ar^{+16} ion density near to the axis is less than mean density of Ar ions when taking into account the low density of Ar^{+16} ions in the centre, $n_{Ar^{+16}}(0) \simeq 0.2\% n_e(0)$, and the fact that the n_e increase (see Fig. 3f) is mainly to connect with Ar ion appearance. The Ar^{+16} intensity is proportional to the injection level while the time behaviour of the intensity is the same and $T_e(0)$ does not change markedly. Thus we believe that $\tau_d(Ar^{+16})$ is a characteristic time for outward diffusion of the heavy impurity of a Fe-type from the centre.

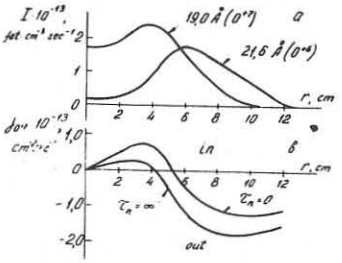

Fig. 2

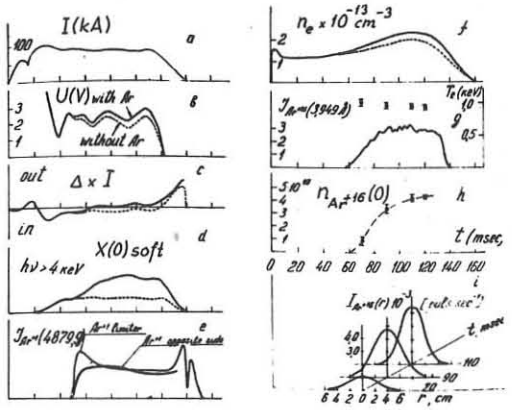

Fig. 3

IMPURITY CONTROL BY MEANS OF A COOL PLASMA BLANKET*

A.Gibson, JET Design Group, Culham Laboratory, Abingdon, Oxon, U.K.
M.L.Watkins, UKAEA, Culham Laboratory (Euratom/UKAEA Fusion Association).

Abstract: A method is presented of controlling the influx of sputtered impurities into tokamaks. A cool plasma blanket (C.P.B.) is formed around the hot core of the discharge to prevent sputtering of wall material by both charged particles and charge-exchanged neutrals. Numerical simulations show that (a) the C.P.B. can be established and maintained by a low energy neutral beam; (b) the C.P.B. is effective in preventing impurity contamination and (c) the resulting clean plasma can be heated by a high energy neutral beam.

1. Introduction. Present tokamak experiments with high ion temperatures show clear indications of impurity production due to the sputtering of wall material by energetic particles from the plasma. It is likely that this process will get worse with still hotter plasmas and it is vitally important to develop methods of controlling the impurity production. We propose an effective method of impurity control based upon establishing and maintaining a COOL PLASMA BLANKET (C.P.B.) which limits sputtering of wall material by both charged particles (by maintaining a sufficiently low plasma edge temperature) and charge-exchanged neutrals (by maintaining the edge region sufficiently hot to ionise the incoming recycled neutrals before they can charge exchange with plasma ions that have energies in excess of the sputtering threshold).

The production of impurities by sputtering is especially serious in injection heated tokamaks where a growing impurity barrier can be formed at the plasma edge. As a result of ion-ion ionising collisions (with a cross-section which increases with the effective ionic charge, Z_{eff}) the injected heating beam can be ionised and captured in the edge region.

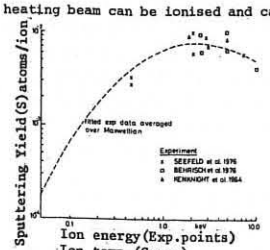

Fig.1 Sputtering Yield (S) for H^+ Ions on 304 Stainless Steel.

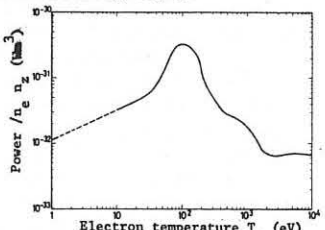

Fig.2 Power Losses by Iron Impurity Radiation.

Eventually the injected beam is no longer able to penetrate the barrier, heating of the plasma core ceases and the central temperature collapses. This effect can seriously limit the useful injection pulse length. Establishing a C.P.B. substantially reduces the impurity influx so that in our calculations no significant impurity build up occurs and the heating beam penetrates freely for the duration (2s) of the simulation.

2. The Transport Model. A 1-D transport code ICARUS is used to follow the development of the plasma. Features are: electron thermal and hydrogen fluxes are 30* pseudo-classical; the hydrogen thermal flux and impurity fluxes are neo-classical; recycled neutrals are treated as in [1]; impurities are introduced by sputtering on an Iron wall (Fig.1); radiation loss (Fig.2) is calculated from [2]. Plasma dimensions approximate those of JET (a=1.28m; R=2.93m, B=3T, I=3MA). Initial Conditions are: $\hat{n}_e=5\times10^{19}m^{-3}$; $n_z=10^{16}m^{-3}$; $\hat{T}=10^2eV$.

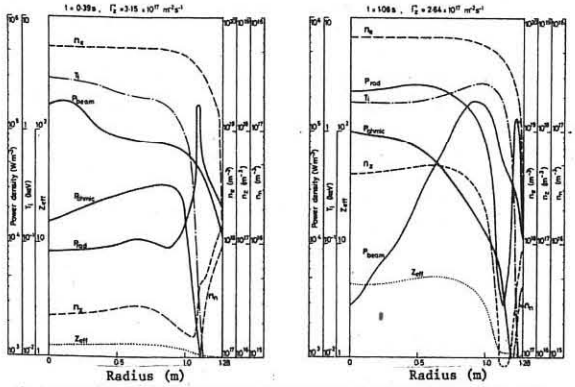

Fig.3 Radial Profiles of Plasma Parameters at Times 0.39s and 1.06s. A Heating Beam of 7MW/80keV is Applied from Time, t = 0s.

Electron density	n_e
Impurity density	n_z
Neutral hydrogen density (excluding component from injected beam)	n_n
Temperature (usually $T_e \simeq T_i$)	T_i
Effective ionic charge	Z_{eff}
Ohmic Power Input	P_{ohmic}
Neutral Beam Power Input	P_{beam}
Radiation Power Loss	P_{rad}

3. Impurity Barrier Formation. Fig.3 shows a case simply heated by an 80keV neutral beam. Sputtering by charge-exchanged neutrals causes a build-up of impurities (input flux $\Gamma_z\sim3\times10^{17}m^{-2}s^{-1}$) which by t=1.06s (when Z_{eff} has reached 5) causes the beam to be attenuated in the outer regions and excluded from the interior, so that the central and mean temperatures collapse (Fig.5).

4. The Cool Plasma Blanket (C.P.B.). Fig.4 shows a repeat of the case in Fig.1, but this time a low energy control beam (3MW, 13keV; perpendicular injection) is applied and forms a C.P.B. Over the outer 0.2m the temperatures are 10eV<T<20eV, that is high enough to ionize incoming neutrals and low enough for edge sputtering to be insignificant. The impurity influx is reduced to $\sim5\times10^{15}m^{-2}s^{-1}$ so that when the heating beam is switched on Z_{eff} is still low ~1.2 and the beam is able to penetrate freely and heat the plasma. The C.P.B. is maintained for 2s and the impurity influx remains typically a factor of a 100 less than in the case without control beam. Fig.5 compares the temporal development of the cases with and without the control beam.

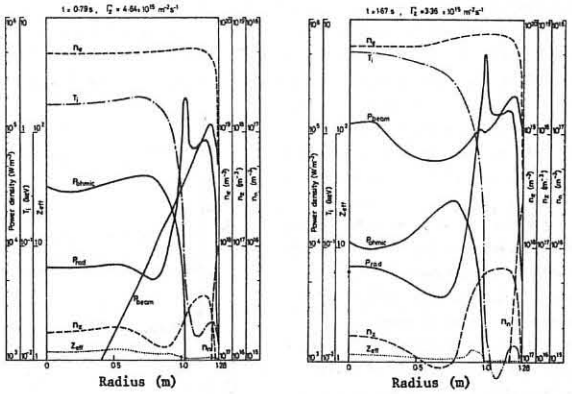

Fig.4 Radial Profiles of Plasma Parameters at Times 0.79s, and 1.67s. A Control Beam of 3MW/13keV is Applied from Time, t=0.15s and a Heating Beam of 7MW/80keV is Applied from Time, t=0.8s. The Control Beam changes to 3.3MW/30keV at 30° from Time 1.37s.

5. Conclusions. Fig.5 shows that a C.P.B. can be established and maintained by low energy injection and that it is extremely effective in reducing the sputtered influx so that the increase in Z_{eff} is prevented. Consequently the high energy neutral beam continues to penetrate and heat the plasma.

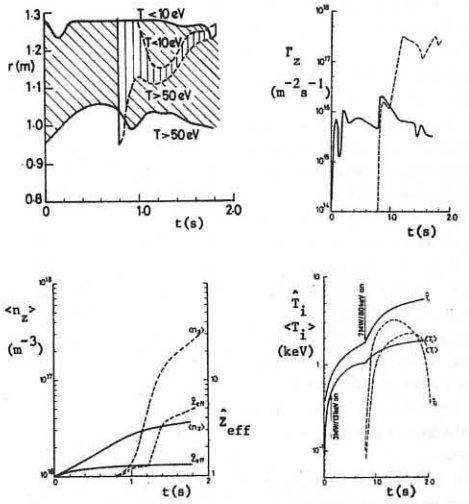

Fig.5 Temporal Evolution of Certain Parameters With (——) and Without (-·-·-) the Low Energy Control Beam (the time origin for case -·-·- is displaced so that comparisons are made from the time of switch on of the heating beam).
(a) The Extent of the Cool Plasma Blanket Defined by the Radii, r(m) at which the Plasma Temperature, 10eV<T<50eV.
(b) The Sputtered Impurity Influx $\Gamma_z(m^{-2}s^{-1})$.
(c) The Maximum Effective Ionic Charge, $\hat{Z}_{eff}$, and mean impurity density $\langle n_z\rangle$.
(d) The Maximum and Mean Plasma Temperatures, $\hat{T}_i$, $\langle T_i\rangle$ (keV).

* Work carried out under EURATOM JET Design Contract/30-74-FUA-C.

[1] Podesta and Engelmann, Proc.3rd.Symp.on Tor.Conf.Garching (1973) C9.
[2] Breton et al Fontenay Report, EUR-CEA-FC-822 (1976).

IMPURITY CONFINEMENT TIME FROM OXYGEN GAS INJECTION EXPERIMENTS ON T.F.R.

T.F.R. Group (presented by C. De Michelis)

ASSOCIATION EURATOM-CEA SUR LA FUSION
Département de Physique du Plasma et de la Fusion Contrôlée
Centre d'Etudes Nucléaires
Boite Postale n° 6. 92260 FONTENAY-AUX-ROSES (FRANCE)

ABSTRACT : Oxygen injection at the current plateau of T.F.R. plasmas results in a decrease of the molybdenum density, due to a decreased molybdenum flux entering the plasma. From the observed density decrease it is possible to deduce the impurity particle confinement time as a function of radius.

We describe here two injection experiments in the T.F.R. Tokamak. They consisted in the injection of cold oxygen gas (either as a short puff or continuously) at the current plateau, when the plasma is in a quasi-stationary state. In both cases the conditions at the injection time were I_p = 160 kA, B_T = 50 kG, T_e (0) = 1.85 keV, $n_e(0) \simeq 5 \times 10^{13}$ cm^{-3}, $Z_{eff}(0)$ between 5.5 and 7, and both n_e and T_e approximately constant in time (the high value of Z_{eff} in these discharges is due to the fact that, due to the injection, more oxygen is present on the liner walls before each discharge, and is released in the first few milliseconds of the plasma lifetime). At the injection $\overline{n}_e$ increases immediately, whereas T_e remains constant.

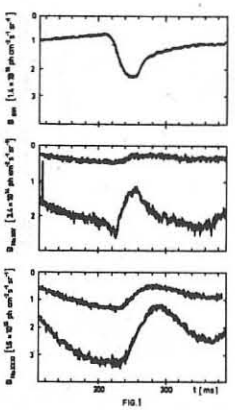
FIG.1

Figure 1 gives the evolution of the radiance (ph cm^{-2} s^{-1} sr^{-1}) of three spectroscopic lines for the puff case : OVI 1032 Å, MoXIV 374 Å and MoXXXI 117 Å (these last two lines with the background to be substracted). The first two lines are both characteristic of the plasma periphery (r = 14-15 cm), and allow to estimate the impurity flux density Γ (cm^{-2} s-1) coming from outside the plasma/1/ ; they show that the oxygen flux density Γ_{ox} increases rapidly due to the injection (the rise-time depending on the injection method), whereas the molybdenum flux density Γ_{Mo} decreases with a delay of $\simeq$ 10 msec. The MoXXXI 117 Å line is, on the other hand, characteristic of the central hot plasma and shows that central molybdenum density decreases with with a delay of ~ 25 msec. Both molybdenum radiances increase again after the end of the increase of Γ_{ox}. Similar results are obtained with the continuous oxygen injection, but in this case the molybdenum radiances do not increase again later in time, since there is a continuous oxygen influx : they tend to arrive to a new (lower) constant value, but the discharge often exhibits a disruptive end.

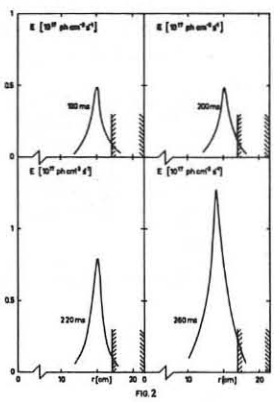

FIG.2

Figures 2 and 3 show the radial profiles of the radiant power density (ph cm-3 s^{-1}) for OVI 1032 Å and MoXXXI 117 Å (obtained after Abel inversion) for the continuous oxygen injection case. Figure 2 shows that as the oxygen increases there is a slight inward movement of the maximum, corresponding to a small cooling of the plasma periphery. Figure 3 confirms that, since $T_e(t)$ is constant in the central region, there is no variation of the corona equilibrium existing in the center (since the ratio $n_{Mo}30+/n_{Mo}31+$ is approximately constant ; the discrepancy at 260msec is due to the fact that at this time the measured radiances are down to a level just above the background noise, thus introducing large inaccuracies in the data processing). Therefore the decrease of the central molybdenum ion radiance must be due to a decrease of the total central molybdenum density.

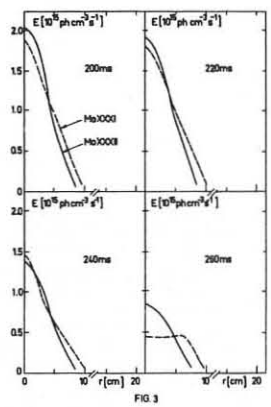

FIG.3

From these measurements, with the help of ionization equilibrium calculations/2/, it is possible to estimate the total central density of molybdenum. From this, and from the central value of Z_{eff} (calculated from the measured T_e), assuming that the only impurities present are oxygen and molybdenum, it is possible to calculate the central density of deuterons and of oxygen (completely stripped). We obtain in this way, for the puff case, the results shown in the Table (before and after injection).

	200 ms	280 ms
$n_e(0)$ (cm^{-3}	$(4.6 \pm 0.2) \times 10^{13}$	$(5.4 \pm 0.2) \times 10^{13}$
$Z_{eff}(0)$	7.2 ± 1.0	5.4 ± 0.8
$n_{Mo}(0)$ (cm^{-3})	$(1.0 \pm 0.5) \times 10^{11}$	$(3.5 \pm 1.7) \times 10^{10}$
$n_{ox}(0)$ (cm^{-3})	$(4.0 \pm 0.8) \times 10^{12}$	$(4.1 \pm 0.3) \times 10^{12}$
$n_{p+}(0)$ (cm^{-3})	$(1.4 \pm 0.5) \times 10^{13}$	$(2.0 \pm 0.2) \times 10^{13}$

The central oxygen density does not increase, in spite of the increase of the peripheral oxygen flux, probably because of its large value before injection.

In the following we shall discuss these results. Before injection, the plasma is in a quasi-stationary state. The oxygen injection results in a decrease of the peripheral molybdenum flux (as shown by the MOXIV radiance), probably as a consequence of a slight cooling of the plasma periphery (alternatively, it is known that in the presence of oxygen contaminated surfaces a large amount of particles is sputtered as ions/3/ ; the sputtered ions are then prevented from entering the plasma by the magnetic field). The molybdenum source being, at least partially, decreased, molybdenum leaves the plasma with a time constant which depends on the impurity particle confinement time (being equal to it only if there is no more source). From Fig.1, we see that this time constant is ~ 50 msec in the central region, and ~ 20 msec at r = 14 - 15 cm, and is therefore a decreasing function of radius.

It is now possible to verify that before injection the inward peripheral oxygen flux density (estimated from the OVI 1032 Å radiance) is equal to the flux density leaving the central region (calculated from the central oxygen density and confinement time). This has the consequence that the impurity confinement time varies approximately as r.n(r). Moreover, when continuously injecticting oxygen, it has been seen (Fig.4) that the peripheral oxygen flux density (estimated from the OVI 1032 Å radiance) increases twice as fact as the flux density at r = 12 cm (estimated from the OVII 1623 Å radiance).

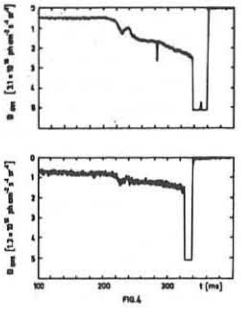
FIG.4

These measurements confirm that, schematically, the plasma is composed of two regions. The central hot region receives an impurity flux which is approximately always the same, independently of the conditions of the cold peripheral region, which has a more or less important impurity flux density depending on the experimental conditions. The transition between these two regions seems to occur in the neighbourhood of the q = 2 surface.

REFERENCES.-

/1/ Equipe T.F.R., Nuclear Fusion 15, 1053 (1975).

/2/ T.F.R. Group, to be published in Plasma Phys.

/3/ BENNINGHOVEN A., Surface Science 53, 596 (1975).

REDUCTION OF POWER LOSS DUE TO HEAVY IMPURITIES IN DIVA

S.Yamamoto, H.Maeda, Y.Shimomura, K.Odajima, M.Nagami, H.Kimura, S.Sengoku, H.Ohtsuka, N.Ueda*, A.Funahashi, T.Matoba, H.Takeuchi, K.Takahashi, S.Kasai, T.Sugie, M.Shiho**, T.Kawakami, K.Kumagai, T.Yamauchi, T.Shoji, T.Tokutake, K.Anno, T.Arai, T.Shibata, H.Hiratsuka, M.Tanaka, Y.Tanaka and S.Kunieda

Japan Atomic Energy Research Institute, Tokai, Japan

*On leave from Mitsubishi Atomic Power Industry, Ohmiya, Saitama, Japan

**On leave from University of Tokyo, Tokyo, Japan

Abstract: The behavior of heavy impurities in light-impurity free plasma is studied in DIVA. The divertor reduces a plasma-wall interaction and therefore reduces the radiation power by a factor of 3. The molybdenum target employed to intercept particle and heat flux to the burial chamber further reduces the radiation loss to less than 30 % of the ohmic dissipation (P_{ohm}).

Discharge conditions described here are the same as those reported in Ref.[1,2]. A 20 kG experiment is scheduled to start on June, 1977.

Power Balance: Energy loss mechanisms from a plasma are divided into two processes. One is a direct energy loss to a wall from the plasma such as radiation and charge-exchange hot neutrals. The other is thermal conduction and convection of the plasma particles. Light impurities are not influential in a power balance of the DIVA discharges, because of its clean wall surface. This situation enables us to study heavy-impurity contamination and its effect on the power balance with and without a divertor.

Power spectrum emitted from the plasma is measured with a grazing incidence vacuum monochrometer calibrated by a branching ratio method (20 Å - 1300 Å). The radiation power from the plasma due to heavy impurities concentrates in the wavelength 120 Å-240 Å (pseudo-continuum). The radiation power including the neutral loss flux is measured with a pyroelectric detector. Power loss by charge-exchange neutrals is calculated by a Monte Carlo code [4]. In the calculations, total neutral influx to the plasma is assumed to be equal to the total loss flux of charged particles from the plasma. The results coincide with experiments within a factor of two.

Power loss to a shell and protection plates (limiter) due to thermal conduction and convection is estimated by ion saturation currents, using a heat transmission rate experimentally obtained. Heat flux to a burial chamber is measured with thermoprobes with a resolving time of 0.2 ms. Table I gives the results of the power balance in the Case A discharge [2]. The results show that the estimation for thermal conduction and convection is consistent with radiation and charge-exchange losses.

Reduction of Heavy Impurities: Application of the divertor to the discharges offers the reduction of power loss due to heavy impurities by a factor of 3 and controlling the boundary plasma with gas injection of small amount is also demonstrated to reduce the heavy-impurity contamination in the case with a divertor [2]. Summaries of the previous experiments are following. The heavy-impurity contamination is caused by evaporation due to the heat flux on copper rods supporting titanium wires and movable shells in the burial chamber (Fig.1). A distribution function of electrons in a scrape-off layer is not a simple Maxwellian, and has a high energy tail. The high energy component of electrons causes a relatively large heat transmission to a floating plate. The small amount of additional gas during the discharge results in dramatic decrease in the high energy component and consequently reduces the heavy-impurity contamination.

However, there remains contamination due to heavy impurities in the Case A discharge. The molybdenum target is employed to intercept particle and heat flux to the lower side with respect to the median plane in the burial chamber. Our experimental setup is sketched on Fig.1. Heat characteristics of molybdenum are better than those of other materials, which are used in DIVA device (Au, Cu and so on). The target electrically insulated is set on the meridian plane across the toroidal magnetic field. The combination of the divertor and the molybdenum target further reduces power loss due to heavy impurities to 60 % of that in the Case A discharge. In the case without the molybdenum target, floating plates in the burial chamber are exposed to the heat flux of 180 watts/cm^2. This value seems to be very small to evaporate materials. These results suggest that surface conditions as well as heat characteristics may play an important role in the evaporation [1,2]. Another possible cause of the contamination is sputtering of wall materials due to charge-exchange hot neutrals or heavy ions, however we have had no evidence that these mechanisms actually take place in the discharge.

Figure 2 shows the relationship between the total radiation power measured with pyroelectric detector (P_{py}) and that measured with the VUV monochrometer (P_{vuv}). Closed circles represent the relationship in the case without the divertor and triangles in the various discharge conditions with the divertor reported in Ref.[2]. An open circle represents that in the optimum condition, that is, in the case with the divertor and the Mo target. The results show that radiation loss due to heavy impurities is comparable with power loss due to charge-exchange hot neutrals in the optimum condition.

Conclusions: DIVA tokamak device with an axisymmetric divertor permits us to study the behavior of heavy impurities in the light-impurity free plasma. Various methods including the control of the plasma boundaries are employed and demonstrated to reduce the heavy-impurity contamination. In the optimum condition with the molybdenum target in the burial chamber, the radiation loss due to heavy impurities is reduced to less than 30 % of the ohmic dissipation, and the energy confinement time has been improved by a factor of 1.3 compared with the previous values [2,3]. In a future large tokamak, the scrape-off layer should be controlled to eliminate serious impurity contamination from a neutralizer plate (or limiter) and vacuum walls.

Table I - Power Balance in DIVA (Case A , t = 10 msec)

	Conduction - Convection			Radiation - Neutral	
	Shell	Limiter	Divertor	Radiation	Neutral
I_s [A]	340	7			
T_e [eV]	15	20			
$F\gamma = q/I_s T_e$	5 (a)	8 (a)	8 - 20 (b)		
Power Loss [kW]	25	1	6.5	< 25 (c)	8 (d); 5.5 (e)
				< 25 (f)	
Total Loss	0.6 P_{ohm}			< 0.4 P_{ohm}	

NB (a): Experimental, (b): Ref.[2], (c): Measured with VUV monochrometer (upper estimation), (d): Calculated by Monte Carlo code, (e): Measured with charge-exchange spectrometer, (f): Measured with pyroelectric detector (upper estimation)

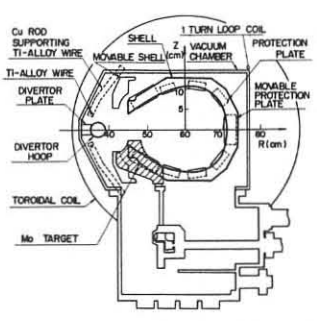

Fig. 1.

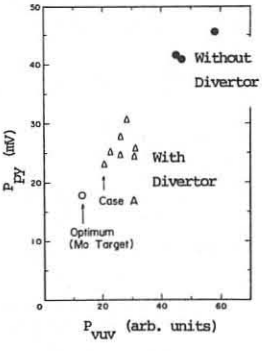

Fig. 2.

References
[1] Maeda, H., et al., Proc. the Berchtesgarden Conf. IAEA-CN-35/A-18 (1976).
[2] Maeda, H., et al., Int. Symp. on Plasma Wall Interaction, Jülich, (1976).
[3] Shimomura, Y., et al., Phys. Fluids 19 (1976) 1635.
[4] Azumi, M., Private communications.

TRANSPORT PROPERTIES AND STEADY STATES OF A TOKAMAK PLASMA WITH IMPURITIES IN THE COLLISION-DOMINATED REGIME

F. Engelmann and A. Nocentini*)
Association Euratom-FOM, FOM-Instituut voor Plasmafysica,
Rijnhuizen, Jutphaas, The Netherlands
*) Guest from University of Trieste, Trieste, Italy

Abstract: Having in mind applications to the cold plasma blanket problem, the transport properties and the steady states of an axisymmetric toroidal plasma containing an arbitrary number of impurity species are derived for the collision-dominated regime, including heat transfer effects.

The transport properties of a collision-dominated tokamak plasma with impurities have been discussed in a number of papers (see e.g. Ref. 1). In the cool, outer part of a tokamak discharge heat transfer not only between the ion species, but also between plasma ions and electrons, matters[2]. For this case, we give here an account of the particle transport properties and of the steady-state profiles following from them. The result is discussed in view of the formation and properties of a cold-plasma blanket.

We consider a tokamak configuration, with magnetic surfaces having concentric, circular cross-sections, in the limit of small inverse aspect ratio $r/R_o < 1$ (where r and R_o are the minor and major radius of the torus, respectively). The collisional regime is defined by

$$r_{Lj} < r, \qquad \omega_{bj} < \nu_j^{tot} < \Omega_j \ , \tag{1}$$

where r_{Lj}, ω_{bj}, ν_j^{tot}, and Ω_j are the Larmor radius, the "bounce frequency", the total collision frequency, and the cyclotron frequency of the species j, respectively.

Conditions (1) allow us to use macroscopic equations for each species. We neglect, as usual, viscosity and inertia, and assume

$$\frac{\partial}{\partial\theta}\left\{\ln T_j\right\} , \qquad \frac{\partial}{\partial\theta}\left\{\ln N_j\right\} < r/R_o \ , \tag{2}$$

where θ is the poloidal angle and T_j and N_j are the temperature and the number density of the species j. The details of the determination of the particle and heat fluxes will be given elsewhere. In most cases of practical interest,

$$(e_I/e_i)^3 \gg \alpha_i^I \ , \qquad m_I/m_i, \qquad \text{and} \qquad e_I > e_i = -e_e \tag{3}$$

hold, where $\alpha_j^j = e_j^2 N_j/e_j^2, N_j$, (we use j = e,i and I to indicate electrons, plasma ions, and impurities, respectively), and m_j and e_j are, respectively, mass and charge of the species j. In case (3), the heat balances for the impurities are dominated by heat transfer with the plasma ions[1], so that the temperature, including its small poloidal dependence, is the same for impurities and plasma ions. Moreover, for the plasma ions and the electrons, the heat balances that determine the θ-dependence of T_e and T_i are formally unaffected by the presence of impurities (which enter only through their effect on the parallel transport properties of the plasma ions and electrons). The determination of the θ-dependences of the temperatures and of the average fluxes of heat and particles (Γ_j) across a magnetic surface can then be performed by a straightforward generalization of the clean-plasma problem[2]. E.g., for the toroidal contribution to the electron flux

$$\Gamma_e = -q^2 \frac{r_{Le}^2}{\tau_{ee}} \frac{1}{T_e} \left\{ \left[C_1(x_e) + \frac{C_2^2(x_e)}{C_3(x_e)} \right] \sum_{j\neq e} \alpha_e^j \left(\frac{dP_e}{dr} - \frac{e_e N_e}{e_j N_j} \frac{dP_j}{dr} \right) + \right.$$
$$- \frac{5}{2} x_e \frac{C_2(x_e)}{C_3(x_e)} \left[N_e \frac{dT_e}{dr} - \frac{s_{ie}^2}{1+s_{ie}^2} \frac{T_i}{T_e} N_i \frac{dT_i}{dr} \right] + \tag{4}$$
$$\left. - \frac{s_{ie}^2}{1+s_{ie}^2} \frac{C_2(x_e) C_2(x_i)}{C_3(x_e)} \frac{x_e}{x_i} \frac{T_i}{T_e} \sum_I \alpha_i^I \left(\frac{dP_i}{dr} - \frac{e_i N_i}{e_I N_I} \frac{dP_I}{dr} \right) \right\}$$

is found, where $q = rB/R_o B_\theta$ is the safety factor,

$$\tau_{jj'} = \frac{3\sqrt{m_j}\, T_j^{3/2}}{4\sqrt{2\pi}\, \ln\Lambda\, e_j^2 e_{j'}^2 N_{j'}} , \qquad x_e = \sum_{j\neq e} \alpha_e^j \ ,$$

$$x_i = \sum_I \alpha_i^I \ , \qquad s_{ie}^2 = \frac{6 x_i}{C_3(x_i)} \left(\frac{m_e}{m_i}\right)^{\frac{1}{2}} \left(\frac{T_i}{T_e}\right)^{3/2} \frac{\alpha_i^e}{(\tau_{ii}\omega_{bi})^2} \ ,$$

C_1, C_2, and C_3 are defined as in Ref. 3, and we have assumed $m_I \gg m_i$. The toroidal contribution to the ion flux, neglecting terms of relative order $\sqrt{m_e/m_i}$, is

$$\Gamma_i = - q^2 \frac{r_{Li}}{\tau_{ii}} \frac{1}{T_i} \left\{ \left[C_1(x_i) + \frac{1}{1+s_{ie}^2} \frac{C_2^2(x_i)}{C_3(x_i)} \right] \sum_I \alpha_i^I \left(\frac{dP_i}{dr} - \frac{e_i N_i}{e_I N_I} \frac{dP_I}{dr} \right) + \right.$$
$$\left. - \frac{5}{2} \frac{x_i}{1+s_{ie}^2} \frac{C_2(x_i)}{C_3(x_i)} N_i \frac{dT_i}{dr} \right\} +$$
$$- q^2 \frac{r_{Le}^2}{\tau_{ei}} \frac{1}{T_e} \left\{ \left[C_1(x_e) + \frac{C_2^2(x_e)}{C_3(x_e)} \right] \left(\frac{dP_e}{dr} - \frac{e_e N_e}{e_i N_i} \frac{dP_i}{dr} \right) + \right. \tag{5}$$
$$\left. - \frac{5}{2} \frac{C_2(x_e)}{C_3(x_e)} \left(N_e \frac{dT_e}{dr} - \frac{s_{ie}^2}{1+s_{ie}^2} \frac{T_i}{T_e} N_i \frac{dT_i}{dr} \right) \right\} \ .$$

Note that the second term on the right-hand side of Eq. (5) (due to collisions of plasma ions on electrons) is not negligible with respect to the first one (due to collisions of plasma ions on impurities) only at very low impurity concentrations, i.e. for $\alpha_i^I \lesssim \sqrt{m_e/m_i}$. The quantity s_{ie}^2 is a measure of the importance of the heat transfer between electrons and plasma ions.

It is interesting to note that, as far as electrons and ions are concerned, the presence of impurities can always be described via <u>one</u> effective impurity species with charge Ze_i and number density N_Z (in general both r-dependent) defined by the following relations

$$ZN_Z = \sum_I Z_I N_I \ , \qquad Z^2 N_Z = \sum_I Z_I^2 N_I \ . \tag{6}$$

This fact allows to readily generalize earlier results on steady-state density profiles[4]. Explicitly, Eqs. (4-6) yield for $\Gamma_e = \Gamma_i = 0$ and $T_e = T_i = T_I = T$ when $s_{ie}^2 \ll 1$

$$\frac{dN_i}{N_i dr} = -\left\{ 1 - \frac{G(x)}{1+x} - \frac{\alpha G(\alpha)}{1+\alpha} \right\} \frac{dT}{Tdr} \ , \tag{7}$$

$$\frac{d(ZN_Z)}{ZN_Z dr} = -\left\{ 1 - z\left[\frac{G(x)}{1+x} - \frac{G(\alpha)}{1+\alpha} \right] \right\} \frac{dT}{Tdr} \ , \tag{8}$$

where $x = x_e = Z_{eff}$, $\alpha = x_i = Z^2 N_Z/N_i$, and $G(x) = (1+0.52x)/(1+0.82x)$. In the highly-collisional regime $s_{ie}^2 \gg 1$ we find instead

$$\frac{dN_i}{N_i dr} = -\left\{ 1 - \frac{G(x)}{1 + Z(1+\frac{2}{\alpha})} \right\} \frac{dT}{Tdr} \ , \tag{9}$$

$$\frac{d(ZN_Z)}{ZN_Z dr} = -\left\{ 1 - \frac{ZG(x)}{1 + Z(1+\frac{2}{\alpha})} \right\} \frac{dT}{Tdr} \ . \tag{10}$$

As far as the collision-dominated plasma layers are concerned, the favourable findings on the appearance of a cool and dense plasma blanket as given in Ref. 4 can, hence be carried over to a plasma containing more than one impurity species, the impurities accumulating on the <u>average</u> close to the plasma edge (for a radially decreasing temperature the steady-state density profiles follow to be as schematically shown in the figure).

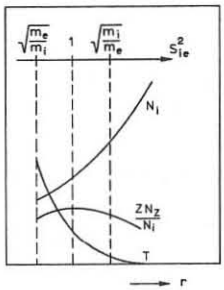

This work was performed under the Euratom-FOM association agreement with financial support from ZWO and Euratom.

References

1. S.P. Hirshman, Princeton Plasma Physics Laboratory, Int. Rep. PPPL-1291 (1976) and to be published.
2. F. Engelmann, A. Nocentini, Nucl. Fusion 16 (1976) 694.
3. P.H. Rutherford, Phys. Fluids 17 (1974) 1782.
4. F. Engelmann, A. Nocentini, 6th Int. Conf. on Plasma Phys. and Controlled Nucl. Fus. Res., Berchtesgaden, B-7 (1976).

HEAT TRANSPORT OF AXISYMMETRIC TOROIDAL LOW-β PLASMAS IN THE COLLISION-DOMINATED REGIME

F. Engelmann and A. Nocentini*)
Association Euratom-FOM, FOM-Instituut voor Plasmafysica,
Rijnhuizen, Jutphaas, The Netherlands
*) Guest from University of Trieste, Trieste, Italy

Abstract: The transport theory of an axisymmetric, toroidal, low-β plasma in the collision-dominated regime is reconsidered. Different subregimes, which are relevant for the outer part of a tokamak discharge, are discussed, in particular with respect to their heat transport properties.

It is well known that, studying the transport properties induced by Coulomb collisions in a tokamak plasma, one is faced with the presence of different regimes, characterized by different expressions for the fluxes of particles and heat across the magnetic surfaces. This is the consequence of the fact that in different regions of the parameter space different phenomena are important.

It is the scope of this paper to discuss a number of subregimes of the collision-dominated regime (defined as that domain of the parameter space where $\nu_j/\omega_{bj} > 1$, ν_j and ω_{bj} being the collision frequency and the bounce frequency of the species j). One of these subregimes is well known since a long time. It is characterized by an enhancement of the transport coefficients, with respect to the cylindrical case, by a factor of the order of q^2 (where $q = rB/R_oB_\theta$ is the safety factor), the so-called Pfirsch-Schlüter enhancement factor[1]. Hence we will refer to it as the usual Pfirsch-Schlüter regime (or subregime I, see the figure). This regime, and the corresponding transport coefficients, are normally assumed to apply to the whole outer part of a tokamak plasma (where $\eta = \nu_i/\omega_{bi} > 1$). Actually, in typical cases, this is true only for a certain region adjacent to the "plateau region". Outside this region, the transport properties change and, in particular, the ion heat conductivity decreases with respect to the usually accepted value (cf. also Ref. 2). Here we shall give an overview of some of the other regimes appearing, focussing our attention on the heat transport properties. As far as the particle transport is concerned, the order of magnitude does not change with respect to the simple Pfirsch-Schlüter result.

Referring to the figure, the collision-dominated regime (where fluid equations can be used to describe the plasma) corresponds to the region at the right of line ①, which separates the collision-dominated regime from the so-called "plateau" regime. We assume concentric, circular cross-sections for the magnetic surfaces, and look for steady states where the number density N, and the temperatures T_e and T_i have (to lowest order in the inverse aspect ratio, taken small) radial gradients. These gradients produce diamagnetic particle and heat flows on the magnetic surfaces (across the magnetic field lines) which are θ-dependent (θ being the poloidal angle), due to the θ-dependence of the magnetic field $\underline{B}$. Hence, poloidal variations of N, T_e, and T_i will appear, which in turn lead to radial components of the diamagnetic fluxes. These are just the "toroidal contributions" to the radial fluxes. The θ-gradients of N, T_e, and T_i are, hence, the crucial physical quantities determining the transport properties of a collision-dominated toroidal plasma. The different subregimes appear because these gradients depend on different physical effects in different domains of parameter space.

As far as heat transport is concerned, these effects are, apart from poloidal dependences of the diamagnetic fluxes induced by the θ-dependence of the toroidal magnetic field,
a) heat flow parallel to magnetic field lines,
b) energy transfer between electrons and ions, and
c) poloidal dependences of the diamagnetic fluxes induced by the (self-consistent) poloidal variation of the plasma parameters (including the effect of the radial fluxes themselves).
The subregimes (see the figure) can now be correlated to the effects which matter:

region I : a)
region II : a) and b)
region III: a) and c)
region IV : a), b), and c)
region V : b) (cf. Ref. 2).

The border lines between these regimes are characterized by certain values of, or relations between, two parameters: the ratio s^2 of the heat transfer between electrons and ions and the heat conduction parallel to $\underline{B}$,

$$s^2 = 3\mu \frac{N}{\tau_e \chi_\parallel^i} \left(\frac{rB}{B_\theta}\right)^2 \approx \sqrt{\mu}\,\eta^2 \quad , \tag{1}$$

and a parameter t measuring the relative importance of the poloidal variations of T_i, with respect to those imposed by B(θ), in the usual Pfirsch-Schlüter regime,

$$t = \frac{5}{2} \frac{cB_\phi r}{\chi_\parallel^i e B_\theta^2} \left\{\frac{d(NT_i)}{dr} - \frac{NT_e}{T_e+T_i}\frac{dT_i}{dr}\right\} \approx \frac{\nu_i}{\Omega_i}\left(\frac{B}{B_\theta}\right)^2 \tag{2}$$

where $\chi_\parallel^i$ is the parallel heat conductivity of the ions, $\mu = m_e/m_i$ the mass ratio, τ_e the electron collision time, B_ϕ and B_θ the toroidal and poloidal magnetic field, e the electronic charge, and r the small the small radius of the toroidal surface. From this is clear that the lines ① (i.e. $s^2 = 1$) and ③ (i.e. $|t| = 1$) limit the usual Pfirsch-Schlüter regime. As in the subregimes I, II, and V the poloidal dependences of the plasma parameters are small (i.e., smaller than 1st order in the inverse aspect ratio), in these regimes the fluxes are linear in the radial gradients. This is no longer the case when going across the lines ③, ④, and ⑧.

The results found for the fluxes (averaged over a magnetic surface) in the different subregimes are

I. $q_r^i = -1.6q^2\chi_\perp^i \frac{dT_i}{dr}$ $\qquad q_r^e = -0.85q^2\chi_\perp^e\left\{\frac{dT_e}{dr} - 0.28\frac{dP}{Ndr}\right\}$

II. $q_r^i = -\left(1+\frac{1.6q^2}{s^2}\right)\chi_\perp^i\frac{dT_i}{dr}$

V. $q_r^i = -\chi_\perp^i\left\{\frac{dT}{dr} + 0.8q^2\sqrt{\mu}\frac{dP}{Ndr}\right\}$ $\qquad q_r^e = 0.24q^2\chi_\perp^e\frac{dP}{Ndr}$

III. $q_r^i = -\left(1+\frac{1.6q^2}{t^2}\right)\chi_\perp^i\frac{dT_i}{dr}$ $\qquad q_r^e = -0.85q^2\chi_\perp^e\gamma\left\{\gamma\frac{dT_e}{dr} + \frac{1-4\gamma}{10}\frac{dP}{Ndr}\right\}$

IV. $q_r^i = -\left(1+\frac{1.6q^2s^2}{t^2}\right)\chi_\perp^i\frac{dT_i}{dr}$ $\qquad$ where $\gamma = \left(1+\frac{N^2}{P}\frac{dT_i}{dN}\right)^{-1}$,

where for the ion heat fluxes the simple cross-field diffusion term has been retained, it can contribute for $q^2 \lesssim \sqrt{m_i/m_e}$.

As a result, leaving the domain of validity of the usual Pfirsch-Schlüter formulae, the main effect is that the ion heat conductivity is decreased either by heat transfer (in region II, IV, and V) or by the additional terms appearing in the diamagnetic heat flux (in region III and IV). In the limit of the lines ⑥ and ⑦ as well as within region V, the toroidal contribution to the ion heat conductivity becomes, order-of-magnitude-wise, equal to that of the electrons. In particular, in region V, the sum of the toroidal terms in q_r^i and q_r^e vanishes so that the total heat loss of the plasma across the magnetic surfaces in a torus is the same as in a cylinder.

We have not considered here effects connected with viscosity, rotating fluxes of the ions, and external sources. In particular, the viscosity of the ions might lead to appreciable modifications of the results for larger Larmor radii (specifically in the uppermost part of region III).

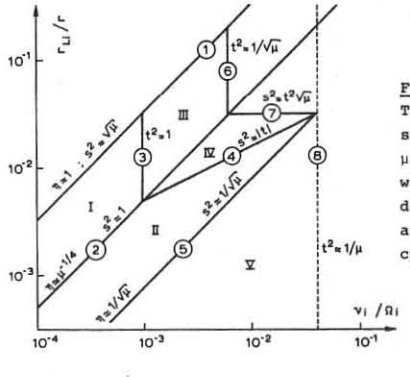

Fig. 1
The ν_i, r_{Li} plane (assuming $B^2/B_\theta^2 = 10^3$ and $\mu = m_e/m_i = 1/1836$); with r_{Li} and Ω_i we indicate Larmor radius and cyclotron frequency of the ions.

This work was performed under the Euratom-FOM association agreement with financial support from ZWO and Euratom.

References

1. D. Pfirsch, A. Schlüter, Max-Planck-Institut für Physik und Astrophysik, Rep. MPI/PA/7/62 (1962).
2. F. Engelmann, A. Nocentini, Nucl. Fusion 16 (1976) 694.

CONTROL OF IMPURITIES BY THE DITE BUNDLE DIVERTOR

S.J. Fielding, M. Hobby, J. Hugill, G.M. McCracken, J.W.M. Paul, N.J. Peacock, B.A. Powell and P.E. Stott

Culham Laboratory, Abingdon, Oxon, OX14 3DB, UK
(Euratom/UKAEA Fusion Association)

Abstract: The divertor is shown to reduce both the low and high Z impurity content of the plasma. However when extra gas is fed in to maintain the same density during diversion, there is an increased desorption of oxygen and no change in Z_{eff}.

The bundle divertor improves the purity of a tokamak discharge, firstly by reducing the flux of plasma particles bombarding the limiter and torus wall and thereby reducing the release of impurities, and secondly by attenuating their influx into the centre of the discharge. The magnetic configuration is complex and is discussed in detail elsewhere [1]. It can be described approximately by saying that there is a central core of undiverted plasma which is surrounded by an annular layer between the separatrix radius a_s = 0.19 m and the torus wall a = 0.27 m, which is connected to the divertor target and will be referred to as the scrape-off layer.

The successful operation of the DITE bundle divertor at a toroidal field B_T = 1.0 T with discharge currents I ≃ 50 kA has been reported previously [2,3]. The present paper extends the earlier results, and discusses their interpretation in terms of three specific divertor effects which contribute to the overall improvement in plasma purity.

(1) The magnetic limiter effect of the bundle divertor transfers the 'plasma-limiter' interaction out of the torus and onto the divertor target. This is demonstrated directly by photographic observation of the diverted plasma striking the target, by measuring the reduced temperature rise of the limiter and the large temperature rise of the target when the divertor is operated. The reduced interaction of the plasma with the molybdenum limiter and stainless-steel torus wall is shown by a reduced influx of heavy metal impurities at the plasma edge. A carbon probe positioned close to the torus wall is exposed to the plasma and later analysed using Rutherford backscattering [4]. When results from diverted discharges are compared with undiverted ones, the combined influx of Fe, Cr, and Ni falls by a factor 4 and the Mo flux by a factor 6. Spectroscopic measurements in the V.U.V., described later, show that the divertor reduces the spectral line intensity of highly-ionized Mo (eg Mo XXII 28.9 Å) to ~ 10% and of Fe (eg Fe XVII, 15.01 Å) to ~ 30%. This confirms that the divertor substantially reduces the influx of heavy metal impurities from the limiter and torus wall, and demonstrates that the backflow of material from the molybdenum target is small.

(2) The divertor exhaust effect removes plasma particles out of the torus and, results in a falling electron density and the need for an increased feed of hydrogen gas to maintain a diverted discharge at a constant density. Fig. 1 shows a density scan with a double Langmuir probe across the mid-plane of the diverted plasma bundle. There is good agreement between the line average density measured with a 4 mm microwave interferometer in the divertor and probe measurements of the density in the scrape-off layer. The shape of the measured density profile fits the computed shape of the magnetic flux bundle, and the measured profiles of the power deposited on the target [5].

(3) The divertor screening effect reduces the flux of impurities into the centre of the discharge, by ionizing a large fraction of them within the scrape-off layer and sweeping them out of the torus. Fig. 2 shows oscillograms of several spectral lines of oxygen and carbon for a discharge when the divertor was switched-on halfway through the current plateau and the density allowed to fall. The intensity of lines from O II and C III, which are easily burnt through in the scrape-off layer, represents the influx of light impurities at the plasma edge. These lines and hence the influxes are reduced to ~ 60% by the action of the divertor. There is a much larger change in the line intensity of the more highly-ionized states, (eg O V falls to ~ 25%) which are burnt through in progressively deeper regions of the plasma and represent impurity influxes inside the separatrix. This clearly demonstrates the screening effect, and an estimate based on the ratio of the intensities of highly ionized to weakly ionized lines gives the screening efficiency $\xi_s \approx 0.5$, which is in reasonably good agreement with calculations based on a simple model of the scrape-off layer [6].

The concentrations of both light and heavy impurities in the centre of the discharge have been measured with a grazing-incidence V.U.V. spectrograph. Using a shutter which opens only during the current plateau, plates are exposed for 10 - 15 identical discharges and measured with a densitometer. The spectrograph can be scanned in a vertical plane to view different chords of the minor cross-section, and the results when Abel-inverted give radial density profiles of the various impurity ions. The analysis of these data is at present incomplete, but the large changes in typical line intensities for Mo and Fe has been quoted earlier. There is little change in the intensity of the oxygen lines (eg O VIII 18.97 Å) when the plasma density is maintained constant during diversion.

In order to maintain the diverted discharges at the same density as the undiverted ones, the hydrogen gas feed must be increased. Unfortunately this increases the plasma recycling and there is a consequent increase in the influx of oxygen desorbed from the wall. This additional influx is sufficient to offset the 50% screening effect, with the result that there is no net reduction in the oxygen level recorded by the V.U.V. spectrometer. The increased oxygen influx also means that there is little change in the value of Z_{eff} calculated from the plasma resistivity and the measured electron temperature profile. The 50 kA undiverted discharge already has a low value of $Z_{eff} \simeq 2$ produced mainly by oxygen, and this does not change significantly when the divertor is operated. However if additional oxygen gas is added to the discharge, without the divertor, Z_{eff} rises to 3 but remains close to 2 with the divertor. The desorption of oxygen, resulting from the gas feed, explains the anomaly, reported earlier [2], that Z_{eff} remains constant although the divertor screens out both low and high Z impurities.

The reduced concentration of heavy metals in the diverted discharge causes the total radiated power loss to fall to ≈ 25% (Fig. 2). The radiation power profile for an undiverted discharge (Fig. 3) is strongly peaked on axis and represents 50 - 100% of the ohmic power input. This substantial radiation loss due to heavy metal, is sharply reduced by the divertor, and there is a major change in the power balance with radiation losses accounting for only 20 - 30% of the ohmic power input, and more than 60% being transferred to the divertor target.

We wish to acknowledge the assistance of the DITE operating and engineering teams.

References

[1] Stott, P.E., Wilson, C.M., and Gibson, A., to be published in Nuclear Fusion and Culham Report No CLM-P474.

[2] Paul, J.W.M., et al, Proc. of 6th Conference on Plasma Physics and Controlled Nuclear Fusion Research, Berchtesgaden, (1976) Paper CN-35/A17.

[3] Stott, P.E., et al, Symposium on Plasma-Wall Interactions, Julich, Paper E3 (1976) and Culham Preprint CLM-P473.

[4] McCracken, G.M., et al, this conference.

[5] Goodall, D.H.J. Symposium on Plasma-Wall Interactions, Julich, (1976).

[6] Stott, P.E., Wilson, C.M., and Gibson, A., to be published.

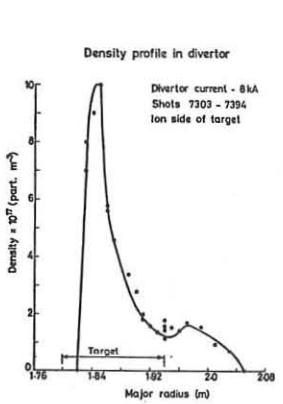

Fig. 1. Density profile in divertor.

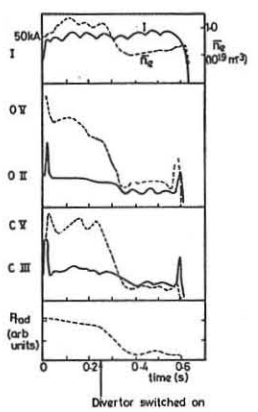

Fig. 2. Behaviour of density and radiation for mid-pulse operation of the divertor.

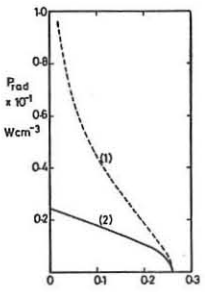

Fig. 3. Radial profiles of radiated power from similar discharges (1) undiverted and (2) diverted.

HIGH DENSITY DISCHARGES WITH GETTERED TORUS WALLS IN DITE

P.E. Stott, J. Hugill, S.J. Fielding, G.M. McCracken, B.A. Powell and R. Prentice

Culham Laboratory, Abingdon, Oxon, OX14 3DB, UK
(Euratom/UKAEA Fusion Association)

Abstract: The limiting density and energy containment time in DITE are improved by a factor > 2 by gettering the torus wall with titanium. This is explained by a reduced influx of low-Z impurities which normally cause contraction of the current channel by cooling the plasma edge.

Electron densities exceeding 10^{20} m^{-3} have been reached in several tokamaks, notably Alcator [1] and Pulsator [7], by feeding hydrogen gas into the discharge. This leads to a decrease of Z_{eff} and an increase of the energy containment time τ_E. In similar experiments in DITE the maximum mean electron density which we had obtained was $\bar{n}_e = 2.3 \times 10^{19}$ in a discharge with I = 180 kA, B_T = 2.7 T and q_a = 4.6 at the limiter radius, a = 0.27 m. The best value for τ_E = 7.8 ms was obtained at I = 67 kA, B_T = 2 T, $\bar{n}_e = 1.7 \times 10^{19}$ m^{-3} and q_a = 9.3. We were prevented from reaching higher densities by disruptive instabilities. We believe that these disruptions are caused by contraction of the current channel when the plasma edge is cooled by an influx of light impurities, chiefly oxygen, desorbed from the torus wall by the recycling plasma. A similar influx of oxygen was observed on Pulsator [7].

To test this hypothesis that the density is limited by the influx of light impurity we have evaporated titanium onto the torus wall. Gettering has previously been shown to reduce both the recycling and the oxygen concentration [3]. In DITE we use a single Varian Ti-ball source which getters some 30 - 40% of the torus wall. The source is evaporated continuously between discharges (for 10 - 20 minutes) and withdrawn from the torus ~ 30 s before a discharge. The evaporation rate of 2×10^{-2} g/discharge is sufficient to pump a quantity of gas several times larger than that introduced.

With the torus wall gettered and an increased feed of hydrogen gas, we have extended the density limit significantly and, for a discharge with I = 150 kA and B_T = 2.7 T, we have obtained a mean density $\bar{n}_e = 7 \times 10^{19}$ m^{-3}, central density $n_e(o) \approx 1.1 \times 10^{20}$ m^{-3}, $\beta_p \approx 0.6$ and $\tau_E \approx 25$ ms. Taking data from a good number of discharges at different currents, the extension of the stable operating region in a plot of I against $\bar{n}_e$ becomes apparent. The stable regions for the ungettered torus, with B_T = 0.9, 2.0 [5] and 2.7 T, coincide with region A in Fig. 1. Here, the axes have been normalised using the scaling given by Murakami [2,6], and the density limits for Ormak with and without gas puffing are shown as M2, M1. Gettering the DITE torus extends the operating region to that shown as B in Fig. 1, which, on the scaled axes, includes the high density discharges obtained on Alcator [1] and Pulsator [7]. The points marked 'a' to 'd' in Fig. 1 refer to typical gettered discharges for which we have measured temperature and density profiles giving the parameters listed in table 1.

Table 1 - Parameters of Typical Gettered Discharges

Point on Figure 1	a	b	c	d
Discharge current (I) kA	100	140	160	230
Toroidal field (B_T) T	2.0	2.65	2.7	2.65
q at limiter	6.2	5.9	5.2	3.6
Mean electron density 10^{19} m^{-3}	3.6	4.4	4.3	4.2
Central electron density $\times 10^{19}$ m^{-3}	5.3	7.0	6.2	6.3
Z_{eff}	1.6	1.4	1.2	1.2
β_{pe} (profiles)	0.28	0.26	0.17	0.12
β_p (diamagnetism)	0.5	0.5	0.4	0.35
Energy containment time (τ_E) ms	10	17	16	19

Oscillograms of the current, loop volts (which gettering reduces by a factor 2) and mean electron density are shown in Fig. 2 for the gettered discharge labelled 'b'. Also plotted are β_p and τ_E calculated from the change in diamagnetic flux and the measured current and loop volts. Radial profiles of electron temperature and density at t = 150 ms are shown in Fig. 3. We have observed that similar hollow temperature profiles are characteristic of low concentrations of light impurities [4]. Assuming Z_{eff} is uniform across the discharge, we calculate the values listed in table 1.

Although the hydrogen gas influx is constant between 0 and 180 ms, the density rise is interrupted by one or more pauses (Fig. 4) lasting 10 - 30 ms when there is increased m.h.d. activity and an increase in internal inductance. We interpret these as major rearrangements of the discharge. A uniform density rise can be maintained through these m.h.d. periods by temporarily increasing the gas influx and this does not seem to change the m.h.d. activity. We also observe that neutral beam injection (200 kW), which changes the electron temperature profile [9], supresses the m.h.d. activity and allows the density to rise smoothly.

The gettering reduces but does not eliminate the oxygen influx which presumably comes from ungettered parts of the torus. During an early stage of the gettered discharge when the density is comparable to an ungettered discharge, the intensity of the O V line (2781 Å) is down by a factor ≃ 9. There are bursts of increased oxygen influx during the density pauses (Fig. 4) and we suppose that with ungettered torus walls these would be larger and would cause disruption at a lower density limit. Even in the gettered torus, the higher density limit is still set by disruption preceded by a sharp rise in oxygen flux. Were this eliminated by some means, there seems no reason why the density limit could not be improved further, at least until ionisation of hydrogen, hydrogenic bremsstrahlung, charge exchange and conduction to the limiter produced a cooling effect equivalent to the radiation by light impurities. However, preliminary results with two getter sources on opposite sides of the torus do not indicate a substantial improvement compared to the results obtained with a single getter.

In general our results are consistent with models of disruption in which ohmic heating is insufficient to prevent cooling of the plasma edge with consequent contraction of the current channel and m.h.d. instability [8].

Acknowledgements: We are indebted to the DITE operating and engineering teams for operation of the machine, and thank R.J. Bickerton and J.W.M. Paul for valuable discussions.

References

[1] Apgar, E., et al, Plasma Physics and Controlled Nuclear Fusion Research, (Proc. of 6th IAEA Conference, Berchtesgaden, 1976) I (1977) 247.

[2] Berry, L.A., et al, Plasma Physics and Controlled Nuclear Fusion Research, (Proc. of 6th IAEA Conference, Berchtesgaden, 1976) I (1977) 49.

[3] Stott, P.E., Daughney, C.C., and Ellis, R.A., Nuclear Fusion 15 (1975) 431.

[4] Hugill, J., et al, this conference.

[5] Paul, J.W.M., et al, IAEA Conference, Berchtesgaden (1976) Paper CN-35/A17.

[6] Murakami, M., Callen, J.D., and Berry, L.A., Nuclear Fusion 16 (1976) 347.

[7] Klueber, O., et al, Nuclear Fusion 15 (1975) 1194.

[8] Rebut, P.H., and Green, B.J., IAEA Conference, Berchtesgaden (1976) Paper CN-35/B6.

[9] Gill, R.D., et al, this conference.

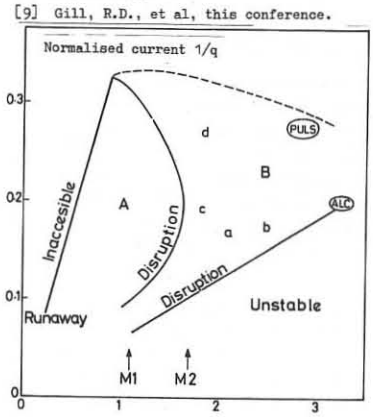

Normalised density $\bar{n}_e R/B_T$ (10^{19} m^{-2} T^{-1})

Fig. 1. Stable operating regimes in normalised I_p, n_e space. A. Without gettering, B. With gettering. M2, M1 Density limits in Ormak with and without gas puff. ALC, PULS operating regimes in Alcator and Pulsator.

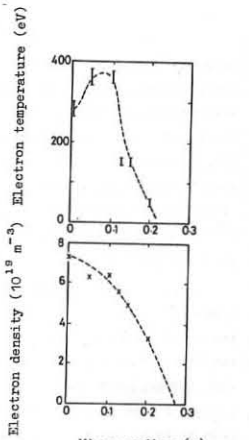

Fig. 3. Photon scattering profiles of T_e, n_e at t = 150 ms in the discharge 'b' of Table 1.

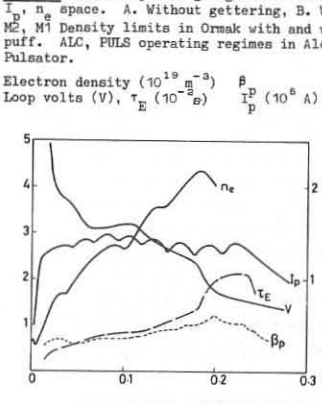

Fig. 2. Time development of I_p, loop volts (corrected for dI_p/dt), n_e and β_p and τ_E from a diamagnetic loop for discharge 'b'. Table 1.

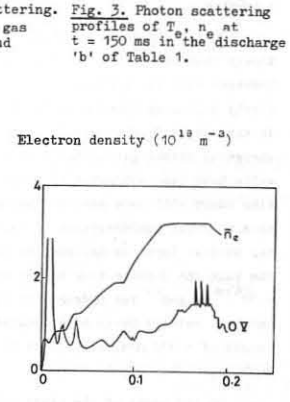

Fig. 4. Time development of mean density and intensity of O V (2781 Å) showing bursts of increased oxygen influx during density pauses.

RECYCLING IN DITE TOKAMAK

S.J. Fielding, G.M. McCracken, S.K. Erents,
A. Pospieszczyk and P.E. Stott

Culham Laboratory, Abingdon, Oxon, OX14 3DB, UK
(Euratom/UKAEA Fusion Association)

Abstract: Recycling has been studied in DITE tokamak by changing the working gas from hydrogen to deuterium. The results show that the recycling gas is composed of approximately equal fluxes of plasma reflected from the wall and gas released from the wall.

The present experiments have been carried out at plasma currents of 50 kA and 100 kA without the divertor or neutral injection. The H/D recycling has been investigated with a scanning Fabry-Perot interferometer to monitor the H_α and D_α lines [1], a mass spectrometer to measure neutral gas concentration and a carbon desorption probe [2] to measure the flux of particles arriving at the torus wall.

Figure 1 shows the behaviour of hydrogen and deuterium as observed by the Fabry-Perot, for the first two discharges in deuterium following many in hydrogen. Also shown are the current, electron density and the deuterium flux ratio $D_\alpha/(H_\alpha + D_\alpha)$. Near the end of the discharge $D_\alpha/(H_\alpha+D_\alpha)$ reaches an equilibrium value and at these times the fluxes of hydrogen and deuterium represent the relative gas concentrations on both the wall and in the plasma. Figure 2 shows that in successive discharges the equilibrium proportion of deuterium slowly rises and approaches asymptotically a value of ~ 0.65. Similar results are obtained from the carbon probe.

After each discharge the hydrogen and deuterium pressures initially rise and then decrease slowly with time, indicating gas being released from the walls.

The results of the Fabry-Perot shows that deuterium, which is ionised at the start of the discharge, is rapidly lost and replaced by hydrogen, indicating that wall recycling is playing a major role during the discharge. We would expect two principal processes to occur (1) reflection of a proportion of the incident particles with an energy dependent reflection coefficient β, (2) release of previously trapped atoms with a probability which depends on an energy dependent cross-section σ and the concentration of atoms in the solid.

Equation (1) describes the change in wall composition on the basis of these two processes.

$$\frac{dN_W}{dt} = (1 - \beta)\frac{N_p}{\tau} - \frac{\sigma}{A} N_W \frac{N_p}{\tau} \qquad \ldots (1)$$

where N_W and N_p are the total number of particles in the wall and plasma phase respectively, τ is an average particle confinement time and A is the area of the wall taking part in the interaction. The first term represents the flux of incident particles trapped in the wall, the second term the flux of atoms back into the plasma. Equation (1) immediately leads to the result that if the plasma density remains constant and no particles are lost from the overall system during a discharge then for the accepted value $\beta \sim 0.6$ [3], the reflected component of the flux is approximately equal to the desorbed component.

We can write similar equations for a system containing two species, hydrogen and deuterium, and this gives for the first discharge in the deuterium, the flux ratio $D_\alpha/(H_\alpha + D_\alpha) = \beta$ at early times. From this and the results of Fig. 1 we obtain the value $\beta \sim 0.6$ which is in good agreement with independent estimates [3]. However the time predicted to reach equilibrium is much shorter than that observed experimentally and we interpret this as being due to a partial loss of deuterium in the wall during the discharge.

Over a series of discharges the hydrogen in the system decays more slowly than exponentially, Fig. 2, indicating an additional source of hydrogen into the system. We interpret this source as being due to hydrogen slowly diffusing from the bulk of the wall material to the surface layer. In any single discharge only those atoms within the range of the incident energetic plasma particles (~ 10 nms) will be desorbed. However if the walls have been subjected to particle bombardment over a long period of time there will have been diffusion into the bulk, resulting in an appreciable hydrogen concentration to some depth in the metal. When hydrogen in the surface layer is depleted by release during a discharge, hydrogen in the bulk can diffuse back to the surface. For a diffusion coefficient of $\sim 10^{-17}$ m^2 sec^{-1} for hydrogen in austenitic stainless steel and a time interval between shots of 6 minutes this gives a characteristic diffusion length of ~ 100 nms, sufficient to replenish the surface layer from the bulk.

On the basis of the above model we have constructed a quantitative description of a series of discharges following a change from one filling gas to another, eg hydrogen to deuterium. We assume that a fixed quantity of deuterium is pulsed into the torus at the start of each discharge, equal to a fraction f of the total quantity of gas in the system. At the end of a discharge all the gas in the system goes to the wall and during the time before the next discharge some of this is desorbed and pumped away, and a fraction $(1 - g_n)$ of the surface layer is replaced by hydrogen diffusing from the bulk, where g_n is a function of shot number n. We then expect that after n discharges, the equilibrium ratio $T_n = D_\alpha/(H_\alpha + D_\alpha)$ is given by $T_n = (1 - f)\, g_{n-1}\, T_{n-1} + f$. From experimental values of T_n we derive that $g_n = 0.73\,[1 - 0.8\,\exp(-0.28\,n)]$ giving the fit to the experimental data shown in Fig. 2. The model predicts that after a series of discharges in deuterium T_n will rise asymptotically to the value 0.66, and that doubling the filling pressure leads to an asymptotic T_n of 0.8. Further if we increase the time between shots we would expect more hydrogen to diffuse from the bulk and replace deuterium on the surface. This all agrees very well with the experimental data.

Finally we note that the two recycling processes reflection and particle induced desorption will give rise to fluxes with different energy distributions. At incident energies less than 1 keV the reflected particles will have energies close to their incident values and will have a high probability of penetrating into the centre of the plasma, whereas the particles released from the wall would be expected to have energies less than 10 eV and will undergo charge exchange or ionisation in the outer regions of the plasma. These results confirm the earlier [2] interpretation of the radial profile of the H_α emission as resulting from approximately equal influxes of low and high energy neutral atoms.

We gratefully acknowledge helpful discussions with Drs J. Hugill and J.W.M. Paul and assistance from the DITE operating team.

References

[1] Pospieszczyk, A., et al, Symposium on Plasma-Wall Interaction, Julich (1976), Paper D3.

[2] Paul, J.W.M., et al, Plasma Physics and Controlled Nuclear Fusion Research, IAEA 6th Conference, Berchtesgaden (1976) Paper CN-35/A17.

[3] McCracken, G.M., Symposium on Plasma-Wall Interaction, Julich (1976).

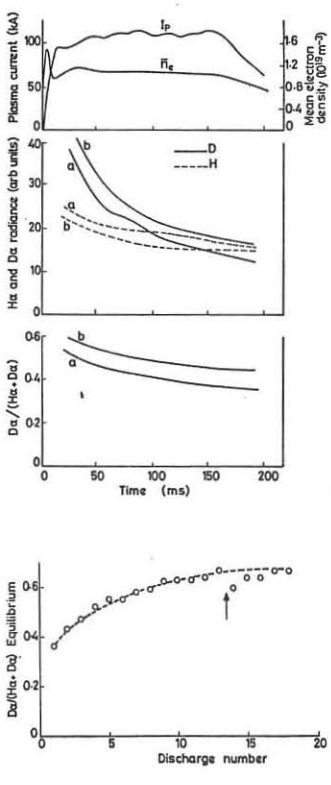

FIGURE 1.

a and b refer respectively to first and second discharges in deuterium.

FIGURE 2.

Dotted line is theoretical curve. Arrow denotes delay of 1 hour between shots.

ORIGIN AND CONTROL OF HOLLOW TEMPERATURE PROFILES IN DITE

J. Hugill, S.J. Fielding, R.D. Gill, M. Hobby, G.M. McCracken, J.W.M. Paul, N.J. Peacock, B.A. Powell, R. Prentice and P.E. Stott

Culham Laboratory, Abingdon, Oxon, OX14 3DB, UK
(Euratom/UKAEA Fusion Association)

Abstract: Hollow temperature profiles associated with centrally peaked total radiation profiles and metallic impurities have been observed recently in DITE. These can be avoided by cooling the periphery of the discharge by various means, by neutral injection heating or by using the DITE divertor.

During the first 10 months of operation of the DITE tokamak the peak electron temperature, T_{eo} in a typical discharge with $I_p \sim 200$ kA, $B_T \sim 2.7$ T fell from $\sim$ 1100 eV to 800 eV. Machine parameters and initial results are given in reference [1]. A few hundred discharges in hydrogen with $I_p \sim 20$ kA, $B_T \sim 0.15$ T were used to condition the vacuum walls each day, and it was thought that their condition had stabilized.

A total radiation thermopile measuring the fraction of ohmic power lost by radiation and charge-exchange gave an almost constant value between 0.5 and 1.0, the uncertainty being due to the thermopile calibration factor. Photospectrographic measurements of radiation between 10 Å and 300 Å showed the principal impurities to be Fe ($\sim 0.004\ n_e$), Cr ($\sim 0.002\ n_e$), Mo($\sim 0.002\ n_e$) and O ($\sim 0.01\ n_e$); similar in composition to the metal-dominated discharges in ST-tokamak [5]. The metals account for $\sim$ 97% of the radiated power and $\sim$ 76% of the mean ion charge excess, $Z_{eff} - 1$.

More recently persistent hollow temperature profiles with $T_{eo} \sim 200$ eV have been observed, occasionally at first, then regularly and reproducibly as shown in Fig. 1. Similar profiles have been observed in Ormak [3].

The radiated power is measured with a thermopile mounted behind a collimator with a spatial resolution of 25 mm which can be scanned across the discharge diameter. It shows a large central peak and little indication of the peripheral radiating layer typical of oxygen dominated discharges in TFR [2]. Indeed, in the centre of the discharge, the radiated power exceeds the ohmic input, calculated from the temperature profiles assuming $j \sim T_e^{\frac{3}{2}}$, by 70%, although the thermopile calibration allows an uncertainty of - 20% + 60% in the values of radiated power given in the figures. This excess of radiated power, mainly line radiation from highly ionized metallic impurities, explains why these hollow profiles persist, but it should be noted that a peaked profile with the same impurity content would also persist because the ohmic input increases more rapidly with T_e (exponent $\sim$ 1.5) than the radiation loss (exponent - 1 to + 0.5). A profile with an intermediate T_{eo} should be unstable [4] and transient. The unstable nature of this thermal equilibrium, possibly augmented by radial diffusion of impurities produced by the strong temperature gradients, explains why relatively slight changes in plasma conditions can replace the hollow by a temperature peak, as discussed below.

It is well known that oxygen, deliberately introduced or as a contaminant, reduces the concentration of metallic impurities [5,6]. In DITE, after exposing the vacuum walls to air for a short time, T_{eo} rises to $\sim$ 1100 eV for a few days, until the low-Z impurities have been removed. A similar effect is produced by adding a small amount of neon. Fig. 2 shows a plot of T_{eo} against neon concentration in the initial gas filling. About 2% is sufficient to raise T_{eo} to $\sim$ 1500 eV. Larger amounts tend to cause disruptive instabilities due to excessive cooling of the discharge periphery [7]. However, a smaller cooling of the edge by low-Z impurities may prevent the formation of hollow profiles by keeping the current-channel compressed in addition to reducing the metal concentration.

The characteristics of discharges with a hollow profile, with air contamination and with 2% of neon are compared in Table 1. Fig. 3 shows the radial dependences, for these discharges, of the ohmic power input and the power radiated in each 10 mm thick annular shell (the areas under these curves being the total power input and radiated). The excess of radiated power in the periphery of discharges 2 and 3, as in TFR [2], must be supported by conduction from the centre resulting in steep gradients of T_e. The thermal instability is limited by outward conduction or flattening of the central peak associated with MHD activity near the q = 1 surface. Similar temperature gradients, but in the opposite direction; arise in the central region of discharge 1 to support the excess radiation loss there, and it is the ohmic power profile, rather than the radiation profile, which changes most. Fig. 4 shows the power radiated per electron, indicating, very approximately, the radial distribution of the strongly radiating impurities. There is no evidence for a marked central peak of impurity concentration in any of these discharges but the resolution of the scanning thermopile is only 25 mm.

Similar effects to injecting low-Z impurities can be produced by inserting a probe 'limiter' into the discharge periphery [1]. It is uncertain whether this acts by reducing metallic impurities, by simply cooling the periphery by conduction, or both.

All the methods of avoiding hollow profiles described above tend to produce disruption by cooling the edge of the discharge, and result in high $Z_{eff} \sim 6$. More satisfactory, and equally successful, is to compensate the power imbalance at the centre by additional neutral beam heating [8] or to use the DITE divertor to screen out metallic impurities [9].

Acknowledgements We are indebted to the DITE operating and engineering teams for reliable operation of the machine and to our colleagues in the physics team for stimulating discussions.

Table 1

	1 (hollow profile)	2 (air contaminated)	3 (2% Neon)
I_p (kA)	176	199	120
V (V)	4.7	3.3	3.3
B_T (T)	2.7	2.7	2.0
$\bar{n}_e$ (10^{19} m^{-3})	1.7	2.1	1.6
Z_{eff}	6.3	6.6	6.3
T_{eo} (eV)	205	1100	940
β_{pe}	0.09	0.14	0.20

References

[1] J.W.M. Paul, et al, 6th Conf. on Plasma Phys. and Controlled Nuclear Fusion, Berchtesgaden (1976) Paper IAEA-CN-35/A17.

[2] T.F.R. Group, 6th Conf. on Plasma Phys. and Controlled Nuclear Fusion, Berchtesdaden, (1976) Paper IAEA-CN-35/A3.

[3] L.A. Berry, et al, 6th Conf. on Plasma Phys. and Controlled Nuclear Fusion, Berchtesgaden (1976) Paper IAEA-CN-35/A4-1.

[4] H.P. Furth, et al, Physics of Fluids, 13 (1970) 3020.

[5] E.B. Meservey, et al, Nuclear Fusion, 16 (1976) 593.

[6] R.E. Clausing, et al, J. Vac. Sci. and Technology, 13 (1976) 437.

[7] J.C. Hosea, et al, Plasma Physics and Controlled Nuclear Fusion Research (IAEA, Vienna, 1971) II 425.

[8] R.D. Gill, et al, this conference.

[9] P.E. Stott, et al, this conference.

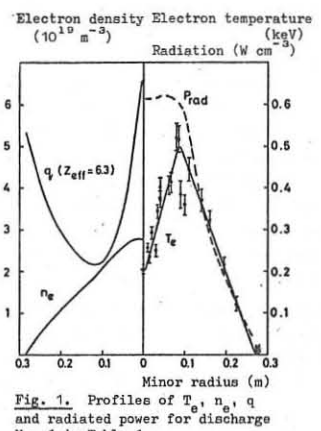

Fig. 1. Profiles of T_e, n_e, q and radiated power for discharge No. 1 in Table 1.

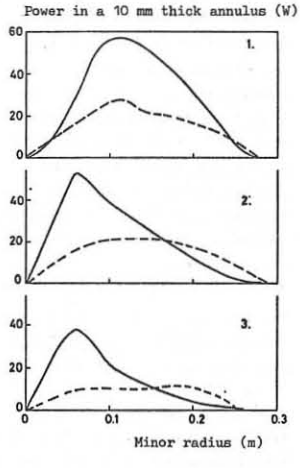

Fig. 3. Profiles of ohmic power input (solid line) and power radiated (broken line) for the discharges in Table 1.

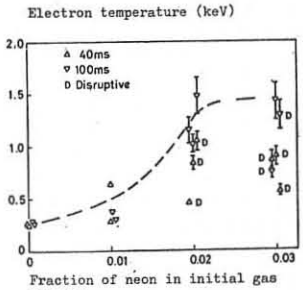

Fig. 2. Variation of central electron temperature with addition of neon in a hydrogen discharge, $B_T = 2.7$ T, $I_p = 200$ kA, $n_e \sim 2 \times 10^{19}$ m^{-3}.

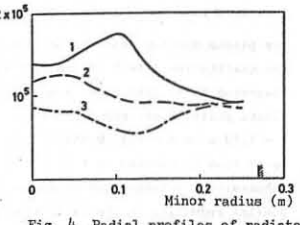

Fig. 4. Radial profiles of radiated power per electron for the discharges in Table 1.

ON THE ORIGIN OF METAL IMPURITIES IN THE DITE TOKAMAK

G M McCracken, G Dearnaley, S J Fielding, D H J Goodall,
J Hugill, J W M Paul, P E Stott, J F Turner and J Vince.

UKAEA/Euratom Assoc., Culham Laboratory, Abingdon, OX14 3DB, England.

ABSTRACT: The metal flux into the plasma has been measured using a time resolved surface technique and optical spectroscopy. On the basis or our results we propose that arcing is the principal mechanism for metal impurity production.

The process whereby metal impurities enter tokamak discharges is not well understood. Possible mechanisms are sputtering, evaporation and arcing. However, two general arguments seem to rule out sputtering. One is the appearance of metals very early in the discharge (∿ 5 ms) when the ion temperature is low. The second is that the metal impurity concentration is very similar in hydrogen and helium discharges [1] when the sputtering coefficients of the two species are about an order of magnitude different. Evaporation due to thermal conduction from the plasma appears very unlikely as a mechanism in normal (undisruptive) discharges on the basis of measurements of the surface temperature of the limiter. [2] In order to investigate the possible processes involved we have made measurements of the flux of metals into and out of the DITE tokamak. In addition we have inserted polished molybdenum specimens into the discharge and obtained direct evidence of arcing.

It is clear from an examination of the optical windows on the torus that metal is removed from the wall and then redeposited in a thin layer over the whole torus wall. The thickness of the deposit varies by only a factor of 2 to 3 along the length of 0.45 m windows, and windows in different azimuthal positions and over different periods of operation of the tokamak have given results which are consistent. The typical composition of these films is Fe 1.8×10^{17}, Ni 2.9×10^{16}, Cr 1.8×10^{16}, Mo 2.0×10^{16} atoms m^{-2} discharge^{-1}. Thus the total amount of metal removed from the wall each discharge is ∿ 3×10^{18} atoms. On the basis of the average density and confinement time the effective removal rate per incident plasma ion is 0.04 atoms/ion compared with the estimated sputtering coefficient for 200 eV H^+ ions on stainless steel ∿ 10^{-4} atoms/ion. The composition of the film is mainly stainless steel (from the walls) with about 10% from the molybdenum limiter. The composition of the stainless steel is different from the bulk material and from that of evaporated stainless steel.

To investigate the material removed from the wall in a more detailed way we have exposed to the plasma carbon probes which are subsequently analysed using Rutherford Backscattering of 3.5 MeV $^{14}N^+$ ions. Some results are shown in Figure 1 of the radial distribution of the atoms collected on the probe. We interpret the surface concentration as a measure of the concentration of impurity ions in the plasma at this radius. The concentration increases with radius as impurity atoms entering the plasma from the wall become ionized and follow field lines until they intersect the probe. The concentration decreases on changing the plasma current from 100 kA to 50 kA and then decreases still further when the divertor [3] is operated.

The time dependence of the metal flux entering the plasma has been measured using the same analytical technique but now using as a collector a carbon disc which rotates once during a discharge. A window of 30° sector in front of the disc allows a time resolution of ≈ 30 ms. The disc is exposed for five similar discharges at a radius of 0.26 m. The results are shown in Figure 2 for a 90 kA discharge. It is found that the metal flux increases roughly in proportion with plasma current and density. Similar results have been obtained at I_p = 140 kA and 180 kA. The results are again inconsistent with either evaporation or sputtering. In both cases the highest metal flux would be expected at the beginning and end of the pulse when the particle flux and the energy flux to the wall will be larger than during the constant current phase. The results are also inconsistent with impurities being produced by runaway electron beams, since these beams reach the wall mainly at the end of the discharge. We believe however that the results are consistent with evaporation due to the type of unipolar arcing observed in pinches [4] since the probability of such arcs occurring increases with both electron density and electron temperature.

The plasma density near the wall has been changed in a number of ways and the qualitative effect on the iron atom flux into the discharge monitored observing Fe II (259.9 nm) spectroscopically. The results of changing the plasma position are shown in Figure 3. By changing the major radius from R = 1.13 m to R = 1.17 m the plasma is moved away from the wall and the Fe II flux is reduced by a factor 3. This has been demonstrated both in successive discharges and by moving the plasma during a discharge. A similar reduction in the Fe II flux can be obtained by turning on the divertor and by introducing a Mo probe into the plasma to a radius of 0.18 m. The metal flux into a discharge can also be controlled by gas "puffing".

The introduction of hydrogen, via a fast gas valve during a discharge results in an immediate reduction in the flux of iron. Similar effects have been observed with hydrogen in PULSATOR [5] and with oxygen in ST [6] and TFR. [7] Although we have not yet made any direct experimental measurements it is suggested that the introduction of cold gas at the edge of the discharge lowers the electron temperature and hence reduces arcing. The fact that the metal flux is reduced by introducing oxygen makes it improbable that light impurity sputtering is responsible for heavy impurities.

The direct observation of arcs on the torus wall has proved difficult because the arcs tracks are small and only readily observed on carefully polished surfaces. Arcs have been directly observed, however, on polished molybdenum probes which have been placed at radii from 0.27 to 0.18 m and subsequently examined in the optical microscope and the scanning electron microscope. Similar arcs have also been observed at the divertor target plate in DITE. They are of two principal types but both tracks run predominantly at right-angles to the B_ϕ field lines. One is fern like, similar in structure to those seen in Zeta, [4] with a total length up to 10 mm. The other consists of tracks typically 20 μm wide and ∿ 10 mm long. The tracks consist of a series of melted blobs ∿ 10 μm diameter.

It is commonly argued that arcing cannot occur in tokamaks because the cross field diffusion leads to the plasma potential being negative with respect to the wall. However, such a condition does not obtain in the region in the shadow of the limiter or at divertor targets. The direct observation of such arcs and the other evidence put forward indicate that arcing must be considered as a potentially serious form of wall erosion both in contemporary tokamaks and in reactors.

ACKNOWLEDGEMENT: We are indebted to the DITE operating and engineering teams for the operation of the machine, in particular to G W Reid and B C Sanders.

REFERENCES:

1. N Bretz et al, Nuclear Fusion 15, 313, 1975.
2. D H J Goodall, Proc 9th SOFT, P523, Pergamon Press, 1976.
3. P E Stott et al, this conference.
4. J L Craston et al, Proc 2nd UN Conf (Geneva) 32, 414, 1958.
5. P Staib and G Staudenmaier, J Nucl Mat 63, 37, 1976.
6. E Merservey et al, MATT 1175, PPL Princeton, Dec 1975.
7. T F R Equipe, Nuclear Fusion to be published.

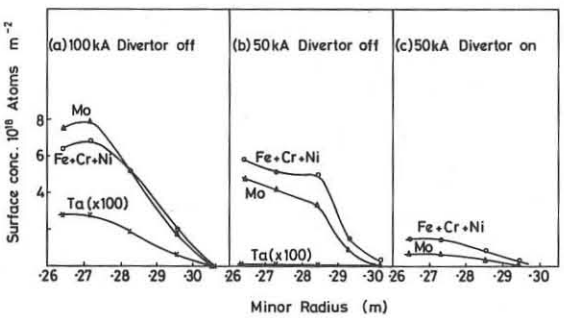

Figure 1. Radial distribution of metal impurities deposited on a probe in DITE discharges.

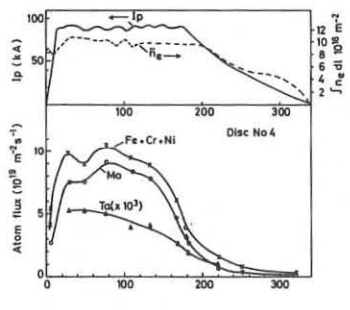

Figure 2. Time distribution of metal impurities arriving on a probe at 0.26 m minor radius during a 90 kA discharge (divertor off).

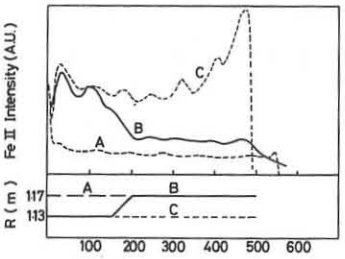

Figure 3. Time dependence of Fe II (259.9 nm) flux entering plasma for different plasma positions (divertor off).

VERTICAL PLASMA STABILITY IN THE T-12 FINGER-RING TOKAMAK WITH TWO POLOIDAL DIVERTORS

A.V. Bortnikov, N.N. Brevnov, S.N. Gerasimov,
V.G. Zhukovskii, V.I. Pergament, L.N. Khimchenko
I.V. Kurchatov Institute of Atomic Energy, Moscow, USSR

T-12 was created for the study of the axial symmetric poloidal divertor in the plasma column with the parameters $n_e = 3.10^{13} cm^{-3}$, $T_e \sim 300$ eV, the discharge current $I_p = 40$ kA and $B_T = 8$ kG. The divertor geometry of the magnetic field is created by the superposition of the plasma current magnetic field, external quadrupole and dipole fields providing equilibrium along the major radius and also by the shell currents. The shape of the copper shell was choosen according to the shape of the equilibrium magnetic surface.

I. Stable Regimes. The vacuum quadrupole field has a zero point in the centre of the chamber for the currents corresponding to Fig. 1. The current I_o is switched on simultaneously with the discharge current (Fig. 2a). The coordinates of the separatrix points z_s and z_s' were determined by means of B_r and B_z components of the poloidal magnetic field measured by magnetic probes (here and on letters with a prime correspond to the lower part of the discharge). The position of "z_s" with time is given at Fig. 2b. The separatrix point moves toward the chamber centre during the first part of the discharge and penetrates into the shell by the 3-d ms; the coordinate z_s is practically constant after the 5-th ms to the end of the discharge. Theoretical behaviour of z_s^T with time is shown in Fig. 2b, too: it was received from the calculation of the equilibrium configuration of the discharge in absence of the copper shell according to the behaviour of $I_p(t)/I_o(t)$. There is a strong divergence in behaviour of z_s and z_s^T that points to the essential influence of the copper shell during the formation and maintenance of the divertor configuration. So, there is a stable magnetic configuration with poloidal divertors at $t \geqslant 5$ ms (Fig. 1). We observed the plasma in divertors channels by means of an interferometer ($n_e d$), bolometer (P) and Langmuir probe (I_{Lp}) after the divertor configuration had been formed (Fig. 2c); the plasma parameters were: $n_e \simeq (0,5 \div 1).10^{12} cm^{-3}$, $T_e = 10$ eV, the divertor layer thickness $d = (0,5 \div 1)$cm. Simultaneously we see that the formation of the poloidal divertor configuration has a strong influence on the character of the discharge (Fig. 3). Thus, the duration of discharge current increased, there were changes in the behaviour and magnitude of the plasma density, and plasma radiation near the limiter decreased. Such an improvment of the discharge characteristics may be connected with divertor operation or with magnetic limiter formation. So these experimental results illustrate the formation of a stable alongated (K=2) plasma column with two magnetic poloidal divertors in the T-12 installation.

II. Unstable Regimes. Besides the stable regimes of the discharge described above it was possible to create those which abruptly vanished due to fast motion of plasma column as a whole in the vertical direction (vertical instability) (2,3). It occurs in T-12 when the magnitude of current in the quadrupole coils exceeds some definite value which is in matching with the poloidal configuration. The oscillograms for the stable (1) and unstable (2) regimes are given together with the quadrupole currents and magnetic probe signal in Figs. 4a,4b,4c. The moment the separatrix point passes through the probe corresponds to the zero magnitude of the signal at the probe. The magnitude of the vacuum magnetic field is given at Figs. 4c,4d by dotted curves. A detectable weak plasma column displacement (Δz) begins (1÷2) ms before the disruption (Fig. 4e); the direction of the displacement is determined by the directions of the scattered magnetic toroidal field and plasma current. Unstable discharges are characterized by the decreasing of the distance between the separatrix points up to a certain bounded value $z_s - z_s' = 25$ cm (Fig. 4f) after which a perturbation mode m=1, n=0 develops. The force influencing the plasma current from the quadrupole fields probably exceeds the stabilising shell force in this case. The instability development characteristic time is sufficiently large (~1 ms) as it follows from Figs. 4e,4f; the latter fact is probably connected with the stabilizing features of the copper shell. A feedback electronic system is able to stabilize such a velocity of the plasma column displacement.

REFERENCES

1 A.V. Bortnikov et al., Preprint IAE-2772, Moscow, 1977.
2 V.S. Mukhovatov, V.D. Shafranov, Nucl. Fusion 11 (1971),605.
3 G. Cima, D.C. Robinson, C.L. Thomas, A.G. Wootton, Sixth Conf. on Plasma Phys. and Contr. Nucl. Fusion Res., Berchtesgaden paper, CN-35/A10-5 (1976).

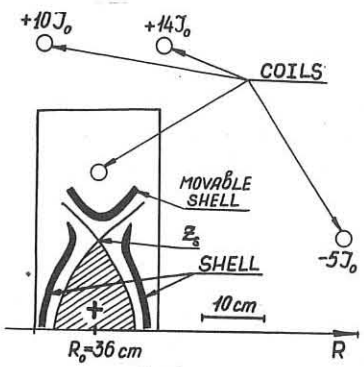

Fig.1.

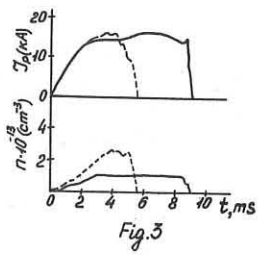

Fig.3

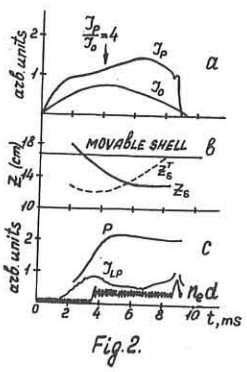

Fig.2.

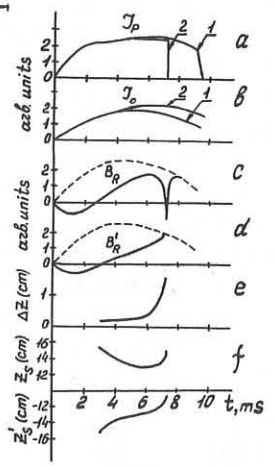

Fig.4.

Equilibrium, stability and confinement of elliptic cross-sectioned tokamak plasmas.

A.J. Wootton and D.C. Robinson

Culham Laboratory, Abingdon, Oxon (Euratom/U.K.A.E.A. Fusion Association)

Abstract: The production and equilibrium of both vertically and horizontally elongated tokamak plasmas is demonstrated. Axisymmetric instability limits permit $0.75 \lesssim b/a \lesssim 1.5$. It is concluded that the observed tearing modes are unaffected by the shaping. Balanced toroidal flux loop measurements are interpreted to show increased β_I with vertically elongated cross sections.

Introduction A small multipole tokamak, TOSCA ($R = 30$, $a \lesssim 10$cm)[1] is used to study non circular plasmas. Results are presented for plasmas with elliptic cross sections. Equilibria, stability and confinement are discussed.

Device A conducting vacuum vessel, $r_v = 10$ cm, is surrounded by 16 equally spaced single turn coils. They induce the plasma current and provide the shaping field. Equilibrium is maintained by a separate vertical field winding. Typical parameters of a discharge, duration ~2ms, are plasma current I_p ~15kA line of site average density ~1×10^{13} cm^{-3}, peak central temperature ~200 ev

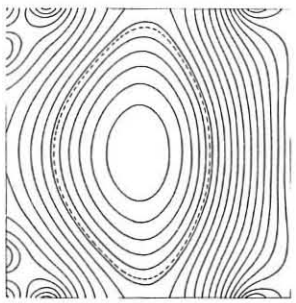

Fig.1 Flux contours

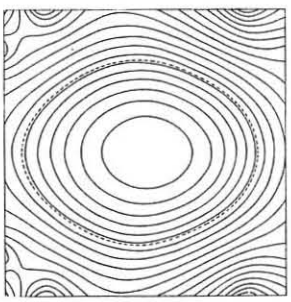

Fig.2 Flux contours

(from laser light scattering measurements), and $\beta_I \sim 0.5$.

Equilibrium An initially circular plasma is produced by the vertical field and primary windings. A quadrupole field is then applied to obtain an ellipse. Figs. 1 and 2 show flux contours, computed for a free boundary equilibrium,[1] using measured winding currents. A flux independent toroidal current distribution is used. The plasma shape is verified by comparing measured and computed plasma current multipole moments[2]. The equilibrium fields are characterized by the decay index $n = -(R/B_\theta).(\partial B_\theta/\partial R)$. An average, $\bar{n} = \int n dS_\beta / \int dS_\beta$, is deduced from measured winding currents, including induced currents: this is related to the semi axis ratio b/a using the free boundary calculation. Curves are shown in figure 5, for flat and peaked current distributions.

Axisymmetric stability For $\bar{n} \lesssim 0$, $\bar{n} \gtrsim 1.5$ axisymmetric modes which terminate the plasma current are identified.[1] The growth times are plotted in figures 3 and 4 as a function of $\bar{n}$ (marked without control). An analytic model[3] is used to predict the critical values of $\bar{n}$ to be 0 and 1.5, as found experimentally. The analytic growth time is shown in figure 3 as a solid line. The vertical motion is well represented. A passive feedback control system allows $-4 \leqslant \bar{n} \leqslant 2$ before the modes are observed. The growth times are shown in Figures 3 and 4 (marked with control): the critical values of $\bar{n}$, related to b/a, are predicted by a rigid shift calculation which includes the effect of induced currents.

For stability with no control $0.85 \leqslant b/a \leqslant 1.05$. With control, $0.75 \leqslant b/a \leqslant 1.5$ before modes are observed in the experimental timescale.

Tearing mode stability. Coils are used to identify helical magnetic structures (Mirnov oscillations). During the current rise, oscillations are observed if q limiter $\geqslant m/\ell$, with m and ℓ the poloidal and toroidal mode numbers. A magnetic probe inserted into the plasma edge shows a B_r signal which does not change sign at the singular surface. Both measurements indicate a resistive mode. Using $q = \pi a^2 B_\phi (1 + b^2/a^2)/(\mu_o I_p R_p)$, and assuming $q \sim m/\ell$, with a, b $\leqslant 8.5$ cm, b/a can be deduced at the mode onset time[4]. The results, plotted as b/a against $\bar{n}$, are shown for $m = 4$, $\ell = 1$ in Fig.5, together with the predictions of the equilibrium calculations. The agreement indicates that the modes are not effected by shaping.

Confinement. Balanced toroidal flux loops are used to determine the plasma pressure. Fig.6 shows the change in β_I, during the risetime of the shaping field (~ 300 μs), plotted against $\bar{n}$ at peak shaping. The results are interpreted assuming $a/R \ll 1$, $b/a \sim 1$. Corrections for the plasma shape[2] reduce β_I^F/β_I^i by about 15% at both $\bar{n} \sim 4$ and -2: it is concluded that a vertical elongation increases β_I. Possible explanations are changes in current density or wall contact.

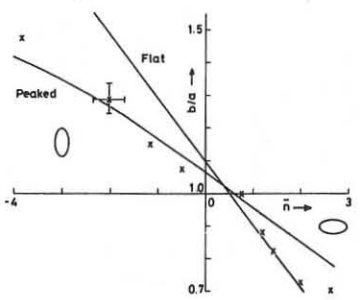

Fig. 5 Semi axis ratio b/a against decay index $\bar{n}$ from mode analysis (points) and equilibrium calculations (solid lines) with two plasma current distributions.

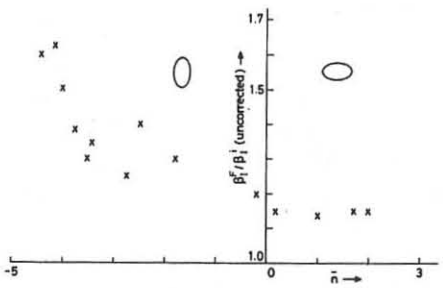

Fig.6. The increase in β_I during the period of shaping as a function of the decay index $\bar{n}$

Conclusions. Using passive feedback control, elliptic cross-sectioned plasmas can be produced with $0.75 \leqslant b/a \leqslant 1.5$. With no control $0.85 \leqslant b/a \leqslant 1.05$. These limits are predicted by rigid shift calculations.

Confirmation of the shape predicted by equilibrium calculations is obtained from field perturbations produced by tearing modes. This implies that the modes are unaffected by the shaping other than by changes in the safety factor.

Initial measurements using balanced toroidal flux loops indicate increases in β_I when the plasma is elongated vertically.

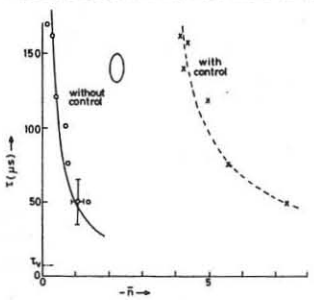

Fig. 3 Axisymmetric mode growth times

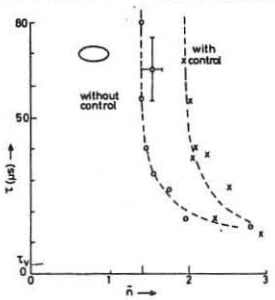

Fig. 4 Axisymmetric mode growth times

References

[1] G. Cima et al. 6th Conf. on Plasma Physics & Contr. Nucl. Fus. Res. Paper CN-35/A10-5 (1976).

[2] L.E. Zakharov, V.D. Shafranov, Sov. Phys. Tech. Phys. 18,151 (1973).

[3] A Fukuyama et al. Japanese Journal of Applied Phys. 14, 871 (1975).

[4] A.V. Bortnikov et al. Fizika Plazmy 1, 931 (1975).

TWO STAGES OF DISRUPTIVE INSTABILITY IN A TOKAMAK AND FEEDBACK STABILIZATION OF IT

V.V.Arsenin

I.V.Kurchatov Institute of Atomic Energy, Moscow, USSR

ABSTRACT In present-day tokamaks peaked current profiles with $q(0)>1$, $q(a)\approx 2$ can be realized, which are stable against rapid MHD-modes (of the surface-wave type). These modes responsible for a disruption develop only in case when a slow "forspike" instability causes flattening of the current profile. The observed rapid MHD-mode growth rate ($\ll\Omega_A$) can be explained by taking into account the dynamics of the passing the instability threshold while the current increases. The dissipative tearing-mode seems to be responsible for the "forspike". On the whole one can eliminate the disruption by the feedback stabilization of the tearing mode.

1. A strong disruptive instability with helical perturbations $\exp(im\theta - in\varphi)$ is observed in a tokamak at $q(a)=\frac{aB_{||}}{RB_\theta(a)}\approx 2$, where a is a minor radius. Theoretically, the most rapid MHD-instability is an instability of an ideally conducting plasma with a free boundary (of the surface-wave type); its growth rate $\sim\Omega_A=\frac{B_\theta(a)}{\sqrt{4\pi\rho}a}$, ρ is the density. However, in spite of the fact that the condition $q(a)=2$ agrees with such an instability criterion for observed $m=2$, $n=1$ perturbations, the growth rate values found experimentally are a few orders of magnitude lower than Ω_A. Detailed experiments have shown /1/ that processes on different time-scales occur during the spike. Two stages have been distinctively revealed.

First a slow $m=2$, $n=1$ instability is excited ($\gamma\sim 10^{-3}\Omega_A$). Data from various tokamaks (the growth rate value, the observation of the phase jump in a radial displacement /2/) cause one to think that this is a dissipative tearing instability. A rapid MHD instability does not arise evidently because the current profile is of the peaked character. And q value in the center is slightly more than unity at $q(a)\approx 2$.

The "forespike" instability causes, according to /1/ the $m=1$, $n=1$ mode in the column center. This mode development results in flattening the profile of temperature and may be of current density.

Further follows the disruptive stage - the proper spike. It is natural to connect it with the rapid MHD instability of the new flat current distribution. We shall show that in spite of the fact that the growth rate observed in this stage is $\ll\Omega_A$, the spike can be interpreted in this way. In fact, the maximum growth rate $\sim\Omega_A$ corresponds to the middle of the instability interval over q (Fig.1). In the experiment the dropping of q occurs gradually and due to the instability disruptive character this value is not achieved: the spike occurs near the $q(a)=2$ instability threshold. To find the perturbation evolution near the threshold one should take into account the time-dependence of q(a). Realizing linear approximation of the $\gamma^2(q)$ dependence near the threshold we get the displacement equation:

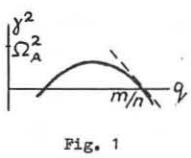

Fig. 1

$$\ddot{\xi} = \alpha\Omega_A^2\,\frac{t-t_0}{T}\,\xi, \qquad (1)$$

where $\alpha\sim 1$, t_0 is an instant of the threshold passing,

$$T^{-1} = -\frac{1}{q}\,\frac{dq}{dt}\Big|_{t=t_0}.$$

The solution of (1) is the following:

$$\xi = C_1(t-t_0)^{1/2}\,J_{1/3}\Big\{i\big[\Gamma(t-t_0)\big]^{3/2}\Big\} + C_2(t-t_0)^{1/2}\,Y_{1/3}\Big\{i\big[\Gamma(t-t_0)\big]^{3/2}\Big\},$$

where $\Gamma=(\frac{4}{9}\,\frac{\Omega_A^2}{T})^{1/3}$, constants C_1, C_2 are determined from initial conditions in the instant $t_1<t_0$.

At $t<t_0$ the solution is of the oscillating character, at $t>t_0$ $\xi\sim\exp\big[\Gamma(t-t_0)\big]^{3/2}$. Thus the characteristic growth time of the perturbation is $\tau\sim\Gamma^{-1}\sim(T/\Omega_A^2)^{1/3}$. For T-4 experiments mentioned above /1/ $\Omega_A\sim 10^7\ s^{-1}$, $T=I/\frac{dI}{dt}\sim 0.1$ s (I is the total current) our estimate gives $\tau\sim 10\ \mu s$ which is in good agreement with observations. Further, the value $\tau\sim 10\ \mu s$ should be generally the characteristic value for present - day tokamaks because the expression for Γ includes the 1/3 power and parameter dispersion for contemporary tokamaks is not large. And this is so in fact.

2. Thus, the disruptive spike can be explained by the "classic" MHD instability of the surface wave type which has been predicted since long. But the spike occurs not in all cases. In the present - day tokamaks (of T-4 type) peaked current distributions can be realized stable against this mode. The spike occurs if the "forspike" results in flattening the current profile. May be, the spike will not occur if the slow forspike instability is suppressed. As was mentioned earlier the tearing instability seems most likely to be responsible for the "forspike". We shall show further that it can be suppressed by a feedback system controlling the magnetic field perturbations outside the plasma.

Tearing instability necessary condition is /3/

$$\Delta = \frac{1}{B_r}\,\frac{\partial B_r}{\partial r}\Big|_{r=r_s+0} - \frac{1}{B_r}\,\frac{\partial B_r}{\partial r}\Big|_{r=r_s-0} > 0, \qquad (3)$$

where B_r is the radial component of the perturbation magnetic field, $r=r_s$ is the surface inside the plasma at which $q(r)=m/n$. Radial profiles of B_r and displacements ξ_r are shown in Fig. 2. It is clear that Δ decreases with approaching to the plasma of the shell. The idea of feedback stabilization consists in the fact that the current $J\sim J\exp(im\theta - in\varphi)$ proportional to the displacement and exceeding the image current in the shell schould be excited between the plasma and the shell. Then due to a steep fall of B_r outside the plasma the value $\Delta<0$ can be achieved.

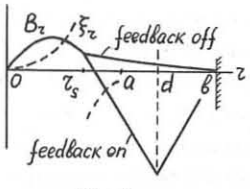

Fig. 2

It is easy to perform analytic calculations for a stepped current distribution: j=const for $r<r_0<a$, a is the plasma radius, j=0 for $r>r_0$. Let the surface density of the stabilizing current be: $J=\frac{I_0}{a}W\xi(r_0)$, (4)

where I is the total current in the column. Then

$$\Delta = -\frac{2m}{1-(r_s/b)^{2m}} + \frac{2m}{m-1-nq(r_0)+\frac{r_0}{r_s}(\frac{r_0}{r_s})^{2m}}\Big[(\frac{r_0}{r_s})^{2m} - \frac{1-(\frac{d}{b})^{2m}}{1-(\frac{r_s}{b})^{2m}}\,(\frac{r_0}{a})^2\cdot$$

$$\cdot(\frac{r_0}{d})^{m-1}W\Big], \qquad (5)$$

where b is the shell radius. For stability ($\Delta<0$) it is sufficient to have

$$W>\frac{1}{\pi}(\frac{r_0}{r_s})^{2m}(\frac{a}{r_0})^2(\frac{d}{r_0})^{m-1}\,\frac{1-(r_s/b)^{2m}}{1-(d/b)^{2m}}. \qquad (6)$$

At $d-a\lesssim a$ for small m the total current in a stabilizing winding $\sim I\,\frac{\xi}{a}$. For a device of T-4 dimensions at $\frac{\xi}{a}\sim 10^{-2}$ the stabilizing current should be of the order of 1 kA.

REFERENCES

1. S.V.Mirnov, I.B.Semenov. VI Intern. Conf. on Plasma Phys. and Contr. Nucl. Fusion Res., Berchtesgaden, 1976.

2. F.C.Jobes, J.C.Hosea, MATT-982(1973). III Intern. Symp. on Toroidal Plasma Confinement, Garching, 1973.

3. H.P.Furth, J.Killeen, M.N.Rosenbluth. Phys. Fluids, 6, 459, 1963.

4. V.D.Shafranov. J. Tech. Phys., 40, 241, 1970.

INTERNAL MODES AND DISRUPTIONS WITH INCREASING ELECTRON DENSITY IN THE PULSATOR TOKAMAK

S.Sesnic, W.Engelhardt, J.Gernhardt, O.Klüber and D.Meisel
Max-Planck-Institut für Plasmaphysik
D-8046 Garching, Fed.Rep.of Germany

Abstract: The paper presents the experimental data on internal modes and disruptions at high densities. The internal disruption at high densities seems to be only a minor energy loss mechanism.

Internal modes and disruptions, first reported on the ST Tokamak /1/, have been observed on almost all other tokamaks. We report some new aspects of these phenomena that are partly associated with the high densities attained in Pulsator /2/.

Most of the data on internal modes and disruptions described here are obtained under one set of discharge conditions:

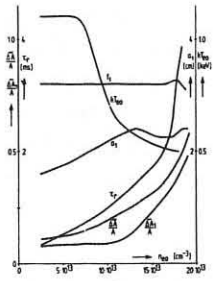

Fig.1:Dependence of electron temperature and internal mode and disruption parameters on density.

$B_\varphi = 27$ kG, $I_{pmax} = 65$ kA, $a_L = 11$ cm, $R_o = 70$ cm, $q(a_L) = 3.5$. A fast gas input at 40 ms increased the peak electron density from 2.0×10^{13} to $1.8 \times 10^{14} cm^{-3}$. For these measurements a set of ten Si surface barrier diodes sensitive to soft X-rays was used. The raw data are summarized in Fig.1. The amplitude modulation of the internal disruption $\frac{\Delta\tilde{A}}{A}$, the relaxation time of the saw tooth τ_r, the amplitude modulation of the m = 1 mode $\frac{\Delta\tilde{A}_1}{A}$ and the radius of the q = 1 surface a_1 all increase with the density. The increase of τ_r is faster than linear. The frequency of the m = 1 mode at low densities is about 22 kHz, but with increased density it quickly drops to about 16 kHz and stays constant. The growth rate of this mode at low densities is $1 - 2 \times 10^4 s^{-1}$ and at high densities $4 - 10 \times 10^4 s^{-1}$. The azymuthal rotation of the mode is in the direction of the electron diamagnetic drift, and the frequency evaluated from this drift is only slightly smaller than the measured frequency. As expected, the toroidal mode number is found to be n = 1.

The electron temperature variation can be evaluated from the sawtooth oscillation signal. Typical electron temperature profiles immediately before (t_1) and after the disruption (t_2), obtained from the Si diodes signals, together with the median profile, obtained by Thomson scattering, are shown in Fig.2 for the high-density case. Soon after the internal disruption the profile is flattened beyond the q = 1 surface up to a minor radius of 4 cm. One can observe during the sawtooth three periods in m = 1 activity: a stationary phase, where neither the amplitude nor the frequency of the m = 1 mode varies, a growing phase just before the internal disruption, where the frequency is decreased, and, finally, a decaying phase after the internal disruption. The radial position of the maximum modulation of this mode, r_1, shown in Fig.3, could be interpreted as the position of the q = 1 surface. t_D is the time in the sawtooth measured from the moment of the internal disruption. During the stationary phase the radius r_1 does not vary. In the growing phase one observes a steady increase in r_1; this could be interpreted as an outward motion of the q = 1 surface caused by electron temperature peaking and accompanying current shrinkage.

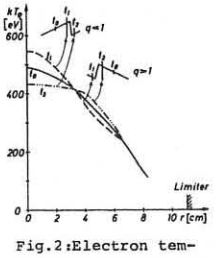

Fig.2:Electron temperature profile for three characteristic times during the sawtooth period.

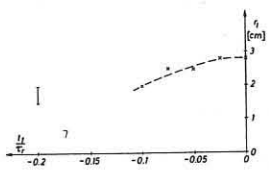

Fig.3: Radial position r_1 of the maximum modulation of the m = 1 mode during its stationary phase (I) and the flowing phase (X) in the sawtooth.

The energy balance inside the q = 1 surface can be evaluated from the electron temperature and density fluctuation in the sawtooth. The absolute and relative values of the electron temperature fluctuation strongly increase with increasing electron density. The relative density fluctuation is a factor of at least four smaller than the corresponding relative temperature fluctuation so that the density fluctuation is not important in the energy balance. Neglecting the profile factors, the electron energy loss during the internal disruption is given by $E_{al} = \frac{3}{2} n_e \Delta kT_e \cdot V_{al}$, where ΔT_e is the temperature drop during the internal disruption and V_{al} is the volume inside the q = 1 surface. This should be compared with the ohmic heating energy accumulated inside the q = 1 surface during one sawtooth period: $E_{ql} = U_L I_{al} \cdot \tau_r$, where U_L is the loop voltage and I_{al} is the current inside the q = 1 surface. As an example, one finds at the highest densities $E_{al} \approx 30$ J and $E_{al} \approx 120$ to 150 J. This means that only one-fourth or one-fifth of the ohmic heating energy inside the q = 1 surface, supplied during one sawtooth period, is lost through the internal disruption, the rest being lost through other loss mechanisms: e.g. energy transfer from electrons to ions and subsequent ion heat conduction loss, stationary electron heat conduction loss etc.

The power balance can also be described in terms of the energy replacement time. In Table I we compare for increasing densities the global electron energy replacement time τ'_{Ee} as obtained from the Thomson scattering measurement with a characteristic time $\tau''_{Ee} = \frac{\tau_r \Delta(nkTe)}{(nkTe)}$ of the internal disruption.

Table I

n_e cm^{-3}	2.5×10^{13}	6.5×10^{13}	10×10^{13}	14×10^{13}	17×10^{13}
τ'_{Ee} ms	2.2	3.6	5.1	5	5.2
τ''_{Ee} ms	4.6	6.5	8.9	14.3	17.0

This characteristic time describes the electron energy replacement time inside the q = 1 surface as given by the electron temperature drop during the internal disruption. At lower densities the ΔT_e value can be strongly in error so that τ'_{Ee} might be overestimated. At high densities the τ''_{Ee} values are quite accurate, so that the conclusion is again that, at least at high densities, the internal disruptions play only a minor role in the energy balance.

References:

/1/ S.von Goeler et al., Phys.Rev.Letters 33, 1201 (1974).
/2/ O.Klüber et al., Nucl.Fus. 15, 1194 (1975)

THE M=1 HELICAL MODE BEHAVIOUR DURING THE DISRUPTION INSTABILITY IN A TOKAMAK

S.V. Mirnov, I.B. Semenov

I.V. Kurchatov Atomic Energy Institute, Moscow, USSR

Experiments were performed for further studies of the disruptive instability in the T-4 Tokamak.

It was stated earlier /1/ that one may distinguish four following stages at this instability development:

1. Slow (during the times exceeding the skin ones) current channel narrowing due to helical perturbation development or radiation cooling of the periphery. The result is the drop of a safety factor q(r) up to 1 in the center and 2 at the periphery.
2. Pre-disruption is helical perturbation (t$\sim$500 μsec) development with m=2 azimuth number. The formation and destruction of the magnetic islands /2/. The process slightly touching the center but appearing outside as characteristic negative loop voltage spikes V(t)(0.5-10 V).
3. Mixturing is temperature and current (q(r), consequently) profile flattening after the pre-disruption. It can be described as m=0, n=0 perturbations.
4. Disruption itself is a nonlinear external helical m=2 mode development following the mixturing process, central plasma region turbulization, the broadening of the plasma column with mode m=2 passing into m=3 and m=4 /3/, a large negative voltage V(t) (up to 500 V) spike generation.

Development of the instability can be stopped itself at any of these stages considered.

Two phenomena are principally important: central mixturing and turbulization. As it was observed /1/ mixturing is followed by an internal perturbation with uneven m (m=1 is the most probable). It was assumed that the mixture is the development of m=1, n=1 /4/. This process is initiated by m=2 at the stage of prespike. It was assumed also that after the mixturing m=2 perturbation spreads all over the plasma column and causes turbulization. To check such a model the measurements of the soft X-rays were undertaken in the T-4 according to the scheme in Fig. 1a. $U_1=U_I-U_{II}$ and $U_2=U_{III}-U_{IV}$ were calculated, the sum difference $U_3=((U_I+U_{II})-(U_{III}+U_{IV}))/2$ and the sum $U_4=(U_I+U_{II}+U_{III}+U_{IV})/4$. U_1 and U_2 values are proportional to the m=1 mode, U_3 to m=2 and U_4 characterizes m=0. The result is given in Fig. 1b (prespike). The m=1 mode is the dominant perturbation near the center of the plasma column at the stage of the prespike. This is a wave propagating along the φ angle in the same direction as m=2 periphery mode. Both perturbations can probably be involved in joint toroidal motion as it was suggested in /5/.

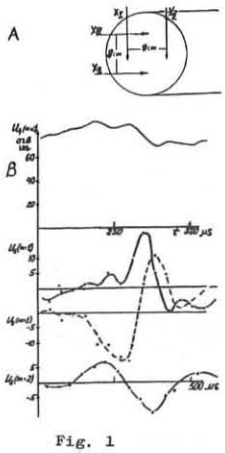

Fig. 1

Behaviour of internal perturbations in the stages of predisruptions and disruption is give in Fig. 2. The dotted field, given in Fig. 2 is curve, normalisated to value U_4. The comparison shows that the difference is in the internal perturbation amplitude the external ones ($\tilde{H}_\varphi$, V, A-A cross-section) are still equal (dotted line - pre-disruption). Joint development of the m=0 and m=1 modes is due the development of the m=1 helical perturbation. As it was stated above /1/, the next rise of m=2 perturbation and appearence of the large negative voltage spike V(t) (an arrow pointing down in Fig. 2 happened 30-100 μsec later the set up of mixturing. In our model it is assumed that the perturbation reaches the plasma column center at the same time. The time variation of the following values for one disruption is given in Fig. 3: U_4(m=0), U_2(m=1), U_2(m=1)/U_4(m=0), U_3(m=2), U_3(m=2)/U_4 (m=0). One can see, that during mixturing (drop of V(t)) m=2 perturbation really reaches the center. However, the accuracy of this method is low at low U_4. Thus we can speek of only the qualitative agreement with the model.

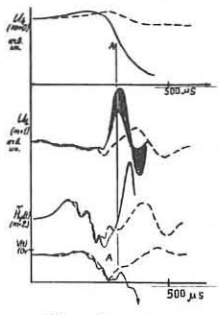

Fig. 2

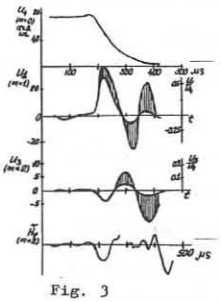

Fig. 3

An example of the strong connection of the m=2 periphery mode and m=1 central one is given in Fig. 4a (the level of m=2 is low in the center). A correlation of both frequencies is usually observed in this case. The example of another kind is given in Fig. 4b (a pre-disruption). The m=2 and m=1 perturbations are obviously connected in the initial stage, but at the next moment this strong connection is broken. In particular, the equality of frequencies is not observed (Fig. 3), or m=1 perturbation exists independently inside the plasma column at a low amplitude of the m=2 perturbation at the perefery. So, it should be noticed that the connection of the external m=2 and internal m=1 perturbations is more complicated than simple toroidal superposition of modes in the developed disruption stage.

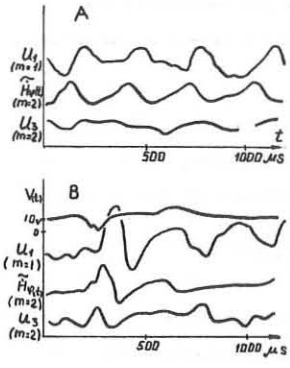

Fig. 4

Finally it is not clear whether the disruption model suggested is the real one. Is the desruption possible at m=2 in the centre and m=3 at the periphery? Really, when the m=3 periphery mode exists the phenomena observed are similar to pre-disruption. Possibly they are caused by the formation and destruction of magnetic islands at the periphery. But the transformation of such pre-disruptions to disruptions was not observed.

REFERENCES

1 S.V. Mirnov, I.B. Semenov, Preprint,IAE-2723, Moscow, 1976

2 S. von Goeler, Proc 7th Int. Conf. Lausanne, 2 (1975), 71

3 V.V. Vlasenkov et al., Proc. 5th Int. Conf. Tokyo 1(1974),33

4 S. von Goeler et al., Phys. Rev. Lett., 33 (1974), 120

5 F. Karger et al., Proc. 6th Int. Conf. Berchtesgaden, IAEA-CN-35/A-7 (1976)

FEEDBACK STABILIZATION OF AXISYMMETRIC MHD INSTABILITIES IN TOKAMAKS

E. Rebhan

Institut für Theoretische Physik, Universität Düsseldorf

A. Salat

Max-Planck-Institut für Plasmaphysik, 8046 Garching bei München

Federal Republic of Germany

Abstract: The possibility of stabilizing axisymmetric instabilities in vertically elongated tokamak plasmas by currents in toroidal loops is investigated.

In tokamaks without material limiters, vertically elongated cross-sections as desired for achieving higher ß values exhibit dangerous axisymmetric instabilities. Theoretically, these instabilities may be stabilized by a superconducting wall surrounding the plasma at some distance. However, in practice there is little chance of having this wall as close as needed.

The effect of stabilizing walls would be due to currents induced in the wall, whose magnetic field impedes the plasma motion. Since these induced currents are not uniformly distributed, some parts of the wall are more efficient than others. Thus, it is tempting to study stabilization by wall segments or simple toroidal conductors, both of these having better chances of technical realization.

As an idealization, in this paper we consider infinitely thin toroidal loops. Furthermore, we do not analyze the time dependent current induction and decay in passive conductors nor the detailed process of current regulation in a feedback control system. Depending on the number N and the position of the loops, we determine whether complete stabilization of all unstable perturbations is possible, what are the necessary loop currents, and what positions are optimum.

In practice, feedback must generally be supported by passive stabilization owing to the fast MHD growth times. Conversely, since passive stabilization can only reduce the growth rates [1], it must be supported by feedback, at least for long-time confinement.

As for the theoretical method, we have only considered linear stability and assumed a linear dependence between the stabilizing currents I_n and the amplitude of the plasma perturbation $\underline{\xi}$. On these assumptions a variational principle was derived:

$$\delta \left(\delta^2 W + \frac{1}{2} \sum_{n=1}^{N} I_n \oint_{\text{Pl.surf.}} y \, B_{\text{pol}} \, \underline{\xi} \cdot d\underline{S} \right) = 0$$

where $y = \underline{t} \cdot (\delta \underline{B}_v^1 - \delta \underline{B}_v^0)$, $\underline{t}$ = poloidal tangent vector, where $\delta^2 W$ and $\delta \underline{B}_v^0$ are, respectively, the usual plasma energy expression and perturbational vacuum field as obtained without external stabilization, while $\delta \underline{B}_v^1$ corresponds to stabilization with unit currents. Using the methods described in [2,3], this variational principle was numerically evaluated for the surface current model (SCM), and for a j = const model with elliptical cross-sections at aspect ratio A = ∞. It can be shown that in elongated plasmas the stabilizing currents must flow in loop pairs with antisymmetric current distribution as indicated in Fig. 1, because otherwise stable symmetric modes may be driven unstable.

If $\delta^2 W$ has only one negative eigenvalue, as was generally found for the SCM, a single pair of loops properly positioned may suffice for full stabilization. For the SCM, Figs. 1-3 show elliptical, triangular and rectangular plasma cross-sections (A = 3, β_p = 1, plasma region dotted, torus axis to the left). The stabilization by a single pair of loops, depending on its position on several concentric surfaces ($d = A/A_{\text{surface}}$), is shown: in the shaded regions stabilization is impossible; outside it is possible for sufficiently large currents. The shaded regions increase with the plasma elongation e until they fill the whole vacuum region (above e ≈ 8 for ellipses). On each surface arrows indicate the optimum loop position: there, among all unstable perturbations, the largest current needed for stabilization is lowest ($I = \max I(\underline{\xi}) = I_{\min}$). For ellipses, Fig. 4 shows $I/I_{\min}$ as a function of the poloidal angle u, and Fig. 5 shows $I_{\min}$ (normalized with the product I_{plasma} × amplitude of $\underline{\xi}$ in $1/(5\pi A)$ units) as a function of d.

Fig. 1

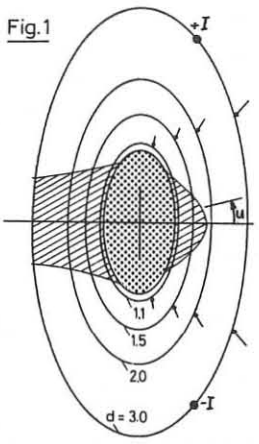

For the j = const model the results are qualitatively similar if e is not too large. For e > 4.5 there are more negative eigenvalues of $\delta^2 W$, and for each of them at least one pair of currents is needed. The pair(s) for each eigenvalue must be capable of reacting independently of the pair(s) for the others.

Fig. 2

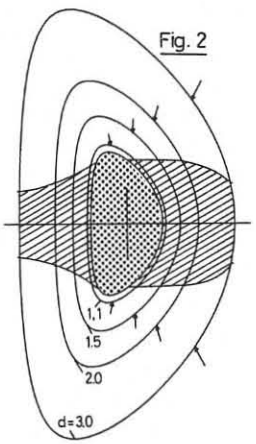

References

[1] Pfirsch, D., Tasso, H., Nuclear Fusion 11 (1971) 259

[2] Rebhan, E., Salat, A., Nuclear Fusion 16 (1976) 805

[3] Rebhan, E., Salat, A., IPP Report 6/150 (1976), to appear in Nuclear Fusion 17 (1977)

Fig. 3

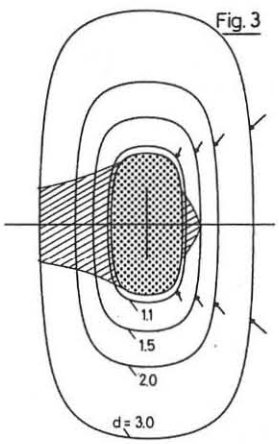

Fig. 4

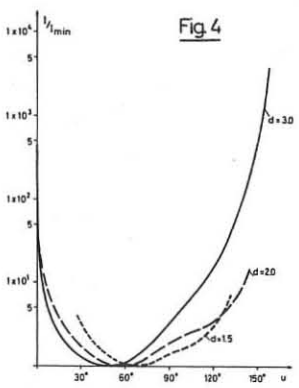

Fig. 5

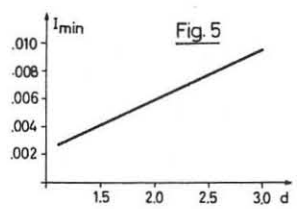

"This work was performed under the terms of the agreement on association between the Max-Planck-Institut für Plasmaphysik and EURATOM".

LOW FREQUENCY RESISTIVE AXISYMMETRIC MODES OF A TOKAMAK PLASMA

T. H. Jensen and W. B. Thompson*

General Atomic Company
San Diego, California, USA

Abstract: A formalism is described for calculating the properties of low frequency axisymmetric modes of a resistive plasma in a tokamak of arbitrary cross section.

1. INTRODUCTION

Generally for the confinement of a tokamak plasma, stability is required against motions on the magnetohydrodynamic (MHD) time scale since feedback stabilization of such modes is difficult. The properties of such fast modes may be calculated assuming that resistivity vanishes. Equilibria stable against these modes may yet be unstable against more slowly growing modes if finite plasma or wall resistance is allowed. One special class of resistive modes growing on a time scale between the MHD and the resistive scale has been described by Furth, Killeen, and Rosenbluth [1]. In the present paper modes with the still lower resistive time scale are considered. These are harder to stabilize, but because of their slow growth rate they are susceptible to feedback control.

2. FORMALISM

We give here a sketch of the ideas involved in the formalism which has been described in more detail elsewhere [2] and for simplicity restrict our arguments to straight geometry.

The unperturbed equilibrium is described by the usual MHD equilibrium equation

$$\nabla^2\psi_o + \mu_o j_o(\psi_o) = 0 \quad , \tag{1}$$

where ψ_o is the flux function, j_o is the z-component of the plasma current, and the symmetry $\partial/\partial z = 0$ is assumed. The perturbation of the flux function and the z-component of the plasma current are denoted ψ_1 and j_1, respectively. Because of the low frequency, inertial forces are neglected, so that the perturbed system is also in MHD equilibrium; therefore we have

$$\bar{\nabla}(j_o + j_1) \times \bar{\nabla}(\psi_o + \psi_1) = 0 \quad . \tag{2}$$

Retaining only first order terms, Eq. (2) provides a relationship between the perturbed quantities

$$j_1 = j_o'\psi_1 + J(\psi_o) \quad . \tag{3}$$

Here ' denotes differentiation with respect to ψ_o and $J(\psi_o)$ is an unspecified function of ψ_o only. First order perturbation of the z-component of Ohm's law,

$$\bar{E} + \bar{v} \times \bar{B} = \eta\bar{j} \quad , \tag{4}$$

and the assumption $\bar{\nabla} \cdot \bar{v} = 0$, which is appropriate for tokamaks with a strong axial magnetic field, allow determination of $J(\psi_o)$

$$J(\psi_o) = - j_o'\langle\psi_1\rangle - i\omega\,\eta_o^{-1}\langle\psi_1\rangle \quad . \tag{5}$$

Here, the flux function average is defined the usual way

$$\langle S\rangle \equiv \oint \frac{S\,d\ell}{|\bar{\nabla}\psi_o|} \Big/ \oint \frac{d\ell}{|\bar{\nabla}\psi_o|} \quad , \tag{6}$$

where the integrals are performed along equilibrium flux surfaces, $i\omega = \partial/\partial t$, and η_o is the equilibrium plasma resistivity assumed a function of ψ_o only. From Maxwell's equation and Eqs. (3) and (4) we get:

$$\frac{1}{\mu_o}\nabla^2\psi_1 + j_o'(\psi_1 - \langle\psi_1\rangle) - i\omega\,\eta_o^{-1}\langle\psi_1\rangle + j_{ex} = 0 \quad , \tag{7}$$

where j_{ex} represents perturbation currents other than the perturbation of the plasma current; j_{ex} may therefore include a source perturbing the plasma, such as currents from a feedback system or currents induced in external conductors. If the plasma is surrounded by a material wall of zero resistivity, induced currents in that wall are most simply taken into account as a boundary condition, namely that ψ_1 vanish at the wall.

Consider an eigenvalue equation closely associated with Eq. (7)

$$\nabla^2\phi_\nu + j_o'(\phi_\nu - \langle\phi_\nu\rangle) - i\omega\,\eta_o^{-1}\langle\phi_\nu\rangle - i\omega\,\eta_w^{-1}\phi_\nu + \lambda_\nu\phi_\nu = 0 \quad . \tag{8}$$

We assume, for example, that the plasma is surrounded by a wall of zero resistivity, and correspondingly the boundary condition for Eq. (8) is that ϕ_ν be zero at that wall. The term involving η_w, which is an arbitrary function of x and y, mimics the effect of axisymmetric resistive material within the perfectly conducting boundary as, for example, a vacuum chamber wall. One can readily show that the eigenfunctions of Eq. (8) have the fortunate property

$$(\lambda_\nu - \lambda_\mu)\int \phi_\nu\,\phi_\mu\,dA = 0 \quad , \tag{9}$$

where the integral is extended over the area, A, inside the conducting wall. This suggests that the eigenfunctions are orthogonal. When only natural modes are considered, i.e., $\lambda = 0$, one can show that ω must be purely imaginary, so that in this case all quantities of Eq. (8) are real. Thus, the equilibrium is unstable with the growth rate Ω_1 ($\equiv i\omega_1 > 0$) if there exists an eigenvalue such that $\lambda_\nu(\Omega_1) = 0$. Since we can show that $d\lambda/d\Omega \geq 0$, it is suggestive that the existence of any negative eigenvalue for $\Omega = 0$ means that the equilibrium is unstable. This has been formally proved by Tasso [3] and this result is very similar to that of the "Energy Principle" [4] for an ideal MHD plasma.

For doublets, it has been found by Chu and Miller [5] that ideal axisymmetric modes are unimportant in the sense that under conditions similar to those of experiments, no unstable modes exist. Using the above-mentioned formalism which allows for a finite plasma resistivity, calculations [6] show that under conditions similar to those of Doublet IIA [7], unstable axisymmetric modes may exist. Under the conditions surveyed, it was found that the most dangerous mode is one with two nodes passing through the elliptic axes. The associated deformation of the plasma corresponds either to an elongation or to compression of the plasma in the vertical direction.

ACKNOWLEDGMENT

This work was supported by the U. S. Energy Research and Development Administration, Contract No. EY-76-C-03-0167, Project Agreement No. 38.

REFERENCES

[1]. H. P. Furth, J. Killeen, and M. D. Rosenbluth, Phys. Fluids 6, 459 (1963).

[2]. T. H. Jensen vs. W. B. Thompson, "Low Frequency Response of a Resistive Plasma to Axisymmetrical Perturbations," General Atomic Report GA-A14334, to be submitted to J. Plasma Phys.

[3]. H. Tasso, Plasma Phys. 17, 1131 (1975).

[4]. I. B. Bernstein, et al., Proc. R. Soc. Lond. A244, 17 (1958).

[5]. M. S. Chu and R. L. Miller, "Wall Stabilization of Axisymmetric Modes in Noncircular Tokamak Plasmas," General Atomic Report GA-A14323, to be submitted to Phys. Fluids.

[6]. T. H. Jensen and F. W. McClain, to be submitted for publication.

[7]. R. L. Freeman, et al., in Plasma Physics and Controlled Nuclear Fusion Research (IAEA, Vienna, Austria, 1977), Vol. I, 317.

*Permanent address: Department of Physics, University of California La Jolla, California, USA

THREE DIMENTIONAL CODE FOR STUDYING OF MHD MOTION OF TOKAMAK PLASMA

A.F.Danilov, D.P.Kostomarov, A.M.Popov
Moscow State University

Yu.N.Dnestrovskii
I.V.Kurchatov Institute of Atomic Energy, Moscow, USSR

Experimental studies of the disruption instability in tokamaks showed that the initiating role of the disruption falls to a helical perturbation with m=2 (precursion), and then in the final stage of process the interaction between modes m=1, n=1 and m=2, n=1 could play an essential role /1/. The study of m=1 mode development considering finite conductivity (internal disruption), together with the formation and evolution of magnetic islands during m=2 mode exitations was investigated in /2-3/. M=2 mode instability was also discussed in /4-5/. The study of m=1, n=1 and m=2, n=1 mode interaction should be done both in cylindrical and toroidal geometry basing on a three-dimentional MHD system. First results of similar studies were reported in /6/. This paper concerns with the development of these simulations.

The system of magneto-hydrodynamics equations including finite conductivity and viscosity was written in the following form

$$\frac{\partial \rho}{\partial t} + \mathrm{div}(\rho\vec{v}) = 0 \ , \quad \frac{\partial \vec{H}}{\partial t} - \mathrm{rot}[\vec{v}\vec{H}] = \nu \Delta \vec{H} \ ,$$

$$\rho\frac{\partial \vec{v}}{\partial t} + \rho(\vec{v}\nabla)\vec{v} = -\nabla P - [\vec{H}\,\mathrm{rot}\,\vec{H}] + \eta \Delta \vec{v}, \quad P = \beta\rho$$

The units of measurement are similar to those in /6/ - they are alfvenous relating to the poloidal field. It is assumed that plasma reaches the conducting shell, the latter having a square cross - section. The boundary conditions are $\vec{v}\big|_\Gamma = 0, \ \vec{H}\big|_\Gamma = \vec{H}\big|_{\Gamma, t=0}$

The computations were made in the cylindrical and toroidal geometry. Equilibrium P and $\vec{H}$ values were obtained by a numerical solution of the equilibrium equation for the poloidal field potential ψ. The exitation of plasma oscillations was determined by the initial velocity distribution.

It is observed during the experiments that the m=2 mode oscillations (precursion) cause m=1 mode development at some definite conditions when $q(a)=2.5-3$, and $q(0) \simeq 1$, which, in its turn, flattens $j(r)$ current profile. In this paper the model of such process is held by means of the system of equations given above. The initial equilibrium state of magnetic field was taken when $q\big|_\Gamma = 2.9$ and $q(0)=1.02$. This state corresponded to the solution of the equilibrium equation when $j(\psi) \sim \psi^2$. The profiles q(x) and $j_z(x,0,L/2)$ are given in Fig.1 for this equilibrium state. There is a resonant surface for the m=2, n=1 mode. The trace of this surface on the x-axis is equal to $x_s=0.7$. There is no resonant surface for the m=1, n=1 mode in the region of plasma. The equilibrium state was initiated by a mixture of two modes: m=1, n=1 with $A_1=0$; 0.1; 0.2 amplitudes and m=2, n=1 with $A_2=0.1$ amplitude. It was suggested that $\nu = 5\cdot10^{-4}$ in the computations.

The main result is the following: the stationary motion of the large amplitude mode m=2, n=1 (in our case when $H_\parallel/H_\perp = 8$ and $x_s=0.7$ the m=2 mode places near the marginal stability level $\omega\sim0$) leads to the formation of current layers, and the current density greatly increases in the vicinity of the center. The current growth and localization lead to a resonant surface appearance at $x_s=0.3$ for the m=1, n=1 mode. Then the m=1 mode instability develops leading to the current flattening. The distribution of the longitudinal current $j_z(x,0,L/2)$ is given in Fig.2 for different time moments. The equilibrium current distribution (t=0) is given in a dotted line, curve II corresponds to a pure m=2, n=1 mode exitation with $A_2=0.1$ amplitude at t=8, curve III corresponds to a mixture of modes with amplitudes $A_1=0.1$, $A_2=0.1$ at t=8.
In Fig.3 one may see the magnetic field profile $H^*(x)=H_y(x,0,\frac{L}{2})-k_z x H_z(x,0,L/2)$ which characterizes the m=1 mode at t=0 (dotted line) and at t=4. The x_s points where $H^*(x_s)=0$ correspond to the m=1, n=1 mode resonant surface.

REFERENCES

1. S.V.Mirnov, I.B.Semenov, preprint IAE-2723, M. 1976.
2. A.F.Danilov, Yu.N.Dnestrovskii, D.P.Kostomarov, A.M.Popov, Fizika Plazmy, 2, 167, 1976; 3, 213, 1977.
3. R.W.Waddel, M.N.Rosenbluth, D.A.Monticello, R.B.White, Nucl. Fusion, 16, 528, 1976.
4. D.Biskamp, H.Welter, 6-th Intern. Conf. on Plasma Phys. and Control. Nucl.Fus.Res. IAEA-CN-35/B2-2, 1976.
5. N.I.Gerlach, N.M.Zueva, L.S.Soloviev, preprint IPM, N84, 1976.
6. A.F.Danilov, Yu.N.Dnestrovskii, D.P.Kostomarov, A.M.Popov, 6-th Intern.Conf. on Plasma Phys. and Contr.Nucl.Fusion Res., IAEA-CN-35/B2-3, 1976.

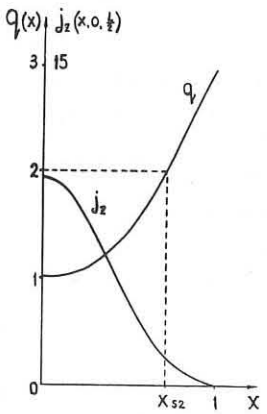

Fig. 1

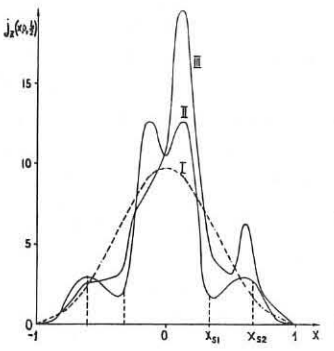

Fig. 2

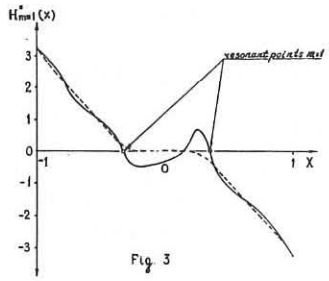

Fig. 3

RELAXATION OSCILLATIONS IN MHD-UNSTABLE PLASMAS

E.K. Maschke

ASSOCIATION EURATOM-CEA SUR LA FUSION
Département de Physique du Plasma et de la Fusion Contrôlée
Centre d'Etudes Nucléaires
Boite Postale n° 6. 92260 FONTENAY-AUX-ROSES (FRANCE)

ABSTRACT : We consider a plasma which is governed by MHD equations with finite viscosity and thermal conductivity, and which is driven unstable by an applied heat source. It is shown that the system may exhibit periodic relaxations of the temperature profile.

In a preceding paper [1] it has been shown that in a weakly unstable plasma governed by MHD equations including viscosity and thermal conductivity, stationary states of large-scale convective motion may exist, which are characterized by strongly anomalous transport. The investigation of ref.1 had been motivated by the discovery of anomalous heat transport in the center of Tokamak discharges [2] when the safety factor q decreases below unity. Later experiments [3, 4] revealed that this anomalous heat transport occurs in the form of periodic relaxations of the electron distribution. Although it is probable that in the experiments (ref.3, 4) the instability includes the formation of magnetic islands, we wish to pursue here the original idea of ref. 1 and show that a simple curvature-driven instability in a shearless magnetic field configuration may give rise to relaxation oscillations.

We consider a cylindrical plasma layer bounded by surfaces $z = 0, L$ and $r = r_o \pm d/2$ (with $d \ll r_o$), and placed in a curved magnetic field $\vec{B} = B\vec{e}_\theta$. We define characteristic times and velocities in terms of the perpendicular viscosity ($\mu_\perp$) and the heat conductivity $\varkappa$ by putting $\tau_{visc} = d^2 n_o m_i/\mu_\perp$, $v_{visc} = d/\tau_{visc}$, $v_{hc} = \varkappa/(n_o d)$. We then normalize as follows :

$$t/\tau_{visc} \to t\,, \quad r/d \to r\,, \quad z/d \to z\,, \quad \vec{v}/v_{hc} \to \vec{v}\,, \quad T/T_o \to T\,, \quad B/B_o \to B\,,$$

and we define

$$\mathcal{P} = v_{hc}/v_{visc}\,, \qquad \Gamma = v_{th}^2/(v_{hc}\, v_{visc})\,, \qquad \beta = n_o T_o/B_o^2\,.$$

We assume that all quantities are independent of θ, and $v_\theta = 0$. Assuming also constant density, $n/n_o = 1$, we use the following equations :

$$\left(\frac{\partial}{\partial t} + \frac{1}{\mathcal{P}}\vec{v}.\nabla\right)\vec{v} = -\Gamma\left[\nabla T + \frac{1}{\beta}\frac{1}{r}\nabla\frac{(rB)^2}{2}\right] - \nabla.\vec{\vec{\Pi}} \qquad (1)$$

$$\frac{3}{2}\mathcal{P}\left(\frac{\partial}{\partial t} + \frac{1}{\mathcal{P}}\vec{v}.\nabla\right)T = \nabla^2 T + S(T) \quad \text{with} \quad S(T) = S_o + S_1 T \qquad (2)$$

$$-\mathcal{P}\frac{\partial B}{\partial t} = r\vec{v}.\nabla\left(\frac{B}{r}\right) \qquad (3) \qquad ; \qquad \nabla.\vec{v} = 0 \qquad (4)$$

Assuming all quantities to be periodic functions of z, an arbitrary quantity X may be written as $X = \langle X\rangle + \tilde{X}$ with $\langle X\rangle = (1/L)\int_0^L X dz$. We assume $\langle\vec{v}\rangle = 0$. Averaging eq.(2) we obtain

$$\frac{3}{2}\mathcal{P}\frac{\partial\langle T\rangle}{\partial t} + \frac{3}{2}\frac{1}{r}\frac{\partial}{\partial r}\left(r\langle\tilde{T}v_r\rangle\right) = \frac{1}{r}\frac{\partial}{\partial r}r\frac{\partial\langle T\rangle}{\partial r} + S_o + S_1\langle T\rangle \qquad (5)$$

We derive two integral relations for $\tilde{T}$ and v. From eq.(2) we obtain :

$$\frac{3}{2}\mathcal{P}\frac{d}{dt}\int_{r_o-1/2}^{r_o+1/2} dr\, r\langle\tilde{T}^2\rangle + \frac{3}{2}\int_{r_o-1/2}^{r_o+1/2} dr\, r\langle\tilde{T}v_r\rangle\frac{\partial\langle T\rangle}{\partial r} = \int_{r_o-1/2}^{r_o+1/2} dr\, r\langle\tilde{T}\nabla^2\tilde{T}\rangle + S_1\int_{r_o-1/2}^{r_o+1/2} dr\, r\langle\tilde{T}^2\rangle \qquad (6)$$

From eq.(1) we find, neglecting terms of order $1/r_o$,

$$\int_{r_o-1/2}^{r_o+1/2} dr\,\langle\tilde{v}.\frac{\partial\tilde{v}}{\partial t}\rangle = -\frac{2\Gamma}{r_o}\int_{r_o-1/2}^{r_o+1/2} dr\,\langle v_r\tilde{T}\rangle + \int_{r_o-1/2}^{r_o+1/2} dr\,\langle v_r\nabla^2 v_r + v_z\nabla^2 v_z\rangle \qquad (7)$$

In the last term (viscosity term) we have used the assumption that r_o is large enough so that $\mu_{//}/r_o^2 \delta \lesssim \mu_\perp$.

The boundary conditions for T are $T = T_1 = \text{const.}$ for $r = r_o - 1/2$, $\partial T/\partial r = 0$ for $r = r_o + 1/2$. The heat source then causes the temperature gradient to increase from zero until the condition for onset of instability is satisfied. This condition, which is derived by linearizing eqs. (1) - (4) [see ref. 1], requires that the "Rayleigh number" $\mathcal{R} = (2\Gamma/r_o)|dT/dr|_m$ exceeds a critical value $\mathcal{R}_{crit}$ ($|dT/dr|_m$ is a suitable mean value of dT/dr). Using the boundary conditions $v_r = 0$, $\partial v_z/\partial r = 0$ at $r = r_o \pm 1/2$, one finds a marginal mode of the form (assuming $|S_1| \ll \pi^2 + k^2$).

$$v_r = A_v \cos\pi(r - r_o)\sin kz\,, \qquad v_z = -\frac{\pi}{k}A_v \sin\pi(r - r_o)\cos kz$$
$$\tilde{T} = -\frac{3}{2}\frac{|dT/dr|_{crit}}{\pi^2 + k^2}A_T \cos\pi(r - r_o)\sin kz \qquad (8)$$

where at the marginal point $A_T = A_v = \text{const.}$ We now assume* that for $\mathcal{R} > \mathcal{R}_{crit}$ the eqs. (8) are still valid if we replace $A_v \to A_v(t)$, $A_T \to A_T(t)$. Introducing this in eq. (7) we obtain

$$\frac{dA_v}{dt} = (\pi^2 + k^2)(A_T - A_v) \qquad (9)$$

Due the large factor $(\pi^2 + k^2) \gg 1$, an approximate solution is

$$A_v(t) \approx A_T(t) \qquad (9a)$$

Using (8) and (9a) in eq. (6) we obtain

$$\frac{dA_T}{dt} = \frac{\pi^2 + k^2}{3\mathcal{P}}\left[G(t) - 1\right]A_T\,, \qquad \text{hence} \qquad A_T = A_o\, e^{(\mathcal{P}/2)y(t)} \qquad (10)$$

where

$$G(t) = \left[\int_{r_o-1/2}^{r_o+1/2} dr\,\cos^2\pi(r - r_o)\left(\frac{\partial\langle T\rangle/\partial r}{|dT/dr|_{crit}}\right)\Big/\int_{r_o-1/2}^{r_o+1/2} dr\,\cos^2\pi(r - r_o)\right] \approx \frac{(\partial\langle T\rangle/\partial r)_{r_o}}{|dT/dr|_{crit}} \qquad (11)$$

and

$$y(t) = \frac{2}{3}\frac{\pi^2 + k^2}{\mathcal{P}}\int_{t_o}^{t}\left[G(t') - 1\right]dt'$$

From eq. (5) we can derive an approximate equation for G(t). Using the variable y(t) rather than G(t) we obtain

$$\frac{d^2y}{dt^2} = \Sigma - \Lambda A_o^2 e^{y} + \alpha\frac{dy}{dt} \qquad (12)$$

where

$$\Sigma = \frac{4}{3}\frac{\pi^2 + k^2}{\mathcal{P}^2}\frac{S_o + S_1 T_1}{|dT/dr|_{crit}}\,, \qquad \Lambda = \frac{2}{3}\frac{1}{\mathcal{P}^2}\,, \qquad \alpha = \frac{2}{3}\frac{1}{\mathcal{P}}\left(S_1 - \frac{4}{3}\right)$$

Let t_o be the time at which the temperature gradient reaches for the first time the critical value for onset of instability, that is, $(dy/dt)_{t_o} = G(t_o) - 1 = 0$. The time behaviour of the system is governed by the solution y(t) of eq. (12). A first integral of (12) is

$$\frac{1}{2}\left(\frac{dy}{dt}\right)^2 + V(y) = \mathcal{E}(t)\,, \qquad \text{with} \quad V(y) = -\Sigma y + \Lambda A_o^2(e^y - 1)\,, \quad \mathcal{E}(t) = \alpha\int_{t_o}^{t}\left(\frac{dy}{dt}\right)^2 dt$$

Interpreting dy/dt as a velocity, V (y) as a potential, $\mathcal{E}(t)$ as total energy, we see that for $\alpha \neq 0$ there are two types of solution :

1. $\alpha < 0$, $\mathcal{E}(t)$ decreases until dy/dt = 0, that is, until a stationary convective state is reached (Fig. 1b).

2. $\alpha > 0$, $\mathcal{E}(t)$ increases with time. The solution oscillates, with the successive maxima of A_T increasing in time and the successive minima decreasing (Fig.1c).

The second type of solution does not correctly describe the physical reality because at successive passages through the marginal situation (dy/dt = G(t) - 1 = 0), y becomes more and more negative so that A_T takes indefinitely decreasing values. Physically, the minimum of the perturbation amplitude is determined by the level of thermal fluctuations. This feature is not contained in our equations, but it can be incorporated in the phase diagram of Fig. 1a by observing that the first cycle of the path describes the physical situation correctly up to the point where y = 0. At this point the path of the physical system follows the (dy/dt) - axis until the origin is reached, where the cycle begins again. This physical path is shown by a full line in Fig. 1c. The forms of G(t) and $A_T(t)$ corresponding to this full line are shown in Fig. 2, from which it appears that G(t) (and thus $d\langle T\rangle/dr$) has the form of periodic relaxation oscillations.

REFERENCES.-

[1] E.K. MASCHKE and R.B. PARIS, Proc. V. Conf. Plasma Physics and Controlled Nuclear Fusion Research, Tokyo 1974 (IAEA, Vienna 1975).

[2] D.L. DIMOCK et al., Nucl. Fusion 13 (1973) 271.

[3] S.v. GOELER, W. STODIEK, N. SAUTHOFF, Phys. Rev. Lett. 33 (1974) 201.

[4] Equipe TFR, Proc. VI. Conf. Plasma Physics and Controlled Nuclear Fusion Research, Berchtesgaden 1976 (IAEA, Vienna 1977).

* The assumption of a single mode, made for reasons of simplicity, is justified in particular geometries (e.g. toroidal) and requires in our case that the cylinder length L be small (L ~ d).

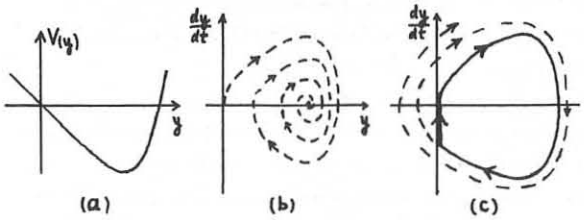

Fig. 1

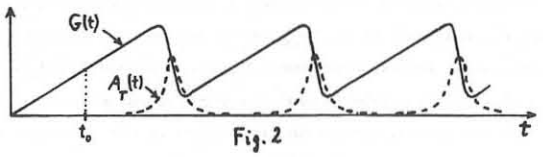

Fig. 2

MHD STABILITY FOR A CLASS OF TOKAMAK EQUILIBRIA WITH FIXED BOUNDARY

W. Kerner

Max-Planck-Institut für Plasmaphysik, 8046 Garching bei München

Federal Republic of Germany

Abstract: The stability limit with respect to internal modes is computed for a class of tokamak equilibria with noncircular cross-sections and essentially flat current profiles. It is found that the Mercier criterion is necessary and sufficient for stability.

Introduction: In this paper we present results obtained with a computer code which solves for the complete spectrum of normal modes in the ideal MHD model. The method consists in extremizing the Lagrangian of the system connected with linearized perturbations around an equilibrium state. The displacement vector is expanded in terms of global Fourier-Bessel functions.

The class of tokamak equilibria considered is defined by the flux function

(1) $\Psi \propto [Z^2(X^2-R^2\delta) + \alpha^2(X^2-R^2)^2/4]$

and is described in detail in Ref. [1], [2] Near the magnetic axis the flux surfaces are ellipses with a half-axis ratio

(2) $e = \alpha/(1-\delta)^{1/2}$, becoming Dee-shaped further outwards. The constant δ, which labels the poloidal current, is restricted to values $\delta < 1-2\varepsilon$, where ε is the inverse aspect ratio.

The first application of the code, Ref. [1] has given the result that toroidal effects are destabilizing with respect to external kinks. In this paper we discuss the stability behavior for fixed boundary (internal) modes. The connection of gross modes with the stability limit of a necessary criterion (Mercier) is examined. It is also discussed whether MHD-stable high-beta equilibria exist.

Results and Discussion: In Ref. [3] a simple form of the necessary criterion for our equilibrium is derived which is valid for a small inverse aspect ratio ε. The value of the safety factor at the axis, which is necessary for stability, is given by

(3) $1/q(0)^2 < 6/(1+e^2) - 4/e(e+1) + Q[4/e(e+1) - 2]$,

where $Q = -\delta/(1+\alpha^2-\delta)$.

We begin the stability analysis for configurations with a large aspect ratio $\varepsilon^{-1} = 10$.

The first interesting result is that for a circular cross-section, $e \equiv \alpha/(1-\delta)^{1/2}=1$, no unstable mode with a toroidal wave number $n = 1$ exists. The stability limit $q(0) = 1$ from equ. (3) is approached by modes with a toroidal wave number $n \to \infty$ and a dominant Fourier component l_o in the poloidal direction $l_o = n - 1$. Instabilities then exist for $q(0) \simeq l_o/n = (n-1)/n$. We are able to find such unstable modes for $2 \le n \le 14$.

Next we keep $n = 1$ and $q(0) = 1$ fixed and vary the elongation e. The marginal points obtained from the code agree better than 2% with the marginal points from the necessary criterion. The corresponding eigenfunctions are global. In Table 1 we have listed the computed critical elongation for marginal stability together with the corresponding critical safety factor from equ. (3). The two marginal points e_{cr} define an interval in e with stability with respect to the $n = 1$ mode. If for an unstable mode the elongation e approaches the value e_{cr}, the interval in q(0) for which instabilities exist shrinks to one point $q(0) = l_o/n$. For $n = 1$ and $l_o = 1$ this point is $q(0) = 1$, which is marginally stable according to Mercier [4]. The conclusion is that the Mercier criterion is also sufficient for stability. This result is confirmed for many different values of n and q(0) where the parameters α and δ are varied.

It is an important question whether additional instabilities occur for a small aspect ratio. It turns out that the toroidicity improves the stability behavior. All the previous results concerning the $n = 1$ mode are also valid for an aspect ratio $\varepsilon^{-1} = 3$ or smaller. No ballooning type modes are found. Therefore, the Mercier criterion is sufficient for stability of internal modes for this entire class of equilibria. Then MHD-stable, high-beta equilibria ($\beta_T > 10\%$) exist. A diamagnetic current profile $1-2\varepsilon > \delta > 0$ is favorable, also a Dee-shaped cross-section.

In Fig. 1 the growth rates of unstable $n = 3$ modes, normalized to the poloidal Alfvén velocity, are plotted versus the safety factor for a JET-like configuration, $\varepsilon^{-1} = 4$ and $e = 2$, with two different values of β_p. The plasma density is kept constant. The two cases with $\delta = 0$ and $\delta = 0.4$ differ in the stability boundary of the necessary criterion, $q_{cr} = 1.36$ for $\delta = 0$ and $q_{cr} = 1.18$ for $\delta = 0.4$. The diamagnetic current distribution ($\delta = 0.4$) stabilizes the $n = 3$ and $l_o = 4$ modes. But the $l_o = 3,2$ and 1 modes are unstable and strongly coupled in both cases.

References

[1] Kerner, W. Nucl. Fusion 16 (1976), 643

[2] Kerner, W., Tasso, H. in Plasma Physics and Controlled Nuclear Research (Proc. 5th Int. Conf. Tokyo, 1974), 1, IAEA, Vienna (1975) 475

[3] Lortz, D., Nührenberg, J. Nucl. Fusion 13 (1973), 821

[4] Mercier, C. Nucl. Fusion 4 (1964), 213

"This work was performed under the terms of the agreement on association between the Max-Planck-Institut für Plasmaphysik and EURATOM".

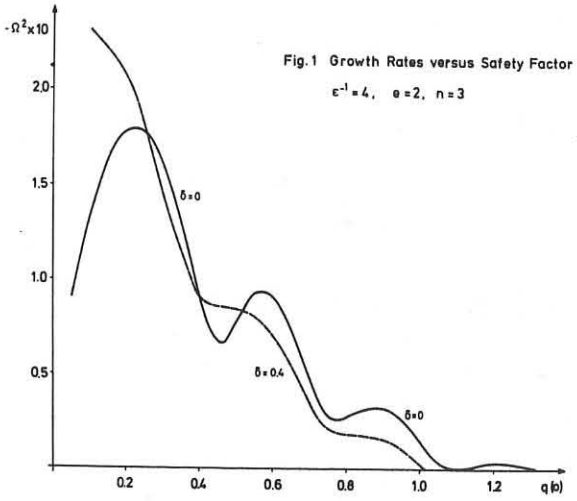

Fig.1 Growth Rates versus Safety Factor
$\varepsilon^{-1}=4$, $e=2$, $n=3$

Table 1: Numerical evidence for sufficiency of the Mercier criterion
$\varepsilon^{-1} = 10$, $n = 1$, $q(0) = 1.0$

δ	e_{cr}(code)	q_{cr}(Mercier)
-2	0.40	1.02
	1.015	1.008
-1	0.56	1.017
	1.015	1.003
0	0.93	1.005
	1.10	1.008
0.5	0.987	1.005
	1.66	1.003
0.75	0.985	1.02
	2.60	1.02

Numerical Study of the Effect of Current Peaking on the MHD Stability of a Small Aspect Ratio Tokamak

D. Berger, R. Gruber, F. Troyon

Centre de Recherches en Physique des Plasmas
Ecole Polytechnique Fédérale
CH-1007 Switzerland

Abstract : We investigate numerically the effect of peaking the current distribution of a small aspect ratio Tokamak with a D-shaped cross section on the MHD stability of the n=1 modes. The evaluation of the most unstable mode is followed as a function of q at the plasma surface, for a fixed value of q on axis. Two different shapes and three values of β_p are examined.

Introduction : The low-n MHD stability of flat current, small aspect ratio toroidal equilibria has been investigated with spectral codes {1,2}. The main results are the sufficiency of Mercier's criterion for internal modes (at least for $\beta_p < 1$) and the presence of external kinks for all values of the safety factor q. In a straight circular system J. Wesson {3} has shown that current peaking eliminates the external kink, leaving presumably the internal kink and the Mercier modes as the most dangerous modes. We investigate numerically the same problem for a class of toroidal equilibria, using the ERATO {4} spectral code.

Equilibrium : An equilibrium is characterized by the shape of the plasma surface and by the derivatives of the pressure $p(\psi)$ and of the toroidal flux $T(\psi)$. The surface is given by the equation

$$\frac{z^2 r^2}{E^2} + \frac{(r^2-R_0^2)^2}{4} = R_0^4/9 \ ,$$

where R_0 is a length which corresponds to the radius of the magnetic axis when the current is flat, and E is the elongation. It corresponds to an aspect ratio of 3. For $p'(\psi)$ and $T'(\psi)$ we take

$$p'(\psi) = p_0 \{ \exp(-\nu\psi^2) - 1\}$$
$$T'(\psi) = R_0^2(1/\beta_p - 1)\ p'(\psi)/T(\psi)$$

where ν characterizes the width of the current distribution and β_p is the poloidal beta. The flux ψ is normalized such that it vanishes at the surface. p_0 is a free parameter. An equilibrium is completely characterized by the safety factor on axis q_0, its value on the surface q_s, β_p and E.

Stability : We study the influence of ν, respectively q_s, on the stability, keeping the other parameters E, β_p and R_0 constant. The equilibrium for each case is computed with the ORNL code and introduced in the stability code. We only look for the n=1 modes, assuming they will be the last ones to be stabilized just as in the straight case.

$E = 1$, $\beta_p = 1$: The results for this case are shown in Figs. 1. The square of the growthrates Γ^2 of the most unstable mode is plotted versus the safety factor at the surface q_s, for two values of q_0. The normalizing frequency ω_T is given by $\omega_T^2 = T^2(\psi_0)/R_0^4\rho_0$. The solid lines are results obtained with an infinite vacuum region surrounding the plasma. The dashed lines are obtained with a conducting shell tight against the plasma surface. For $q_s < 2.5$ the mode is an external kink. Each magnetic surface gives a negative contribution to the potential energy. As the peaking increases the mode changes its character, becoming progressively internal. Extrapolating the sharp drop in growthrate of the kink (dotted line) we can define the point where it cuts the q_s axis as the stability limit for the kink. It corresponds to $q_s/q_0 \approx 2.8 q_0$. In the straight case it is $q_s/q_0 = 2.0$ {3}. For larger values of q_s the mode structure depends on q_0. For large values of q_0 the kink limit is the stability limit. As q_0 decreases towards 1, the stability limit moves up from the kink limit and for $q_0 < 1$ the instability remains for all q_s. When $q_0 > 1$ and $q_s > 2.8 q_0$ the modes are called ballooning because they correspond to q_0 larger than Mercier's limit ($q_m \approx 1$). The negative contribution to the potential energy mainly comes from the region inside the q=2 surface. For $q < 1$ the residual mode is definitely an internal kink with most of the destabilizing contribution coming from the region inside the surface $q = 1$. It is interesting and surprising to note that peaking destabilizes the internal modes (dashed lines). For each case characterized by a fixed value of q_0, the stability limit in q_s corresponds to a maximum value for $\bar{\beta}$. For example, for $q_0 = 1.1$, the marginal point at $q_s \approx 4.2$ gives an average β limit of $\bar{\beta}_{max} \approx 1.1\%$.

β-limitation : Because of the computing effort required (1 point=1 high resolution equilibrium) we have not yet been able to vary continuously the parameters β_p and E but we do have some results which show definite trends. Increasing β_p leads to a wider unstable region for the ballooning modes and a shift to higher q_s of the whole curve, thus partially offsetting the expected gain in $\bar{\beta}_{max}$. Increasing the elongation from 1 to 2 does not change the stability limit for the kink but destabilizes the internal modes. The results for $\bar{\beta}$ obtained in these runs are shown in Figure 2. They show the maximum value of $\bar{\beta}$ which can be reached for a given value of q_0 by optimizing the current profile. We see that increasing the elongation and the poloidal beta increases $\bar{\beta}$, but more work is needed before we can ascertain the dependence of β_{max} on these parameters.

We thank the staff of the Computing Center for their help and understanding. This work is supported in part by the Swiss National Science Foundation.

References

{1} W. Kerner, Nuclear Fusion 16, 643 (1976)

{2} D. Berger, L.C. Bernard, R. Gruber and F. Troyon, IAEA VI, Berchtesgaden, Paper CN-35/B11-4 (1976)

{3} J. Wesson, VIIth European Conference on Controlled Fusion and Plasma Physics, Vol. 2, p. 102

{4} D. Berger, R. Gruber, F. Troyon, 2nd European Conference on Computational Physics (1976), C3

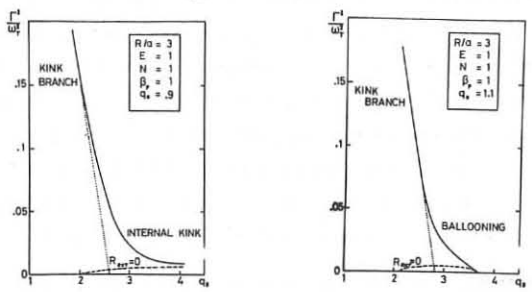

Figure 1. Dependence of the normalized growthrate Γ^2/ω_T^2 of the most unstable n=1 mode on q_s, for two values of q_0. No shell ——— . Shell against the plasma ------- .

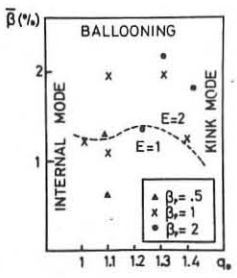

Figure 2. Representation of the optimized average beta value $\bar{\beta}$ versus q_0 for different values of β_p and E. The values below the dashed line are for E=1 and those above for E=2.

Numerical MHD Stability Calculations of a D-Shaped Elongated, Small Aspect Ratio Tokamak

D. Berger, L.C. Bernard, R. Gruber, F. Troyon
Centre de Recherches en Physique des Plasmas
Ecole Polytechnique Fédérale
Ch-1007 Lausanne, Switzerland

Abstract : We report here on a numerical study of the MHD stability of a specific equilibrium met in the design of a variable configuration Tokamak (TCV) characterized by $\beta_p = 0.5$, an elongation of 2, an aspect ratio of 3 and which appears to be stable up to a $\bar{\beta}$ of the order of 2%.

1. Introduction : One of the main objectives of the present Tokamak fusion program is to show the possibility of increasing the maximum β value. The FCT concept {1} relies on an increase in β_p hoping that the stability limit will not change. Another possibility consists in changing the shape of the plasma. Reducing the aspect ratio and increasing the elongation are generally believed to increase the maximum β.

2. Equilibrium : Figure 1 shows the surfaces of constant magnetic flux in the upper half plane of such a TCV equilibrium with an aspect ratio of 3 and an elongation of 2. The plasma is surrounded by a rectangular limiter and held by 4 outer and 8 inner poloidal field coils. The values besides the coils denote the currents normalized to the total current in the plasma. The equilibrium has been calculated by the ORNL equilibrium code {3}. The two arbitrary functions $p(\psi)$ and $T(\psi)=rB_{tor}$ are given by $p(\psi) = p_0 + p_1\psi + p_2\psi^2 + p_3\psi^{L+1}$ and $T^2(\psi) = T^2_{lim} + 8\,R_0^2\,(1/\beta_p - 1)\,p(\psi)$. The parameters p_0, p_1, p_2, p_3, L and β_p are chosen such that the pressure p, its derivative with respect to ψ, p', and the toroidal current density j_φ are zero on the plasma boundary. The half width of the current profile is 0.5.

3. Axisymmetric modes : Using our general purpose spectral code ERATO {3}, we find that the described equilibrium is unstable to n=0 perturbations when no conducting shell surrounds the plasma. The growthrates are typical of external kinks, too fast to be held directly by a feedback system. These modes can be stabilized by a conducting wall. A shell at a constant distance of $(R_{ext}-1)$ times the plasma radius is moved from ∞ to $R_{ext} = 1.5$. The growthrate squared is plotted in Fig. 2 as a function of R_{ext} and shows a stabilization of the n=0 mode for $R_{ext} \approx 1.6$. This means that these modes can in principle be stabilized by a feedback system which only serves to compensate the Ohmic losses of the wall.

4. Low n-modes : In Fig. 3, the growthrate of the most unstable n=1 mode is plotted versus q_0, the safety factor on axis, for the case there is an infinite vacuum region around the plasma. An uncertainty remains as to the precise location of the marginal point due to the number of mesh points used (48x24) in these computations, hence the stability limit could be slightly lower. As q_0 decreases, the mode initially located near the axis becomes more extended and, for much lower q_0 values, will eventually become an external kink. Near the marginal point, the mode seems to localize itself around the q=1 surface. The stability limit for n=1 is around q_0=0.85 which corresponds to a $\bar{\beta} = 2.3\%$. The n=2 modes, however, are found not to be unstable in the range $q_0 \gtrsim 0.5$. For n=3 the large number of singular surfaces within the plasma (13 for $q_0 \lesssim 1$) precludes any reliable conclusions with our present resolution.

5. High n-modes : For large values of n, Mercier's criterion provides a necessary stability condition which is in our case more stringent than the low-n stability requirement. This had been observed already for the Solovev equilibrium with a rigid boundary {4}, but there was no reason to believe it was general. Mercier's criterion is local and it can be tested at all radii. The region where it is violated is shown in Fig. 4 as a function of q_0. For $q \gtrsim 1$ it is satisfied everywhere. For $q_0 < 1$ there is an unstable region between the centre, where $q = q_0$, and a surface characterized by $q = q_\ell$. Since q at the surface is of the order of 4 times q_0, we see that these modes are not important. Even at high n, Mercier's criterion is not sufficient as there may be ballooning modes. No information is available on these modes, which are expected to be important only at higher values of β_p.

6. Conclusions : For a $\beta_p = 0.5$ and an elongation of 2 the stability limit for $n \neq 0$ is of order of $q_0 = 1$, just as in the circular case. With increasing current, the first modes to become unstable are localized Mercier modes or high n ballooning modes near the axis, whereas n = 1 is stable up to $q_0 = 0.85$, corresponding to $\bar{\beta} = 2.3\%$. The n=0 modes have to be stabilized by a feedback system combined with a shell.

This work has partly been supported by the Swiss National Science Foundation.

References :

{1} J.F. Clarke, D.J. Sigmar, Phys.Rev.Lett. 38 (1977) 70

{2} J.D. Callen, R.A. Dory, Phys.Fluids 15 (1972) 1523

{3} D. Berger, R. Gruber, F. Troyon, 2nd Europ. Conf. on Comp. Phys., Garching (1976), Paper C3

{4} D. Berger, L.C. Bernard, R. Gruber, F. Troyon, Proc. 6th Int. Conf. Plasma Phys., Berchtesgaden (1976) Paper B11-4

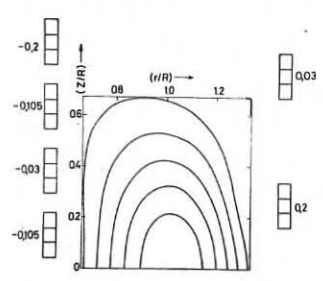

Figure 1. Equilibrium configuration showing the coils and the magnetic surfaces. The current flowing in each coil, normalized to the total current, is shown next to the coil.

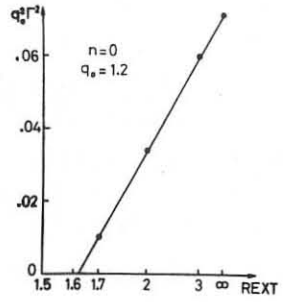

Figure 2. The growthrate of the n=0 mode as a function of R_{ext}, showing the wall stabilization effect.

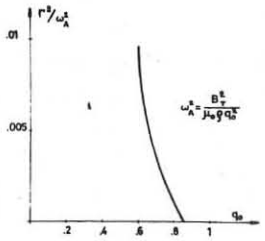

Figure 3. Growthrate Γ of the fastest growing n=1 mode as function of the safety factor on axis q_0.

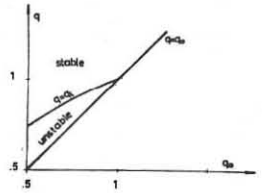

Figure 4. Mercier's criterion. The unstable region, limited by q_0 and q_ℓ is plotted versus q_0. The plasma extends from q_0 to $4q_0$.

LASER THERMONUCLEAR INSTALLATION "DELFIN"

N.G.Basov, O.N.Krokhin, Yu.A.Mikhailov,
G.V.Sklizkov and S.I.Fedotov

P.N.Lebedev Physical Institute of Academy of Sciences of the USSR. Leninsky prospect 53, Moscow, USSR

An examination of different schemes of LCTR results in the necessity of construction of lasers with pulse energy at least 10^4 J and pulse duration of 0.1-10 ns. Moreover, lasers must comply with a number of demands, such as high degree of radiation contrast $10^7 \div 10^8$, small divergence $10^{-4} \div 10^{-3}$ [1,2], high temporal synchronization of optical beams, a great number of output beams and a possibility of pulse shaping.

These requirements have been taken into account in the creation of 12-channel Nd-glass laser installation "DELFIN" [2] described. This installation is intended for a spherical heating of a thermonuclear target and these investigations should enableus to optimize the conditions of the heating and to reach sufficiently high thermonuclear yield.

The installation "DELFIN" has been constructed (Fig.1) on the basis of successive-parellel disposition of amplifiers. A general view of the optical hall with laser system, vacuum chamber and diagnostic arrangement is shown in Fig.2.

A subnanosecond pulses are formed by Nd-glass master-oscillator operating in the periodic pulse Q-switching regime. A nanosecond pulses are generated by the single-mode Nd-glass Q-switching oscillator and high-speed pulse formation system.

In the installation "DELFIN" we have chosen the following splitting coefficients from stage to stage:n=2;2;3;2;3;3(Fig4).

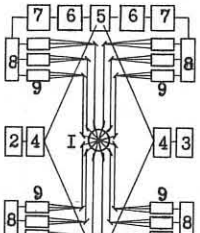

Fig.1. A block-diagram of the installation "DELFIN". 1 - target chamber; 2,3 - nanosecond and subnanosecond master oscillators; 4 - stages LPSA; 5÷7-stages PSA I÷II and PFSA I÷III; 8 - beams splitting arrangements; 9 - stages OSA.

Fig.2. General view of the optical hall.

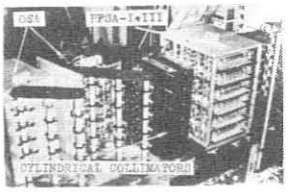

Fig.3. General view of poweful stages of amplification.

A general view of powerful stages of amplification is shown in Fig.3. Each output stage of amplification represents a module with overall dimensions 72 x 96 x 135 cm^3 containing 18 laser heads with active rods Ø 45 mm. There are 12 such modules in the whole "DELFIN" providing 216 laser beams with equal energy in each beam. The basic laser parameters of the installation "DELFIN" are given in Table 1.

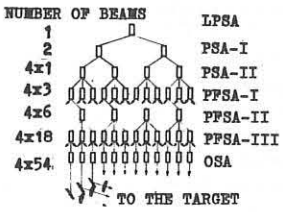

Fig.4. Optical scheme of beam multiplication.

From each of 12 output modules OSA 18 beams converge to the multi-prism "mirror", which forms one big composite beam with aperture 285 mm.

At present two-lens objectives are used to focus composite beam. The diameter of a focal spot is 300 μm.

In agreement with,the principle goals of laser-thermonuclear plasma diagnostics [3,4] the planned investigations at "DELFIN" installation are measurement of light energy conversion into the thermal ion energy in coronal area ($n_e \lesssim 10^{21}$ cm^{-3}), a study of comulation processes in the target core ($n_e > 10^{22}$ cm^{-3}), and the investigation of thermonuclear burning conditions.

Table 1.

Stage	Number of beams	Energy,J	Divergence, rad	Brightness, W/cm^2 ster
LPSA	1	30	$1 \cdot 10^{-4}$	$6.5\ 10^{16}$
PSAI	2	70	-"-	-"-
PSAII	4	180	-"-	-"-
PFSAI	3	120	-"-	-"-
PFSAII	6	320	$2 \cdot 10^{-4}$	$2.8\ 10^{16}$
PFSAIII	18	880	-"-	-"-
OSA	3x18	2500	$5 \cdot 10^{-4}$	$4 \cdot 10^{15}$
OUTPUT	12	10 000	-"-	$3 \cdot 10^{15}$

The plasma diagnostic technique at the "DELFIN" can be divided into the following groups:

1. optical diagnostics in the wavelenght range 0.35÷1.06μm;
2. spectroscopy in the region of VUV and soft X-ray $\lambda = 1 \div 10^3$ Å;
3. energy distribution of hard X-rays $\lambda < 1$ Å;
4. corpuscular diagnostics.

At present the preliminary start of the first part of the installation "DELFIN" (3 composed beams - 54 beams Ø 45 mm) have been carried out. The summary laser radiation energy in 3 composed beams is ≈ 650 J, and light pulse duration is $\approx 10^{-9}$s. The pumping energy value is ≈ 21 kJ per 1 rod active element with Ø 45 mm and pumped part lenght ≈ 560 mm. The averaged value of light divergence is not more than 10^{-3} rad. The contrast ratio is not less than 10^5.

References.

1. O.N.Krokhin, Yu.A.Mikhailov, G.V.Sklizkov, S.I.Fedotov Kvantovaya Electronika, 3, 3, 636 (1976).
2. N.G.Basov, O.N.Krokhin, Yu.A.Mikhailov, G.V.Sklizkov, S.I.Fedotov in "Laser Interaction and Related Plasma Phenomena", Plenum Press, IY(1977).
3. N.G.Basov, E.G.Gamaly, O.N.Krokhin, Yu.A.Mikhailov, G.V.Sklizkov, S.I.Fedotov in "Laser Interaction and Related Plasma Phenomena", Plenum Press, III B, 553 (1974).
4. N.G.Basov, Yu.A.Zakharenkov, N.N.Zorev, A.A.Kologrivov, O.N.Krokhin, A.A.Rupasov, G.V.Sklizkov, A.S.Shikanov Zh.Eksp.Teor.Fiz., 71, 5(11), 1788 (1976).

MULTIKILOJOULE CO_2 LASER HEATING OF POLYTHENE PELLETS

A.C. Walker, M.W. McGeoch, T. Stamatakis, S. Ward, B.L. Willis and I.J. Spalding

Euratom-UKAEA Fusion Association, Culham Laboratory, Abingdon, OX14 3DB, United Kingdom.

Abstract: A multikilojoule CO_2 laser ('TROJAN') has been used to heat $\frac{1}{2}$-1 mm polyethylene cubes at incident intensities $\lesssim 4 \times 10^{12} Wcm^{-2}$, in preliminary assessments for a laser plasma stellarator-filling experiment. Measurements of transmission through the resulting laser-plasma, and of refraction and back-reflection, indicate energy losses of $\lesssim$ 1, 10 and 5% respectively. These and other measurements will be discussed.

1. INTRODUCTION

Ohmic-heating typically generates a plasma having an energy content of ~ 300J in CLEO Stellarator.[1] This paper examines the efficiency with which multikilojoule CO_2 lasers may be used to create laser-plasmas, as an alternative means of filling CLEO and other toroidal traps.[2] Earlier measurements of reflection from plane carbon targets[3] have indicated that back-reflection can be small, since absorption is significantly stronger than that attributable to inverse-bremmstrahlung alone;[4,5] the present work extends such observations by investigating transmission and refraction losses when finite targets are irradiated. It is hoped to use free-falling cryogenic deuterium targets[6] for this cooperative Euratom programme, but for these preliminary assessments the targets were (suspended) polythene cubes.

2. EXPERIMENTAL TECHNIQUE

The experimental arrangement is illustrated in Fig.1. The electrical characteristics of the electron beam preionized laser ('TROJAN') have been described previously.[5] For the present experiments the system was filled with gas at one standard atmosphere, with a $He:N_2:CO_2$ ratio of 0:1:2; its active volume was ~ 180 cm x 20 cm x 25 cm. An unstable confocal optical resonator having a magnification of 2.8 was used to ensure low-order transverse mode, gain-switched, output pulses. The initial spike typically had a peak power of $\gtrsim$ 30 GW and exhibited mode beating; its envelope had a duration of 50 ns (FWHM) and a tail lasting some 2 μs. The energy contained in this tail could be conveniently controlled by adjusting the duration of the electron-gun pulse; Fig.2 illustrates typical pulse shapes generated for the present experiments. The incident power and energy were monitored by the photon-drag (P1) and large area pyroelectric (E1) detectors illustrated in Fig.1; similarly P2 and E2 measured the power and energy back-reflected from the target. The effective (17 x 20 cm^2) cross section of the laser beam was focused by a 4.5m focal length spherical mirror on to the target; the focal spot size, determined by a grating technique,[7] was 750 μm (FWHM). The polythene targets were hand cut from sheet, and stuck with a minimum of epoxy resin to 10 μm diameter glass fibres supported on a micromanipulator within the target chamber at a vacuum pressure of 10^{-4} - 10^{-5} torr.

3. EXPERIMENTAL RESULTS

Energy balance measurements have been made in which 0.6 - 1.5 kJ laser pulses, of duration 50 ns to 2 μs respectively (cf Fig.2), have been focused centrally on to both 1 mm and $\frac{1}{2}$ mm polythene cubes. These have given reproducible results showing, for all cases, high coupling of the laser energy into the pellet plasma.

Detector E2, sampling light directed back through the focusing optics with an effective aperture of f/17, indicated $\lesssim$ 5% direct energy reflection. A cone calorimeter, E3, placed behind the target and matched in size to the beam diameter gave a response typically < 8% of that recorded with no pellet in position. Such a device, however, considerably underestimates the magnitude of high energy (unattenuated) pulses, because of plasma formation at its entrance aperture. To investigate further, calibrated film was placed behind the pellet to give a spatial measure of the energy density of both transmitted and refracted CO_2 laser radiation. (The calibration was obtained by directing various known intensities of 10 μm radiation on to the film, in vacuum, and observing the colour of the resulting burn.) Fig.3 illustrates typical energy density contours, derived in this way, for CO_2 radiation transmitted and refracted through the plasma. It indicates that the direct transmission is < 1% of the incident energy, but that refraction, confined to a cone of (full) angle $\lesssim 60°$, contributes the major energy loss, of $\lesssim$ 10%. Film placed at other positions within the target chamber gave no detectable response except when close to the laser beam direction, indicating that additional back-scattered light not reaching the focusing optics amounted to no more than 1% of the incident energy.

Detector P2, sampling the reflected intensity, showed enhanced back-reflection of the long μs tail of the pulse, relative to the intense (50 ns) initial spike (Fig.4).

4. CONCLUSION

These energy balance measurements demonstrate that small, submillimetre, $(CH_2)_n$ targets can be efficiently heated using (relatively slow) kilojoule CO_2 laser pulses. Measurements of total charge, using ion probes, etc., are in hand to establish whether pre-pulses of the type discussed in ~ 100J Nd laser heating experiments[6,8] will be necessary to ensure full ionization in the present higher energy, microsecond duration experiments. (A highly simplified model suggests that this practical complication may be avoided,[5] or perhaps restricted to the use of only a 10.6 μm prepulse.[9])

REFERENCES

1. ATKINSON, D.W. ET AL - 'Plasma Physics and Controlled Nuclear Fusion Research 1976', Nucl.Fusion Suppl.1977, IAEA-CN-35/D1.
2. Culham Study Group on Heating and Injection (1970); and SPALDING, I.J. - Kuantovaya Elektron 4, 40 (1972)
3. DONALDSON, T.P. ET AL - Phys.Rev.Lett.37, 1348 (1976)
4. DONALDSON, T.P., SPALDING, I.J. - Phys.Rev.Lett.36, 467 (1976)
5. SPALDING I.J. ET AL - 'Plasma Physics and Controlled Nuclear Fusion Research 1976', Nucl.Fusion Suppl.1977, IAEA-CN-35/G3-3
6. BAUMHACKER, H. ET AL - Appl.Phys.Lett.30, 461 (1977)
7. MARQUET, L.C. - Appl.Opt.10, 960 (1971)
8. GREIG, J.R., PECHACEK, R.E. - Appl.Phys.Lett.29, 798 (1976) and J.Appl. Phys.48, 596 (1977)
9. cf DONALDSON, T.P. ET AL - Culham preprint CLM-P480 (1977)

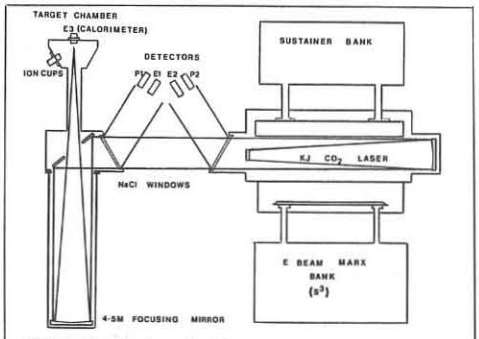

FIGURE 1 Plan-view of experimental arrangement

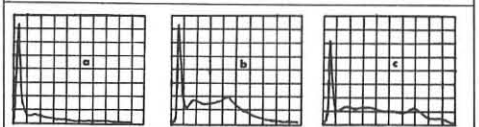

FIGURE 2 Time variation of 'TROJAN' output power, using an electron beam of (a) 0.8, (b) 1.6 and (c) 2 μs duration. (Vertical: ~ 3 GW/div., horizontal: 200 ns/div.)

FIGURE 3 Distribution of transmitted and refracted laser radiation on a plane 7.5 cm behind a $\frac{1}{2}$ mm polythene cube irradiated by a 1.5 kJ (2 μs) pulse. Numbers indicate average energy density in joules/cm^2 between contours. Circles show cone (full) angles relative to pellet position.

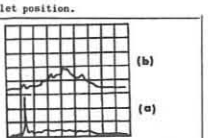

FIGURE 4 Incident (a) and back-reflected (b) pulse shapes for experiment of Fig.3 (500 ns/div).

EXPERIMENTS ON NEODYMIUM LASER PULSE INTERACTION WITH SLAB TARGETS IN THE PICOSECOND REGIME

J.A. Zimmermann, J.E. Balmer, T.P. Donaldson, P. Wägli
Institute of Applied Physics, University of Berne,
CH-3012-Berne/Switzerland

Abstract Experiments are described on the interaction with solid targets of a short neodymium laser pulse at intensities up to 10^{15} watts cm^{-2}. The dependence of reflectivity and electron temperature on laser intensity was determined and the effects of pre-pulses and self-focused filaments were investigated.

Introduction Of considerable relevance to laser fusion are scaling laws for electron temperature and plasma reflectivity. Scaling of coronal electron temperature with incident laser intensity in the long pulse (nanosecond) regime has been fairly well established by several groups using neodymium in-glass lasers (1,2). However, in the short pulse (picosecond) regime not many results on electron temperature scaling have been published, and plasma reflectivity results are not fully in agreement (3,4,5). Scaling laws for short pulses are reported here and the influence of prepulses from the laser has been investigated.

Experiment and Diagnostics Laser pulses of 35 psec duration were generated by a neodymium:YAG mode locking oscillator. A single transverse mode pulse was selected and amplified by a Nd:glass chain which included a discrimination amplifier (6) to ensure that any noise or prepulse intensity was less than 10^{-6} of the main pulse intensity. Thus well "characterised" laser pulses were focused onto slab targets located in vacuo. An f/3.75 aspheric lens produced a focal spot of ∿80 μm diameter and an intensity of 10^{15} watts cm^{-2}. Simultaneous measurements of X-ray emission were made with two identical pairs of scintillator foil detectors using 12.5 μm and 25 μm Be foil absorbers. Temperatures were derived from signal ratios of each detector pair, and from absolute intensity values. These were compared for consistancy (1). Electron temperature (T_e) was derived from signal ratio (R>1) using (7):

$$T_e = 0.50(E_B-E_A)\left(1 + \sqrt{1 + 0.073\ \ell n\ R(E_A+E_B)/(E_A-E_B)}\right)/\ell n\ R$$

valid for $1 < (E_A/T_e$ and $E_B/T_e) < 10$ and a foil with no edge in the transmission band, E_A and E_B are cut-off energies of the thin and thick foils respectively. The electron temperatures of plasmas generated from transparent perspex and opaque carbon targets were measured and compared. Examination of the transparent targets after the interaction revealed the presence of self-focusing filaments which were non linearly refracted as they entered the perspex. The effect of laser intensity on the angle of refraction of the filaments was measured, see figure 1.

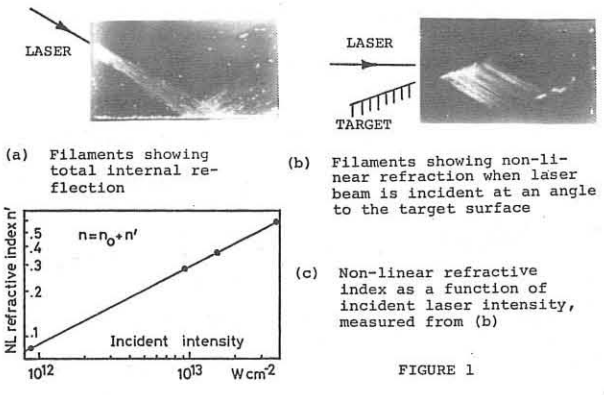

(a) Filaments showing total internal reflection

(b) Filaments showing non-linear refraction when laser beam is incident at an angle to the target surface

(c) Non-linear refractive index as a function of incident laser intensity, measured from (b)

FIGURE 1

To determine if self-focusing of the laser beam was initiated before a stable critical surface was formed, a perspex target was coated with a thin gold layer (< 500 Å), preventing the initial part of the laser pulse from reaching the perspex; thus the critical surface was established before the main part of the pulse "burnt through" the gold to the perspex. No filaments were observed, implying that self-focusing began in the early stages of the laser pulse before a stable critical surface was established. It was estimated that up to 5 % of the laser radiation energy was lost in these filaments. Laser radiation backreflected into the solid angle (0.35 sterad) subtended by the focusing lens was measured. Figure 2 shows the dependences of plasma reflectivity and electron temperature on the peak incident laser intensity (I). To observe the effect of prepulses on plasma parameters, a controlled prepulse of $3x10^{-2}$ I was introduced ∿1 nsec before the main laser pulse.

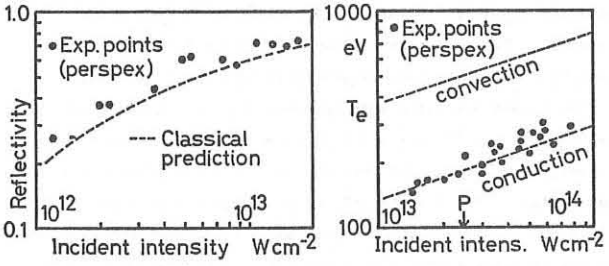

FIGURE 2

Discussion Electron temperature measurements for the range 10^{12} - 10^{14} watts cm^{-2} lie between theoretical predictions based on two limiting plasma energy losses: conduction (8) and convection (9). The point (P) where these losses should balance was calculated (see figure 2). The measured electron temperature scaling; $T_e \propto I^{0.44 \pm 0.05}$ agrees with the theoretical scaling of 0.44 (8,9,10). On the basis of these results the electron thermal conductivity is thought to be close to classical for $I < 10^{14}$ watts cm^{-2}, and the measured temperature scaling of plasma reflectivity conforms to classical absorption predictions, assuming a density scale length ∿ 2 μm. Absolute reflectivity values of up to 70% correspond more closely to the results of (4) and (5) rather than those of (3). Note the contrast with the results in (11) where long pulse (50 nsec) CO_2 lasers were used and backscattered reflectivity was ∿ 3-4%. The high short pulse reflectivity can be explained by the characteristically short density scale lengths in the plasma. When the pre-pulse was introduced the density scale length had time to grow before the main laser pulse arrived, and the reflectivity was seen to fall dramatically from 70% to 40%, while the electron temperature increased correspondingly. Filaments were not seen in this case because the solid perspex was shielded by the critical surface. It is concluded from these results that laser prepulses significantly affect the absorption of laser energy and therefore it is very important to characterise the exact temporal evolution of the laser radiation impinging on the target for the interpretation of absorption measurements. Further work is in progress to extend the range of these measurements.

(1) T.P. Donaldson, R.J. Hutcheon, M.H. Key, J. Phys. B. 6, 525 (1973)
(2) Naval Research Laboratory, Laser Fusion Report, 3315, P123 (1976)
(3) B.H. Ripin et al., Phys. Rev. Lett., 33, 634 (1974)
(4) C.G.M. van Kessel et al., IPP Garching Report IV/94 (1976)
(5) R.A. Haas et al., Phys. Fluids, 20, 322 (1977)
(6) W. Seka and E. Stüssi, J. Appl. Phys., 47, 3538 (1976)
(7) T.P. Donaldson, to be published
(8) A. Caruso and R. Gratton, Plasma Phys., 11, 839 (1969)
(9) H. Puell, Z. Naturforsch., 25a, 1807 (1970)
(10) E. Cojocaru and P. Mulser, Plasma Phys., 17, 393 (1975)
(11) T.P. Donaldson, M. Hubbard, I.J. Spalding, Phys. Rev. Lett., 37, 1348 (1976)

DIRECT MEASUREMENT OF A FLUX LIMIT IN A LASER HEATED PLASMA

D.R. Gray and J.D. Kilkenny

Blackett Laboratory, Imperial College, London SW7 2BZ

Abstract: A homogeneous plasma of density 6.10^{16} cm^{-3} is heated by a 2ns CO_2 laser pulse. The heat flux is directly measured by ruby laser scattering and is limited to≃4% of the free steaming limit. The maximum T_e/T_i is 6 and heat flux driven ion acoustic turbulence is seen.

We report an experiment where a homogeneous, underdense plasma of density 6.10^{16} cm^{-3} is heated by a 2ns CO_2 laser pulse of peak intensity 3.10^{11} Wcm^{-2}. Classical thermal conduction is not expected. Space and time resolved electron temperature (T_e) and density (n_e) are measured by ruby laser scattering. These results are compared with numerical simulations by varying the thermal conductivity and absorption.

The plasma used is a weak hydrogen z pinch. The initial n_e and T_e are 6.10^{16} cm^{-3} and 4 eV respectively. A 400 MW CO_2 laser pulse is focussed into the centre of the plasma by a 17 cm doublet. The diameter of the focal spot is measured to be 350 ± 50 μm. Both the CO_2 laser and the diagnostic ruby laser are incident radially on the pinch column, the radii being separated by 45°. The ruby pulse is much longer than the CO_2 pulse and sychronisation is achieved with subnanosecond jitter by electro-optically switching both lasers from a common spark gap.

On the length and time scale of the heating experiment the plasma is essentially homogeneous, constant and unmagnetised. Thus there is cylindrical symmetry about the CO_2 laser beam.

The scattered light is resolved by a grating spectrometer. Time resolution is achieved by a 1.2 ns risetime photomultiplier. Reproducibility is good enough to plot spectra on a shot to shot basis. The spatial resolution is 200μm and results are taken with various displacements (δ) from the centre of the CO_2 beam. The scattering vector is usually parallel to ∇T_e, i.e. radially outwards from the CO_2 laser beam. Data is taken for δ=0, δ= 400 μm , δ= 700 μm and δ= 1200 μm. The electron feature is used to derive values for n_e and T_e from Salpeter curves.

A one dimensional two fluid simulation is used to compare with the experiment. The ponderomotive force and the saturation of inverse bremsstrahlung absorption are including since $v_r = eE_o/m\omega_o \lesssim v_{th}$. As in previous work (1) the multiples w(absorption) and s (thermal conductivity) (2) are varied to fit the experimental results. Thus s=1, w=1 is the purely classical situation. Alternatively, the experimental results can be compared with a simulation using an artificial limit (f) to the heat flux (q), so that q cannot exceed $f\ (n\bar{c}/4)\ 2\ kT_e$.

For previous low power results (1) the best fit was achieved with s=0.4, w=1. However, these results can also be interpreted (3) with f=0.06 and w=1. Some of the present results are shown in Fig. 1. The density changes very little. These results can be fitted by varying s and w. The fit is poor but is best for s=0.1 , w=1. A better fit is obtained by varying f and as shown in Fig. 2, the best fit is with f=0.04±0.02, w=1±0.2 .

By fitting the experimental data for several different displacements both the absorption and the conduction have been measured. It is interesting that we can interpret both experiments with a similar flux limit.

The values of n_e and T_e deduced from the measured electron feature defines a thermal level for scattering in the ion feature (S_{ith}). The observed ion feature (S_{io}) is enhanced to >10. S_{ith} at the peak of the CO_2 laser pulse as shown in Fig. 3. This is interpreted as ion acoustic turbulence driven by the conduction return current along ∇T_e. This was not observed in the low power experiment presumably because there the long timescale (70ns) allowed equilibration of T_i and T_e. In contrast for the present experiment T_i is constant to 10% during the electron heating. Thus we expected T_e/T_i to be as large as 6 , and ion acoustic waves to be driven by the return current.

Although, the ion acoustic turbulence could be inhibiting the thermal conduction for the high power experiment, this could not explain the flux limit seen in the low power experiment. A more consistent explanation might be that the degree of turbulence is insufficient to greatly inhibit conduction and that the flux limit of ~5% is due to collisional effects. It should be noted that Spitzer's (2) perturbation treatment of transport coefficients becomes invalid when $q > 0.1\ (\frac{n\bar{c}}{4})\ 2kT_e$. Under these conditions the total distribution function becomes negative in the region of velocity space where the net heat flux occurs ($1.5v_{th} < v < 3v_{th}$).

Acknowledgement Thanks are due to M.S.White for help in the early stages of this work, A.W.R.E. for the use of their CO_2 laser, and the S.R.C. for supporting this work.

References

1.M.S.White, J.D.Kilkenny, A.E.Dangor, Phys.Rev.Lett., 35, 524 (1975).

2. L. Spitzer, and R. Harm, Phys.Rev. 89, 977 (1953).

3.D.R.Gray, J.D.Kilkenny, et al, 6th. Int. Conf. on Plasma Physics and Controlled Nuc. Fusion, (I.A.E.A.-Berchtesgaden, 1976), G4-2.

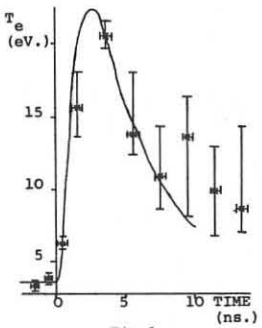

Fig.1

Time history of T_e at δ=0. Solid curve is computational fit (f=0.03, w=1)

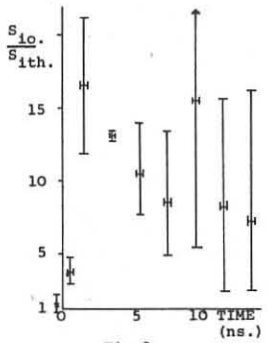

Fig.3

Enhancement above thermal of scattering in the ion feature.

(In Figs.1 and 3 the 2ns. CO_2 pulse starts at time zero)

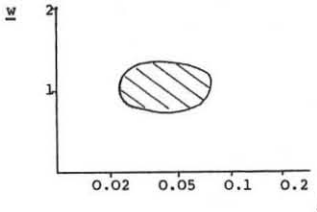

Fig.2. The shaded region shows the area of w,f space where computations fit the experimental results.

SELF-SIMILAR DEFLAGRATION IN LASER HALF-SPACE PLASMAS

J.R. Sanmartín and A. Barrero

E.T.S.Ingenieros Aeronáuticos

Universidad Politécnica de Madrid, Madrid-3, Spain

Abstract: The self-similar motion of a half-space plasma, generated by a linear pulse of laser radiation absorbed anomalously at the critical density, has been studied. The resulting plasma structure has been completely determined for [pulse duration × (critical density)^2/maximum irradiation] large enough.

In laser fusion schemes, laser radiation is absorbed in a plasma at electron densities less than, or around, the critical density n_c. If $\varepsilon \equiv n_c/n_o \ll 1$, n_o being the initial density, absorption occurs in a hot and rarefied corona, ablated by the laser [1]. Entropy (which is generated there) should be kept low inside the dense plasma, where mass and energy should converge efficiently; in addition the energy coronal outflow should be minimized. Thus, hydrodynamics plays an essential part in microfusion.

We have studied the self-similar motion of a plasma under irradiation of a laser pulse linear in time [2], [3]. The plasma at t=0 is assumed to occupy the half-space x>0, with uniform density n_o and negligible temperature; the pulse irradiation

$$\phi = \phi_o\, t/\tau \quad , \qquad 0<t\leq\tau \tag{1}$$

is assumed absorbed at the plane where the electron density n_e equals n_c. The analysis allows for electron thermal conductivity and different temperatures, T_e and T_i (an electron flux limiter, viscosities, and ion heat conduction could be also included in the self-similar solution); we consider neither nuclear fusion, nor radiation pressure and emission.

We make the ansatz (verified in the solution) that the plasma is both quasineutral and collision-dominated. From $n_e = n_i \equiv n$ we then get equal ion and electron velocities, $v_e = v_i \equiv v$. For the electron thermal conductivity and the ion-electron relaxation time we may use the classical results [4]

$$K_e \equiv \overline{K}_e T_e^{5/2} \quad , \qquad t_{ei} = \overline{t}_{ei} T_e^{3/2}/n$$

where the Coulomb logarithms in $\overline{K}_e$ and $\overline{t}_{ei}$ are assumed to remain constant.

Defining appropriate dimensionless variables

$$\xi = x/w\tau\,(t/\tau)^{4/3} \quad , \qquad u(\xi) = 3v/4w\,(t/\tau)^{1/3}$$
$$\overline{n}(\xi) = n/n_o, \quad \theta_j = T_j/T_o\,(t/\tau)^{2/3}, \quad \alpha = 9kT_o/4m_i w^2 \tag{2}$$

the equations of continuity for either species, momentum for the ion-electron fluid, and entropy for each species, read

$$(\xi-u)\,d\overline{n}/d\xi = \overline{n}\,du/d\xi$$
$$u - 4(\xi-u)\frac{du}{d\xi} = -\frac{\alpha}{\overline{n}}\frac{d}{d\xi}\left[\overline{n}(\theta_e+\theta_i)\right]$$
$$\overline{n}\left[\theta_i\left(1+\frac{4}{3}\frac{du}{d\xi}\right) - 2(\xi-u)\frac{d\theta_i}{d\xi}\right] = 4.3\,\alpha\,\overline{n}^2\,\frac{\theta_e-\theta_i}{\theta_e^{3/2}} \tag{3}$$
$$\overline{n}\left[\theta_e\left(1+\frac{4}{3}\frac{du}{d\xi}\right) - 2(\xi-u)\frac{d\theta_e}{d\xi}\right] = \frac{d}{d\xi}\left(\theta_e^{5/2}\frac{d\theta_e}{d\xi}\right) - 4.3\,\alpha\,\overline{n}^2\,\frac{\theta_e-\theta_i}{\theta_e^{3/2}} + \delta(\xi-\xi_c)$$

with boundary condition

$$\theta_e = \theta_i = u = \overline{n}-1 = 0 \qquad \text{at} \quad \xi = \infty$$
$$\overline{n} = u - \xi_v = 0 \qquad \text{at} \quad \xi = \xi_v \tag{4}$$

where ξ_v is the position of the plasma-vacuum boundary and ξ_c is given by

$$\overline{n}(\xi_c) = \overline{n}_c \equiv \varepsilon \quad .$$

In Eqs. (3) we have chosen w and T_o to satisfy

$$w = (\phi_o^{\,5}\overline{K}_e^{\,2}/k^7 n_o^{\,7}\tau^2)^{1/9}, \quad T_o = (\phi_o^{\,2}\tau/\overline{K}_e k n_o)^{2/9}$$

and then

$$\alpha = (9k/4m_i)(k^2 n_o^{\,2}\tau/\phi_o\overline{K}_e)^{2/3} \quad ;$$

k is Boltzmann's constant and m_i the ion mass.

Assuming $\alpha \gg \varepsilon^{-4/3}$ [that is, $\alpha_c \equiv \alpha(n_c/n_o)^{4/3} \gg 1$] we find that the flow presents three main regions. An isentropic compression to the right, beginning at a shock bounding the undisturbed plasma at ξ_f, and ending at $\overline{\eta}\xi_f$, where

$$\xi_f = .53\varepsilon^{1/6}\alpha^{1/3} \quad , \qquad \overline{\eta} = .82 \quad .$$

A much larger isentropic expansion to the left, lying between $\overline{\eta}\xi_f$ and $\xi_v = -2.19\varepsilon^{-1/2}\xi_f$, so that in this region, $\overline{\eta}\xi_f$ is indistinguishable from zero. A deflagration layer (where absorption occurs, conduction is important, and $\theta_e \neq \theta_i$) separating the isentropic regions; its width is of the order of $\varepsilon^{-5/2}\alpha^{-3/2}\xi_f$, so that deflagration and isentropic expansion merge into each other when $\alpha = 0(\varepsilon^{-4/3})$, while the relative size of the deflagration and the isentropic compression depends on the value of $\varepsilon^{-5/2}\alpha^{-3/2}$ Detailed results are given in the figure.

REFERENCES

[1] J. Nuckolls, L. Wood, A. Thiessen and G. Zimmerman, Nature 239, 139 (1972).

[2] S.I. Anisimov, Zh. Eksp. Teor. Fiz. Pis'ma Red. 12, 414 (1970) |JETP Lett. 12, 287 (1970)|.

[3] A. Barrero and J.R. Sanmartín, Phys. Fluids 20 (July) 1977.

[4] L. Spitzer, Physics of Fully Ionized Gases (Interscience, New York, 1962).

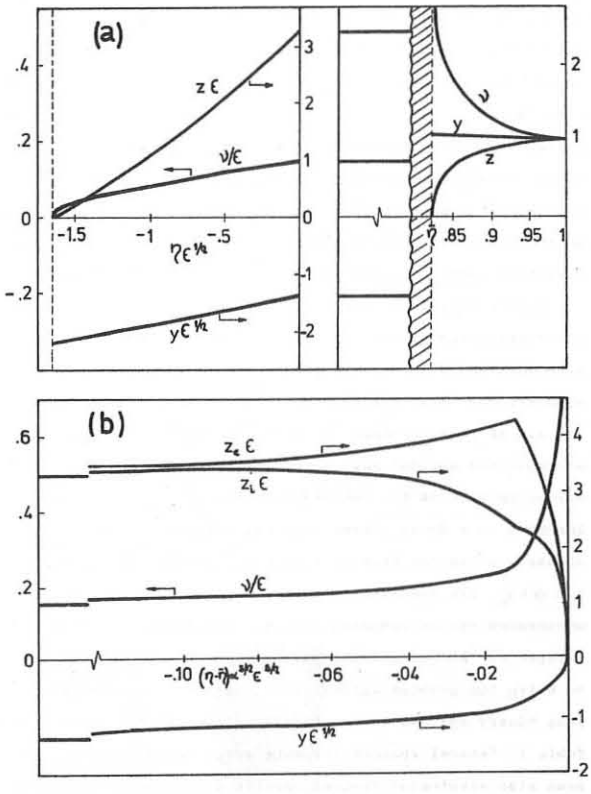

a) Isentropic expansion and compression regions, b) Deflagration layer; $\eta = \xi/\xi_f$, $y = 4u/3\xi_f$, $z_j = 8\alpha\theta_j/3\xi_f^2$, $\nu = \overline{n}/4$.

COMPUTATIONAL STUDY OF SOME RADIATION AND NUCLEAR PROCESSES IN LASER-PRODUCED PLASMAS

L. Drska, R. Dragila, J. Krepelka

Faculty of Nuclear Science and Physical Engineering, Technical University of Prague, Brehova 7, 115 19 Praha 1, Czechoslovakia

Abstract: Results of two computational studies in the field of laser-produced plasmas are presented: (1) Absorption and reflection of solid spherical targets irradiated by laser light. (2) Electron screening factors for nuclear reactions in inertial confinement systems.

(1) Correct treatment of the absorption and reflection of laser light leads to the solving the consistent system of the hydrodynamical and Maxwell equations, as there is some cut-off neighbourhoud where the geometrical approximation fails /1/. In present work, the problem analogous to that treated in /2/ is dealt with, but for a spherical system and with the flux limited ion thermal conductivity. - The absorption mechanisms taken into account are both collisional inverse bremsstrahlung and collective effects, the latter through the effective collision frequency ν_{ef}. Generally, the collision frequency is defined as $\nu_{ef} = \max(\nu_e^c, \nu_e^a)$, where ν_e^c is the usual value of the collision frequency corresponding to the inverse bremsstrahlung mechanism and $\nu_e^a = \nu_{ef}$ or 0, according to /2/. - To check the role of the collective effects, the calculations have been done for the cases without and with the anomalous absorption respectively. The reflectance $/V_T/^2 = /V/^2 R_o(t)$, the laser pulse and prepulse (dashed line) versus time for both cases are plotted in Figure 1. - To demonstrate some possibilities to optimalize the laser pulse for given size of the target and laser energy, several shapes of the laser pulse have been chosen. Two examples are given in Figure 2. The absorbed energy E_a and compression ratio ρ_{max}/ρ_o evaluated for these cases were as follow: (a) 85 % , 242 ; (b) 95.5 % , 4200. - All details concerning this study are given in /3/. The results of the study will be used in a more general code for the simulation of radiation processes in laser-generated plasmas /4/.

(2) Calculations of rates of thermonuclear reactions in laser-generated plasmas (and in inertial systems generally) have been based on the assumption that the Coulomb interaction with all the other nuclei and electrons can be neglected. It is the aim of present paper to check this assumption regarding advanced and special inertial systems. - The calculation of screening effects for nuclear reaction of charged particles immersed in a dense plasma requires the evaluation of the electron screening factor $f = \langle\sigma v\rangle_s / \langle\sigma v\rangle_o$, where $\langle\sigma v\rangle_s$ and $\langle\sigma v\rangle_o$ are reaction rates per particle for screened and unscreened system respectively /5/. - General methodology developed for astrophysical applications /6/, /7/ have been used to solve the problem. Illustrative results of calculations for some binary systems being of interest in CTR are presented in Table 1. Several speculative, more complicated systems have been also examinated, typical results are given in the Table 2. - All details of the calculations are explained and more general aspects of the problem (two-temperature systems etc.) are studied in /8/.

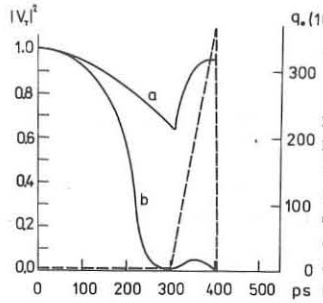

FIG. 1. Reflectance $/V_T/^2$ versus time. Dashed line represents laser pulse. - Curve a: Inverse bremsstrahlung only. Curve b: Anomalous effects included. - Target: CD_2, 120 μm. Laser: Nd, 36 J.

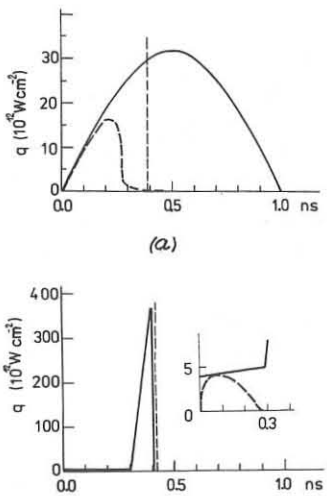

FIG. 2. Impinged and reflected (dashed line) pulses illustrating the optimalization of the absorption process: (a) Gaussian pulse (τ_L = 1 ns, τ_P = 0). (b) Triangle pulse (τ_L = 405 ps , τ_P = 300 ps). The vertical dashed line represents the time when the maximum compression occurs. - Target : CD_2 , 120 μm. Laser: Nd, 36 J.

TABLE 1. SCREENING FACTORS OF BINARY SYSTEMS

SYSTEM	⟨Z⟩	N_i/cm^{-3}	T/K		
			1.000 +7	1.000 +8	1.000 +9
DD/TD	1.0	1.0 +26	1.034	1.002	1.000
		1.0 +27	1.510	1.002	1.000
		1.0 +28	2.678	1.016	1.000
		1.0 +29	3.738 +1	1.073	1.001
Li6D	2.0	1.0 +26	1.624	1.013	1.001
		1.0 +27	3.390	1.042	1.002
		1.0 +28	7.212	1.189	1.004
		1.0 +29	8.524 +2	1.564	1.014
B11H	3.0	1.0 +26	2.439	1.039	1.002
		1.0 +27	4.686	1.160	1.005
		1.0 +28	3.270 +1	1.384	1.012
		1.0 +29	2.154 +3	2.348	1.041

TABLE 2. SCREENING FACTORS OF COMPOUND SYSTEMS

SYSTEM	⟨Z⟩	N_i/cm^{-3}	T/K		
			1.000 +7	1.000 +8	1.000 +9
TD+B11H	2.0	1.0 +26	1.272	1.005	1.000
		1.0 +27	1.747	1.018	1.001
		1.0 +28	2.204	1.062	1.002
		1.0 +29	6.305	1.249	1.006
TD+Fe	13.2	1.0 +26	5.355	1.198	1.012
T:0.4		1.0 +27	3.994 +1	1.579	1.037
D:0.4		1.0 +28	3.035 +3	2.108	1.069
Fe:0.2		1.0 +29	-	5.355	1.196
B11H+U	20.8	1.0 +26	5.068	1.216	1.016
B11:0.4		1.0 +27	3.452 +1	1.692	1.051
H:0.4		1.0 +28	-	2.081	1.078
U:0.2		1.0 +29	-	5.068	1.225

References:

/1/ GINZBURG V.L., Rasprostranenie elektromagnitnych voln v plazme, Nauka, Moskva 1967, p.186
/2/ AFANASIEV JU.V., DEMCHENKO N.N., KROKHIN O.N., ROZANOV V.B., ZhETP 72 (1977) 170
/3/ DRAGILA R., KREPELKA J., Laboratory Report FNS-LP-11, Faculty of Nuclear Science, Prague 1977
/4/ DRSKA L., BITZAN P., KASPAR V., Laboratory Report FNS-LP-12 (under preparation)
/5/ CLAYTON D.D., Principles of Stellar Evolution and Nucleosynthesis, McGraw-Hill, New York 1968, p.357
/6/ DE WITT H.E., GRABOSKE H.C., COOPER M.S., Astrophys.J. 181 (1973) 439
/7/ GRABOSKE H.C., DE WITT H.E., GROSSMAN A.S., COOPER M.S., Astrophys.J. 181 (1973) 457
/8/ DRSKA L., Laboratory Report FNS-LP-13 (under preparation)

THE REXIMPLO EXPERIMENT: HIGH FREQUENCY
PULSED COMPRESSION OF PRE-IONIZED DEUTERIUM GAS

E. Panarella
National Research Council, Ottawa, Canada, K1A 0R6

Abstract: REXIMPLO is a new plasma compression experiment characterized by high-frequency explosive and implosive discharges that respectively preheat and compress deuterium gas in cylindrical geometry. The main features of the design of the experiment as well as the technological innovations will be described and initial results will be shown.

REXIMPLO is an acronym for the repetitive-explosion-implosion experiment of the National Research Council of Canada. Basically, the experiment aims at heating deuterium gas in a cylindrical vessel by means of a rapid succession of compression waves each preceded by an ionizing expansion wave that drives the gas towards the wall of the vessel thus creating a strong density gradient towards the centre of the vessel. The idealized phases of the process are summarized in Fig. 1. At time t=0 a linear discharge along the axis of the vessel is triggered via two electrodes plugged into the centre of the end windows. The linear discharge generates a diverging wave which, at the time it reaches the wall of the vessel ($t=t_1$), produces a distribution of gas density decreasing from the wall to the centre of the vessel. At this particular time the first converging shock wave is launched by means of a theta-pinch discharge. The imploding wave travels now in a decreasing density medium, hence, it accelerates and, at collapse time $t=t_3$, a large thermal energy is obtained from the conversion of the kinetic energy of the ordered gas motion. Immediately after this cycle a second linear discharge is fired. The shock wave moves outward and redistributes the gas density according to the figure ($t=t_4$). At $t=t_5$, when the diverging wave has reached the wall of the vessel, the density distribution appears as at $t=t_1$. A second imploding shock wave is now launched and the entire succession of events as previously described is repeated. This scheme promises that the temperature of a gas can be increased by periodical energy dumping. The experimental apparatus designed to achieve this result is described in Fig. 2. Basically, it is made up of three parts: the explosion and implosion circuits, the discharge control unit and the flow visualization system. The explosion and implosion circuits are in all respect the same. A 24 μF condenser bank (Main Bank) is charged to 10 KV. A much smaller condenser bank (Secondary Bank, 2 μF) receives periodically a charge from the Main Bank through a 5 μH inductance and is discharged into a single turn coil (in the implosion circuit) or into the linear axial circuit (in the case of explosion). The flow visualization system is made up of a Mach-Zehnder interferometer, a Nd:glass laser and an image converter camera operating in the streak mode. The discharge control unit has the purpose of triggering alternately explosions and implosions. To this end, two photomultipliers are coupled by fiber optics light guides to an interferogram of the discharge. A differentiating circuit (Logic) coupled to the photomultipliers produces a strong signal only at the time of detection of passage of a shock wave which, on the interferogram, appears as a rapid shift of the fringes. Hence, by positioning the fiber optics light guides near the axis and the wall of the vessel, an explosion and an implosion can be triggered respectively. In operation, the entire apparatus works as follows (see lower right part of Fig. 2). At t=0 the laser is fired and the light pulse is monitored through a photodetector. This is coupled with a Triple Delayed Pulse Generator. The first pulse (A) triggers the spark gap switch of the Main Bank of the Explosion Circuit. After ∿5 μsec a second pulse (B) appears that triggers the Main Bank of the Explosion Circuit. At the peak of the charge of the Secondary Bank of the Explosion Circuit a third pulse appears that triggers the first explosion. After this, all other discharges are triggered by the Discharge Control Unit and the firing ceases when the voltage of the Main Bank is reduced to the point where the Quenched Spark Gap Switch of the Secondary Banks cannot become conductive any more. These switches are the main technological innovation of the apparatus. They have been described in detail in ref. [1]. Basically, they are high voltage spark gap switches where the single switching spark has been replaced by a series of elementary sparks separated by a set of copper plates. The elementary sparks, being in contact with the copper plates, are cooled and deionized as soon as the current flow reduces to zero in the oscillatory circuit. Hence, the current flowing in the circuit, rather than being a long damped oscillation, lasts only for the time of the first halfwave (Fig. 3). The switch is then ready to fire again immediately thereafter and the firing frequency can be as high as several hundreds kilohertz. The second fundamental innovation of the apparatus is the insertion of an intensity stabilized laser system, described in detail in ref. [2]. Basically, it is a Nd:glass high power laser on which an electronic feedback system is inserted in order to convert the spiky light emission into a smooth near rectangular output of adjustable intensity and duration. Figure 4 shows a typical pulse out of the modified laser where the light pulse has a power of 150 KW and a duration of ∿14 μsec.

Some preliminary experimental results are shown in Fig. 5. Figure 5a shows an image converter streak photograph of the plasma luminosity during the first cycle of the discharges, i.e. an explosion followed by an implosion. The gas used has been deuterium at 200 mTorr pressure. The most notable result is that an implosion can occur at a gas pressure which, without preionization, would not allow it. The current sheet (or shock front) velocity is quite high, $\sim 4 \times 10^6$ cm.sec^{-1}. Figure 5b shows a streak interferogram of the same discharge. From the shift of the interference fringes, which is due to the refractivity of free electrons, it appears that the gas (deuterium) is fully ionized at collapse time.

[1] E. Panarella and V. Guty, Journ. Phys. E: Sc. Instr. 7, 835 (1974).
[2] E. Panarella and L.L.T. Bradley, IEEE Journ. Quantum Electr. May 1975.

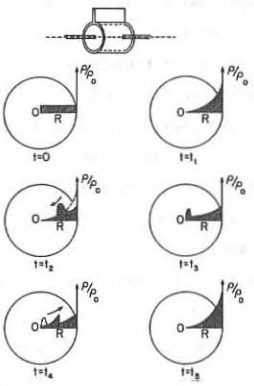

Fig. 1 - Phases of REXIMPLO Experiment

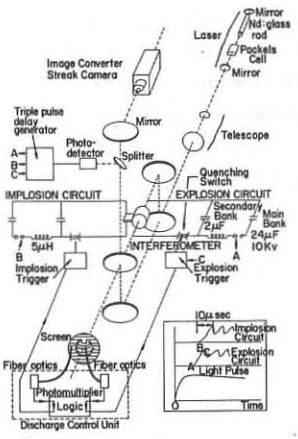

Fig. 2 - Experimental Apparatus

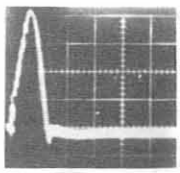

Fig. 3 - Current Pulse in the Secondary Circuit with the Quenched Spark Gap Switch Time Scale 1 μsec/div

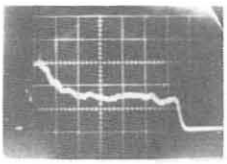

Fig. 4 - Intensity Stabilized Laser Output. Time Scale 2 μsec/div; Intensity 107 KW/div

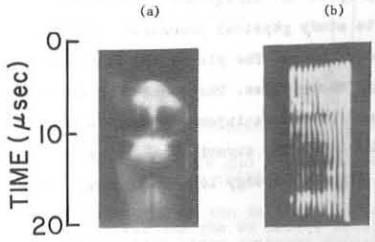

Fig. 5 - (a) Streak Photograph of Plasma Luminosity; (b) Streak Interferogram of Discharges

MODELING OF AN INERTIAL SYSTEM WITH GAS-KINETIC CONFINEMENT OF MAGNETIZED PLASMA

S.G.Alikhanov, V.P.Bakhtin, I.S.Glushkov, A.D.Musychenko and V.P.Novikov

The Kurchatov Institute of Atomic Energy.

Inertial confinement by liner is an inherent approach for almost all pulsed thermonuclear systems at present. Differences between these systems are mainly in the techniques of liner acceleration and, also, isolation and heating of plasma. Here, the scheme is considered /1/, where the plasma confinement and heating are achieved by means of cumulation of a cylindrical shell, i.e. liner. The presence of an axial magnetic field considerably reduces heat conduction in radial direction and as it has been shown earlier /2/ a plasma flow to the wall originates, which is necessary to compensate the radiative losses from the dense plasma being in contact with the wall (nT=const, $\beta \gg 1$). The calculations performed show that ~ 10 Mj energy storage is required to get the efficiency needed for practical application ($n\tau \geq 10^{15}$ sec/cm^3). For realization of this considerable progress should be made in developing fast energy storages, low inductance energy leads, initial plasma production, etc. Therefore, in the nearest future only modeling experiments at available energy levels are possible aimed at obtaining a 1% burnup of $D-T$ mixture at 10 kev.

The calculations were done for a 30 kj storage capacitor with $U = 300$ kv and $t_0 \simeq \sqrt{LC} \simeq 2 \cdot 10^{-8}$ sec. The 1% burnup has been shown to require a plasma with the following parameters: $n_0 = 2 \cdot 10^{20}$, $H_0 \simeq 200$ kG and $T_0 = 400$ eV in the volume $d \simeq \ell \simeq 0.2$ cm. Such a plasma could be easily produced by laser irradiation ($Q \simeq 500$ j) of D-T targets placed at the opposite ends of the cylinder to be compressed. At the initial moment of cumulation the liner cuts off the inlets for laser beams. Since the mean free path of particles is less than the cylinder length there are no problems associated with plasma thermal relaxation by shock waves. Figure 1 shows the calculated density distribution at the moment of maximum compression ($T_{max} = 12$ keV, $H_{max} = 2 \cdot 10^8$ G).

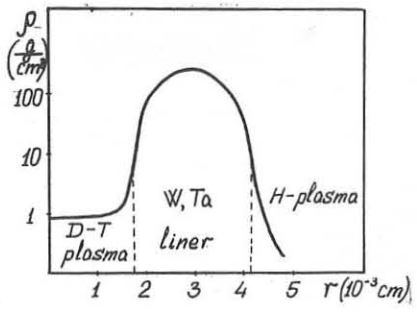

Fig.1.

The experimental results on the plasma injection into the chamber D=L=12 cm and liner acceleration up to 10^6 cm/sec are given below. These model experiments enable to study physical processes forming the basis of the scheme under development. The plasma was injected by two coaxial electric duscharge shock tubes. The shock wave velocity amounted to 10^7 cm/sec. The plasma jets were injected into the chamber through the circular slits at the ends. The experimental value of $p=f(t)$ (Fig.2) agrees with the expected energy loss mechanism, i.e. electron thermoconductivity along the magnetic field (H_0=10 kG). Though the streak camera spectrum (Fig.3) shows the impurities to be negligible, one cannot be assured that the radiative energy losses are due to the hydrogen only.

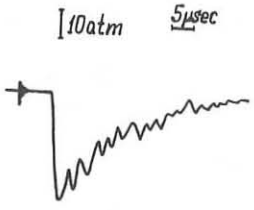

Fig.2.

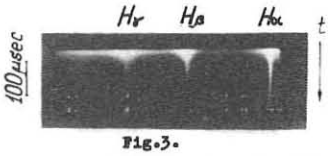

Fig.3.

Acceleration by means of a magneto-compressed discharge has been proposed for a real pulsed reactor with Z-pinch liner; however, for modeling experiments a well-checked technique of metal liner acceleration can be used making the velocity up to as high as possible. The maximal velocity is limited by liner heating by currents in it. Since the increase in the temperature and momentum of the accelerated liner is proportional to the current squared, then for a planar case one can define the so-called current integral which relates the velocity at a given thickness to the temperature and phase state /3/. In a cylindric geometry the liner thickness is not constant. In this case the maximum attainable velocity is certain to be higher. Indeed, a value of 10^6 cm/sec has been obtained which doubles the maximum one for a planar case. The photos made with a high speed framing camera distinctly show that the liner does not explode till the stop. All the measurements including those on the amplification of the initial longitudinal magnetic field and the singularity on the current curve are in good agreement with the calculations.

The authors thank E.P.Velikhov for support and interest in the work.

References

1. S.G.Alikhanov et.al. The Paper on the Joint Soviet-American Seminar on Pulsed Fusion Reactors, NIIEFA, Leningrad, 1975.

2. S.G.Alikhanov and I.S.Glushkov. Proc.of the European Conf.on Control. Fusion and Plasma Physics. Switzerland, 1975.

3. H.Knoepfel. Pulsed High Magnetic Fields, North-Holland Publishing Company. Amsterdam. London, 1970.

PLASMA EFFECTS ON THE ABSORPTION SPECTRUM FOR THE ORDINARY MODE IN A MAGNETIZED PLASMA

T. A. Casper and J. L. Shohet
The University of Wisconsin, Madison, Wisconsin 53706 USA
and
J. A. Tataronis
Courant Institute, New York University, New York, NY 10012 USA

Abstract: The rate of energy absorption for electrons in a plasma is calculated from the emission, including plasma effects through the index of refraction. The net absorption is obtained for the case of propagation perpendicular to an applied dc magnetic field. The dispersion relation for cyclotron harmonic waves is solved numerically.

The net absorption [1], that is, absorption minus stimulated emission, for waves in a magnetized plasma has been obtained for the special case of propagation perpendicular to the dc magnetic field. The plasma is assumed to consist of a single species of electrons in a neutralizing background of infinitely massive ions. The electron temperatures are considered to be relativistic with electron density high enough so that the electric and magnetic fields produced by the plasma may not be neglected.

The coefficient of spontaneous emission from which the absorption is determined corresponds to cyclotron emission from the electrons in a dc magnetic field. The plasma effects are incorporated into the calculation through the index of refraction resulting from the plasma dispersion relation.

As a measure of the net absorption, the coefficient, $\alpha_\omega(S)$, is calculated which gives the decrease in intensity along a ray S in units of reciprocal length as determined from the difference between the stimulated and spontaneous emission and absorption. For the case of a relativistic, anisotropic plasma, the emissivity associated with the ordinary mode ($\theta=\pi/2$) can be written as (Ref. 1, p. 193),

$$\eta^o_\omega(\pi/2) = \frac{ne^2\omega^2}{8\pi^2\varepsilon_0 c}\sum_{\ell=1}^{\infty}\beta_n^2 J_\ell^2(\ell\beta_\perp)\,\delta(\ell\omega_0-\omega) \quad . \tag{1}$$

Using this in the definition of the absorption coefficient (Ref. 1, p. 60), the ordinary wave absorption can be expressed as,

$$\alpha^o_{\omega\perp} = \frac{2\pi^2 m_o^4\omega_{co}^3\omega_{po}^2}{c|\mathrm{Re}(k)|^4}\sum_{\ell=1}^{\infty}\ell^3\int_I \frac{\beta_n^2}{\beta_{\perp\ell}}J_\ell^2(\ell n\beta_{\perp\ell})\left.\frac{\partial f_o}{\partial p_\perp}\right|_\beta d\beta_n \tag{2}$$

where $\beta_{\perp\ell}=[1-\beta_n^2-(n\omega/\ell\omega_{co})^2]^{1/2}$ must be a real valued parameter to prevent the occurrence of imaginary velocities. This results in the range of integration, I, for β_n becoming smaller than -1 to +1. Also, the above makes use of the symmetry present at $\theta=\pi/2$ in equating the ray refractive index with the index of refraction, that is,

$$n_{r\perp}^2 = |n|^2 = |c\ \mathrm{Re}(k)/\omega|^2 \quad . \tag{3}$$

The remaining unspecified parameter is the wave number k. This is determined from the plasma dispersion relation which at $\theta=\pi/2$ can be written as,

$$(-n^2+\varepsilon_{zz})[\varepsilon_{xx}(-n^2+\varepsilon_{yy})-\varepsilon_{yy}^2] = 0. \tag{4}$$

The ordinary mode then satisfies the dispersion

$$-n^2 + \varepsilon_{zz} = 0. \tag{5}$$

For a hot plasma, the permittivity tensor elements involve infinite sums of Bessel function integrals [2]. Since numerical results to be presented here only involve the ordinary mode, the pertinent quantity is

$$\varepsilon_{zz}=1+\frac{\omega_{po}^2}{\omega^2}2\pi m^4c^4\sum_{n=-\infty}^{\infty}\int_0^1\int_{-1}^1 J_n^2\left(\frac{kc\beta_\perp}{\omega_c}\right)(\omega-n\omega_c)^{-1}$$
$$\times\left((\omega-n\omega_c)\frac{\partial f_0}{\partial p_n}\right|_\beta + n\omega_c\frac{\beta_n}{\beta_\perp}\left.\frac{\partial f_0}{\partial p_\perp}\right|_\beta)\gamma^5\beta_\perp\beta_n d\beta_n d\beta_\perp. \tag{6}$$

The infinite summations can be converted to finite integrals by use of Bessel function densities and analytic continuation. Employing the identity

$$\frac{1}{\omega-n\omega_c} = i\int_0^\infty \exp[-i(\omega-n\omega_c)t]dt; \quad \mathrm{Im}(\omega) < 0 \tag{7}$$

the infinite sums are converted to integrations between 0 and ∞ valid for all Im(ω). The Bessel function periodicity allows the elimination of the infinite integration yielding,

$$\varepsilon_{zz}=1+\frac{a_0}{\omega}\int_0^1\int_{-1}^1\gamma^5m^4c^4\beta_n\beta_\perp\left(\left.\frac{\partial f_0}{\partial p_n}\right|_\beta - \frac{kc\beta_n}{\omega_c\sin(\omega\pi/\omega_c)}\right.$$
$$\times\left.\frac{\partial f_0}{\partial p_\perp}\right|_\beta\int_0^\pi\sin\left(\frac{\omega\tau}{\omega_c}\right)\sin\left(\frac{\tau}{2}\right)J_1(\xi)d\tau)d\beta_n d\beta_\perp \tag{8}$$

with $a_o = 2\pi\omega_{po}^2/\omega$, $z = \gamma kc\beta_\perp/\omega_{co}$, $\xi = 2z\cos(\tau/2)$.

The complicated nature of the dispersion relation and absorption coefficient presented in the previous section requires a numerical approach to find the absorption. A zero search for complex k roots of the dispersion relation provides values of k required in the evaluation of $\alpha^o_{\omega\perp}$. The absorption spectrum ($\alpha^o_{\omega\perp}$ vs ω) is obtained for a range of frequencies, temperature and density assuming a 1 kG dc magnetic field. For the results presented here we have used an isotropic Maxwellian distribution truncated at a circle of radius c. No attempts have been made to renormalize the distribution nor to remove the effects of truncation.

The search process involved in evaluating the absorption coefficient effectively solves the dispersion relation thus providing k(ω) including the self-consistent fields. The dispersion relation for a temperature of 100 keV at various densities are shown in Figure 1. The "noisy" wave numbers at frequencies below the plasma frequency are due to a lack of sufficient precision in the numerical integration scheme. The existence of low frequency propagation bands is consistent with results presented by Tataronis [2]. Absorption obtained for the 100 keV case is shown in Figure 2 at various densities.

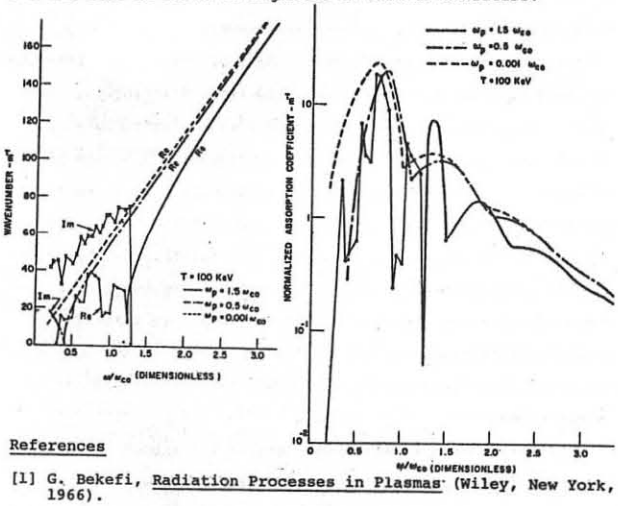

References

[1] G. Bekefi, Radiation Processes in Plasmas (Wiley, New York, 1966).

[2] J. A. Tataronis and F. W. Crawford, J. Plasma Phys. 4, 231 (1970); 4, 249 (1970).

Work supported by the National Science Foundation under grant ENG 75-11168 and the US Energy Research and Development Administration under contract E(11-1)2387 and E(11-1)3077.

POLARIZATION OF X-RAYS FROM LASER-PRODUCED PLASMAS

J.L. Shohet
The University of Wisconsin, Madison, Wisconsin 53706 USA
and
D.B. vanHulsteyn, S.J. Gitomer, J.F. Kephart and R.P. Godwin
Los Alamos Scientific Laboratory, Los Alamos, NM 87544 USA

Abstract: The first measurement of polarized X-rays from a laser-produced plasma is reported. The degree of polarization is related to the net anisotropy of the hot electron velocity distribution.

It is the purpose of this paper to show the first successful measurement of the polarization of the X-radiation from laser-produced plasmas, and to show the relationship between the anisotropy of the velocity distribution and the degree of polarization of the X-rays.

The experimental apparatus is shown in Fig. 1. A 5 joule Nd-glass laser was used to produce plasma using a flat polyethylene target. The laser system is a mode-locked Nd:YAG oscillator from which one 30 psec pulse is switched out and amplified by two Nd:YAG rods followed by two Nd:glass amplifier rods. The f/3.5 focusing optics yielding incident intensities of the order of 10^{15} W/cm^2 at the target. An 8 percent energy prepulse was introduced 30 psec or more in advance of the main laser pulse.

The polarimeter incorporates five scintillator-photomultiplier detectors. Detector #5 is arranged to detect unscattered X-rays. The remaining detectors are divided into two separate polarimeters: one set has covering foils of 0.1 mm Al. X-rays incident on the scatterer which are polarized horizontally are scattered vertically, due to the Compton effect, into the top and bottom detectors (#2 and #4) while vertically polarized X-rays are scattered horizontally into the two side detectors (#1 and #3). The Al absorbers result in a lower energy cutoff for the X-rays of about 6 KeV. An upper energy cutoff for detection of the X-rays is at about 200 KeV.

In order to select an appropriate observation angle, some initial assumptions regarding the nature of the hot electron velocity distribution were made. It was assumed that the distribution was either an anisotropic Maxwellian with the $T_\parallel > T_\perp$. ($\parallel$ & $\perp$ refer to the target normal, or a drifting Maxwellian with $V_{D_\parallel}$ superimposed on an isotropic Maxwellian distribution function). Free-free electron-ion bremsstrahlung produces X-rays of varying intensity and polarization depending upon the angle of observation relative to the target normal. The intensity, and more strongly, the polarization are affected not only by the anisotropy of the electron velocity distribution, but also according to whether the X-rays are produced by small or large angle scatterings, and whether the electrons are relativistic or non-relativistic. Given the distribution function mentioned, the X-ray polarization should be predominantly parallel to the target normal.

Figure 2 shows experimental results for a shot in which polarization was measured at an observation angle 5° with respect to the target surface. The traces correspond to signals measured by calibrated detectors #1, #2, #3 and #4. Detectors #2 and #3 have the Al absorbers. Note that the signals on detectors #2 and #4 are larger than those on detectors #1 and #3, respectively. This implies that the X-rays are polarized predominantly parallel to the target normal. A comparison of the unscattered to scattered X-ray intensities indicated a scattering efficiency of roughly 1 percent. Single photons could be detected, but in the case shown here, all the detectors were measuring at least some tens of photons. The degree of polarization seems to be roughly the same for either the uncovered or Al covered detectors.

The intensity of X-radiation produced per shot depends on the energy of the laser pulse. In fact, X-ray intensity appears to be greatest for laser energies below the highest energy available from the system. This may be due to self-focusing of the laser beam at the higher energies, thus cutting down the intensity of laser light striking the target. Given a sufficiently large measured X-ray intensity, the polarization was always parallel for the orientation shown in Fig. 1.

Two additional angles of observation were used. The first was such that the polarimeter observed X-rays emitted along the target normal. In this configuration, no trend to the polarization was observed. The second orientation placed the polarimeter so that it observed X-rays emitted parallel to the target surface but perpendicular to the plane of the laser beam and the target normal. The indicated polarization again appeared to be parallel to the target normal.

By computing both average polarization from the experiment and a comparable average from theory for a range of perpendicular temperatures and anisotropies (anisotropic Maxwellian distribution function assumed), we conclude that the experimental polarization data implies a net anisotropy $T_\perp/T_\parallel \approx 0.2$-0.3. Such anisotropy is in reasonable agreement with particle simulation results [1,2] and may indicate that resonant absorption [2] is the process by which laser light is absorbed and hot electrons produced.

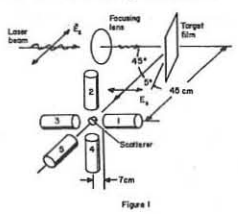

Figure 1

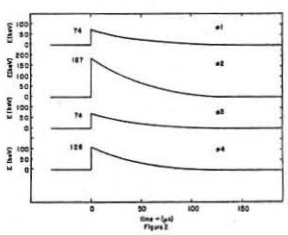

References

[1] D. W. Forslund, J. M. Kindel, Kenneth Lee, E. L. Lindman and R. L. Morse, Phys. Rev. All, 679 (1975).

[2] J. P. Freidberg, R. W. Mitchell, R. L. Morse and L. I. Rudsinski, Phys. Rev. Lett. 28, 795 (1972).

Work performed under the auspices of the United States Energy Research and Development Administration and the National Science Foundation under grant ENG 75-11168.

INVESTIGATION OF ENERGETIC ION BEAMS
IN THE PLASMA FOCUS DISCHARGE

N.V.Filippov, V.A.Bezbatchenko, I.F.Belyaeva, T.I.Filippova
I.V.Kurchatov Institute of Atomic Energy, Moscow, USSR

ABSTRACT Studies of the characteristics of a high current deuteron beam (DB) was carried out by three methods of the "time-of-flight" spectrometer, of nuclear emulsions and by activation methods on the base of C^{12} (d,n) N^{13} and Al^{27} (d,p) Al^{28} reactions. The energy distribution (maximum near E_d = (1... 1.5) MeV) has a reproducible fine structure close to a periodical type.

Scale of the current beam is 3.10^4 Å and time of it's generation 15 ns.

As it was shown before /1/ there are regimes in system of Plasma Focus (PF) type which are determined by slipping of current shell along the electrode surface in which current contraction takes place without noticeable common contraction of substance. Energy and intensity of generated under such conditions high power electron beam (EB) are determined by the value and density of contracted current and also by thermophysical properties of a contact anode zone.

Studies of characteristics of a high current deuteron beam /2/ propagating towards cathod has been continued in regimes close to the conditions of EB generation. The increase of the length of the current contracting zone and stopping of its direct contact with the anode allowed to get DB substantially exceeding the previously observed ones in intensity and bardness /3/.

The purpose of the present paper is the comparison of results of DB studies by activation methods on the base of C^{12} (d,n) N^{13} and Al^{27} (d,p) Al^{28} reactions and by nuclear emulsion method. Fig. 1 presents a scheme of measurements. A drift tube (2) is mounted on the discharge chamber (1) of the "MG" device /4/ which operates at p_o = 0,6-0,8 torr D_2 + 0,15 mtorr Xe; U_o = 15-17 kV, $W_o \sim$ 80 kJ. Deutron flux originated in "PF" having covered the distance of S=245cm reach the target (3) (Al, C or Al+C), β - activity of which is measured by a counter (4). A combined target is made of double ribbon (a graphite cloth and an aluminum foil) which is stretched between the barrel for realing of the working section of the area of 6 x 8 cm^2. Original number of Al^{28} and N^{13} atoms is found from the curve of radioactive decay (the sum of two exponents of T/2 = 138 sec. and T/2 = 600 sec.). In the case of monochromatic DB their ratio determines the energy of deuterons and in the present studies it determines representation of the hard (E_d = 2 MeV) part of the spectrum. From curves similar to those represented in Fig. 2 the DB hardness and power can be preliminarily evaluated.

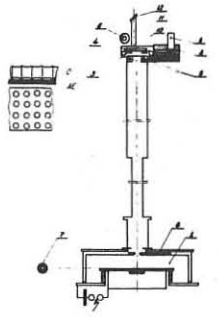

Fig. 1

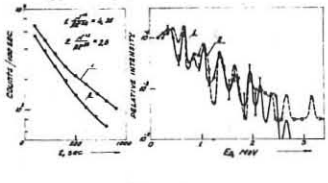

Fig. 2

The neutron irradiation intensity of the C^{12} (d,n) N^{13} reaction of the carbon target was registrated by photoscintillation detector (5) in the method of the "time-of-flight" spectrometer. As it was shown in paper /2/ the instant of DB appearing coinsides with the pulse of hard X-ray radiation and the generation length (10-15 ns) is small compared with the path time to a target. The pulse oscillogram dN_n/dt (Fig. 3,a) was treated using the dependence of the reaction section on deuteron energy. Fig. 3 (3) presents differential energy spectrum of deuterons obtained by the above method. An absolute scale of similar distributions was found from calibration in terms of a standard source (gold-activated foil of the area of 6 x 8 cm^2) and was checked by direct measurement of the number of neutrons from the target by a counter (6) with the help of an ordinary method of silver activation (Ag^{109}). The counter (6) is quite identical to the block (7) used for measuring the bulk neutron yield from PF which influence on the counter reading (6) was determined while the beam was interrupted by a lid (8). DB symmetry was checked by four β - counters (9) which was placed behind aluminum screens limiting the beam section in front of the target.

Exposure of nuclear emulsions was carried out simultaneously with activation methods of measurements in the chosen regimes of operation. A part of DB through the window (10) near the target center (3) was taken out through an opening (11) 15μ in diameter (in a plate 0,1 mm thick) and got on a nuclear emulsion (12) set at an angle of 45° to the beam axis. Obtained energy spectra are shown in Fig. 3 (1,2). (3,2) and (3.3) spectra correspond to one and the same discharge. The absolute value of a carbon target activity in the discharge (3,1) is approximately one order of magnitude higher than that in the case (3,2). One should pay attention to fine and close to a periodic one structure of a spectra reproducible in a set of discharges. In spite of some averaging resulting from the procedure of the photoelectric signal treatment of a neutron pulse the same structure is noticed in the spectra (3.3). This states a sufficient adequacy of the "time-of-flight" spectrometry method. Periodic structure of deuteron spectra can result from the discreteness of the acceleration zone. It is interesting to note that in the given regimes a PF natural neutron radiation is characterized by high degree of stability ($\sim$ 10%) and its value ($\sim 1.5 \times 10^{10}$) is not connected with the presence or absence of DB.

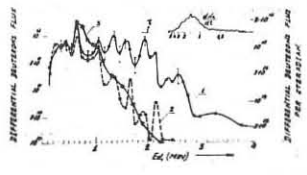

Fig. 3

In conclusion the authors would like to express their gratitude to V.V.Komissarov, O.S.Kudryashov and R.A.Tyulyaeva for their assistance in carrying out the experiments.

REFERENCES

1. K.G.Gureev, V.S.Imshennik, N.V.Filippova, "Fisika plasmy", 1, 192, 1975.
2. N.V.Filippov, T.I.Filippova, JETF, Pis'ma, 25, 262, 1977.
3. N.V.Filippov et.al., Nucl. Fusion, Suppl., p. 169, 1975.
4. V.I.Agafonov et.al., Plasma Phys. and Contr. Nucl. Fusion Res., IAEA, Vienna, 2, 21, 1969.

ANOMALOUS RESISTIVITY AND SUBSEQUENT FAST PARTICLES IN THE PLASMA FOCUS

A. BERNARD, A. COUDEVILLE, J.P. GARCONNET, A. JOLAS, J. de MASCUREAU, C. NAZET

Commissariat à l'Energie Atomique, Centre d'Etudes de Limeil
B.P. n° 27 - 94190-VILLENEUVE SAINT-GEORGES - FRANCE

Abstract : Magnetic probe measurements show that the electrical singularity is caused by a resistive effect occuring in a large volume current sheath. Later the current is carried by fast particle beams.

Previous experiments have shown /1,2/ that the current sheath is a broad structure. A small part of the current (about 15 %) flows in the dense and luminous front, the largest fraction flows behind in an extended zone of lower density. Recent results also obtained with magnetic probes are clear evidence of a strong resistive term in the plasma impedance. This effect is followed by the acceleration of fast electrons and ions.

Various types of probes have been used to measure $\frac{dB}{dt}$. Two are drawn in Fig. 1, their risetime is about 1 ns. It is difficult to have probe holders in glass or ceramic withstand the shock caused by the focus discharge, mainly when they are located to observe the radial phase close to axis. The second type, with small outer diameter and metallic strength, is well suited to observation in this zone.

Measurements have been done with a 530 kA, 40 kV, 27 kJ machine operated at 3 Torr H_2 with inner electrode positive. Electrode diameters are 50 and 100 mm, length is 250 mm.

Typical waveforms of $\frac{dB}{dt}$ are shown in Fig. 2 for probes located in the axial propagation phase of the discharge. For all waveforms shown the $\frac{dB}{dt}$ negative peak coincides in time with the $\frac{dI}{dt}$ negative peak (as measured from a Rogowski coil outside the plasma chamber) which allowed the time positionning of the various probes in Fig. 2. With the probe located at z = - 20 mm the first part of the signal between t_1 and t_2 reflects essentially the passing of the current sheath, as the current intensity is then a slowly varying function of time. From the constant sheath velocity V_z (1.2×10^7 cm s^{-1} as measured with the probes) it results that $\frac{dB}{dt}$ is directly proportional to the radial current density j_r. After the current sheath has gone by the probe entirely ($\frac{dB}{dt}$ returns to 0) one observes later at t^* (Fig.2) that $\frac{dB}{dt}$ becomes negative. Now the variation of B is due to that of the current I flowing in the anode at z = - 20 mm.

The change in $\frac{dB}{dt}$ waveforms as a function of probe location is shown in Fig. 2. For probes at z = - 10 , = - 5 , = 0 the two phenomena are not time separated any longer. Rather the decrease of current occurs while the sheath, approximately constant in width in that propagation phase, is still passing across the probe.

The same observation is done on $\frac{dB}{dt}$ waveforms taken with probes located to look at the radial phase (Fig. 3). On the three probe signals the decrease of $\frac{dB}{dt}$ is correlated to the negative peak in the total current time derivative $\frac{dI}{dt}$. Approximate sketches of the current sheath (with the dense and tenuous zones) are drawn in Fig. 2 and 3. It is then quite clear that the strong increase of the plasma impedance typical of the singularity (negative peak in $\frac{dI}{dt}$, overvoltage measured across the insulator) is not caused by an inductive effect, which implies gathering the current sheath on diameters of 1 mm or so, but rather by a high value of the plasma ohmic resistance.

Each series of measurements was done with the same probe. Quite similar results have been obtained on a smaller machine (250 kA ; 40 kV ; 3.4 kJ) with other probes. Relative calibration only is assumed in the measurements just discussed. As there is complete consistency between all of them it is worth while to consider the absolute calibration as well. From the probe located at r = 20 mm the current gathered in front of the anode on a 40 mm diameter zone is only 200 kA. It corresponds to an average current density j_z of 15 kA.cm^{-2}. Following Ref. 2 the voltage across the pinch reaches approximately 100 kV. It develops on distances of a few centimeters which makes the field E,1 to 5 times 10^4 V.cm^{-1}. So that the conductivity is in the range of 10^{12} to 2×10^{11} sec^{-1}, to be compared to Spitzer's value of 2×10^{15} sec^{-1} at T_e = 50 eV. Even though T_e is not known precisely the resistivity is strongly anomalous.

It is observed experimentally that the emission of hard X-rays and neutrons (when D_2 is used) usually starts at the $\frac{dI}{dt}$ negative peak. The probe signals at that time display a positive surge (Fig. 4,a) which is absent when the machine does not emit X rays and neutrons (Fig. 4,b). The current increase is due to the lower impedance met by the beams of particles that carry the current at that time. Thus there appears to be two current régimes - resistive or beam - in the same discharge. In poor discharges the beam régime is practically absent. In other discharges the beam régime occurs a few times (2 to 4) which accounts for the multiple X-ray and neutron pulses.

Let us summarize the main conclusions. The current sheath is a very broad structure extending over more that the central electrode area. Strongly anomalous resistivity takes place creating a large voltage drop between the anode and the cathode (or a virtual cathode). This plasma diode is suddenly shorted by fast beams of electrons and ions leading to the emission of X rays and neutrons.

References

/1/ A. BERNARD, A. JOLAS, J.P. GARÇONNET, J. de MASCUREAU, C. NAZET, A. COUDEVILLE, A. BEKIARIAN, Commissariat à l'Energie Atomique, France, Report CEA-R-4807 (1977).

/2/ A. BERNARD, A. COUDEVILLE, J.P. GARÇONNET, A. JOLAS, J. de MASCUREAU, C. NAZET, in Plasma Physics and Controlled Nuclear Fusion Research (I.A.E.A Vienna 1977, Berchtesgaden 6-13 Oct. 1976 CN - 35 E 18-4).

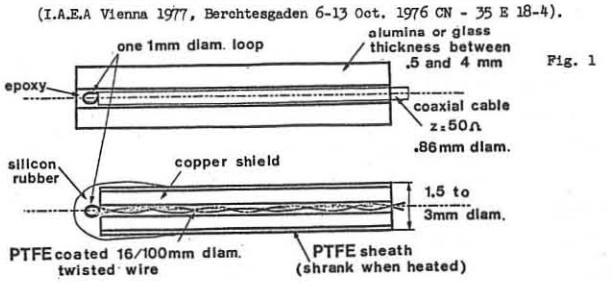

Fig. 1

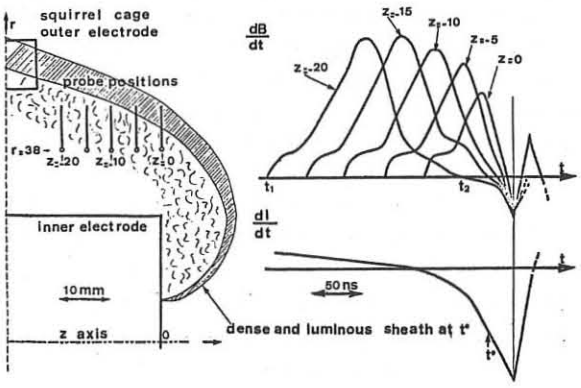

Fig. 2

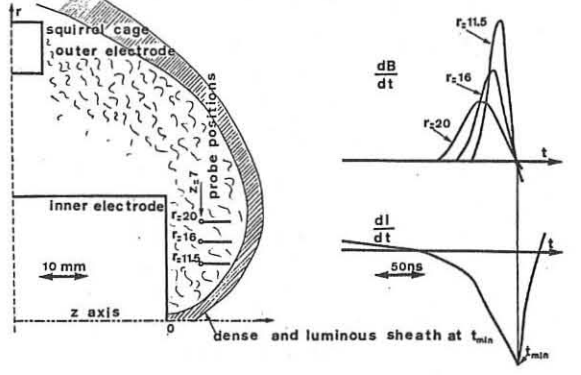

Fig. 3

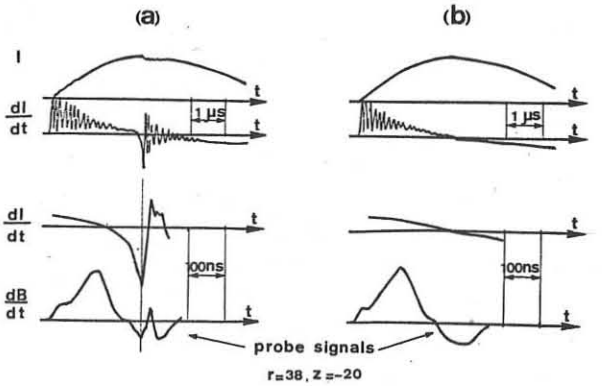

Fig. 4

ENHANCEMENT OF NEUTRON YIELD FROM FOCUS DEVICES

Y.H. Chen[+], G. Decker, L. Flemming, W. Kies, T. Oppenländer, G. Proß, B. Rückle, H. Schmidt, M. Shakhatre, M. Trunk

Institut für Plasmaforschung, Universität Stuttgart
Federal Republic of Germany

Abstract: Enhancement of neutron yield by the following methods was investigated: Variation of voltage, geometry, pressure and gas mixture. The gain of an 85 kV device (12 kJ) in comparison to a 20 kV device of equal energy is 3. Reduction of radius of the center electrode of a 20 kV device permits operation at increased pressure values with a gain of 1.5. Argon addition does not improve the yield for an optimized device.

Efforts in the low to middle energy range have been undertaken /1/ to improve the remarkable neutron yield of focus devices. It is hoped that the trends found here may further the yield and application also of large devices.

1. From MHD calculations we conclude that the available pinch current for condensor banks of constant energy may be increased by using banks with higher voltage than used typically so far, maintaining as low external inductance L_0 as possible /2/. Enhanced current should result in enhanced neutron yield Y /3/. These devices will have inherently short quarter cycles for the current scaling with $\tau/4 \sim 1/U$ for L_0 = const. or $\tau/4 \sim 1/\sqrt{U}$ for $L_0 \sim U$. To test the technical feasibility and the predictions as to enhanced yield, we operated an 85 kV device (HV device) with L_0 = 35 nH, 12 kJ, $\tau/4 \approx 600$ nsec. For comparison, we used our 20 kV, L_0 = 50 to 70 nH, 12 kJ device "Minifokus" with $\tau/4 \approx 3$ µsec.

We found that for our HV device it was necessary to adjust the plasma dynamics to the current quarter cycle not only by varying length and filling pressure as usual but also a variation of center electrode radius r was necessary for the following reason: Due to the short quarter cycle, the radial compression takes up an appreciable part of the available time. Experimental efforts to match the motion of the plasma by using very low filling pressures failed due to spoke formation and current loss in the accelerator. No neutron yield for r = 33 mm for the broad length and pressure range investigated, an average value of $4 \cdot 10^8$ per shot for r = 25 mm (filling pressure ≈ 1 torr) and an average value of $\approx 3 \cdot 10^9$ for r = 12.5 mm (pressures between 7 and 15 torr) were obtained. Figure 1 shows the improvement (factor 3) obtained for the energy values 6 kJ, 9 kJ and 12 kJ if the energy scaling law according to Rapp /4/ is employed. The scaling with current fits into the $Y \sim I^{3.3}$ law established by Bernard /3/. The discharge current was increased from 420 kA ("Minifokus") to 560 kA for the HV focus partly due to the decreased inductance but also due to decreased accelerator dimensions leading to less damping of the current.

2. Operating at comparatively high filling pressures and small c.e. radii with the HV focus has led to good reproducibility and high yield. Therefore, we tried to improve our "Minifokus" by reducing the c.e. radius. Figure 2 shows that indeed a shift to higher operating pressures can be obtained (from 1.8 torr to 10 torr) and an increase of the neutron yield by a factor 1.5 is found. For comparison the pressure range and neutron yield of the HV device with the corresponding radii are indicated. Additionaly, we studied the following parameters and ascertained their effect on neutron yield and operating range: o.e. diameter (quoted as example in Figure 3), o.e. structure (bars are better than perforated material), o.e. length (weak influence for bars), c.e. length (may be used for fine tuning), c.e. material (copper and silver giving about equal yield, silver less standard deviation, aluminium less yield and high standard deviation).

3. It seems likely that the important breakdown phase and the following current transfer /5/ and possibly also the pinch formation and neutron yield may be influenced by adding different gases /6/. Figure 4 indicates that for certain operating ranges (higher and lower than optimum pressure) an increase of Y is possible but the maximum yield never could be surpassed.

For operation with c.e. negative (which normally produces very few neutrons) an enhancement by a factor of 30 was found. Generally the effect was the stronger the less the device was optimized.

In conclusion we may say that higher voltage clearly results in higher maximum current and thus increased neutron production. On the other hand, there is evidence that high voltage has other effects such as improved breakdown behavior, current transfer and reproducibility, culminating in increased neutron production. The different efforts to improve focus devices will, however, eventually have to be accompanied by appropriate diagnostics in order to understand the influence of all parameters investigated here on the neutron production and neutron production mechanism in general.

1. Decker, G. et.al., IAEA-CN-35/E18-1, 6th Int. Conf. on Plasma Phys. and Contr. Fus. Research, Berchtesgaden 1976

2. Trunk, M., Plasma Physics 17, 237 (1975)

3. Bernard, A., Paper C1.1, Third Top. Conf. on Pulsed High Beta Plasmas, Culham (1975)

4. Rapp, H. et.al., 6th Europ. Conf. on Contr. Fusion and Plasma Physics, Moscow 1973, 1, 371

5. Oppenländer, T., to be published in Plasma Physics: The plasma focus current in the compression phase

6. Rückle, B., Report IPF-76-1, Stuttgart 1976

[+] Guest researcher from University of Kuala Lumpur, Malaysia

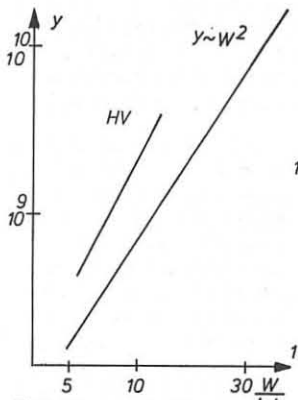

Fig.1: Energy-Scaling of the HV focus

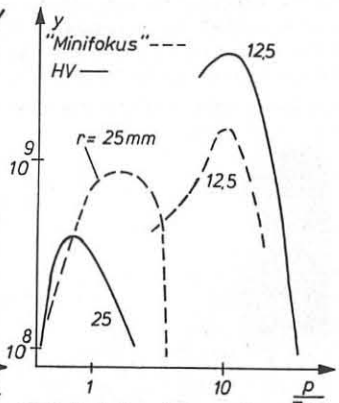

Fig.2: Variation of the center electrode radius and voltage

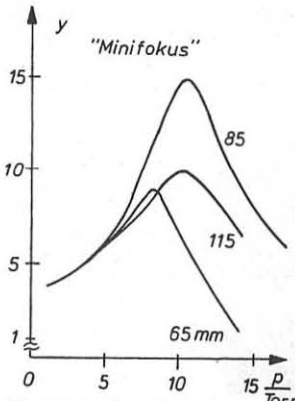

Fig.3: Variation of the diameter of the outer electrode

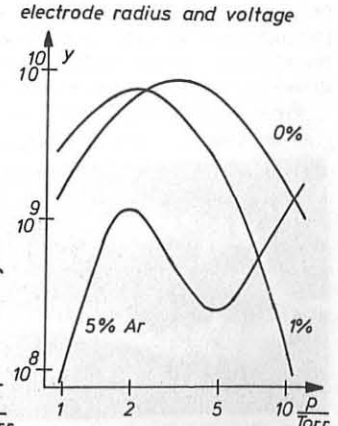

Fig.4: Variation of Ar-admixture for "NESSI" device (45kJ, 20kV)

PLASMA FOCUS DISCHARGE INVESTIGATIONS IN A ZETA-PINCH GEOMETRY

N.G.Reshetnyak, R.D.Meladze

Sukhumi Institute of Physics and Technology of the State Committee on Utilization of Atomic Energy, Sukhumi, USSR

Abstract. The paper deals with the experimental results of studies on a short zeta-pinch. It is shown that during a single discharge pulse, plasma can have several states with high energetic parameters accompanied with intense neutron and hard X-ray emissions. The experimental data allow us to conclude that the neutron emission is related with the accelerated deuton beam interacting with a gaseous target.

The discharge system described in/I/ has been used in the experiments. The discharge was ignited between the tubular electrodes (the inner diameter and the length of hollow electrodes being 6 ÷ 10cm and 20cm, respectively). The gap between the electrodes (I ÷ 3cm) is shorter than their diameter. The electrodes have been located within the vacuum chamber of large volume. Gas pumping into the interelectrode gap is accomplished by means of a pulse valve. In the process of compression the plasma configuration becomes noncylindrical. This leads to appearing axial cumulative jets. At the moment of the plasma layer compression at the system axis there arises an anomalous high resistance of the current channel related with the turbulent processes. This stage of the discharge is called the plasma focus (PF).

The main results are obtained in the device with the following parameters: the voltage at the condenser bank is 20 kV, the discharge current is I MA, the discharge halfcycle is close to 9 μsec and the energy stored amounts to ~ 38 kJ.

The discharges have been investigated in different gases (D_2, H_2, He) with various distribution types of neutral gas densities in the interelectrode gap. Magnetic probe measurements obtained in the discharge optimum regimes show that there is no secondary ignition of the discharge in the system after the maximum compression stage for ~ 3 msec. This result is confirmed by streak photoes of the discharge. A typical streak photo of the discharge taken from the side with the slit oriented the axis is shown in Fig.1.

Figl. The discharge streak photo showing the absence of secodary ignitions for ~4 μsec. Time scanning performed left to right.

After bright flashing at the moment of the maximum compression the luminosity vanishes in a visible area of the spectrum. "A dark pause" takes place. The "dark pause" duration during which the neutron emission is observed amounts to ~3 μsec. It should be noted that the "dark pause" has been observed by several authors studying the systems of plasma focus type /2,3/; however, its duration (0,1÷0,3 μsec) has been coincided with the neutron pulse duration. The subsequent bright flash of luminosity corresponds to visual appearing of ionized vapours of electrode materials.

Fig.2 shows typical current-voltage characteristics illustrating the type of discharge current and voltage variations.

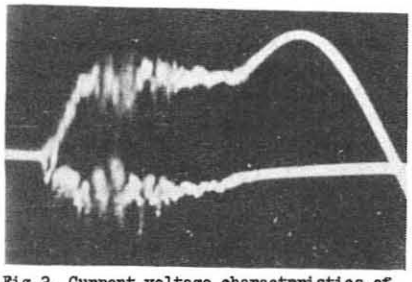

Fig.2. Current-voltage characteristics of the discharge forming PF ($5 \cdot 10^9$ neutrons/discharge). Upper trace shows the discharge current; lower trace reflects the voltage.

The current-voltage characteristics indicate that the current radial compression to the axis is accompanied with the voltage sharp splash of 50÷80 keV and the discharge current drop. The first singularity appears in voltage and current curves. After this characteristic moment of time, the currentt rapidly increases up to the former level (~400 KA) and past a short interval of time, the current drop and the voltage growth reappear, resulting in the second singularity and so on.

In optimum stages of the discharge, the current curve shows four or five subsequent singularities. Up to the moment of the maximum compression, the voltage divider reflects the plasma shell dynamics with a sufficient accuracy. At the moment of the current shell stopping close to the system axis the voltage should drop down to zero (if to neglect the active resistance). When the plasma column expands the voltage should change in sign. However, this does not occur. Examination of the splash shape on the voltage curve shows that the voltage drop takes nearly 250 nsec. That means that after the maximum compression stage, a considerable growth of the current channel ohmic resistance occurs. /4/. In optimum regimes of the discharge, the neutron emission total duration is I ÷ 2 msec, while hard X-ray radiation takes ~4 ÷ 5μsec. For the discharge regime investigated, four or five neutron pulses are characteristic; the pulses do not much differ in amplitude and duration, each of them existing for 250 ÷ 300nsec and being accompanied by the splash of hard X-ray radiation (Fig.3).

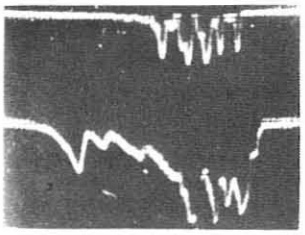

Fig.3. Traces of neutron (upper trace) and hard X-ray emission pulses.

The present results allow to draw a conclusion about an entire character of the mechanism resulting in generation of hard X-ray and neutron radiations.

PF is a source of soft X-rays. On a photo in soft X-rays, the accumulation zone appears as a fibre stretched along the axis. Lateral and longitudinal dimensions of fibers are ~ 0,6cm and I ÷ 3 cm, respectively. The electron temperature in plasma changes from 0,8 to 1,2 keV. Electron and ion beams forming during the discharge are measured directly.

The mass-spectrometric analysis of the ion beam extracted along the discharge axis (towards the cathode) showed that the energy of accelerated deutons is in the region of ~ 80keV. It is comparable to the energy of accelerated electrons defined from the hard X-ray measurements, and corresponds to the splash amplitude value of the voltage curve.

The experimental data indicate that in PF regimes investigated, neutron fluxes towards the zeta-pinch axis (Φ_{0°) are 1,4 times greater than in the perpendicular direction Φ_{90°. The anisotropy factor is $k = \frac{\Phi_{180^\circ}}{\Phi_{90^\circ}} \sim 0,6$.

The neutron output observed (~ $5 \cdot 10^9$ neutrons per discharge) can be accounted for by the interaction of intense deuton beams generated due to the considerable rise of the discharge channel resistance with a gaseous target.

It has been experimentally demonstrated that there is a relation between the discharge current drop depth, the beam current magnitude and the neutron output level.

The present experimental results witness that during a single pulse of the discharge, plasma can have several states with a high density and high energetic parameters. In such states plasma is an intense source of neutron and hard X-ray emissions.

REFERENCES

1. Н.Г.Решетняк, Р.Д.Меладзе. Материалы III Всесоюзной конференции по плазменным ускорителям. Минск, 1976, 110.
2. Jalufka N.W., Lee J.H. Phys.Fluids, vol.15, No 11, 1954 - 1958, 1972.
3. Toepfer A.J., Smith D.R., Beckner E.H. Phys.Fluids, vol.14, No 1, 52 - 61, 1971.
4. И.Ф.Кварцхава, Э.Ю.Хаутиев, М.Л.Нинидзе. Физика плазмы, т.2, вып.1, 1976, 40-43.

PLASMA-FOCUS DYNAMICS INVESTIGATIONS BY MEANS OF MULTIFRAME INTERFEROMETRY AND SHADOWGRAPHY

S.Denus, S.Kaliski, A.Kasperczuk, S.Kowalski, M.Paduch, L.Pokora, Z.Wereszczyński
Institute of Plasma Physics and Laser Microfusion, Warsaw, Poland
and M.Sadowski
Institute of Nuclear Research, Otwock-Świerk, Poland

Abstract. The paper presents results of interferometric and shadowgraphic studies performed on the F-150 plasma-focus device. The velocities of current layers and plasma expansion are determined. Also determined are electron concentration distributions. Multiple generation of plasma bubbles is shown.

A diagram of the experimental setup is shown in Fig.1. The measurements were performed on the Focus device /PF/ with copper electrodes of the following dimensions: ϕ_e=100mm, ϕ_k=50mm in diameter and 200mm long [1]. In the face of the central electrode there was made 8-mm-i.d. hole enabling introducing the CO_2-laser beam /during the focus-laser experiments [2] /. To supply the setup use was made of a condenser bank of a capacity C=112μF and nominal energy E_n=150kJ. The studies under consideration were conducted at a smaller energy of about 60kJ. Formation and dynamics of the plasma-focus were studied with a laser Mach-Zehnder interferometer which enabled a series of three interferograms to be made in the course of one discharge. Time-lags between the diagnostic laser pulses were controlled by changing the distances between the mirrors of the delay line /LO/. The interferometric or shadowgraphic images were registered with the aid of a special three-frame camera /KF/. The light source in the interferometric setup in question was provided by a ruby laser [3] which generates pulses of about 2ns duration. When synchronizing the laser with the plasma discharge, the onset of the pulse of the hard X-ray radiation /X_h/ way considered as the moment t=0. Fig.2 presents an example of a series of shadowgrams. In Fig.3 a sequence of interferograms

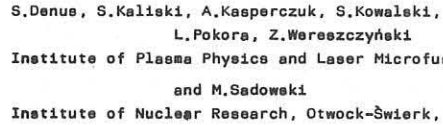

Fig.1

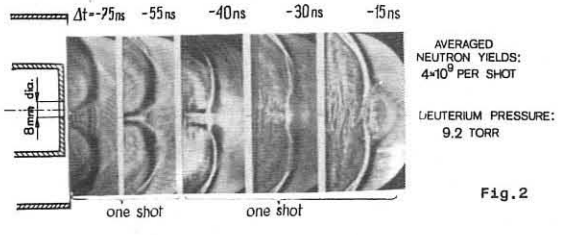

Fig.2

there is shown in correlation with the neutron-radiation pulse averaged on the basis of 20 discharges .

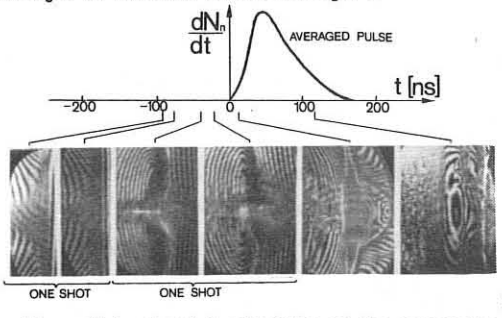

Fig.3

The radial and axial velocities of the converging current layer, as determined on the basis of the interferograms and the shadowgrams, were v_r=/1.4±0.2/×10^{7}cm/s and v_z=/0.8±0.2/×10^{7}cm/s respectively. The value of v_z was approximately constant, whereas the of v_r varied both in time and space. The maximum value of v_r was about 2.5×10^{7}cm/s and was observed at some distance from the central electrode /about 0.5 - 0.8 cm/.

The convergence phase under study was followed by the collapse of the current layers on the symetry axis. As a result of this collapse there occurred a formation of a high-density plasma focus of a length of 0.8 - 1.2 cm and approx. 2mm in diameter. In the last phase of this process a very fast /$V_z > 10^8$cm/s/ axial outflow of plasma in the direction from the electrodes was observed.

The lifetime of plasma of a maximum density was estimated to be only about 10 ns. After the plasma attains its maximum density, there is observed its quasistable radial expansion at a velocity of about 1.5 x 10^{7}cm/s. At the first onset of the expansion there occur the hydrodynamic instabilities of the m = 0 type. The examplificatory spatial distribution of electron concentration, determined on the basis of a chosen interferogram, is presented in Fig.4. The fast, axial outflow of plasma gives rise to the formation of the plasma bubbles. Numerous instances were observed of the formation of a few bubbles which propagate along the axis at a velocity of /1.0 - 2.5/x10^{7}cm/s. Fig.5 illustrates such a multiple generation of the plasma bubbles.

On the basis of the measurements performed it has been found that, in the course of the axial expansion of plasma, as early as about 40ns after the maximum compression has been attained, there is formed at the central electrode, a layer of contamined plasma wherein violent turbulence takes place. The thickness of this region along the symmetry axis increases with the time and attains about 2cm. After about 120ns this layer starts to detach itself from the central electrode. In the later stages of the discharge the release is observed of increasingly larger amounts of plasma which is likely to contain a large quantity of impurities resulting from the erosion of the electrode surface. This plasma is formed in the shape of a conic stream and can exist for a few microseconds.

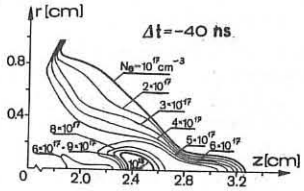

Fig.4

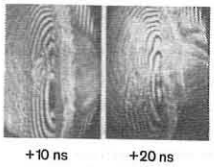

Fig.5

All phases of the plasma-focus were investigated from the moment of the collapse of the current layer up to the disintegration of plasma. The results of the studies under consideration are consistent with those presented in Refs [4] and [5], but special attention should however be paid to the observed multiple generation of the plasma bubbles. The measurements have also demonstrated that, for the purpose of heating the plasma-focus along the symmetry axis, it would be profitable to use a CO_2-laser pulse shorter than 40ns, since after this period a layer of plasma can be teared off from the central electrode and screen the plasma-focus. Further detailed investigations of plasma-focus dynamics are being continued especially in connection with focus-laser experiment.

[1] M.Gryziński, A.Jerzykiewicz, J.Nowikowski - Bull.de l'Academic Polonaise des Sciences, Ser.Des Sciencies Techniques XXII, 2, 1974.
[2] S.Kaliski, J.Baranowski, M.Borowiecki, S.Denus, M.Gryziński, K.Jach, A.Jerzykiewicz, M.Kielesiński, S.Kowalski, J.Kubicki, Z.Kurzyński, J.Nowikowski, P.Parys, T.Rusinowicz, M.Sadowski, J.Wawer, J.Wolski, J.Wołowski, - Journ.Techn.Phys., 16, 4, 1975
[3] A.Kasperczuk, M.Paduch, L.Pokora, Z.Wereszczyński - Biul. WAT 26, 2, 1977;
[4] A.Bernard, A.Coudeville, A.Jolas, J.Launspach, J.de Mascureau Phys.of Fluids 18, 2, 1975;
[5] H.Schmidt, M.Salzmann, H.Stromwald - Appl.Optics 16, 9, 1975.

HIGH-BETA TOKAMAKS SURROUNDED BY FORCE-FREE FIELDS

D.A. D'Ippolito, J.P. Freidberg*), J.P. Goedbloed, J. Rem
Association Euratom-FOM, FOM-Instituut voor Plasmafysica,
Rijnhuizen, Jutphaas, The Netherlands
*) Los Alamos Scientific Laboratory, Los Alamos, U.S.A.

Abstract: An MHD-analysis of the surface-current model of a toroidal high-beta tokamak shows that shaping of the cross-section favourably affects the equilibrium, while force-free currents make a new stability region accessible when the cross-section is elongated without increasing the curvature.

Application of the high-beta ordering in an MHD-analysis of the sharp-boundary model of an axisymmetric tokamak has been shown to provide a reasonable description of global kink modes[1]. Here we report on some results concerning effects of shaping the cross-section and addition of force-free fields on the equilibrium and the stability of elliptical and racetrack-like cross-sections. The equilibrium quantities describing the plasma are:

$$p = \text{constant}\ , \qquad \underline{B} = B_\phi \hat{e}_\phi\ , \qquad B_\phi = R_o B_o / R\ . \tag{1}$$

On the plasma surface C, currents produce a jump in the magnetic field components such that the pressure is balanced:

$$p + \tfrac{1}{2}B_\phi^2 = \tfrac{1}{2}\hat{B}_p^2 + \tfrac{1}{2}\hat{B}_\phi^2\ , \tag{2}$$

where hats refer to quantities in the exterior region. In the latter region force-free currents are permitted to flow:

$$\underline{\nabla}\times\underline{\hat{B}} = \alpha\underline{\hat{B}}\ ; \qquad \alpha = \text{constant}\ . \tag{3}$$

In the high-β ordering the various quantities are ordered as follows:

$$\varepsilon = a/R_o \ll 1\ , \qquad B_\phi/B_o \sim \hat{B}_\phi/B_o \sim 1\ ,$$
$$\hat{B}_p/B_o \sim \varepsilon\ , \qquad \beta \equiv 2p/B_o^2 \sim \varepsilon\ , \qquad \alpha a \sim \varepsilon\ . \tag{4}$$

Application of the ordering to (2) leads to:

$$\hat{B}_p/\varepsilon B_o = \frac{2}{k}\sqrt{\beta/\varepsilon}\left[1-\frac{k^2}{2}(1-x)\right]^{\frac{1}{2}}\ ,$$
$$B_\phi/B_o = \hat{B}_\phi/B_o = \left[1+\varepsilon x\right]^{-1}\ , \tag{5}$$

where $x = (R-R_o)/a$ (see Fig. 1). The parameter k^2 represents the freedom that we still have to choose the toroidal current or the safety factor q. It is chosen so that $k^2 = 0$ corresponds to low-β ($\beta = 0(\varepsilon^2)$) and $k^2 = 1$ corresponds to the maximum allowable β, i.e. the beta for which the separatrix touches the surface ($x = -1$).

It is tempting to choose as physical parameters describing the equilibrium: β, the safety factor q, and αR. There is, however, a serious disadvantage in selecting q. This quantity varies strongly when the separatrix approaches the plasma surface while the quantity that really is fixed in an experiment, the current, varies only little. This has led us to introduce a new quantity q^*, related to the current:

$$q^* \equiv 2\pi a c \hat{B}_\phi / I_\phi \approx \varepsilon B_o / \langle \hat{B}_p \rangle\ , \tag{6}$$

where c is the elongation of the cross-section with respect to the circle: $c = L/2\pi a$ and $\langle \hat{B}_p \rangle$ is $\hat{B}_p$ averaged along C; L = length of circumference $= \oint dl$. This definition has the advantage that at low β the stability boundary is in the neighbourhood of $q^* \approx 1$ (Fig. 2).

It is now logical to measure the pressure with respect to q^{*2}, i.e.

$$\varepsilon\beta_p \equiv 2\varepsilon p/\langle \hat{B}_p \rangle^2 = (\beta/\varepsilon)q^{*2} \tag{7}$$

instead of with respect to $\hat{B}^2$; similarly the force-free field is measured by $\Gamma = \alpha R_o q^*$.

Table 1

$\varepsilon\beta_{p,crit} = \frac{1}{2}\left[\frac{1}{L}\oint\sqrt{1+x}\,dl\right]^{-2}$			b = 0	c = 1	b = 1	b → ∞ c → ∞
circle	2 ←2→	$\varepsilon\beta_{p,crit} = \pi^2/16$	—	.617	.617	—
ellipse	2b		.563	.617	.617	.673
racetrack	2b	$\left(\frac{b-1+\pi/2}{b+1}\right)^2$	—	.617	.617	1
triangle	2b	$\left(\frac{3b+3\sqrt{b^2+4}}{6b+4\sqrt{b^2+4}}\right)^2$	.563	.426	.422	.360
triangle	2b	$\left(\frac{3b+3\sqrt{b^2+4}}{4\sqrt{b^2+4}}\right)^2$	.563	1.14	1.18	2.25

Since $\varepsilon\beta_{p,crit} = \varepsilon\beta_p(k^2=1)$ corresponds to the equilibrium limit, this relationship points out that any β is possible if q^* is not restricted by stability. Table I contains $\varepsilon\beta_{p,crit}$ for various cross-sections. It shows that shaping of the cross-section can yield a gain of a factor 2 to 3 in $\varepsilon\beta_{p,crit}$. A D-shape with the flat side at the inside of the toroid is seen to be the most favourable.

The force-free currents do not affect the equilibrium. Their influence on the stability is, however, quite pronounced. Figure 3 shows the results for an ellipse with b/a = 3. Qualitatively this stability diagram is similar to that for the circular cross-section (Ref. 2). The two stability regions, one at large q^* and one at small q^*, are seen to approach each other when Γ is increased from a low value to a value between 1-2, whereafter the left region remains stationary and the other region withdraws to large q^*. Since the stability diagram is valid for any toroidal mode number n one must conclude that the stability region for small q^* is inaccessible and that the maximum possible β is found at the intersection of the right-hand-side stability boundary with the equilibrium limit. Consequently, there is an optimum value of Γ.

From plots of the marginally stable surface perturbation of an elliptical cross-section at various values of the parameters q^*, Γ, and b/a the following picture emerges. At low values of Γ the perturbation is localized near the top and bottom of the cross-section, the more so the larger the elongation. Increasing Γ diminishes the localization and the perturbation becomes that of an m = 1 kink mode. Together with the stability results this suggests that elongation as well as force-free currents enlarge the range in β and q^* where the plasma is stable, and that for an elliptical cross-section the stability decreases when b/a is large, due to the increasing curvature at the top and bottom of the cross-section. The results for the racetrack b/a = 2.7 (Fig. 4), with the same value of c as the ellipse with b/a = 3, confirm this. These results also show a basic change in the behaviour of the two stability regions. There is now a range in Γ for which both regions overlap, so that, as far as the global kink modes are concerned, almost the entire β-q^* space is stable (Figs. 4 and 5).

This work was performed under the auspices of FOM, ZWO, Euratom, and USERDA.

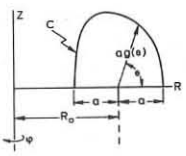

Fig. 1

References

1. J.P. Freidberg and W. Grossmann, Phys. Fluids 18 (1975) 1494.
2. D.A. D'Ippolito, J.P. Freidberg, J.P. Goedbloed, J. Rem, Proc. 6th Int. Conf. on Plasma Phys. and Contr. Nucl. Fusion Res., Berchtesgaden, I, IAEA (1977) 523.

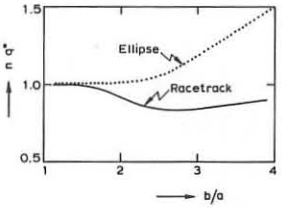

Fig. 2 nq^* at marginal stability versus b/a for elliptical and racetrack-like cross-sections at Γ = 0, β/ε = 0.

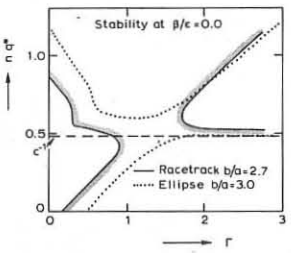

Fig. 5 Effect of force-free currents on stability regions at β/ε = 0.0 for ellipse and racetrack.

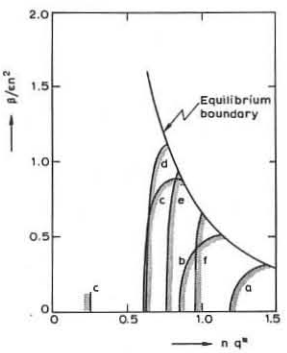

Fig. 3 Stability ellipse b/a = 3., c = 2.1.

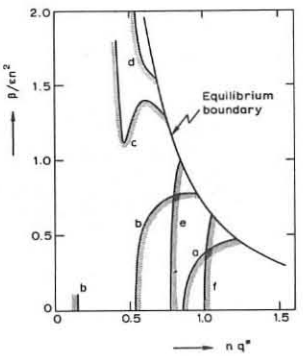

Fig. 4 Stability racetrack b/a = 2.7, c = 2.1.

Curves a, b, c, d, e, f, indicate stable regions, shaded side, for the values of cΓ = 0, 1, 2, 3, 4, 5.

APPLICATION OF IDEAL MHD STABILITY CODE ERATO
TO HIGH BETA TOKOMAK EQUILIBRIA

R.A. Dory, D.B. Nelson and Y-K. M. Peng
Oak Ridge National Laboratory, Oak Ridge, Tennessee 37830

D. Berger, L.C. Bernard, R. Gruber and F. Troyon
Centre de Recherches en Physique des Plasmas
Ecole Polytechnique Fédérale, 1007 Lausanne, Switzerland

Abstract: An initial survey of the MHD stability of FCT equilibria has been done with the ERATO {1} spectral code. When the plasma is surrounded by vacuum extending to infinity, a β-limit of 1-2% is found. A conducting shell at about 1.1-1.2 times the plasma radius can stabilize the ballooning modes and increase the β-value to 3-4% for an unoptimized case.

The ERATO code {1}, written by the Swiss authors of this paper, analyzes the stability of an axisymmetric plasma toward small perturbations. The model used is an evaluation of the quadratic perturbation energy δW from ideal (non-resistive) magnetohydrodynamics. This evaluation uses a two-dimensional finite hybrid element technique {2} with the resulting matrix solved by vector iteration, which can provide as eigenvalues the (squared) growth rate, $\gamma^2 = -\omega^2$, and as eigenfunctions, the mode structure of the perturbation.

The high beta equilibria {3} found at Oak Ridge and used in this study are for plasmas shaped by external lumped conductors. Figure 1 shows the plasma boundary (outermost solid line) and two locations considered later for placement of a "conducting" shell supposed to be effective in the time scale of the instability. (The shell is assumed to carry images of the perturbation plasma currents, but is not required for equilibrium.) The equilibria are characterized by the values for $\bar{\beta}$, the volume-averaged plasma pressure scaled by the vacuum magnetic pressure $B_o^2/2\mu_o$ at the center $R = R_o$ and $Z = 0$, of the discharge cross section, and by the value q_a/q_o, ratio of safety factor (inverse rotational transform) at the plasma edge and magnetic axis. The usual Oak Ridge scaling {4} is applied so that one equilibrium calculation can be used for many values of q_o and corresponding values of $\bar{\beta}$. This scaling varies the total plasma current, while holding fixed the geometry, toroidal field outside the plasma, and the shape of the pressure profile.

Figure 2 presents growth rate curves for five ostensibly different equilibria from a sequence approximating the FCT model {3} of tokamak response to strong external heating. Curves labelled FCT 2, 4, 6...represent cases with $q_a/q_o = 3.7$, and $\bar{\beta}_1$ values of 2, 4, 6...12% (the subscript 1 means that the $\bar{\beta}_1$ value applies to the case $q_o = 1$). It will be seen that, in units of the Alfven velocity (using B_o) divided by the major radius of the torus, the growth rates of the modes are as high as 0.6 for the higher $\bar{\beta}$ cases when the conducting shell is removed to infinity except for the conducting line along the cylinder axis $Z = 0$. A single case (FCT9) is also shown in dashed lines to indicate the behaviour when the shell lies directly at the plasma edge (no vacuum). The change of $\bar{\beta}$ with q_o complicates the interpretation of these data, so a cross plot has been made in Figure 3. Here the data between $q_o = 1$ and $q_o = 1.5$ are shown in a graph of γ versus the appropriately scaled values $\bar{\beta}$. The near-coincidence of the lines for the case FCT6, 9 12 motivates the "ostensibly" used early. Values of γ well above zero suggest extrapolation to give a $\bar{\beta}$ limit of 1-2%.

Corresponding data are also shown for the case with shell at the plasma edge suggesting that the $\bar{\beta}$ threshold can be raised substantially by taking advantage of stabilization by a nearby conducting shell. The threshold $\bar{\beta}$ appears to be about 3-4%, somewhat in agreement with conclusions in Ref. 4, and it is tempting to think that higher values may obtain as we test other plasma shapes

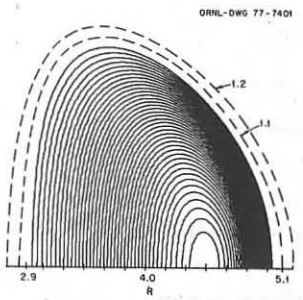

Fig. 1 Typical configuration treated. Dashed lines show conducting wall location for stability runs. Solid lines are magnetic surfaces.

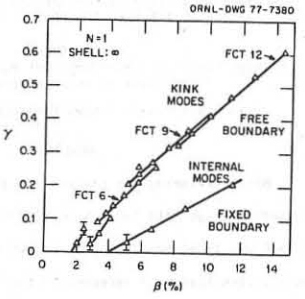

Fig. 3 Growth rate as function of β for $1 < q_o < 1.5$, and infinite vacuum. Also shown is the case with shell at the plasma surface.

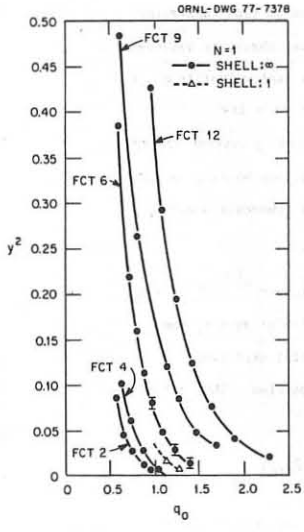

Fig. 2 Growth rate curves as function of q_o for several cases, with infinite vacuum and one case (FCT9) with shell at the plasma surface.

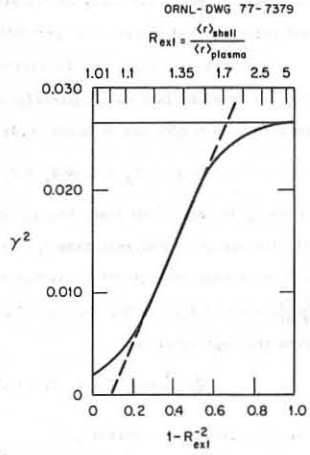

Fig. 4 Growth rate of a case near threshold as function of radius of conducting shell.

and as we vary q_a/q_o, a measure of the profile widths. We may hope also that broadening the current distributions will make the system more stable near the threshold where the modes have a somewhat localized ballooning nature, relying on proximity of the conducting shell to control the global kink modes. Since the ERATO code has provision for analyzing the effect of conducting shell at a finite distance from the plasma, we have studied this for the FCT6 case with $q_o = 1.22$. The data in Figure 4 show that the transition from infinite vacuum region to no vacuum is essentially complete when the ratio of average shell radius to average plasma radius is reduced to about 1.1-1.2.

It should be mentioned that the indicated uncertainties in the γ values result from artificial restraints (computer time, money, etc.) on the resolution of the present calculations and that work is underway to reduce the uncertainty by a better resolution of the equilibrium, by an improvement of the analytic treatment around the axis and by a judicious choice of grid intervals. This is specially necessary for high $\bar{\beta}$ cases where the distortion of the magnetic surfaces is great.

Future study is needed of optimization vis a vis cross section shaping and control of the plasma pressure profile width.

---

*Research sponsored by the Fonds National Suisse de la Recherche Scientifique and by Energy Research and Development Administration under contract with Union Carbide Corporation.

{1} D. Berger, L.C. Bernard, R. Gruber and F. Troyon, IAEA VI, Berchtesgaden, Paper CN-35/B11-4 (1976)

{2} R. Gruber, Jrnl.of Comp.Physics, (1977) to appear

{3} (a) R.A. Dory and Y-K. M. Peng, Nuclear Fusion 17, 21 (1977)
(b) J.F. Clarke and D.J. Sigmar, Phys.Rev.Lett. 38, 70 (1977)

{4} R.G. Bateman and Y-K. M. Peng, Phys.Rev.Lett. 38, 829 (1977)

PROGRESS IN EQUILIBRIUM AND TRANSPORT THEORY OF THE FLUX CONSERVING TOKAMAK*

D. J. Sigmar
Oak Ridge National Laboratory, Oak Ridge, Tennessee, USA
(on leave of absence from MIT)
and ORNL Fusion Energy Division Theory Group

ABSTRACT

After reviewing the physical origins of the idea of flux conserving high beta Tokamak equilibria and recalling their basic global and local properties we report on recent advances. The equilibrium theory is extended to include the time dependent coupling of the inner (plasma) solution to the outer (vacuum) solution, as will be required in any strong beam heating experiment. After showing a numerical simulation of flux conserving adibatic heating to high beta, the transport theory is extended to study the resistive decay of the safety factor profile $q(\psi,t)$ and poloidal flux driven by a generalized Ohm's law.

The physical origin of the flux conserving tokamak concept derives from the fact that successful auxiliary heating to "high" beta (i.e. $\beta \sim a/R$) has to occur under the timescale ordering

$$\tau_A < \tau_h < \tau_E < \tau_s \tag{1}$$

where τ_A is the Alfven time, the heating time $\tau_h^{-1} = \eta_\parallel j^2 + P_{aux})/nT$, the energy containment time $\tau_E^{-1} = \kappa_\perp T/a^2 nT$ with $\kappa_\perp$ the effective heat conductivity, and the poloidal skin time $\tau_s^{-1} = \frac{1}{\psi}\frac{\partial \psi}{\partial t}$, where $\psi(R,z)$ is the poloidal flux function. This follows from the heat equation

$$\frac{\partial}{\partial t}\ \frac{3}{2}\, nT - \nabla \cdot \kappa_\perp\ \nabla T = \eta_\parallel j^2 + P_{aux}, \tag{2}$$

the flux diffusion equation [1]

$$\frac{\partial \psi}{\partial t} = \frac{\eta_\parallel c^2}{4\pi}\ \Delta^* \psi - \underline{V} \cdot \nabla \psi \tag{3}$$

and the experimental evidence that for typical ohmically heated higher density Tokamak plasmas $\kappa_\perp$ is close to the neoclassical ion heat conduction and $\eta_\parallel$ is practically the classical resistivity. From (2), the ratio $\tau_h/\tau_E \ \alpha\ (1 + \frac{P_{aux}}{P_{oH}})^{-1}$ can be made small with large auxiliary power and from (3) it follows that $\tau_E/\tau_s < 1$, thus confirming Eq. (1). Recalling the definition of the safety factor as

$$4\pi^2\, q(\psi) = F(\psi) \oint_\psi \frac{d\ell}{B_p R^2}$$

where $F(\psi) = RB_\phi$,

it follows that also $q(\psi)$ decays on the resistive timescale (3) so that if the auxiliary heating is faster than τ_s the flux is frozen in.

The solution of the equilibrium equation is then obtained with $p'(\psi)$ determined by auxiliary heating and $q(\psi)$ frozen to its initial low β profile [2]. Such a choice of the two free functions with increasing $p'(\psi)$ profiles yields a series of neighboring equilibria with novel and desirable properties [2,3], such as complete absence of the so called equilibrium limit $\beta_I \simeq R/a$ (since the separatrix cannot enter the plasma on a timescale faster than τ_s), a pressure driven rise in toroidal plasma current and onset of an absolute minimum B region in the vicinity of the magnetic axis. This can be gleaned from the resultant form of the poloidal field [2]

$$RB_p = 2\,\frac{\psi_o}{a^2}\,\rho/(1 + d\cos\theta) \tag{4}$$

where $d \equiv 2\,\frac{\psi_o}{a^2}\,\rho\,\frac{d\delta}{d\psi}$, $\delta(\psi)$ being the pressure driven Shafranov-shift of the flux surface ψ such that for high beta $d \to -1$. (ψ_o is the flux at the boundary $\rho = a$.) Consequently, at the outside of the torus ($\rho = a$, $\theta = 0$) one obtains $B_p/B_T = \frac{a}{Rq}/(1 + d)$, which can become of $O(1)$, thus compensating for the R^{-1} drop of B_T.

For a more complete understanding of strongly beam heated Tokamak plasmas it is necessary to connect the "inner" solution (4) to the vacuum solution, including the effect of a casing and/or external field windings. For low beta equilibria where the denominator in Eq. (4) can be readily Fourier expanded, this has been accomplished by Shafranov et al. [4]. However, as $d \to -1$ in the high beta limit of the flux conserving Tokamak, the Fourier series does not converge. Following the generalization of the circular cross section work of Ref. [2] to an elliptic cross section [5] the scaling with β of the self consistent vertical field inside an elliptical casing is presently under investigation. Numerical calculations [6] indicate that the dependence on major radius R of the field index $-(R/B_\perp)(dB_\perp/dR)$ changes from positive to negative, as β exceeds a few percent. The ensuing vertical stability problem and its dependence on plasma elongation is also under investigation.

For the questions discussed so far, knowledge of the standard global plasma parameters β_I, μ_I, ℓ_i and of the function B_p on the plasma surface were sufficient. The <u>local</u> values of the plasma current and pressure profile so important for MHD stability are controllable via the heat deposition profile of the neutral injection system. By tailoring the beam direction and penetration depth, a wide variety of more or less stable profiles can be produced. Numerical solutions [7] using the adiabatic heating theory of Grad, Hu and Stevens [8] will be shown. (The linear and nonlinear stability behavior, particularly with respect to pressure driven kink-ballooning modes [9] will be presented in a separate paper.)

Assuming MHD stable equilibria have been obtained under the constraint of flux conservation it is then of interest to study their diffusive decay. In particular, from Eq. (3) one expects the edge region to diffuse relatively more rapidly than the center, and the safety factor profile to change, thereby affecting the MHD stability properties. Hirshman [10] has recently derived the equation

$$\left.\frac{\partial}{\partial t}\right|_\psi q(\psi,t) = -\frac{c}{4\pi^2}\,\frac{\partial}{\partial \psi}\, V'(\psi)\, \left[< \underline{E} \cdot \underline{B} > - V(t)\, F < R^{-2} > \right] \tag{5}$$

where $V(\psi)$ is the plasma volume, $\underline{E}$ the electric field in the plasma, $V(t)$ the induced voltage on the plasma surface, and the angular brackets denoting a flux surface average. When Eq. (5) is combined with a simple [1] or generalized Ohm's law [11] to express $< \underline{E} \cdot \underline{B} >$ in terms of $j_\parallel$ and pressure and temperature gradient driven collisional fluxes one obtains an analytic estimate of the β-dependent decay time of $q(\psi,t)$. Supporting exact numerical solutions obtained by Hogan [12] will be shown.

* Research sponsored by Energy Research and Development Administration under contract with Union Carbide Corporation.

[1] H. Grad, J. T. Hogan; Phys. Rev. Lett. 24, 1337 (1970).
[2] J. F. Clarke, D. J. Sigmar; Phys. Rev. Lett 38, 70 (1977).
[3] R. A. Dory, Y-K. M. Peng, Nucl. Fusion 17, 21 (1977).
[4] V. S. Mukhovatov, V. D. Shafranov, Nucl. Fusion 11, 495 (1971).
[5] T. Mizoguchi, T. Kammash; to be published.
[6] Y-K. M. Peng; ORNL/TM, to be published.
[7] D. Nelson, ORNL/TM, in preparation.
[8] H. Grad, P. Hu, D. Stevens; Proc. Natl. Acad. Sci. USA 72, 3789 (1975).
[9] G. Bateman, Y-K. M. Peng; Phys. Rev. Lett. 38, 829 (1977).
[10] S. P. Hirshman, private communication.
[11] A. A. Ware; Nucl. Fusion 13, 793 (1973).
[12] J. T. Hogan; Controlled Fusion Theory Conf. 1977, paper E10.

INFLUENCE OF PREDISCHARGE CONDITIONS IN SPICA

A.A.M. Oomens, C. Bobeldijk, J.A. Hoekzema,
A.F.G. van der Meer and D. Oepts
Association Euratom-FOM, FOM-Instituut voor Plasmafysica,
Rijnhuizen, Jutphaas, The Netherlands

Abstract. A study of the predischarge conditions in SPICA[1] has been started to improve the reproducibility of the screw-pinch discharges. Measurements on three types of predischarge plasmas are reported, together with a first comparison of the associated main discharges, characterized in the most favourable type by peak β-values of 0.2.

Introduction. In an earlier publication of the SPICA results[2] it was reported that a marked difference in behaviour of the screw-pinch plasmas was observed with the same external conditions. It seemed therefore appropriate to study the values and the reproducibility of the plasma parameters resulting from different predischarges.

Predischarges. Three types of predischarges, summarized below, have been studied. Here t_1 is the start of the predischarge, t_2 is the start of the bias field, both with respect to the main discharge, and τ_E the time in which 90% of the energy content (9.0 kJ) of the predischarge bank is dissipated. Density profiles in the outer half of the torus were measured at t=0 μs by means of Thomson scattering. The results are given in Fig. 1 for p_o = 10 mtorr and p_o = 5 mtorr. Type H has an approximately Homogeneous density profile, good reproducibility and a high degree of ionization. Type E also shows good reproducibility, but a very Eccentric density profile. Type L is not reproducible and has a Low degree of ionization. The electron temperatures are the same for L, H, and E (about 3 eV) and constant over the tube radius. At p_o = 2 mtorr breakdown is not reproducible, but for all types the plasmas seem to be homogeneous and fully ionized.

Type	t_1	t_2	τ_E (μs)
L	-100	-110	55
E	-150	-110	30
H	-100	-110	30

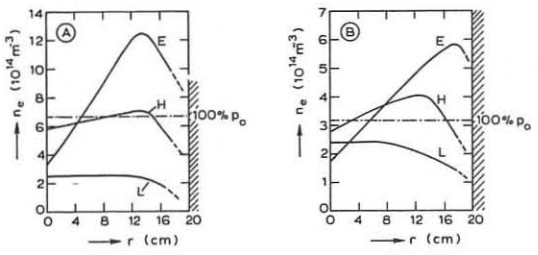

Fig. 1. n_e-profiles in the outer half of the torus obtained in three types of predischarge. The dashed line represents a 100% ionized homogeneous plasma. a) p_o = 10 mtorr, b) p_o = 5 mtorr.

Main discharges. The main discharges following the L, H and E predischarges have been compared at p_o = 10 mtorr, $B_\phi \approx 1.2$ T, $I_{zp} \approx 250$ kA, and an initial bias field B_o ranging from 0.1 to 0.15 T. Most of the discharges were done with type H, some with E and only a few with L. The time behaviour of the electron temperature and the local β are shown in Fig. 2. Up till 26 μs there seems to be no difference in time behaviour for the three types: T_e remains constant and there is a slight decrease in the measured value of β. This decrease may be due to energy loss but can be explained as well by a broadening or shift of the profiles. Another common feature of the discharges is the large D-shaped deformation of the plasma column at times early in the discharge, as derived from poloidal field measurements.

Type E. Most of these main discharges show a gradual loss of equilibrium at times varying from 20 to 50 μs. Measurements of $\int n_e dl$ confirm these lifetimes. The frequency of the m=1, k=0 oscillations as observed on the streak pictures indicates that the mass in the column equals the total mass of the filling gas. The poloidal field fluctuations indicate a current-carrying region extending to 15 cm (Ref. 3).

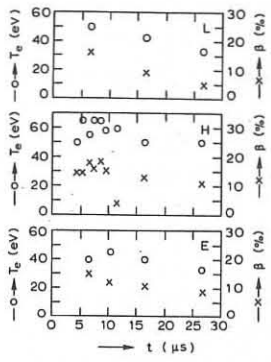

Fig. 2.
Measured values of T_e and β at different times in the main discharge for the three types of predischarge.

Type H. Main discharges of this type are always unstable. At low values of B_o this often leads to violent wall contact, visible on the streak pictures and giving rise to strongly increased impurity radiation (mainly Si). There is always an abrupt loss of compression at times varying from 10 to 50 μs. A stabilizing effect on the plasma is obtained by an increase of B_o or q_{wall}.

Type L. The main discharges associated with this type of predischarge are the same as those described in Ref. 2, except for an increase in bias field from 0.12 to 0.15 T. Again stable and unstable discharges are observed; better preionized plasmas are more likely to be stable. Some parameters of a stable discharge are presented in Fig. 3. As compared to Ref. 2, the time during which the plasma is in equilibrium and shows no MHD-instabilities is increased from 100 to at least 200 μs. From the inductance measurement we conclude that the radius of the current-carrying region is comparable, but the rate of decrease is considerably less.

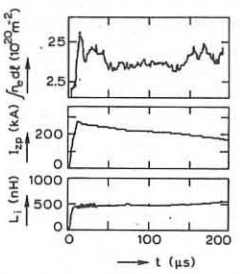

Fig. 3.
Toroidal plasma current, plasma inductance, and $\int n_e dl$ measured in the equatorial plane as functions of time for a stable discharge.
p_o = 7.9 mtorr D_2, B_ϕ = 1.2 T, B_o = 0.15 T, q_{wall} = 1.5.

Theoretical developments. As was shown in Ref. 2, force-free currents surrounding the main plasma core substantially raise the equilibrium and stability limit of β in a high-β tokamak. An extension of the theory towards non-circular cross-sections[4] shows that vertical elongation (racetrack) enhances this tendency with respect to the stability limit. For the equilibrium limit an additional weighting of the shape of the cross-section towards the axis of toroidal symmetry is favourable. Equilibrium calculations taking into account a circular conducting wall and force-free currents in the screw-pinch mode (roughly constant pitch fields) have shown[5] that this elongated D-shape of the minor cross-section quite naturally appears in a screw-pinch discharge, in accordance with the above-mentioned experimental observations. It is possible that this can be further improved by reshaping the conducting wall into a moderately elongated one.

Conclusions. Stable screw-pinch discharges have been obtained with a predischarge plasma having a homogeneous density profile and an ionization degree of 40%. These discharges with q ≈ 1.5 and a peak β of 0.2 are in equilibrium and show no gross MHD-instabilities during about 200 μs. The electron temperature (≈ 40 eV) remains constant during the first 25 μs, the measured values of β slightly decrease.

Acknowledgement. The machine has been skilfully operated by D.J. Maris, P.H.M. Smeets and G. van Dijk. Further assistance was given by W. Kooijman (data handling), P.J. Busch (Thomson scattering), H.W. Luijsterburg (magnetic measurements) and P.R. Jonkers (X-ray measurements). This work was performed under the Euratom-FOM association agreement with financial support from ZWO and Euratom.

References.

1) R.J.J. van Heijningen et al., Proc. 8th Symposium on Fusion Technology, Noordwijkerhout (1974) 341.
2) C. Bobeldijk et al., Proc. 6th Int. Conf. on Plasma Phys. and Contr. Nucl. Fusion Res., Berchtesgaden 1976, Suppl. Nucl. Fusion (1977) 493.
3) M. Mimura et al., Rijnhuizen Report R.R. 76-99.
4) D.A. D'Ippolito et al., this conference.
5) J.A. Hoekzema, Proc. 3rd Topical Conf. on Pulsed High Beta Plasmas, Culham 1975, Suppl. Plasma Phys. (1977) 535.

FINITE-GYRORADIUS EFFECTS IN SCREW PINCHES*

H. Ralph Lewis, Leaf Turner, and Mary Menzel

University of California, Los Alamos Scientific Laboratory
P. O. Box 1663, Los Alamos, New Mexico 87545
USA

Abstract: The effects of finite ion gyroradius on the behavior of screw pinches are being studied numerically and analytically in the context of the Vlasov-fluid model.

The effects of finite ion gyroradius on the behavior of screw pinches are being studied numerically and analytically in the context of the Vlasov-fluid model [1,2]. Of particular interest are the modifications of the predictions of ideal MHD theory and the guiding-center-plasma model due to finite gyroradius. Under study are instabilities in screw pinches and, more recently, the possibilities of magnetoacoustic heating.

In our Vlasov-fluid model [1,2], the ions are treated as collisionless (Vlasov approximation), the electrons are treated as a massless fluid, charge neutrality is assumed, and displacement current is neglected. We are investigating the model computationally and analytically. The computational approach is based on a numerical method that has been developed for linearized systems in which one or more components are collisionless [2-4]. This method has been applied to the $m = 2$ instability of a sharp-boundary screw pinch [2], and the computer code is being modified to treat screw pinches with diffuse profiles. Two analytic approaches are being used for the Vlasov-fluid model applied to a screw pinch. For a sharp-boundary screw pinch, a theory has been developed which relies on certain assumptions regarding the region within about an ion gyroradius of the boundary [5,6]. With these assumptions, the theory is valid for small values of kr_L and ω/ω_c compared to unity, where ω is the eigenfrequency, ω_c is the equilibrium cyclotron frequency, and k is the largest relevant wavenumber. This theory has provided valuable insight into the physics of the model, and good agreement between the theory and numerical computations has been obtained for the $m = 2$ instability when the conducting cylinder surrounding the pinch is infinitely far away [2]. However, discrepancies between the theory and computations have been noted when the conducting wall is near the plasma, and some difficulties have been encountered with convergence of the numerical method in that case.

The problems that have been encountered with a conducting wall close to a sharp-boundary pinch may be clarified by another analytic treatment of the Vlasov-fluid model [7]. This theory is applicable to diffuse-profile screw pinches as well as to the sharp-boundary case. The Liouville equation is solved for small values compared to unity of kr_L and ω/ω_c. Finite gyroradius effects are kept to first order; and, in the case of a sharp boundary, the solution is valid up to the boundary, so that no further assumption is required for the boundary region of the size of r_L. This theory is expected to provide a good set of expansion functions for $\underline{\xi}$ ($\underline{A}^{(1)} = \underline{\xi} \times \underline{B}^{(0)}$) that can be used in the numerical code for the diffuse case as well as the sharp-boundary case. It also provides a differential equation for $\underline{\xi}$, valid in both cases, that is a finite-gyroradius correction to the MHD equation for $\underline{\xi}$.

Currently, both analytic treatments are also being applied to study the possibility of useful magnetoacoustic heating of pinches.

---

*Work performed under the auspices of the United States Energy Research and Development Administration.

[1] J. P. Freidberg, Physics of Fluids 15, 1102 (1972).

[2] H. R. Lewis and L. Turner, Nuclear Fusion 16 993 (1976).

[3] H. R. Lewis and K. R. Symon, Bulletin of American Physical Society 19, 924 (1974); also, to be published.

[4] B. L. Buzbee, G. H. Golub, and H. R. Lewis, in Proceedings of the 7th Conference on Numerical Simulation of Plasmas (Courant Institute, New York University), pp. 196-198.

[5] L. Turner, Physics of Fluids 20, 654 (1977).

[6] L. Turner, Physics of Fluids 20, 662 (1977).

[7] H. R. Lewis, to be published.

PLASMA FORMATION IN THE BELT-SHAPED SCREW PINCH SP IV

E.J.M. van Heesch, A.E. Prinn* and A. Verheul
Association Euratom-FOM, FOM-Instituut voor Plasmafysica,
Rijnhuizen, Jutphaas, The Netherlands
(*University of Liverpool, during part of the experiment guest at Jutphaas)

Abstract. The SP IV experiment investigates the possibilities for elongation in a force-free current screw pinch. The first results show that relatively high ellipticities and β-values can be obtained. The currents observed between conducting wall and central plasma may be responsible for this favourable behaviour.

Introduction. In a new experiment the well-known screw-pinch configuration with force-free currents[1] is combined with an elongated minor plasma cross-section. From theory it can be concluded that equilibrium[2] as well as stability[3] are improved by this combination. A high ellipticity of the plasma is possible by the presence of a copper shell. The quartz vacuum vessel fits closely in the copper shell, thus allowing force-free currents to be induced[1]. High-β values are obtainable by the applied implosion mechanism. The geometry of SP IV is given in Fig. 1. The copper shell and the vacuum vessel have a minor cross-section shaped like a racetrack with ellipticity e = b/a = 4. The primary windings, wound helically around the copper shell, are connected to a 40 kV, 120 kJ capacitor bank. Since plasma current $I_{\phi p}$ and toroidal magnetic field B_ϕ are generated simultaneously, the q-value at the wall is approximately constant in time. The ringing main discharge has a quarter period T/4 = 10 μs. For the described experiments the initial pressure p_o = 30-50 mtorr H_2. Pre-ionization is accomplished by h.f. pulses (30 MHz, 50 kV) and a toroidal predischarge (20 kJ, 80 kHz). A toroidal bias field (B_{io}) can be trapped in the plasma to control β.

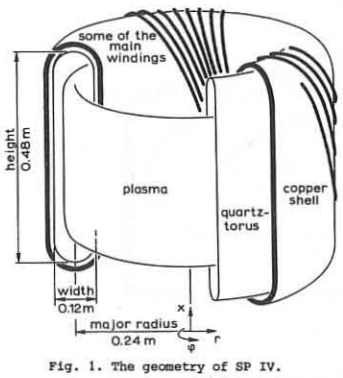

Fig. 1. The geometry of SP IV.

Results. The results presented here are obtained at $I_{\phi p}$ up to 220-260 kA, $q^* = B_\phi \ell^2_{pol}/\mu_o I_{\phi p} \ell_\phi$ between 1.8 and 2.0 and $\overline{B_\phi}$ up to 0.73 T. n_e varies from 1 to 2×10^{22} m^{-3} and T_e from 10 to 60 eV at p_o = 30 mtorr. The first quarter period of the main discharge is characterized by a formation stage including implosion and compression (6 μs) followed by a more stationary period which terminates in a fast decay after 10-12 μs. We can distinguish two reproducible major types of plasma (see Fig. 2); type-A shows: 1) weak implosion, 2) radial compression slowly reaching 2a ≈ 3 cm after 4 μs, 3) very high elongation obtained after a weak vertical compression which reaches 2b ≈ 27 cm after 7 μs, 4) low-β value during the quasi-stationary phase. Type-B plasmas show: 1) strong effective implosion, 2) radial dimensions relax to 2a ≈ 3-4 cm, 3) comparatively low elongation caused by a strong vertical compression which stops after 6 μs at 2b ≈ 15 cm, 4) high β-value during the quasi-stationary phase. The properties of the implosion are investigated by means of streak photographs. Besides, during an effective implosion the diamagnetic signal Δφ shows strong oscillations due to inertia effects (see Fig. 2). The efficiency of the implosion in sweeping up mass has been estimated for type-B plasmas from the radial oscillation frequencies immediately after the implosion. According to a simple model $T = \nu\{c(p_o/e)^{0.5}\}/\overline{B_\phi}$, where c is equal to 1.89×10^{-7} for SP IV; ν depends on the shape of the density profile and equals one for a homogeneous profile. We find ν = 0.93 which indicates that a large mass fraction is swept up. A characteristic of type-A implosions is given by the difference $\Delta\phi_x$ found between $2\pi/B_x \int r dr$ and $\int V_{loop,tor} dt$. At 9 μs this difference, which is caused by ohmic dissipation in the initial stage, amounts to 0.01 Tm^2. The compression following after the implosion can be seen clearly on the streak photographs and also influences the measured value of $L_{i\phi} \equiv 2\pi/B_x \int r dr/I_{\phi p}$. The measured values of $\Delta L_{i\phi}/\Delta b$ (-4.3 nH/cm at p_o = 30 mtorr and -3.1 nH/cm at 40 and 50 mtorr) are in reasonable agreement with a simple model. During the quasi-stationary phase we determined volume average β-values by application of the relation between β and Δφ. In the A-type discharge the β-value of 6% ± 3% is mainly due to a B_x-correction whereas in the B-type the Δφ-term dominates, resulting in β = 15% ± 2% at p_o = 30 mtorr, B_{io} = 0, down to 11% ± 2% at p_o = 50 mtorr, B_{io} = 32 mT. These values indicate that in (B) the column-β is close to unity.

The poloidal magnetic field profile (type A) at 9 μs is given in Fig. 3. The toroidal current profile and q-profile are also presented. The q-profile in the low pressure outside region was evaluated by solving the equation $\nabla \times B = \alpha B$ (Ref. 2), where α was determined from the probe measurements in the midplane and the shape of the central plasma from the streak pictures. Comparison of streak photograph and current profile shows that some 50% of the total toroidal plasma current flows in the region outside the dense central column. This fact as well as the flatness of the q-profile in a region around the central plasma confirm the presence of a well-conducting and probably low density plasma in a part of the outer region of this elongated discharge type for at least 9 μs. The conditions that lead to the reported different discharge types have been investigated. The properties of the initial plasma at t=0, especially the initial degree of ionization γ and the homogeneity, have a dominating influence on the subsequent behaviour of the main discharge. The bias field as well as the predischarge energy have a strong influence on γ. The highly elongated plasmas are produced after a weak preheating, while plasmas with moderate elongation are preceded by a very effective predischarge.

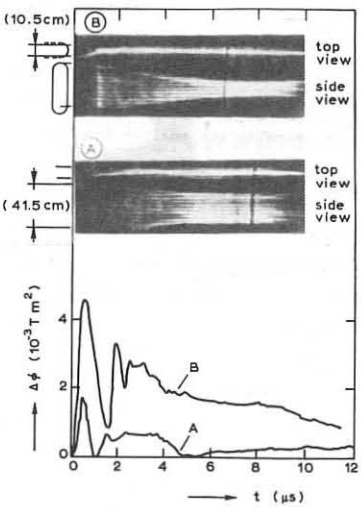

Fig. 2. Streak photograph and diamagnetic signals of two plasma types.

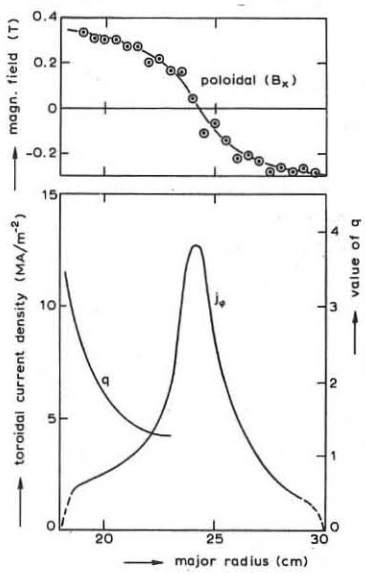

Fig. 3.
Results of magnetic probe measurements at 9 μs in (A).

Acknowledgement. This work was performed under the Euratom-FOM association agreement with financial support from ZWO and Euratom.

References.

1) Bobeldijk, C. et al., Proc. 6th Int. Conf. on Plasma Phys. and Contr. Nucl. Fusion Res., Berchtesgaden 1976, Suppl. Nucl. Fusion (1977) 493.
2) Hoekzema, J.A., Proc. 3rd Topical Conf. on Pulsed High Beta Plasmas, Culham 1975, Suppl. Plasma Phys. (1977) 535.
3) D'Ippolito, D.A. et al., Proc. 6th Int. Conf. on Plasma Phys. and Contr. Nucl. Fusion Res., Berchtesgaden 1976, Suppl. Nucl. Fusion (1977) 523.

STATIONARY MAGNETIC FIELD CONFIGURATION
IN NON-CIRCULAR CROSS SECTION SCREW PINCH, TPE-1a

K. Sugisaki
Electrotechnical Laboratory
Mukodai-machi 5-4-1, Tanashi, Tokyo, Japan

Abstract: A magnetic field configuration desirable to confine a high beta plasma is obtained in a stationary stage of a non-circular cross section screw pinch with a metal shell, TPE-1a. No global modes are observed.

Introduction: It has been shown that in an axisymmetric toroidal system with a moderately elliptical cross section, the beta value of the plasma can be higher than in a system with circular cross section [1]. Additional increase of critical beta value is expected in a plasma with a broad current profile as in a screw pinch with a metal shell. The positional instability can be avoided in case of use of the metal shell.

Apparatus: The schematic diagram of TPE-1a [2] is illustrated in Fig. 1. A quartz discharge chamber is 40 cm in length,

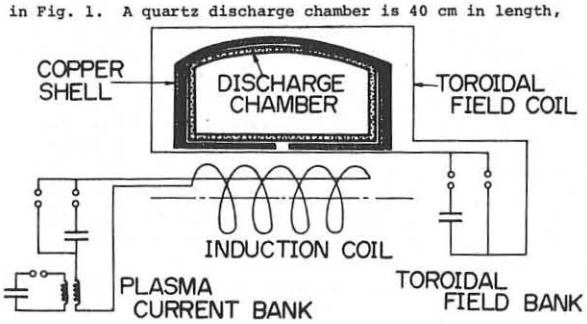

Fig.1 Schematic diagram of TPE-1a.

while the major and minor radii are 13.5 cm and 6 cm, respectively. The copper shell of 1.5 mm thickness covers the discharge chamber. A toroidal magnetic field and plasma current are induced by separate capacitor banks of 30 KJ. The maximum toroidal field of 6 KG and plasma current of 120 KA are generated with rise time of 8 μs. The experiments are almost carried out for deuterium of 10 mTorr.

Dynamic stage: After implosion and subsequent large displacement toward the wall, the plasma column returned rapidly near the center of the discharge chamber. At the stationary stage, the toroidal shift of the plasma column was 1.5 cm. The plasma temperature determined from pinch speed was 70 eV. The electron temperature determined from the soft x-ray foil absorption technique was about 40 eV at 10 μs.

Stationary stage: The plasma current was kept nearly constant for 50 μs by power crowbar circuit. The magnetic field configuration was also unchangeable during this stage. The typical magnetic profiles on the medium plane are shown in Fig. 2. The plasma current density was nearly uniform over the discharge chamber. The plasma paramagnetism was also observed during this stage. The beta value of the plasma was about 3 % from magnetic field measurements. The magnetic flux surfaces obtained from magnetic field measurements are shown in Fig. 3. The safty factor q was 2 on the flux surface A and 3.5 on the flux surface B. The electron density integrated on the medium plane was measured with a He-Ne laser interferometer and was $2 \times 10^{15}/cm^2$. The electron temperature at this stage was determined from the ratio of D_β line to continuum and was 5 eV. For $q < 3$, magnetic probe measurements indicated the existence of small amplitude plasma motions with n=0 mode (axial displacement) and n=1 mode (kink-like deformation). These plasma motions were not growing but oscillatory. The streak pictures taken axially did not indicate the existence of global modes during this stage. The flux surfaces were approximately

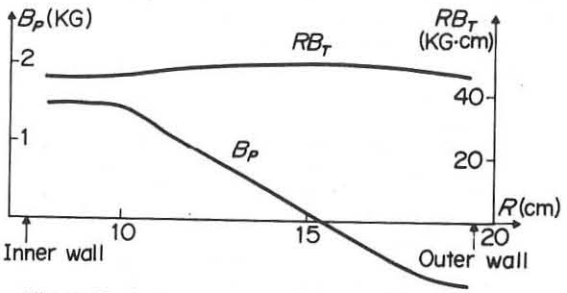

Fig.2 Typical magnetic field profiles.

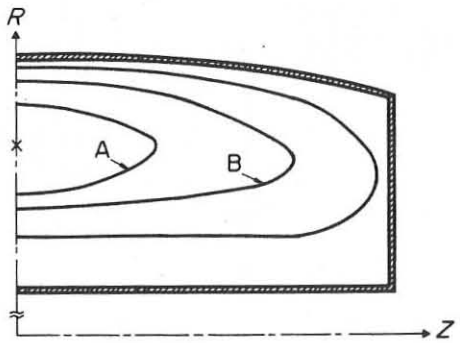

Fig.3 Typical magnetic flux surfaces.

symmetric in regard to the medium plane in this stage.

Decaying stage: The plasma current begins to decay at 50 μs. In this stage, magnetic field measurements showed that the plasma current decayed rapidly in the outer region, while it decayed slowly in the inner region. Therefore, the current flowing region was limited near the magnetic axis and the cross sections of the flux surfaces tended to be circular. The plasma current channel was separated from the wall and the poloidal magnetic field is stronger at the outer wall than at the inner wall as in an ordinary Tokamak configuration. The toroidal field profile tended to be vacuum field like.

Conclusion: The magnetic field configuration at the stationary stage should be able to confine a high beta plasma. However, the beta value obtained experimentally was smaller than that predicted theoretically. The beta value and electron temperature decayed rapidly at the transition phase (10 ~ 20 μs) from the dynamic to stationary stage. The decay time was not affected by the small amplitude plasma oscillations. Therefore, it seems that the beta value is limited not by a stability condition but by energy transports.

REFERENCES

[1] J.P. Freidberg and W. Grossmann, Phys. Fluids 18 (1975) 1494.

[2] T. Shimada and others, 6th Conf. on Plasma Physics and Controlled Nuclear Fusion Research, CN-35/E4, Berchtesgaden (1976).

Measurement of the Poloidal Configuration in the Lausanne Belt Pinch

J.-M. Peiry, M. Altmann, G. Tonetti, F. Hofmann

Centre de Recherches en Physique des Plasmas
Ecole Polytechnique Fédérale
CH-1007 Lausanne, Switzerland

Abstract : The three components of the magnetic field (B_r, B_θ, B_z) were measured in the plasma of the Lausanne belt pinch, as functions of radius, axial distance and time. Maps of the poloidal flux function ψ and the toroidal current density j_θ, as well as radial profiles of the safety factor q are presented. The results show that the poloidal field diffuses axially through the plasma.

Introduction : Belt pinch plasmas are still far from being understood. Axial contraction {1,2,3}, radial compression ratio {4,5}, and axial displacement instabilities {6} are just a few of the phenomena that have not yet been satisfactorily explained. In the Lausanne belt pinch, plasma parameters have been measured in the midplane (z=0) but up to now little was known about their dependence on axial distance. In the present paper we report the first detailed measurements of magnetic fields in a belt pinch plasma, as functions of radius, axial distance and time.

Measurements : Experimental parameters for the set of measurements reported here were as follows: Charging voltage of the main capacitor bank: 30 kV, filling pressure: 20 mTorr D_2, maximum toroidal field at r=16 cm: 7.5 kG, $\tau/4 = 5$ µs, $n_{e_{max}} = 6\times10^{15}cm^{-3}$, $T_{e_{max}}$=40 eV. Access to the plasma in the Lausanne belt pinch is difficult. There is only one radial port at z=0. Therefore, the field measurements had to be done by introducing a long probe through one of the axial ports. The probe has two small pick-up coils in its tip. It can be rotated about its axis to permit measurement of either (B_r,B_z) or (B_θ,B_z). It can also be moved radially and axially, such that one half of the poloidal cross-section (z>0) can be completely scanned. The field components, B_r,B_θ and B_z, were measured by radial scanning at 6 different axial positions (z=0, 100, 200, 250, 300, 350 mm). The radial resolution was 5 mm in the dense plasma and 10 mm in the tenuous plasma near the walls. Vacuum fields were also measured at each point. The measurement of B_r is extremely sensitive to the alignment of the probe. A very small error in the orientation of the probe produces a large error in B_r, since $B_\theta \gg B_r$.

The flux function ψ was computed by assuming a polynominal expansion of the form

$$\psi = \sum_{i=0}^{m} \sum_{j=0}^{n} a_{ij}\, r^i z^j$$

with m=6 and n=5. The coefficients a_{ij} were obtained from a least-squares fit to the measured data. Fig. 1 shows the ψ = const. surfaces for z>0, at various times during the discharge. It should be noted that the last frame in Fig. 1 is taken at a time after the onset of the axial displacement instability. Since the onset time is not exactly reproducible from shot to shot, this last frame had to be composed of measurements taken at ξ = const., rather than t = const., where ξ is the axial displacement obtained from a differential probe (Fig. 3). The differential probe signal also shows that, at t = 15 µs, the configuration is still symmetric with respect to the midplane (z=0).

Discussion of results : It is quite obvious from Fig. 1 that, during the stable phase of the discharge, there is a rapid axial contraction of the ψ = const. surfaces. The plasma itself, however, does not undergo an equivalent axial contraction . We deduce this from the following observations : (1) the electron density at z=0 decreases with time, (2) the radial pressure profile at z = 200 mm indicates a beta value of 5-10%, at time t = 15 µs, and (3) the toroidal current density, as shown in Fig. 2, remains rather high near the ends, its axial distribution being very wide. We must, therefore, conclude that the poloidal field diffuses axially ghrough the plasma. Assuming the plasma to be stationary, one can compute a "loop voltage", $V = 2\pi \frac{\delta\psi}{\delta t}$. At t = 15 µs and z = 200 mm, we find V ≈100 Volts, which corresponds to a Spitzer temperature of ∿ 10 eV. This is consistent with rough estimates of the energy balance at that point.

Fig. 1 also shows that, at t = 15 µs, a large fraction of the poloidal field lines intersect the walls of the discharge vessel. This is due to the absence of a conducting shell. Consequently, the ends of the plasma must be cooled by thermal conduction along the field lines. This effect could easily explain the "axial contraction" observed in the Garching experiments {1,2}. In our case, the shrinkage of the plasma due to the cooling of the ends cannot be observed during the short time available (20 µs) before the onset of the axial displacement instability. In summary, we note that the poloidal field configuration changes rather drastically during the "stable" phase of the discharge (Fig.1.), and it is not too surprising that the pinch switches from a stable to an unstable phase at t ∿ 20 µs {6}.

Fig. 4 shows radial profiles of the safety factor, q. They were computed by integrating along the ψ = const. lines, according to the prescription

$$q = \frac{1}{2\pi} \oint \frac{B_\theta\, ds}{r\sqrt{B_z^2 + B_r^2}}$$

It is interesting to note that q at the wall reaches values which are usually considered dangerous for belt pinches {1}, whereas q on axis always remains above the critical value for internal modes, i.e. $q_{axis} \sim 1$.

This work has been supported by the Swiss National Science Foundation.

References :

{1} H. Krause, Garching Report IPP 1/150 (1974)

{2} O. Gruber et al. in Plasma Physics and Controlled Nuclear Fusion Research (Proc. 6th Int. Conf. Berchtesgaden, 1976)

{3} F. Hofmann, L. Bighel and J.M. Peiry, 7th European Conf. on Contr. Fusion and Plasma Physics, Lausanne, 1975, Vol. II, p. 137

{4} L. Bighel, F. Hofmann, Third Topical Conference on Pulsed High Beta Plasmas (Culham 1975), Pergamon Press, Oxford (1976), 507

{5} A. Kadish, Nuclear Fusion 13 (1973) 756

{6} F. Hofmann, L. Bighel, J.M. Peiry, A. Simik, Plasma Phys. and Contr. Nucl. Fusion Research (Proc. 6th Int. Conf. Berchtesgaden 1976) 1, IAEA, Vienna (1977), 305.

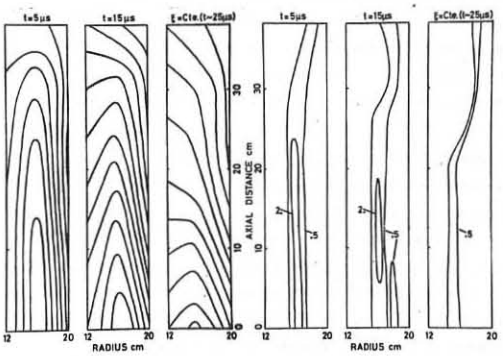

Fig. 1. Lines of constant ψ ($\Delta\psi$ between adjacent lines = 25 kG x cm^2)

Fig. 2. Lines of constant toroidal current density, j_θ (1 unit = 800 A/cm^2)

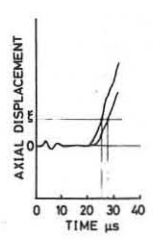

Fig. 3. Axial displacement as seen by the differential probe.

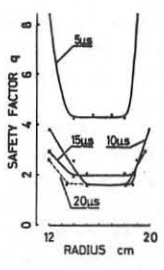

Fig. 4. Radial profiles of q, at various times.

Toroidal Confinement with Reduced Energy Losses in Belt-Pinch IIa

G. Becker, O. Gruber, H. Krause, F. Mast, R. Wilhelm
Max-Planck-Institut für Plasmaphysik, 8046 Garching, Fed.Rep.Germany
EURATOM Association

Abstract: In the Garching Belt-Pinch IIa discharges with strongly reduced impurity content resulted in improved energy confinement ($\tau_{1/e} \approx 60$ µs, initial parameters $T_e + T_i \approx 100$ eV, $n_{e\,max} \approx 3.5 \times 10^{14}$ cm^{-3}, $\langle\beta\rangle \approx 0.6$). With a modified multipole system vertical displacement instabilites could be avoided. At q-values above 2.5 no signs of external kink instabilites were observed for plasma elongations $b/a \approx 5 - 10$.

Introduction: In recent years growing interest in the optimization of the cross-sectional shape for axisymmetric configurations led to the Belt-Pinch experiments in Garching. They produced high-ß plasmas whose energy content decayed in some 10 µs dominantly caused by impurity line radiation /1/. In this paper we present results of discharges in Belt-Pinch IIa with light impurities (C and O)the content of which was reduced from 7% to 1% only. This allows now to observe the effects of additional energy loss mechanisms, like neutral gas cooling or an enhanced energy transport due to internal MHD-modes. Furthermore, modifications of the multipole system resulted in a clear separation of the plasma ends from the walls. Under these new conditions plasma confinement and equilibrium are studied and compared with theoretical investigations. The stability behaviour will be discussed.

Experimental results: The BP IIa device /1/ has a toroidal coil system of rectangular cross-section: coil height $2\,b_c = 260$ cm, distance between inner and outer coil: $2\,a_c = R_o - R_i = 47$ cm and average torus radius: $R_T = (R_o + R_i)/2 = 52.5$ cm. In all cases a maximum shock voltage of 140 kV is applied and a filling density of 2 mtorr deuterium is used. Typical confinement parameters at the end of the dynamic phase at 10 µs are given in Figs. 1, 2, 3, 4 and in the following table:

toroidal field	$B_t(R_T)$	= 1 kG	$\langle\beta\rangle$	= 0.6
toroidal plasma current	I_t	= 150 kA	β_p	$= 8\pi \langle p \rangle / \overline{B_p}^2 = 4.1$
plasma height	2 b	≈ 220 cm	$\langle p \rangle$	$= \int p\,df / \int df$
plasma width	2 a	≈ 22 cm	$\overline{B_p}$	$= 2\pi I_t / (2a + 2b)$

The radial profiles of the toroidal and poloidal magnetic fields measured by probes in the torus midplane and the evaluated pressure and toroidal current density are shown in Fig. 1. As the β_p-value is comparable with the plasma aspect ratio A the toroidal current density maximum is strongly shifted to the torus outside with respect to the magnetic axis, which coincides with the maximum plasma pressure, Note, that the toroidal plasma current already has a smooth profile at this early time and does not resemble a surface current. The q-value at the plasma boundary is $q_b = \oint \frac{B_t\,dl_p}{2\pi R B_r} \approx 4.5$, whereas the q-value on the magnetic axis is above 1 according to equilibrium calculations.

Fig. 2 shows the radial profiles of the electron density at 10 µs measured by Ashby interferometry. According to the broader pressure profile from the magnetic probe measurements the sum of the electron and ion temperature should have a hollow structure. The n_e-profile shows further that about 80% of the initial filling density is ionized. The ionization of the neutral gas outside the dense plasma and/or an additional gas influx from the walls produce shoulders in the n_e-profile. (Due to limited access for the end-on density measurements only the shoulder on the right hand side could be observed at t = 10 µs). The shoulders rise with time to about 60% of the central electron density at 25 µs due to neutral gas capture. At 40 µs the line density corresponds to nearly 100% of the filling density and does not decrease for the rest of the discharge.

In order to maintain the strongly non-circular equilibrium a too large radial compression ratio has to be avoided. With the vertical coil system used the present compression ratio of $a_c / a \approx 2$ results in a modest axial contraction. This can be seen in Fig. 3 where vertical B_z (z) - profiles near the outer (B_{zo}) and inner (B_{zi}) coils are plotted for three different times. The corresponding equilibria are investigated by means of a free boundary equilibrium code /2/ which matches the measured B_z (z) - profiles and the $\langle\beta\rangle$ and β_p - values. For t = 10 µs and $\beta_p \approx$ A the plasma boundary is roughly race-track shaped with tapered ends ($b/a \approx 10$) and the toroidal current density is "flat" with small ψ - ingredients (ψ poloidal flux function). This results in extremely elongated inner flux surfaces with a half-axis ratio of about 25. Fig. 2 shows that at later times (90 µs) the plasma contour deviates from the race-track shape with $2\,b \approx 130$ cm, $b/a \approx 5$ and $q_b = 2.5$. Detailed equilibrium calculations are in progress.

Plasma confinement and stability: As a consequence of reduced impurity level an evident improvement of the confinement properties has been achieved. From diamagnetic flux measurements it has been derived that the plasma energy of 7 kJ at 10 µs decays to 1/e in about 60 µs. This energy loss is consistent with the time behaviour of the central electron temperature measured by Thomson scattering (Fig. 4). At the beginning $T_i \gg T_e$ holds and T_e rises due to ion-electron energy transfer. After 30 µs both T_e and T_i decrease consistent with the measured energy decay. The obtained data are not in agreement with preliminary results from a numerical transport code /3/, which predicts larger 1/e decay times. Moreover, the experimental increase of plasma line density due to external neutrals exceeds the predictions from the present theoretical model. Nevertheless, the development of shoulders on the n_e-profiles is demonstrated by the transport code. A more detailed particle and energy balance will be presented at the conference.

The main result on plasma stability again is the fact that fast growing external modes are not observed. Obviously, a vanishing current density at the plasma boundary combined with a high shear (according to $q_b / q_o > 2$ to 3) is sufficient in order to suppress external kink modes even for strong elongations and high beta. This result, which is qualitatively confirmed by recent numerical calculations /4/ clearly indicates that most of the previous stability calculations, e.g. /5/ are not able to give an adequate description of the elongated high-beta tokamak.

On the other hand, a certain influence of internal modes on energy confinement cannot be excluded. One indication for the occurrence of such modes are fluctuating B_r-fields inside the plasma at about 50 µs which amounts to 20 to 30% of the local poloidal field. At approximately the same time there is a rapid decay of the diamagnetic signal and a drop of the electron temperature from 25 eV to ≈10 eV.

The problem of vertical displacement instabilities has been solved by modifying the vertical coil system. It has been shown that these axisymmetric modes are sensitive to the current distribution in the outer short-circuited multipole windings. A suitable current distribution has been found, which, due to the stabilizing properties of the outer flux conserving shell, provides stability at least for the experimental time scale. The restrictions on strength and position of multipole currents do not appear to be very stringent.

References:

/1/ O. Gruber, R. Wilhelm, Nucl. Fusion 16, 243 (1976)
/2/ G. Becker, K. Lackner, Nucl. Fusion, to be published
/3/ G. Becker, D. Düchs, Nucl. Fusion 16, 763 (1976)
/4/ R. Gruber, private communication
/5/ J.B. Freidberg, F.A. Haas, Phys. Fluids 17, 440 (1974)

Fig. 1 Radial profiles of the magnetic fields and resulting pressure and toroidal current density

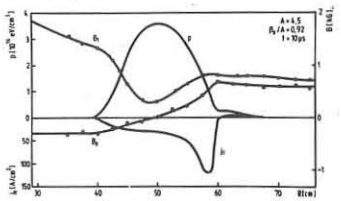

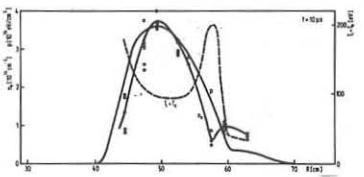

Fig. 2 Radial profiles of the electron density, pressure and resulting plasma temperature

Fig. 3 Axial profiles of the vertical field at the coil surfaces

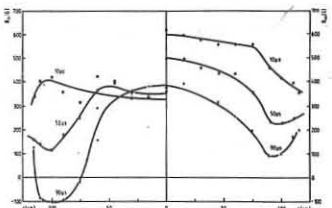

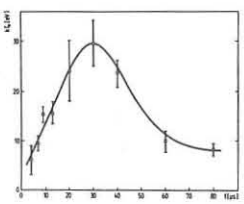

Fig. 4 Time behaviour of the electron temperature in the plasma centre

EXPERIMENTAL INVESTIGATIONS OF THE STABILITY OF A BELT-PINCH TO VERTICAL DISPLACEMENTS

E. Graffmann, F. Hoenen, A. Kaleck, L. Könen, M. Korten and J. Schlüter
Institut für Plasmaphysik der Kernforschungsanlage Jülich GmbH
Assoziation EURATOM-KFA, 5170 Jülich, Federal Republic of Germany

Abstract: In the belt-pinch TENQ stability to axisymmetric modes can be obtained now at low densities, where ion temperatures larger than 100 eV are observed. This density regime was made accessible by an appropriate shaping of the preionized plasma and by compressing the plasma near the outer cylindrical shell, thus stabilizing it to vertical displacements.

Introduction: Recently, confinement with beta values larger than 20 % has been reported from different belt-pinches [1], [2]. However, the density in all these experiments was so high, that temperatures larger than 30 eV were not obtainable. Instability to vertical displacements, which should be expected for the geometries studied, was normally not detected. On the other hand, at low densities stable confinement was not observed up to now. Either only the heating by shock-waves was studied [3], or a closed configuration could not be obtained [2]. In the following we report on some alterations of the experimental set-up of TENQ, which should facilitate the accessibility of stable equilibria at low densities.

Apparatus: The vertical field configuration (fig. 1) is produced by a multipol coil system S_o, S_1 and S_2. S_o is a helical part of the main coil, which generates a toroidal field B_T up to 7 kG at the magnetic axis. The plasma current ($I_p \leq 110$ kA) is induced by the currents in S_o, S_1 and S_2. In all 4 coils the currents are flowing in the same direction, thus providing an octopol configuration. After crowbarring S_o, S_1 and S_2 at current maximum, S_1 and S_2 become opaque, whereas S_o remains transparent to the poloidal magnetic field. In the course of our investigations the length of the vessel was reduced from 116 cm to 80 cm. The major radius

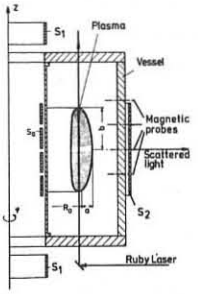

Fig. 1 Apparatus

R_o was varied between 40 cm and 55 cm, the lengths of the half-axes were $a \approx 7$ cm, $b \leq 30$ cm at q-values of 3.5 - 4.5.
T_e and n_e were measured by Thomson scattering, T_i by Doppler broadening of impurity lines. Radial profiles of B_p, B_T, j_T and p were obtained from measurements with local magnetic probes. The axial position of the plasma column was measured by streak photos and external magnetic probes. The data acquisition system consists of a PDP 8e computer with 20 k core and a CAMAC instrumentation with 200 ns ADC's, store and amplifier modules.

Results: At low densities the axis ratio b/a exceeded in the initial phase of the discharge a critical value ($b/a_{crit} \approx 5$) resulting in a fast loss of the plasma in the region of strong curvature. This is shown in curve I of fig. 2: after a short axial compression, the axis b increases, indicating the fast end-losses. To avoid large b/a-ratios during the initial phase, the compression length (not the linear compression ratios) should be equal both in radial and in axial direction, e.g. 2h - 2b = 2d - 2a (2d = width of the vessel). To fullfill this condition, the vessel height 2h was reduced from 116 cm to 80 cm. Curve II in fig. 2 shows, that now the half-axis b reaches an equilibrium value.
With low densities now the m=1 instability (vertical displacement) could be observed with growth-rates larger than $10^5 sec^{-1}$. On a first glance, wall-stabilization seems to be not promising in a belt pinch, where the compression results in a large plasma-wall distance. However, by lowering the vertical field, the compressed plasma might be positioned near the outer coil S_2. Then image currents in S_2 might prohibite a vertical displacement of the plasma column.

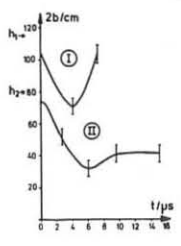

Fig. 2 Time dependence of b for large (I) and small (II) height of the vessel

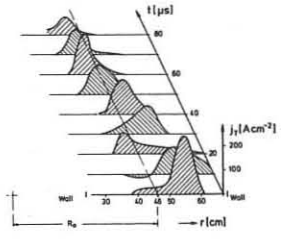

Fig. 3 Profiles of the toroidal current density

This presumption was confirmed by the experiments. Fig. 3 shows the time development of the current density profile. In the initial phase, the plasma is compressed near the outer wall, $R_o \approx 60$ cm (the radius of the coil S_2 is 75 cm). Then the major radius R_o shrinks monotonically due to the decreasing ß. The difference ΔB_r in the values of the radial magnetic field measured at $z = \pm 46$ cm and R = 50 cm remains zero for 50 µsec (fig. 4b), indicating that there is no vertical displacement of the plasma column. At t = 50 µs ($R_o \approx 50$ cm), the plasma starts to move in vertical direction, ΔB_r is now increasing. Side-on streak pictures (fig. 4a) demonstrate this transition from stable to instable behaviour even more convincingly. End-on framing pictures -not reproduced here - show axisymmetry all the time, e.g. the instability is identified as the m=1, k=0-mode. The sign of $\Delta B_r \sim \Delta z$ in different discharges might be positiv or negativ. This behaviour was observed down to filling pressures of .8 mT D_2 at axis ratios $2 \leq b/a \leq 3$.

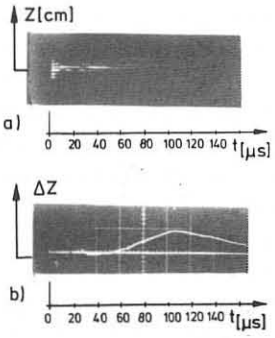

Fig. 4 a) Streak-picture side-on
b) Oszillogram of $\Delta B_p \approx \Delta z$

The Doppler broadening of the 2297 Å CIII-line (fig. 5) gives $T_{imax} = 160$ eV at $\bar{n}_e = 5 \cdot 10^{14} cm^{-3}$. T_i decreases with an e-folding time of 10 µsec. For technical reasons, T_e and n_e could be measured by Thomson scattering only at R = 46 cm, z = 0 cm, e.g. only on the slopes of the corresponding profiles because $R_o > 50$ cm for $t < 50$ µsec (see fig. 3). The measured

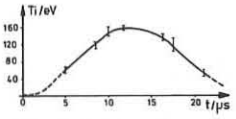

Fig. 5 Ion Temperature

T_{emax} (≈ 30 eV) can therefore be considered as a lower limit for T_e. It decreases with an e-folding time of 40 usec.

Conclusions: In belt-pinches, where an octopol field is superimposed on the vertical field, confinement and stability to vertical displacements can be obtained also in the low density-high temperature regime, where the plasma parameters are approaching the Tokamak regime. The equilibrium configuration can be achieved by a fast magnetic compression, if a strong elongation of the plasma cross-section is avoided during the compression. Stabilization of the axisymmetric m=1 mode is possible, if the plasma torus is surrounded by a cylindrical conducting shell. The distance l of the plasma boundary from this shell should fullfill the condition $l \leq 1.5\, a$ for b/a = 3.
It is interesting to note, that Haas [4] calculated nearly exactly the same condition for the plasma wall distance at z = 0, however, he assumed the plasma to be surrounded totally by an elliptical conducting shell. Also we want to mention the results reported from the Lausanne belt-pinch [5], where the plasma-wall distance was presumably too large for an effective stabilization.

References:

[1] O. Gruber et al., Nucl. Fusion Suppl. 1977, p. 311

[2] E. Graffmann et al., Nucl. Fusion Suppl. 1977, p. 351

[3] F. Söldner, K.H. Steuer, Proc. of the III. Top. Conf. on Pulsed High Beta Plasmas, Culham 1975, Pergamon Press, Oxford, 1976, p. 527

[4] F.A. Haas, Nucl. Fusion 15, 407 (1975)

[5] F. Hofmann et al., Nucl. Fusion Suppl. 1977, p. 305

FIELD REVERSAL IN PINCHES

A. Sykes and J.A. Wesson
Culham Laboratory, Abingdon, Oxon, UK
(Euratom/UKAEA Fusion Association)

The aim of this paper is to describe a numerical simulation which shows (i) how the axial magnetic field in a pinch can become reversed through a helical instability, (ii) how the configuration can return to a more axisymmetric state and (iii) that this reversed field configuration can remain indefinitely.

A three dimensional simulation has been carried out using the non-linear, resistive mhd equations with ohmic heating and an energy loss term included[1]. The calculation is carried out in a straight system of square cross-section, and the code uses a Lax Wendroff technique based on a 14 × 14 × 13 grid. The neglect of toroidal effects is appropriate in the case of a large aspect ratio pinch since the poloidal magnetic field B_θ is of the same magnitude as the toroidal magnetic field B_φ and the square cross-section does not introduce any essential differences from the circular cross-section of the experiments. The length of the box is πa (where a is the half width of the cross-section) and can be regarded as a section of a large aspect ratio system.

The conductivity is taken to be paramagnetic, so that $\sigma_\perp = \frac{1}{2}\sigma_\parallel$, and is proportional to $T^{3/2}$. Initially the axial plasma current has the form $j_z = j_{zo}\cos(\pi x/2a)\cos(\pi y/2a)$ with a central value of $\sigma_\parallel = 16/aV_A$. The energy loss term includes a part proportional to the plasma pressure and a part giving an approximate radiation loss.

The axial flux, $\int B_z\,ds$, is kept constant and an axial electric field is applied at the surface according to the chosen circuit conditions. The unit of time is $\tau = a/(B_{zo}/\rho_o^{\frac{1}{2}})$, B_{zo} being the initial uniform axial magnetic field and ρ the initial density.

Figures 1 and 2 give the results of a calculation which show all of the effects described above. Figure 1a gives the form of the imposed current variation, the current being kept constant after the initial rise, and also gives the applied voltage required to produce this current. Figure 1b shows the time variation of $\langle B_{za}\rangle$, the average value of B_z at the surface of the plasma. It is seen that during the time up to $t = 5$ $\langle B_{za}\rangle$ is considerably reduced. This is due to a combination of pinching and the paramagnetic effect.

During this time the plasma column has remained almost axisymmetric. This and the subsequent deviations from axisymmetry can be seen in figure 2 which gives the trajectories of related magnetic field lines as viewed from the side of the box. The lines shown are chosen on the basis of their proximity to the magnetic axis at the end plane of the box. At time $t = 1.1$ the configuration is close to the initial state and is still axisymmetric. At $t = 4.8$ a single wavelength helical instability is just appearing. The growth of this instability is shown in figure 1c where the kinetic energy of the plasma is plotted.

It is seen that just after $t = 5$ the kinetic energy grows rapidly and at this time $\langle B_{za}\rangle$ reverses strongly. The reason for this is the helical form of the current channel which acts as a solenoid, increasing the flux within it and, because total flux is conserved, removing flux from the outer region. The form of the helix at $t = 5.3$ is shown in figure 2.

At $t \simeq 9$ the helical plasma column itself becomes unstable to a mode having half the wavelength of the initial instability. The growth of this $n = 2$ instability is clearly seen from the growth in kinetic energy and from the magnetic field structure at $t = 9.8$.

The second instability is followed by a remarkable change in the magnetic field structure. It can be seen from figure 2 that by $t = 13.1$ the plasma has become almost axisymmetric again, but now the magnetic field at the surface has the more stable reversed magnetic field configuration. This increased axisymmetry is borne out by a detailed analysis of the overall magnetic field. The process by which this has occurred is indicated by the magnetic field plot at $t = 10.7$ where the magnetic axis is seen to have formed two loops. It seems that these loops neck off and decay resistively leaving an almost straight magnetic axis.

Because the structure is now almost axisymmetric the reversed field starts to decay resistively, being almost lost at $t = 14$. In the absence of further instability the reversed magnetic field would disappear completely. However this process is prevented from occurring by further instability and the reversed field is, in fact, then maintained by a series of damped relaxation oscillations as can be seen in figure 1b. It appears therefore that a reverse field configuration can be maintained indefinitely, the key question then being whether the loss of confinement arising from the level of instability required to maintain the reversal is acceptable or not.

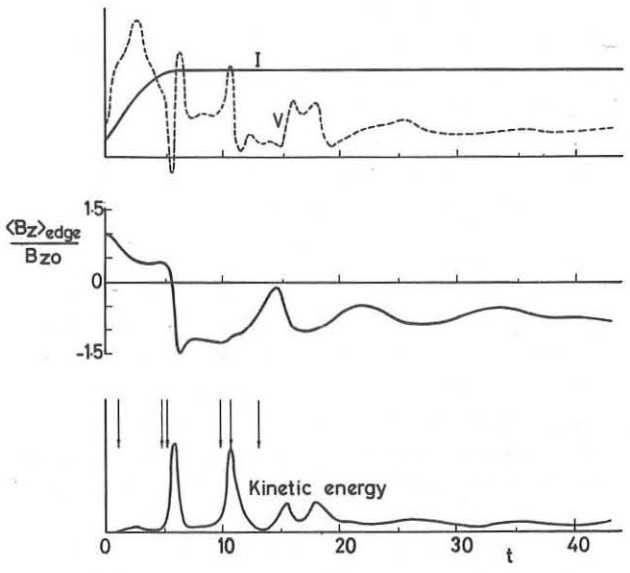

Fig. 1
Time variation of plasma parameters. The six arrows indicate the times of the field line plots of Fig. 2.

(a) Total axial current I maintained by applied voltage V.

(b) Surface average of axial magnetic field B_z.

(c) Total kinetic energy. The small increase around $t = 2$ is due to pinching. The first peak at $t \approx 6$ is the large $m = 1$ $n = 1$ instability which, due to the solenoidal effect of the helix, produces the rapid reversal of $\langle B_z\rangle_{edge}$. The second peak at $t \approx 11$ is the secondary $m = 1$ $n = 2$ instability which culminates in a return to approximate axisymmetry. Resistive diffusion then causes the $\langle B_z\rangle$edge to decay until, at $t \sim 14$, the reversal has almost disappeared. However the plasma now becomes unstable again and the reversed field is restored. At large times diffusion and instability produce a series of damped relaxation oscillations which maintain the reversal indefinitely.

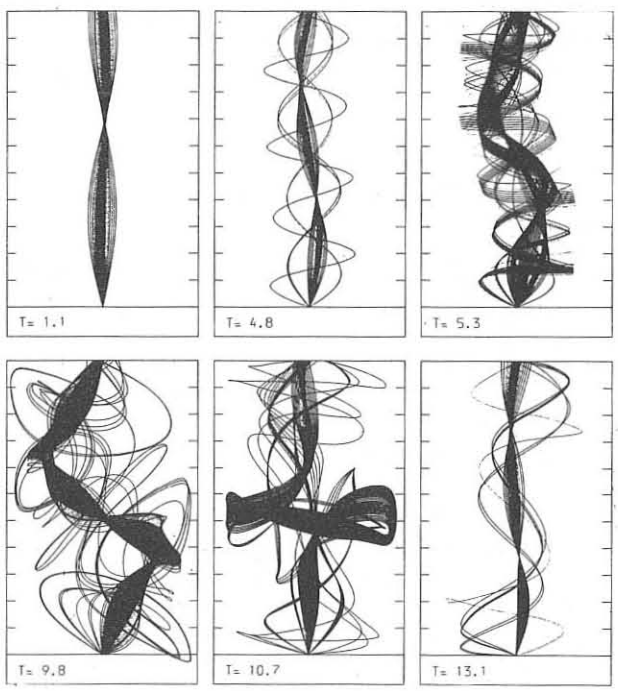

Fig. 2
Trajectories of selected field lines viewed from the side of the box at the six different times indicated by arrows on Fig. 1.

T = 1.1 : Initial axisymmetric compression phase
T = 4.8, 5.3 : development of $m = 1$ $n = 1$ helical instability
T = 9.8 : start of $m = 1$ $n = 2$ kink on fully developed $n = 1$ helix
T = 10.7 : combination of $n = 1$ and $n = 2$ helices : 'necking off' process starting in centre
T = 13.1 : 'necking off' completed : return to axisymmetry as at $T = 1.1$ but now with reversed B_{za}.

Reference

(1) A. Sykes and J.A. Wesson, Phys. Rev. Letts. 37, 140 (1976).

CHARACTERISTICS OF SPONTANEOUSLY GENERATED RFP IN ETA-BETA

A. Buffa, S. Costa, R. De Angelis, G.F. Nalesso, S. Ortolani and G. Malesani
Centro di Studio sui Gas Ionizzati
del Consiglio Nazionale delle Ricerche e dell'Università di Padova
(Associazione Euratom - CNR) - Padova (Italy)

Abstract: Studies of RFP produced by spontaneous reversal have been done under different conditions of current rise time (τ_I) and filling pressure. Two regimes are found: at 40 mtorr and $\tau_I \sim 1-10$ μs an instability is associated with the reversal; at 5 mtorr and $\tau_I \sim 10$ μs a turbulent regime is observed during the whole time of the discharge.

Introduction: The spontaneous relaxation of a pinch to a Reverse Field Pinch (RFP) configuration has been observed in many experiments [1, 2, 3]. The most relevant evidence has been obtained in ZETA where after the field reversal a quiescent phase was observed [1]. The theory for the relaxation of a pinch to a minimum energy state has been discussed by Taylor [4], however as pointed out by Kadomtsev [5] the basic phenomena related with this process are common to a wider class of magnetically confined plasmas (e.g. Tokamaks). Experimental studies on this subject have been done recently on devices [HBTX1 at Culham and ETA-BETA] designed primarily for the study of programmed RFP. The expected phenomenon of spontaneous reversal has been observed, but its characteristics are quite different from the one observed in ZETA mainly because of the low temperature (i.e. low magnetic Reynolds' number $S = \tau_\eta/\tau_A$, typically 100) which does not allow to reach a quiescent phase and because of the large external flux reservoir which imposes a large internal flux enhancement to obtain the field reversal.

In this paper we describe experiments performed on ETA-BETA with various current rise times and filling pressures. In this way we could obtain conditions which differ for the ratio τ_I/τ_A where τ_A is the Alfvén time which is a measure of the timescale for the instability and the relaxation process to occur. In particular by modifying the connection between the condenser bank and the load it was possible to obtain the following conditions: a) $\tau_I \sim 1$ μs ($\tau_I/\tau_A \sim 2$ at 40 mtorr); b) $\tau_I \sim 6$ μs ($\tau_I/\tau_A \sim 10$ at 40 mtorr); c) $\tau_I \sim 10$ μs ($\tau_I/\tau_A \sim 20$ at 40 mtorr; $\tau_I/\tau_A \sim 60$ at 5 mtorr).

Experimental results: The results obtained in the case (a) have been reported elsewhere [3] and show that a strong kink instability is usually associated with the appearance of the reversal which occurs after the current maximum and is subsequently lost on a short time scale due to disruption of the magnetic configuration. We point out that with the same machine conditions it is possible to obtain by field programming RFP configurations which decay without instabilities [6].

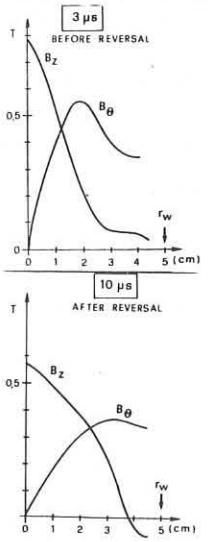

fig. 1

In the case (b) the characteristics of the configurations obtained by spontaneous reversal can be summarized as follows. The reversal is attained during the current rise, lasts for about 20 μsec and is usually limited by field diffusion which eventually leads to an instability. As in case (a) a highly compressed configuration has to be produced before the reversal due to the large flux reservoir. Field profiles before and after the reversal are drawn in figure 1. The ideal MHD stability analysis gives gross fast growing kink modes ($\gamma \sim 10^6$ sec^{-1}, $k \sim 45$ m^{-1}) for the profiles measured before the reversal, whereas only localized slowly growing modes ($\gamma \sim 10^5$ sec^{-1}) are found for the profiles measured after the reversal. The radial component of the magnetic field shows an instability, with growth rates and axial wavenumber in reasonable agreement with the theoretical analysis, starting ~1 μsec before the spontaneous reversal. After the strong unstable phase, which characterizes the period before and immediately after the reversal, a RFP configuration is obtained and the fluctuation level of the magnetic signals is substantially reduced (by a factor of 5-10).

For the case (c) we report here the results obtained with 5 and 40 mtorr of filling pressure. At 40 mtorr the results are similar to those discussed previously for the case (b). As we see in figure 2 there is a clear kink instability before the reversal. The local B_θ field measured just inside the vacuum chamber, the sinusoidal coils signal, the radial field component (near the axis) and the light signal of an O II line are well correlated in time and all show a gross instability. The current e-folding time is about 20 μsec as in case (b).

At 5 mtorr of filling pressure a quite different behaviour is observed. In particular, as is seen in figure 3, during the whole time of the discharge a turbulent behaviour characterized by high frequency fluctuations is observed. The current e-folding time is less by more than a factor of 2 as compared to the 40 mtorr case. The losses associated with the magnetic field fluctuations [7] and the anomalous transport due to microinstabilities are more important in this case and could then account for the observed behaviour.

The oxygen impurity concentration has been evaluated by measuring the intensity of O II and O III lines. As long as the plasma does not hit the wall an impurity concentration corresponding to 0.1 mtorr is generally deduced. This impurity level is consistent with the limitations of the present vacuum system. When the plasma interacts with the wall the discharge is in all the cases contaminated by several percentages (3 - 5% at 40 mtorr) of oxygen. A quantitative difference between the various cases discussed is not deducible within the experimental errors.

Conclusions: RFP configurations generated by spontaneous reversal have been obtained in a wide range of values for the current rise time and the Alfvén time. Different characteristics in the plasma behaviour have been observed. At 40 mtorr in the range of $\tau_I/\tau_A \sim 1-20$ a strong instability is associated with the reversal. In particular for $\tau_I/\tau_A \gg 1$ the reversal clearly follows the instability and afterwards a RFP configuration characterized by a low level of magnetic field fluctuations is obtained which decays similarly to programmed RFP with comparable parameters [6].

A different regime, characterized by high frequency fluctuations, is found at lower values of the filling pressure (5 mtorr, $\tau_I/\tau_A \sim 60$). The situation is in this respect somewhat similar to the one preceeding the quiescent phase in ZETA but on the other hand it is very different because the energy limit of the machine and the large energy losses lead to a very low temperature plasma with short lifetime.

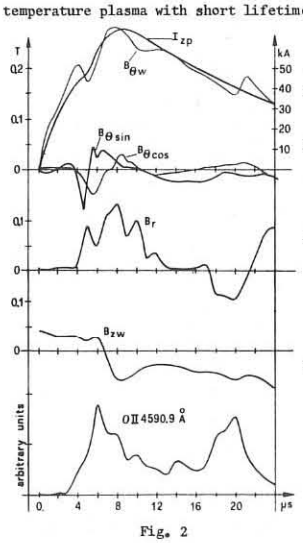

Fig. 2

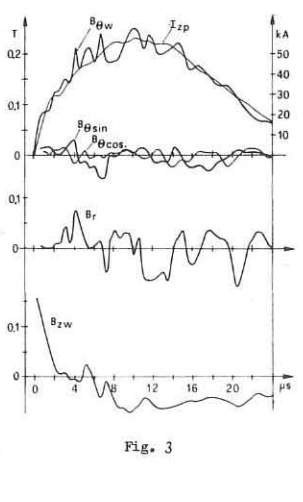

Fig. 3

References:

1 Robinson, D.C. and King, R.E., 2nd IAEA Conf., Novosibirsk (1968), CN-24/B-8.
2 Gowers, C.W. et al., 6th IAEA Conf., Berchtesgaden (1976), CN-35/E2.
3 Buffa, A. et al., 7th EPS Conf., Lausanne, I, 40.
4 Taylor, J.B., 3rd Top. Conf. on Pulsed High Beta Plasmas, Culham (1975) B1.6.
5 Kadomtsev, B.B., 6th IAEA Conf., Berchtesgaden (1976), CN-35/B1.
6 Buffa, A. et al., 6th IAEA Conf., Berchtesgaden (1976) CN-35/E3.
7 Robinson, D.C., 3rd Top. Conf. on Pulsed High Beta Plasmas, Culham (1975) B1.7.

PERFORMANCE PREDICTIONS FOR REVERSED FIELD PINCHES

J P Christiansen and K V Roberts

Culham Laboratory, Abingdon, Oxfordshire, UK
(Euratom/UKAEA Fusion Association)

Abstract. The time evolution of two slow reversed field pinches is studied during the current sustainment phase, starting from a low-β force free Taylor state. The calculations use a 1DMHD equilibrium and diffusion code, with anomalous transport coefficients chosen to simulate a central Suydam-unstable core surrounded by MHD-stable region with enhanced electron thermal conductivity.

1. Introduction. The reversed field pinch (RFP) is a high-β containment configuration. Formation of an RFP during the setting-up phase is complicated, but theoretical predictions by Taylor [1] and Kadomtsev [2] suggest that a force-free Bessel-function RFP configuration should tend to develop as the plasma tries to relax towards a minimum energy state. Starting from this configuration

$$B_z = B_o J_o\left(2\,\Theta\,\frac{r}{a}\right) \quad , \quad B_\theta = B_o J_1\left(2\,\Theta\,\frac{r}{a}\right) \qquad (1)$$

we use a 1DMHD equilibrium and diffusion code to study the evolution during the subsequent current sustainment phase. Here B_o is the axial magnetic field, a is the minor radius, and the pinch parameter $\Theta \equiv B_\theta(a)/\overline{B}_z$. The initial β is assumed small.

Configuration (1) with β = 0 is ideal MHD stable for $\Theta \leq \Theta_I = 1.587$ and tearing-mode stable for $\Theta \leq \Theta_T = 1.552$. Limiting values $\Theta_I(\beta)$, $\Theta_T(\beta)$ can be calculated by adding pressure while conserving magnetic flux [3], and the maximum Suydam-stable axial $\beta_o \equiv \beta(o)$ is obtained by inward integration of the marginally stable pressure gradient

$$\nabla p_S = -\,(r/8\mu_o)B_z^{\,2}(\nabla P/P)^2 \qquad (2)$$

with $P = rB_z/B_\theta$. Fig.1 shows the maximum value β_S for β_o, and the maximum value Θ_I for Θ. (Tearing-mode stability [3] requires only slightly smaller Θ). We study which of the high-β configurations can be reached and maintained during the sustainment phase starting from (1) with $1.2 < \Theta < 1.6$.

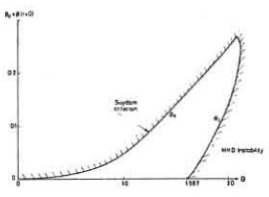

Fig.1
Maximum values (β_S, Θ_I) of (β_o, Θ) for the pressure inflated Bessel function model

2. MHD equations. The plasma is described by electron density n, temperatures T_e, T_i and effective charge and mass numbers Z, A. It evolves through a sequence of states in pressure equilibrium with the fields B_θ, B_z. Each new equilibrium $\nabla p = J \times B$, $p = nk(T_e + T_i/Z)$ is reached after solving the equations

$$\partial \underline{B}/\partial t - \nabla \times \underline{V} \times \underline{B} = -\,\nabla \times (\underline{\eta} \cdot \nabla \times \underline{B})/\mu_o \qquad (3)$$

$$nk/(\gamma-1)\; DT_e/Dt = -\,\nabla \cdot \underline{F}_e - K + Q_e \qquad (4)$$

$$nk/(Z(\gamma-1))\; DT_i/Dt = -\,\nabla \cdot \underline{F}_i + K + Q_i \qquad (5)$$

where D/Dt is a Lagrangian derivative. The resistivity $\underline{\eta}$ includes parallel and perpendicular terms $\eta_\parallel$, $\eta_\perp$. The transverse thermal fluxes $\underline{F}_e$, $\underline{F}_i$ have the form $\kappa\, \partial T/\partial r$. K is the equipartition rate and the terms Q_e, Q_i include ohmic and turbulent heating and Bremsstrahlung.

3. Transport coefficients. The coefficients used are

$$\eta_\parallel = \eta_\parallel^o \;;\; \eta_\perp = \eta_\perp^o + 4\beta\,\mu_o\, D_T' \;;\; \kappa_e = \kappa_e^o + nk(D_T'' + D_a) \;;\; \kappa_i = \kappa_i^o + n/Zk\; D_T''' \qquad (6)$$

where (o) denotes classical. Turbulent diffusion (T) is switched on locally in Suydam-unstable regions and is discussed in [4]. Anomalous (a) electron thermal conductivity is given two alternative forms $D_a = C_e\, D_e^o$ (pseudo-classical, $D_e^o = \kappa_e^o/nk$), and $D_a = C_\theta\, D_\theta$ (poloidal Bohm, $D_\theta = \kappa T_e/16e\, B_\theta$), the constants C_e, C_θ being adjusted to straddle energy-loss values determined from empirical Tokamak scaling laws.

4. RFP device parameters. Two proposed devices HBTX1A and RFX are discussed, both using programmed wall fields $B_\theta(a)$, $B_z(a)$, with parameters:

Parameter		HBTX1A	RFX
Liner Radius a	[m]	0.26	0.6
Major radius R_o	[m]	0.802	1.8
Current I_z	[MA]	0.3 - 0.5	0.7
$B_o \equiv B_z(o)$	[T]	0.6 - 1.0	0.55
Line density N	[m^{-1}]	2.5×10^{19}	2.5×10^{19}

The RFX calculations vary the anomalous electron transport using $0 < C_e < 100$ or $0 < C_\theta < 0.15$, while the HBTX1A calculations vary I_z and use $C_e = 100$, (corresponding to an energy containment time τ_E below half the empirical Tokamak value). In both cases Z = 2.5, A = 4.

5. Predicted performance. In the tables $\beta_\theta = 16\pi^2(\gamma-1)W/(\mu_o I_z^{\,2})$ where W is the total plasma energy, and the configuration time τ_c is the time at which $\Theta > \Theta_I$. Times in ms, axial temperatures in eV, β_θ in %, current in MA. Values of τ_E, T_e, T_i, β_θ are calculated for HBTX1A at $t = \tau_c$ and for

I_z [MA]	HBTX1A				
	τ_E	τ_c	T_e	T_i	β_θ
0.3	0.75	0.8	174	156	17.1
0.4	1.50	1.5	295	261	16.0
0.5	2.46	2.4	438	383	15.1

Electron thermal transport	RFX				
	τ_E	τ_c	T_e	T_i	β_θ
Classical	81	60	898	645	16.9
C_θ = 0.05	19	25	720	609	13.5
C_θ = 0.1	14	20	651	585	12.5
C_θ = 0.15	11.5	15	608	565	11.9
C_e = 50	15	12	754	617	12.5
C_e = 100	12	10	702	603	11.8

RFX at t = 20 ms. The current I_z is maintained constant. If I_z is allowed to decay τ_c can be prolonged but at somewhat reduced temperature.

The main conclusion is that HBTX1A should attain central temperatures of order 300 eV with a stable lifetime 1 - 2 ms. Corresponding figures for RFX are 600 eV and 15 - 20 ms. The case $I_z = 0.3$ MA for HBTX1A corresponds to RFX if I_z scales with minor radius a, so our results emphasize a strong dependence of the performance upon a.

References

[1] Taylor J B (1974). Phys.Rev.Lett. 33, 1139.

[2] Kadomtsev B B (1976). 6th Int.Conf.on Controlled Fusion and Plasma Physics, Berchtesgaden. CN-35/B1.

[3] Robinson D C (1976). Ibid, CN-35/E2.

[4] Christiansen J P and Roberts K V (1977). 'Turbulent Behaviour of the Reversed Field Pinch'. This conference.

TURBULENT BEHAVIOUR OF THE REVERSED FIELD PINCH

J P Christiansen and K V Roberts

Culham Laboratory, Abingdon, Oxfordshire, UK
(Euratom/UKAEA Fusion Association)

Abstract. The central region of the reversed field pinch (RFP) has a small shear but a high ohmic heating rate and is expected to become Suydam unstable during the current sustainment phase. This paper discusses the turbulent transport coefficients to be used in a 1DMHD equilibrium and diffusion code which simulates the time evolution of the RFP. Arguments are based on numerical calculations of linear eigenmodes and estimates of subsequent non-linear behaviour.

1. Introduction. A qualitative picture of the RFP in low-β cylindrical approximation is provided by the Bessel function model [1] which exhibits an essential feature of this type of system: the ohmic heating rate $\sim |\underline{J}|^2$ has a maximum at $r = 0$ where the shear $\nabla\mathcal{P} \equiv \nabla(rB_z/B_\theta)$ is zero. During the current sustainment phase we therefore expect the Suydam condition $\Sigma \equiv \nabla p/\nabla p_S - 1 < 0$ to be consistently violated near the axis so that the RFP should have an MHD turbulent central core. Here p is the plasma pressure and

$$\nabla p_S = -\,(r/8\mu_o)B_z^{\,2}(\nabla\mathcal{P}/\mathcal{P})^2 \qquad (1)$$

is the marginally Suydam-stable pressure gradient.

To predict the performance of the RFP we follow its evolution through the sustainment phase using a 1DMHD equilibrium and diffusion code [2], and this paper discusses the turbulent transport coefficients to be used when $\Sigma > 0$. Ideal MHD stability theory is used to compute growth rates and eigenfunctions of unstable linear modes and §2 summarizes results from numerical calculations. We conjecture in §3 what happens in the non-linear regime and estimate the turbulent transport in §4. The evolutionary behaviour is however expected to be insensitive to the turbulent transport coefficients over a wide range and this is confirmed in practice. Numerical values refer to a toroidal device with minor/major radii 0.6/1.8 m, axial field 0.55 T and central density 3×10^{19} m^{-3}.

2. Pressure-driven instabilities. Departure from equilibrium is described by a Lagrangian displacement vector $\underline{\xi}$ which in the linear regime can be analysed into eigenmodes

$$\underline{\xi} = \sum_{m,k} \underline{\xi}_{mk}(r)\ \exp\, i(m\theta+kz-\omega t) \qquad (2)$$

each eigenmode satisfying an equation of motion $-\rho\omega^2\underline{\xi} = \underline{F}\{\underline{\xi}\}$ where ω is the frequency and ρ the density. To study Suydam-unstable modes we construct pressure equilibria with $\Sigma(r) > 0$ in the centre to represent the overheating due to high current density in a low-shear region and solve this equation numerically. This is done for a sequence of pressure equilibria with $\Sigma(r)$ chosen as

$$\Sigma(r) = -\,\sigma_1 + \sigma_2 \exp(-(r-r_1)^2/r_2^{\,2}) \ . \qquad (3)$$

For given (m,k) there is an infinite set of radial eigenfunctions $\xi \equiv \xi_r$ characterized by node number n, but the growth rate γ decreases exponentially [3] as n increases so that only $n = 0$ is important. For fixed k/m (i.e. a given singular surface r_s) γ reaches an asymptotic limit as $m \to \infty$ [3] if non-ideal effects are ignored. Fig.1 shows $\xi(r)$ for $m = 1,2$ and 5. In a toroidal device of major radius R_o only surfaces with $k = \ell/R_o$ (ℓ integer) are allowed, but the critical m-value at which finite Larmor radius stabilizes a mode is likely to be sufficiently high that in practice a large number of localized modes will compete.

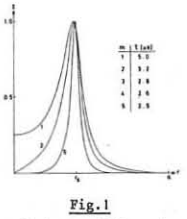

Fig.1
$n = 0$, $ka = -5/3$ m eigenfunctions of Suydam unstable modes with $m = 1,2,5$

3. Rearrangement of field topology. When a mode of the type shown in Fig.1 grows the field structure undergoes the Lagrangian transformation

$$\underline{r} \to \underline{r}^* = \underline{r} + \underline{\xi} \ . \qquad (4)$$

Eventually the Jacobian $\partial\underline{r}^*/\partial\underline{r}$ can become zero or unbounded so that (4) becomes singular. This will happen if the radial Jacobian $\partial r^*/\partial r = 1+\partial\xi/\partial r$ approaches zero corresponding to $|\partial\xi/\partial r| = 1$, which will occur when $\xi(r)$ has grown to the order of its width Δ in the neighbourhood of r_s. Fig.2 sketches the rearrangement of the magnetic field structure which is conjectured to occur near the singular surface. Modes which are not affected by FLR have comparable growth rates [3] but $|\partial \log \xi/\partial r|$ increases with m. The change in topology shown in Fig.2 should therefore occur first for some radially localized mode $m > 1$. Outside the region $r_s \pm \Delta$, the functions ξ, $\partial\xi/\partial r$ remain small so that the topology remains unaltered. Therefore the radial transport of plasma and thermal energy is expected to be confined to the immediate neighbourhood of the singular surface for each individual mode, justifying the use of a turbulent diffusion coefficient which depends on the local stability criterion.

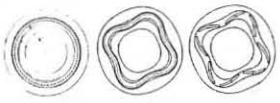

Fig.2
Qualitative interpretation of the transformation (4) corresponding to $|\partial\xi/\partial r| \to 1$. Arrows show the direction of the field component transverse to $\underline{B}$ at r_s

4. Turbulent diffusion coefficient. The usual $D_I = \gamma/k^2 = \gamma\Delta^2$ estimate for the diffusion coefficient is difficult to apply in our calculations since γ is exponentially small near $\Sigma = 0$, so that D_I would start small and then increase rapidly as the excess pressure gradient built up. A marginal stability argument is also not straightforward, since once the sequence in Fig.2 has occurred starting from $\Sigma > 0$, the turbulent transport should flatten the local profiles resulting in $\Sigma = -1$. Subsequent 'healing' of the magnetic surfaces may restore $\Sigma > 0$. Hysteresis may therefore be expected so that the marginal condition $\Sigma = 0$ is satisfied only as an approximate time average. A further complication is that flattening of the profiles near r_s will steepen them on adjacent surfaces, so triggering off a random sequence of 'microdisruptions'.

Numerical estimates for a number of modes show that D_I is of the order of the Bohm diffusion coefficient $D_\theta = kT/16e\ B_\theta$; in fact using the Bennett pinch relation we find the scaling $D_\theta \propto D_I(\beta N^{-\frac{1}{2}})$ where N is the line density. We model the hysteresis and healing effects by turbulent diffusion coefficients

$$D_T = \begin{cases} C_T \dfrac{\Sigma}{1+\Sigma} D_\theta & (\Sigma > 0 \ , \ \text{unstable}) \\ 0 & (\Sigma < 0 \ , \ \text{stable}) \end{cases} \qquad (5)$$

where C_T is a constant of order unity which may be different for different transport processes. This switches on the turbulent diffusion smoothly as Σ increases from zero. Results from the evolutionary calculations [2] are found, as expected, to be insensitive to the values of C_T over a wide range.

References

[1] Taylor J B (1974). Phys.Rev.Lett. 33, 1139.

[2] Christiansen J P and Roberts K V (1977). 'Performance Predictions for Reversed Field Pinches'. This conference.

[3] Goedbloed J P and Sakanaka P H (1974). Phys.Fluids 17 908.

EXPERIMENTAL STUDY OF MAGNETIC FIELD DIFFUSION IN A HIGH-β-PLASMA OF A 7 m θ-PINCH AT LOW DENSITIES

K. Höthker and J. Downing+
Institut für Plasmaphysik der Kernforschungsanlage Jülich GmbH
Assoziation EURATOM/KFA, D 517 Jülich, Germany

Abstract: The magnetic field diffusion of a broad sheath ($>c/\omega_{pi}$) for $T_e/T_i < 1$ is measured to be two to three orders of magnitude faster than classical. The diffusion seems to be faster for the lower β region than for the higher β region. The results are compared with theory.

1. Introduction: The confinement of a high-β-stellarator is largely determined by the time development of β. It has e.g. a major effect on the equilibrium and stability of a high-β-stellarator /1/. It is therefore of particular interest to study the processes which dominate the change of β, e.g., the energy losses by charge exchange neutrals and magnetic field diffusion. The sheath width ($>c/\omega_{pi}$) and the temperature ratio ($T_i/T_e > 1$) in these devices are such that ion sound turbulence is not expected. Nevertheless, there had already been experimental indication that in a sheath of a helically shaped high-β-plasma with the above mentioned properties magnetic field diffusion occurs significantly faster than classical /2/. In the present paper we present more detailed experimental investigations on the magnetic field diffusion. We have done the investigations on a plasma with a low compression ratio, which is required for a wall stabilized high-β-stellarator of reasonable dimensions /1/.

2. Apparatus and diagnostics: The plasma is produced in "HELIX", a straight discharge tube of 900 cm length and 30 cm diameter which is surrounded for the presented measurements by a straight coil of L=700 cm length and 2 R_o=38 cm diameter /2/. It was of interest for the magnetic field diffusion studies to generate an initial plasma with negligible temperature gradient in the compressed plasma and with neutral density as low as possible so that charge exchange neutrals had no dominant influence on the sheath properties of the compressed plasma. The scattering of laser light was used to measure the electron density n_e and electron temperature T_e. Radiation measurements were employed on charge exchange neutrals to determine the velocity distribution of the ions . Magnetic probes determined the magnetic field profiles./2/.

3. Results, 3.1 General properties of the plasma: The filling pressure was 0.5 mTorr D_2 and the initial density was n_{e1}= $4\cdot10^{13}$ cm^{-3}. The radial compression ratio was $R_o/a \approx 2$. The properties of the plasma at the beginning of the quasistationary phase are typical of theta pinches, e.g. anisotropic velocity distribution of the ions $T_{i\parallel} < T_{i\perp} \approx 350$ eV and $T_i > T_e \approx 50$ eV. A $\beta_o = 1-B^2(o)/B^2_{ext} \approx 1$ plasma is generated along the axis at the time of maximum current. The time development of β_o is shown in Fig.1. We note that β_o stays constant for $t > 6/\mu s$. Corresponding measurements with the same initial density but 1 mTorr D_2 filling pressure showed a continuously decreasing β_o. This difference may be due to the different densities of neutrals. The average value $\beta = 16\pi \int_o^{R_o} dR R nkT/R_o^2 B^2_{ext}$ decreases all over the observation time. There is no substantial temperature gradient across the radius. This feature persists during the rapid decline of the temperature with time eventhough the gyroradius of the ions becomes distinctly smaller than the sheath width by the end of the observation time. Fig.2 shows the decrease of $T_\perp$. We note that the rate of decrease of the local value $T_\perp$ is practically the same as the rate of decrease of the line energy E_L, which is an average across the radius.

3.2 On the diffusion of the magnetic field: The sheath width 2a increases slightly at the beginning of the postimplosion phase and scales as $2a \sim (7\text{-}8)c/\omega_{pi}$. The ratio v_d/v_{T_i} increases across the radius from 0 at the center to ≈1 at the edge (v_d=azimuthal drift velocity, v_{T_i}=thermal ion velocity). $T_{\perp i}/T_e > 1$ for $t < 10/\mu s$ and becomes $T_{\perp i}/T_e < 1$ for $t > 10/\mu s$. The diffusion coefficient D_M, has been determined by two procedures. In the first one the equation $\int_o^R dR'R' \partial B/\partial t = D_M \int_o^R dR'R' \partial^2 B/\partial R^2$ was evaluated for the experimental profiles B(R). The integration has been extended to different radii R, to give some information on the radial dependence of the diffusion coefficient. Results for D_M are shown in Fig.3. We observe that all the measured diffusion coefficients are by more than two orders of magnitude larger than the classical one. Eventhough, the accuracy of the measurements is expected to be not better than a factor 2, a general characteristic can be determined from the measurements. The diffusion coefficient obtained for a larger limit of integration R is systematically larger than for smaller R. We conclude that there is substantial diffusion of the magnetic field at the low-β-edge of the plasma. In addition, the observation that β_o is constant for $t > 6/\mu s$ (cf. Fig.1) indicates that there is no significant diffusion in the high-β-center of the plasma. As a second method, the diffusion coefficient was obtained by comparing the difference between the measured change in the radius of the plasma and the expected change. The expected change was calculated from the change of $\Delta T_\perp$, ΔB_{ext}, and ΔN (N=line density). The resulting diffusion coefficients are also shown in Fig.3. These values are, too, at least two orders of magnitude larger than the classical diffusion coefficients; but they are systematically smaller than those from the first procedure. This is expected if the diffusion at the edge is faster than in the center of the plasma. The Bohm diffusion coefficient is $D_B \lesssim 10^7$ cm^2/s. The collision frequency related to the experimental diffusion coefficient from the first procedure is of the order of ω_{pi}. Preliminary results on the electric field fluctuations show that the turbulence level is distinctly higher than the thermal one.

Summary and discussion: The measurements show that the sheath in the postimplosion phase of a theta pinch exhibits a diffusion which is by two to three orders of magnitude faster than the classical one. The sheath width is larger than c/ω_{pi} and the diffusion is stronger in the low β part of the sheath than in the high β part. Although the sheath width becomes ≈4 times the ion gyroradius, the radial temperature profile appears to remain uniform in the radial direction until the end of the observation time. Comparing the experimental results from the first procedure with theory /3/ an order of magnitude agreement is found for D_M, when Fowler's estimate for the turbulence level is used.

References:

/1/ H. Grad and H. Weitzner, Phys. Fluids 12, 1725 (1969)
M.N. Rosenbluth, J.L. Johnson, J.M. Greene and K.E. Weimer Phys. Fluids 12, 726 (1969)
/2/ P. Bogen, E. Hintz, K. Höthker and A. Pospieszczyk, 6th Conf. Plasma Physics and Contr. Nucl.Fus. Res., Berchtesgaden 1976 (IAEA, Wien 1977) Vol. I, p. 539
/3/ P.C. Liewer and R.C. Davidson, University of Maryland, preprint 606P002 (1976)

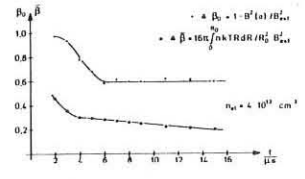

Fig. 1. Time dependence of maximum and avaraged beta

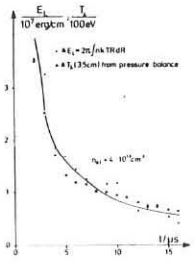

Fig. 2. Energies perpendicular to magnetic field as functions of time

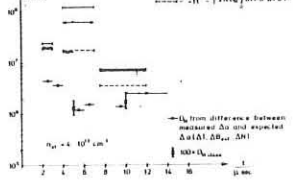

Fig. 3. Diffusion coefficients of magnetic field

+Permanent address: University of California, Los Alamos Scientific Laboratory, Los Alamos, New Mexico 87545, USA

EXPERIMENTS ON END-LOSS PHENOMENA AND MATERIAL END PLUGS IN A 5-M LINEAR THETA PINCH

K. F. McKenna, R. J. Commisso, C. A. Ekdahl, K. B. Freese
R. Kristal, W. E. Quinn, and R. E. Siemon

Los Alamos Scientific Laboratory
University of California
Los Alamos, New Mexico USA

ABSTRACT. End loss from a collisionless theta pinch plasma has been studied interferometrically and with a local pressure sensitive diagnostic. The results are compared with theoretical predictions. End stoppering experiments, using quartz end plugs, are reported.

I. INTRODUCTION. The linear theta pinch is an attractive alternative approach to a fusion reactor due to its ease of plasma heating, high plasma beta and density, demonstrated plasma equilibrium and neutral stability properties, and simple geometry. However, particle and energy loss from the ends presents a fundamental limitation on the plasma containment time. The Scylla IV-P theta pinch was constructed to facilitate studies of end loss physics and to investigate end-stoppering schemes.

II. EXPERIMENTAL ARRANGEMENT. Scylla IV-P has a maximum energy storage of 2 MJ at 60-kV main bank voltage. Six-hundred 1.85-μF capacitors feed the 500-cm long 11.2-cm diam compression coil. Bank operation at 45 kV generates an E_θ of 0.6 kV/cm at the inner wall of the 8.8-cm i.d. quartz discharge tube and a peak crowbarred compression field of 50 kG is obtained 3.3 μs after discharge initiation. Plasma experiments were carried out at 45 kV main bank voltage and with a 10 mTorr D_2 fill pressure.

III. PLASMA PARAMETERS. The plasma parameters measured at the coil midplane at maximum compression are: 1) plasma density $\sim 1.6 \times 10^{16}$ cm^{-3} from end-on interferometry; 2) plasma radius of ~ 1.0 cm from luminosity profiles; 3) plasma electron temperature of 600 eV from Thomson scattering; 4) plasma ion temperature of 1.8 keV from both pressure balance and prompt neutron diagnostics; and 5) plasma beta on axis $\beta_A \simeq 0.6$ from excluded flux and luminosity data. The plasma stability characteristic at the coil midplane were identified with a side-on viewing streak camera. A low amplitude (~ 1 plasma diam) m=1 "wobble" instability was observed with an onset time of 4-5 μs after discharge initiation. The wobble never totally damps out.

IV. END-LOSS MEASUREMENTS. The particle end-loss time was obtained using the standard end-on interferometric technique.[1,2] Figure 1 presents the time history of the plasma column electron inventory. In the interferogram data analysis, the plasma contained in the low density "halo" which surrounds the main plasma column was not included in the electron inventory. Also neglected were the fringe-shifts near the discharge tube wall which are beleived to result from the plasma-wall interaction at the theta-pinch ends. For $t \geq 5$ μs, the data yield an e-folding end-loss time τ of 13.1 ± 1.0 μs. The period of zero inventory decay rate, $t \leq 5$ μs, has also been observed in previous experiments.[1,2] The plasma flow near the theta pinch ends was studied with a 2 mm diam acoustic delay line piezoelectric pressure sensor. The pressure probe was inserted axially into a 20-cm diam, 50 cm long vacuum vessel located at the theta pinch coil end. Figure 2 presents the measured pressure profiles at t = 5 μs; Z = 0 defines the coil end and -Z values indicate positions external to the coil. The ejected plasma does not rapidly expand, as is usually assumed, but remains radially confined with 1/e radius less than the discharge tube radius. The radial confinement of the ejected plasma results in the initial period of constant electron inventory.

In Fig. 3, taken from Ref. [3], the theoretically predicted normalized end-loss time $\eta = \tau/L(L/2)(m/2T)^{1/2}$, where T is the total plasma temperature and L is the coil length, is plotted against β. The experimental data, analyzed as discussed above, for the present and previous experiments are shown as barred points and the X's mark the results of a recent numerical MHD computation.[3] The only experimental result which agrees with theory is that obtained in the collision dominated Scylla I-C device [4], the collisionless plasma results are not well described by exixting theories.

V. END STOPPERING EXPERIMENTS. In the present experiment 5-cm diam, 3.8 cm thick quartz plugs were used as end stoppers. The front face of each plug was inserted 5 cm inside the theta pinch coil ends. Stereo-streak camera photographs (viewing the plasma from the coil top and front simultaneously), taken at the coil midplane are shown in Fig. 4. The plugs result in the stabilization of the m=1 "wobble" instability and increase the lifetime of the observed plasma light intensity 20-30% over that obtained without plugs. Time integrated photographs of the end vacuum vessel show that the intense light generated by the end flow plasma is completely absent when the plugs are inserted, indicating that end-flow is eliminated. Axially arrayed time-integrated neutron counters show that the presence of the plugs has no significant effect on the total neutron yield; a slight increase in neutron yield is observed near the coil ends. The plugs showed very little visible damage after twenty-nine plasma discharges, the plug surface being slightly glazed with small pit marks barely visible to the naked eye. The plasma energy per unit length at the coil midplane, $a^2\beta_A B^2/8$ where a is the plasma radius and B the external field, was determined from excluded flux and luminosity measurements. The time history of the central energy line density is shown on Fig. 5. The line energy maintains a higher value for a longer time and the instantaneous decay rate (slope of the curve) is less with the plugs inserted.

REFERENCES

[1] K. S. Thomas, et.al., Phys Fluids 17, 1314 (1975).

[2] R. F. Gribble, et.al., Phys Fluids 14, 2042 (1971).

[3] J. U. Brackbill, et.al., Third Topical Conference on Pulsed High Beta Plasmas, Culham, England (Permagon Press, Oxford and New York, 1975) p. 775.

[4] K. F. McKenna and T. M. York (to be published in Phys Fluids).

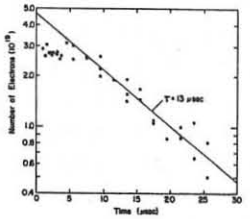

FIGURE 1

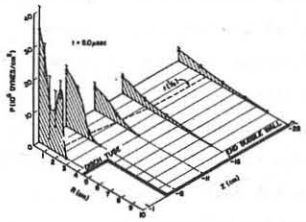

FIGURE 2

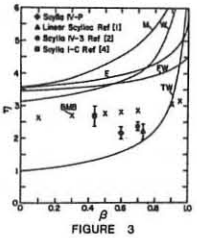

FIGURE 3

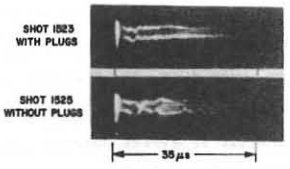

FIGURE 4

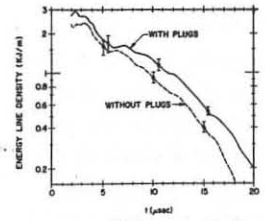

FIGURE 5

FIG. 1: TOTAL ELECTRON INVENTORY TIME HISTORY

FIG. 2: PLASMA PRESSURE PROFILES IN END VACUUM VESSEL Z=0 IDENTIFIES END OF COIL

FIG. 3: COMPARISON OF THEORETICAL AND EXPERIMENTAL END LOSS TIMES, η VS β

FIG. 4: STEREOSCOPIC STREAK PHOTOGRAPH

FIG. 5: TIME HISTORY OF PLASMA ENERGY PER UNIT LENGTH

INVESTIGATION OF DENSE PLASMA HEATING IN LINEAR THETA-PINCH WITH STRONG FAST-RISING MAGNETIC FIELD

D.V.EFREMOV SCIENTIFIC RESEARCH INSTITUTE OF ELECTROPHYSICAL APPARATUS, LENINGRAD, USSR

Burtsev V.A., Berezin A.B., Zukov A.P., Kubasov V.A., Litunevski V.N., Ljublin B.V., Ovsjannikov V.A., Smirnov A.G., Smirnov V.G., Fediakova V.P.

ABSTRACT. The paper presents the results of the heating of dense deuterium plasma in linear θ -pinch. For producing the strong fast rising magnetic fields in the one turn coil the inductive energy accumulation has been exploited with switching of the current into the load by using fast foil breakers. As a charging device for the inductive accumulation the low inductive condenser bank has been applied.

In recent experiments carried out on θ -pinch "Utro" [1-3] it was shown that application of strong fast rising magnetic fields(B_z= 40 kgs, $\tau \simeq 0.2$ μsec) allows to obtain in linear theta-pinch without preliminary ionization the sufficiently hot ($T \simeq 1$ keV) and dense ($n_e \simeq 3 \cdot 10^{16} cm^{-3}$) plasma column with a small coefficient of the radial compression ($\alpha = 2 \div 3$).

This paper presents the results of the further experimental study of the staged heating of the dense plasma by the strong fast rising magnetic field. These experiments were carried out at the disconnected condenser bank, using which the initial reverse biased field has been formed in the previous set of experiments. Equivalent electric circuit of the device is shown in fig.1. The basic parameters of the device "Utro" are presented in the table below.

U_{o1} (kV)	40	I'_{1max} (MA)	1,2
C_1 (μF)	288	B_{max} (kG)	30
W_o (kJ)	230	ℓ_{coil} (cm)	50
L_{o1} (nH)	2	d_{coil} (cm)	7
L_1 (nH)	50	C_3 (μF)	2
L_{coil} (nH)	10	U_{o3} (kV)	75
dB/dt (G/s)	$7 \cdot 10^{10}$	L_3 (nH)	40

Unlike the preceeding experiments the device has been supplied by the system of the gas preionization, consisted of 2 electrodeless discharges excited in the vacuum chamber at the distance 10 cm from the ends of the solenoid. The vacuum chamber was made of high quality UV -quartz. The filling pressure was 200 mtorr of deuterium. Applied diagnostics were: two frame holographic interferometry, spectroscopy in visible region with image conversion, X-ray diagnostics using aluminium absorbing filters with limited appertures, neutron yield measurements.

Fig.2 shows the oscillogramm traces of the currents in the various circuits of electric set up (I_1, I'_1, I''_1), X-ray flux emitted by plasma (γ) and neutron yield. X-ray detector registered the γ -quante with the energies above 10 keV. Measurements of the relative intensities of X-ray fluxes passing through the aluminium filters of various thickness (10÷1000 μm) allowed to estimate the mean energy of electron responsible for observed X-ray flux which has been found in the range 4-6 keV. Seeking of the solution of the problem wich fraction of plasma electrons really posess by the given average energies requires further study. Spatial resolution of X-ray measurements in the insert to this figure. The distribution of the $\mathcal{D}_\beta$ line broadening on the hight of the frame reflects the distribution of the density across the chamber. Coefficient of radial compression of the plasma column in the stage confinement $\alpha \simeq 3$.

Fig.4 presents typical examples of hologrammes obtained during one discharge using ruby laser emitted two light pulses separated in space and time.

Literature

1. A.B.Andresen et al. 7th Europ.Conf. on Contr.Fusion and Plasma Physics, Lousanne, 1975, paper 47.
2. V.A.Burtsev et al. Preprint K-0290, NIIEFA, 1976.
3. V.A.Burtsev et al. 6th Int.conf.Plasma Physics and Cont. Nucl.Fusion Res., 1976, Berchtesgaden, paper IAEA-CN-35.

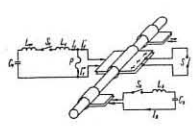

Fig. 1

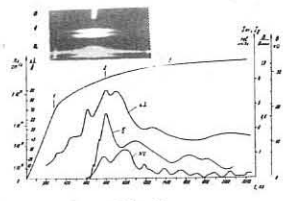

Fig.3

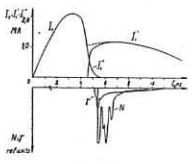

Fig.2

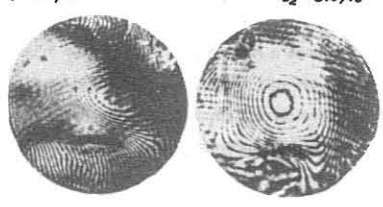

Fig.4 (axial zone d=3 cm)

FORMATION OF LONG-EXISTANCE DENSE PLASMA CONFIGURATIONS IN ZETA-PINCH ("Magnetic Press" regime)

Yu.V.Matveev, I.F.Kvartskhava

Sukhumi, Institute of Physics and Technology of the State Committeee on Utilization of Atomic Energy, Sukhumi, USSR.

Abstract. The experimental data are given indicating the possibility of forming a MHD stable plasma configuration called a multishell Zeta-pinch.

The analysis of the experimental data has led us to the conclusions that stable Zeta-pinches are observed, as a rule, in the presence of well developed plasma wall shells which arise as a result of secondary breakdowns of the discharge gap /I/. In such regimes the central plasma stable state is maintained for 20 μsec. The state arises due to the stabilizing effect of a wall-side plasma which acts as a conducting casing close to the pinch. For stable regimes R/r = 3-4 ratio is typical (R is the wall-side plasma radius and r is the pinch radius).

States with secondary breakdowns are natural for pinch devices since there occurs an incomplete snow-ploughing of gas; the wall is intensely bombarded by ultraviolet and soft X-rays; there arise considerable electric fields at the periphery, etc /I,2/. The secondary breakdown process developes for $\sim 10^{-7}$ sec. As a result, the current increases at the chamber wall ($\dot{I} > 10^{12}$ amp/sec), evaporating it. After the breakdown, the pinch is turned off from the external circuit.

Similar situations arise in other thermonuclear devices (Theta-pinches, tokamacks) also on increasing the power supply. This is one of the difficulties for the present stage of investigations on plasma magnetic confinement.

In Paper /2/, a device is offered with an evaporating pure gaseous wall compressing a closed current loop which developes in the Zeta-pinch chamber after the secondary breakdown. Compressing the current loop, we can increase the current in the pinch and ensure the plasma Joule and adiabatic heating. Here, magnetic press ratio $p_n = p_1(R/r)^{\zeta}$ is in action, where p_n is the field pressure onto the pinch and p_1 is the field pressure onto the gaseous wall.

The initial experiments studied the influence of wall-side plasma processes on the life-time of the current loop. A condenser bank with W = 10 kj (V_0 = 0 - 25 kV) has been used. The experiments have been performed in a porcelain chamber with the inner diameter and length equal to 28 cm and 50 cm, respectively. The electrodes were shorted along the chamber axis by a copper rod ("rigid pinch").

Depending on D_2 pressure p_0, the gas breakdown initiation can be displaced in any halfcycle of the condenser discharges through the rod (Ø 8 mm). The magnitude and the direction of the loop-trapped (rod-electrodes - wall-side plasma) "exciting" magnetic field have been changed in such a manner. The discharges ignited in the first cycle of the current flow through the rod have been studied in more detail.

The gas breakdown in the first quarter of a cycle ($p_0 = 10^{-1}$ torr) results in subsequent appearance of two or three plasma shells compressing to the axis. The long-existance current loops develop turned off from the external circuit in the chamber after formation of closed loops in the wall-side layer (~ 1 cm) and does not penetrate the inner regions of the chamber (Fig.1). We obtain a stable MHD configuration- a multishell Zeta-pinch. A full period of the current loop existance is 90 μsec (the current e-folds). Diffuse decay of the plasma shells "pressed" between the rod and the wall-side plasma takes place for 30 - 40 μsec.

The first shell of the plasma presses to the rod with an average velocity $V_{aver.} = 3.10^6$ cm/sec and ensures fivefold growth of the current (up to 10^5 amp) in the first closed loop (rod- electrodes + compressing plasma). The second and the third plasma shells compress with less velocities.

It follows from results of magnetic probe measurements that a magnetic energy cumulation takes place in skin-layers. Thus, in the thickness of the first plasma shell, a magnetic field H_φ, corresponding to the current I_s > 300 kamp (the current in the external circuit is I = 200 kamp) is recorded. These phenomena hawe been discussed earlier /3/. In the present case the field cumulation is observed in an outer skin-layer of the plasma shell.

The condition of trapping the peak "exciting" current (H_φ field) is realized at $p_0 = 2.10^{-2}$ torr. In this case deuterium breakdown occurs nearly at the peak current in the rod. The wall-side plasma compression takes place in the second half-cycle up to r = 8 - 9 cm with $V_{aver.} \leq 10^6$ cm/sec and is not accompanied with a pronounced pressing of the magnetic field. The current loop life-time is 80 μsec.

The cases of fast heating of the plasma by shock waves have been studied at lower p_0 and small $I_{exciting}$. Reduction of P_0 down to $\leq 10^{-2}$ torr allowed to accomplich gap breakdowns at the end of the first and in the beginning of the second halfcycles of the current in the rod. The gas breakdown at the end of the first halfcycle at $I_{exciting} < 0{,}23\ I_{peak}$ does not lead to the stable current loop formation. The plasma compression took place in the second halfcycle and H_φ field rapidly vanishes from the first halfcycle. In these unstable regimes neutron emission generates (Fig.2). Gas breakdowns in the beginning of the second halfcycle ensure the stable regime accompanied with the flush of soft X-rays (Δt = 1 - 5 μsec).

The neutron emission characteristics are close to the characteristics found in the experiments with classical pinches (pressure range, duration, occurence moments, intensity growth towards the cathode, etc). Now, they are distinguished by their larger intensities (20 - 30 times) and occurence regularities in the first and the second singularities. The neutron output was reduced by the rod diameter increase up to 30 mm. The results obtained are contradictory with the widely spread opinion on neutron generation on developing the pinch narrowing (m = 0). It's interesting to note that there was recorded a low neutron emission in the case of a quartz rod too (Ø 10 mm).

Thus, model experiments indicate the opportunity of obtaining a MHD stable (to m=I and m=0) plasma formation - a multishell Z-pinch (Fig.3). The unique feature of a Z-pinch as a trap and its higher MHD stability result in the necessity of further exploring this design. The calculations show that in an energy balance of the closed current loop, the main kind of losses is represented by the emission from the wall-side plasma ($T \leq 10eV$). Therefore, in the experiments with the multishell Z-pinch pressed by a purely gaseous piston, plasma paramaters (T and τ) increase. To this end, we have constructed a chamber called "Condensate" where the operating gas on the wall can be freezed. The gaseous piston used for pressing the plasma will allow to create multishell Z-pinches in toroidal chambers too.

We would like to thank N.V.Philippov for indicating the neutron generation mode.

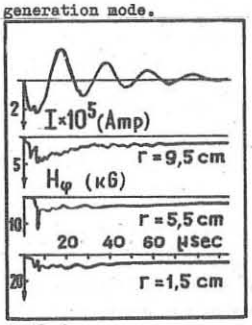

FIG. 1

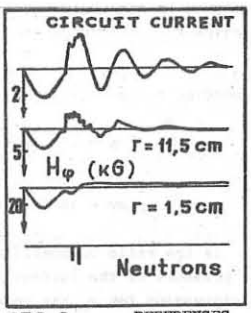

FIG.2

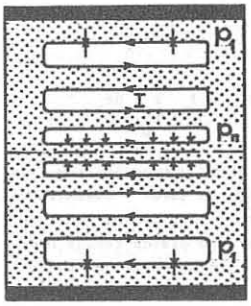

FIG.3

REFERENCES

1. Kvartskhava I.F., Matveev Yu.V. Nucl.Fusion, II (1971) 385.
2. Кварцхава И.Ф., Матвеев Ю.В. Письма в ЖЭТФ, 18, в.I (1973)
3. Кварцхава И.Ф., Матвеев Ю.В., Бутов И.Я. и др., in "Plasma Phys. and Contr. Nucl. Fus. Res. 3 (1974) 149, IAEA, Vienna 1975.

THE FORMATION OF HIGH DENSITY PINCHES

by

David Potter

Physics Department, Imperial College, London S.W.7.

Abstract

The formation of a z-pinch is analysed theoretically. A slug model describing the plasma between shock and piston is developed and the final pinch structure resolved. It is shown that such a formation inevitably produces a weak compression. By profiling the current in time, quasi adiabatic compression can be produced and plasmas of very high density and temperature achieved.

Introduction

Analysis of the plasma focus suggest that, in the absence of an increased voltage, scaling of the conditions of the dense plasma is very weak. On the other hand, the technology of Blumlein sources now permits the production of pinches at very large voltages and currents over short timescales. The formation of such a pinch has been demonstrated experimentally (Choi et al., 1977). This paper analyses the formation of such a pinch theoretically. By profiling the current in time, thermonuclear plasmas of density $n \sim 10^{20}$ cm^{-3} and temperatures of $T \sim 1$ keV are obtainable with currents of 400 kAmps. and voltages of 800 kvolts.

The conventional snowplough model of the formation of a pinch is inadequate in describing the transient plasma structure, the final pinch radius, or the final pinch structure. A slug model of the formation of a pinch has been developed which defines the plasma structure in space and the final pinch radius.

By varying the applied current in time, very large compressions and a dense pinch of small radius can be obtained.

Slug Model of the formation of a Pinch

Streak photographs of a fully ionised hydrogen pinch suggest that, unlike the snowplough model or shock reflexion models, the piston comes uniformly to rest as the shock meets the axis (Choi et al., 1977). This suggeststhat as the shock approaches the axis it emits outgoing sound waves which slow down the piston. Any reflected shock is very weak. Comparing the transit time of sound waves between shock and piston with the pinch time suggest a slug model in which the plasma pressure between piston and shock is uniform in space but not time. At any instant in time, the volume V of plasma between the shock radius $r_s(t)$ and piston radius $r_p(t)$ is compressed adiabatically

$$\gamma p dV + V\, dp = 0$$

where according to the strong shock boundary conditions imposed at $r_s(t)$:

$$dp = 2p \frac{dv_s}{v_s}$$

and

$$dV = 2\pi \left(r_p\, dr_p - \frac{2r_s}{\gamma+1} dr_s\right)$$

where γ is the ratio of specific heats. Combining these equations with the pressure of the current I at the magnetic piston to give an expression for v_s the velocity of the shock,

$$v_s = \left\{\frac{p_o}{\rho_o}\right\}^{\frac{1}{2}} (\gamma+1)^{\frac{1}{2}} \cdot \frac{I}{4\pi r_p},$$

yield for the constant current case a relationship between the shock and piston radius:

$$\left\{\frac{\gamma-1}{\gamma} + \frac{1}{\gamma}\frac{r_s^2}{r_p^2}\right\} dr_p = \frac{2}{\gamma+1}\frac{r_s}{r_p}\, dr_s$$

It is apparent that for $\gamma > 1$, as the shock approaches the axis ($r_s/r_p \to 0$), the piston velocity tends to zero. Furthermore, the plasma comes to rest and the final pinch radius and structure are defined. The solutions for the piston radius and shock radius are drawn in Figure 1. Solution of the above

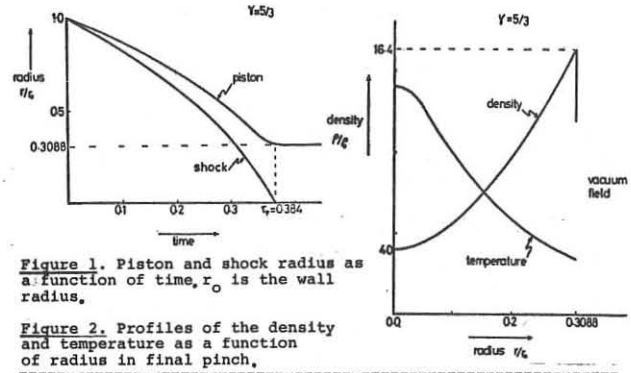

Figure 1. Piston and shock radius as a function of time, r_o is the wall radius.

Figure 2. Profiles of the density and temperature as a function of radius in final pinch.

equation shows that the final pinch radius a is simply related to the wall radius r_o and γ:

$$a = r_o \left\{\frac{\gamma}{\gamma+1}\right\}^{\frac{\gamma}{\gamma-1}}$$

For the important limit $\gamma = 5/3$, $a = 0.31\, r_o$ so that the compression is very weak. With the aid of a Lagrangian solution we can solve for the density and temperature as a function of radius, the solutions of which are shown in Figure 2.

High Compression by Programming the Current in Time It has been shown above that when a z-pinch is formed by a large constant current, a weakly compressed pinch is formed when $\gamma = 5/3$. This is due to the properties of a strong shock across which a limiting value of the compression is reached of 4. To produce a high compression small radius pinch, the compression must occur adiabatically. If we consider the limiting case where the moving piston produces a series of inwardly travelling adiabatic pressure pulses which only meet at the axis, the compression will be a maximum. If u is the velocity of the piston and the plasma adjacent to the piston and v the velocity of sound waves there, the condition for coincidence is:

$$\frac{d}{dt}\left\{(u+v)(\tau - t)\right\} = -u$$

where τ is the time at which maximum compression occurs. With the adiabatic hydrodynamic equations, we obtain the solution for the required pressure of the piston:

$$p(t) = p_o \left(1 - \frac{t}{\tau}\right)^{\frac{-2\gamma}{\gamma+1}}$$

and the required profiles of the current:

$$I(t) = I_o \left\{\left(\frac{\gamma+1}{\gamma-1}\right)\left(1 - \frac{t}{\tau}\right)^{\frac{2-\gamma}{\gamma+1}} - \left(\frac{2}{\gamma-1}\right)\left(1 - \frac{t}{\tau}\right)^{\frac{1}{\gamma+1}}\right\}$$

where I_o is the initial current and p_o the initial uniform pressure of the plasma. (Figure 3). To apply these conditions, the plasma and field must first be in equilibrium. The initial equilibrium is produced by shock formation with current I_o. Thereafter the main strong compression is produced by such a rising current (Figure 4).

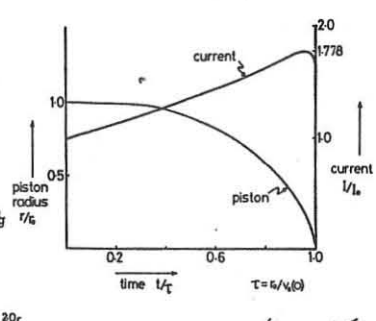

Reference:

Choi, P., Folkieski, A., and Dangor, A.E. (1977) private communication

Figure 3 (top). Current profile for singular compression.

Figure 4 (right). Suggested current for maximum compression.

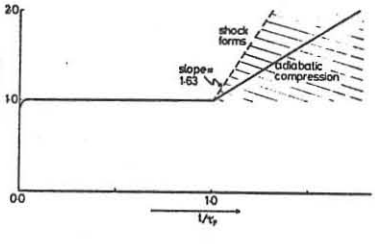

SCALING RELATIONS FOR HIGH-β PLASMA COOLING

G.E.Vekstein
Institute of Nuclear Physics
630090, Novosibirsk-90, USSR

Abstract. Various regimes of a dense high-β plasma cooling are considered. The energy confinement time is estimated as a function of plasma parameters (density, temperature, magnetic field) and dimensions of a system.

The high-β plasma is suggested to be used in different types of fusion systems. In this report we examine some peculiarities of such a plasma in solenoidal devices with nonmagnetic (or wall) confinement. The detailed survey of these installations is given in [1].

Let us consider infinitely long cylindrical tube of radius R with homogeneous hot plasma and axial magnetic field H_o. Plasma density and temperature are n_o and T_o. Magnetic pressure is small: $\beta_o \equiv 16\pi n_o T_o / H_o^2 \gg 1$. The only role of the magnetic field is to suppress transverse heat conductivity. It means that plasma is strongly magnetizied, so even for ions the parameter $\delta_o \equiv (\omega_{Hi}\tau_i)_o \gg 1$. Plasma density decreases in time due to heat conductivity and bremmstrahlung (radiation power per unit volume $Q_r = An^2T^{1/2}$). It turns out that the energy confinement time τ_E is quite different for plasmas with $\beta \lesssim 1$ and $\beta \gg 1$. The reason is that confinement time for the cases of practical interest greatly exceeds inertial time R/C_s (C_s - sound velocity). It means that for high-β plasma $\frac{\partial}{\partial r}(nT) = 0$ is valid every moment. As a result, plasma flow to walls arises while cooling. Besides that the radiation losses increase because Q_r is proportional to $T^{-3/2}$ upon the condition $nT = const$ and radiation becomes large in the cold boundary layer.

To separate various regimes of cooling for plasma with $\beta \gg 1$ it is convenient to consider dependence of τ_E on radius. For small enough R radiation is negligible and heat transport equation takes the form [2]:

$$3\frac{\partial(nT)}{\partial t} = -\frac{1}{r}\frac{\partial}{\partial r} r\left(5nTv - \varkappa \frac{\partial T}{\partial r}\right) \qquad (1)$$

(v - plasma radial velocity, $\varkappa$ - thermal conductivity). As $nT = const$, the whole heat flux $q = 5nTv - \varkappa \frac{\partial T}{\partial r}$ is r. Near the wall where v goes to zero, heat conductivity contribution is principal. In this near-wall layer whose thickness Δ is much less than R we have:

$$q = -\varkappa \frac{\partial T}{\partial r} = const \qquad (2)$$

Plasma heat conductivity $\varkappa$ essentially depends on the ion magnetization parameter $\delta = \omega_{Hi}\tau_i$ is $HT^{-3/2}/n$. The magnetic field changes due to plasma motion. The corresponding equation is [2]:

$$\frac{d}{dt}\left(\frac{H}{n}\right) = \frac{1}{nr}\frac{\partial}{\partial r} r\left(\frac{c^2}{4\pi\sigma}\frac{\partial H}{\partial r} + \frac{c\beta_\Lambda^{uT}}{en}\frac{\partial T}{\partial r}\right) \qquad (3)$$

(σ - plasma conductivity, β_Λ^{uT} - coefficient connected with Nernst effect). For high-β plasma Nernst effect is more important than magnetic field diffusion. But magnetic field remains approximately frozen into the plasma: $\Delta\left(\frac{H}{n}\right) \sim \frac{H}{n}\left(\frac{m}{M}\right)^{1/2}$. The reason is that characteristic time corresponding to ion heat conductivity is small enough.

So $\delta = \delta_o (T/T_o)^{3/2}$. For $T > T_1 \sim T_o \delta_o^{-2/3}$, when $\delta > 1$, the heat conductivity $\varkappa \sim n_o \chi_o \left(\frac{T_o}{T}\right)^{1/2}$ (χ_o - hot plasma temperature conductivity). And for $T < T_1$ we have $\varkappa \sim n_o \chi_o \delta_o^2 (T/T_o)^{5/2}$. After that from eq.(2) it is easy to find the profiles of T, n and the boundary layer. Let us write the constant in eq.(2) $q = const = \alpha n_o \chi_o T_o / R$. Then the total number of particles in layer is $N_\Delta \sim n_o R^2 \delta_o^{4/3}/\alpha$, so the heat flux to the wall mu lar-ge enough:

In the hot plasma with $T \sim T_o$ the heat conductivit is small and such a flux can be provided only by convec flow of the plasma. For the time of the order of magnit its density drops, roughly speaking, by one-half, so th number of particles in the layer N_Δ becomes of order n_o means that $\alpha \sim \delta_o^{4/3}$ and the energy confinement time $\tau_E \sim$ The thickness of the boundary layer $\Delta \sim R/\delta_o^{4/3}$.

This is valid until the total radiation losses W $2\pi\int_0^R Q_r r\,dr$ are less than q. The main contribution t comes from the region with temperature $T \sim T_o \delta_o^{-2/3}$ where w $W_r \sim n_o T_o R^2 \delta_o^{4/3}/\tau_r$ ($\tau_r = 3n_o T_o / A n_o^2 T_o^{1/2}$ - radiation cooling tim the hot plasma). So the radiation becomes important for For $R \gg (\chi_o \tau_r)^{1/2}$ energy losses may be described as "cooli ve" motion from the cold walls to the centre [3]. It m that energy radiated from the boundary layer is compens the convective energy flux from the hot plasma. The geo may be considered as plane. Then for the stationary "co wave" we have:

$$5n_o v_o \frac{dT}{dx} = \frac{d}{dx}\left(\varkappa \frac{dT}{dx}\right) - Q_r$$

(n_o and v_o - density and velocity of the hot plasma). city v_o is determined by the total radiation losses: $\frac{1}{5n_o T_o}\int Q_r\,dx$. It is easy to obtain that the main c bution to radiation comes from region with temperature and the hot plasma velocity $v_o \sim \delta_o^{4/3}(\chi_o/\tau_r)^{1/2}$. For the time we have $\tau_E \sim R/v_o \sim R(\tau_r/\chi_o)^{1/2}/\delta_o^{4/3}$. Time τ_E increas nearly with R until the total hot plasma radiation is than radiation from the boundary layer. It is so if $R <$ For larger R time τ_E becomes equal to τ_r.

All previous estimations were obtained for the pla negligible magnetic pressure, that is for large enough such a case the time τ_E doesn't depend on β_o, and the parameter is the ion magnetization value δ_o. The transi low-β plasma ($\beta_o \lesssim 1$) occurs as follows. For the froze ic field its pressure increases when temperature drops $\frac{H_o^2}{8\pi}\left(\frac{T_o}{T}\right)^2$ and becomes equal to the plasma pressure at Since the whole pressure $\frac{H^2}{8\pi} + 2nT$ is homogeneous, it mea for $T < T_o \beta_o^{-1/2}$ density n and magnetic field H becomes con and $\beta < 1$. It is obvious now that our previous results lid if this temperature $T_o \beta_o^{-1/2}$ is less than $T_o \delta_o^{-2/3}$ or $\beta_o^{1/2} \geq$ the opposite case the region with $T \sim T_o \beta_o^{-1/2}$ is important must change the quantity $\delta_o^{4/3}$ on $\beta_o^{1/4}$ in our formulas.

These peculiarities of the high-β plasma coolin of course, connected with the concrete dependence of c heat conductivity $\varkappa$ on n, T and H. They may be absent different $\varkappa(n, T, H)$, for example, of Bohm type, when $\varkappa$

In conclusion we want to mention that our analyti mations for high-β plasma cooling are in good agreem computer results [4].

References

[1] Budker G.I. Proc. VI Europ.Conf. on Controlled Fus Plasma Physics, vol.2. p.136 (Moscow, 1973).
[2] Braginski S.I. Rev. Plasma Physics. N.Y., 1965, vo
[3] Vekstein G.E. IAMTP (ПМТФ)(in Russian), No6, p.3,
[4] Vekstein G.E. et al. Paper IAEA-CN-35/E-21 (Bercht 1976).

SCALING RELATIONS FOR HIGH-β PLASMA COOLING

G.E.Vekstein
Institute of Nuclear Physics
630090, Novosibirsk-90, USSR

Abstract. Various regimes of a dense high-β plasma cooling are considered. The energy confinement time is estimated as a function of plasma parameters (density, temperature, magnetic field) and dimensions of a system.

The high-β plasma is suggested to be used in different types of fusion systems. In this report we examine some peculiarities of such a plasma in solenoidal devices with nonmagnetic (or wall) confinement. The detailed survey of these installations is given in [1].

Let us consider infinitely long cylindrical tube of radius R with homogeneous hot plasma and axial magnetic field H_0. Plasma density and temperature are n_0 and T_0. Magnetic pressure is small: $\beta_0 \equiv 16\pi n_0 T_0 / H_0^2 \gg 1$. The only role of the magnetic field is to suppress transverse heat conductivity. It means that plasma is strongly magnetizied, so even for ions the parameter $\delta_0 \equiv (\omega_{Hi}\tau_i)_0 \gg 1$. Plasma density decreases in time due to heat conductivity and bremmstrahlung (radiation power per unit volume $Q_r = An^2T^{1/2}$). It turns out that the energy confinement time τ_E is quite different for plasmas with $\beta \lesssim 1$ and $\beta \gg 1$. The reason is that confinement time for the cases of practical interest greatly exceeds inertial time R/C_s (C_s - sound velocity). It means that for high-β plasma $\frac{\partial}{\partial t}(nT) = 0$ is valid every moment. As a result, plasma flow to walls arises while cooling. Besides that the radiation losses increase because Q_r is proportional to $T^{-3/2}$ upon the condition $nT = const$ and radiation becomes large in the cold boundary layer.

To separate various regimes of cooling for plasma with $\beta \gg 1$ it is convenient to consider dependence of τ_E on radius. For small enough R radiation is negligible and heat transport equation takes the form [2]:

$$3\frac{\partial (nT)}{\partial t} = -\frac{1}{r}\frac{\partial}{\partial r} r \left(5nTv - \varkappa \frac{\partial T}{\partial r}\right) \qquad (1)$$

(v - plasma radial velocity, $\varkappa$ - thermal conductivity). As $nT = const$, the whole heat flux $q = 5nTv - \varkappa \partial T/\partial r \sim r$. Near the wall where v goes to zero, heat conductivity contribution is principal. In this near-wall layer whose thickness Δ is much less than R we have:

$$q = -\varkappa \partial T/\partial r = const \qquad (2)$$

Plasma heat conductivity $\varkappa$ essentially depends on the ion magnetization parameter $\delta = \omega_{Hi}\tau_i \sim HT^{3/2}/n$. The magnetic field changes due to plasma motion. The corresponding equation is [2]:

$$\frac{d}{dt}\left(\frac{H}{n}\right) = \frac{1}{nr}\frac{\partial}{\partial r} r \left(\frac{c^2}{4\pi\sigma}\frac{\partial H}{\partial r} + \frac{c\beta_\wedge^{uT}}{en}\frac{\partial T}{\partial r}\right) \qquad (3)$$

(σ - plasma conductivity, $\beta_\wedge^{uT}$ - coefficient connected with Nernst effect). For high-β plasma Nernst effect is more important than magnetic field diffusion. But magnetic field remains approximately frozen into the plasma: $\Delta(H/n) \sim H/(m/M)^{1/2}$. The reason is that characteristic time corresponding to ion heat conductivity is small enough.

So $\delta = \delta_0 (T/T_0)^{3/2}$. For $T > T_1 \sim T_0 \delta_0^{-2/3}$, when $\delta > 1$, the heat conductivity $\varkappa \sim n_0 \chi_0 \left(\frac{T_0}{T}\right)^{1/2}$ (χ_0 - hot plasma temperature conductivity). And for $T < T_1$ we have $\varkappa \sim n_0 \chi_0 \delta_0^2 (T/T_0)^{5/2}$. After that from eq.(2) it is easy to find the profiles of T, n and H in the boundary layer. Let us write the constant in eq.(2) as $q = const = \alpha n_0 \chi_0 T_0 / R$. Then the total number of particles in this layer is $N_\Delta \sim n_0 R^2 \delta_0^{4/3}/\alpha$, so the heat flux to the wall must be large enough:

In the hot plasma with $T \sim T_0$ the heat conductivity is small and such a flux can be provided only by convective flow of the plasma. For the time of the order of magnitude τ_E its density drops, roughly speaking, by one-half, so the total number of particles in the layer N_Δ becomes of order $n_0 R^2$. It means that $\alpha \sim \delta_0^{4/3}$ and the energy confinement time $\tau_E \sim R^2/\chi_0 \delta_0^{4/3}$. The thickness of the boundary layer $\Delta \sim R/\delta_0^{4/3}$.

This is valid until the total radiation losses $W_r = 2\pi \int_0^R Q_r r\, dr$ are less than q. The main contribution to W_r comes from the region with temperature $T \sim T_0 \delta_0^{-4/3}$ where $\omega_{Hi}\tau_i \sim 1$: $W_r \sim n_0 T_0 R^2 \delta_0^{4/3}/\tau_r$ ($\tau_r = 3n_0 T_0 / A n_0^2 T_0^{1/2}$ - radiation cooling time for the hot plasma). So the radiation becomes important for $R \geq (\chi_0 \tau_r)^{1/2}$. For $R \gg (\chi_0 \tau_r)^{1/2}$ energy losses may be described as "cooling wave" motion from the cold walls to the centre [3]. It means that energy radiated from the boundary layer is compensated by the convective energy flux from the hot plasma. The geometry may be considered as plane. Then for the stationary "cooling wave" we have:

$$5n_0 v_0 \frac{dT}{dx} = \frac{d}{dx}\left(\varkappa \frac{dT}{dx}\right) - Q_r \qquad (4)$$

(n_0 and v_0 - density and velocity of the hot plasma). Velocity v_0 is determined by the total radiation losses: $v_0 = \frac{1}{5n_0T_0}\int Q_r\, dx$. It is easy to obtain that the main contribution to radiation comes from region with temperature $T \sim T_0 \delta_0^{4/3}$ and the hot plasma velocity $v_0 \sim \delta_0^{4/3}(\chi_0/\tau_r)^{1/2}$. For the cooling time we have $\tau_E \sim R/v_0 \sim R(\tau_r/\chi_0)^{1/2}/\delta_0^{4/3}$. Time τ_E increases linearly with R until the total hot plasma radiation is less than radiation from the boundary layer. It is so if $R < \delta_0^{4/3}(\chi_0\tau_r)^{1/2}$. For larger R time τ_E becomes equal to τ_r.

All previous estimations were obtained for the plasma with negligible magnetic pressure, that is for large enough β_0. In such a case the time τ_E doesn't depend on β_0, and the large parameter is the ion magnetization value δ_0. The transition to low-β plasma ($\beta_0 \lesssim 1$) occurs as follows. For the frozen magnetic field its pressure increases when temperature drops: $\frac{H^2}{8\pi} = \frac{H_0^2}{8\pi}\left(\frac{T_0}{T}\right)^2$ and becomes equal to the plasma pressure at $T \sim T_0 \beta_0^{1/2}$. Since the whole pressure $\frac{H^2}{8\pi} + 2nT$ is homogeneous, it means that for $T < T_0 \beta_0^{1/2}$ density n and magnetic field H becomes constant and $\beta < 1$. It is obvious now that our previous results are valid if this temperature $T_0 \beta_0^{1/2}$ is less than $T_0 \delta_0^{-2/3}$ or $\beta_0^{1/2} \gtrsim \delta_0^{4/3}$. For the opposite case the region with $T \sim T_0 \beta_0^{1/2}$ is important and we must change the quantity $\delta_0^{4/3}$ on $\beta_0^{1/4}$ in our formulas.

These peculiarities of the high-β plasma cooling are, of course, connected with the concrete dependence of classical heat conductivity $\varkappa$ on n, T and H. They may be absent for some different $\varkappa(n, T, H)$, for example, of Bohm type, when $\varkappa \sim nT/H$.

In conclusion we want to mention that our analytical estimations for high-β plasma cooling are in good agreement with computer results [4].

References
[1] Budker G.I. Proc. VI Europ.Conf. on Controlled Fusion and Plasma Physics, vol.2. p.136 (Moscow, 1973)
[2] Braginski S.I. Rev. Plasma Physics. N.Y., 1965, vol.1,p.205
[3] Vekstein G.E. IAMTP (ПМТФ)(in Russian), No6, p.3, 1976
[4] Vekstein G.E. et al. Paper IAEA-CN-35/E-21 (Berchtesgoden, 1976)

The Influence of Anisotropic Ion Pressure on Non-Axisymmetric Toroidal High-Beta Equilibria

J. Neuhauser, F. Herrnegger, M. Kaufmann, G. Schramm, J. Sommer
Max-Planck-Institut für Plasmaphysik, 8046 Garching, Fed.Rep. Germany
EURATOM Association

Abstract: The influence of an anisotropic ion pressure on nonaxisymmetric toroidal high-ß equilibria, e.g. the High-ß Stellarator, is discussed. Experimental results concerning mirror instabilities and isotropic or slightly anisotropic high-beta stellarator equilibria are presented.

Introduction: Toroidal high-ß stellarator equilibria were calculated using small parameter expansions and, recently, 3D-computer codes. These calculations were based on the ideal MHD equations and assumed a scalar isotropic pressure. Experimentally, high-ß stellarator equilibria were established in moderately hot toroidal theta-pinches for a limited time because of the occurrence of $m \geq 1$ instabilities [e.g. 1]. One feature inherent in the shock heating scheme is that initially only the perpendicular ion energy is increased, while the parallel energy rises on a relaxation time scale governed by collisions and instabilities. An important consequence is the occurrence of mirror instabilities (short wavelength m = 0 modes). In addition, the anisotropic ion pressure will influence the amplitude of the periodic corrugations in toroidal high-beta stellarators and will change the toroidal force balance.

Mirror instabilities in theta-pinches: Mirror instabilities were theoretically predicted long ago and observed for the first time experimentally in the ISAR I straight 1.5 m long theta-pinch [2]. They were also found in the 5.4 m theta-pinch and recently in the ISAR T1 B toroidal high-ß stellarator experiment for the lowest filling pressure ($\lesssim 10$ mtorr D_2) and a bank energy of 1.5 MJ. At present, a toroidal theta-pinch (or screw-pinch) is being operated on the ISAR I bank, called TORIX ($R = 1.35$ m, $r_{coil} = 11$ cm, $r_{tube} = 8$ cm), where the preionization and shock compression for HBS II-like conditions [3] is investigated. Even with a reduced bank energy of 0.5 MJ a hot plasma is obtained with a comparatively low filling pressure of 3 mtorr D_2 (preliminary data for $t \approx 3$ µs: $T_i \gtrsim 500$ eV, $T_e \lesssim 300$ eV; $n_e \approx 3 \times 10^{15}$ cm^{-3}, oxygen impurity content: 0.5 %; ion-ion collision time $\tau_{ii} \gtrsim 5$ µs). Mirror instabilities were indicated by strong variations in local measurements, e.g. a factor 2 for the fringe shift of the infrared interferometer or a factor of up to 10 in the O VI and C V spectral line intensity. The line intensity of lower ionization stages (O III, IV, V) occurring earlier ($t < 2$ µs) was less pronounced (less than a factor 2). As proof a multislit window (14 slits) was used to observe the plasma shape in a 134 mm long segment. In Fig. 1 framing pictures are shown for filling pressures of 3 and 10 mtorr at $t = 2$, 2.5 and 3 µs (exposure time 50 ns). Mirror instabilities are clearly observed for 3 mtorr with a wavelength comparable with or longer than the plasma diameter. The formation time is below 500 ns. For $t < 2$ µs there are no large amplitude mirrors. As in our linear experiments, the plasma column is not destroyed by the mirror instabilities. These investigations are being continued.

Toroidal equilibrium in ISAR T1 B: A toroidal high-ß stellarator equilibrium was achieved for a wide range of plasma parameters in ISAR T1 B ($R = 135$ cm, $B_{max} = 30$ kG) [1,4]. Fine correction of the equilibrium was provided by $\ell = 2$ windings in addition to the $\ell = 1$, $\ell = 0$ and $\ell = 2$ fields produced by a shaped coil. For $T_i < 500$ eV the correction factor α with respect to the sharp boundary model (as defined in [5], Sec. 9) was $\alpha = 1.4 \pm 0.25$, while there was rough agreement with recent results of numerical 3D codes [6]. However, for $T_i \approx 500$ to 800 eV and $\tau_{ii} = 1$ to 3.5 µs on axis the plasma was rapidly driven inwards with the same external fields, and for equilibrium a smaller $\alpha = 1.2$ was derived. The difference in equilibrium between the collision dominated case and that with $\tau_{ii} > 1$ µs might be due to a moderate increase in ß. But, experimentally, a very strong antiparallel bias field ($B_o \approx 400$ Gauss) producing a $ß \approx 1$ on axis instead of $ß = 0.65$ was necessary in order to produce a comparable effect at low ion temperature. We suppose, therefore, that the ß-dependence of the equilibrium is weaker than predicted by the sharp boundary model, and that the ion pressure anisotropy indicated by occasional mirror instabilities causes, at least partly, the change in the toroidal equilibrium.

Discussion: The close connection between mirror instability and the existence of a periodic high-ß equilibrium is quite obvious: The equilibrium corrugation represents a finite plasma disturbance which is unstable above a certain degree of anisotropy. A strong change of the plasma corrugation is already expected for a pressure anisotropy below that limit. This means that an equilibrium can again be obtained by adjusting the external magnetic field, but it will be quite different from that with an isotropic pressure ($P_\perp = P_\parallel$).

In order to demonstrate this behaviour more quantitatively, we treat the straight bumpy theta-pinch ($\ell = 0$) in a very crude model (sharp boundary; mirror force included; $\varkappa$ = wall radius r_w / plasma radius r_p; normalized bump amplitude $\delta_o \ll 1$; r_w, $r_p \ll$ period length λ) and get for fixed wall shape (Fig. 2)

$$\delta_o(r=r_p) \Big/ \delta_o(r=r_w) = \varkappa^2 \Big/ \left[1 + (\varkappa^2 - 1)\left(1 - \beta \frac{P_\perp}{P_\parallel}\right)\right], \quad \beta = \frac{2\mu_o P_\perp}{B_{ext}^2}$$

With increasing anisotropy but fixed external magnetic field corrugation, the bump also increases and blows up when the anisotropy approaches the mirror stability limit $P_\perp / P_\parallel = \varkappa^2 / [ß(\varkappa^2 - 1)]$. Beyond this limit we get formally an unstable equilibrium which is of no physical interest and does not exist in a more realistic model.

The curvature of the magnetic field lines, which is less significant for $\ell = 0$, must be included for $\ell \geq 1$ symmetry. Straight guiding centre plasma equilibria with $\ell = 0$ [7] and $\ell = 1$ [8] symmetry and their stability were investigated and again a strong influence on equilibrium and $m = 1$ stability is found.

Experimentally, it is well documented that short wavelength mirror instabilities are harmless and may even help to accelerate the relaxation process. The question is, whether longer wavelength m = 0 modes, especially the mode corresponding to the external corrugations, can reach a dangerous amplitude before the ion pressure anisotropy is sufficiently reduced by collisions, short wavelength mirror instabilities or other turbulent effects. Taking only collisional relaxation as the worst case, it is required that the ion-ion self-collision time be smaller than the growth time of the long wavelength mirror instability, which, for large anisotropy, is approximately equal to the wavelength divided by the perpendicular (!) ion velocity. This condition would be violated for HBS II standard parameters. To study this question in more detail, an appropriately designed experiment with a single bump will be conducted in TORIX.

References:

1 E. Fünfer et al., 7th Europ. Conf. on Contr. Fusion and Plasma Physics, Lausanne 1975, Vol. II, p. 151
2 M. Kaufmann, J. Neuhauser, H. Röhr, Z. Physik 244, 99 (1971)
3 W. Braun et al., Plasma Physics and Contr. Nucl. Fusion Research, Vienna 1975, IAEA-CN-33 / E2, Vol. III, p. 25
4 J. Neuhauser et al., Nucl. Fusion 17, 3 (1977)
5 E. Fünfer et al., Nucl. Fusion 15, 133 (1975)
6 D.C. Barnes et al., Plasma Physics and Contr. Nucl. Fusion Research, Vienna 1977, IAEA-CN-35 / E - 11
7 M.J. Schmidt, G. Vahala, Phys. Fluids 19, 1405 (1976)
8 M.J. Schmidt, G. Vahala, Bull.Am.Phys.Soc., Ser. II, 21, 1091 (1976)

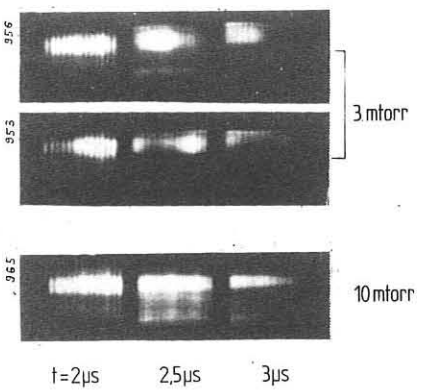

Fig. 1: Framing pictures of a 135 mm long segment of the toroidal plasma column in TORIX

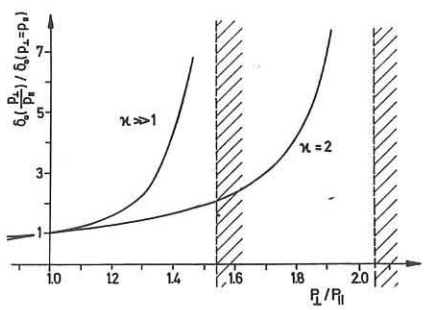

Fig. 2: Plasma bump amplitude δ_o as a function of the ion pressure anisotropy for different wall distance ($ß = 0.65$)

STABLE TOROIDAL MHD EQUILIBRIA WITH ROTATIONAL TRANSFORM AND WITHOUT LONGITUDINAL CURRENT

D. Lortz, J. Nührenberg

Max-Planck-Institut für Plasmaphysik, 8046 Garching bei München

Federal Republic of Germany

Abstract: Stable toroidal MHD equilibria with rotational transform and without current density on the magnetic axis are investigated. Conditions are formulated for the possibility of obtaining high stable β-values. New explicit existence conditions for three-dimensional equilibria with rational rotational transform on the magnetic axis are calculated.

Three-dimensional toroidal magnetohydrostatic equilibria raise various questions which necessitate a variety of investigation methods [1-6]. In this paper we use the expansion of a toroidal configuration around its magnetic axis to study the equilibrium and stability of three-dimensional equilibria [6] with rotational transform and without current density on the magnetic axis. The latter condition allows us to use a sufficient stability criterion [6] which provides complete stability with a vacuum surrounding the plasma column.

The β-values which can be obtained in the simplest type of $\ell = 2$ stellarator [7] and in equilibria with vanishing rotational transform [8] are rather low. The theory of the simplest $\ell = 2$ stellarator without current density on the magnetic axis [7] is dominated by the following facts. An increase in rotational transform decreases the part of the magnetic well that is independent of the third order form of the flux surfaces. A decrease of the rotational transform, with fixed pressure gradient $[\dot{p}(0)]$, increases the magnitude of the transverse fields, moves the stagnation points in the third order flux surfaces towards the magnetic axis and thus decreases the equilibrium β-value. Formally, this may be seen from the following equations:

$$b' + i\left(K_0' - \alpha'\right)b = -\varepsilon \exp(i\alpha)\, c_0^{-\frac{3}{2}} \varkappa \left(e^{-\frac{1}{2}} \cos\alpha - i e^{\frac{1}{2}} \sin\alpha\right) \qquad (1)$$

($' = d/d\ell$, ℓ arc length along the magnetic axis, $K_0(L) - K_0(0)$ rotational transform on axis except for an integer, α turning angle of the elliptical cross-section of half-axes ratio e, c_0 field on axis, $\varkappa$, τ curvature and torsion of the magnetic axis)

and

$$\mathcal{L}\Sigma = F\left(\varkappa, c_0, e, K_0', \alpha', \tau\right) + \dot{p}(0)\, G\left(b\right) \qquad (2)$$

where $\Sigma = (S^*, s^*, \Delta^*, \delta^*)$ describes the third order deformations of the flux surfaces, $\mathcal{L}$ is a linear differential operator in ℓ and F and G are functionals of the quantities indicated. Eq. (1) shows that the equilibrium is lost as $\iota \to 0$, which expresses the fact that the q = const surfaces are created by rotational transform alone.

For $\iota = 0$ equilibria [8-10] the situation is quite different. The destabilizing effects associated with those quantities generating rotational transform (current density on the magnetic axis, α', τ) are absent. In the simplest case, $K_0 = \alpha = \tau = 0$, eq. (1) is solved by imposing an integral side condition on $\varkappa$, e, c_0:

$$\oint \varkappa\, c_0^{-\frac{1}{2}}\, e^{-\frac{1}{2}}\, d\ell = 0 \,, \qquad k' = \varkappa\, c_0^{-\frac{3}{2}}\, e^{-\frac{1}{2}}$$

This means that the gross plasma form is chosen in such a way that q becomes stationary on the magnetic axis without the help of rotational transform. Nevertheless the stable β-values are not high (10% for reasonable geometry) because the condition that q be a function of volume alone to the order required in the framework of the present theory

$$q = q(0) + \dot{q}(0)\, V + O\left(V^{\frac{1}{2}}\right) \qquad (3)$$

imposes a severe additional integral side condition on the choice of functions compatible with $\dot{q}(0)/q(0) < 0$ (which is necessary for stability):

$$\oint d\ell \Big\{ c_0 k'^2 (e^2-1) + \tfrac{3}{4}\tfrac{c_0'^2}{c_0^2 e}(e^2-1) + \tfrac{1}{4}\tfrac{e'^2}{c_0^2 e^3}(e^2-1) - \tfrac{c_0'}{c_0^3}\tfrac{g'}{e^3}(e^2+1) + 3 c_0 e e' k k'$$

$$- c_0' k k' e^2 + \tfrac{4\pi}{L} k S^{*\prime}(e^2+1) + 4\pi q(0)\dot{p}(0) e k^2 \Big\} = 0 \qquad (4)$$

Obviously, a possible way out is provided by keeping the conditions for stationary q, introducing as little rotational transform as possible, and as much as in necessary to relax condition (4).

As a first step in the procedure outlined above we check whether the β-value becomes larger if we drop the side condition (4) without considering a nonvanishing rotational transform. The β-value does in fact become large, as is seen from the following example. Choosing

$$k = k_1 \sin x \,, \quad e = e_0 (1 + a^2 - 2a\cos x)^{-2} \,, \quad c_0 \propto e^{\frac{1}{2}} \,, \quad S^* = S_1^* \cos x$$

we obtain for a torus with 20 periods, $e_0 \approx 5$, $a = 0.1$, a β-value of about 1 for a local aspect ratio which is at least about 2. More details will be presented at the conference.

We now have to make the above procedure consistent by calculating the generalization of the side condition (4) for small values of ι. To this end we obtain the conditions for eq. (3) to be true for rational values of ι on axis. The lowest order conditions, i.e., that q be stationary on axis, are [9,10]

$$\oint \varkappa\, c_0^{-\frac{3}{2}} \left(e^{\frac{1}{2}} \sin\alpha \sin K_0 + e^{-\frac{1}{2}} \cos\alpha \cos K_0\right) d\ell = 0$$

$$\oint \varkappa\, c_0^{-\frac{3}{2}} \left(e^{\frac{1}{2}} \sin\alpha \cos K_0 - e^{-\frac{1}{2}} \cos\alpha \sin K_0\right) d\ell = 0$$

so that the variables $\varkappa$ and α may be eliminated:

$$\varkappa \cos\alpha = c_0^{\frac{3}{2}} e^{\frac{1}{2}} \left(k_1' \cos K_0 - k_2' \sin K_0\right)$$

$$\varkappa \sin\alpha = c_0^{\frac{3}{2}} e^{-\frac{1}{2}} \left(k_1' \sin K_0 + k_2' \cos K_0\right)$$

where k_1 and k_2 are arbitrary periodic functions of ℓ. The next order conditions appear to be rather tedious. We have already shown that they can be written as direct generalizations of eq. (4) and are integrals involving $e, c_0, \tau, K_0, k_1, k_2$ and the third- order quantities $S^*, s^*, \Delta^*, \delta^*$. Explicit formulae will be presented at the conference and will allow not only the consistency of the above β-calculation to be discussed, but also, more generally, existence properties of smooth three-dimensional equilibria with rational rotational transform on axis, such as stellarators with and without ohmic heating current and racetrack tokamaks.

References

[1] Grad, H., Phys.Fluids 10 (1967) 137.

[2] Brackbill, J.U., Barnes, D.C., Bull.Am.Phys.Soc. II, 21 (1976) 1074.

[3] Betancourt, O., Garabedian, P., Proc.Nat.Acad.Sciences, USA, 73 (1976) 984.

[4] Chodura, R., Schlüter, A., 2nd Eur.Conf.on Comp. Physics, Garching (1976) C2.

[5] Mercier, C., Nucl.Fusion 4 (1964) 213.

[6] Lortz, D., Nührenberg, J., Z. Naturforschung 31a (1976) 1277.

[7] Lortz, D., Nührenberg, J., Nucl. Fusion 17 (1977) 125.

[8] Lortz, D., Nührenberg, J., IAEA-CN-35/E9.

[9] Shafranov, V.D., Soviet Atomic Energy 22 (1967) 449.

[10] Lortz, D., Nührenberg, J., 3rd Int. (Kiev) Conf. on Plasma Theory, Trieste (1977) B-1/1-2.

"This work was performed under the terms of the agreement on association between the Max Planck-Institut für Plasmaphysik and EURATOM".

FEEDBACK STABILIZATION EXPERIMENTS USING $\ell = 2$ EQUILIBRIUM WINDINGS IN SCYLLAC

R. R. Bartsch, E. L. Cantrell, R. F. Gribble, K. B. Freese
L. E. Handy, R. Kristal, G. Miller, W. E. Quinn

Los Alamos Scientific Laboratory
University of California
Los Alamos, New Mexico USA

ABSTRACT. The confinement time in the Scyllac Sector Feedback Experiment has been extended with a pre-programmed equilibrium compensation force. This force was produced by driving a current with a flexible waveform in an additional set of $\ell = 2$ windings.

I. INTRODUCTION. Scyllac feedback experiments have been performed on a 120° sector of the 4-m major-radius toroidal theta pinch. Plasma parameters for the present set of experiments are the same as previously reported.[1] The configuration of the initial discharge has been altered from that of [1] to eliminate the helical oscillations of the plasma column. This has been accomplished by the use of a helical discharge tube which permits the initial implosion to create the plasma column in the helical configuration which it would otherwise dynamically approach in time.[2] The $\ell = 0,1$ sector, which is shown schematically in Fig. 1, has 13 wavelengths of the equilibrium fields with a 5 position feedback sensor system which locally drives the $\ell = 2$ feedback windings to stabilize the long wavelength, m=1 instability.[3] An additional programmable force system using an additional set of $\ell = 2$ windings is incorporated to allow for optimization of the equilibrium.

II. SECTOR END EFFECTS. Since the plasma behavior in the end regions of the sector is characterized by large displacements and accelerations, confinement time limitation due to the propagation of m=1 waves from the end regions to the center of the system has been investigated.[4] The calculated trajectory of the plasma column has been compared to the measured change in column trajectory at several positions along the sector when a step function force is applied to wavelength 10. The measured and calculated trajectory at the location of position detector No. 3 are shown in Fig. 2, and illustrate that the propagation of gross-column motion disturbances is at approximately the Alfvén velocity in agreement with the sharp boundary theory.

III. EQUILIBRIUM STUDIES. Analysis of column trajectories in the plane of the torus has indicated the need for a time-programmed force, in addition to the feedback force, to counteract an equilibrium force imbalance. Factors which influence the observed equilibrium force imbalance are (a) transients in the toroidal equilibrium force, $F_{1,0}$, due to $\ell = 0$ shape oscillations of the plasma column,[5] (b) the diffuse radial profile of the experiment which reduces the $F_{1,0}$ force from the sharp boundary design value, [6] (c) sector end effects propagating into the center of the system, and (d) decreases of β due to, for example, loss of particles from radial diffusion which, for the T_e = 100-eV Scyllac plasma, can cause a 10% drop in β in 11 μs based on classical effects alone.

The programmed equilibrium compensation force is generated with a Weibel-Jones-type circuit driving $\ell = 2$ trimming coils wound on top of the $\ell = 2$ feedback coils. Plasma trajectories and $\ell = 2$ trimming fields for two discharges are shown in Fig. 3. A small change in the amplitude of the trimming force is observed to drastically alter the trajectory. The relationship between the applied force and the observed motion can be interpreted using sharp boundary theory in terms of an effective plasma β, which is ~ 1/2 of the β on axis determined from the plasma diamagnetism and luminosity profile. This can at least partly be attributed to diffuse profile effects.

IV. FEEDBACK STABILIZATION RESULTS. The feedback system for stabilization of the m=1 long wavelength has been operated with the plasma column held near its equilibrium position by the trimming system. An improvement in confinement time to 40-50 μs is shown in the streak photograph of Fig. 4, where the column is observed to remain centered in the discharge tube for many instability growth times with feedback stabilization applied. The feedback system can generate forces on the order of 0.2 of the toroidal equilibrium force and has a risetime of 0.4 times the instability growth time. The feedback system is arranged in 5 independent arrays along the length of the 13 wavelength, 120° sector for each of the orthogonal transverse coordinates.

V. $\ell = 1,2$ CONFIGURATION. The Scyllac feedback sector has been converted to an $\ell = 1,2$ equilibrium configuration to eliminate transient effects on the toroidal force balance due to the $\ell = 0$ field and provide a less β-dependent equilibrium. The helical shape of the plasma column has been increased to a helical radius of ~ 3.0 cm to minimize the growth rate of the m=1 instability and increase the effectiveness of the feedback stabilization. The sector has been lengthened by 40% to an arc length of 168° to increase the time before end effects influence the plasma behavior. The feedback system for the $\ell = 1,2$ sector includes the capability of driving each wavelength with an individual signal which represents the sum of the required feedback forces at that location for all unstable modes.

REFERENCES

[1] E. L. Cantrell, et. al., Seventh European Conference on Controlled Fusion and Plasma Physics (1975, Vol. 1, p. 48.

[2] E. Funfer, M. Kaufmann, J. Neuhauser, G. Schramm, Seventh European Conf. on Controlled Fusion and Plasma Physics, Vol. II, p. 151.

[3] F. L. Ribe and M. N. Rosenbluth, Phys. Fluids 13, 2572 (1970).

[4] E. L. Cantrell, et. al, submitted to Nuclear Fusion.

[5] G. Miller, to be published, Physics of Fluids.

[6] D. C. Barnes and J. U. Brackbill, to be published, Nuclear Science and Engineering.

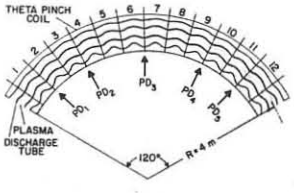

FIGURE 1 – LAYOUT OF THE ℓ=1.0 SCYLLAC FEEDBACK SECTOR

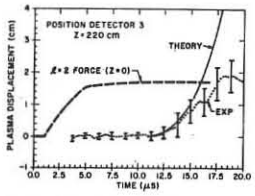

FIGURE 2 – THE PLASMA COLUMN TRAJECTORY CHANGE DUE TO A STEP FUNCTION ℓ=2 FORCE APPLIED 220cm FROM THE DETECTOR

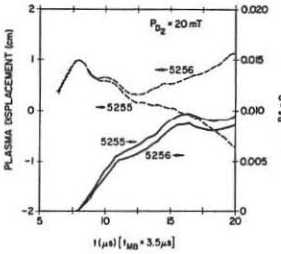

FIGURE 3 – PLASMA DISPLACEMENT VERSES TIME FOR TWO DIFFERENT AMPLITUDES FOR THE ℓ=2 EQUILIBRIUM CORRECTION FIELD

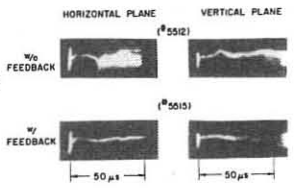

FIGURE 4 – STREAK PHOTOGRAPHS WITH AND WITHOUT ℓ=2 FEEDBACK STABILIZATION

Anomalous Transport in Shock Produced Plasmas

R. Chodura, C.T. Dum [+], F. Söldner, K.-H. Steuer
Max-Planck-Institut für Plasmaphysik, 8046 Garching, Fed.Rep.Ger.
EURATOM Association

Abstract: Fast shock heating in a toroidal belt-pinch produces a highly elongated, weakly compressed high-ß plasma with electron and ion temperatures in the keV range. Electron heating is attributed to ion sound turbulence. The effective drift velocity for wave growth is increased due to distortion of the electron distribution by strong density and temperature gradients. The measured temperature-, density - and magnetic field profiles are in good agreement with numerical results of a fluid-particle hybrid code which includes the gradient effects and the influence of the neutral background gas.

In this paper we report on fast shock heating of a low density toroidal plasma to keV electron and ion temperatures. The electrons are heated by ion sound turbulence. We show that the distortion of the electron distribution function by density and temperature gradients significantly changes the anomalous resistivity and heat conduction. The gradient effects as well as the influence of neutral particles are included in a hybrid code which, then, fits rather well the experimental results. The experiments were performed in the Garching High-Voltage Belt-Pinch /1/ which is a shock heated high-ß tokamak with highly elongated cross-section. The shock compression has been investigated in detail for two cases with initial densities of $n_{eo} = 3 \cdot 10^{13}$ cm^{-3} and $n_{eo} = 7 \cdot 10^{13}$ cm^{-3}, respectively. The magnetic field penetrates the entire plasma at the lower density and an average ß-value of 0.4 is obtained after compression. The electron temperature rises up to 1 keV with the incoming magnetic field. In the sheath region the electrons are heated to 3 keV. At the higher initial density the radial motion of the magnetic piston is slowed down by the pressure of the compressed plasma and a central ß = 1 plasma is formed. While the electron temperature stays low in the central ß = 1 - plasma ($T_e \lesssim$ 50 eV), strong electron heating is observed in the piston region with temperatures up to 1 keV. In both cases, steep electron temperature gradients are retained after implosion.

Electron heating and magnetic field penetration cannot be explained by Coulomb collisions. There are a number of observations from which we conclude that ion sound turbulence should dominate the implosion phase /2/. The electron temperature is large compared to the ion bulk temperature. The ion distribution develops a weak tail which results in a critical drift velocity for ion sound of typically $v_{crit} \approx 2.5\,(T_e/m_i)^{1/2}$. For ion sound the electron distribution is expected to relax from an initial Maxwellian to a flat topped distribution /3/. This fact and the distortion of the distribution function by gradients in temperature and density are of crucial importance for wave excitation and anomalous transport. For this distorted function the effective drift velocity $v_{d,eff}$ for wave growth and momentum transfer $R_e = -n_e m_e \nu_{eff} v_{d,eff}$ differs very substantially from the relative electron-ion drift $v_{d,i}$, as seen from Figs. 1, 2.

$$\underline{v}_{d,eff} = (\underline{\underline{I}} - \underline{\underline{\varrho}}\underline{\underline{u}}) \cdot \underline{v}_{d,i} - \underline{\underline{\varrho}}_{T_e} \cdot \underline{\nabla} T_e - \underline{\underline{\varrho}}_{n_e} \cdot \underline{\nabla} n_e ,$$

where $\underline{v}_{\nabla n_e}(\nabla T_e) = v_{th,e}^2 / \nu_{eff}\, \underline{B}/|\underline{B}| \times \underline{\nabla} \ln n_e(T_e)$, $v_{th,e} = (T_e/m_e)^{1/2}$ and the $\underline{\underline{\varrho}}$'s are transport coefficients dependent on ν_{eff}/Ω_e (Ω_e = electron gyro-frequency) and the shape of the energy distribution. In fact, only the gradient related terms make instability over the entire piston region possible, especially for higher initial density (Fig. 2).

Since R_e enters also magnetic field penetration and electron heating rate ($R_e v_{d,i}$) they are also modified correspondingly. The heat flux for the self-consistent distribution is related, in a similar manner as R_e, to the drift and the gradients of temperature and density. It should be mentioned that the anomalous transport theory for ion sound /4/ also explains the reduction of axial heat flow /5/ and the rotation of the spectrum with respect to $v_{d,i}$ observed in linear devices. Classical transport dominates in front of the piston and anomalous transport in the unstable sheath region where $\nu_{eff}/\Omega_e = 0$ (1). It is not possible to simply add anomalous and classical transport.

An earlier fluid-particle hybrid code /6/ has been modified therefore to provide a transition between classical and anomalous transport which depends on the local ratio $v_{d,eff}/v_{crit}$. The total effective collision frequency for all transport effects e.g. takes the form

$$\nu_{eff} = \nu_{cl} + \nu_{an} \left(1 - e^{-(v_{d,eff}/v_{crit})^2}\right)$$

where $\nu_{an} = 10^{-2}\,\omega_{pe}$ from simulation results /7/. A similar transition is carried out for transport coefficients in momentum transfer and heat flux. The switch on/off condition for anomalous transport may be justified by the fact that the growth time of the instability is short compared to the particle transit time t_t through the turbulent piston region $\gamma t_t \approx 15$. Furthermore, the code has been extended to include the effects of ionization, multiple charge exchange and neutral particle diffusion. The neutral hydrogen atoms at rest are treated as a fluid and the fast charge exchange neutrals are treated as particles in the same manner as the ions.

The dynamics of the piston is slowed down and damped considerably due to the interaction between plasma and neutrals. The compression sheath is broadened and agrees much better with experimental findings. The most sensitive feature is the electron temperature profile, as seen in Fig. 3. The enhanced electron density due to ionization and the larger density gradient reduce the effective drift $v_{d,eff}$ in the front region of the piston resulting in a smaller collision frequency thereby lowering the electron temperature due to reduced heating and radial heat conduction in that region.

Conclusion: An analysis of shock experiments and comparison with theory of ion sound turbulence show that the effective drift velocity for wave growth differs substantially from the relative electron-ion drift due to distortion of the electron distribution by density and temperature gradients. Simulation calculations with a fluid-particle hybrid code including anomalous heating and transport and the interaction between plasma and neutral hydrogen background show good agreement with the experimental results.

References:

/1/ Söldner, F., K.-H. Steuer, 6th IAEA Conf. on Plasma Physics and Contr. Nucl. Fusion Res., Berchtesgaden, CN 35/E 13-2 (1976)
/2/ Söldner, F., C.T. Dum, K.-H. Steuer, submitted to Phys. Rev. Lett.
/3/ Dum, C.T., IPP Report 6/153, submitted to Phys. Fluids
/4/ Dum, C.T., IPP Report 6/154, submitted to Phys. Fluids
/5/ Chodura, R., C.T. Dum, M. Keilhacker, M. Kornherr, H. Niedermeyer, R. Protz, F. Söldner, K.-H. Steuer, 5th IAEA Conf. on Plasma Physics and Contr. Nucl. Fusion Res., Tokyo, Vol. III, 397 (1974)
/6/ Chodura, R., Nucl. Fusion 15, 55 (1975)
/7/ Dum, C.T., R. Chodura, D. Biskamp, Phys. Rev. Let. 32, 1231 (1974)

[+] C.T. Dum, Max-Planck-Institut für Physik und Astrophysik, Institut für Extraterrestrische Physik, 8046 Garching

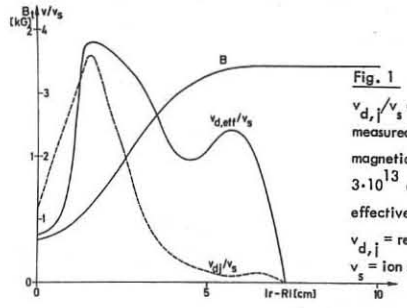

Fig. 1 Radial profiles of $v_{d,eff}/v_s$, $v_{d,i}/v_s$ and magnetic field B from measured density, temperature and magnetic field profiles for $n_{eo} = 3 \cdot 10^{13}$ cm^{-3} at t = 0.3 µs. $v_{d,eff}$ = effective drift for wave growth, $v_{d,i}$ = relative electron-ion drift, v_s = ion sound velocity

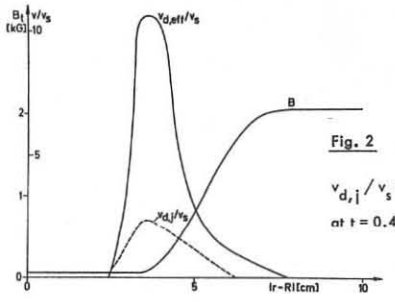

Fig. 2 Radial profiles of $v_{d,eff}/v_s$ $v_{d,i}/v_s$ and B for $n_{eo} = 7 \cdot 10^{13}$ cm^{-3} at t = 0.4 µs.

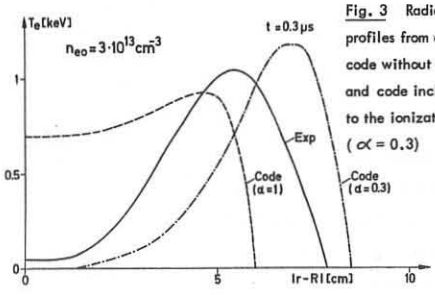

Fig. 3 Radial electron temperature profiles from experiment (solid curve), code without neutral background ($\alpha = 1$) and code including neutrals according to the ionization degree in the experiment ($\alpha = 0.3$)

SECTOR EXPERIMENT OF THETA-PINCH PLASMA IN MODIFIED BUMPY TORUS

Y.Osanai, K.Saito, Y.Nogi, H.Gesso, G.Todoroki, S.Shiina
H.yoshimura.

Department of Physics and Atomic Energy Research Institute,
College of Science and Technology, Nihon University,
Kanda-surugadai, Chiyodaku, Tokyo, Japan.

Abstract: In Modified Bumpy Torus, the toroidal equilibrium is achieved with main surface distortion of ℓ=±1 magnetic fields. The results of 1/4 sector experiment show the confined plasma is in stable equilibrium at 3 mtorr filling pressure and unstable weakly to m=2 like-mode at 10 mtorr filling pressure.

Introduction: The asymmetric toroidal equilibrium of high-beta plasma has been achieved in Scyllac and High Beta Stellarator with main surface distortion of ℓ=1 helical field[1,2]. The confinement time of highly compressed plasma is limited by m=1 mode instability. To confine a more stable plasma, we had propossed a new type of magnetic configuration with the main surface distortion of ℓ=±1 magnetic fields, which has no rotational transform and different from M&S configuration with the main surface distortion of ℓ=0 bumpy field. In order to examine the existence of M.B.T. equilibrium, the 1/4 sector experiment was carried out,following the experiment in linear geometry[3,4,5]. The preliminary results showed the plasma was in stable equilibrium[6]. Here are reported the more detailed experimental results and discussed comparing with theoretical predictions[7].

Experimental Arrangement: The schematic arrangement of 1/4 sector experiment is shown in Fig. 1. The device parameters reported here are listed in Table 1. The magnetic field distortions of ℓ=±1, ±2, etc. fields are induced by means of inserting a gaped copper shell, which modifies the ℓ=0(bumpy) field produced by the z-dependent, periodical theta current fed to compression coil. The induced field distortions depend on gaped angle θ_0, shell radius r_s, periodic length L and mirror ratio R_m(on coil axis without a gaped shell). The value of gaped angle, $\theta_0=120^0$ gives a relatively large surface distortion of ℓ=±2 fields.

Fig. 1 Schematics of 1/4 M.B.T. sector device.

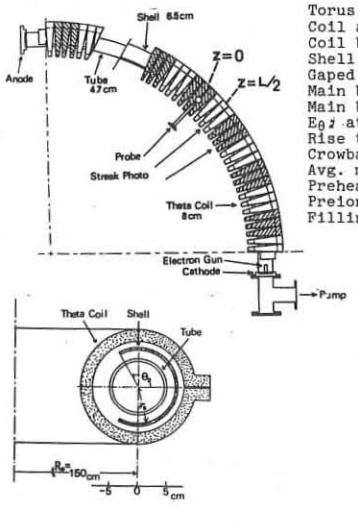

Table 1 Device parameters

Torus major radius(R_0)	150 cm
Coil arc length	230 cm
Coil bore radius	8 cm
Shell radius(r_s)	6.5 cm
Gaped angle of shell(θ_0)	120°
Main bank voltage	35 kV
Main bank capacitance	37.5 μF
E_θ at 4.5 cm	98V/cm
Rise time of mag. field	2.2 μs
Crowbar decay time(L/R)	25 μs
Avg. mag. field	6 kG
Preheating(z-type)	20 kV
Preionization(Electron Gun)	15 kV
Filling pressure(H_2)	50~3 mt

Experimental Results: Streak photographs taken through horizontal(top view) and vertical(side view) slits showed the plasma behavors depend on initial filling pressure.

At 3 mtorr filling pressure, the confined plasma was in stable equilibrium. The m=1 mode instability was not observed during the confined stage. The equilibrium positions of plasma column were nearly constant with time, kept to be 1 cm outer-side off coil axis at z=0 plane (convex region of field lines) and 0.6 cm inner-side at z=L/2 plane (concave region of field lines). Photographs indicate also a large ellipticity of plasma column cross section. To compare with these experimental results, the constant surface of $\int \frac{dl}{B}$ (integral of magnetic specific volume along field line) was numerically calculated under the assumption of near-axis and low-β approximations($2\pi r/L \sim [r/R_0]^{\frac{1}{2}} \sim \beta^{\frac{1}{2}}$), as shown in Fig.2. The numerical results are qualitatively consistent with the experimental results, although the plasma column shifts as a whole to more outer-side than observed equilibrium positions at any z-plane. The quantitative deviation can not yet be sufficiently explained, maybe as a high beta effects. However it is remained as problem to resolve experimentally and theoretically.

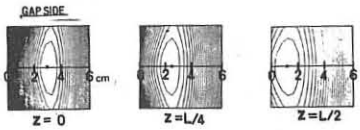

Fig.2 The constant surface of $\int dl/B$ at each z-plane. r=0 is position of coil axis, r>0 outer-side.

At 10 mtorr filling pressure, streak photographs showed the plasma split into two parts and contact weakly with tube wall. Fig.3 shows the radial profiles of the diamagnetic signal in horizontal plane, measured with method of cancelling the signals of internal and external magnetic probes. It is found that a m=2 like-mode instability occurs and then the plasma contacts weakly with the outer-side of tube wall. Furthermore,the decay rate of diamagnetic signals is larger at z=0 plane than at z=L/2 plane. This fact indicates an axial plasma dynamics so that the plasma contracts to z=L/2 plane from z=0 plane.

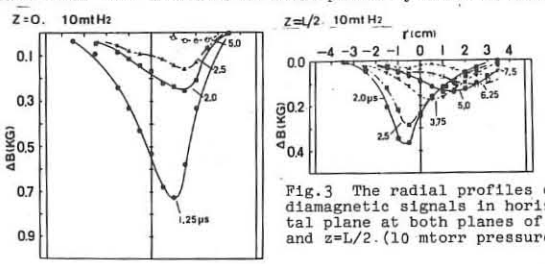

Fig.3 The radial profiles of diamagnetic signals in horizontal plane at both planes of z=0 and z=L/2.(10 mtorr pressure).

Discussion: The total temperature of confined hydrogen plasma is of 30-50 ev depending on initial filling pressure, determined from the simple toroidal drift observed. The maximum value of β, ratio of plasma pressure to magnetic pressure, is of 0.2 from diamagnetic measurment. The Alfven wave velocity is of 2.5 x 10^7 cm/sec in maximum. The small surface distortion($\delta_\ell \ll 1$) model predicts a growth time of 2~3 μsec against m=1 mode instability for sharp boundary plasma. Therfore, the observed stable plasma may result from some stabilizing effects as end effect, axial plasma dynamics and finite surface distortions.

REFERENCES

(1) R.R.Bartsch, F.L.Ribe, etal., Sixth IAEA Conf. on Plasma Physics and Contr. Fusion Research(Berchtesgaden, 1976), CN-35/E-10.
(2) E.Funfer, M.Kaufmann, J.Nëühauser, G.schramm, 7th Europ. Conf. on Contr. Fusion and Plasma Physics(Lausanne, 1976), vol 11, p.151.
(3) T.Itagaki, S.Shiina, etal., 5th IAEA Conf. on Plasma Phys. and Contr. Fusion Research(Tokyo, 1974),CN-33/E7-3.
(4) S.Shiina, etal., 7th Europ. Conf. on Contr. Fusion and Plasma Physics(Lausanne, 1976), vol 1, p.52.
(5) S.Shiina. etal., 3rd Pulsed High Beta Plasmas(Culham, 1976), p.147.
(6) J.Todoroki, S.shiina, Sixth IAEA Conf. on Plasma Physics and Contr. Fusion Research(Berchtesgaden, 1976),CN-35/E-12
(7) J.Todoroki, Plasma Physics, vol.18, p.137, 1976.

Pulsed Fusion Reactor with Evaporating Wall

Tetsu Miyamoto

Department of Physics, College of Science and Technology,
Nihon University, Kanda-Surugadai, Chiyoda-ku,Tokyo,Japan

Abstract: An evaporating wall is proposed in order to abate the radiation damage of a first wall in a pulsed fusion reactor. The evaporated gas can compress and heat the plasma.

General Concept of Evaporating Wall: In the common conceptual design of a fusion reactor, the first wall receives intensive radiations directly. It is well known that the irradiation of the fast neutrons is severe for the wall. This is even more serious for the pulsed fusion reactor. In the present paper we propose the evaporating wall of the following roles in order to solve this problem and to give a prospect for the pinch fusion reactor.

(1) The evaporating wall protects a vacuum wall in terms of slowing down the fast neutrons and absorbing them.

(2) The wall material evaporates to produce the high temperature and high pressure gas which expands inwardly and compresses the confinement magnetic field and the plasma.

(3) The resultant gas and the residual wall further absorb the fusion power and transport the energy to a heat engine.

Conditions for Evaporation: The wall materials must naturally be a good moderator of neutrons. Table 1 shows properties of few good moderators. It is necessary for slowing down neutrons that the ice wall is only about 10 cm in thickness.

In order that the wall evaporates and the evaporated gas can compress the plasma, the neutron energy emitted from the reactor $P_n t$ must be larger than the heat energy required for the evaporation of the wall material. We assume that the wall material evaporates instantaneously after it reaches the critical state at time t_e(see Fig.1). Then we have

$$P_n t_e \cdot V_{pi} \cdot \xi\Sigma_s \Delta r \gtrsim 4.2\cdot 10^6 \,(854 - T_{gi}) \cdot S_{gi} \Delta r$$

where T_{gi}(°K) and S_{gi} are the initial temperature and the area of the inner surface of the wall. Hereafter, we consider the axially symmetric configuration of infinite length. Then the inequality gives

$$n_{Ti} n_{Di} t_e \gtrsim 8.9\ 10^{41}\ r_{gi}/r_{pi}^2 \quad \text{for the DT reaction, } D_2O \text{ ice and } T_{pi} = 10 \text{ keV}$$

$$n_{Di}^2 t_e \gtrsim 1.5\ 10^{43}\ r_{gi}/r_{pi}^2 \quad \text{for the DD reaction, } H_2O \text{ ice and } T_{pi} = 50 \text{ keV}$$

for T_{gi} = 173 °K. The condition for the DD reaction is very severe. In the following, however, we assume the instantaneous evaporation. Because it seems to be possible to evaporate the wall by alternative methods.

Moderator		H_2O	D_2O
Macro scattering cross section	$\Sigma_s(m^{-1})$	90	43
Macro absorption cross section	$\Sigma_a(m^{-1})$	2.2	0.009
Energy logarithm	ξ	0.92	0.57
Slowing down power	$\xi\Sigma_s$	135	26
Fermi age	τ (m^2)	0.003	0.012
Diffusion length	l_d (m)	0.029	1.0
Migration length	l_m (m)	0.064	1.01
Slowing down time	$t_s(\mu s)$	6.8	35
Diffusion time	t_d(ms)	0.21	53

Table 1

r_o (m)	2.0	
r_{gi} (m)	1.8	
r_{pi} (m)	1.3	
$n_{pi}(m^{-1})$	10^{22}	$5\cdot10^{22}$
T_{pi} (K)	10^8	10^8
t_e (ms)	9.5	0.38
r_{pl} (m)	0.76	0.41
$n_{pl}(m^{-3})$	$3\cdot10^{22}$	$5\cdot10^{23}$
T_{pl} (K)	$3\cdot10^8$	10^9
τ (ms)	8.1	4.3

Table 2

Free Expansion Process: The inner surface of vapor implodes to the axis with the thermal speed from time t_e till it becomes conductive in terms of the irradiation, the surface discharge and Joule heating by the induced electric field (several kV/m), and so on. We distinguish the gas and plasma quantities by the suffixes g and p, and also add the suffix α to quantities at time $t = t_\alpha$. Then we can obtain

$$T_{gc} = T_{ge}(1 + 3\pi^{1/2} q\ (r_{ge} - r_{gc})/c_s^3)^{2/3}$$

$$p_{gc} = (N_g k T_{ge}/V_{ge})(1 + 3\pi^{1/2} q\ (r_{ge} - r_{gc})/c_s^3)^{2/3}$$

at the end of the free expansion process ($r_g = r_{gc}$ and $t \fallingdotseq t_c$), where $q = P_n/m_g N_g$, $c_s = 2kT_{ge}/m_g$, and m_g and N_g are the mass of imploding gas molecular or atom and the number density of gas.

Compression Process: If the plasma pressure p_{pc} is less than the gas pressure p_{gc}, the plasma is compressed after $t \gtrsim t_c$. In the simplified case that the magnetic field freezes to the plasma and the inner surface of gas, and that the production and conduction of heat can be neglected, we can obtain the compression ratio of plasma.

$$v_p = V_p/V_{pc} = (1/2)((v_{p1} + v_{p2}) + (v_{p2} - v_{p1})\ \sin(\omega(t - t_c) - \phi))$$

where v_{p1} and v_{p2} are the ratio for the minimum and maximum volume. When $p_{pc}/p_{gc} \ll 1$, they are given by

$$v_{p1} \sim (2/3)(1 - V_{gc}/V_o)(1 - (V_{gc}/V_o)^{2/3})^{-1}(V_o/V_{gc})(p_{pc}/p_{gc})$$

$$v_{p2} \sim (3/2)((V_o/V_{gc})^{2/3} - 1)(1 - V_{gc}/V_o)^{-1}$$

The angular frequency ω, the period τ and the phase angle φ are

$$\omega^2 = (12\pi/M_g)(V_{gc}/V_o)^{5/3} p_{gc}\ , \qquad \tau = 2\pi/\omega$$

$$\phi = \arcsin((v_{p1} + v_{p2} - 2)/(v_{p2} - v_{p1}))$$

For simplicity, we put γ = 2 for the plasma in the avove treatment. Using these results we have

$$p_p/p_{pc} = v_p^{-2}\ , \quad T_p/T_{pc} = v_p^{-1} \quad \text{and} \quad V_m/V_{mc} = B_c/B = v_p$$

The plasma is finally quenched by the vapor. Table 2 shows the estimations for the DT reactor and the D_2O ice.

Concluding Remarks: The evaporating wall can be applied only to the pulsed reactor in principle and give a new prospect. It however, seems that an alternative evaporator of the wall is requires for the DD reactor. We can point out a laser fusion as an example of appropriate evaporators. The break-even energy balance is not required for this laser fusion, but the neutron flux of $> 2\cdot10^7\ S_{gi}$ joule will be required.

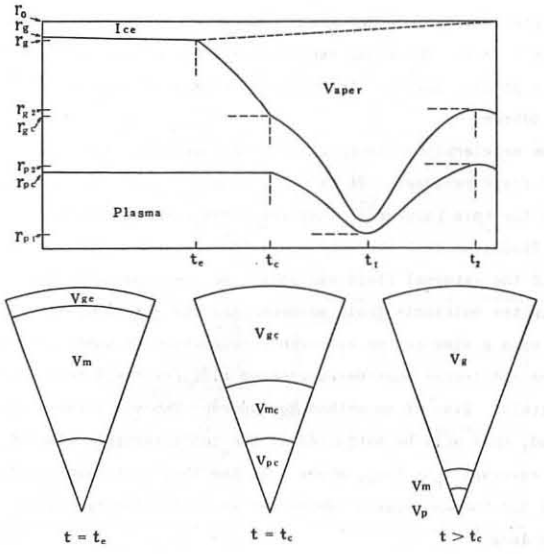

Fig. 1

Possibility of Astron-like Theta Pinch

Tetsu Miyamoto

Department of Physics, College of Science and Technology,
Nihon University, Kanda-Surugadai, Chiyoda-ku, Tokyo, Japan

Abstract: It is discussed to produced the Astron-like configuration in terms of a theta pinch with a multipole field.

Introduction: The reversed field configurations appears at a theta pinch. They are magnetohydrodynamically unstable. In the low initial pressure regime the reversed field also vanishes fastly due to micro-instabilities. Therefore, they have not been noticed with a view to confining plasma. They can, However, be produced easily in the linear machine and suppress the end losses. They are same magnetic field configuration with the Astron,[1] in which the reversed field is produced by the relativistic E-layer. On the other hand it is produced by the diamagnetic current consisted mainly of the non-relativistic electrons in the theta pinch. If the relativistic electron components can be produced in the theta pinch, the stability of its reversed field configuration will be improved. So far the high energy electron components have been observed in the low pressure regime of theta pinch.[2,3] It is the purposes of this paper to study whether the Astron-like configuration can produced by the theta pinch, and to propose the theta pinch with a multipole field as one of the methods.

Requirements for Astron-like Theta Pinch: It is necessary to accelerate electrons to a relativistic energy at any phase of the theta pinch in order to realize the Astron configuration. It will be the initial phase where the field varys rapidly. However, the field is reversed at this phase, so that the plasma expands outwardly and is pushed to the wall. Thus, it is necessary to satisfy the following requirements.

(1) The plasma (or a part of it) must not be dissipative but reactive at the accelerating phase and region. It means there

$$\delta_a \sim \delta_{cl} >> \delta_r \quad \text{or} \quad n \sim 2.7\times10^{13}\delta_a^{-2} \text{ and } \omega >> \gamma$$

where δ_a, δ_{cl}, δ_r, ω and γ are the characteristic width of accelerating region, the collisionless skin depth, the resistive skin depth, the characteristic angular frequency of pinch field and a growth rate of current driven instabilities, respectively. It is possible by increasing the initial plasma temperature to satisfy $\omega >> \gamma$. The above density seems to be very severe for a theta pinch. However, it will not be impossible in the following scheme.

(2) The accelerating electrons must be confined during the period of field reversal. It is promissing to apply the multipole fields for this purpose.[4] They are independent of the theta pinch field, so that they can exert the pressure on the plasma, even if the external field vanishes. We are especially interested in the multipole field accompanying the azimuthal closed field with a view to the electron acceleration as shown in Fig.1.

(3) The end losses must be suppressed till the field reverses completely. Even if no method to suppress the end losses is applied, this will be satisfied if the characteristic time of field reversal $t_r << L/v_{th}$ where L is the length of system and v_{th} is the thermal speed. Hereafter we assume the system is enough long.

Theta Pinch with Multipole Field: Let us consider the theta pinch superposed by the multipole field of Fig.1. We assumed that the high temperature plasma is produced in the interior of the inner multipole rods at the initial phase by any method. Then we can expect the followings: (i) The density is enough lower in the exterior of the inner rods than in the interior, and the plasma is low β in the exterior. (ii) The high temperature plasma is confined in the interior of the closed azimuthal field line during the phase of field reversal. (iii) The field changes mainly in the region between two sets of current rods during that phase. (iv) The betatron condition are satisfied at some place, and the electrons run away along the azimuthal field in other region, too. (v) When the external field increases sufficiently, the accelerating electrons are pushed into the interior region in terms of the similar process with the retarded theta pinch.[5] Each rod current must be enough large to be able to recoil the accelerating electrons from its neighbor. If these expectation are satisfied, the theta pinch superposed by the multipole field as Fig.1 can be one of the methods to realize the Astron-like configuration.

Schmatical Model for Fusion Reactor: It may be claimed that the use of such inner conductor is inadequate to the fusion reactor. However, we notice that the reactor concept of Fig.2 is also possible. The evaporating wall will be useful at the burning region.

References: (1) N.C.Christfilos : Proc. Second U.N.International Conf. on Peaceful Use of Atomic Energy, Geneve 32 (1958) 279 ; (2) K.Sato et al : J.Phys. Soc. Japan 19 (1964) 1244 ; (3) K.Sato et al : Kakuyugo Kenkyu (in Japanise) 21 (1968) 121 ; (4) Y.Nogi and T.Miyamoto : J. Phys. Soc. Japan 34 (1973) 1059 ; (5) and (6) T.Miyamoto : To be presented in this conf.

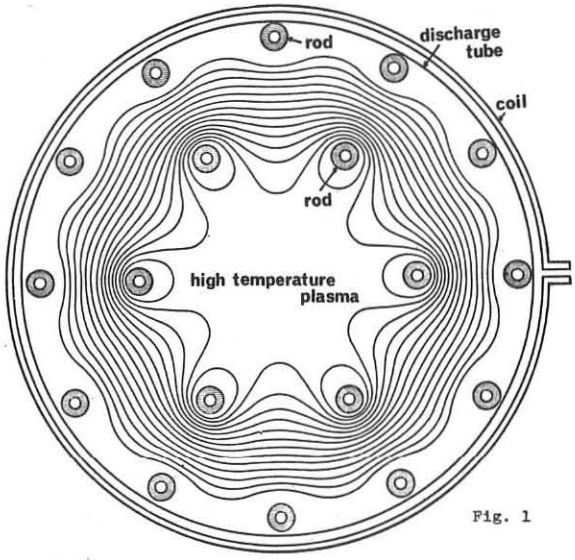

Fig. 1

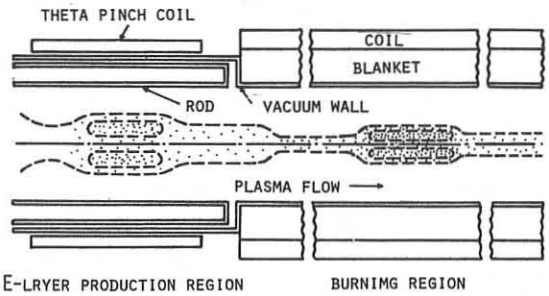

Fig. 2

Retarded Theta Pinch

Tetsu Miyamoto

Department of Physics, College of Science and Technology,
Nihon University, Kanda-Surugadai, Chiyoda-ku, Tokyo, Japan

Abstract: It is proposed and studied to retard the implosion of a theta pinch in order to increase the energy coupling between the plasma and the coil.

Introduction: The fast theta pinch is a powerful method to produce a fusion plasma. The technical difficulties, however, increase in order to obtain the large amount of a high temperature and high density plasma. The energy coupling between the coil and the plasma (or the mutual inductance) decreases with the implosion of plasma. In order to strengthen the energy coupling, we must retard the implosion of the plasma (or the current layer) till the magnetic field increases to enough large value. The retardation of implosion happens naturally in some theta pinches. A fast theta pinch and a reversed field configuration are the examples. In the former the magnetic field increases to a large value before the implosion finishes. On the other hand the implosion is not retarded by decreasing the initial pressure, though the high temperature plasma can be produced. There are several limitations in these natural retardations. For example, the reversed field is mainly dissipated by the electron heating and triggers instabilities. The theta pinch, in which the implosion is artificially retarded, is also possible. We call it "the retarded theta pinch". The staged theta pinch is a sort of retarded theta pinch.[1] In this paper we propose the retarded theta pinch by the multipole field.

Retardation of Implosion by Inner Multipole Field: Let us consider the multipole field produced by two sets of longitudinal current rods arranged on the cylindrical surfaces, as shown in Fig.1. It is independent of the theta pinch field, and exerts the average radial pressure on the plasma layer[2]. Figure 2 shows schematically the whole processes presumed in the theta pinch with the multipole field. The plasma will be produced between two sets of rods at first. The inner set of current rods enclosed by the plasma layer can produce the average outward pressure which supports the inward pressure of pinch field and interrupts the implosion of plasma. When the number of rods 2N is enough large, this pressure can be approximated by

$$P_{mult} \approx \mu_o (IN/\pi r_p)^2 \, (r_m/r_p)^{2N-1}$$

When the pinch field increases and the inner set of the rods can not support its pressure, the plasma collapses to the axis through the separations of rods. In other words, the collapse happens when the impedance along the azimuthal current path becomes larger in the path enclosing the inner rods than in the unenclosed one. The common theta pinch starts after the current path changes.

When the current of each rod flows to the opposite direction as shown in Fig.1 alternatively, the multipole field has the tendency to interrupt the electrical break-down. The retardation time is not only limited by the outward pressure of the rods, but also by the cusp losses. When the current flows to the same for all rods, the closed azimuthal field appears outsides of the inner multipole rods and the break-down become easy, but the outward pressure becomes weak. It will be useful to choose the appropriate combination of rod currents.

Simple Analysis of Retarded Theta Pinch: We are not interested in the detailed processes but in the total energy which the plasma can obtain finally. Therefore, we consider only the difference between the initial and the final states under the following assumptions. (1) The plasma is perfectly conductive, cylindrically symmetric and infinite in length. (2) The initial plasma energy is negligibly small. (3) The external flux increases to maximum value before the start of implosion, but is constant during and after the implosion phase. (4) The plasam is sustained initially at a radius r_{pi} by some forces and results to an equilibrium radius r_{pf} finally after the forces vanish instantaneously. We distinguish the quantities in the initial and the final states by the suffixes i and f. We have the final plasma radius from the conservation of total energy anf the pressure balance.

$$\xi_f^2 = 1 - \xi_i (1 - \xi_i^2)^{1/2} \cdot (\xi_i^2 + b_i^2 (1 - \xi_i^2))^{1/2}$$

where $\xi = r_p/r_c$ and b_i = (the flux trapped in the plasma)/(the external flux). The ratio of the final plasma energy $W_{pf} = W_{mi} - W_{mf}$ to the initial magnetic energy W_{mi} is given by

$$W_{pf}/W_{mi} = (\xi_f^4 - b_i^2 (1 - \xi_f^2)^2)/\xi_f^2$$

Both quantities are displayed as a function of ξ_i and b_i in fig. 3 and 4. The results show that a few×10 percent of total magnetic energy can be transformed to the plasma energy under suitable parameters, not taking Joule heating into considerations.

References:

(1) J.P.Freidberg et al.: Symp. Tech. of Controlled Thermonuclear Fusion Experiment and Engineering Aspects of Fusion Reactors, Austin, Texas, Nov. 20-22, 1972.

(2) T.Miyamoto et al.: Phys. Soc. Japan 30(1971) 591; Y.Nogi et al.: ibid 34 (1973) 1059

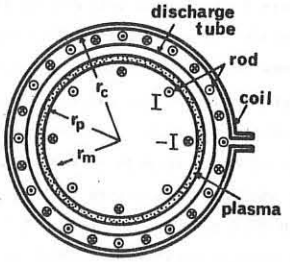

Fig. 1

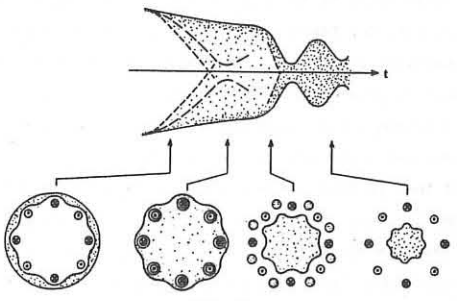

Fig. 2

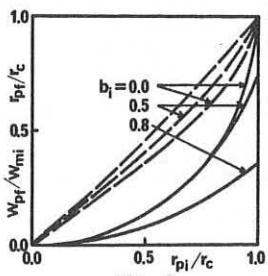

Fig. 3

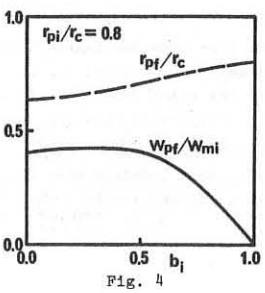

Fig. 4

STABILIZATION OF DRIFT-CYCLOTRON LOSS CONE INSTABILITY IN THE TRAP WITH AMBIPOLAR MIRRORS

A.A.Ivanov, G.V.Roslyakov

Institute of Nuclear Physics

630090, Novosibirsk-90, USSR

Abstract. It is shown here that the contact between cold and hot "cone" plasmas leads to normal mode of the system with the wave length along the magnetic field of the same order as the hot plasma length. If this length is small enough ($L \lesssim R_p$), the plasma density gradient becomes unimportant and instability turns into the high-frequency convective "loss-cone" mode.

One can hope to get great values of $Q \approx 10 \div 10^2$ in open trap with ambipolar mirrors proposed by G.I.Dimov /1/ in the absence of instabilities. However, the elementary components of such a device are two extreme mirror traps containing plasma with ion velocity distribution of "loss-cone" type and the question arises whether plasma will be stable. One of the most dangerous instability in mirror trap is the drift-cyclotron loss cone instability (DCLC) /2/ . For driving of this instability sufficiently small density gradient is needed. The presence and possibility of damping DCLC were demonstrated in experiments on open trap 2XIIB /3/ when a hot confined plasma with $T_i \approx 10$ keV contacted with a cold plasma ($T_i \approx 10$ eV) if the density of cold plasma was the same order of magnitude as a hot plasma density. In these experiments the confinement time of a mirror-confined plasma has been greatly increased. This method of stabilizing DCLC instability can result in great energy losses in usual mirror machine. On the other hand, in the case of a device with ambipolar mirrors the contact of warm "Maxwellian" plasma confined in the central trap (the plasma produces the main part of thermonuclear power) with "cone" hot plasma in extreme traps is an integral part of the experimental scheme. The present explanation of stabilization DCLC mechanism in 2XIIB experiments /3/ is connected with penetration of small amounts of cold ions in the traps and based on the stabilization method by partial filling of the loss cone with cold plasma proposed in /4/ . It must be mentioned that the density gradient in 2XIIB device is high enough and in accordance with analysis /6/ the drift-cyclotron instability /5/ must occur even for Maxwellian ion velocity distribution.

In present paper the attempt is made to explain stabilization DCLC in presence of the contact of hot "cone" plasma with cold plasma without assumption that some amounts of cold plasma penetrate into a hot one. Stabilization is due to the fac t that in such systems unstable flute-type drift wave ($k_\parallel = 0$) cannot exist. The presence of longitudinal wave number ($k_\parallel \neq 0$) leads to convection of the perturbation along the magnetic field lines. Thus, instability will not be of importance for sufficiently short plasma length in the absence of reflection at the ends of plasma.

Let us consider dense $\omega_{pi}^2/\Omega_i^2 \gg 1$ "cone" plasma with $T_c = 0$ and density n_h bounded to the left from point $z=0$ by vacuum, and to the right from $z=L$ by cold ($T_h = T_c = 0$) plasma with density n_c . Dispersion relation for DCLC at $k_\parallel = 0$ is /2/ (notations from /2/)

$$\varepsilon_{\perp h} = 1 + \frac{\omega_{pi}^2}{\Omega_e^2} - \frac{\omega_{pi}^2 \varepsilon_c K}{\omega \Omega_e K^2} + \left(\frac{\omega_{pi}^2 \omega}{K^2 \langle v_\parallel^3 \rangle} + \frac{\omega_{pi}^2 \varepsilon_c}{K^2 \langle v_\parallel \rangle \Omega_i} \right) \cot \frac{\pi \omega}{\Omega_i} = 0 ; \qquad (1)$$

Assuming some longitudinal variation we have equation for perturbed potential in the form:

$$\frac{d}{dz} \left(1 - \frac{\omega_{pe}^2(z)}{\omega^2} \right) \frac{d\varphi}{dz} - K^2 \varepsilon_\perp \varphi = 0 ; \qquad (2)$$

Then, putting $\varepsilon_{\perp c} = 1 - \frac{\omega_{pi}^2}{\omega^2 - \Omega_i^2}$ for cold plasma and utilizing continuity of potential and $\left(1 - \frac{\omega_{pe}^2}{\omega^2}\right) \frac{d\varphi}{dz}$ over the boundaries we obtain the dispersion relation for localized modes in hot plasma

$$\frac{\omega}{\omega_{pe}} \varepsilon_{\perp h}^{1/2} K_\perp L \cdot \operatorname{tg} \left(\frac{\omega}{\omega_{pe}} \varepsilon_{\perp h}^{1/2} K_\perp L \right) = -i \frac{n_c}{n_h} K_\perp L \left(\frac{m_e}{M_i} \frac{\omega^2}{\Omega_i^2 - \omega^2} \right)^{1/2} \qquad (3)$$

Here $\varepsilon_{\perp h}$ is given by eq.(1) and $\frac{\omega_{pi}^2}{\omega^2} \gg 1$ is taken into account. Let, firstly, $\omega > \Omega_i$ and $\frac{n_c}{n_h} K_\perp L \left(\frac{m_e}{M_i} \right)^{1/2} \gg 1$, then we have from (3)

$$\varepsilon_{\perp h} - \frac{\omega_{pe}^2}{\omega^2} \frac{(2N+1)^2 \pi^2}{4 K_\perp^2 L^2} = 0 ; \quad (N = 0, 1, 2 \ldots) \qquad (4)$$

This dispersion relation differs from (1), it contains term $\frac{\omega_{pe}^2}{\omega^2} \frac{k_\parallel^2}{K^2}$ describing longitudinal electron conductivity and corresponding to the standing wave with $K_\parallel = \frac{2N+1}{2} \pi \frac{1}{L}$. If $\frac{\omega_{pe}^2}{\omega^2} \frac{(2N+1)}{4 K_\perp^2 L^2} \pi^2 \gg \frac{\omega_{pe}^2 \varepsilon_c k_\perp}{\omega \Omega_e K_\perp^2}$, $\frac{\omega_{pi}^2 \varepsilon_c}{K^2 \langle v_\parallel \rangle \Omega_i}$ gradient becomes unimportant and instability turns into convective loss-cone mode discussed previously in /7/ . This corresponds to the conditions $\frac{M_i}{m_e} \frac{\Omega_i}{\omega} \frac{\pi^2}{4} \frac{R_p}{K_\perp L^2} \gg 1$ and $\frac{M_i}{m_e} \frac{\Omega_i^2}{\omega^2} \frac{\pi^2}{4} \frac{R_p \langle \Omega_i \rangle}{L^2} \gg 1$; here we define $R_p = \epsilon^{-1}$. If $\frac{n_c}{n_h} K_\perp L \left(\frac{m_e}{M_i} \right)^{1/2} \ll 1$ we have such dispersion relations $\varepsilon_{\perp h} - \frac{\omega_{pe}^2}{\omega^2} \frac{\pi^2 N^2}{K_\perp^2 L^2} = 0 ; (N = 1, 2)$ and $\varepsilon_{\perp h} - \frac{n_c}{n_h} \frac{\omega_{pe}^2}{\omega^2} \frac{1}{K_\perp L} \left(\frac{m_e}{M_i} \right)^{1/2} = 0$. The first relation corresponds to (4) with somewhat different value of $K_\parallel$, and in the second one gradient can be neglected if conditions $\frac{n_c}{n_h} \frac{\Omega_i}{\omega} \left(\frac{M_i}{m_e} \right)^{1/2} \frac{R_p}{L} \gg 1$ and $\frac{n_c}{n_h} \frac{\Omega_i^2}{\omega^2} \left(\frac{M_i}{m_e} \right)^{1/2} K_\perp \langle a \rangle \frac{R_p}{L} \gg 1$ are fulfilled. Let us note that the case $\omega > \Omega_i$ corresponds to wave reflection from cold plasma (on the length $\sim \left(\frac{M_i}{m_e} \right)^{1/2} \frac{1}{K_\perp}$. If $\omega < \Omega_i$ wave penetrates into cold plasma and in that case dispersion relation becomes

$$\frac{\omega}{\omega_{pe}} \varepsilon_{\perp h}^{1/2} K_\perp L \cdot \operatorname{tg} \left(\frac{\omega}{\omega_{pe}} \varepsilon_{\perp h}^{1/2} K_\perp L \right) = -i \frac{n_c}{n_h} \left(\frac{m_e}{M_i} \right)^{1/2} K_\perp L \frac{\omega}{\Omega_i}$$

Assuming $K_\perp L \left(\frac{m_e}{M_i} \right)^{1/2} \frac{\omega}{\Omega_i} \ll 1$ we may put the dispersion relation in the form $\varepsilon_{\perp h} = -i \left(\frac{M_i}{m_e} \right)^{1/2} \frac{\omega_{pi}^2}{\omega \Omega_i} \frac{1}{K_\perp L} \frac{n_c}{n_h}$. When $\frac{n_c}{n_h} \left(\frac{M_i}{m_e} \right)^{1/2} \frac{R_p}{L} \gg 1$ the gradient terms may be neglected and the remaining instability is the same as it has been investigated in /8/ . In particular case, when $K_\perp L \left(\frac{m_e}{M_i} \right)^{1/2} \frac{\omega}{\Omega_i} \gg 1$ dispersion relation is an analog of (4). The conditions obtained above contain $\omega, K_\perp$ and for estimation it's natural to take extreme frequency and $K_\perp \langle a \rangle$ for instability arising from radial density gradient. If critical density gradient is greatly exceeded, DCLC described by (2) occurs for $K_\perp \langle a \rangle \leq K_\perp \langle a \rangle_{crit} \approx \left(\frac{M_i}{m_e} \right)^{1/2} \frac{\langle a \rangle}{R_p}$, then $R_e \omega \approx \operatorname{Im} \omega \approx \Omega_i \cdot K_\perp \langle a \rangle \left(\frac{\langle a \rangle}{R_p} \right)^{1/2}$. For previous conditions this implies that $\frac{\pi^2}{4} \frac{R_p^2}{L^2} \gg 1$, $\frac{\pi^2}{4} \frac{R_e^2}{L^2} \left(\frac{R_e}{\langle a \rangle} \right)^{1/2} \gg 1$, $\frac{R_p}{L} \left(\frac{R_p}{\langle a \rangle} \right)^{3/4} \gg \frac{n_h}{n_c}$, $\frac{R_e}{L} \left(\frac{R_e}{\langle a \rangle} \right)^{5/6} \gg \frac{n_h}{n_c}$ respectively, and these expressions should be valid for $n_c \approx n_h$ and $R_p \sim L$. Thus, if the contact between cold plasma and hot "cone" one with $R_p \sim L$ exists inherent localized modes have the dispersion equation with gradient terms which may be neglected and, therefore, the instability has to transform into high frequency one /7/ . Such perturbations are absorbed at the end of the machine and if scale length is sufficiently small, the instability will not arise. This question has been discussed previously /9/ , the stabilization criterion for all inherent modes of high frequency instability has been obtained. This criterion requires plasma length to be sufficiently small.

We have benefited from useful discussions with G.I.Dimov and M.E.Kishinewsky.

References

1. G.I.Dimov et al, Fizika Plazmy, 2, 597, 1976
2. R.F.Post, M.N.Rosenbluth, Phys. Fluids, 9, 730, 1966
3. Logan B.G. et al. Phys. Rev. Letters, 37, 1468, 1976
4. R.F.Post. Mirror confinement and its optimization VCRL-70681, 1967
5. A.B.Mikhailowsky, Nucl.Fusion, 5, 125, 1965
6. M.I.Gerver, Phys. Fluids, 19, 1581, 1976
7. M.N.Rosenbluth, R.F.Post, Phys. Fluids, 8, 547, 1965
8. H.L.Berk et al., Phys. Rev. Letters, 22, 876, 1969
9. H.L.Berk et al., Phys. Fluids, 15, 891, 1972

STABILIZATION OF THE DRIFT-CONE INSTABILITY (DCI)
BY LOW-ENERGY IONS

M.S. Ioffe, B.I.Kanaev, V.P. Pastukhov, E.E. Yushmanov
I.V. Kurchatov Institute of Atomic Energy, Moscow, USSR

The PR-6, PR-7 and 2XII experiments (1,2) have demonstrated the possibility of stabilizing DCI by a cold plasma stream or by neutral gas. These two methods are based on the Post's idea that a small addition of low energy ions to the hot plasma should stabilize DCI (3). It should be pointed out, however, that these earlier experimental results cannot be considered as conclusive evidence of the realization of just this stabilizing mechanism, because the instability was only partially suppressed but not fully stabilized. It may be caused, in particular, by the low electron temperature established there as a result of cooling the electrons by the plasma stream or by neutral gas rather than by the modification in the ion distribution function.

This paper reports results of new PR-6 experiments which allowed us to establish with sufficient certainty the stabilization effect due to a small amount of slow ions introduced into the plasma. As in our earlier experiments, the hot hydrogen plasma is created by HF heating and trapping the ions from a plasma stream injected axially along the magnetic field. The plasma parameters were as follows: the initial plasma density $n_o = 2.10^{12} om^{-3}$, $T_i = 200eV$, $T_e = 10eV$, plasma diameter = 10cm. An intense burst of DCI is developed as usually on PR-6 during the plasma free decay 150-200msec after the beginning of the decay. Special experiments have shown that the delay of the instability results from a stabilizing action of the residual plasma stream which penetrates into the trap after the end of the discharge in the plasma source. If this stream is cut off the instability appears immediately with decay. The cutting off is provided by a small pulsed coil breaking the stream just before it enters the trap.

The cut.off technique enabled us to repeat the previous experiments on DCI stabilization by the anisotropic overheated electrons (4) under new and more clean conditions and to check the given explanation of the observed stabilization effect.

This effect was previously attributed to the accumulation of slow ions in the electrostatic well, formed due to the presence of a group of fast electrons in the central part of the trap. It was assumed at the same time that those ions originate in the ionization and charge exchange processes in the residual neutral gas.

However, the present experiments similar to the previous ones except for using the cut-off technique revealed that this conclusion was erroneous. They have shown that if the afterinjection stream is cut off before the microwave power pulse for electron heating is turned on the instability remains to be unstabilized in spite of the conditions for forming the potential well and filling it with ions formed from the neutral gas mantain the same as before (Fig.1). Such results are obtained under the vacuum conditions typical of PR-6 (the basic pressure of 2.10^{-8}torr, freshly gettered vacuum surfaces.) They indicate that the ions trapped from the afterinjection stream could be the determining factor in stabilization under these conditions rather than the ions formed in the neutral gas. Another conclusion may also follow from these observations. If a potential well is really formed and the Post's idea about stabilization of DCI by a small amount of slow ions is valid it should be expected that by cutting off the afterinjection stream the stabilization would set in with deterioration of the vacuum conditions. To verify this conclusion experiments have been performed, in which the afterinjection stream was cut off while the neutral gas pressure is controllably raised from pulse to pulse. Hydrogen was used as a neutral gas in the main set of the experiments. The results justified our expectations: the instability disappeared as the pressure was increased. In this case the dependence of the oscillation amplitude on the hydrogen pressure was found to have a steplike form (Fig.2a). Because the density of the ions accumulated in the potential well due to ionization and charge exchange is proportional to the pressure, such a steplike curve should be considered as an evidence of a threshold transition

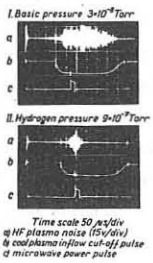

Fig. 1

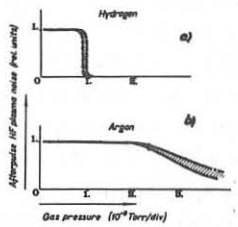

Fig. 2

from the unstable to stable state taking place as soon as the slow ions reached a quite definite critical density. This density can be evaluated by the known hydrogen pressure at the transition point and the parameters of hot plasma. In this case it was found to be 3-5% of the hot plasma density, this is consistent with numerical calculations made for similar plasma conditions (3).

Experiments with argon as a neutral gas are also of interest. As the argon ions strongly differ from those of hydrogen in their cyclotron frequency, they do not seem to be a "sutable material" for improving the ion distribution function of the hydrogen plasma. Therefore, no similar relationship between the oscillation amplitude and pressure should be expected in this case. In fact, instead of a steplike transition to the stable state at a certain critical density the oscillations slowly weaken with pressure, beginning with higher pressure than that in the case of hydrogen (Fig.2b). The curve in Fig.2b indicates that it is practically impossible to stabilized the instability with argon completely; the instability only can be partially suppressed.

In conclusion: it is shown in accordance with the theoretical predictions that, in fact, DCI can be stabilized if a hot plasma is added with a small amount of slow ions of the same kind (not less than 3-5%). Unlike the previous experiments the stabilization observed cannot be explained by some other factors except an addition of low energy ions.

1. Yu.T.Baiborodov et al.,6-th Europ.Conf.on Controlled Fusion and Plasma Physics,Moscow, 1973, v.2, p.122.
2. F.H.Coensgen et al.,Phys.Rev.Letters, 37,(1976),1468.
3. R.F.Post, Livermore Report UCRL-70681, 1968.
4. M.S.Ioffe et al., Zh.Eksp.Teor.Fiz., 67 (1974), 2145.

SUPPRESSION OF THE LOW DENSITY PLASMA CYCLOTRON INSTABILITIES BY EXCITED PLASMA OSCILLATIONS

V.A. Zhil'tsov, V.Kh. Likhtenstein, D.A. Panov,
V.A. Chuyanov, A.G. Shcherbakov
I.V. Kurchatov Institute of Atomic Energy, Moscow, USSR

Experiments were carried out at the Ogra-3 device /1/. The plasma was initiated by injection of 20 keV hydrogen atoms beam into a magnetic field of a simple mirror configuration, a field strength in the trap center being 21.6kG. The plasma radius was 5cm, the plasma length along the magnetic field was determined by beam dimensions and was 3-4cm. A flute instability occured at the density of $1x10^{8}cm^{-3}$. It could be suppressed by a feedback system/1/. Two regions of oscillations on the fundamental cyclotron frequency have been found in the investigated density range /2/. The first region threshold is $\sim 3x10^{7}cm^{-3}$ and corresponds to the conditions for development of an anisotropic cyclotron instability (ACI) $W_{pe} \approx W_{Bi}$, in this case $K_{II}\rho_i \approx 0.8$, $K_{\perp}\rho_i \approx 0.7$, azimuthal mode m=1 and the oscillation structure is simmetric relative to a central plane. The second region threshold depended on the plasma anisotropy and was $(0.4-1)x10^{9}cm^{-3}$. There were two oscillation branches in this region. The first branch frequency was lower than W_{Bi} in the device center-$W_{Bi}(0)$, $K_{II}\rho_i \approx 1$, $K_{\perp}\rho_i \approx 0.5$, m=0, the second branch frequency was higher $W_{Bi}(0)$, and $K_{II}\rho_i \approx 1$, $K_{\perp}\rho_i \approx 0.7$, m=1. These two branches had threshold values close to each other and they caused the limitation of the plasma density.

In the present work the influence of the excited plasma oscillations on cyclotron instabilities has been investigated. The scheme of the experiment is presented in Fig. 1. The signal from the generator (G) was amplified (PA) and supplied in opposite phase to two rings disposed at the device ends. Fig. 2 shows the amplitude φ distribution of the excited oscillations along the magnetic field. Dotted line represents the distribution of the oscillation potential without plasma. It can be seen that large - scale oscillations have been excited, the oscillation amplification by a factor of 10-20 taking place in the plasma. Fig. 3 represents dependence of the density region of the oscillation excitation (shaded area) on the ring voltage U_g and on the generator frequency W_g. The lower threshold of the excitation region in the density band corresponds to the condition $W_g \approx W_{pe}$, where in the calculation of W_{pe} an average plasma density n was taken. The upper boundary depends nonlinearily on the amplitude U_g and increases with the increase of U_g.

The influence of the excited plasma oscillations on ACI is shown in Fig. 4. The ACI threshold is lower than that of the flute instability and therefor feedback system for suppresion of the flute instability was switched off. Under these conditions losses due to ACI were observed to be approximately equal to the charge-exchange losses. In presence of the excited plasma oscillations cyclotron losses disappeared (Fig. 4).

ACI suppression has been observed over all the region of the oscillation excitation at a suffiolently high value of U_g, the cyclotron oscillation amplitude A has been decreased by a factor of more than 100.

The influence of the excited oscillations on the cyclotron oscillations in the second region at densities $\sim 10^{9}cm^{-3}$ is more complicated. Oscillations with azimuthal mode m=0 have been fully suppressed, but m=1 oscillations were presented in the explored region of U_g (up to 10V). The plasma density increased by ~20% but it remained limited by m=1 cyclotron oscillations.

ACI and m=0 oscillation suppresion is likely to be connected with heating of the electrons by plasma oscillations and absorption of the cyclotron oscillations due to Landau damping. Remaining m=1 instability was identified as a modified negative mass instability.

REFERENCES

1 Zhil'tsov V.A., et al., Plasma Phys. and Control Nucl. Fusion Res., IAEA Vienna, 1 (1975), 355.
2 Zhil'tsov V.A., et al., Fizika Plasmy, 3(1977), 37.

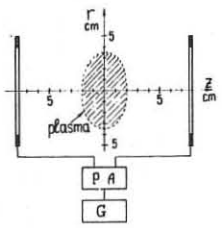

Fig. 1

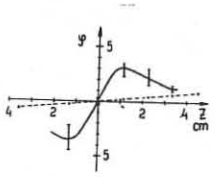

Fig. 2

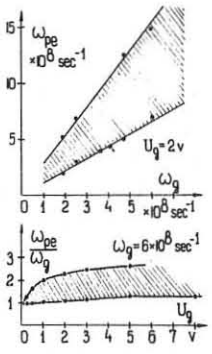

Fig. 3

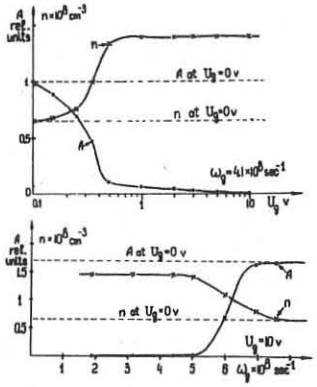

Fig. 4

PLASMA DRIFTS IN THE POLYTRON

H. Chuaqui

Blackett Laboratory, Imperial College, London SW7 2BZ

Abstract: The outward toroidal drift in the Polytron has been suppressed by the addition of a vertical magnetic field, none the less vertical drifts are present which prevent further Hall acceleration.

Previous results (1) have shown that the plasma column in the Polytron has a toroidal outward drift. The addition of a vertical field prevents this drift. Nonetheless, a decrease in the reaction force on the cusp coils and toroidal velocities is observed, probably due to a vertical shift of the plasma.

The Polytron is a toroidal Hall accelerator with 36 cusps. A schematic of the apparatus is shown in Figure 1. The accelerating electric field is provided by discharging a capacitor bank through a set of induction rods. This set of rods also provides the vertical magnetic field which prevents the radial outward toroidal drift (2). Ions are preferentially accelerated as the ion Larmor radius is larger than the cusp separation (for argon is the present device), where electron Larmor radius is small, except near the cusp magnetic axis where they can flow freely. Off axis the electrons are tied to the magnetic field lines. For perfect conductivity, the magnetic field lines are effectively equipotentials. Thus, the electric field can exist only in the ring cusp region. (3)

The radial and vertical motion of the plasma in the minor cross section have been investigated by measurements of the distribution of line emission from AII, AIII, and AIV and by external magnetic probes. The line emission measurements show a well defined narrow channel (1 cm diameter) that stays centered on the major radius, but show a vertical drift of up to 8mm at late times. Figure 2 is a typical plot of plasma position with respect to time. Within the margin of experimental accuracy the vertical shift does not seem to depend on the direction of either the toroidal electric field or cusp magnetic field. Also shown in the figure is the reaction force on the cusp coil. From these measurements the decrease of the reaction force on the cusp coils seems to be associated with the vertical shift, presumably due to the fact that the Hall currents in the ring cusp can no longer close.

Figure 3 shows the ion toroidal velocity as a function of time. The ion velocity measurement was obtained by a differential Doppler shift method (2). Note that the ion velocity changes only after the reaction force begins to decrease. At this time there appears to be a reduction in the ion number density on axis, as inferred from the AIII and AIV line emission, shown in Figure 3. This seems to be consistent with the vertical drift shown in Figure 2.

Line profile measurements show that there is a Doppler broadening which is larger near the ring cusp region than at the point cusps. This indicates that the broadening is not wholly thermal, but that there is a large contribution due to directed ion motion in the ring cusp region, in agreement with particle trajectory calculations (4).

Loss of particles through the ring cusp and thickness of the loss region have been investigated by a faraday cup probe positioned near the wall. These measurements show that after an initial loss (1.5 to 3 μs) there is little further loss. The loss width is between 3 and 8 mm, which is between an electron and ion Larmor radii and is consistent with resistive sheath calculations (3).

The measurements indicate that the radial outward motion has been suppressed by a vertical magnetic field. However, there is a vertical shift which limits further Hall acceleration. The observed shifts are comparable with the radius of the plasma.

column.

References:

1. Kilkenny, J.D., Dangor, A.E., Haines, M.G., Plasma Physics, 15, pp 1197-1220 (1973)
2. Chuaqui, H., Ph.D Thesis, London University (to be submitted)
3. Kilkenny, J.D., Proc. 5th Conf. on Controlled Fusion and Plasma Physics, Grenoble, 1, 101, (1972)
4. Kilkenny, J.D., (1972) PhD. Thesis, London University

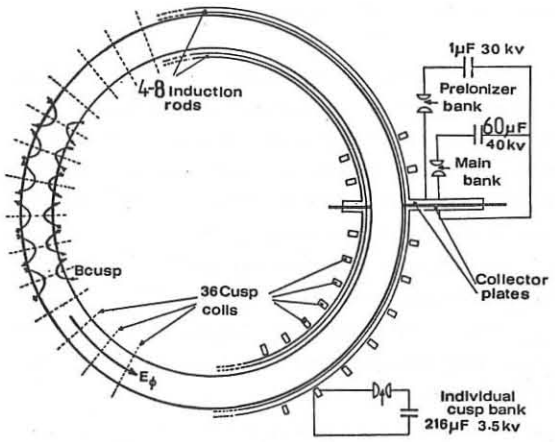

FIGURE 1. SCHEMATIC OF THE POLYTRON

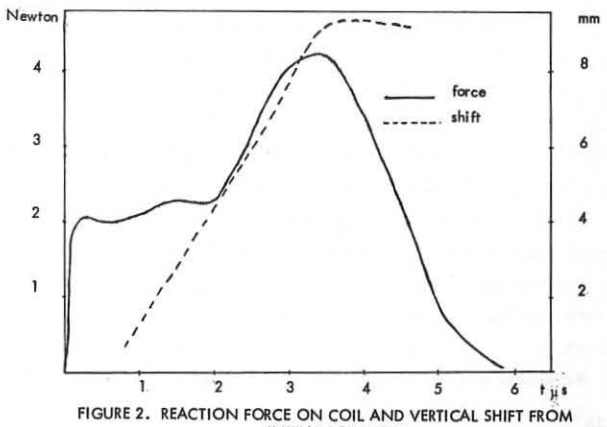

FIGURE 2. REACTION FORCE ON COIL AND VERTICAL SHIFT FROM INITIAL POSITION

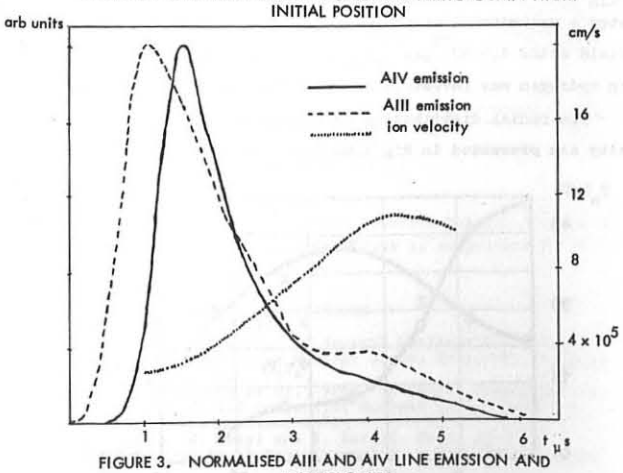

FIGURE 3. NORMALISED AIII AND AIV LINE EMISSION AND ION VELOCITY

LOW PRESSURE DISCHARGE AT ECR IN THE MAGNETIC BOTTLE

V.D.DOUGAR-JABON, K.S.GOLOVANIVSKY, V.D.SCHEPILOV
Plasma Phisics Laboratory
Patrice Lumumba University
Moscow W-302, U.S.S.R.

A possibility of creation of three-dimensional well for ions in the mirror configuration, added by h.f. field on electron cyclotron resonance (ECR) was experimentally investigated. Experiments were carried out with hydrogen at pressure $7\ 10^{-5}$ torr. It was shown that such a potential well with a depth of 50 - 60 v was formed at the generator power level 75 watt.

This work presents the experimental investigation of one of the possibilities of creating three dimensional electrostatic potential well for ions by acting on the magnetised electron component by external microwave field near electron gyroresonance. The idea of the experiment is as follows. Let the plasma be contained in a magnetic bottle, in the central plane of which is created a microwave field with the electric component perpendicular to the magnetostatic field. Since the field in such a trap is radially inhomogenious the condition $\omega = \omega_{ce}$ is realized on a certain axially symmetrical surface, the radius of which may be varied.

Perpendicular heating of electrons takes place mainly on this surface, hence the electron mean energy here will be considerably higher that in the other regions of plasma. Due to intensive diffusion of hot electrons, plasma on resonance surface acquires a positive potential with respect to the central part, thus creating a radial well for ions. In the longitudinal direction, anisotropically heated electrons are held back by the increasing magnetic field, which enables to hold back ions electrostaticaly in the longitudinal direction.

In this case the life time of ions in such a three-dimensional well should increase by exp ($Ze\varphi/kT_i$) times, where Ze - the ion charge, φ - height of potential barrier, T_i - ion temperature, and the ions flow from the well decreases by the same amount.

Experiments were carried out in a mirror device with R=1,5. B_{min}=(850 - 880) gs. In the central part of the trap is situated a cylindrical cavity, in which TE_{III} right hand rotating field at $\omega = 1{,}5\ 10^{10}\ sec^{-1}$, P_{gen} = 75 wt was excited. Discharge in hydrogen was investigated at a pressure $7\ 10^{-5}$ torr.

The radial distribution of electron temperature and density are presented in Fig I. Maximum electron temperature was

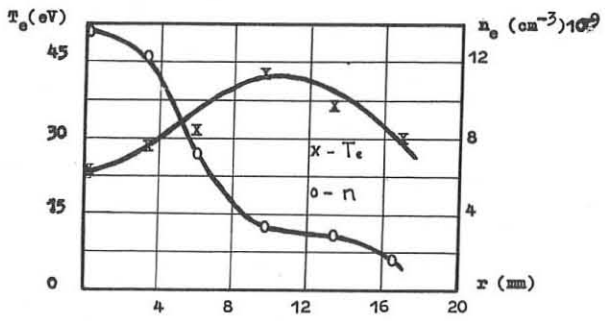

Radial distribution of n_e, T_e
Fig 1

observed in the ring zone with r = 10 mm. In the same zone X - ray radiation, coresponding to electrons of 5 Kev energy was also observed. Radial distribution of plasma potential is presented in Fig 2. In Fig 3 is given the longitudinal distribution of plasma potential. At pressure higher than $1\ 10^{-4}$ torr in the condition of our experiments longitudinal potential is not formed. In this way, inside the cavity at sufficiently low electron collision frequency, a three-dimentional potential well for ions is formed with a depth 45 v in the longitudinal direction, and 60 v in the perpendicular direction.

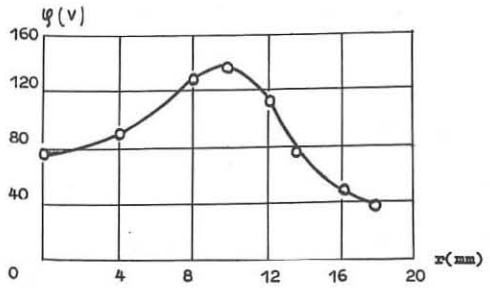

Fig 2

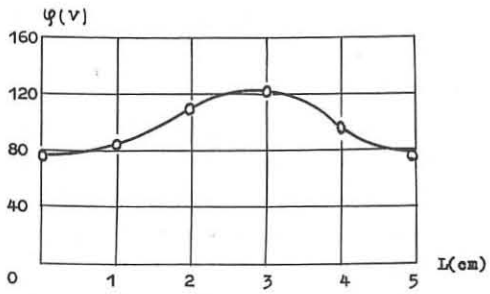

Fig 3

The existance of a three-dimentional potential barrier for ions results in an increase of density in the central region of discharge. In our experiments the plasma density is six times higher in the well than in the hot ring as shown in the Fig 1.

Since the main chanell of charged particles loss is diffusion, we can estimate the ion life time by the expression

$$\tau = \frac{n V}{I} ,$$

where n, V and I are, respectively, the plasma density, volume and the full diffusion flow out of this volume. This diffusion ion loss is compensated for by the ionisation of neutral atoms which takes place troughout the plasma volume, with the greatest intensity in the zone of maximum potential. The calculated ionisation flow into the three-dimentional well agrees with the experimentaly measured flow of ions from the well. The ion life time averaged over the well volume is 60 mcsec. This is over 10 times the ion life time outside the well and in the same volume.

Thus, it is experimentaly shown that ECR discharge in the field of mirror bottle at sufficiently low pressure formes a three-dimentional potential well for positive ions, the depth of which is determined by the microwave power level and the magnetic field geometry.

RADIO-FREQUENCY PLUGGING OF MIRROR AND POINT CUSP ENDS

T.WATARI, R.KUMAZAWA, S.HIDEKUMA, T.AOKI, M.INUTAKE, S.HIROE
A.NISHIZAWA, K.ADATI, T.SATO, H.OBAYASHI, T.HATORI, T.WATANABE
K.TAKAYAMA

INSTITUTE OF PLASMA PHYSICS, NAGOYA UNIVERSITY, NAGOYA, JAPAN

Abstract: Mirror end loss can be suppressed by applying an rf field at the mirror throat through low impedance coils. This method is verified to be effective even when plasma density amounts to 10^{14} cm^{-3}.

When an rf electric field is applied perpendicularly to a magnetic field, the combined effect of the electric field and a spatial variation of the magnetic field is such as to exert a force on a charged particle in the direction of decreasing magnetic field. Such force is applicable to suppress the end loss of an open system. In so far our experimental works[1] have been concentrated on plugging of the line cusp end. In this paper we confine ourselves to the plugging of an open end of cylindrical geometry like mirror and point cusp. There are two typical ways to produce an rf electric field: electrostatic field by a pair of parallel plates, and electromagnetic field by a coil. In the plugging experiment on the line cusp, the former type has been used. In this experiment, however, we adopt the latter and three types of coil shown in Fig.3 are examined. Type 1 is an ordinary 7-turn solenoid, type 2 a pair of half turn coils. Type 3 is similar to the one used by Ovchinnikov et al. in the heating of a stellarator plasma.[2]

The experiment is carried out in a mirror magnetic configuration (see Fig.1). The magnetic field intensity of the throat and the center of the mirror are 5.84 kG and 1.8 kG, respectively. A hydrogen plasma is produced by a TPD source for the density less than 10^{13} cm^{-3}, while an MPD source[3] is used for higher densities. It is known that the ion and electron temperatures of plasma produced by these plasma sources are nearly equal. The plasma is introduced through one of the mirror throat into the center of the mirror. An rf field is applied on the other mirror throat to reduce the plasma loss. The rf field is fed by a 500 kW rf oscillator. Applied rf frequency (6.2 MHz) is lower than the local ion cyclotron frequency (7.55 MHz) inside the coil. The plasma density at the center of the mirror is measured with a 70 GHz microwave interferometer, a diamagnetic loop and a double probe. The loss flux is measured with another diamgnetic loop set up behind the rf coil and a multigrid energy analyzer used as an ion collector. Figure 2 shows the signal of the multigrid

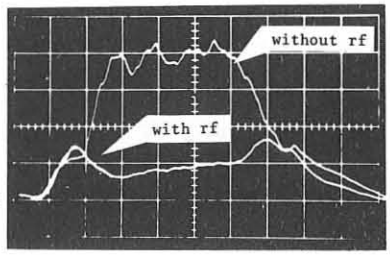

Fig.2 Loss flux with and without rf field.
Time scale: 200 μs/div.

analyzer. It must be noted that remarkable decrease of loss flux is achieved when rf field is applied. Relations between the plasma density n and rf voltage V_{rf} to keep a given value of the plugging efficiency is experimentally obtained and shown in Fig.3 for the three coils. It is read that $V_{rf} \propto n^{0.9}$ for type 1, $V_{rf} \propto n^{0.5}$ for type 2, and $V_{rf} \propto n^{0.1}$ for type 3. Type 3 coil needs the least rf voltage for high density plasma. Both type 1 and type 2 coils produce rf field in azimuthal direction and there is no intrinsic difference between them. Type 2 coil is more effective than type 1 coil, because induced electric field is inversely proportional to the number of turns. Type 3 coil differs from the others in producing a non-vanishing electric field component inside the plasma, which is effective for the plugging. Type 1 and 2 coils give the electric field vanishing on the axis. The result of type 3 coil is remarkable in its very weak dependence on the density, and this is quite meaningful for the future application of rf plugs to fusion plasmas.

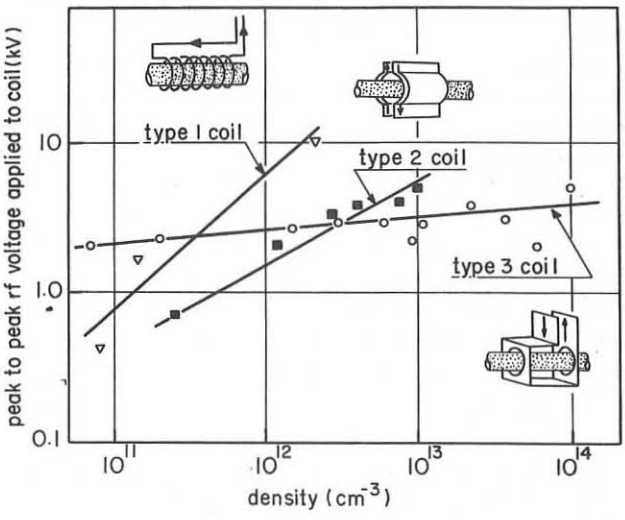

Fig.3 The experimentally obtained relation between the plasma density and the rf field when loss flux is suppressed to 10 %.

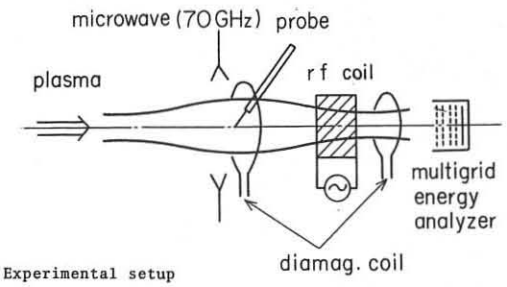

Fig.1 Experimental setup

REFERENCES

(1) S. Hiroe et al., Proc. of Seventh Conference on Plasma Physics and Controlled Nuclear Fusion Research, CN-35/H5, Berchtesgaden, Oct. 1976.
(2) S. S. Ovchinnikov et al., Proc. of Fourth Conference on Plasma Physics and Controlled Nuclear Fusion Research, Vol.III, p.597, Madison, 1971.
(3) M. Inutake, H. Ikezi and K. Kuriki, Proc. of Tenth International Shock Tube Symposium, p.714, Kyoto, 1975.

R. F. Plugging and Heating of a Magnetized Sheet Plasma

Kazuya Uehara*, Akiyosi Itakura, Shigeo Hagiwara and Shoji Kojima

Institute of Physics, The University of Tsukuba, Ibaraki, Japan.

*Division of Thermonuclear Fusion Research, Japan Atomic Energy Research Institute, Tokai Establishment, Ibaraki, Japan.

Abstract: R. f. plugging and heating of a magnetized sheet plasma is confirmed experimentally to be effective at a frequency of a series resonance in the r.f. circuit including the plasma, the sheath and the oscillator. The frequency is not the characteristic frequency of infinite plasma.

Recently a radio frequency electric field in a plasma has come to play an important role with respect to stabilization of instabilities, heating and confinement in plasmas aiming at the thermonuclear fusion reactor. Many efforts have been made to supply r.f. powers to give energy to the charged particles in plasmas. When the r.f. electric field E_p is excited in the plasma, the plasma forms a quasi-potential ϕ, which is expressed by[1]

$$\Phi = \frac{1}{2}\varepsilon_0 \frac{(\omega_{pi}^2+\omega_{pe}^2)(\omega^2-\omega_0^2)}{(\omega^2-\omega_{ci}^2)(\omega^2-\omega_{ce}^2)} E_p^2 \qquad (1)$$

where $\omega_0=((\omega_{pi}^2\omega_{ce}^2+\omega_{pe}^2\omega_{ci}^2)/(\omega_{pi}^2+\omega_{pe}^2))^{+1/2}$ and ε_0 is a dielectric constant in vacuum. Therefore, when ϕ has a derivative with respect to the space, that is, the spatial gradient of the magnetic field and/or of the density exists in the plasma, the charged particles in the plasma should feel a pondermotive force $F=-\nabla\phi$, and are accelerated effectively. At the same time the plasma is heated.[2,3] Experimental investigations[4], however, do not completely support above predictions. When the dielectric constant becomes zero, which is the eigen resonance of the plasma, the total impedance of the r.f. circuit becomes infinitely large and the efficiency of a power absorption into the plasma is not always good. While, when the series resonance of the system occurs, which corresponds to the case of the sheath resonance, the r.f. field in the plasma becomes large. Then, the plasma plugging is very effective in the resonance. In this paper, the experimental study on the sheath resonance is reported from the aspect of the r.f. plugging and the heating of a magnetized sheet plasma.[5]

Experimental apparatus is shown in Fig.1. Magnetic field configuration is a mirror type with a ratio 2.3. A plasma produced by ECRH near the mirror point diffuses out to the mirror center and is made a sheet type by a pair of alminium limiters inserted perpendicularly to the magnetic field. The parallel electrodes for supplying the r.f. power are placed in the region where the magnetic field gradient is large and the spacing of the electrodes can be changed widely so as to vary a sheath thickness. The field strength at the center of the electrodes is about 1.0 kG. A grid type electriostatic energy analyser is placed at the down stream of the plasma in order to examine the particle loss, and the ion sensitive probe is inserted in the mirror center. The plasma density at the mirror center is about 10^{10} cm^{-3}, and the electron and ion temperature at the same position are 5-10 eV and 0.3-0.8 eV, respectively.

Following results are obtained : When the series resonance occurs in the circuit, the total impedance of the system takes minimum and the phase shift of the r.f. current to the voltage becomes zero, then the ion saturation current on the analyser decreases resonantly. On the other hand, the ion saturation current on the ion sensitive probe increases correspondingly to this decrease, and the increment of the ion temperature is also observed. As shown in Fig.2 and Fig.3, these resonance frequencies change by varying the spacing of the electrodes d, where the plasma parameters are kept constant. The resonant frequency is clearly above the ion cyclotron frequency and below the lower hybrid resonant frequency.

Above experimental results can be explained by using a simple model of the sheath and the plasma. The equivalent circuit is assumed as shown in Fig.1. For simplicity the sheath is assumed to be completely vacuum. The impedance of the sheath, $\dot{Z}_s$, and the plasma, $\dot{Z}_p$, are $\dot{Z}_s = 1 / j\omega C_s$ and $\dot{Z}_p = 1 / j\omega C_p$, where C_s and C_p are the effective capacitance of the sheath and the plasma, respectively. Then $C_s = \varepsilon_0 A / s$, $C_p = \varepsilon_0\varepsilon_\perp A / p$, where A is the area of the electrode, s the sheath thickness, p the plasma thickness and $\varepsilon_\perp$ the perpendicular dielectric constant. As the total impedance of the system is described by $\dot{Z} = 2\dot{Z}_s + \dot{Z}_p + r$, the r.f. electric field in the plasma is expressed as $E_p = (\dot{Z}_p / \dot{Z})(V_{rf} / p)$, where V_{rf} is the voltage applied between the parallel electrodes. The value r in $\dot{Z}$ is the real resistance which may contain the total r.f. circuit. The plasma forms a quasi-potential derived from E_p :

$$\Phi_1 = \frac{1}{2}\varepsilon_0 V_{rf}^2 \frac{(\omega_{pi}^2+\omega_{pe}^2)(\omega^2-\omega_0^2)(\omega^2-\omega_{ci}^2)(\omega^2-\omega_{ce}^2)}{(r\varepsilon_0 A\omega(\omega^2-\omega_{LH}^2)(\omega^2-\omega_{UH}^2))^2+(d(\omega^2-\omega_{LG}^2)(\omega^2-\omega_{UG}^2))^2} \qquad (2)$$

where ω_{LH}, ω_{UH} are the lower and upper hybrid resonant frequency and ω_{LG}, ω_{UG} are the frequency of the sheath resonance. When $\omega = \omega_{LG}$, $\omega = \omega_{UG}$, then $\dot{Z}$ takes minimum value and E_p , Φ_1 and F takes the maximum value, so the r.f. plugging and the heating of the plasma may be expected at these points. ω_{LG} versus G is calculated graphically in Fig.4 putting the density as a parameter, where G is the geometrical factor : G = p/d. When the sheath is absent (G = 1), then ω_{LG} becomes ω_{ci} and when the plasma is absent (G = 0), then ω_{LG} becomes ω_{LH}.

The ion heating is well explained by a Joule heating process of a radio frequency resistance. From the equation of the energy balance and using the conductivity in a magnetic field, the increment of the ion temperature is estimated

$$\Delta T_i = \frac{e^2 E_p^2}{m_i \omega^2} \nu \tau_{ic} \qquad (3)$$

where ν is the collision frequency, m_i the mass of ions and τ_{ic} is the energy confinement time of ions.

In conclusion, an r.f. plugging and heating of a magnetized sheet plasma occurs more effectively at the sheath resonant point, but not at the ion cyclotron frequency or at the lower hybrid frequency.

References

1) L.D.Landau and E.M.Lifshitz : Electrodynamics of Continuous Media (Addison Wesley Reading Press 1960) p.68.

2) D.G.Dow and R.C.Knechetli : J. Electron Control 7 (1959) 316.

3) C.J.H.Watson and L.G.Kuo-Petravic : Phys.Rev.Letters 27 (1968) 1231.

4) T.Watari, S.Hiroe, T.Sato and S.Ichimaru : Phys. of Fluid 7 (1974) 2105.

5) K.Uehara, A.Itakura, S.Hagiwara and S.Kojima : J.Phys.Soc.Japan 42 (1977) 539.

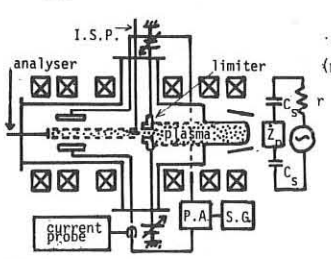

Fig.1 Experimental apparatus and the equivalent circuit of the r.f. system.

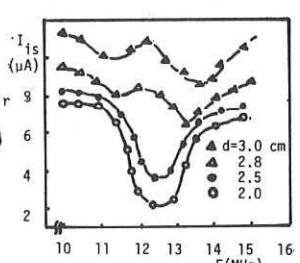

Fig.2 Ion saturation current on the analyser versus the r.f. frequency.

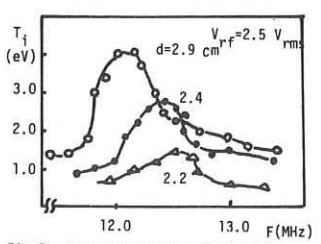

Fig.3 Ion temperature obtained by the ion sensitive probe.

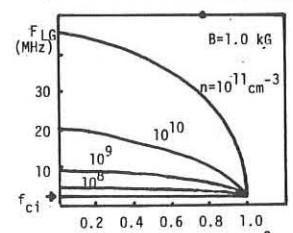

Fig.4 The calculated values of ω_{LG} versus G.

THE INFLUENCE OF HEAVY GAS ENDPLUGS ON THE ENERGY CONFINEMENT TIME

H.J. Hopman, J.A. Markvoort, E.H.A. Granneman and P. de Jagher

Association EURATOM-FOM

FOM-Instituut voor Atoom- en Molecuulfysica,
Kruislaan 407, Amsterdam/Wgm., The Netherlands

Abstract: An analytical expression for the electron heat conduction in a linear plasma column of constant pressure predicts an increase in the energy confinement time of roughly a factor $\lambda(Z/4)$ when endplugs are used; λ is the fractional length and Z the ion charge of the endplug.

Introduction: In linear fusion experiments such as laser or REB heated plasma solenoids the energy confinement time is determined by electron heat conduction along the magnetic field [Green et al.]. In case the particle lifetime is determined by multiple mirror magnetic confinement [Lichtenberg et al.] one can show that the ratio of energy confinement time τ_E and the particle loss time τ_m is given by [Benford; Budker et al.]

$$\tau_m/\tau_E \approx Z^2 \, (T_e/T_i)^{5/2} \sqrt{m_i/2m_e} \, , \qquad (1)$$

where Z is the charge of the plasma ions. Eq. (1) shows that $\tau_E \ll \tau_m$, unless $T_e \ll T_i$, valid for linear θ-pinches. To reduce the electron heat conduction it has been suggested [Dawson et al.] to use endsections filled with a heavy gas such as Kr or Xe. The coefficient for electron heat conduction $\kappa_\parallel$ is proportional to the electron-ion collision time τ_{ei} and therefore proportional to Z^{-1},

$$\kappa_\parallel = a \, n_e T_e k^2 \, \tau_{ei}/m_e; \; \tau_{ei} = b \, T_e^{3/2}/Z_i n_e \, . \qquad (2)$$

If the heavy gas is multiply ionized, the large value of Z reduces the electron heat conduction and τ_E is increased. In E-beam heated plasmas T_e, reaches values above 1 keV within a few nanosec [Jurgens et al.]. In plasma with $T_e \gtrsim 1$ keV and $n_e = 10^{22} m^{-3}$ one can obtain Z = 10 [Mattioli] in about 100 ns, which is presently the duration of E-beam injection. Therefore it is worthwhile to look carefully at the influence of high Z endplugs on the energy confinement time.

Formation of endplugs: E-beam heated plasmas are ideally suited to do experiments with gaseous endplugs. The beam is injected into the plasma chamber through a metallic foil separating the plasma area and the diode from which the E-beam is extracted. If the beam current density exceeds ≈ 1.5 kA cm^{-2}, these foils are ruptured during beam injection. Two foils in succession make up a gas chamber. On firing the beam both foils are ruptured and the gas is released and is ionized by the beam. This way an endplug is established with precisely known initial values such as density, location and type of gas.

Reduction of heat conduction: Because $\tau_m \gg \tau_E$ we assume that the particle density is constant in time. In case of E-beam heating electrons are heated preferentially. Therefore we do not take into consideration the plasma ions. Furthermore we assume that the kinetic pressure nkT is only weakly dependent on the axial distance z. Because of the boundary condition that the temperature at the ends of the plasma column is very small we have the kind of z-dependence for n and T sketched below.

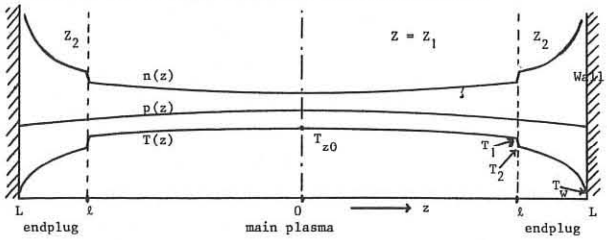

In the main plasma we have $Z = Z_1$. In the endplugs, located between $z = \ell$ and $z = L$, we have $Z = Z_2$. We assume a sharp interface between plasma and endplug with no mixing of particles. We allow for the formation of a sheath with a jump in density and temperature but with pressure continuous. We neglect any dependence on radius.

If only electron heat conduction is considered and all other loss mechanisms are neglected, it is possible to derive an analytical expression for the endplug heat loss reduction. When the electron heating pulse is over, the energy flow in our one-dimensional system is described by,

$$\partial \, nT/\partial t = d \, \partial^2 T^{7/2}/\partial z^2 \; ; \; d = 4\kappa_\parallel/21k. \qquad (3)$$

Because n is time independent we have an equation in T, which can be solved by separating the temperature in a time and a position dependent part, $T = T_t(t) \; T_z(z)$,

$$T_t^{-7/2} \, \partial T_t/\partial t = (d/nT_z) \; \partial^2 T_z^{7/2}/\partial z \equiv 2A/5 \, , \qquad (4)$$

where A is the separation constant. The time dependent part can be integrated directly and the spatial part can be integrated if we assume that nT_z, which is essentially the pressure p, is a known function of z. The boundary conditions taken into account are,

1) At $z = \ell$ both pressures p and heatflow $q = -\kappa_\parallel \partial T/\partial z$ are continuous.

2) At the interface at $z = \ell$ a sheath may develop. We define a parameter $\alpha \equiv \{T_{z1}(\ell)/T_{z2}(\ell)\}^{5/2}$. Subscripts 1 and 2 refer to main plasma and endplug, α is treated as an unknown which must be derived from other considerations. We assume α is constant in time.

3) At $z = 0$, $T_{z1}(z) \equiv T_{z0}$, $\partial T_{z1}/\partial z = 0$; at $z = L$, $T_z(z) \equiv T_w$. The initial pressure in the centre of the column $p(0,0) = n(0)kT(0,0)$ is taken equal to $n(0)kT_z(0)$; $T_t(0) = 1$.

With these conditions the solution for the time dependent part T_t for a plasma column with endplugs becomes,

$$T_t(t) = (1 - At)^{-2/5}, \qquad (5)$$

$$A = \frac{5}{2} \, d_1 k \left[\frac{-(\alpha^{-7/5} \, T_{z0}^{7/2} - T_w^{7/2})}{\alpha^{-7/5} \, C(\ell) + (d_1/d_2) \; \{(L-\ell)B(\ell) + C^*(L)\}} \right], \qquad (6)$$

where,

$$B(z) = \int_0^z p(z',0)dz', \; C(z) = \int_0^z B(z')dz', \; C^*(z) = \int_\ell^z dz' \int_\ell^{z'} p(z'',0)dz''.$$

In the limit that $\ell \to L$ and $\alpha \to 1$, eq. (6) gives the solution for a uniform Z_1-plasma column. A decay time for the temperature is obtained from $T_t(0)/T_t(\tau) = e$, giving $\tau = -(e^{5/2} - 1)/A$. Next we calculate the ratio of the decay time τ in a homogeneous column and τ^* in a column with endplugs. Simplifying the result by taking $T_w = 0$ and a constant pressure $p(z,0) = p_0$ we find,

$$\frac{\tau^*}{\tau} = \left[\frac{\ell^2}{L^2} + \alpha^{7/5} \, \frac{d_1}{d_2} \, \left(1 - \frac{\ell^2}{L^2}\right) \right]. \qquad (7)$$

With $Z_2 \gtrsim 20$ and $Z_1 = 1$ we have $d_1/d_2 \approx Z_2/4 \approx 5$. Then taking $\ell = 0.8 \, L$ and $\alpha = 1$ we obtain $\tau^* = 2.5 \, \tau$.

Conclusions: At first sight endplugs help in reducing heat conduction losses but marginally.

The ratio τ^*/τ is proportional to Z_2. The ratio τ^*/τ is proportional to $\alpha^{7/5} = (T_1/T_2)^{7/2}$. α comes from the temperature jump at the interface of Z_1 and Z_2-plasma. The kind of jump sketched in the figure is favourable for energy confinement. Because of the large 7/2 power it is worthwhile to develop methods to enhance this effect.

The pressure profile has little influence on τ^*/τ.

Remarks: The useful length of the endplug is limited by the demand that the heat flow from the main plasma is convected to the end walls and not lost by other means such as radiation.

The lifetime of the endplug is limited by diffusive mixing of the ions from the Z_1 and Z_2 plasma.

This work was performed as a part of the research program of the association agreement of EURATOM and the "Stichting voor Fundamenteel Onderzoek der Materie" (FOM) with financial support from the "Nederlandse Organisatie voor Zuiver-Wetenschappelijk Onderzoek" (ZWO) and EURATOM.

References:

J. Benford, unpublished.

G.I. Budker et al., JETP Letters 14 (1971) 212.

J.M. Dawson et al., Plasma Physics and Controlled Nuclear Fusion Res., IAEA, Vienna (1971), vol. I, p.673.

T.S. Green et al., Phys.Fluids 10 (1967) 1663.

B. Jurgens et al., Plasma Phys. 18 (1976) 821.

A.J. Lichtenberg et al., Phys.Fluids 17 (1974) 1291, 1302.

M. Mattioli, report EUR-CEA-FC-761 (Febr. 1975).

EXPERIMENTAL STUDIES OF LASER-PRODUCED PLASMAS WITHIN THE SPHERICAL MULTIPOLE TRAP

J.Baranowski, S.Chyrcsakowski, K.Czaus, K.Meissacki, M.Sadowski, E.Składnik-Sadowska, and S.Ugniewski
astitute of Nuclear Research, 05-400 Otwock-Świerk, Poland

tract: The paper reports investigations on plasma production containment within the spherical multipole /SM/ trap. Re-ts of interferometric and spectroscopic measurements are gi-. A leakage aperture is determined from probe measurements.

spherical multipole /SM/ configurations have been extensive-investigated [1,2] since they form true minimum-B traps with-linear loss-gaps. The concept of plasma containment with h-order multipole fields [1] has also been exploited in cy-drical machines [3] used for basic studies of quiescent plas-. In our initial experiments [1,2] with the SM fields and smas produced by injectors an increase in the containment e was observed as compared with a conventional spindle-cusp tem, but more detailed investigations [4,5] have shown that y a portion of plasma injected into the SM field can be ef-tively captured. Therefore it was of interest to investigate er methods of filling up the trap. Particular attention was d to a laser method since it provides a relatively clean sma and makes possible to reduce a particle leak [6]. In the restigations to be described, use was made of a new Kaktus II vice [7]. A layout of this facility is shown in Fig.1. The 23-i.d. spherical chamber has been equipped with a new oil-less uum system and a set of modified SM coils. These coils were plied from a 2.000 μF, 10 kV, condenser bank and made possi-

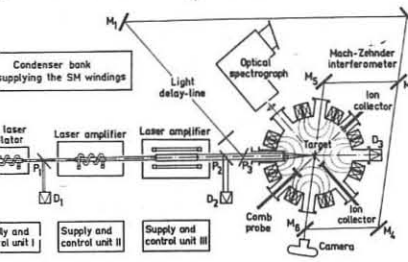

Fig.1.

ble to generate pulsed magnetic fields up to 100 kG at the chamber wall [8]. The experiment described has however been performed with elds up to 24 kG only. Plasma was generated by 1 J, 40 ns, by laser pulses focussed on a polyethylene-foil target pla-d at the center of the trap. Since the HWHM of the SM-coil rrent pulse was about 1 ms, the magnetic field during laser lse was practically constant. Thickness of the target was rried from 25 to 250 μ. When a 250-μ foil s used, some assymetry in integral visible diation /see Fig.2/ has been observed, but larger portion of laser energy was then ab-rbed. All the measurements were performed a pressure of 10^{-5} Tr. To ensure appropri-

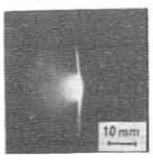

Fig.2.

e reproducibility, laser energy was controlled and the target s shifted a little after each shot. A photo of a typical la-r crater is shown in Fig.3. The dark places correspond to car-bon layers, and the central hole proves that plasma could penetrate through the target im-mediately. An amount of hydrogen atoms vapor-ized during a shot, as determined from the cra-ter dimensions, was about 5×10^{18}. More de-tailed informations about the initial stage

Fig.3.

of plasma expansion were obtained by means of a Mach-Zehnder interferometer /see Fig.1/ and optical spectroscopy. A typical interferogram, taken at t = 40 ns, is shown in Fig.4. The fringe shifts observed correspond to the maximum electron concentration $\sim 5 \times 10^{17}$ cm^{-3} and the total number of electrons $\sim 2 \times 10^{16}$. These numbers can be compared with results of spectroscopic measurements performed at various distances from the target /see Fig.5/. The electron concentrations determined from the H_α line, are approx. one order smaller than those assessed from interferometry /i.e., 1.4×10^{17} cm^{-3} at the focus, 0.3×10^{17} cm^{-3} at z = 0.5 mm, and 2.1×10^{16} cm^{-3} at z = 1.0 mm/. This can be interpreted by an increase in temperature and excitation of carbon ions. Hence, it can be shown that during the initial stage temperatures increased from 1 eV to 7 eV. It should however be noted that spectroscopic measurements have also demonstrated carbon ions expanding with velocities of 5×10^6 cm/s, what corresponds to energies of several hundred eV. Substantial informations about plasma interaction with the SM field were obtained with a comb probe and ion collectors placed within the loss-cones regions, as shown in Fig.1. Typical signals obtained from two different pins of a comb probe, are presented in Fig.6. Results of detailed probe measurements performed with and without the magnetic field, are shown in Fig.7. It can be easy seen that the half-width of the leakage aperture of plasma ions escaping through the point cusps, was about 0.9 cm. This means that the leakage aperture was somewhere between the hybrid gyroradius $/r_e r_i/^{1/2}$ for carbon ions and the ion gyroradius r_i for protons. This is principally consistent with the existing theory and results of other laser experiments carried out with a standard spindle-cusped configuration [6]. In order to check whether it is possible to reduce the leakage aperture in the SM trap below the hybrid gyroradii, it is necessary to perform a detailed mass- and energy-analysis of escaping ions. An improvement in spherical symmetry of the experiment as well as measurements for larger values of β, are also required. Further investigations on these subjects are being continued.

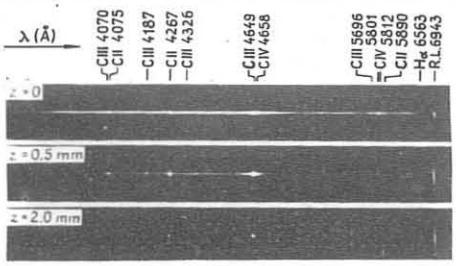

Fig.5.

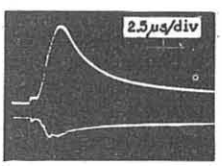

Fig.6.

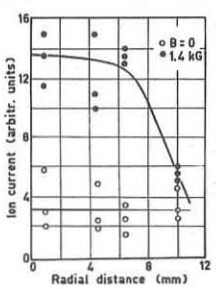

Fig.7.

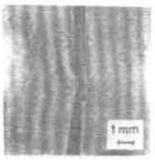

Fig.4.

1. M.Sadowski, Phys. Lett. 25A, 695 /1967/; 27A, 435 /1968/.
2. M.Sadowski, J. Plasma Phys. 4, 1 /1970/.
3. R.Limpaecher, R.K.MacKenzie, Rev. Sci. Instr. 44, 726 /1973/.
4. M.Sadowski et al., Proc. 5th European Conf., Grenoble 1972.
5. M.Sadowski et al., Proc. 6th European Conf., Moscow 1973.
6. A.Kitsunezaki et al., Phys. Fluids 17, 1895 /1974/.
7. World Survey of Major Fac. in CFR, Nucl. Fusion Suppl. 1976.
8. K.Czaus, M.Sadowski, Proc. 6th Intern. Conf. on Magnet Techn., Bratislava 1977 /to be published/.

ENERGY DEPOSITION IN NEUTRAL HYDROGEN BY AN INTENSE RELATIVISTIC ELECTRON BEAM

A.K.L. Dymoke-Bradshaw, A.E. Dangor, J.D. Kilkenny, L.J. Phillips
Blackett Laboratory, Imperial College, London, United Kingdom

Abstract: Measurements of the energy dissipated by the return current induced when an intense relativistic electron beam is injected into neutral hydrogen are compared with the observed plasma diamagnetism and the electron energy obtained by laser scattering. These show that there is either a high energy electron tail or that the ions are heated preferentially.

In a previous paper (1) we reported that the energy deposited in a plasma by a relativistic electron beam injected into neutral hydrogen was primarily due to return current dissipation, the evidence being a close correlation between W_{OHM} ($= \int J_p . E_z . dt$) and W_{DL} the plasma diamagnetic energy. In this paper we report further evidence for this and measurements of low $\alpha (= 1/k_s \lambda_D)$ scattering to determine the electron number density and the low energy electron velocity distribution. Simultaneous W_{OHM} measurements were performed. The radial distribution of B_θ outside the beam channel has been investigated by a double probe arrangement.

The beam, whose parameters, as in (1) are 350kV, 50kA, 100ns, 2 cm diameter, is injected through a 12.5μm aluminised mylar foil into a 7.6 cm diameter chamber immersed in an axial magnetic field of ~ 1.5 Tesla. Filling pressures varied from 0.1 to 1 Torr hydrogen. Scattering was performed with a 400MW ruby laser incident perpendicular to the beam. The light scattered perpendicular to both the laser and the electron beam was spectrally resolved with a 7 channel polychromator over 12 nm on the blue side of 694.3 nm. Scattering was restricted to filling pressures in the range 0.1 to 0.2 Torr where high values of W_{OHM} have been obtained. B_θ probe measurements indicate that the axial current outside the beam channel is small, typically 60 amps/cm^2 at 0.1 Torr, compared with 8kA/cm^2 in the beam channel. This confirms the assumption made for calculating W_{OHM} in (1), that the return current is confined to the beam channel. Analysis shows that the resistivity is 10 Ω-cm, giving $n_e \lesssim 10^{-4}\, n_{neutral}$ outside the beam channel. This resistivity is a factor 5 times larger than can be derived from data in (2).

Results of some shots are summarised in Table 1 and some typical scattering data shown in Figure 1. This shows a non-Maxwellian velocity distribution at early times, which has been interpreted as a two temperature component plasma. Figure 1 also shows that at late time relaxation to a Maxwellian is observed. Ionization greater than 20% was observed in all shots, increasing to $\gtrsim$50% at late times. The observed energy W_{the} (including ionization) in the electron velocity distribution sampled in the scattering experiment is ~ 20% of W_{OHM} as can be seen in the table. The largest value of W_{OHM} measured was found to be associated with a low degree of ionization.

Measurements of W_{OHM} and peak W_{DL} as shown in the Table are in reasonable agreement. So is their temporal variation as shown in (1). This indicates that there is no rapid loss of energy from the system due to radiation or thermal conduction. The discrepancy in the observed energies, W_{OHM} and W_{the}, must be due either to energetic ions or to a very high velocity tail in the electron distribution.

Electron tails have been predicted, (3) and there is some experimental evidence for this from X ray emission, (2). However, spectral profile measurements of the H_α and H_β emission lines which were previously reported, (1) suggest that the energy could be in the ions. The lines have typical f.w.h.m. of 0.56 nm. H_α broadening is a factor of 10 larger than that due to thermal Stark effects for the measured n_e. If the broadening is interpreted as a Doppler width this corresponds to energies $\gtrsim$200 ev thus accounting for the observed discrepancy. A high α scattering experiment is in progress to measure the ion temperature to check this.

References:

(1) A.K.L. Dymoke-Bradshaw, A.E. Dangor, J.D. Kilkenny 6th IAEA Conference on Plasma Physics and Controlled Nuclear Fusion September 1976

(2) D.S. Prono et. al., Physics International report PIFR-557 February 1975

(3) L.E. Thode and R.N. Sudan Phys. Rev. Lett. 30, 732 (1973)
K. Papadopolous Phys. Fluids, 18, 1769 (1975)

TABLE 1.

Shot No.	W_{OHM} eVcm^{-3}	W_{DL}(max) eVcm^{-3}	$n_e(t)$ cm^{-3} (ns)	T_{e1} eV	T_{e2} eV	W_{the} eVcm^{-3}
1	$7.0 .10^{17}$		$5.0 .10^{15}$ (170)	5.2		$1.1 .10^{17}$
2	$2.3 .10^{18}$		$1.6 .10^{15}$ (120)	0.9	10.7	$3.6 .10^{16}$
3			$5.0 .10^{15}$ (144)	3.4	8.4	$1.2 .10^{17}$
4	$7.5 .10^{17}$	$5.5 .10^{17}$				
5	$1.4 .10^{18}$	$1.2 .10^{18}$				

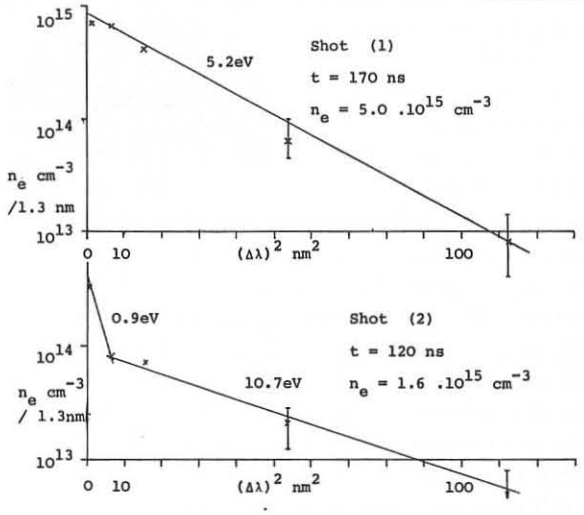

Fig. 1 Showing scattered light spectra of table 1.

PLASMA HEATING AND ION ACCELERATION BY A RELATIVISTIC ELECTRON BEAM - REB ACCUMULATION

P.Šunka, K.Jungwirth, I.Kováč, V.Piffl, J.Stöckel, J.Ullschmied
Institute of Plasma Physics, Czechoslovak Acad. Sci., Prague 9

ABSTRACT: Results on REB interaction with an inhomogeneous magnetized plasma are reported. The maximum efficiency of plasma heating is found if a virtual cathode is created near the end of the system. In the virtual cathode regime also partial reflection and accumulation of beam electrons and ion acceleration from a free plasma boundary is observed.

Measurements were performed on the improved REBEX machine [1] (I_b= 10-20 kA, U_b= 450 kV, Q_b= 150-300 J, t_i= 70 ns). A gun (aperture diameter 7cm) placed 30cm apart the foil anode fills the whole interaction region (L=210 cm) with a hydrogen plasma ($n \lesssim 3.10^{13}cm^{-3}$) only after a time delay of 60μs. For time delays between plasma and beam injection $t_d \lesssim$ 35μs the plasma density remains negligible near the collector.

PLASMA HEATING

Plasma energy content Q after the beam injection is measured by three diamagnetic loops (placed at z=50,100,140 cm) at various t_d. In Fig.1 the z-dependence of transverse plasma energy $nE_\perp S$ is shown for t_d=40,80,200μs. Assuming an isotropic heating the REB-plasma energy coupling efficiency of about 50%,30%,20%, respectively, is achieved. As return current heating is negligible in our system ($I_b < I_A$, $L \ll t_i v_b$) excitation of strong plasma waves near the upper hybrid ($\omega_o^2 \approx \omega_{pe}^2 \gg \omega_{ce}^2$) represents the only effective channel for the REB-plasma energy coupling. Energy of these waves (localized within the beam channel) is rapidly absorbed by plasma electrons via parametric-decay instabilities. Rough estimates based on [2,3] suggest for the plasma core (3cm in diameter, $n=3.10^{13}$ cm^{-3}) heated by a propagating beam ($n_b/n=10^{-2}$) the following typical values: $t_i \nu_{eff} \approx 16\pi nE_\perp/E_o^2 \gg 1$, where the wave electric field $E_o \approx 100$ kVcm^{-1}, threshold plasma length $L_{th} \approx 50$ cm, $nE_\perp \approx 3.10^{17}$eVcm^{-3}, $\nu_{eff} \approx 4.10^9$ s^{-1}, Q = 0,2Q_b.

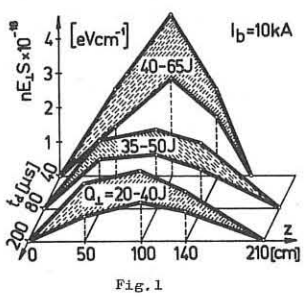

Fig.1

By shortening t_d ($t_d \lesssim 80$ μs) the heating efficiency increases regardless the increase in the plasma density n and in its inhomogeneity dn/dz. The highest efficiency is measured at t_d=40μs when a virtual cathode is created and a significant part of the beam electrons multipasses the system. For t_d<40μs we were not able to determine the plasma energy content as strong r.f. cscillations ($\omega \lesssim 6.10^9$s^{-1}) appear on diamagnetic loops placed in the virtual cathode region. Signal from the loop at z=50cm, however, continues to grow. The maximum value of $nE_\perp S \approx 5.10^{18}$eVcm^{-1} is reached for magnetic fields B_o=4-6kG and 10μ thick aluminized mylar anode foil. (Most measurements were done with 30μ Al foil at B_o= 4,7 kG.)

The plasma core is overheated at the end of the beam injection ($\beta_i = 8\pi nE_\perp/B_o^2 \gtrsim 1$) and tends to expand radially towards a new pressure equilibrium. If a dense plasma is heated rapidly ($f_{ac} \lesssim \min(f_{ci}, 1/2t_i)$) a strong magnetoacoustic wave with frequency $f \approx f_{ac}$ is expected to be excited by the expansion. Its presence is demonstrated by regular damped oscillations of the diamagnetic signals (Fig.2). By decreasing the plasma density f_{ac} approaches the ion gyrofrequency f_{ci} and the oscillations become strongly damped. Then, energy of the magnetoacoustic wave $Q_{ac} \approx \beta_i Q/2(2+\beta_i)$ should be effectively absorbed by plasma ions and heat them to keV energy. (For $n=5.10^{13}cm^{-3}$, B_o= 4,7kG and $nE_\perp S=5.10^{18}$eVcm^{-1} it is $\beta_i=3/2$, $Q_{ac} \approx Q/5$, el. field E_{ac}=300Vcm^{-1}.)

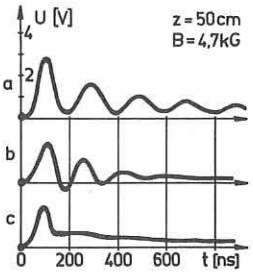

Fig.2: Oscillograms of diamagnetic signals $nE_\perp S$
a) t_d=40μs, $n=6.10^{13}cm^{-3}$
b) 60μs, $4.10^{13}cm^{-3}$
c) 160μs, $2.10^{13}cm^{-3}$

Measurements of fast neutrals escaping radially indicate that the ions are heated up to keV "temperatures". At higher densities an appreciable part of ions is heated to several hundreds eV, whereas at lower densities only a small part of ions is heated, but to higher energies (T_i=8-10 keV) Ions can get comparable energy also in radial electric fields arising in the hot electron plasma due to its expansion as well as due to longitudinal losses of overthermal electrons.

ACCUMULATION OF REB ELECTRONS AND ACCELERATION OF IONS

To detect the accumulated beam electrons X ray bremsstrahlung from the foil anode was monitored. It increases with the decreasing plasma length. The maximum observed enhancement was about 6times for the foil-terminated plasma and about 3times for a longer plasma column with a free boundary relative to the beam propagation mode. A similar result was obtained by measuring the current from a foil placed closely (2mm) to the terminating foil, indicating that the number of fast electrons increases 3-4times. The multipassage of these electrons through the anode foil results in an increase in the net diode current.

In the virtual cathode regime energetic ions (E_i > 100keV) accelerated from a free plasma boundary both axially and radially were detected. The total number of axially accelerated ions $N_{i\parallel}$ as well as their energy $E_{i\parallel}$ is maximum if the beam multipasses a short plasma column (L_p<50cm, max $E_{i\parallel}$=1MeV, $N_{i\parallel}$ = 2.10^{13} detected 2m downstream). If the plasma boundary becomes smooth (L_p>50cm) the radial dependence of potential in virtual cathode region causes the radial acceleration of ions to be more effective than the longitudinal one. The initial focusation of ions towards the axis leads to a drastic change of the potential distribution and ions with energies comparable to eU_b can then be ejected. Bursts (20ns) of such ions with transverse energy $E_{i\perp}$>400keV were registered. The total number of ions accelerated from a smooth boundary should exceed significantly that from a sharp boundary. Thus, at least for low density plasmas, this direct conversion of energy from REB to the plasma ions could be of practical interest.

REFERENCES

[1] P.Šunka et al.: Paper G2-2, Plasma Phys. and Contr. Nucl. Fusion Research, Berchtesgaden, 1976
[2] P.Šunka, K.Jungwirth: Czech. J. Phys. B25 (1975) 404
[3] A.A.Galejev et al.: Zh.exp.teor.Fiz. 72 (1977) 507
[4] C.Ekdahl et al.: Phys. Rev. Lett. 33 (1974) 346
[5] Yu.I.Abrashitov et al.: Zh.exp.teor.Fiz. 66 (1974) 1324
[6] D.D.Rjutov et al.: Zh.exp.teor.Fiz. (Lett) 24 (1976) 19
[7] D.A.Phelps et al.: IEEE Trans. Plasma Sci. PS-4 (1976) 246

THE ENERGY LOSS OF A RELATIVISTIC ELECTRON BEAM MEASURED BY MEANS OF A SCINTILLATOR AND A PHOTODIODE

B. Jurgens, P.H. de Haan, H.J. Hopman and P.C. de Jagher

Association EURATOM-FOM

FOM-Instituut voor Atoom- en Molecuulfysica, Kruislaan 407, Amsterdam/Wgm, The Netherlands

Abstract: A plastic scintillator and a photodiode have been used to obtain the energy loss of a 500 keV, 500 A REB being injected into a plasma, having $10^{11} < n_e < 10^{12} cm^{-3}$. There is good agreement between this experiment and recent theory predicting the energy loss by beam plasma instabilities at ω_{pe}.

Introduction: Plastic scintillators convert about 3% of the kinetic energy of a single electron into light, provided the electron is stopped within the scintillator. The light output per electron is linear with energy in the range from 120 keV [1] to over 100 MeV [2,3]. The light intensity is proportional to the number of electrons striking the scintillator per unit of time, thus in total with the power of an incident electron beam. We measured the photon output as a function of time. The method is similar to one described in [4].

Above a certain power density the photon production behaves nonlinearly and tends to saturate [5]. Literature gives no specific data for the type of scintillator (NE104) which we used. We therefore did some measurements ourselves. Because of the insulating properties of the scintillator plastic charge accumulation and internal breakdown can occur, at high current densities. We found for our 500 keV beam that 5 A/cm^2 corresponding to 10^{-7} C/cm^2 per shot gives a safe upper level for both effects. Since the current density in our beam-plasma experiment exceeds this level we had to reduce it. This was done by spreading part of the beam over a larger area.

Experimental setup: The experimental setup [6,7] consists of a 260 cm long 3 cm diameter plasma column produced by a microwave source (17 in fig. 1) at 2.45 GHz. The plasma is confined in a 0.2 T magnetic mirror field. The plasma density ranges from 10^{11} to $10^{12} cm^{-3}$. A 500 keV, 500 A, 20 ns, 3 cm diameter electron beam is injected (at z = 0) into the plasma through a 30 μm Ti foil and leaves the plasma (at z = 260) through a 30 μm Ti foil (19). The beam is stopped on a 3 mm thick Pb collector (21) having a hole of 3 mm diameter on axis. Part of the beam passes the collector and expands in the diverging magnetic field, before it strikes the scintillator (23). A collector (22) intercepts half of the beam just in front of the scintillator to measure the current. The other half of the beam produces light that is measured by a photodiode (24). Time resolution is about 7 ns. Since faster variations occur we integrate the signals over the beam pulse duration. The photo diode signals are calibrated with the same beam being injected into vacuum. In this case we know the beam energy from measurements with a magnetic energy analyser [8].

Experimental results: When we compare the integrated current and light signals measured if we inject the beam either into vacuum, or into plasma, we notice that in the latter case both charge and light output have changed. A change in light output is generally the result of a change in the number of electrons striking the scintillator and a simultaneous change in the energy of these electrons. To show both effects the integrated light intensity E has been plotted against the charge Q (see fig. 2). In this figure (X) represents shots into vacuum and other symbols originate from different plasma densities. At each condition several shots are shown separately to give an impression of the shot to shot variations. In fig. 2 a pure energy loss gives a shift (vacuum compared to plasma) downwards, whereas a decreasing number of electrons give a shift in the direction of the origin. The average energy of the electrons in a particular shot is given by the quotient $\varepsilon = E/Q$. If the beam loses energy in the plasma then ε_p, the average energy of the beam electrons after having passed through the plasma, will be smaller than ε_v, the average energy after passing the vacuum. In fig. 2 the solid lines give the relation between E and Q for fixed ε.

Discussion: All our measurements are summarized in one figure by plotting the relative energy loss against $S = \beta^2 \gamma \sqrt[3]{n_b/2n_e}$, the strength parameter of Thode and Sudan [9]. The energy loss is normalized to the total beam energy, $n_b \gamma m_e c^2$, for comparison with theory. The measured energy loss is shown in fig. 3 for a 30 μm Ti foil (X) and a 10 μm stainless steel foil (O). Solid lines represent the theory of Thode [10]. This theory predicts the beam energy losses due to a hydrodynamic beam plasma instability at the plasma frequency in case the velocity vectors of the beam electrons have an angular distribution. Such a distribution arises from scattering in the anode foil of the diode which produces the beam. The energy loss depends on the mean scattering angle $\bar{\theta}$, defining the angular width of the velocity distribution. Moreover it depends on the beam energy and the beam to plasma density ratio. For our experimental parameters (viz. $\gamma = 2$, $\bar{\theta} = 28^o$ for a 30 μm Ti foil and $\bar{\theta} = 20^o$ for a 10 μm stainless steel foil) the predicted energy loss, according to equation (11) of ref. [10], is plotted against S. Averaging over all measurements we find $\Delta E_{experiment}/\Delta E_{theory} = 0.6$ both for the 30 μm Ti foil and for the 10 μm stainless steel foil. The foil thickness has indeed the expected influence on the energy loss. Agreement between experiment and theory is within a factor of 2 on the average.

REFERENCES

[1] Von Schmeling, Zeitschr.für Physik 160 (1960) 520.
[2] Evans and Bellamy, Proc.Phys.Soc. 74 (1959) 483.
[3] Gooding and Pugh, Nucl.Instr.& Methods 7 (1960) 189.
[4] Ellis R.E. and Carllson N.W., Rev.Sc.Instr. 32 (1961) 1367.
[5] Stevens J. and Knowlen R.B., IEEE Trans.on Nucl.Sci. NS-15 (1968) 136.
[6] Jurgens B., Sinman A., Hopman H.J., de Jagher P.C., VII Eur.Conf.on Contr.Fusion and Pl.Phys., Lausanne 1975.
[7] Jurgens B., Hopman H.J., de Jagher P.C., Sinman A., Vrijdaghs J.B., Plasma Physics 18 (1976) 821.
[8] Jurgens B., Hopman H.J., de Haan P., de Jagher P.C., Kistemaker J., VI Intern.Conf.on Pl.Physics and Contr.Nucl.Fusion Research, Berchtesgaden, 1976.
[9] Thode L.E. and Sudan R.N., Phys.Rev.Lett. 30 (1973) 732.
[10] Thode L.E., Phys.of Fluids 19 (1976) 831.

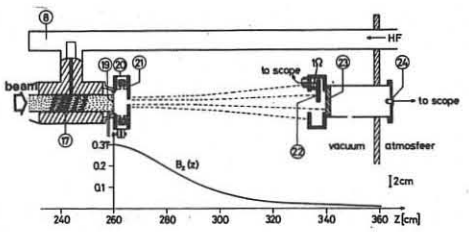

Fig. 1 - Terminating section of the beam-plasma experiment. The beam comes from the left after travelling through a 2.4 m long plasma column. Numbers are referred to in the text.

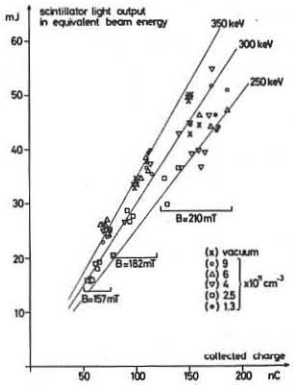

Fig. 2 - Time integrated scintillator response on single shots of the beam, for 3 values of the magnetic field strength.

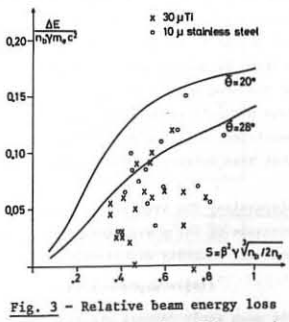

Fig. 3 - Relative beam energy loss as a function of beam and plasma parameters. $\Delta E = \varepsilon_v - \varepsilon_p$; $n_b \gamma m_e c^2$ is the total beam energy; $\bar{\theta}$ is the mean scattering angle.

RELATIVISTIC ELECTRON BEAM SCATTERING DUE TO BEAM-PLASMA INTERACTION

P.H. de Haan, B. Jurgens, H.J. Hopman and P.C. de Jagher

Association EURATOM-FOM

FOM-Instituut voor Atoom- en Molecuulfysica, Kruislaan 407, Amsterdam/Wgm., The Netherlands

Abstract: The measurement of a plateau like energy distribution of a 550 keV, 500 A relativistic electron beam, having interacted with plasma, suggests saturation of beam-plasma instabilities by beam trapping. The mean angle, $\bar{\theta}$, between the velocities of the beam electrons and the magnetic axis, with $\bar{\theta} \approx 42^{\circ}$ are obtained from the total current to the energy analyser.

Experiment: A relativistic electron beam is injected into a microwave created plasma of $2.5 \times 10^{17} m^{-3}$. The plasma column is 3 cm in diam., 2.6 m long and confined by a magnetic field of 0.15 T. The beam has a maximum energy $eV_b = 550$ keV, a maximum current $I_b = 500$ A, a pulse duration of 20 ns (FWHM) and a diam. of ca. 2 cm. The plasma is prevented from entering the diode by a 30 μm Ti foil. At the end of the column, the beam is stopped on a collector with a small opening on the axis of 3 mm diam. Through this hole part of the beam reaches an energy analyser, after travelling through a drift space of 1.2 m.
The 180° magnetic analyser is equipped with pin diodes as current detectors. A time resolution better than 2 ns permits the measurement of a time resolved beam energy spectrum.
Only electrons with their velocity vector within an angle $\theta_a = 1^{\circ}$, with respect to the guiding magnetic field are accepted by the analyser.

Experimental results: In fig. 1 we show beam energy spectra, integrated over 3 ns long time intervals, for two interesting times, t = 26 ns, at the maximum of V_b and I_b, and t = 35 ns. The spectrum, obtained when the beam passes through vacuum (thick line) is compared with the spectrum of the beam, having interacted with the plasma (dotted area). By summing the measured current over all energies, we obtain the time dependence of the total current that reached the analyser. Fig. 2 gives both the current in the vacuum case (thick line) and in the plasma case (dotted area).
We note from fig. 1, that at t = 26 ns the narrow peak of 550 keV electrons in the vacuum case is spread out into a broad energy spectrum, ranging from 120 to 700 keV.
The same feature repeats at t = 35 ns, when the beam energy eV_b has reduced to 300 keV. Secondly, the spectral area is generally smaller in the plasma case than in the vacuum case (fig. 2). Because a current is a product of density and velocity, both retardation of the beam particles and scattering out of the 1° velocity cone, accepted by the analyser, contribute to this effect. By averaging over the energy spectrum the mean energy and velocity of the beam electrons can be obtained, as a function of time [2]. From the mean particle velocity and the current we can calculate the density of beam particles, that are accepted by the analyser. Fig. 3 presents the ratio of that beam density in the plasma case, n_p, and the vacuum case n_v.

Discussion: The beam electrons are scattered in the 30 μm Ti foil at the entrance of the plasma chamber. A plausible form for the angular part of the beam velocity distribution is [1],

$$f(\theta) \propto \exp(a \cos \theta). \qquad (1)$$

The mean angle between the beam electron velocities and the magnetic axis $\bar{\theta}$, is then given by $\bar{\theta} = \sqrt{2/a}$. Diamagnetic loop measurements give a mean angle due to scattering in the foil, $\bar{\theta}_f = 30^{\circ}$. After interaction with the plasma $\bar{\theta}$ has changed [3]. We call this mean angle between the velocity vector and the axis $\bar{\theta}_p$. Assuming that the scattering of beam electrons in the plasma is isotropic, i.e. eq. (1) remains valid, then the number of particles in the velocity cone, θ_a, accepted by the analyser, is determined by the mean angle. For $\theta_a \ll \bar{\theta}_f, \bar{\theta}_p$, eq. (1) leads to the simple relation

$$\bar{\theta}_p = \bar{\theta}_f \sqrt{n_v/n_p} \; . \qquad (2)$$

In fig. 3 we converted the ratio n_p/n_v by means of relation (2) to a mean velocity angle $\bar{\theta}_p$. We observe a strong fluctuation in $\bar{\theta}_p$ suggesting a rapid succession of the instabilities, with a 10 ns repetition rate. Large angles $\bar{\theta}_p$ coincide with a strong broadening of the energy spectrum.
For t > 80 ns the beam current is very small and data are no more reliable. For t < 60 ns, the time averaged value of $\bar{\theta}_p$ is ca. 42°, which agrees with time averaged measurements of the angular distribution by Greenspan [4].
In case the unstable wave is saturated by trapping of beam electrons, Thode [1] calculated the maximum wave amplitude that can be expected. Inserting values of our experimental parameters, n_e, I_b, V_b, at t = 26 ns, we find the theoretical amplitude of the electric field to be E = 8.4 MV/m. For an initial energy of 300 keV, at t = 35 ns, we find E = 4.2 MV/m.
The width of the broad beam distribution, resulting from trapping of the beam, is determined by the wave field, and the initial beam velocity v_b and wave phase velocity v_ϕ. Dispersion theory gives $v_\phi = 0.9\, v_b$. From a maximum energy of 700 keV, obtained from the distribution of fig. 1, we find the wave electric field at t = 26 ns, E = 1.8 MV/m. From the broadening of the spectrum at t = 35 ns we find, E = 1.6 MV/m. Thus, the measured value for the electric field is smaller than the theoretical prediction.
From other experiments we know that strong beam plasma interaction is limited to the first 50 cm [3,4]. Over this length the trapped beam electrons execute at most two bounce oscillations in the unstable wave. This short length may be the explanation for the fact that the measured electric field is below the predicted value. The bumpiness of the energy spectrum (fig. 1), too, could be caused by the short coherence length of the instability.

REFERENCES

[1] L.E. Thode, Phys.Fluids, 19 (1976) 305, 831.
[2] B. Jurgens, P.H. de Haan, H.J. Hopman, P.C. de Jagher, to be published.
[3] B. Jurgens, H.J. Hopman, P. de Haan, P.C. de Jagher, J. Kistemaker, Proc.6th Int.Conf.Plasma Phys.and Contr.Nucl.Fusion Res., Berchtesgaden (1976), to be published.
[4] M.A. Greenspan, Ph.D. Thesis, Cornell University, Ithaca, N.Y. (1976).

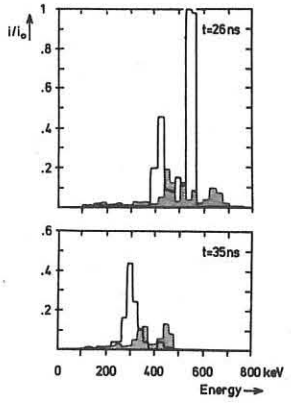

Fig.1-Beam energy distribution for two interesting times.

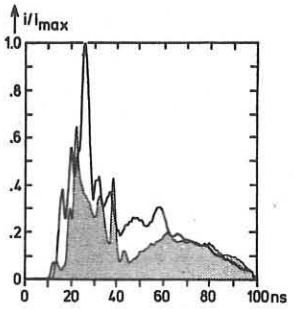

Fig.2-Total current reaching the analyser.

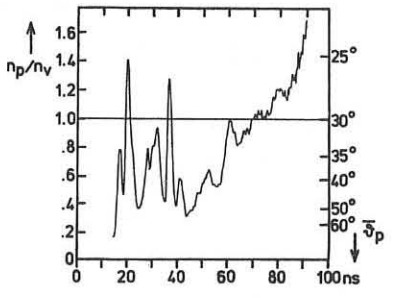

Fig.3-The ratio n_p/n_v, c.q. mean angle between the velocity vector and the axis, $\bar{\theta}_p$.

RETURN CURRENT DRIVEN INSTABILITIES IN A RELATIVISTIC ELECTRON BEAM - PLASMA SYSTEM

P. Vrba

Institute of Plasma Physics, Czechosl. Acad. Sci.,

Prague 9, Czechoslovakia

Abstract: The numerical analysis of general dispersion relation for the charge and current compensated relativistic electron beam and the plasma leads to the new synchronism predictions. The return current's slow space charge wave and return current's slow cyclotron wave are synchronous with the ion plasma wave.

The dispersion relation in electromagnetic approximation for monoenergetic relativistic electron beam - cold plasma system was derived. Plasma waveguide confinement and the presence of external magnetic field were taken into account. Our dispersion relation contains certain terms more than Adlam's one [1]. These terms result from non zero oscillating magnetic field and from full charge and current compensation presumptions. The evaluation of complex roots of dispersion relation was get by the numerical solution of equivalent matrix eigenvalue problem. Resulting dispersion characteristics of system studied can be seen from Fig.1. Characteristic parameter α is the ratio of beam electron density n_0 and plasma ion density N_0, β is the ratio of beam electron velocity u_0 and velocity of light c, B_c is normalized magnetic flux-density, Ω is normalized complex frequency, K and T are normalized longitudinal and transversal wave vector, repectively.

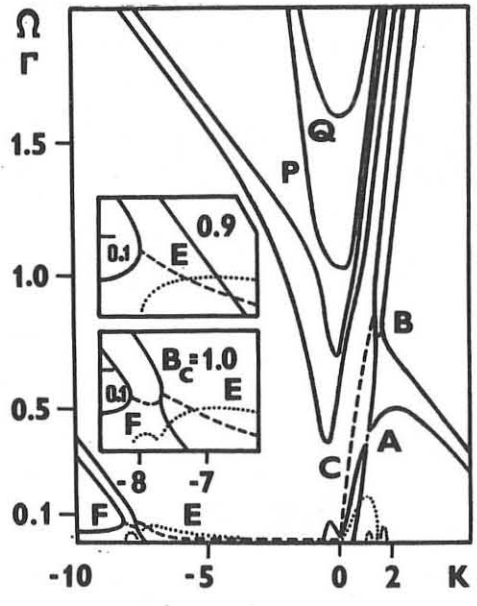

Fig.1: Dispersion characteristics of cold relativistic electron beam - plasma system, charge and current compensation supposed $\alpha = 0.138$, $\beta = 0.82787$, $T = 0.39$, $B_c = 1$ ($B_c = 0.9$). Dashed and dotted lines represent the real and imaginary parts of the frequency Ω , respectively.

There are two salient diretions in K-Ω plane. One of them corresponds to the velocity of relativistic eletrons, the other is the direction given by the velocity of return current. Well known anomalous Doppler effect instabilities ($\Omega - \beta K \simeq -\sqrt{1-\beta^2}\beta_c$) and Cerenkov instability ($\Omega - \beta K \simeq 0$) are excited in regions A,B and C respectively. Coupling between the return current's slow space charge wave and ion plasma wave in a wide region E results in so called Bunneman instability ($\Omega + \frac{\alpha}{1-\alpha}\beta K \simeq 0$). The maximal value of increment $\Gamma_{max} \simeq 2\,\Omega_{pi}$ is reached in the vicinity of ion plasma frequency Ω_{pi}. An interesting interaction occurs in region F, where the return current's slow cyclotron wave is synchronous with the ion wave ($\Omega + \frac{\alpha}{1-\alpha}\beta K \simeq -\beta_c$) Owing to this synchronism the low frequency short wavelength electromagnetic wave ($Re\,\Omega \doteq 2{,}5\,\Omega_{pi}$, $K \gg 1$) could be excited. Whenever $\Omega_{ce} < \Omega_{pe}$, the unstable region F disappears (see the detail sketches for $B_c = 0.9$ and $B_c = 1$, Fig.1.). In a case of $\Omega_{pe} < \Omega_{ce}$ especially when the external magnetic field increases (or $\beta_{ep} = -\frac{\alpha}{1-\alpha}\beta$ decreases) the unstable region F is shifted to very high value of K, see Fig.2.

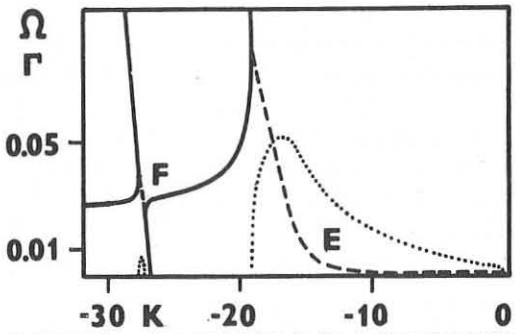

Fig.2: Dispersion characteristics in the region of synchronism of ion wave with return current's slow waves. $\alpha = 0.1$ $\beta = 0.5$, $T = 2$, $B_c = 1.5$

$\alpha = 0.138$, $\beta = 0.82787$, $(\beta_{zp} = -0.133)$
$B_c = 1$, $T = 0.39$

Region	Re Ω	K	Γ	v_{ph}/c
A	0.391	1.11	0.008	0.352
B	0.787	1.61	0.044	0.489
C	0.736	1.07	0.167	0.688
E	0.034	-7.00	0.052	-0.0049
F	0.058	-7.90	0.020	-0.0074
$B_c = 0.9$				
E	0.039	-7.20	0.050	-0.0056

Representative numerical results are summarized in the table. Maximal values of increment Γ for all unstable regions and appropriate values of real part frequency $Re\,\Omega$ longitudinal wave vector K and normalized phase velocity $\beta_{ph} = \frac{v_{ph}}{c}$ are there compared. It can be seen that the maximal increment Γ of Cerenkov instability (region C) is three times greater than Bunneman's one (region E), in this case.

I would like to express my thanks to dr.P.Šunka, dr.K.Jungwirth, for valuable comments and to dr.J.Lacina, P.Jarošová, J.Schrötter and Š.Kořbel for numerical evaluations.

References

[1] J.H.Adlam, Plasma Physics 13,/1971/,329-345

[2] G.Küppers, A.Salat, H.K.Wimmel, Plasma Physics 15, /1973/, 429-439

RECENT PROGRESS ON THE FIELD-REVERSING ELECTRON RING EXPERIMENTS AT CORNELL

H. H. Fleischmann, H. A. Davis, S. C. Luckhardt, and D. J. Rej
Laboratory of Plasma Studies, Cornell University
Ithaca, New York 14853, U.S.A.

Abstract: Stable field-reversal times in RECE-Christa have been extended to over 450 μsec, and field-reversal has been attained also by combining two rings of 44 and 68% strength. In RECE-Berta, the addition of quadrupole components leads to loss enhancement over the normal collisional decay.

As envisioned in the Astron and Ion Ring Compressor[2] schemes[1,2] field-reversing rings of high-energy ions trapped in a mirror may be used for plasma confinement and heating. Similarly, field-reversal has been proposed for end closure in mirror machines. In the respective Livermore Astron experiment using relativistic electrons, rings with 40% of field-reversal strength were obtained,[4] but a combination ("stacking") of rings to attain full field-reversal appeared to fail. On the other hand, stably decaying, field-reversing electron rings have been obtained in the three separate RECE-experiments at Cornell,[5] with field-reversal times ranging up to 200 μsec. The present paper is to report a further extension of the reversal time in RECE-Christa and the attainment of field-reversal via a successful stacking of electron rings. In addition, further results on a multipole stabilization[6] of the precessional mode in RECE-Berta are reported.

As described earlier,[5] in RECE-Christa (Fig. 1) an intense electron beam pulse (typically 2.5 MeV, 30 kA, 80 nsec) is injected nearly perpendicularly into a magnetic mirror trap ($B_o \approx 500$ Gauss, 300-700 mTorr H_2 filling) augmented with a toroidal magnetic field $B_\theta \approx (1 - 2)B_o$. In order to extend the collisionally determined field-

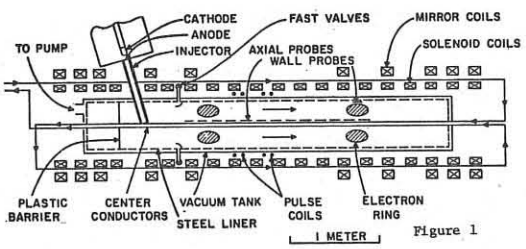

Figure 1

reversal times (so far up to 200 μsec), a number of changes were made so that rings trapped in a transient gas cloud near the injector could be moved axially into a high-vacuum region. These changes (Fig. 1) included exchanging the normal copper liner (L/R-time ≈ 15 μsec) with a stainless steel mesh (7 μsec), the addition of four pulsed gas valves (total output ≈ 150 at·cm^3) and the addition of two pulsed field coils (1.2 kHz, $\Delta B \leq \pm$ 50 Gauss). Experiments have been started recently. First, trapping experiments were performed without ring movement (using crowbarred pulse coils producing two separate field minima, and with a relatively large delay (1.8 msec) between gas puffing and beam injection so that a median gas pressure (30-100 mTorr) prevailed at the downstream field minimum at the time of injection. In this case, often two separate rings were trapped in the field minima. Due to the lower gas pressure, the decay rate of the downstream rings was reduced, and strong rings ($\delta B/B_o \sim 150\%$) with field reversal times of up to 450 μsec have been obtained (Fig. 2: 200 μsec/div, 250 Gauss/div.). The initial decay of these layers is slower than in our earlier experiments by about a factor 3 in rough agreement with the pressure reduction. The decay acceleration after about 800 μsec is caused by a rapid increase in background pressure.

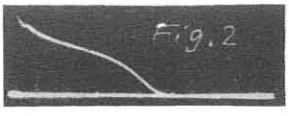

Ring moving experiments were performed both with steady gas pressure and with gas puffing. In both cases, (Fig. 3a and b) the rings moved over distances of up to 1.5 m, i.e. about 10 times the ring radius. Average ring speeds of 1-2 cm/ sec are in good agreement with theoretical expectations, with weaker rings moving faster than strong ones. The mentioned simultaneous trapping of two separate rings provided the opportunity to investigate the stacking of rings under the conditions of our experiment. As shown in Fig. 3c, two strong rings (in this case 44% and 68%) readily combine forming a field-reversing ring ($\delta B/B_o \approx 106\%$). This constitutes a marked improvement over the Livermore experiment in which only layers of less than 25% could be obtained and maintained by stacking.

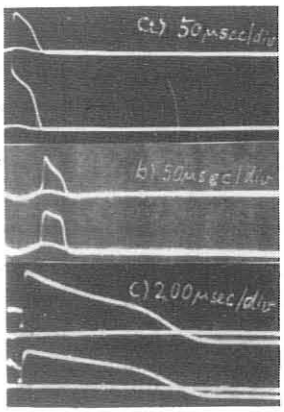

Fig. 3

On RECE-Berta, further experiments were performed on the precessional ring stabilization by additional multipole Ioffe fields. The enhanced decay of strong rings in quadruple Ioffe fields observed earlier was reconfirmed (Fig. 4a), and investigated in more detail. It appears that the critical ring strength at which the mini-dumps occur is independent of the quadrupole field strength (Fig. 4b) and of other external parameters. The decay anomaly factor (relative to the normal collisional decay rates) observed for rings with strengths above these critical levels is strongly dependent on the quadrupole field (Fig. 4c), but independent of the pressure. Overall, the results appear consistent with an orbital resonance of the fast electrons, in which case such losses may occur quite generally in near field-reversed rings in quadrupole stabilized mirrors, as for instance in the 2XIIB experiments. First experiments with hexapole stabilization indicate about normal losses.

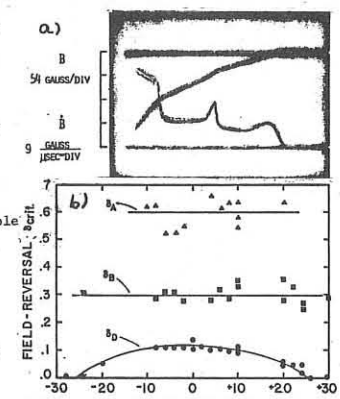

Fig. 4

*Work supported by US-ERDA under Contract EY-76-S-02-2319.*000.

1. N. C. Christofilos, 2nd U.N. Intern. Conf. Peaceful Uses of Atomic Energy, 1958, Vol. 32, p. 279; J. R. M Nally, Jr., ORNL 3392 (1962),

2. H. H. Fleischmann, Conf. Electrost. and Electromag. Confinement of Plasmas, N. Y. Acad. Sci. New York, March 1974.

3. W. C. Condit, T. K. Fowler, and R. F. Post, UCRL-52008 (1976).

4. R. J. Briggs et al., Phys. Fluids 16, 1934 (1973); H. L. Berk, and L. D. Pearlstein, Phys. Fluids 15, 2396 (1972); N. C. Christofilos et al., 4th Intern. Conf. Plasma Physics and Contr. Fusion, Madison, 1971 Paper CN-28/A-9.

5. J. J. Bzura et al., Phys. Rev. Letters 29, 256 (1972); R. E. Kribel et al., Plasma Physics 16, 113 (1974); H. A. Davis et al., Phys. Rev. Letters 37, 542 (1976) and others.

6. D. M. Woodall et al., Phys. Rev. Letters 34, 260 (1975); and S. C. Luckhardt et al., Phys. Rev. Letters 35, 1758 (1975).

SPACE CHARGE NEUTRALIZATION OF ION BEAMS

A J T Holmes

Culham Laboratory, Abingdon, Oxon. OX14 3DB, U.K.
(Euratom/UKAEA Fusion Association)

ABSTRACT: The space charge of ion beams is severely modified by the presence of a neutralizing gas. A model is presented which describes the behaviour of the beam space charge which agrees well with experimental results. The theory indicates how the effect of space charge expansion of the beam can be minimised.

INTRODUCTION: Neutral beam injection is a major method of plasma heating in CTR. The power transfer from the ion source to the fusion plasma is maximised if the ion beam and resulting neutral beam are highly collimated. Most of the residual beam divergence except that due to space charge expansion can be virtually eliminated by careful design. Using a model of the beam plasma described below, we have been able to reduce this component of the divergence to below the fundamental emittance limit whose value is determined by the temperature of the extracted ions.

2. PHYSICAL MODEL: For simplicity we consider the case of a collimated monoenergetic beam passing through a gas filled volume bounded by conducting walls at infinity. Ionization and charge-exchanging collisions produce a dilute plasma of low energy ions and electrons which modifies the vacuum potential of the beam by trapping the electrons and expelling the slow ions. A complete description of the beam plasma can be obtained from the continuity equation for these particles, their energy balance and Poisson's equation.

2.1 The Continuity Equation: The continuity equation is used to obtain the slow ion and electron densities as discussed below.

a) Slow ions: These are produced by charge exchange and ionization. The motion is purely radial and controlled by the electric field. Integration of the continuity equation gives an axial density of

$$n_{io}^{\circ} = n_{bo}\sigma n v_b r_o / 0.26\ \phi_\omega\ (2e/m_i)^{\frac{1}{2}} . \qquad \ldots (1)$$

This value of the slow ion density is only finite if the potential well near the axis has a parabolic form.

b) Electrons: Since the electrons produced by ionization are born with very low kinetic energy (assumed to be zero), they can only escape from the potential well via diffusion in velocity space until their kinetic energy exceeds their binding potential. For a Maxwellian electron distribution, the time required to diffuse over a velocity increment σ_x by electron electron collisions is proportional to σ_x^2. Hence the electrons can be considered to move with a uniform velocity in "potential" space and the continuity equation can be applied. If the solution is transformed back to real space, and neglecting the radial distribution, the axial density is

$$n_{eo} = \left[\frac{0.62\pi\varepsilon_o^2}{e^3 \ln \Lambda} \left(\frac{eT}{m_e}\right)^{\frac{1}{2}} n\, n_{bo}\sigma_i v_b \phi_\omega \right]^{\frac{1}{2}} . \qquad \ldots (2)$$

2.2 The Fokker-Planck Equation When an electron-ion pair is created, by ionization, the slow ion removes approx. $2e\phi_\omega/3$ as it escapes. The electron must hence absorb an equal amount of energy from the beam by coulomb drag to restore equilibrium before it also escapes. The ions created by charge exchange are not involved in this energy balance [1]. The beam ion energy loss is controlled the low velocity part of the electron distribution which is enhanced over the Maxwellian distribution because of electron production by ionization and the near equality of the electron-electron collision time and the beam containment time. We have calculated the velocity distribution, assumed to be a perturbed Maxwellian using the Fokker-Planck equation, and find an enhancement at low velocities which has the form $A \ln(v_s/v)$. The energy absorbed by this distribution function can be easily found and equating it to the energy loss caused by the slow ions leads to an electron temperature of $n_{eo}^2\phi_\omega/2.2\, n_{bo}^2$.

2.3 Poisson's Equation: The complete solution involves the substitution of eqs.(1) and (2) and the electron distribution function into Poisson's equation together with an assumed beam profile, which results in an integro-differential equation which can only be solved by numerical techniques. If spatial dependence is ignored and Poissons equation is reduced to plasma neutrality on axis re-arrangement gives

$$\frac{0.41\pi\varepsilon_o^2\sigma_i\phi_\omega}{e^3 \ln \Lambda} = \frac{n_{bo}\sigma r_o}{0.26}\left(\frac{m_i}{2m_e}\right)^{\frac{1}{2}} + \frac{n_{bo}}{nv_b}\left(\frac{e\phi_\omega}{m_e}\right)^{\frac{1}{2}} \qquad \ldots (3)$$

The solution of this equation is compared with experiment in Fig.1 and fairly good agreement is obtained which is further improved if the full Poisson's equation is used. The electron temperature can also be derived and is found in good agreement with experimental results. It should be noted that the potential ϕ_ω depends only on the beam density and not the radius at low pressure as opposed to the vacuum beam where ϕ_ω scales as $n_{bo}r_o^2$. If ϕ_ω is incorporated in the paraxial ray equation after allowing for the effects of beam divergence and charge exchange on the value of n_b; the numerical solution for the target radius r_T, of the beam envelope shows that r_T declines with increasing values of beam waist, R subject to $r_T > R$. This is a direct consequence of the scaling of ϕ_ω with R. This effect has been used to build large single aparture beam extraction systems. The results are shown in Fig.2 where the divergence, defined as $(r_T - R)z_T$, declines with beam aperture radius. It is not practical to use still bigger apertures because of the anode hole effect.

4. CONCLUSIONS: The virtual elimination of the effects of beam space charge arises from the scaling of the radial potential on beam radius which differs completely from the scaling of the vacuum potential. Hence large diameter, low divergence beams can be created at high energies and current densities applicable to CTR.

ACKNOWLEDGEMENT: The author wishes to thank Dr E Thompson for helpful discussions throughout this work.

REFERENCES

[1] Green, T S, Private Communication.

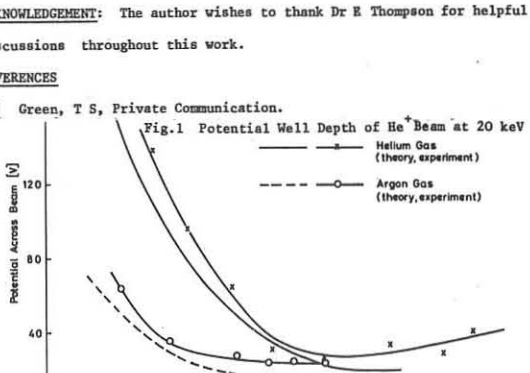

Fig.1 Potential Well Depth of He^+ Beam at 20 keV

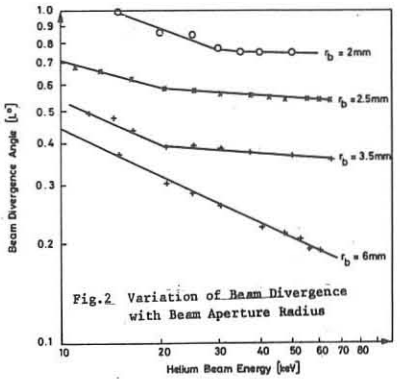

Fig.2 Variation of Beam Divergence with Beam Aperture Radius

PARTICLE BALANCE IN A PICKET FENCE ION SOURCE

A Goede, T S Green and B Singh
Euratom-UKAEA Association for Fusion Research
Culham Laboratory, Abingdon, Oxon. United Kingdom.

ABSTRACT. Electrical efficiency and factors relating to instability have been investigated in a picket fence ion source.

1. INTRODUCTION. In the design of high current ion sources, for neutral injection systems it is important to obtain high electrical efficiency whilst maintaining uniformity and stability of the source plasma. In a plasma generated by primary electron impact ionisation, the efficiency is dependent on the containment time of the ionising electrons[1], which can be enhanced using magnetic fields. However, magnetic fields may adversely affect the plasma uniformity and stability.

One approach to enhancing containment whilst maintaining good uniformity, is to use a configuration in which the anodes are shielded by localised magnetic fields, as for example the periplasmatron[2] and the picket fence source[3].

In evaluating source designs we have investigated the properties of a cylindrical picket fence source studying the containment time and the factors which may influence the stability of the source. The experimental data are compared with a simple model based on the assumption of ionisation by primary electrons developed from reference 1.

2. EXPERIMENTAL ARRANGEMENT. The experimental arrangement is shown in Fig.1. A simple reflex source (monopigatron) has been modified by inserting, a copper cylinder of 15 cm diameter and 15 cm length which is lined with permanent magnets. These magnets are arranged to form a 24-pole line cusp field, similar to that originally employed for the production of Q-plasmas[4]. The field strength in the cusps, at the cylinder wall is about 800 Gauss decreasing exponentially to a value of 10 Gauss at 2.5 cms from the wall. The source can be operated with this cylinder as an anode, or with a simple non-magnetically shielded anode or with a combination of the two. Electrodes other than the anodes are biased 30 V negative with respect to the cathode thus ensuring reflection of the primary, ionising electrons and providing the possibility of collecting and measuring the ion flux to these electrodes.

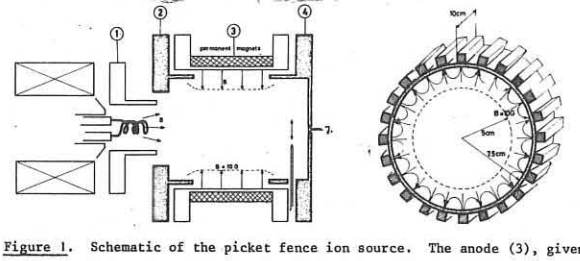

Figure 1. Schematic of the picket fence ion source. The anode (3), given in sectional view, is magnetically shielded by a 24-pole line cusp field.

The source has been operated at pressures of a few millitorr with an arc voltage of 90 V and an arc current of 50 A, limited by power supply. The ion current density at the extraction plane was 200 mA/cm^2, uniform to $\pm$ 5% over a 7 cm diameter circle, thus providing about 7 A of ions.

3. THEORETICAL MODEL. We consider the balance between production and loss of the three species of particles in the discharge i.e. primary electrons, thermal electrons and ions, assuming ionisation is due to primary electrons and not thermal electrons, an assumption justified by the low values of electron temperature measured.

(a) Primary electrons

$$I_e = \frac{e\, n_b\, V}{\tau_e} + e\, n_b\, n_o\, \langle\sigma v\rangle_{IN}\, V$$

(b) Thermal electrons

$$e\, n_b\, n_o \left[\langle\sigma v\rangle_{IN} + \langle\sigma v\rangle_{ION}\right] V = \frac{n_e\, v_e}{4} A_a \exp\left[-\frac{e\phi}{kT_e}\right]$$

(c) Ions

$$e\, n_b\, n_o\, \langle\sigma v\rangle_{ION}\, V = \frac{e\, n_+\, V}{\tau_+} = I_+$$

(d) charge neutrality $\quad n_+ = n_e + n_b \sim n_e$

where n_e is the density of thermal electrons, n_+ the density of ions and n_b the density of the primary electrons, n_o the density of neutrals, I_e is the emission current (primary electron flux), I_+ the current of ions to the walls, V the volume, A_a the anode area, τ_e the containment time of the ionising electrons, $\langle\sigma v\rangle_{IN}$ the rate coefficient of inelastic scattering of electrons to energies below the ionisation threshold, $\langle\sigma v\rangle_{ION}$ the rate coefficient for ionisation, ϕ the plasma potential with respect to the anode, T_e the electron temperature and τ_+ the ion lifetime.

Dividing these equations through leads to the relations

$$\frac{I_e}{I_+} = \frac{\langle\sigma v\rangle_{IN}}{\langle\sigma v\rangle_{ION}} + \frac{1}{n_o\, \tau_e\, \langle\sigma v\rangle_{ION}} \qquad (1)$$

and

$$\frac{e\phi}{kT_e} = \log\left[\frac{v_e\, \tau_+}{4} A_a \left\{1 + \frac{\langle\sigma v\rangle_{IN}}{\langle\sigma v\rangle_{ION}}\right\}^{-1}\right] \qquad (2)$$

Equation 1, previously derived in reference 1, enables one to derive τ_e, the containment time of the primary electrons from the measured values of I_e/I_+ as a function of the neutral gas pressure. Equation 2 relates $e\phi/kT_e$ which is measured experimentally, to the arc voltage (via $\langle\sigma v\rangle_{IN}/\langle\sigma v\rangle_{ION}$), to the anode area and to the source pressure (via τ_+).

4. MEASUREMENTS. 4.1 Containment time and Anode area. Following the approach proposed in reference 1, the measured variation of I_e/I_+ with the inverse pressure may be used to derive relative values of τ_e, as shown in Fig.2. Because τ_e is inversely proportional to the effective anode area, this leads to an assessment of the effective width of the line cusps in the picket fence for primary electron collection. The value obtained is 2.6 mms which is about two times the Larmor diameter of 90 eV electrons evaluated one Larmor diameter away from the wall.

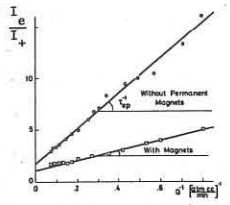

Fig.2. Increase in electron containment using a picket fence anode.

4.2 Plasma Potential. The parameter variations of plasma potential are shown in Fig. 3, 4 and 5. The electron temperature ranges from 1.5 to 2.5 eV. In plotting $e\phi/kT_e$ versus anode area, we have used the effective areas derived from measurements of the primary electron containment time. The agreement implies that the effective area for the thermal electrons is close to that for the primary electrons. More extensive measurements are required to confirm this point. The voltage dependence, via the term $(1 + \langle\sigma v\rangle_{IN}/\langle\sigma v\rangle_{ION})$ is shown in figure 4. Values of the reaction rate coefficient used are taken from reference 1.

The pressure dependence arises from the variation of τ_+ with pressure. The experimental data, figure 5, are consistent with the proposal that τ_+ varies inversely as the drift velocity of the ions which at low pressures varies as $p^{-\frac{1}{2}}$ (5,6). The implication is that the ion motion in the source is governed by diffusion processes.

5. CONCLUSION. The measurements of electrical efficiency and plasma potential are consistent with predictions of a model based on ionisation by primary not thermal electrons. The evaluation of primary electron containment time leads to an assessment of effective anode area and thus scaling laws for picket fence ion sources, the containment time being inversely proportional to effective anode area.

The observed plasma potential variation predicts a minimum anode area beyond which the plasma potential becomes negative, a factor known to relate to the onset of instability[6,7]. Preliminary experiments indicate that there are lower limits to anode area, source pressure and arc voltage in agreement with this concept; this problem will be the subject of a later publication.

REFERENCES

1. GREEN, T.S. et al, 7th Eur. Conf. Fus. Pl. Phys., Lausanne 1 (1975) 93.
2. FUMELLI, M. and VALCKX, F.P.G., EUR-CEA-FC-809 (1976).
3. STEWART, L.D. et al, ORNL-5154 Ann. Rep. (1976) 118.
4. BRAKENHOFF, G.J. and GOEDE, A., Plasma Phys. 12 (1970) 815.
5. ROSE, D.J., J. Appl. Phys. 31 (1960) 643.
6. GREEN, T.S. et al, NID (1976) 8.
7. MARTIN, A.R., Plasma Phys. 14 (1972) 123.

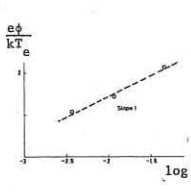

Figure 3

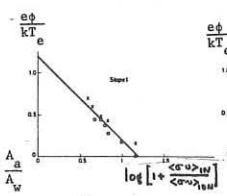

Figure 4

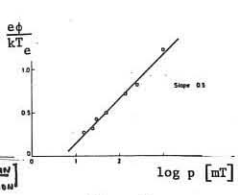

Figure 5

Variation of plasma potential with anode area, arc voltage, and source pressure. Drawn lines are the predictions by equation 2.

DEVELOPMENT OF NEUTRAL INJECTORS AT FONTENAY-AUX-ROSES

A.Bariaud, R.Becherer, J.F.Bonnal, J.P.Bussac, J.Druaux, M.Fumelli, R.Oberson, P.A.Raimbault, F.P.G.Valckx.

ASSOCIATION EURATOM-CEA SUR LA FUSION
Département de Physique du Plasma et de la Fusion Contrôlée
Centre d'Etudes Nucléaires
Boite Postale n° 6. 92260 FONTENAY-AUX-ROSES (FRANCE)

ABSTRACT : The experimental activity on fast neutral injectors at Fontenay-aux-Roses is briefly reviewed, with emphasis on the development of periplasmatron ion sources and of direct energy recovery systems.

The experimental work on neutral injectors at Fontenay-aux-Roses is directed toward providing injection lines for plasma heating in the T.F.R. experiment and development work mainly inspirated by the requirements of the Joint European Tokamak (J.E.T.) experiment. A collaborative development programme is carried out at Culham and at Fontenay-aux-Roses with the objet of realizing a prototype injector for J.E.T. ; the main objectives at Fontenay-aux-Roses being the development of the periplasmatron ion source and of energy recovery systems for the un-neutralised fraction of the beam. In connexion with this programme a considerable work is also done on water cooled extraction systems, high voltage fast protection systems and ion trajectories computational studies.

THE NEUTRAL INJECTORS ON T.F.R.

The neutral injection on T.F.R. is realised with ten injectors based on the O.R.N.L. duopigatron sources. With the ten injectors operating simultanensly a neutral beam power of 570 KW has been injected into T.F.R. for a total extracted ion beam power of 2 MW (D^+ beam at ~30 keV) [1], [5]. By enlarging the diameter of the extraction grid from 8 to 10 cm and using an additional gas imput in the expansion chamber to compensate the transitory decrease of the neutral gas pressure in this region owing to the discharge pumping effect, the performances of an injector uniton the test bed were improved by about a factor 2. These modified injectors will be used for T.F.R. 600 experiment.

THE PERIPLASMATRON ION SOURCES

The basic ideas of the periplasmatron design are : (i) Insure the plasma homogeneity over a large extraction surface by injecting the primary electrons (emitted by a multifilament cathode) from the oter border of the plasma chamber. (ii) Provide containment of these electrons by magnetic shielding of the anodes in a cusp-like magnetic field configuration. This type of source can be built in circular or rectangular form. A schematic view of the last model of the circular periplasmatron [2] is given in Fig.1. An ion current up to 35 A has been extracted at 30 KV from this source with a multi aperture three electrode system of 14,5 cm diameter (see table I). This source is mounted on a complete neutral injection line and it serves presently to produce intense beams for the energy recovery studies. It was assembled at the end of 1974 and operated till now without any failure.

A rectangular version of the periplasmatron capable of illuminating a 38 x 12 cm^2 extraction area has been constructed for the needs fo the J.E.T. The discharge and the plasma properties of this source are actually under investigation. The discharge has been operated till now up to 700 A, 100 V arc current and voltage, 1 sec pulse length and an ion flux of 200 mA/cm^2, this flux being roughly proportional to the discharge current. This source operates in a regime very comparable to the circular source. In table I we summarize the expected performances of this injector.

The positive points of the periplasmatron desing are the following :

I) The peripheral disposition of the filaments allows to use a large number of them. Futhermore placing a 1Ω resistor in series with each, eliminates most problems with filament burn-out due to localised discharges.

II) The cusped magnetic field provides the containment of ionising electrons without affecting the plasma homogeneity and stability.

III) The first grid of the extraction system does not receive direct thermal radiation from the filaments.

IV) The filaments and the insulators are well protected against back streaming energetic electrons coming from the accelerating structure.

ENERGY RECOVERY

In a neutral injector it is possible to recover the energy of the un-neutralised beam fraction emerging from the neutraliser by decelerating and collecting the ions on a suitable electrode biased near the ion source potential. The problem in this case is to prevent the acceleration of the neutraliser plasma electrons toward this electrode. A solution is to create a negative electric potential barrer for these electrons at the exit of the neutraliser. In initial experiments [3] this barrer was created by means of a negatively biased plane grid placed across the beam. A new methods has been developed in wich instead of a plane grid is used a long cylindrical suppressor grid surrounding the beam [4]. The operation of this grid has been tested on the circular periplasmatron neutral injector and for extracted ion beam currents up to 35 A at 30 kV (about 10 A of residual ion beam). In these experiments the additional electrical power required to create the potential barrer for the electrons was of order of 13 % of the power needed to accelerate the beam.

Two slightly different energy recovery schemes based on the cylindrical suppressor grid system are studied at Fontenay-aux-Roses. In the first (see Fig. 2a) a screen grid is used across the expanded residual ion beam. The region situated between the suppressor grid and the screen grid is almost equipotential and the ion trajectories are straigth lines. The main contraint on the system is the thermal loading of the grid. In the second system (Fig. 2b) the screen grid is absent. The ion trajectories are controlled by the potential applied on a conical deflector electrode and are made to focus on the recovery plate. This system can have smaller dimension than the previous one, thermal loading problems are reduced, however the space charge effects are important and the control of the ion trajectories can be delicate.

REFERENCES.-

[1] TFR Group, Report EUR-CEA-FC-834.

[2] M. FUMELLI, F.P.G. VALCKX, Nuclear Inst. and Methods 135 (1976) 203.

[3] M. FUMELLI, F.P.G. VALCKX, Proc. ind. Symp. as Ion Sources, Berkeley, California (1974).

[4] M. FUMELLI, Ph. RAIMBAULT, Proc. 9th Symp. on Fusion Technology Garmisch Partenkirchen (1976).

[5] J.F.BONNAL, J.DRUAUX, R.OBERSON, Proc. 9th Symp. on Fusion Technology Garmisch Partenkirchen (1976).

TABLE I

	Circular Periplasmatron	Rectangular Periplasmatron
EXTRACTION SURF. (cm^2)	160	450
EXT. CURRENT (A)	35	(60)*
EXT. CURRENT DENSITY (A/cm^2)	0,35	(0,2)*
OPERATING PRESSURE (mT)	5 - 10	5 - 10
GAS EFFICIENCY	60 %	-
PULSE LENGTH (s)	0,5	1
DISCHARGE CURRENT (A)	450	700 A
DISCHARGE POWER	40 kW	70 kW
FIL. HEATING POWER	10 kW	17 kW
SPECIES (%) H^+, H_2^+, H_3^+	70, 25, 5	-

* expected values

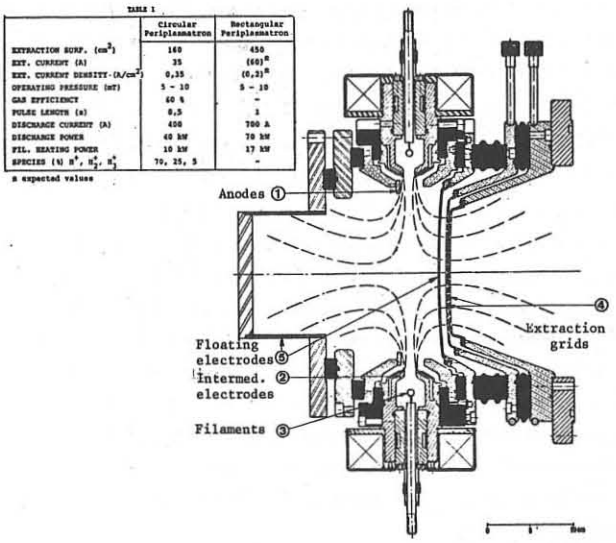

FIG.1 : THE PERIPLASMATRON ION SOURCE

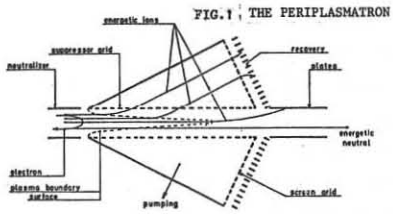

fig.2a

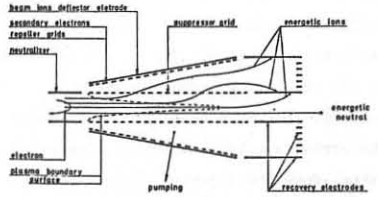

fig.2b

Negative Ions Produced from Clusters for Plasma Heating

E.W. Becker, H. Falter, O.F. Hagena, W. Henkes, R. Klingelhöfer, H.O. Moser, W. Obert, I. Poth

Institut für Kernverfahrenstechnik, Kernforschungszentrum Karlsruhe, P.O.B. 3640, D-7500 Karlsruhe 1, Federal Republic of Germany

Abstract: Negative ions to be used for heating plasmas can be produced by dissociation and charge exchange of an accelerated cluster ion beam on a Cs vapour target. Cluster ion beams are particularly suited to produce high particle current densities at the low energies required for efficient conversion into negative ions.

Supplementary heating of large tokamaks by neutral injection requires a high particle energy, in the case of a fusion reactor of the order of 1 MeV. To produce these particles it has been proposed to accelerate D^- ions that may be neutralized with high efficiency[1]. D^- ions may either be produced by direct extraction, together with a certain amount of electrons, out of special ion sources[2], or by charge exchange of positive ions on an alcali vapour target. For the latter method the best efficiency of conversion - about 30 %[3] - is obtained by passing D^+ ions of an energy of 0.5 keV or lower through cesium vapour. At higher energy the yield drops off sharply, e.g. to 6 % at 5 keV. The current density of conventional ion sources, however, is quite low at these low energies. To overcome this problem we have proposed[4] to use cluster ion acceleration, a method that is under development at Fontenay-aux-Roses and at Karlsruhe. Because of the low charge density cluster ion beams have less space charge problems so that high particle current densities of the order of 1 A_o/cm^2 at 0.1 - 1 keV/atom should be possible.

The equilibrium fraction of negative ions for a thick Cs target has been shown to be independent of the nature of deuterium particles, e.g. D^+, D_2^+, and D_3^+ of the same speed[5]. Hence the equilibrium fraction for cluster ions D_n^+ should be the same. The target density required to reduce cluster ions to small neutral fragments, most probably hydrogen molecules, was found to be one order of magnitude smaller than that required to reach the equilibrium for D^- [6]. Thus the disintegration of clusters and the conversion into negative ions may be executed in one step in a Cs target with the same target density as required for D^+ primaries.

Generally cluster ions have a broad distribution of masses. Figure 1 shows for example the mass spectrum of a hydrogen cluster ion beam with a mean size of $\langle N \rangle$ = 900 atoms/cluster. This distribution results in a correspondingly broad distribution of the energy per atom after acceleration. To obtain the efficiency for conversion into negative ions, the energy distribution must be folded with the energy dependence of the thick target yield. If we assume the beam of figure 1 to be accelerated by 1 MV, we compute the conversion efficiency to be η = 28 %. The mean size of cluster ions is easily controlled by the parameters of the cluster production and ionization process[7]. Therefore its value may be adjusted to result in a mean energy/atom of around 0.5 keV after acceleration with the voltage which is used to accelerate the negative ions. Thus the injection system can be envisaged as a tandem accelerator, as shown in the schematic drawing of figure 2. Contrary to our present system, the cluster

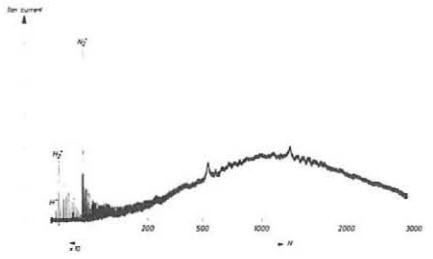

Fig. 1. Mass spectrum of a hydrogen cluster ion beam. N = number of H atoms per cluster ion. Mean size $\langle N \rangle$ = 900 atoms/cluster.

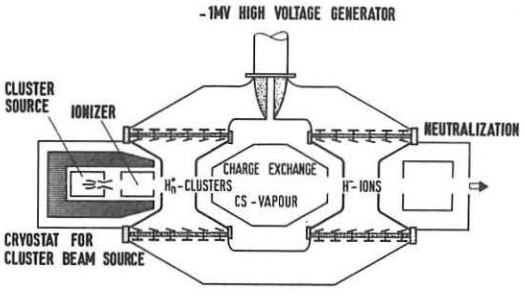

Fig. 2. Schematic drawing of a tandem accelerator for production of 1 MeV D^- ions from a cluster ion beam with a mean cluster size of $\langle N \rangle$ = 1000 atoms/cluster.

ion beam generation will be on ground potential, which greatly simplifies its construction and operation. Positive cluster ions are accelerated into the negative terminal, housing the Cs vapour cell, where they are in part converted into negative ions which subsequently are accelerated through the second acceleration tube to ground potential. The power carried by the cluster ion beam is only $1/\eta \langle N \rangle$ of that of the negative ion beam, for the figures of this paper less than 1 %. Thus the main expenditures will be those of the negative ion accelerator, the cluster section comprising only a modest fraction.

References

1) A.C. Riviere, D.R. Sweetman, APS Meeting (Nov. 1970), paper 4E2

2) Yu.I. Belchenko, G.I. Dimov, V.G. Dudnikov, Nucl. Fusion 14 (1974), 113.

3) Equilibrium fractions according to A.S. Schlachter et al., private communication. The numerical values of the present paper are based on these new data and therefore differ from those of ref. (4).

4) E.W. Becker, H. Falter, O.F. Hagena, W. Henkes, R. Klingelhöfer, H.O. Moser, W. Obert, I. Poth, Nuclear Fusion, in print.

5) F.W. Meyer, L.W. Anderson, Phys. Rev. A, 11 (1975), 589.

6) O.F. Hagena, W. Henkes, U. Pfeiffer, Proc. of the 9th Symp. on Fusion Technology, Garmisch Partenkirchen, 1976, page 885.

7) W. Henkes, V. Hoffmann, F. Mikosch, Review of Scient. Instr., in print.

STATISTICS OF AMPLITUDE AND TIME-INTERVALS ASSOCIATED WITH SEQUENCES OF ELECTRON CYCLOTRON BURSTS

J.A.C. CABRAL, M.E.F. SILVA and C.A.F. VARANDAS
Laboratório de Electrodinâmica - Complexo Interdisciplinar
Instituto Superior Técnico - Lisbon - Portugal

ABSTRACT - The sequence of electron cyclotron bursts of a beam-plasma system is analysed by the experimental determination of its time-interval and amplitude statistical distributions.

1.- INTRODUCTION: - The understanding of the physical mechanisms which determine burst-like radiation from plasmas can be important for the development of thermonuclear research. Indeed, in some TOKAMACS strong cyclotron radiation occurring in bursts has been detected in regimes in which the runaway electrons can behave like high energy electron beams [1][2]. To get an extra insight into the nature of the electron cyclotron instability we analyse its statistical behaviour. In our interaction chamber (L=75 cm, ϕ=8 cm) an electron beam (U_b=2000 eV, i_b= 0- 20 mA, ϕ= 0.4 cm) creates its own Helium plasma ($n \sim 10^9$ cm^{-3}, $T_e \sim 5$ eV) under low pressure regimes ($p_{He} = 4.2 \times 10^{-4}$ Torr) in weak magnetic fields ($B_o \sim 0.01$ Wb m^{-2}). Under these conditions the cyclotron instability is characterized by the spontaneous emission of rapid bursts (~ 100 ns) with frequencies of the order of 400 MHz. Single sweep oscillograms usually show sequences of bursts with variable amplitude and irregular time intervals between consecutive bursts.

2.- AMPLITUDE STATISTICS: - They were determined in the following manner:- A pin probe receives the rf bursts which after amplification are sent to a quadratic detector whose output is fed into a multichannel analyser directly yielding the amplitude distribution p(E) as a function of E^2. Fig.1 shows typical results (B_o= 0.006 Wb m^{-2}):- For weak interactions (i_b= 6 mA) all the bursts have practically the same amplitude (c). As we increase the interaction strength (i_b= 8 mA) the distribution broadens mainly to the high energy side(b). For a stronger interaction (i_b= 10 mA) the distribution is very broad (a) showing the existence of small amplitude bursts which result from the non-linear evolution of the high amplitude ones [3].

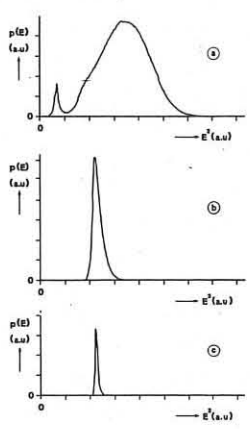

Fig.1

3.- TIME-INTERVAL STATISTICS:- They were obtained as follows:- The cyclotron bursts were amplified and then sent to the quadratic detector whose output is fed into a constant fraction discriminator. This unit gives a sharp pulse whenever a burst arrives with a power exceeding some discriminating level. This new pulse sequence is then sent to a time-to-amplitude converter whose output is fed into the multichannel analyser. In this way we obtain the distribution of time intervals between consecutive occurrences of bursts with a power exceeding some threshold level. Fig.2 shows typical results (B_o= 0.009 Wb m^{-2}, i_b= 10 mA):- Curve (a) was obtained with the detection system as sensitive as possible (discriminating level 0% with 100% cutting the complete distribution). We see that $p(\tau)$ is strongly peaked at a certain value of τ. Curve (b) was obtained with a small discriminating level (25%) and we note more clearly that $p(\tau)$ has a periodical structure. Curve (c) had a higher discriminating level (75%) and we see that the maximum of probability is now found at a higher value of τ. Curve (d) shows the complete disappearence of the small time intervals when we only analyse bursts with large amplitude (disc. level of 90%). For weak interactions the distribution approaches a single sharp peak occurring at the 1st maximum of $p(\tau)$.

4.- A LOWER HYBRID WAVE Varying the axial magnetic field we made similar measurements. Assuming that the cyclotron instability is excited in the neighbourhood of the upper hybrid frequency ($f_o \sim f_{uh}$) we determined for each case the approximate value of f_{pe}. Plotting the inverse of the periods (T_o) observed on the time-interval statistics against f_{pe} we verified that the experimental points lie on a straight line. Measurements made with other noble gases (Ar, Ne) showed that the periodicity in the time interval distribution results from the excitation of an ion wave with $f \sim f_{pi}$, as $1/T_o$ is for all cases very close to f_{pi}. This result was already assumed in [4]. This ion wave can be independently excited by the electron beam. Indeed, the theoretical study of the dispersion of a cold beam-plasma system of finite radial extent, when allowance is made for ion motion, shows that there is a propagation band extending from a cutoff at $f = f_{lh}$ to a resonance at $f = f_{pe}$ or $f = f_{ce}$ whichever is lower [5]. In the cases we are considering ($0 \leq f_{pe} \leq f_{ce}$) the lower hybrid frequency varies from f_{pi} ($f_{pe} \to 0$) to $f_{pi}/\sqrt{2}$ ($f_{pe} = f_{ce}$). The slow space-charge wave of a weak beam will then interact with the plasma waves at $f \sim f_{pi}$ and k comprised between ω_{pi}/v_{ob} and $(\omega_{pi} + \omega_{pb})/v_{ob}$, v_{ob} being the beam axial velocity. Therefore the unstable mode will develop as a standing wave since the wavelength will be of the order of or greater than the length of the interaction chamber ($f_{pi} \sim 4$ MHz, $f_{pb} \sim 100$ MHz, $v_{ob} = 2.65 \times 10^9$ cm s^{-1}). Hence, due to the action of this lower hybrid wave, the plasma density will vary periodically in time with a frequency close to f_{pi}. The interpretation of the results of this statistical analysis and the explanation of the role played by the lower hybrid wave on the nonlinear development of the electron cyclotron instability will be presented in [3].

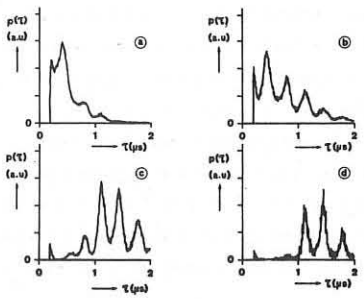

Fig.2

REFERENCES

[1] - STONE, D.S. (1976) M.I.T. RLE Progress Rapport 118, 170.
[2] - SPONG, D.A. et al (1974) Nuclear Fusion 14, 397.
[3] - CABRAL, J.A.C. et al (1977) 8th Europ. Conf. Controlled Fusion and Plasma Physics, Prague.
[4] - CABRAL, J.A.C. (1976) Plasma Physics 18, 719.
[5] - BRIGGS, R.J. (1964) "Electron stream interaction with plasmas", M.I.T. Press, Cambridge, Mass. U.S.A., pg 87.

NONLINEAR INTERACTION BETWEEN A LOWER HYBRID WAVE AND THE ELECTRON CYCLOTRON INSTABILITY

J.A.C. CABRAL, M.E.F. SILVA and C.A.F. VARANDAS
Laboratório de Electrodinâmica - Complexo Interdisciplinar
Instituto Superior Técnico - Lisbon - Portugal

ABSTRACT - The interpretation of the statistics of amplitude and of time-intervals associated with sequences of electron cyclotron bursts reveals the profound influence of a lower hybrid wave on the nonlinear development of the cyclotron instability.

1.- INTRODUCTION: - In another publication [1] we have shown that a lower hybrid wave was detected in our beam-plasma system in close correlation with the temporal statistical behaviour of the electron cyclotron instability. To analyse the influence of the plasma density variations, caused by that wave, on the linear characteristics of the cyclotron instability we made, neglecting ion motion, a computer study of the real-k solutions of the dispersion equation for a cold beam-plasma system filling a cylindrical waveguide immersed in an axial magnetic field [2].

$$p^2\left\{1-\frac{\omega_{pe}^2}{\omega^2-\omega_{ce}^2}-\frac{\omega_{pb}^2}{(\omega-kv_{ob})^2-\omega_{ce}^2}\right\}+k^2\left\{1-\frac{\omega_{pe}^2}{\omega^2}-\frac{\omega_{pb}^2}{(\omega-kv_{ob})^2}\right\}=0,$$

corresponding to the following parameters:- f_{ce}= 300 MHz, f_{pb}= 110 MHz, p= 0.6 cm^{-1}, v_{ob}= 2.65 x 10^9 cm s^{-1} and different values of f_{pe}. Considering only the numerical values relating to the most unstable cyclotron mode we verified that ω_r, k and the growth rate ω_i all increase monotonically with the plasma density. A second computer study was made in which we varied f_{pe} in a similar way but keeping now a constant ratio f_{pb}/f_{pe}. The numerical results show that ω_r, k and ω_i are now more sensitive to the plasma density.

2.- WEAK INTERACTIONS:- In these cases (low values of i_b) we can state now that the instability is characterized by a relaxation process originated by the lower hybrid wave which produces a steady state variation of the plasma density (Fig.1-b). As soon as the instantaneous density n exceeds the threshold level n_c [3], temporal exponential growth starts with an ever increasing growth rate. When the density begins to decrease the growth rate also decreases and this stabilization mechanism leads to the quenching of the instability. The rapid decrease of the bursts amplitude is most probably due to cyclotron damping:- indeed, if we compute, based on the above mentioned numerical study, the energy $U_{cy}= m_e v^2/2$ of the electrons which experience the instability electric field at cyclotron resonance ($\omega_r - k\,v = \omega_{ce}$) we realize that the damping is produced by electrons which belong to the bulk of the velocity distribution ($U_{cy} < 4$ eV, $T_e \sim 3$ eV). Therefore we can expect that the cyclotron damping rate will be large. This mechanism justifies the existence of a density threshold for the excitation of the cyclotron instability:- the growth rate, which increases with the plasma density, must exceed the strong cyclotron damping rate. We have experimentally verified that the weak interactions present burst sequences similar to that depicted on Fig.1-b, which are typical of a relaxation oscillation with its almost δ-function distributions both in time-intervals and in amplitude [1].

3.- INTERMEDIATE INTERACTIONS: - When the interaction strength is increased the burst sequences lose gradually their regularity, and the distributions p(E) as well as p(τ) broaden. The increase in the bursts amplitude results from two converging causes:- (i) an increase in the growth rate and (ii) a decrease of the cyclotron damping rate ($U_{cy} \sim 5$-10 eV, $T_e \sim 4$ eV).

4.- STRONG INTERACTIONS: - This situation corresponds to the conditions of our former publication [4]. Fig.1-a shows the schematic evolution of the instability:- For t=0 the plasma density varies smoothly and the system permits the growth of a large amplitude burst. As it was previously shown the cyclotron wave (ω_o, k_o) decays into a new cyclotron wave ($\omega_1 < \omega_o, k_1 > k_o$) and into a low frequency electron plasma wave ($\omega_2, k_2 < 0$). The growth of the wave (ω_2, k_2) originates strong and relatively fast variations of the plasma density causing the decoupling of the cyclotron wave from the beam slow space-charge wave. The burst becomes the only energy source for the growth of the two new waves and vanishes while the electron plasma wave reaches its maximum of amplitude. Based on Fig.1-a we can predict that whenever n exceeds n_c, short small amplitude bursts can be excited and this explains the existence of the small peak at rather low energy in the amplitude distribution [1]. When the plasma density, averaged over ω_2, is high, the excitation of moderate amplitude modulated bursts becomes possible, as experimentally observed. These bursts however do not lead to additional parametric interactions. Therefore the electron plasma wave damps in about 2-3 ion wave periods and afterwards a new high amplitude burst may start growing. These considerations are in agreement with the broad amplitude distributions observed in these regimes [1]. We have also seen in [1] that the time interval between consecutive bursts of high amplitude has its maximum of probability for a value of τ corresponding to 3-4 ion wave periods, in agreement with the present qualitative description of the interaction (Fig.1-a). We can therefore state that, for the strong interactions, there is a double mechanism involved:- (i) the relaxation process considered above and (ii) the parametric decay of the bursts with high amplitude. These high amplitudes are attained because:- (i) the growth rate is large and (ii) the cyclotron damping is almost inexistent ($U_{cy} \sim 22$ eV, $T_e \sim 5$ eV).

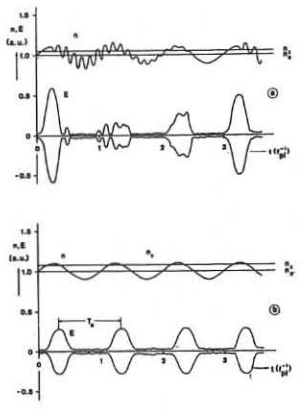

Fig.1

Concluding the paper we can stress that these results open the possibility of controlling the instability development by artificial plasma density variations, not only in time but also in space (multi-mirror configurations). Eventually these instability suppression mechanisms might result in additional plasma heating.

REFERENCES

[1] - CABRAL, J.A.C. et al (1977) 8th Europ. Conf. Controlled Fusion and Plasma Physics, Prague.

[2] - BRIGGS, R.J. (1964) "Electron stream interaction with plasmas", M.I.T. Press, Cambridge, Mass. U.S.A. pg. 84.

[3] - CABRAL, J.A. and HOPMAN, H.J. (1970) Plasma Phys. 12, 759.

[4] - CABRAL, J.A.C. (1976) Plasma Physics 18, 719.

ECR AND UPPER-HYBRID HEATING IN THE CULHAM LEVITRON

A C Riviere, M W Alcock and T N Todd

Culham Laboratory, Abingdon, Oxon. OX14 3DB, U.K.
(Euratom/UKAEA Fusion Association)

ABSTRACT: The electron temperature and density profiles have been measured for microwave heated plasmas in the Culham Levitron. At power levels ≈ 10 W the heating is spatially located at $\omega_{ce} = \omega_{RF}$, whereas at higher power levels heating occurs between ω_{ce} and the upper hybrid resonance. The profiles remain unchanged for changes in the plane of polarization of the microwaves.

Electron cyclotron resonance (ECR) heating has been used extensively for heating plasmas and recently it has been used to raise the bulk temperature of the electrons in the T3 Tokamak[1]. With high power sources becoming available[2] and with the observation of ion heating through parametric decay processes[3] microwave radiation could be useful for heating large plasmas. Preliminary studies of plasmas produced by microwave heating in the Culham Levitron are described for field strengths up to 5.8 kG and with plasma in which $\omega_{pe} \approx \omega_{ce}$.

The Culham Levitron is an axisymmetric machine with a strong poloidal field provided by a superconducting ring winding with major and minor diameters of 60 cm and 9.3 cm respectively. Flux surface shapes are determined by external vertical field coils and the toroidal magnetic field is provided by a 72 turn winding. Steady state plasmas were produced during 3.5 sec pulses of microwave power.

The electron temperature (T_e) and density (n_e) profiles were measured with a double Langmuir probe with spherical tips 2 mm in diameter spaced 5 mm apart. The probe tips were aligned approximately parallel to the magnetic field. The probe voltage was swept at 10 kHz and a continuous measure of T_e and I_s was obtained by means of a recently developed system[4]. The values of n_e calculated from T_e, I_s and probe area were normalised by a factor 1.5 or less to the value of $\bar{n}_e$ obtained with the 4 mm interferometer.

Profiles of n_e and T_e were recorded for several power levels with the ECR point at 1.2 cm from the ring (I_R = 110 kAT, f_{RF} = 10 GHz). Those for 11, 18 and 130 W at a helium gas pressure of 1.0×10^{-5} Torr are shown in Fig.1. The interesting feature of these profiles is that at low power (11 W) the T_e profile shows that the heating is located at the surface in which $\omega_{RF} = \omega_{ce}$ but at the higher powers it moves to where $\omega_{ce} < \omega_{RF}$. The ratio of field strengths between the inner and outer edges of the plasma was 1.7. The upper hybrid resonance point, where $\omega_{RF}^2 = \omega_{UH}^2 = \omega_{pe}^2 + \omega_{ce}^2$, is marked on each T_e profile and the heating appears to occur between where $\omega_{RF} = \omega_{ce}$ and ω_{UH}. In the central region of the density profiles the ratio $\omega_{pe}^2/\omega_{ce}^2$ is almost independent of position but increases with power level (0.6, 0.8 and 1.1 for 11,18 and 130 W respectively).

This is further illustrated in Fig.2 by profiles taken at a power level of 1000 W. Here the resonance is 1.3 cm from the ring, I_R = 180 kAT, f_{RF} = 16.25 GHz and the hydrogen gas pressure is 5.10^{-6} Torr. The upper hybrid resonance is well separated from the ECR point where a second maximum in T_e is observed. The ratio $\omega_{pe}^2/\omega_{ce}^2$ has a nearly constant value of ≈ 1.7 in the central part of the profile suggesting a sharp threshold for an electron cyclotron instability[5] or additional damping as n_e approaches a critical value.

The plane of polarization of the microwave radiation was rotated from $E_{\parallel}B$ to $E_{\perp}B$ but the effect on the measured profiles was less than a few per cent even for the narrow profiles centred on ω_{ce}. The polarization from the horn measured in the open laboratory was better than 95% but scattering of the radiation by the metal components around the plasma may account for the lack of sensitivity to polarization. This effect has been invoked in Tokamak experiments to explain the lack of polarization observed in the inverse process of the emission of electron cyclotron harmonic radiation[6].

The power absorbed by the plasma was calculated from the T_e, n_e profiles, gas density and energy loss per ion pair for hydrogen. The microwave power was separately calibrated calorimetrically. Efficiencies up to 70% were observed without including additional losses due to thermal conductivity or impurity radiation. The experiments of Porkolab et al.[7] were carried out in the same frequency, electron density and temperature range and the parametric instabilities they observed may also be present in our case leading to the efficient absorption of power.

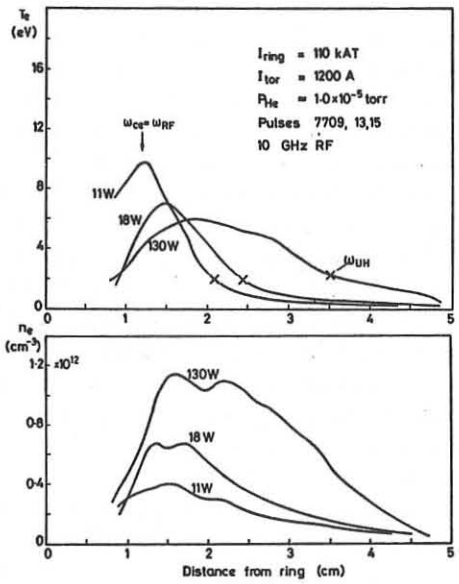

Fig.1 T_e and n_e profiles at power levels of 11, 18 and 130 W

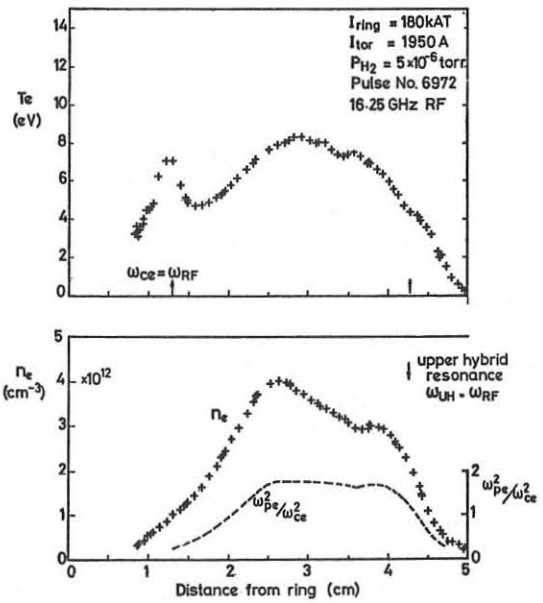

Fig.2 T_e and n_e profiles at a power level of 1000 W

ACKNOWLEDGEMENTS: The authors gratefully acknowledge the contribution to this work made by members of the Levitron team led by D R Sweetman and in particular by M F Payne, T Edlington, P R Collins and N R Ainsworth.

REFERENCES

[1] V V Alikaev et al., Soviet J. Plasma Phys. 2 212 (1976).
[2] V V Alikaev et al. 3rd Int. Meeting Theor. Exp. Aspects of Heating of Toroidal Plasmas, Grenoble, 2, 375 (1976).
[3] M Okabayashi, K Chen and M Porkolab, Phys. Rev. Lett. 31, 1113 (1973).
[4] D E T F Ashby, W H W Fletcher and T N Todd - to be published.
[5] F W Crawford, Radio Science 69D, 789 (1965).
[6] P Brossier et al. VIth Conf. Plasma Phys. and Contr. Nucl. Fus. Res. 1976, Paper IAEA-CN35/A13-2, Nucl. Fus. Suppl. vol.1,p.409, 1977.
[7] M Porkolab et al. Princeton University Plasma Physics Laboratory Report, MATT-1160 (1975).

LOW FREQUENCY ELECTROSTATIC WAVES IN THE CULHAM LEVITRON

D E T F Ashby, E M Jones, D F H Start

Culham Laboratory, Abingdon, Oxon. OX14 3DB, U.K.
(Euratom/UKAEA Fusion Association)

TRACT: Low frequency (< 250 kHz) waves present in an ECRH-produced
.ium plasma in the Culham Levitron have been investigated using probes
measure floating potential. A band of frequencies typically centred
50 kHz is identified as drift waves. Large amplitude waves near
kHz are attributed to the temperature gradient instability.

RODUCTION: The Culham Levitron[1] consists of a levitated superconduct-
ring of major radius 30 cm, minor radius 4.8 cm. Toroidal and vertical
elds are superimposed on the poloidal ring field to give high-shear axi-
mmetric field configurations ($L_s \sim 10$ cm, $|B| \simeq 3$ kG, $B_\theta/B_\phi \approx 10$).
evious fluctuation measurements[2,3] in the machine have been concerned
th decaying plasmas and the effect of ohmic heating current. This paper
als with steady-state helium discharges produced by ECRH (~ 180 W at
GHz) giving $n_e \simeq 5\times10^{11}$cm^{-3} and $T_e \simeq 5$ eV.

AGNOSTICS: Mean plasma parameters were measured from HeI light emission
d a microwave interferometer, but major reliance was placed on probes. A
ept double probe was used to measure n_e and T_e as a function of position;
e Figs.1(a) and 1(b). Fluctuations in floating potential were measured
ing probes with 0.6 mm diameter platinum spheres. Groups of up to four
obes were used thus allowing k_θ, k_ϕ and k_r to be determined. The signals
re digitalized using fast ADCs and then Fourier analysed to give amplitude
d phase spectra.

SULTS: Power spectra at three different distances from the ring are shown
Fig.2 together with the relevant plasma and magnetic field parameters.

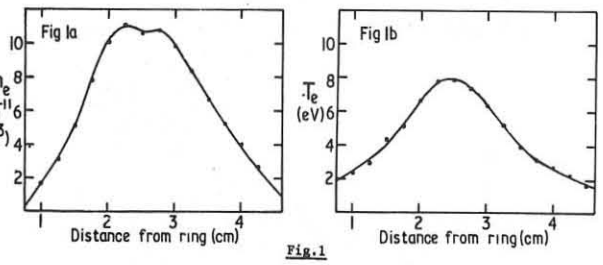

Fig.1

On the outside of the plasma the spectrum is dominated by a peak near 40 kHz. Measurements at 1 mm intervals show that this peak progressively changes in amplitude and frequency across the plasma. At 3.5 cm from the ring it appears occasionally and is completely absent at 3.0 cm. Phase measurements at this peak give $k_\phi a = 0.3$ and $k_r a \simeq 0.2$–0.6, where $a = \sqrt{kT_e/M_i}$; it is attributed to a drift wave, which in toroidal geometry need not be shear-stabilized[4]. Its disappearance in Fig.2(c) agrees with the change in $\eta_e = d(\log_e T_e)/d(\log_e n_e)$ which stabilizes the drift wave[5]. The frequency of the peak implies a Doppler shift due to a guiding centre velocity, v_{gc} which is $\simeq 1.3\times10^5$cm/sec for Fig.2(b).

Applying this value of v_{gc} to the spectrum near 10 kHz shows that these ves are characterised by $\omega_{gc} \simeq 0$ where ω_{gc} is the frequency in the station- guiding centre frame. Assuming that $T_i = T_e$, so that $\eta_i = \eta_e$, then the haviour of the low frequency wave is consistent with the collisional tempera- re gradient wave[6] which has $\omega_{gc} \simeq 0$ and is unstable if $\eta_i > 2/3$. Measure- nt shows that $k_\phi a \simeq 0.1$ and $k_r a \simeq 0.5$. The collisional temperature gradient ve requires $k_\parallel \lambda_{mfp} < 1$ which becomes $k_\phi a < L_s/\lambda_{mfp}$ if shear imposes the con- raint $\frac{k_\phi}{k_r} \simeq k_\parallel L_s$ and thus makes $k_\phi \simeq a^{-1}$; these expressions are satisfied perimentally. A further requirement is that $\omega_{*e} = k_\phi v_{de} > k_\parallel \sqrt{kT_i/M_i}$; this equality may be written $k_\phi a > k_\parallel L_n$, which is also satisfied ($L_n^{-1} = n^{-1}dn/dx$) e spectrum at these low frequencies is dominated by a single frequency whose

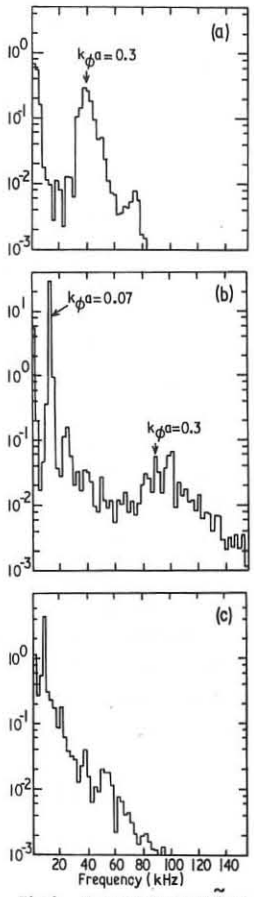

Distance from ring = 4.0 cm
$\eta_e = 0.5$
a = 0.12 cm
Electron drift vel. $v_{de} = 1.3\times10^5$cm/sec
Mean free path $\lambda_{mfp} = 38$ cm
$|B| = 2.6$ kG
Pitch length $L_p \simeq 33$ cm
Average shear length $\bar{L}_s \simeq 11$ cm

Distance from ring = 3.5 cm
$\eta_e = 1.0$
a = 0.14 cm
Electron drift vel. $v_{de} = 1.3\times10^5$cm/sec
Mean free path $\lambda_{mfp} = 49$ cm
$|B| = 2.9$ kG
Pitch length $L_p \simeq 20$ cm
Average shear length $\bar{L}_s \simeq 17$ cm

Distance from ring = 3.0 cm
$\eta_e = 1.4$
a = 0.17 cm
Electron drift vel. $v_{de} = 1.1\times10^5$cm/sec
Mean free path $\lambda_{mfp} = 84$ cm
$|B| = 3.0$ kG
Pitch length $L_p \simeq 14$ cm
Average shear length $\bar{L}_s \simeq 23$ cm

Fig.2 Power spectra of $\tilde{\phi}$ at different distances from the ring.

coherence length is greater than the toroidal circumference of the machine.

DISCUSSION AND CONCLUSION: In the present experiments drift waves dominate the fluctuation spectrum near the edge of the plasma where η_e is small. Further into the plasma, where $\eta_i \simeq \eta_e \geq 2/3$, the drift waves are replaced by large amplitude low frequency waves whose characteristics are consistent with the collisional temperature gradient instability. In connection with other machines it is worth noting that for the temperature gradient wave the dominant fluctuating parameters are $\tilde{T}_i$ and $\tilde{v}_\parallel$, the plasma velocity along the field lines. Typically $\tilde{T}_i/T_i \approx \tilde{v}_\parallel/v_i \gg \tilde{n}/n_e = e\tilde{\phi}/kT_e$, where $v_i = \sqrt{kT_i/M_i}$ and $\tilde{\phi}$ is the fluctuating plasma potential. Since the floating potential is proportional to $\tilde{v}_\parallel$, the temperature gradient wave can be detected easily by probes; however it will be less obtrusive using scattering techniques which measure $\tilde{n}/n$.

ACKNOWLEDGEMENTS: The authors gratefully acknowledge the contribution to this work made by the members of the Levitron Team, led by D R Sweetman, and by J G Cordey and R J Hastie on the theory of drift waves.

REFERENCES

[1] A C Riviere, D R Sweetman, Proc. 5th Eur. Conf. on Controlled Fusion and Plasma Physics, Grenoble, 1972, p.95.

[2] N R Ainsworth et al. Proc. 6th Eur. Conf. on Controlled Fusion and Plasma Physics, Lausanne, 2 (1975), p.127.

[3] M W Alcock et al. Sixth Conf. on Plasma Phys. and Controlled Fusion Research, Berchtesgaden, 1976, IAEA-CN35/D12.

[4] J G Cordey and R J Hastie, CLM-P476 (1977) - to be published in Nucl. Fusion, also:
J B Taylor, Sixth Conf. on Plasma Phys. and Controlled Fusion Research, Berchtesgaden (1976), IAEA-CN35/D10.

[5] A A Rukhadze and V P Silin, Sov. Phys. Uspekhi, 11, No.5 (1969), p.659.

[6] C W Horton and R K Varma, Phys. Fluids, 15, No.4 (1972) p.620.

STUDY OF MAGNETIC SHAPING IN A SHELL-LESS HYBRID TOKAMAK WITH OCTOPOLE

T. Okuda, Y. Tanaka*, K. Sakurai and K. Nakamura

Department of Electronics, Nagoya University, Nagoya 464 JAPAN

A positionally stable plasma with D-shape can be produced in a hybrid tokamak with octopole conductors. Also the poloidal distribution of ion flux to the limiter exhibits a good convergence into the corners of the square magnetic surface.

In order to attain a stable confinement without a conducting shell, an axisymmetric magnetic field configuration with a shaping field produced by external conductors has been proposed[1]-[5].

In our hybrid tokamak, a non-circular magnetic surface is realized by octopole conductors wound outside the vacuum vessel and has a separatrix. The separatrix may act as an immaterial limiter and provides axisymmetric poloidal divertors, which is required for solving the impurity problem.

(a) Apparatus

In order to verify the possibility and the predicted properties of such a hybrid tokamak configuration, we constructed a compact toroidal machine (HYBTOK I-a) which is shown in Fig. 1. This machine has no conducting shell and the vacuum vessel V is made of stainless steel bellows of 0.2 mm thick. The magnetic skin time of the vessel is about 30 μsec.

Three axisymmetrical external conductor systems C_M, C_J, C_V are placed inside the toroidal magnetic field coils. The octopole conductors C_M are used for shaping the magnetic surface. The vertical field produced by the C_M conductors is compensated by the vertical field conductors C_V in order to keep the equilibrium position of the plasma.

The experimental parameters are as follows; the toroidal field B_T = 3 kG, the major radius R = 30 cm, the minor radius of a molybdenum limiter L, a = 8 cm, the working pressure of He, P = 1.4 x 10^{-4} torr.

At the time 80 μsec after firing the discharge by injecting an initial plasma produced by two coaxial guns into the vessel which is filled with helium, the octopole field is applied. The plasma current reaches a maximum value 10 kA at 0.6 - 0.7 msec after the initiation of the discharge. The electron density is 3 x 10^{13} cm^{-3} (measured by a 50 GHz interferometer), the mean conductivity temperature is 20 eV (under the assumption that the effective charge Z_{eff} = 2).

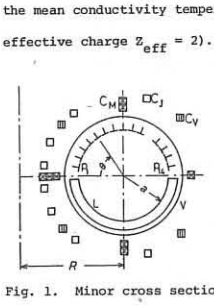

Fig. 1. Minor cross section of HYBTOK I-a.

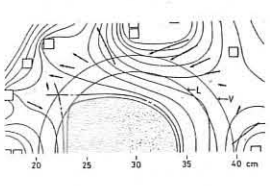

Fig. 2. An example of poloidal-field measurements for the case of D-shaped cross section. The values of the current flowing in C_M, C_J and C_V are 3.0 kA per one conductor, 5.1 kA and -0.18 kA, respectively, and the plasma current is -8.0 kA.

(b) Equilibrium

A typical example of the observed poloidal field just outside the vacuum vessel at 0.4 msec is shown in Fig. 2. The thin lines show the magnetic surfaces computed by the technique previously proposed by us[3] and the arrows indicate the direction and the relative amplitude of the measured poloidal magnetic field. Both patterns fairly agree with each other.

Thus, one conclude that the cross sectional shape of the plasma column at that time is D-shape with two neutral points of the poloidal magnetic field located on the inner wall of the vacuum vessel.

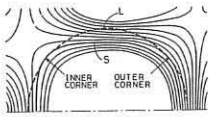

Fig. 3. Magnetic field configuration for the case of square cross section. The values of the current flowing in C_M, C_J and C_V are 1.7 kA per one conductor, 3.0 kA and -0.04 kA, respectively, and the plasma current is -5.0 kA.

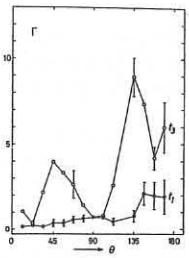

Fig. 4. Experimental results of the time variation of the poloidal distribution of the radial ion flux Γ (10^{21} $m^{-2}s^{-1}$) to L. θ(deg.) is the poloidal angle indicated in Fig. 1. t_1 = 50 μsec and t_3 = 250 μsec are the time after the discharge firing.

(c) Particle Transport near the Separatrix

A magnetic configuration with square cross section as shown in Fig. 3 can be obtained at the earlier time. In this case, the neutral points are outside the limiter surface L and the magnetic surface S which touches tangentially with L acts as a separatrix for the particle transport along the magnetic line of force.

For this reason, the particles diffusing out of such a magnetic surface are expected to converge into the corners, but spread to the extent of $d = (DqR/\sqrt{T_e/M})^{1/2}$, where D, q, T_e and M are the diffusion coefficient, safety factor, electron temperature and ion mass, respectively. To verify this, the angular distribution of ion flux Γ to L is measured by the plane collectors (P_1 to P_{14}) as shown in Fig. 1. The results obtained at 50 and 250 μsec after the initiation of the discharge are shown in Fig. 4.

From the figure, it is seen that the particle flux is converged into the corners, i.e. θ = 45° and 135°, in accordance with the prediction. The peak value corresponding to the outer corner is larger than that corresponding to the inner corner. This is explained by the toroidal effect of B_T and the position of the plasma. The diffusion coefficient $D = (a/\langle n_e \rangle)\Gamma$ is found to be 8.7 m^2/s from the averaged value of Γ, shown in Fig. 4. The extent d described above is therefore expected to be d = 2.9 cm (q = 5, T_e = 10 eV), which is reasonable as the width of the two peaks at the corners.

Conclusion

We presented the experimental results confirming that a positionally stable toroidal plasma with a D-shaped cross section can be maintained in the hybrid shell-less octopole tokamak. In connection with the shaping of the magnetic surface, the poloidal distribution of the ion flux diffusing out from the most outer closed magnetic surface was studied. From the fact that two peaks of the particle flux appeared at the corners, it was found that this magnetic surface plays a role of a separatrix, along which particles are diverted.

* Present address: Japan Atomic Energy Research Institute.

(1) T. Matsui, Y. Tanaka and T. Okuda, Nuclear Fusion 13 (1973) 671.

(2) W. Feneberg and K. Lachner, Nuclear Fusion 13 (1973) 549.

(3) K. Sakurai, Y. Tanaka and T. Okuda, J. Phys. Soc. Japan 37 (1974) 1108.

(4) K. Sakurai, Y. Tanaka and T. Okuda, Phys. Letters 14 (1974) 331.

(5) K. Sakurai, Y. Tanaka and T. Okuda, Plasma Phys. 17 (1975) 261.

ON THE STATE OF LOWEST ENERGY IN IDEAL MHD

G. O. Spies

Max-Planck-Institut für Plasmaphysik, 8046 Garching bei München
Federal Republic of Germany

Abstract: The state of lowest energy in toroidal MHD plasmas depends discontinuously on certain parameters which are related to the topology of the magnetic field lines. This fact is demonstrated and discussed.

In many physical systems, stable equilibria are states of lowest potential energy. This "energy principle" is considered so fundamental that it is sometimes postulated as a definition of stability even when its relation to the equations of motion is unknown, as is the case in nonlinear ideal MHD. The nonlinear energy principle of MHD [1] has recently found increased attention in connection with numerical computations of stable toroidal equilibria [2,3]. The potential energy, $U = \int d\tau (\frac{1}{2}B^2 + \frac{1}{\gamma-1} p)$, $\gamma = 5/3$, is minimized by varying the solenoidal magnetic field B and the pressure p subject to the boundary condition $B_n = 0$ and subject to the constraint of accessibility: the states in competition are connected with some reference state by a path which conserves mass, entropy, and flux. Clearly, the resulting stable equilibrium (if it exists at all) depends upon the reference state. It is the purpose of the present note to point out that this dependence is not continuous.

Let us first, as an illustration, consider the one-dimensionally constrained motion of a particle in a two-dimensional potential, $\ddot{y} = 0$, $\ddot{x} = -\partial U(x,y)/\partial x$. Here, the parameter y represents the reference state. Equilibria are characterized by $\partial U/\partial x = 0$. An equilibrium is stable if, in addition, U has a local minimum with respect to x. If the potential is a smooth function of x and y, a stable equilibrium depends continuously on y whenever $\partial^2 U/\partial x^2 > 0$, so that discontinuities can only occur at marginal points. Linearizing about a stable equilibrium, one finds that the spectrum (which in this case consists of two eigenvalues of opposite sign) includes the origin, and that there are linearly growing solutions whenever the dependence on y is discontinuous. Obviously, this is a somewhat exceptional situation.

It is well known that this situation is common in linearized ideal MHD: the spectrum is never bounded away from the origin [4], and there are always linearly growing solutions [5] (with the possible exception of equilibria with no closed magnetic field lines or with constant pressure). Furthermore, the stability criteria [6,7] derivable from the second variation of the potential [8] behave discontinuously (a family of shearless equilibria depending on the rotation number μ can be constructed such that rational μ implies stability, but irrational μ implies instability). These pathological features of the linear theory suggest that the parameter dependence of the state of lowest energy in the nonlinear theory is always discontinuous. To show that this is indeed the case we demonstrate that for arbitrary equilibria (except for those mentioned before) a neighboring (inaccessible) state exists from which an accessible path of monotonically decreasing potential leads to a non-neighboring state. The demonstration is based on two theorems.

Theorem 1. For every equilibrium (with the above restrictions) arbitrarily small magnetic field perturbations with continuous first derivatives can be found such that the resulting field lines perform finite excursions from the pressure surfaces. This perturbation is associated with a change in topology, and hence not accessible; it usually leads to a more complicated topology (if the equilibrium field lines are closed, the perturbed ones are ergodic; if the equilibrium field lines form nested magnetic surfaces, the perturbed ones exhibit an island structure).

Theorem 1 is nontrivial only if the equilibrium field has shear. It follows from Takens's counterexample [9] to Moser's well-known twist theorem [10]. Moser's theorem implies that perturbing fields with sufficiently many derivatives do not allow finite excursions of field lines. Takens's result implies that perturbing fields with one derivative do. Obviously, our reasoning depends on allowing field perturbations with discontinuous higher derivatives. From the point of view of physics this is not at all objectionable because higher derivatives, unlike first derivatives which define forces, have no physical meaning.

Theorem 2. Starting from an arbitrary initial state, minimization of the potential with respect to the pressure in an infinitesimal flux tube with fixed magnetic field yields constant pressure along field lines. The potential decreases monotonically from the initial state to the corresponding final state.

Since the quantity to be minimized is $\langle p \rangle$, where $\langle \cdots \rangle$ is the volume average, and since the appropriate constraint (which follows from the conservation of mass and entropy) is fixed $\langle p^{1/\gamma} \rangle$, the first part of Theorem 2 follows from Hölder's inequality, $\langle p \rangle \geq \langle p^{1/\gamma} \rangle^{\gamma}$ for $\gamma > 1$. The second part is proved by considering a family of pressure functions, $p_\lambda = (\lambda p^{1/\gamma} + (1-\lambda)\langle p^{1/\gamma} \rangle)^{\gamma}$, so that the final (minimizing) pressure is obtained from the initial (arbitrary) pressure by decreasing the parameter λ from one to zero. Then, $d\langle p_\lambda \rangle / d\lambda = \langle \phi(u) \rangle$, where $u = p^{1/\gamma} - \langle p^{1/\gamma} \rangle$, $\phi(u) = \gamma u(\langle p^{1/\gamma} \rangle + \lambda u)^{\gamma-1}$, and Jensen's inequality, which asserts that $\langle \phi(u) \rangle \geq \phi(\langle u \rangle)$ for convex functions ϕ, is used to show that $d\langle p_\lambda \rangle / d\lambda \geq 0$.

Now, considering an arbitrary equilibrium (which, of course, has constant pressure along field lines), we construct a neighboring state by perturbing the magnetic field according to Theorem 1. In this state, the pressure variation along field lines is finite. Therefore, the corresponding state with constant pressure along field lines, which according to Theorem 2 is accessible along a path of decreasing potential, is not neighboring.

To discuss the implications we recall that the nonlinear energy principle is based on an imagined experiment [1] in which the heat generated by some small viscosity is "somehow magically" removed until the state of lowest potential is reached. We have shown that the change of the final state caused by a continuous change of the initial state which breaks the topology is discontinuous. An immediate consequence is that the imagined experiment is irreproducible, and hence unphysical. By the same token, a strict distinction between stable and unstable equilibria is also unphysical. However, it should be stressed that the time-dependent MHD equations are not unphysical because these define a well-posed initial value problem. It should also be stressed that MHD stability still is a useful concept: Our result is compatible with the statement that stable equilibria are always acceptable, but that a decision as to whether an unstable equilibrium is acceptable depends on information not obtainable from the energy principle.

As to numerical minimizations of the energy, these should not be impeded by our result as long as the topology is well-defined and accurately conserved. This is the case in recent calculations [2] where an ergodic constraint ensures that there are nested magnetic surfaces (to which fixed values of mass, entropy, and rotation number are then assigned.) The present result shows that such a constraint is not just an expedient for simplifying the problem, but also a necessity in order to have a computable problem at all. However, it also indicates that imposing the ergodic constraint and simultaneously [2] assuming that all field lines are closed (i.e. assigning the same rational rotation number to all surfaces) should yield a final state totally different from the final state obtained by taking the same initial state, but imposing the non-ergodic constraint [11] appropriate to closed-line systems.

References

[1] M.D. Kruskal and R.M. Kulsrud, Phys. Fluids 1, 265 (1958)
[2] O. Betancourt and P. Garabedian, Proc. Nat. Acad. Sci. USA 73, 984 (1976)
[3] R. Chodura and A. Schlüter, 2nd European Conf. on Computational Physics, Garching (1976)
[4] H. Grad, Proc. Nat. Acad. Sci. USA 70, 3277 (1973)
[5] H. Grad, private communication
[6] G.O. Spies, Phys. Fluids 17, 400 (1974)
[7] D.B. Nelson and G.O. Spies, Phys. Fluids 17, 2133 (1974)
[8] I.B. Bernstein et al., Proc. Roy. Soc. A244, 17 (1958)
[9] F. Takens, Indagationes Mathematiae 33, 379 (1971)
[10] J. Moser, Nachr. Akad. Wiss. Göttingen, Math.-Phys. Kl. 2, 67 (1970)
[11] G.O. Spies, Phys. Fluids 17, 1188 (1974)

"This work was performed under the terms of the agreement on association between the Max-Planck-Institut für Plasmaphysik and EURATOM".

Nonlinear Properties of Tearing Modes in Tokamaks

D. Biskamp, H. Welter

Max-Planck-Institut für Plasmaphysik, 8046 Garching bei München
Federal Republic of Germany

Abstract: Theoretical and numerical investigations of the nonlinear behavior of tearing modes are reported. The 2D helical model includes heat transport, viscosity and diamagnetic drift effects. The non-linear interaction of m = 1 and m = 2 modes is studied in a 3D model.

Experimental observations in tokamaks show that the processes associated with a major or external disruption may be characterized by two phases:
1. growth of the m = 2 tearing mode on the resistive diffusion time scale;
2. the rapid disruption phase, where m = 2 strongly couples to m = 1. In this paper the previous theoretical investigations [1] have been extended to cope with the particular aspects of these two phases.

1. The helical model described in Ref. 1,

$$\frac{\partial\psi}{\partial t} + v\cdot\nabla\psi = \eta j - E_o,$$

$$(1)\quad \frac{\partial\nabla^2\phi}{\partial t} + v\cdot\nabla\nabla^2\phi = (\nabla\psi \times \nabla\nabla^2\psi)_z ,$$

$$v = e_z \times \nabla\phi, \quad j = \nabla^2\psi + 2kB_o ,$$

yields the result that the nonlinear evolution of the m = 2 tearing mode on the resistive time scale is determined by the properties of the resistivity $\eta(\psi,t)$, in particular within the islands, where the change of the flux, $\partial\psi/\partial t$, is dominated by resistive diffusion. A stationary island configuration requires that $\eta(\psi)\, j\,(\psi) = E_o$. It is found numerically that $\partial j/\partial\psi > 0$ within the island (current maximum at the O-point) even for rather large island size, which is a generalization of the property of the linear solution j_1, $j = j_o + j_1 \cos m\theta$

$$j_1 = \frac{d^2\psi_1}{dr^2} \propto \frac{\psi_+' - \psi_-'}{\lambda} = \frac{\Delta'}{\lambda}\psi_1 > 0 , \qquad \text{for} \quad \psi_1 > 0,$$

since $\Delta' > 0$ for instability (λ = resistive layer width). Hence for stationary islands $\partial\eta/\partial\psi < 0$ is required in the islands, i.e. T_e must be larger in the center of the island than at the separatrix. Hence the island size is determined by the electron energy transport equation, which in the case of infinite parallel heat conductivity, $T_e(\psi,t)$, reads

$$\frac{\partial T_e}{\partial t} + \left\langle \frac{\partial\psi}{\partial t} \right\rangle T_e' = \kappa_\perp \left\langle |\nabla\psi|^2 \right\rangle T_e''$$

$$+ \left(\kappa_\perp \langle \nabla^2\psi \rangle + \kappa_\perp' \left\langle |\nabla\psi|^2 \right\rangle\right) T_e' + S,$$

where $\kappa_\perp(\psi)$ and $S(\psi)$, the latter representing the various sources and sinks such as ohmic heating, radiation losses and heat transfer to the ions. In the case $\kappa_\perp = S = 0$, $T_e(\psi,t)$ in the islands is determined by energy conservation. For small island size we obtain $\partial T/\partial\psi = 0$ in the islands, turning to $\partial T/\partial\psi < 0$ for larger island size, which is consistent with the numerical finding that no saturation of the tearing mode occurs in this case.

For general $\kappa_\perp$, S, a stationary solution of (2) and (1)) implies that the temperature profile in the islands is completely determined by the source term S in the islands. For a rounded current profile with the q = 2 surface well within the hot plasma, S should be positive in the islands, since ohmic heating is strong and radiation losses weak, giving rise to a (rather small) island size. As the current profile becomes more peaked, the q = 2 surface moves into the colder outer plasma layers, where conditions are opposite and hence S negative, leading to (unlimited) island growth. Quantitative investigations using appropriate models for S will be reported.

In addition, diamagnetic drift effects are taken into account. The linear dispersion relation is obtained by integrating the linearized equations in time. For $\omega^* > \gamma_t$, γ_t = tearing mode growth rate, significant deviations from the analytic dispersion relation $\omega(\omega - \omega_i^*)\,(\omega - \omega_e)^3 = i\,\gamma_t^5$ appear owing to finite size effects and viscosity.

The corresponding nonlinear equations are

$$\frac{\partial\psi}{\partial t} + v\cdot\nabla\psi = \eta j - \frac{T_e(r) + T_i(r)}{n(r)}\alpha\left[\nabla\psi \times \nabla n\right]_z - E_o$$

$$\frac{\partial n}{\partial t} + v\cdot\nabla n = \alpha\left[\nabla\psi \times \nabla\nabla^2\psi\right]_z - \frac{T_i}{n}\alpha\left[\nabla\psi \times \nabla n\right]_z$$

$$\frac{\partial w}{\partial t} + v\cdot\nabla w = \left[\nabla\psi \times \nabla\nabla^2\psi\right]_z - \left[\nabla\frac{v^2}{2} \times \nabla n\right]_z$$

$$w = \nabla\cdot(n\nabla\phi), \qquad \alpha = \frac{c}{\omega_{pi}qR} .$$

These equations are discussed and solve numerically. A large nonlinear frequency shift is found which may even reverse the sign of ω. The saturation island width is not significantly different from that obtained for $\omega^* \ll \gamma_t$, and hence the model (1), (2) should have a rather broad range of validity.

2. As the amplitude of the m = 2 mode becomes large nonlinear coupling to the m = 1 mode is to be expected, particularly if $q(0) \lesssim 1$. To study this effect and in the hope of obtaining a qualitative description of the disruption process, a three-dimensional code has been set up.

Considering the case where q(0) < 1 and the m = 2 being unstable and nonsaturating, strong interaction between m = 1 and m = 2 is found. This process will be analysed in detail. Finite parallel heat conduction is included to account for the rapid energy depletion of the central part of the plasma.

1) D. Biskamp, H. Welter, Plasma Physics and Controlled Nuclear Fusion Research, 1976, Vol. I, p. 579

"This work was performed under the terms of the agreement on association between the Max-Planck-Institut für Plasmaphysik and EURATOM".

EFFECT OF FLUCTUATING ELECTRIC FIELDS ON SUPERBANANA DIFFUSION OF PLASMA IN A STELLARATOR

V.S. Voitsenya, A.Yu. Voloshko, S.S. Kalinichenko, S.I. Solodovchenko, A.F. Shtan'

It is shown that the excitation of electric fields of a wide noise spectrum in the appropriate frequency range results in $30 \div 40\%$ increase of the low collisional plasma containment time at the $l = 3$ stellarator Saturn.

It follows from the neoclassical theory [1], that the observed increase of transport coefficients, when plasma collision frequency decreases, is connected (in closed magnetic traps) with the presence of trapped particles. This effect should manifest itself most strongly when a collisionless plasma is confined in configurations with local inhomogeneities of the magnetic field – stellarators and rippled tokamaks [2].

By now such an increase of plasma diffusion coefficient has been observed in modelling experiments at several devices of the stellarator type (see review [3]). One can believe that it is possible to effect plasma transport coefficients in toroidal magnetic traps by changing, in an appropriate way, the movement of localized particles. One feasible method [4,5] consists of transferring some part of localized particles into passing ones by means of fluctuating electric fields. The frequency of the field time change must be equal (or be multiple) to the localized particle bounce frequency.

For the particle to be transferred into a passing one (due to the fluctuating electric fields) the longitudinal velocity addition value may be very small ($\tilde{v}_{\parallel}/v_{th} \sim 0.1$) as compared with the thermal velocity because $v_{\parallel}$ itself is small for localized particles ($v_{\parallel}/v_{th} < \sqrt{\varepsilon}$ where ε is the relative inhomogeneity of the magnetic field).

In this Letter we present some results of studying the effect of fluctuating electric fields on low collision frequency plasma at the $l = 3$ toroidal stellarator Saturn [3]. The experiment has been done in the regime of a very low collision frequency when the increase of the plasma diffusion is observed.

The hydrogen plasma with initial density $\sim 10^{10}\,cm^{-3}$ was produced by a titanium plasma gun located between the last magnetic surface and the vacuum chamber wall. To measure parameters of plasma and its lifetime τ the double electrical probe was used. The lifetime was defined from the decay of ion saturation current to the probe starting with a time instant when:

$n_e \simeq 10^9\,cm^{-3}$, $T_e = 5 \div 8$ev, $T_i = 15 \div 20$ev, $\nu_{en} \lesssim \nu_{ei}$.

The bounce frequency of localized particles is $f_\ell \simeq \dfrac{v_{th}\sqrt{\varepsilon_h}}{2\pi N R}$

where N is the number of the magnetic field periods, R is the torus major radius, ε_h is the relative value of the helical inhomogeneity of the magnetic field, v_{th} is the particle thermal velocity. In the $l = 3$ stellarator ε_h depends on the minor radius of the magnetic surfaces [2], therefore, the localized particle bounce frequencies would be different for different radii of the plasma column cross-section. For the stellarator Saturn ($N=8$, $R=36$cm) in the range of radii between 2 and 5.5cm where the main part of the localized electrons $\delta n \sim n_e(r)\sqrt{\varepsilon_h(r)}$ is concentrated, the bounce frequency changes from 0.2 MHz to ~1.2 MHz (for $v_{the} = 1.7 \cdot 10^8$cm/sec). For this reason, the noise generator of the stochastically modulated signal, similar to that described in [6], was used. The frequency range of this generator was $0 \div 10$ MHz and the band width $\lesssim 2$MHz. The HF voltage was applied to the exciting electrodes (EE) as shown in Fig.1 so that mainly the longitudinal electric fluctuating fields should be excited in a plasma [7].

Fig.2 shows the dependence of τ on the amplitude of the HF voltage, $\tilde{U}$, applied to EE when only one pair of EE was used. The spectrum of the HF voltage and the method of its measurement are shown in the insertion of Fig.1.

It is seen from the graph of Fig.2 that the confinement time increases with $\tilde{U}$ up to the maximum value (at $\tilde{U} \simeq 100$mV) and then begins to reduce. This maximum value of τ remains unchanged (30÷40% more as compared with $\tilde{U}=0$) but it moves into the region of lower HF voltage amplitude ($\tilde{U} \simeq 60$mV) when two pairs of EE were used apparently due to the better coupling between EE and a plasma in the last case.

At fixed $\tilde{U}$, an effect of τ increase (Fig.2) has a resonance character on the RF spectrum position dependence in the frequency range 0÷10MHz, as shown in Fig.3 (two pairs of elements, $\tilde{U} \simeq 60$mV). The resonance position is shifted, as compared to the range of the bounce frequency of localized electrons, the range being calculated on the basis of $\bar{\varepsilon}_h(r)$ for stellarator Saturn (this range is marked in Fig.3 as Δf_ℓ). On supplying a monochromatic signal to EE, a slow decrease of τ is observed as HF voltage grows, Fig.4.

The τ growth was not also observed in the case when electron collision frequency was increased (by addition of neutral helium) to the values conforming to plateau regime of the neoclassical theory.

And finally it should be noted, that according to estimation, the amount of energy delivered to EE from the generator in τ time makes up only several per cent (at $\tilde{U} \simeq 100$mV) of the plasma energy content and therefore cannot more or less essentially change plasma parameters.

Thus, the observed increase of τ (30÷40%) can be explained by untrapping some part of the localized electrons and the corresponding plasma loss decrease.

The τ drop at the further increase of $\tilde{U}$ takes place, apparently, through the increase of losses connected with turbulent diffusion, or through other effects [8] caused by a rather high level of oscillations in a plasma.

REFERENCES

1. B.B. Kadomtsev, O.P. Pogutse, Nucl. Fus., 11, 67, (1971).
2. T.E. Stringer, 3-d Int. Symp. on Toroid. Plasma Confinem., Garching 1973, paper F 1-1.
3. V.S. Voitsenya, A.Yu. Voloshko, S.I. Solodovchenko, V.A. Suprunenko, V.T. Tolok, A.F. Shtan', IAEA, Tokyo 1974, v.2, p.63, Vienna 1975.
4. R.A. Demirkhanov, M.A. Stotland, Sh.V. Hil', ZhTF, 42, 1419, (1972).
5. M. Dobrowolny, A. Orefice, R. Pozzoli, Nucl. Fus., 13, 485 (1973).
6. S.S. Kalinichenko, O.M. Shwets, Radioelektronika, 18, 120, (1975).
7. A.Yu. Voloshko, et al. Pis'ma v ZhETF, 16, 80, (1972).
8. L.M. Kovrizhnykh, Pis'ma v ZhETF, 17, 369, (1973).

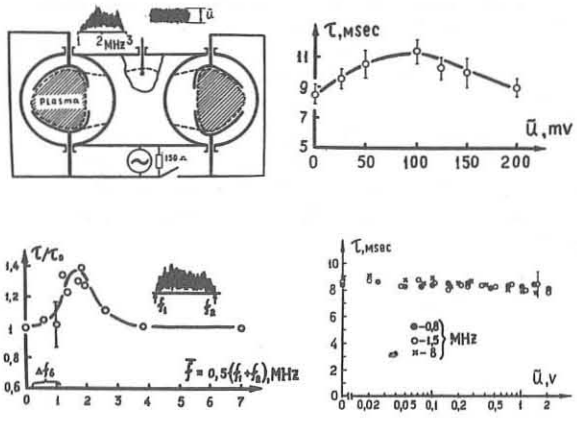

EXPERIMENTAL INVESTIGATIONS OF CURRENT DISHARGE PLASMA CONFINEMENT IN L=1 TORSATRON IN THE REGION OF LOW-FREQUENCY COLLISIONS

V.K. Bocharov, V.L. Berezhny, E.D. Volkov, B.V. Kravchin, V.G. Konovalov, V.I. Kononenko, V.A. Rudakov, E.A. Sukhomlin, V.A. Suprunenko, A.M. Ternopol.

Recently in experiments on the torsatron "Vint-20" [1] the confinement of currentless model plasma produced by titanium injectors ($T_e \simeq 5 \div 10$ev, $n \simeq 10^9 \div 10^{10} cm^{-3}$) has been investigated in the region of low-frequency collisions ($\nu_{eff} = \nu_{ee} + \nu_{ei} + \nu_{en} < \varepsilon_t^{3/2} \frac{v_{Te}}{R}$). It has been shown in this case that the lifetime of plasma particles is in satisfactory qualitative agreement with the neoclassical theory developed for the case $\varepsilon_h > \varepsilon_t$ [2].

In the given work the results of investigations on thermal insulation and confinement in "Vint-20" device of current-carrying plasma with parameters ($n \simeq 3 \cdot 10^{12} cm^{-3}$; Te up to 80 ev) have been pressented.

The experiments were performed with the helium plasma under initial pressure of neutral gas $6 \cdot 10^{-5}$ torr. The discharge initiation was accomoplished by means of a titanium injector. The current in plasma was excited through an electric field induced by the torsatron helical winding itself while changing the basic magnetic field in time. All obtained results apply to case of summation of current rotational transform with the main rotational transform through the ohmic heating current field. The distinguishing feature of the given experiment lies in a very low level of impurities (the authors did not succeed to register carbon and oxygen spectral lines at a sensitivity limit of apparatus). This is apparently caused by design features of the machine, nevertheless, an appreciable anomaly of the current discharge plasma conductivity is observed. Fig.1 shows conductivity anomaly $\frac{\sigma_{coll}}{\sigma}$ for two discharge regimes, differing in values of density and magnetic field amplitude versus E/Ek. Here $E = \frac{V - V_L}{2\pi R}$, $E_k = \frac{m_e v_{Te} \nu_{coll}}{e}$ is Draicer critical field, $\sigma_{coll} = \frac{ne^2}{m\nu_{coll}}$ $\sigma = \frac{I \cdot 2\pi R}{S(V - V_L)}$, I - current in plasma, S - plasma co-lumn cross-section, V - system by-passvoltage, V_L - its inductive component.

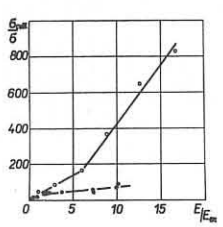

Fig.1

The energy content of plasma both in case of strong and weak anomalies is proportional to $i_\Sigma I$ (fig.2), where i_Σ is a summary angle of rotational transformation. This relationship complies with the pseudoclassical law of thermal losses. For the strong resistance anomaly case $\frac{U}{v_{Te}} < 0.1 \simeq \bar{\theta}$ (U and v_{Te} are current and thermal electron velocities, $\bar{\theta}$ is an average shear parameter), the coefficient of proportionality "a" in the formula $\chi = a^2 \rho^2 \nu_{eff}$ equals 3.5 and in the case of weak anomaly $\frac{U}{v_{Te}} > 0.1 \simeq \bar{\theta}$ it attains 10. The demarcation of regimes is observed at $\frac{U}{v_{Te}} \simeq \bar{\theta}$.

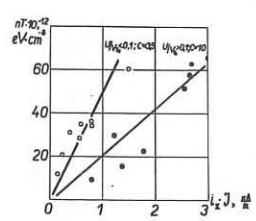

Fig.2

While measuring the lifetime of charged particles τ_n, primary emphasis was given to the revealing of functional relationships and their correlation with the neoclassical theory.

The collision frequency range ($5 \cdot 10^4 \div 5 \div 10^5$ sec^{-1}) in given experiment for the torsatron "Vint-20" complied with a superbanana region of the diffusion curve for which according to the theory we have $D_\perp$ sb $Te^{7/2}/H^2$. The results of experimental investigations of such kind of relationships are shown in Figs.3 and 4. Straight lines on the graphs comply with neoclassical theory predictions.

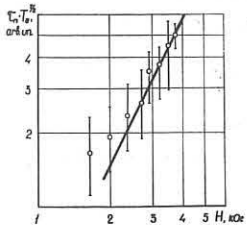

Fig.3

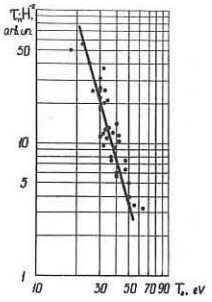

Fig.4

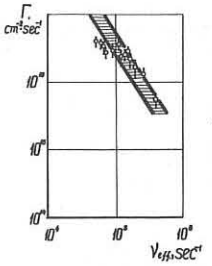

Fig.5

Experimental and theoretically calculated fluxes were also compared between themselves.

In Fig.5 the shaded band conforms to the formula [2]:

$$\Gamma = -4.34 \frac{\varepsilon_t^{3/2}}{\nu_{eff}} \left(\frac{c T_e}{eHR}\right)^2 n \left[\left(1 + \frac{T_i}{T_e}\right)\frac{n'}{n} + 3.37\frac{T_e'}{T_e} + 3.44\frac{T_i'}{T_i}\right]$$

assuming that $T_1 \ll T_e$, $\frac{n'}{n} = \frac{T_e'}{T_e} = \frac{T_i'}{T_i} = \frac{1}{r_0}$

The points conform to the measured diffusion flux $\Gamma = -\frac{r_0 n_e}{2\tau_n}$ in temperature range 20 to 70 ev. Over the range $10^5 < \nu < 5 \cdot 10^5$ sec^{-1} a satisfactory agreement between theory and experiment is observed. A decrease of experimentally measured flux at low frequencies can be explained by existence of the radial electric field $E_r \sim \frac{T_e}{e r_0}$ which must cause disruption of superbanana motion. The value of radial electric fields measured in this experiment were of the order of $5 \div 10$v/cm.

Thus, in the torsatron with high inhomogeneity of magnetic field some pseudoclassical losses of current plasma energy are observed and the particle confinement is described by the law approximating the neoclassical one.

REFERENCES

1. Voitsenya V.S. et al., Voprosi atomnoy nayki i tekhniki (USSR), 1(2), 76 (1974), Kharkov.
2. Stringer T.E., Third Intern. Symp. on Toroidal Plasma Confinement, F - 1, (1973), Munich.

MAGNETOHYDRODYNAMIC INSTABILITIES IN A STELLARATOR

K. MATSUOKA, K. MIYAMOTO, K. OHASA and M. WAKATANI
Institute of Plasma Physics, Nagoya University,
Nagoya 464, Japan

Abstract: Stability diagrams on kink and resistive tearing modes are presented in a linear stellarator for the parabolic current profile and various helical fields.

In a stellarator kink instabilities [1] and the effect of finite resistivity on m.h.d. modes [2] have been studied by many authors. Here we present more detailed stability diagrams on these modes.

We treat a pressureless plasma in a linear stellarator with an ohmic heating current. The current has the parabolic distribution: $j_z(r) = j_0(1 - r^2/a^2)$, where a is the minor radius of the plasma column. The external region from r = a to r = b is filled with vacuum, where b is the wall radius. We consider the following rotational transform angles: $\iota^\delta(r) = \iota_0^\delta$ (1), $\iota^\delta(r) = \iota_0^\delta(0.286 + 0.714\ (r/a)^2)$ (2), $\iota^\delta(r) = \iota_0^\delta(r/a)^2$ (3), where ι_0^δ is the rotational transform angle at the plasma surface. Helical fields given by Eqs.(1), (2) and (3) correspond to those of WVIIA and JIPP T-II, L-2 and CLEO stellarators.

The Euler equation $\frac{d}{dr}(r\frac{d\psi}{dr}) - \frac{\alpha}{r}\psi = 0$ is obtained from the energy integral which is derived under the stellarator expansion [1]:

$$2\delta W = \frac{8\pi^2}{k}\left\{\int_0^a r\,dr\left[\left(\frac{d\Psi}{dr}\right)^2 + \frac{\alpha}{r^2}\Psi^2\right] - \frac{1}{a}\frac{d}{dr}\left(r^2\iota^{(\sigma)}\right)\frac{\Psi^2}{\nu}\Big|_{r=a} + m\Psi^2(a)\frac{1+(a/b)^2}{1-(a/b)^2}\right\},$$

$$\Psi = -\frac{krB_0}{2}\nu\xi, \quad \nu = -\frac{2\pi n}{m} + \iota^{(\sigma)}(r) + \iota^{(\delta)}(r), \quad \alpha = m^2 + \frac{1}{r\nu}\frac{d}{dr}\left(r^3\frac{d\iota^{(\sigma)}}{dr}\right),$$

where ξ denotes the radial displacement of the plasma column and $\iota^{(\sigma)}(r)$ is due to the plasma current. Here pressure term and several terms of the order of $(kr/m)^2$ are neglected. We obtain the stability criterion of kink and resistive tearing modes, following the theorem given by Newcomb[3] and the numerical procedure by Furth et al.[4], respectively. In our calculations the length is normalized by the plasma radius (a=1, b=1.44, 3.0).

In order to understand the stability properties of kink modes, the Euler equation can be shown in terms of ξ:

$$(r^3\nu^2\xi')' - \{(m^2-1)r\nu^2 - (3r\iota^{\delta\prime} + r^2\iota^{\delta\prime\prime})r\nu\}\xi = 0. \qquad (4)$$

The derivative of ξ is given by

$$\xi' = \frac{1}{r^3\nu^2}\int_0^r\left\{(m^2-1)r\nu^2 - (3r\iota^{\delta\prime} + r^2\iota^{\delta\prime\prime})r\nu\right\}\xi\,dr. \qquad (5)$$

Equation(4) is simplified in special cases as follows:

ℓ=2, m=1 $\quad (r^3\nu^2\xi')' = 0,$ (6)

ℓ=2, m>1 $\quad (r^3\nu^2\xi')' = (m^2-1)r\nu^2\xi,$ (7)

ℓ=2 + ℓ=3, m=1 $\quad (r^3\nu^2\xi')' = -(3r\iota^{\delta\prime} + r^2\iota^{\delta\prime\prime})r\nu\xi.$ (8)

The solution of the Euler equation is given by $\xi \sim r^{m-1}$ near the origin and ξ=const.(small solution) near the singular point r_s. We see from Eq.(5) how ξ behaves in the subinterval, i.e., whether ξ crosses zero or not.

In the ℓ=2 case horizontally striped areas are unstable regions against external kink modes which mean the instability due to the singular point in the vacuum. Dotted areas refer to unstable regions against the tearing mode. The m=1 internal kink mode is marginally stable within the assumptions used here, since ξ=const. near the origin and $\xi' = 0$ from Eq.(5). The m=2 and m=3 tearing modes are stable for $\iota_0^\delta > \pi$.

When an ℓ=3 helical component exists, the stability criterion is determined essentially by the ℓ=3 helical field. From the negative derivative of ξ given in Eq.(5), the m=1 external kink mode becomes unstable even without singular points in the region $0 < r < b$, which is shown by the horizontally striped areas by dashed lines. The unstable m=1 'external kink mode' with the singular point inside the plasma (in this case the plasma surface is perturbed) is also explained by the similar account. It should be noted that the m=1 internal kink mode which is shown by vertically striped areas becomes more unstable than tokamak. When $\iota_0^\delta = 0$ (corresponds to tokamak), the mode is marginally stable in accordance with the ℓ=2 case. The m=2 and m=3 internal kink modes also can become unstable if the condition $(m^2 - 1)\nu < 3r\iota^{\delta\prime} + r^2\iota^{\delta\prime\prime}$ is satisfied. Therefore these modes become unstable for ι_0^δ which is larger than a critical value as shown in the figures.

The unstable ranges of the m=2 and m=3 tearing modes as a function of r_s are shown for the ℓ=3 case. When $\iota_0^\delta = 0$, values of Δ' are same as those of the ℓ=2 field. The effect of the wall location is also shown in the case of $\iota_0^\delta = 0$. For the m=3 mode the wall effect is too slight to be seen on the graph.

Stability diagrams with various current profiles will be reported elsewhere[5].

References

[1] SINCLAIR, R.M., YOSHIKAWA, S., HARRIES, W.L., YOUNG, K.M., WEIMER, K.E., JOHNSON, J.L., Phys. Fluids 8 (1965) 118.

[2] JOHNSON, J.L., GREENE, J.M., COPPI, B., Phys. Fluids 6 (1963) 1169.

[3] NEWCOMB, W.A., Ann. Phys. 10 (1960) 232.

[4] FURTH, H.P., RUTHERFORD, P.H., SELBERG, H., Phys. Fluids 16 (1973) 1054.

[5] MATSUOKA, K., MIYAMOTO, K., OHASA, K., WAKATANI, M., IPPJ-287 (Research Report of Institute of Plasma Physics, Nagoya University, 1977) to be published.

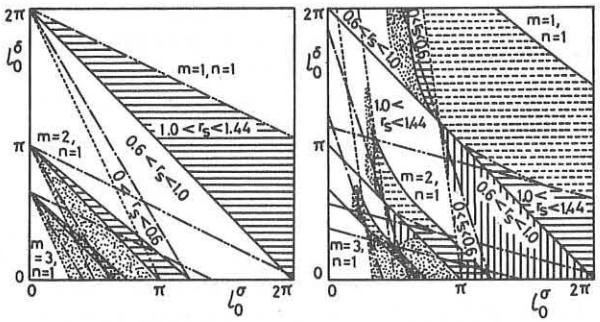

l=2 l=2 + l=3

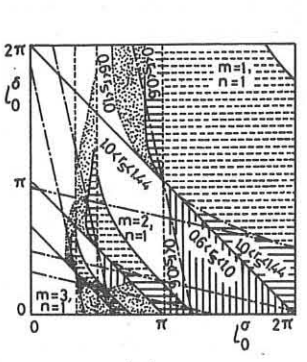

l=3

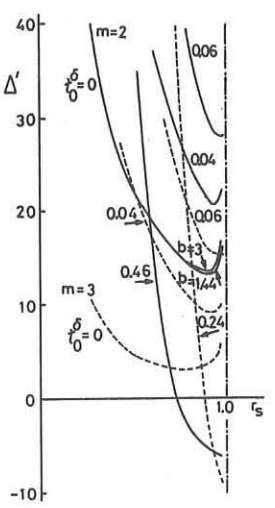

On Sawtooth Oscillations and MHD-Modes in the W VII A Stellarator

W VII A Team[+)]
Max-Planck-Institut für Plasmaphysik, EURATOM-Ass.
D-8046 Garching, Federal Republic of Germany

Abstract: For discharges with plasma currents constant in time evidence is given on sawtooth oscillations in the W VII A stellarator; MHD modes of m = 3, n = 2 and m = 2, n = 1 are identified at different plasma parameters.

First experimental results of the W VII A stellarator were presented at the Berchtesgaden conference /1/. At that time experiments were performed with a transient plasma current whereas now stationary plasma parameters are maintained /2/ for $\gtrsim$ 0.3 s. A study of sawteeth and MHD modes still is hindered by technical imperfections: very high plasma densities and feedback control of the vertical field are not yet available. During current built-up, when passing rational values of ι at the plasma edge, strong effects are observed on various diagnostics /1/. In this paper, effects occurring during the current plateau of the discharge are studied exclusively. Table I lists the diagnostics relevant for the present investigation.

Plasma Signals	Wall Signals	Magnetic Signals
Soft X	Limiter Signals	B_θ-Coils
μ-Wave Interf.	Langmuir Probe	Rogowski Coil
HF-Probe	Hard X	Loop Voltage
Diamagn. Loop	Bolometer	Position

Table I

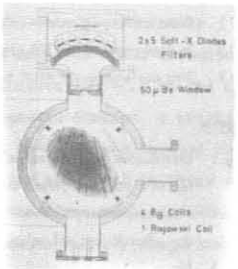

Fig.1:
Soft X diode array and B_θ-coils

The arrangement of the soft X-ray detectors and B_θ-coils is shown in Fig.1. Fig.2 shows the behaviour of external MHD modes detected by the magnetic pickup coils, in correlation with internal disruptions as seen by the soft X-ray diodes, $\tau_{\text{saw}} \approx 1.3$ ms. The distortion caused by the 600 Hz-ripple of the OH system is also visible on the Rogowski signal. The stationary phase of the discharge is dominated by a m = 3, n = 2 mode at f/m $\approx$ 7 kHz. The total rotational transform at the plasma edge is $\iota(a) = 0.57$. Therefore, this mode can be attributed to a MHD instability at the

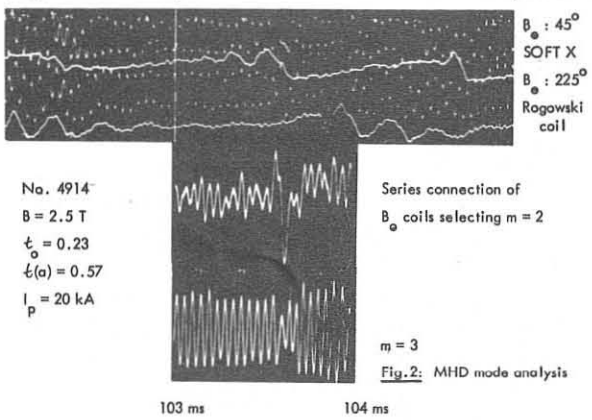

Fig.2: MHD mode analysis

ι = 2/3 surface. Since in /1/ the complete diagnostic equipment was not yet available, this mode has been misinterpreted as m = 1. During the internal disruption a m = 2 mode appears here for a short time, as observed by a proper series connection of the B_θ-coils providing a simple Fourier analysis.

In the case of a rotational transform $\iota(a) \leq 1/2$ and $\iota_o = 0.11$ a transition from m = 3, n = 2 to m = 2, n = 1 has been observed with frequencies f/3 $\approx$ 7 kHz and f/2 = 4 - 5 kHz during the internal disruption. This feature could indicate a change of the radial current density profile in accordance with an observation of negative voltage swings during this time and a modulation of the plasma current. These phenomena are also expected by theory /3/.

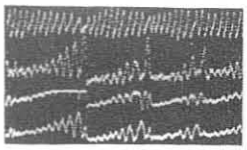

Fig.3: No.4094
Mode coupling of internal m = 1 and external m = 2 modes, $\iota_o = 0.11$, $\iota(a) \lesssim 1/2$
B = 2.75 T, ι = 100 ms.

Fig.3 exhibits the growth of the internal m = 1 modes ($\gamma \sim 10^3$/sec) between the relaxations and a strong mode activity m = 2, $\delta B/B \approx 2 \cdot 10^{-3}$ at the outside. A mode coupling can be seen between the B_θ-signals and the soft X-rays near the ι = 1 surface.

For all cases studied the modes propagate in the direction of the electron diamagnetic drift. For the discharge in Fig.3 the observed frequencies agree within 30% with those calculated from the laser profiles.

Sawtooth relaxations play an important part in energy transport. Taking the soft X-ray flux $\sim (n_e T_e)^2$ - approximately valid for a plasma with $T_e \sim 300$ eV and ≈ 1 % of fully ionized oxygen - the losses by the sawtooth relaxations only yield a confinement time $\tau_E^{saw} = 2 \tau_{saw} / (\Delta A_{saw}/A)$, where τ_{saw} are the relaxation period and $\Delta A_{saw}/A$ the relative (peak to peak) sawtooth amplitude, respectively. For several discharges with $n_{eo} \sim 2 \cdot 10^{13}$ cm^{-3} the values of τ_E^{saw} are larger by a factor 2 - 3 than $\tau_E' = (3/2\, n_e T_e)/(\eta \cdot j^2)$. This means a substantial loss by the sawtooth relaxations, even at a moderate density.

In addition to the conventional diagnostics discussed above, in W VII A several outer diagnostics (see Table I) show a marked correlation with the sawteeth. Shortly after each relaxation the characteristic of a Langmuir probe situated in the limiter shadow reveals enhanced ion and electron fluxes. The potentials of the four insulated limiter segments, as well as the signals of a photo transistor viewing the limiter region are correlated /1/ with the internal relaxations and show superimposed high frequencies.

This feature is shown in Fig.4, top and centre trace, under discharge conditions similar to that of Fig.2. Connecting the two limiter segments as shown in the left part of Fig.4 introduces currents of the order of 1 A which are modulated by about 2 A in correlation with the internal disruption (Fig.4, bottom trace).

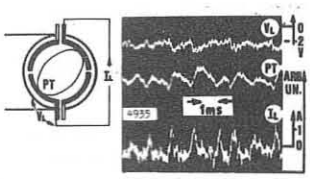

Fig.4: Limiter Signals, t = 120 - 130 ms

Generally, the mode activity seems to decrease, when increasing the external rotational transform. Especially, the m = 2, n = 1 mode diminishes, which mode is believed to play an important part in the disruptive instability. At $\iota_o = 0.23$ and $\iota(a) > 1/2$ (equivalent to q(a) < 2) a disruptive instability is never observed, even at high densities. The stellarator field has been seen to improve both the stability behaviour regarding tearing and kink modes /4/ as well as the plasma equilibrium.

References

/1/ Proceedings of Berchtesgaden Conference (1976), W VII Team, paper D 2.
/2/ This conference, paper presented by H.Renner.
/3/ Proceedings of Berchtesgaden Conference (1976), paper A 8.
/4/ K.Lackner, H.Wobig, private communication.

[+)] G.Cattanei, A.Cavallo, D.Dorst, A.Elsner, H.Hacker, H.Jäckel, R.Jaenicke, J.Junker, R.-C.Kunze, F.Leuterer, S.Marlier, G.Müller, F.Rau, H.Renner, H.Ringler, J.Saffert, J.Sapper, P.Smeulders, M.Tutter, A.Weller, H.Wobig, E.Würsching, M.Zippe

Ohmic Heating in the Wendelstein VII A Stellarator

W VII A Team[+)]
Max-Planck-Institut für Plasmaphysik, EURATOM-Ass.
D-8046 Garching, Federal Republic of Germany

Abstract: In ohmically heated discharges at high rotational transform the temperature and density profiles are flattened out by internal disruptions within the $q = 1/\iota = 1$ - surface. The current density is limited to $j \leq \frac{2B_o}{\mu_o R}(1 - \iota_o)$. This leads to a correlation between the energy confinement time of electrons, τ_E' and the central plasma parameters $n_e(o)$, $T_e(o)$, and Z_{eff}.

Introduction

At the Berchtesgaden conference [1] first results on Ohmic heating in the Wendelstein W VII stellarator were presented (R = 2.0 m, a = 0.1 m; helical windings l = 2, m = 5, external rotational transform $0 < \iota_o \leq 0.23$, without shear). After installation of the control system for the primary current of the air core transformer the plasma current I_p (t) is now programmable. The available OH-flux $\phi = 2.5$ Vs allows a duration of the discharge up to 0.5 s. To maintain the density for H_2 discharges an additional neutral flux $\Gamma(t)$ is necessary.

Electron Energy Confinement

As shown in [1] for high values of $\iota I_p = (\iota_o + \iota_p(a)) \cdot I_p \geq 8$ kA the pseudoclassical scaling of the energy density $nkT \sim (\iota_o + \iota_p) I_p \cdot B_o$ [2] does not hold anymore. We will demonstrate that the growing effect of the internal fluctuations which changes the profiles may be responsible for this deterioration.

From the density and temperature profiles, obtained by Thomson scattering, the current profiles are calculated under the assumption of Spitzer resistivity and $Z_{eff} = \text{const}$.

Fig.1 shows from top to bottom radial profiles of electron temperature, density and current density for $\iota_o = 0.23$ (heavy lines) and $\iota_o = 0.055$ (fine lines) and identical plasma current $I_p = 17$ kA. The q = 1 surface together with the current density limit $j(o) = \frac{2B_o}{\mu_o R}(1 - \iota_o)$ are indicated. An experimental coefficient for the heat conductivity χ_e can be derived by a numerical code from analytical curves fitted to the measured points of T_e and n_e [3], (Fig.2). For comparison the coefficient D_{PCL} for pseudoclassical transport has been plotted. The diameter of the q = 1 surface enclosing a region with enhanced transport widens with increasing external ι_o. Increasing the plasma current has the same effect.

A simple correlation between the electron confinement time τ_E' and the central plasma parameters $n_e(o)$, $T_e(o)$ and $j(o)$ can be derived. Similar to TFR [3] the variation of $\tau_E'(r)$ across the plasma radius is small: $\tau_E'(a) \approx \tau_E'(o)$, therefore,

$$\tau_E'(a) = \frac{\int n_e kT_e \, r\,dr}{\int \eta j^2 \, r\,dr} \approx \frac{n_e(o)\, kT_e(o)}{\eta(o) j(o)^2} = 0.19 \, \frac{n_e(o)\,(kT_e(o))^{5/2}}{Z_{eff}(1-\iota_o)^2 B_o^2} \text{ [sec]}$$

where n_e is in 10^{13}cm^{-3}, kT_e in keV, and B_o in Tesla.

Note that this correlation does not imply a $\frac{1}{B_o^2}$ scaling of τ_E', since $n_e(o)$, $T_e(o)$, Z_{eff} and B_o are interdependent.

Fig.3 shows that the experimental data confirm this relation. Estimations of the energy confinement based on sawtooth oscillations [4] demonstrate the importance of the internal instability for the confinement. Similar to the current density the power density is also limited in the plasma center. Under the conditions $Z_{eff} < 2$, $B_o = 2.5$ T, $\iota_o = 0.23$ a maximum electron temperature of 300 eV was found.

Behaviour of Plasma Density

For $n_e > 10^{13}\text{cm}^{-3}$ the recycling is not sufficient to maintain the plasma density, therefore, a constant neutral gas inflow is necessary. During a discharge the density could be varied between $8 \cdot 10^{12}\text{cm}^{-3} - 8 \cdot 10^{13}\text{cm}^{-3}$ by additional neutral flux $\Gamma(t)$.

The increase of the density is connected with decrease in temperature and Z_{eff}. Applying an additional neutral flux stationary conditions are reestablished in the discharge after 50 ms. The particle replacement time $\tau_A = \frac{\int n dV}{\Gamma}$, which is an upper limit for the particle confinement time, varies between 9 and 50 ms.

For $B_o = 25$ kG, $\iota_o = 0.23$ we have studied the plasma confinement with $\iota(a) = 0.5$ at the edge of the plasma. A stationary discharge without enhanced MHD oscillations and current disruptions could be maintained. But still enhanced losses were observed. In low density discharges they lead to a small reduction of density and an increase of kT_e and Z_{eff}. In discharges with stationary gas inflow Γ, Z_{eff} and kT_e remain practically constant, whereas the density drops by a factor of about 2 compared with discharges at $\iota(a) \gtrsim 0.5$ (Fig.4). During the transition phase additional plasma loss is also indicated by the enlarged probe signals at a position outside the last magnetic surface. The regime of enhanced losses is rather small, $\frac{\Delta J}{J} = \frac{\Delta \iota}{\iota} \approx 10\,\%$. The same effect can be achieved by small variations of the vertical field. This is an indication that the additional losses at $\iota(a) = 0.5$ may be due to magnetic islands in contact with the limiter or due to stationary convective cells originating from MHD instabilities.

References

[1] Proc. of Berchtesgaden Conference (1976), W VII Team, IAEA-CN-35/D2
[2] Proc. of Tokyo Conference (1974), H.Hacker et al., IAEA-CN-33/B1.
[3] Invited paper of the TFR Group, Proc. of Lausanne Conf. II, p.1-13 (1975)
[4] This conference, W VII A team, paper presented by A.Weller.

Figures

Fig.1 Distribution for temperature, electron and current density for different ι_o but with the same plasma current.

Fig.2 Heat conductivity derived from temperature and density profiles for different ι_o. Pseudoclassical values for comparison.

Fig.3 Normalized energy confinement time τ_E' as a function of the central electron temperature. Dashed curve: correlation given above.

Fig.4 Temperature and density distributions for $\iota(a) \lesssim 0.5$ ($q \gtrsim 2$), #5048, along with plasma current and energy content as a function of time.

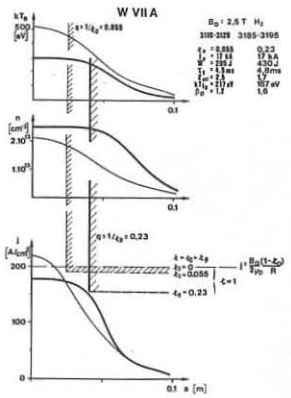

Fig. 1

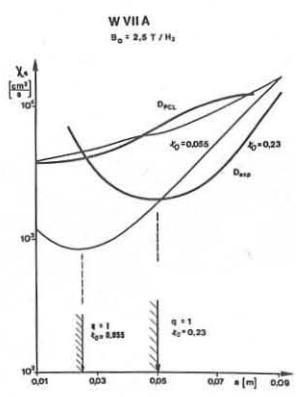

Fig. 2

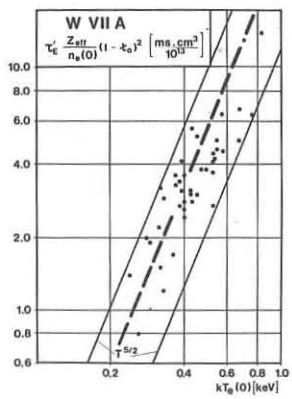

Fig. 3

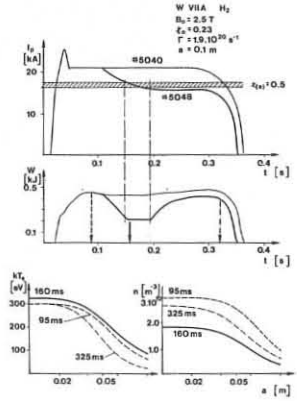

Fig. 4

+) G.Cattanei, A.Cavallo, D.Dorst, A.Elsner, H.Hacker, H.Jäckel, R.Jaenicke, J.Junker, R.C.Kunze, F.Leuterer, S.Marlier, G.Müller, F.Rau, H.Renner, H.Ringler, J.Saffert, J.Sapper, P.Smeulders, M.Tutter, A.Weller, H.Wobig, E.Würsching, M.Zippe

SOME CHARACTERISTICS OF OHMIC HEATING PLASMA IN THE L-2 STELLARATOR

D.K.Akulina, E.D.Andryukhina, M.S.Berezhetsky, G.S.Voronov, S.E.Grebenshchikov, M.S.Rabinovich, I.S.Sbitnikova, O.I.Fedyanin, Yu.V.Kholnov, A.V.Khudoleev*, I.S.Spigel.

Lebedev Institute of the Academy of Sciences, Moscow, USSR

The first ohmic heating experiments [1] on the L-2 Stellarator have shown the possibility of creation a plasma with sufficiently high parameters comparable with the parameters in tokamaks of corresponding sizes. The existance of the critical current was also discovered in these experiments which corresponds to the achievement of the total rotational transform angle equal to 2π in the centre of plasma column. This work is devoted to the more detailed study of plasma parameters, energy and particle confinement time in the current region essentially lower than the critical one.

The L-2 Stellarator has $\ell = 2$ helical magnetic field, the major radius of the torus R=100 cm; the mean plasma radius $\bar{a}$ =11,5 cm; the maximum longitudinal magnetic field strength B_0=20 kG. The angle of rotational transform $\iota_\phi(0)$=0.2 on the axis, and $\iota_\phi(a)$ = 0,7-0,8 on the boundary magnetic surface. A quasi-stationary current with a pulse duration 16-22 ms was induced in a plasma. The following plasma diagnostics were used in these experiments: electrotechnical methods, the diamagnetic measurements of the plasma energy and mean plasma density measurement. The electron and ion plasma temperatures were determined by X-ray and charge exchange atoms spectra. The behaviour of the hydrogen and impurities lines in the visible spectrum part was also studied. In Fig.1 the time-dependence of the main characteristics of the discharge is given: the plasma current I, loop voltage V, mean plasma density $\bar{n}$, plasma conductivity σ, ohmic heating power P, electron T_e and ion T_i temperatures, and plasma energy W. All plasma parameters achieve the stationary values for the time 7-10 ms depending on plasma density. Within the ranges of the magnetic field (9-16 kG) and initial gas pressure ($0.4\text{-}2.10^{-4}$ torr) at heating currents 9-20 kA a stationary discharge with $\bar{n}$=0.4 - 2 = 10^{13} cm^{-3},

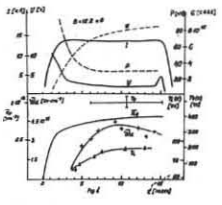

T_e=250-700 ev and T_i=65-120 ev was obtained. Fig.2 shows that T_e decreases with a density while T_i increases, i.e. the difference between ion and electron temperatures reduces. At present we have not yet information on density and temperature radial distribution. The parabolic distribution is supposed at all estimations of the energy content and the lifetimes. As Fig.2 shows the plasma energy content obtained by the diamagnetic measurements W_d with the accuracy of 30% coincide with the value calculated according to the measured electron and ion temperatures for $\bar{n}=7.10^{12}$ cm^{-3}. At low densities the discrepancy between these values is observed. It is difficulty now to say definitely of the cause of this. The energy lifetime is practically not changed with a density. As the ohmic heating current increases (Fig.3) the plasma energy and the lifetime increase.

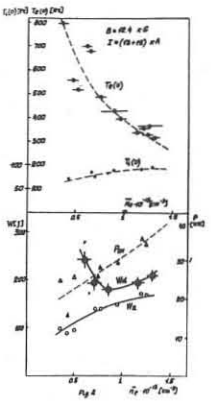

However, this rize is limited at the ratio I/B=1,3 when the toal angle of rotational transform $\iota_\phi + \iota_I$ =1 (ι_I - due to current) appears on the plasma boundary. The plasma confinement time decreases as the surface with $\iota = 1$ moves from the boundary to the centre of plasma column. The abroupt increase of ohmic heating power after I/B=1,3 indicates to the column resistance rise. This and some other features in the high current range permits us to make assumption about the change of the radial distribution corresponding to decrease of the effective plasma dimensions. Calculation of the power transfered from electrons to ions and absolute measurement of flux of the charge exchange atoms escaping the plasma shows that up to 30-40% of this power may escape due to charge exchange. The ion energy lifetime corresponding to the theoretical coefficients for the plateu region prove to be close to the experimental one (4-4,5 ms at B=12 kG), exceeding it 1,5-2 times. The functional dependence of the ion temperature on the plasma density and the magnetic field strength do not contradict to the Artsymovich formula. Calculations of the penetration of neutral atoms in a plasma and the integer charge exchange atoms flux was made. Its normalisation by the experimentally measured flux permited us to evaluate the neutral density in the plasma column. Simultaneously, the neutral density on the boundary was determined from H_α line intensity. Both methods gave coincoiding values and permitted us to calculate both local and mean particles lifetimes in a plasma. The local particles lifetime at the centre of plasma column at B=12 kG is ~80 msec and falls to the plasma boundary. The mean particle and energy lifetime as a function of a magnetic field is shown in Fig.4. The circles correspond to the values calculated for the T_e and T_i measured, the crosses - to the diamagnetic measurements. The solid curve II corresponds to the empirical scaling law $\tau_E \sim a^2 B_\theta$, where B_θ - is the sum of helical and plasma current poloidal fields, the former in our case being the dominant. Both particle and energy confinement time increases with increasing of the magnetic field. The confinement for stellarator case is essentially better due to the external poloidal field. However, the better confinement leads to the plasma conductivity increase and decreases the ohmic heating power input in a plasma. In this connection investigations of other methods of plasma heating in stellarators are of particular importance.

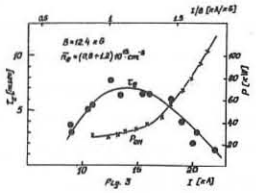

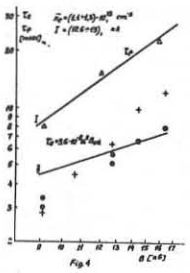

* Permanent address: Ioffe Physical-Technical Institute, the Academy of Sciences, Leningrad, USSR.

1. D.K.Akulina et al. Paper to the VI International Conference on Controlled Fusion and Plasma Physics, Berchtesgaden, 1976.

PARTICLE CONFINEMENT IN HF-HEATED PLASMA IN THE "URAGAN-2" STELLARATOR

A.G. Diky, V.G. Konovalov, B.V. Krawchin,
O.S. Pavlichenko, G.P. Pavlova, O.M. Shvets.

Particle confinement in a plasma heated by the ion-cyclotron waves in the "Uragan-1" stellarator were studied earlier [1]. One of results of these experiments was a conclusion about the neaclassical particle diffusion in ICRH plasma. The drawback of these experiments was a lack of data concerning magnetic field dependence of particle confinement time. In this report we present data concerning this question.

Parameters of the "Uragan-2" stellarator were described earlier [2]. The wave launching system was mounted inside of vacuum chamber on the straight part of the stellarator. This system was excited on the frequency 5.7 Mc/s. Changing the magnetic field strength from 3.6 kOe to 9.6 kOe it was possible to excite in the hydrogen plasma ion-cyclotron, ion-ion hybrid and Alfven waves. In these experiments electron density was measured by the 8-mm interferometer, plasma pressure n(Te + Ti) - by the diamagnetic loop, electron temperature - from helium lines ratio (5 ÷ 10% of helium was added in the hydrogen plasma).

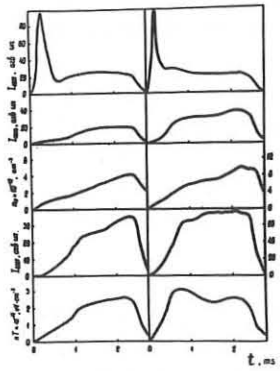

Fig. 1.

Particle confinement time τ_n was calculated from the electron balance equation [3]. Fig.1 shows the time behaviour of measured parameters for two values of magnetic field strength - 3.6 kOe (left column) and 9.6 kOe (right column) with HF pulse duration Δt = 2.5msec. Particle confinement time was measured at the moment $\Delta t \leq$ 1ms. Experimental data on τ_n were compared with these predicted by the neoclassical theory. In the experiment the electron temperature was in a range: 20ev $\leq$ Te $\leq$ 40ev. It means that our data correcponded to the plateau regime of theory ($0.1 \leq \frac{\nu_{ei}}{\nu_{pg}} \leq 0.5$; $\nu_{pg} = \frac{v_{Te}\theta}{r_c}$). Fig.2 shows experimental values of the diffusion coefficient $\mathcal{D}_{exp}$ ($\mathcal{D}_{exp} = a^2/(2.4)^2\tau_n$) normalized on values of the diffusion coefficient $\mathcal{D}_{st}$ [4], calculated for the case when $\alpha = \frac{\rho_{ni}}{a_n\theta} > 4$ and plotted against the normalized electron collision frequency. Here $\frac{\mathcal{D}_{exp}}{\mathcal{D}_{st}} = 1$ (solid line) correspond to the theory for the axially symmetric systems. The dashed line ($\frac{\mathcal{D}_{exp}}{\mathcal{D}_{st}} = 2.6$) takes into account the helical inhomogeneity of the magnetic field [5]. Closed circles are related to data obtained for the magnetic field range 3.6 kOe $\leq$ Ho $\leq$ 7.2 kOe, opened ones - for the range 8kOe $\leq$ Ho $\leq$ 9.6 kOe.

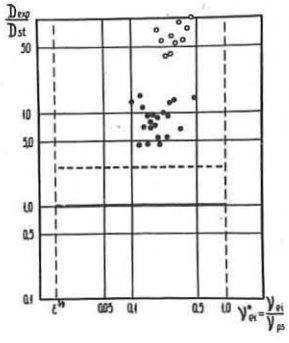

Fig.2

If to take into account the fact that the additional particle flux connected with electron and ion temperature gradients (the thermodiffusion) wasn't taken into account, one can consider data for lower part of magnetic field range as a good correspondance with theory predicted ones. Data for higher magnetic field indicate the factor 20÷40 amomaly of the particle diffusion.

Trying to clear the reason of this anomaly up, wehave analyzed the particle confinement dependence on plasma parameters.

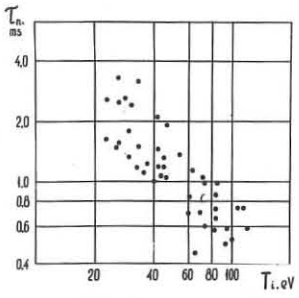

Fig.3

Fig.3 shows that the particle confinement time decreases with th the increase of ion temperature. This fact is in a qualitative agreement with the theory prediction.

The magnetic field dependence of the particle confinement time (Fig.4) showes that in the range 3.6kOe $\leq$ Ho $\leq$ 7kOe the particle confinement time increases as $\tau_n \sim Ho^2$. The saturation of τ_n in the range 7kOe $\leq$ Ho $\leq$ 9.6kOe reflects the above mentioned anomaly of the diffusion process. We dan't have any simple explanation of the observed anomaly yet. Trying to understand this phenomenon we paid attention to the fact that starting with the excitation of ion-cyclotron waves we passed to the excitation of Alfven waves ($k_{\parallel} \to 0$) (H_{ci} = 3.6kOe). Recent experiments on Alfven wave heating of plasma in the "Protoclec" stellarator [6] indicated that the anomalous particle diffusion accompanied the excitation of these waves. We shall study this phenomenon in detail in our future experiments.

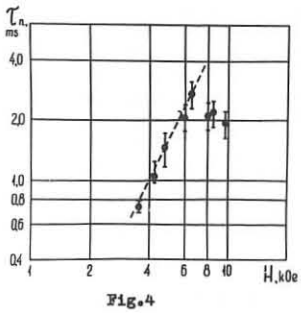

Fig.4

Physical-Technical Institute
Kharkov, USSR

REFERENCES

1. В.Г.Коновалов и др. Физика плазмы, т.3, вып. 2, стр. 311(1977)
2. А.Г.Дикий и др. Вопросы атомной науки и техники, вып. 1(2), Харьков, 1974.
3. В.Г.Коновалов, О.С. Павличенко, Г.П. Павлова, ЖТФ, 42, 1854 (1972).
4. T.E. Stringer, Phys. Fluids, 13, 1586 (1970).
5. T.E. Stringer, Phys. Fluids, 13, 810, (1970).
6. S.N. Golovato, J.L. Shohet, J.A. Tataronis, ECE-76-11, October 1976.

PLASMA HEATING BY ALFVEN WAVES IN THE PROTO-CLEO STELLARATOR

S. N. Golovato and J. L. Shohet
The University of Wisconsin, Madison, Wisconsin 53706 USA

Abstract: The shear Alfvén wave has been excited in plasmas in the Proto-Cleo stellarator. Doubling of both the electron and ion temperatures was observed. Evidence of the presence of a resonant surface in the plasma, which leads to the heating, was obtained. Some enhanced plasma loss was also seen.

The shear Alfvén wave has been excited in plasma confined in the Proto-Cleo ℓ=3, 7 field period stellarator. The experiment has a major radius of 40 cm and a plasma minor radius of about 5 cm. The confining magnetic field is 3 kG. Plasma was produced either with a titanium gun or by RF breakdown of neutral hydrogen. The gun produced plasma had a peak density of about 10^{12} cm^{-3} and electron and ion temperatures of 5 eV and 10 eV respectively. The RF-produced plasma had a peak density of about 10^{10} cm^{-3} and an electron temperature of 10 eV. The Alfvén wave was excited by a helical launching structure which was positioned at a minor radius of 7 cm and makes 3 revolutions of the major axis in one revolution of the minor axis. Figure 1 shows the experiment. The helical coil could be driven with RF at 1-2.5 MHz, in pulses of 0.4-1.2 msec at power levels up to 200 kW.

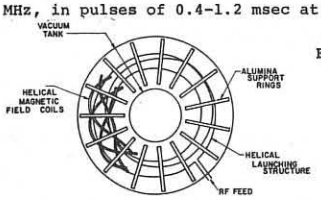

FIG. 1. The experimental configuration for the Proto-Cleo stellarator.

With application of 1 kW of RF power, a doubling of both the electron and ion temperatures was observed [1]. The electrons and ions must be heated independently by the wave, since energy equilibration by collisions was too slow to account for the heating of one species by the other. As well, the ratio T_i/T_e remained approximately the same after heating. The heating efficiency, measured as the ratio of the change in total plasma energy to the total RF energy applied, was about 6% with the majority of the rest of the RF lost in the wave launching helix itself.

The experimental results were compared with theoretical predictions of energy absorption using the analysis of Tataronis and Grossmann [2,3]. In their theory, energy absorption should occur in the vicinity of a resonant layer in the plasma defined where the applied RF frequecy equals the local Alfvén frequency,

$$\omega_A^2 = \frac{\left(\frac{m}{r}\right) B_\theta + kB_z)^2}{\rho_m \mu_o} ,$$

where m and k are the poloidal and toroidal wave numbers, B_θ and B_z are the poloidal and toroidal fields and ρ_m is the mass density. B_θ, B_z and ρ_m were assumed functions of minor radius only. Radial profiles of electron temperature and the wave magnetic field were made and showed no strong peaking as might be expected at the resonant layer. This may be explained by the fact that stellarators are not axisymmetric devices and the resonant layers are not closed toroidal surfaces. In Proto-Cleo, the diagnostics were located in a region that did not cross the resonant layer. The dependence of the heating on density and RF frequency for a gun produced plasma are shown in Figure 2. It is predicted by the theory that heating should be better at lower densities and lower frequencies for Proto-Cleo parameters. This effect is seen in Figure 2.

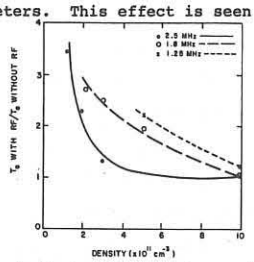

Fig. 2. Ratio of electron temperature with rf to electron temperature without rf versus density at three frequencies.

Along with plasma heating, enhanced plasma loss was observed when the wave was applied. The loss only occurred during the RF pulse and showed the same dependence on density and frequency as the heating. The enhanced loss increased linearly with wave amplitude.

Plasma was also produced by applying high power RF, up to 200 kW, to break down neutral hydrogen. The resulting plasma had a density of about 10^{10} cm^{-3} and an electron temperature of 10 eV. Radial profiles of density, electron temperature and the wave magnetic field showed strong peaking as shown in Figure 3. This indicated the existence of the resonant layer as predicted by theory. The peaking was more visible in the RF produced plasma case since the plasma was being created at the resonant layer where the wave fields were highest and because higher RF powers could be used. The RF peaks at a larger minor radius than n and T_e due to the non-axisymmetry of the stellarator equilibrium.

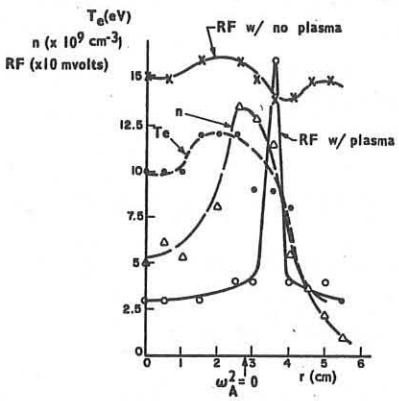

Fig. 3. Radial profiles of n, T_e, and RF amplitude with and without plasma for the RF produced plasma.

The results of this experiment show that plasma electrons and ions may be heated efficiently by Alfvén waves at frequencies below the ion cyclotron frequency. The existence of a resonant layer and the agreement with theory as parameters were varied indicate that the energy absorption was due to the effect known as Alfvén wave heating [2,4]. If the accompanying enhanced plasma loss can be controlled, this heating technique shows great promise for fusion reactor applications.

References

[1] S. N. Golovato, J. L. Shohet and J. A. Tataronis, Phys. Rev. Lett. 37, 1272 (1976).

[2] J. A. Tataronis and W. Grossmann, Nucl. Fusion 16, 667 (1976).

[3] S. N. Golovato, J. L. Shohet and J. A. Tataronis, IEEE Trans. on Plasma Science (to be published).

[4] A. Hasegawa and L. Chen, Phys. Rev. Lett. 32, 454 (1974).

Work supported by the National Science Foundation under grant ENG 75-11168.

ROTATING PLASMA IN THE "TORNADO-650" TRAP

J.Bergström, A.B.Beresin, V.M.Kuznetsov,
B.Lehnert, B.P.Peregood
A.F.Ioffe Physico-Technical Institute, USSR,
Leningrad K-2I, Politechnicheskaya 26 - jointly with
The Royal Institute of Technology, Sweden,
S-I00 44, Stockholm 70, Teknikringen 3I

Results of the first experiments on behaviour investigation of plasma created by means of crossed magnetic and electric fields discharge in the Tornado trap are reported. These are first experiments where plasma rotation is driven in a closed magnetic bottle.

The experiments were prepared and carryed jointly by the Royal Institute of Technology (Stockholm-Sweden) and the A. F.Ioffe Physico-Technical Institute (Leningrad-USSR). Results of works which had been carryed within the frames of programmes "Tornado" (PTI) and "Fiasco" (RIT) have played a role of prerequisites for the joint work raising.

There was ascertained by the works on "Tornado" programme that the trap field is closed and belongs to the class of fields having a spherical separatrix [1,2,3]; that inside the region limited by the separatrix there is a volume with the field strength increasing everywhere towards its boundary [4,5]; that plasma of $n \simeq 10^{12} - 10^{14}$ I/cm^3, $T \simeq$ I eV is hydromagnetically stable inside the trap and its behaviour and losses are determined by the classical diffusion [6,7].

Features of the behaviour of plasma rotating in the magnetic field which has field lines crossing an insulator surface were studyed while realising the "Fiasco" programme at devices F-I, F-2 and F-2a [8].

This new joint (RIT - PTI) programme is aiming at:

I.Production of plasma rotating in the magnetic field which has no field line escaping the system or crossing its constructional elements.

2.Behaviour investigation of plasma produced this way in the Tornado trap during the plasma decay. Statement of the lifetime dependence on temperature within the range of temperature up to several tens eV.

3.Investigation of possibility to exceed the Alfven plasma rotation velocity limit [8,9], restricting the rotation velocity for systems having end losses.

The experiments had been performed at the Tornado-650 apparatus (650 mm - separatrix diameter), equipped with systems of radial electric field production inside the trap and manipulating it.

There were measured: plasma current, total over the spectrum (3000 - 8200 Å) plasma light radiation dependence on time, integral over the time spectrum of the radiation in the range of 3600 - 8000 Å and microwave radiation in the range of 6 - 8 mm. Besides the plasma was photographed in its own light without time resolution.

Briefly, the results gained are following:

I.After several training discharges the discharge inside the trap becomes stable-ignited, the reproducibility of plasma and discharge parameters is good.

2.On the time-integral photos of plasma there was not noticed any inhomogeneity of discharge or plasma.

3.The short (50 μs) intense microwave radiation is registered at the starting instant of the discharge. During all later time of plasma rotation and decay this radiation is absent.

4. There are no oscillations or pulses on the current and total light radiation oscillogrammes. These time dependence curves are perfectly smooth (Fig.I).

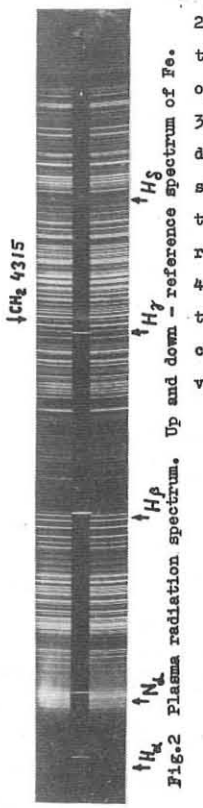

Fig.2

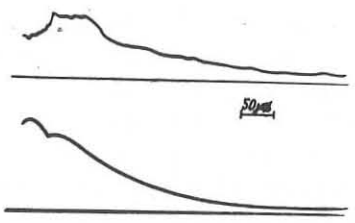

Fig.I Upper curve - total over the spectrum radiation (3000 - 8200 A), lower curve - plasma current.

5.Many times reproduced plasma radiation spectrum photos (5 - II expositions each time) have atomic hydrogen radiation lines predominantly: H_α, H_β, H_γ, H_δ (Fig2).

Presumable interpretation of the results performed with the help of some preliminary estimations is following:

I. Plasma density is of the order of 10^{14} cm^{-3}.

2. Ionization percentage is high in the central region. Neutral gas temperature around the plasma body near its surface is higher than hydrogen molecules dissociation temperature.

3. In the course of rotation and decay plasma has no large-scale disturbances.

4. Rotating plasma, presumably, have no contact with the conducting constructional elements of the trap for the phenomenon of plasma cleaning of heavy impurities due to the rotation can not be completely responsible for the cleanness of the plasma produced.

References:

I. B.Lehnert, Physica Scripta, 12, I66, I975.
2. B.P.Peregood, A.A.Semenov, ЖТФ, 4I, 2297, I97I.
3. B.P.Peregood, et.al. ЖТФ, 4I, 23I6, I97I.
4. K.B.Abramova, et.al. ЖТФ, 36, I426, I966.
5. A.N.Kozyrev, B.P.Peregood, ЖТФ, 40, 950, I970.
6. G.A.Galechan, B.P.Peregood, ЖТФ, 39, I996, I969.
7. A.N.Kozyrev, B.P.Peregood, ЖТФ, 44, 743, I974.
8. B.Lehnert, Nuclear Fision, II, 484, I97I.
9. H.Alfven, "On the origin of the Solar System", Clarendon Press, Oxford, I954.

FIRST RESULTS ON THE CONFINEMENT OF A LASER-PRODUCED PLASMA IN THE W IIb STELLARATOR

H.Baumhacker, H.Brinkschulte, K.Büchl, M.Hashmi, S.F. Marlier, W. Riedmüller, and M. Salvat

Max-Planck-Institut für Plasmaphysik, 8046 Garching, FRG.

Abstract: Isolated deuterium pellets were irradiated with a focused Nd glass laser beam at the axis of the stellarator W IIb. The plasma density in the torus reaches a maximum within 50 μs. At a toroidal magnetic field strength of 0.25 Tesla a space averaged density of 7 x 10^{12} cm^{-3} decaying within several msec has been detected.

The production of a plasma by irradiating matter with high power lasers offers the possibility of filling a stellarator with a plasma of high energy density and low degree of impurities without ohmic heating current. This method was studied earlier at the Lebedev Institute (1) using a large lithium disk and in Culham (2) using suspended wires of different materials as targets. In order to reduce the large amount of neutral gas produced if extended targets are irradiated, we used isolated deuterium pellets at the axis of the W IIb stellarator.

W IIb (2) is a stellarator with a $\ell = 2$ helical field and has a major radius of 0.5 m. It has a built-in limiter with a diameter of 0.12 m. A laser plasma production system consisting of a deuterium pellet droper, a triggering system and the energy laser was developed. Pellets about 300 μ in diameter and 500 μ in length containing about 2 x 10^{18} deuterium atoms were produced by cutting off the lower end of an ice stick (see Fig. 1). The pellets fall freely (0.3 m) down into the stellarator. If the pellet is detected by a triggering laser focused close to the axis of the stellarator, the energy laser is fired. It is a Nd glass laser, which delivers single or double pulses with selectable time distance and energy ratio, a half width pulse duration of 25 ns and a total energy of ~100 J. More details are given in (4). In order to find out the initial conditions of the laser-produced plasma, we measured the total number of ions by means of ruby laser interferometry and the energy of the ions by means of the time-of-flight method with electrostatic probes in a separate vacuum chamber without magnetic field. The results pertaining to single pulse laser shots are shown in Figs. 2 and 3 as a function of the laser energy and the radiation energy hitting the pellet respectively.

Fig 1

The plasma expansion velocity increases slightly with increasing laser energy and exceeds 2 x 10^5 m/s corresponding to more than 500 eV per ion. We have performed an optimization of the number of laser-produced ions with respect to the relative position of the laser focus and the pellet position. The maximum ion number was obtained when the pellet was hit 1.5 mm before or behind the laser focus, where the cross-section of the laser beam is about equal to the pellet cross-section. The number of the ions increases with increasing laser energy. Even in the optimum pellet position only about 2 x 10^{17} ions were detected corresponding to an ionization degree of ~10 % of the pellet. This is in agreement with the result of numerical calculations (5). Longer pulses or double pulses are required for full ionization of the pellet (6, 7, 8). Most of the experiments in the stellarator itself were therefore performed using two successive laser pulses (Δt = 70 nsec, $E_1/E_2 \sim 1/2$, $E_1 + E_2 \sim 80$ J). In the torus cross-section that is situated opposite the focus of plasma production we measured the space averaged electron density by means of a microwave interferometer as a function of time. Fig. 4 shows that the density reaches a maximum value 50 μs after the lasershot. The density decreases within a time of 1 to 2 msec depending on the toroidal magnetic field strength to values below 1 x 10^{11} cm^{-3}. Until now, only fields up to 0.25 Tesla have been applied. A maximum density - averaged along the limiter diameter - of 7 x 10^{12} cm^{-3} was found at B_{tor} = 0.25 T. At the stellarator axis a density higher than 10^{13} cm^{-3} can be assumed if allowance is made for a density profile. Taking into account the volume within the limiter of the W IIb stellarator of 3,6 x 10^4 cm^3, a maximum total number of electrons captured in the stellarator of 3.6 x 10^{17} is found. This number increases with increasing toroidal magnetic field strength (Fig. 5) and exceeds by a factor of 3 the maximum total ion number produced with single pulse laser shots. The current in the helical windings was varied from 0 to 1000 A. At low magnetic field strength and with t = 0 to t = 0.3 the plasma capture seems to depend only weakly on the rotational transformation. No signal exceeding noise is obtained by Thomson-scattering from an axial volume at 50 μs and later. This indicates that the electron temperature is less than 5 eV at an electron density of 5 · 10^{12} cm^{-3}.

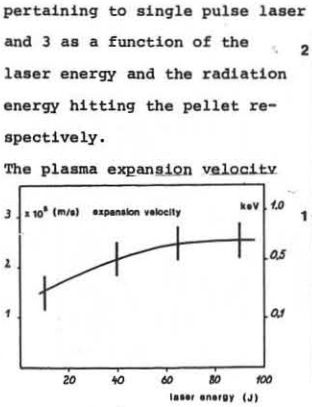

Fig 2

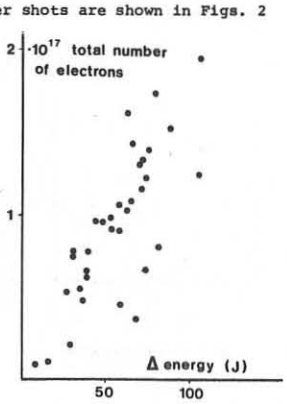

Fig 3

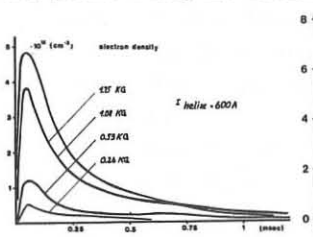

Fig 4

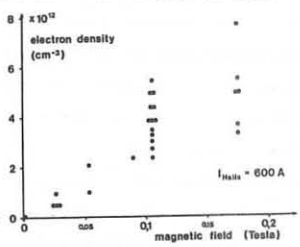

Fig 5

Conclusion: The largest part of the deuterium plasma produced by laser irradiation from isolated pellets on the stellarator axis is captured by the magnetic field.

(1) E.D.Andryukhina et al.: ZhETF Pis.Red. 14, 5, 317-320.
(2) R.A.E.Bolton et al.: IAEA-CN-28/H-6 Proc. IV Conf.(1971) on plasma phys., Madison, 79-82
(3) H.Hacker et al.: Plasma Phys.and Contr.Nucl.Fus.Res. II,3 (1974)
(4) H.Baumhacker et al.: Fusion Techn.,Proc.9th Symp.873-878(1976).
(5) L.L.Lengyel, Plasma Phys. 18, 929-945 (1976).
(6) L.L.Lengyel, IAEA-CN-35/G3-2, Berchtesgaden (1976).
(7) A.F.Haught,D.H. Polk:Phys.Fluids 13, 2825 (1970).
(8) J.R. Greig, R.E. Pechacek: Appl.Phys.Lett 29, 12, 798-800, (1976)

DC Current Generation by RF Travelling Field in a Magnetized Plasma

Masaji FUKUDA and Kiyokata MATSUURA
Institute of Plasma Physics, Nagoya University, Nagoya, Japan

Absract: The DC toroidal current driven by RF travelling field is studied experimentally in connection with the absorbed RF power and the plasma resistance in a magnetized plasma. The DC current distribution and the RF field distribution are measured.

An RF travelling field can produce a unidirectional current in a steady state/1-3/. The mechanism of the current generation is that the RF travelling field transfers not only RF power but also momentum to electrons in the plasma/4/. The force balance between the electromotive force produced by RF travelling field and the frictional force due to electron-ion collisions leads the following equation/4,5/

$$\frac{P_a}{(-N_e e V_p)} = \eta J_{DC} \qquad (1)$$

where P_a is the absorbed RF power, V_p is the phase velocity and η is the plasma resistivity. This current generation is expected to be applicable to the current sustaining of tokamak /5/. In this paper, we report experimental results for the DC toroidal current in a low magnetic field: (1) relation between the generated current I_t and the absorbed RF power P_a, (2) DC current distribution and RF field distribution.

Experiments were carried out by a tokamak device named Synchromak/3/. The schematic diagram of the device is shown in Fig.1. The major radius of the discharge tube is 25 cm and minor radius is 5 cm. The plasma is limited by a metallic limiter of 4 cm in radius. A stationary toroidal magnetic field B_t up to 3 kG is applied. The RF travelling field is generated by a transmission line which is set up locally on a glass discharge tube. The phase velocity of the field V_p is 1.9×10^6 m/sec, which corresponds to the electron thermal velocity of 11 eV. The RF power, from 200 kW nominal output oscillator, is fed to the line for a duration of 1.0∿2.0 msec. The RF frequency is 3.6 MHz. The argon plasma is produced by the RF field itself.

We measure I_t, N_e, P_a and plasma resistance R as a function of electron collision frequency ν_e at a constant magnetic field B_t = 0.3 kG, where ν_e is varied by changing the gas pressure. Here ν_e is calculated from the relation $\nu_e = \eta(N_e e^2/m)$. The plasma resistance R is measured by a current response to a weak pulse induction field which is generated by a current transformer with iron core(0.02 V·sec). The electron density is inferred from the fringes of 50 GHz microwave interferometer. Typical values at B_t = 0.3 kG and $P = 1.9 \times 10^{-4}$ torr are as follows: I_t = 200 A, $N_e = 8 \times 10^{12}$ cm^{-3}, P_a = 90 kW and R = 24 mΩ. Figure 2 shows the voltage P_a/I_o produced by RF travelling field and the voltage $R \times I_t$ due to the frictional force, where $I_o = -N_e e V_p S$ and S is the cross section of the plasma column. Both voltages decrease with increasing ν_e and indicate almost the same dependence. The voltage P_a/I_o is nearly equal to $R \times I_t$ within the experimental ranges of $\nu_e = 3$∿7×10^7 rad/sec. This result is consistent with eq.(1). Therefore we see that the force balance relation is satisfied in a collisional plasma.

The radial profile of DC current is measured by a magnetic probe. Figure 3 shows the profile $J_{DC}(r)$ at B_t = 0.3 kG and $P = 7.5 \times 10^{-4}$ torr. The current profile shows a hollow structure even for a quasi-steady state. From measurements of Langmuir probe, the profile of plasma density is observed to be fairly flat and not to be hollow structure. Therefore the structure is not due to electron density profile. Figure 4 shows radial profiles of RF magnetic field $\tilde{B}_r$, $\tilde{B}_\theta$ and $\tilde{B}_z$, which are measured by magnetic probes underneath the exciting coil. The field $\tilde{B}_z$ penetrates in the plasma with increasing B_t and then a bell-shaped profile develops/3/. The field $\tilde{B}_\theta$ is generated in the plasma and the amplitude is comparable to or higher than the field B_r. These RF field profiles indicate that there is an excitation of a proper mode of plasma wave. From dispersion relation of cold plasma, the wave is thought to be a Whistler mode. The perpendicular wave length is estimated from the shape of RF field to be 17 cm, while the value calculated from the dispersion relation is 8.2 cm for $N_e = 6.4 \times 10^{12}$ cm^{-3} and B_t = 0.3 kG.

From these components of RF magnetic field, the RF electric field can be calculated. The ratios among the amplitude of components thus obtained are

$$|\tilde{E}_r| : |\tilde{E}_\theta| : |\tilde{E}_z| = 1 : 0.5 : 2 \times 10^{-3}$$

The RF electric field $\tilde{E}_z$ is very small compared with the fields $\tilde{E}_r$ and $\tilde{E}_\theta$. Since the fields $\tilde{E}_r$ and $\tilde{E}_\theta$ are approximated by a Bessel function $J_1(k_\perp r)$, the absorbed RF power has hollow structure. Therefore we see that the generated current has also hollow structure since the plasma density and plasma resistance are fairly uniform.

References: /1/ K.Hirano et al.: Phys.Letters 36A (1971) 215.
/2/ S.M.Osovets and I.A.Popov: Proc.5th.Europ.Conf. on Contr. Fusion and Plasma Phys. Grenoble, 1972.
/3/ M.Fukuda et al.: J.Phys.Soc. Japan 41 (1976) 1376.
/4/ R.Klima: Plasma Phys. 15 (1973) 1031.
/5/ D.J.H.Wort: Plasma Phys. 13 (1971) 258.

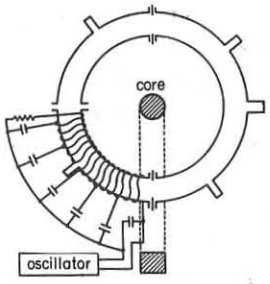

Fig.1. Schematic diagram of Synchromak.

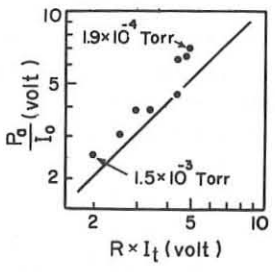

Fig.2. Voltages P_a/I_o and $R \times I_t$ at B_t = 0.3 kG

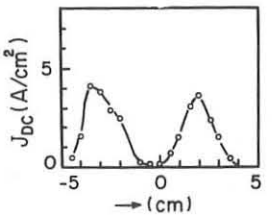

Fig.3. DC current profile at B_t = 0.3 kG.

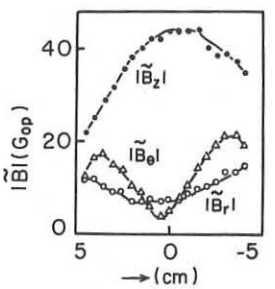

Fig.4. RF magnetic field profiles at B_t = 0.3 kG.

DIRECT TOROIDAL CURRENT GENERATED BY MICROWAVES

R. Klíma, V. Kopecký, J. Musil, F. Žáček
Institute of Plasma Physics, Czechoslovak Academy of Sciences,
Nademlýnská 600, 180 69 Prague 9, Czechoslovakia

Abstract: Generation of direct toroidal current by travelling microwaves is demonstrated experimentally. At parameters used, this current is apparently carried by fast electrons. The experimental results can be interpretted satisfactorily on the basic of previous theory.

The recent experiments [1] support the idea of the "peristaltic" stationary tokamak [2] by using low-frequency waves. The purpose of the present contribution is to give first preliminary results of (i) the excitation of the toroidal current in a magnetoactive plasma by microwaves and (ii) the comparison of the experimental data with the theory [3].

The study was carried out on the toroidal device INTERMEZZO, Fig. 1. Basic parameters of this device are: stainless

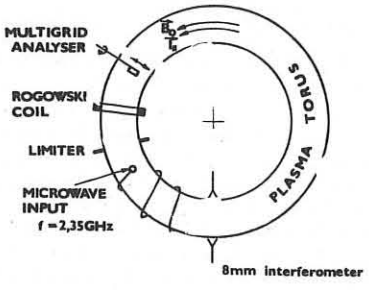

Fig. 1

steel vacuum toroidal chamber with major radius R = 35 cm and minor radius 4.7 cm, limiter radius 3 cm, steady toroidal magnetic field up to 2.5kG. A helical slow-down structure placed inside the vacuum chamber is fed from the magnetron 60 SA 51 ($\omega/2\pi$ = 2.35 GHz, P = 0÷5kW) in 200-500usec pulses with 50Hz repetition frequency. The initial plasma is generated by a directly heated cathode. The plasma density n, the toroidal current $I_{\parallel}$ and electron distribution function are measured by an 8 mm interferometer, Rogowski coil and electrostatic multigrid analyser. Experiments were carried out in hydrogen at $\omega_{ce}/\omega \simeq 1.7$, ω_{ce} being electron cyclotron frequency.

The experimentally found dependences of $I_{\parallel}$ and plasma density ω_p^2/ω^2 on the microwave power P are given in Fig. 2.

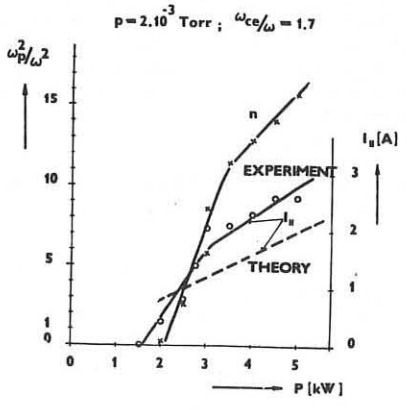

Fig. 2

Hydrogen pressure was p = 2x10^{-3}torr. Fig. 3 shows the dependences of $I_{\parallel}$ and P on hydrogen pressure for fixed density $\omega_p^2/\omega^2 = 7$. The data given by the electrostatic multigrid analyser (p = 2.2x10^{-3}torr, P = 5kW), see Fig. 4, demonstrate the presence of electrons with high parallel velocities $v_{\parallel}$ of the order of hundreds eV.

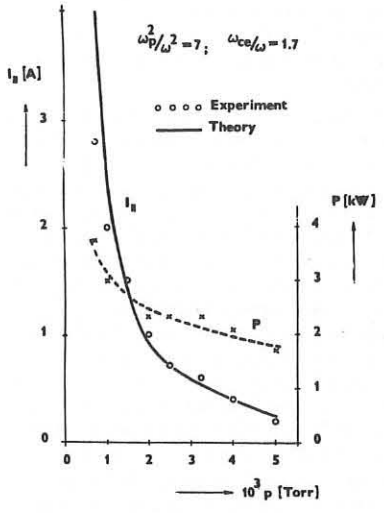

Fig. 3

According to the theory [3], the value of the toroidal current generated by a travelling wave is, in CGS elst. units,

$$I_{\parallel} \simeq e k_{\parallel} P / 2\pi R m \nu_e \omega \quad ,$$

where e and m are the charge and the mass of an electron, $k_{\parallel}$ is the longitudinal (here the toroidal) wave number of the wave excited in the plasma torus, ν_e is the effective collision frequency of electron momentum transfer. From the cold plasma dispersion theory $k_{\parallel} \simeq 2.5$ in the range of parameters

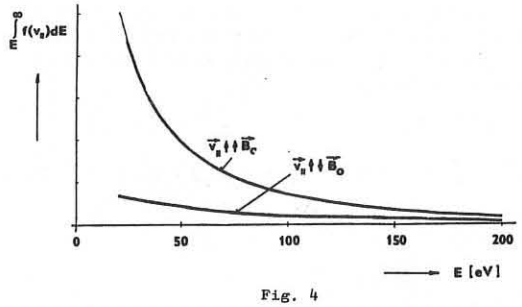

Fig. 4

used. According to Fig. 4, we suppose that $I_{\parallel}$ is created by fast electrons with energies about 100 eV and, therefore, $\nu_e \simeq 2\text{x}10^9 p$ [torr] is given by electron-neutral collisions [4]. The theoretical values of $I_{\parallel}$ found this way are also given in Fig. 2 and 3. It is obvious that the agreement with the experimental values is satisfactory.

We note that the wave excited by the slow-down structure (whistler wave) propagates antiparallelly to the magnetic field $\vec{B}_o$. This fact is given by the non-reciprocity theorem established in [5].

References:

[1] M.Fukuda et al.: J. Phys. Soc. Japan 41 (1976), 1376
[2] D.J.H. Wort: Plasma Phys. 13 (1971), 258
[3] R. Klíma: Plasma Phys. 15 (1973), 1031
[4] P.Laborie et al.: Electronic cross-sections and macroscopic coefficients, vol.1. Dunod, Paris 1968, p.42
[5] P.I. Kurilko et al.: ŽTF 43 (1973), 1142

ON THE STABILITY OF ELECTROMAGNETIC MODES IN THE BOUNDARY LAYER OF A GAS INSULATED PLASMA

D. Ohlsson
Royal Institute of Technology, 10044 Stockholm 70, Sweden

Abstract. In gas insulated plasmas large density and pressure gradients are likely to arise close to the boundaries on account of plasma neutral gas interaction effects. In this paper the stability of gravity driven electromagnetic modes in the boundary region is investigated.

Introduction. In order to fulfill power density requirements in future steady-state fusion reactors the ion density in central parts must be of the order $10^{21} m^{-3}$. In such systems high density neutral gas will surround the hot plasma, provided the flux of neutral particles from the plasma is not continuously removed by external means. From investigations of the equilibrium properties of gas insulated plasmas it is found that large driving sources for plasma instabilities will be localized to the narrow partially ionized boundary layers surrounding the hot fully ionized plasma. The stability properties of these layers therefore become essential for the whole gas blanket concept, in particular since minimum-average-B and shear properties of the magnetic field are likely to become less effective, on account of insufficient magnetic-line-tying due to large resistivity and the small localization region of the modes being considered.

Basic Equations. We use the ordinary dissipative MHD equations for a three-component plasma consisting of ions, electrons and neutrals. Conventional notation is used. The plasma and neutral gas are coupled through the exchange of directed momentum. The plasma also indirectly affects the neutral gas through the viscosity tensor in a way previously described by Lehnert [1].

Dispersion Relation. We make a localized perturbation analysis in cylindrical geometry assuming all quantities to vary as $\exp[i(k_r r+m\theta+\frac{n}{L}z-\omega t)]$. We define $k_\theta=m/r$ and $k_z=n/L$. We will only consider modes for which the lines of force are curved but not compressed or expanded. The magnetic field is in the polar direction. Plasma neutral gas interaction is reconsidered as compared to earlier investigations [1] and expressed in terms of the mass and viscosity tensors. The plasma-neutral gas coupling is generally highly anisotropic. Thus the final dispersion relation can be written

$$F(\omega,\bar{k}) = \omega^3+\omega[\omega_\Gamma^2-\omega_r(\omega_\mu+\omega_{\eta p})-\omega_A^2] + i[\omega^2(\omega_\mu+\omega_{\eta p}+\omega_r) + \omega_r\omega_\Gamma^2 -(\omega_{\eta p}+2\omega_{\mu p})\omega_A^2] = 0 \quad (1)$$

Here $\omega_\Gamma^2=\omega_g^{*2}-\omega_\mu\omega_{\eta p}$ (2); $\omega_g^{*2}=(1-\frac{\omega m_c k_1^2 n}{eBk_z\nabla n}-i\frac{\mu_c k_2^4}{eBk_z\nabla n})\omega_g^2$ (3)

$\omega_r=\frac{n_n k_i^2}{\mu_o}$ (4); $\omega_g^2=\frac{4k_z\nabla B\gamma e\omega_n}{m_c k_1^2}$ (5); $\omega_n=\frac{k_z kT\nabla n}{neB}$ (6); $\omega_\mu=\frac{\mu_c k_2^4}{nm_c k_1^2}$ (7)

$\omega_A^2=\frac{B^2 k_i^2}{\mu_o nm_c k_1^2}k_\theta^2$ (8); $\omega_{\mu p}=\frac{\gamma kT\mu_c k_2^4}{ne^2B^2}$ (9) $\omega_{\eta p}=\frac{2\gamma p n_i k_i^2}{B^2}[1-\frac{3(\gamma-1)}{4\gamma}]$ (10)

$m_c k_1^2 = m_r^* k_z^2 + m_z^* k_r^2$ (11); $\mu_c k_2^4 = (\mu_r^* k_z^2 + \mu_z^* k_r^2) k_i^2$ (12)

Here m_r^*, m_z^*, μ_r^* and μ_z^* represent the diagonal elements of the mass and viscosity tensors. Generally these elements are complicated functions of the defined parameters including the frequency. For the case when $\omega_r \ll \omega_A$ the electrostatic and electromagnetic modes are strongly coupled and the dispersion relation splits up into two equations

$$\omega_{1,2}^2 + i(\omega_\mu+\omega_{\eta p}+\omega_r)\omega_{1,2}+\omega_\Gamma^2-\omega_r(\omega_\mu+\omega_{\eta p}) - \omega_A^2 = 0 \quad (13)$$

$$\omega_3 = i\frac{\omega_r\omega_\Gamma - \omega_{\eta p}\omega_A^2}{\omega_A^2 + \omega_r(\omega_\mu+\omega_{\eta p}) - \omega_\Gamma^2} \quad (14)$$

We have here neglected the frequency dependence of the coupling coefficients, inertia and frictional drift motion. The interpretation of Eq. (13) and (14) is straight forward. Note the strong stabilizing effect represented by the term $\omega_r(\omega_\mu+\omega_{\eta p})$. Here ω_μ becomes strongly enhanced due to plasma-neutral gas interaction. This example should, however, merely be considered as special application of the general dispersion relation. For typical neutral gas blanket data we actually find for a wide range of parameters, that the electromagnetic and electrostatic modes decouple. The electromagnetic modes become strongly damped on account of large resistivity along the lines of force, and the stability properties are determined by the low frequency electrostatic modes. The general dispersion relation, Eq. (1) has been investigated by the Nyquist technique, taking into account the frequency dependence of the mass and viscosity tensor components (due to plasma-neutral gas interaction) and also inertia and frictional drift motion effects.

Results. The stability criterion becomes

$$\Delta = (1-\frac{\omega_f}{\omega_{ci}^*})\omega_g^2 - \omega_\mu\omega_{\eta p} + \omega_f^2 - \frac{(\omega_{\eta p}+2\omega_{\mu p})}{\omega_r}\omega_A^2 < 0 \quad (15)$$

Here $\omega_f = \frac{\omega_r\omega_\mu\omega_g}{\omega_{ci}^*[\omega_\mu\omega_{\eta p}-\omega_g^2+\omega_r(\omega_\mu+\omega_{\eta p})+\omega_A^2]}\omega_g$ (16) $\omega_{ci}^*=\frac{eB}{m_c}\frac{k_z k_n}{k_1^2}$ (17)

Note that this general criterion also applies to cases when the electrostatic and electromagnetic modes couple. The tensorial mass elements should be evaluated for $\omega=\omega_f$. The result is

$m_c k_1^2 = m(1+\frac{n_n m_n}{nm})k_i^2$ and $\mu_c k_2^4 = (\mu+\mu_{ii})k_i^4$

Here the driving source for the modes considered is associated with the term ω_g^2 which arises on account of the "bad" curvature of the magnetic field. This term is reduced by a factor ω_f/ω_{ci}^*. The term ω_f/ω_{ci}^* is associated with plasma density expansion and compression effects due to the inertia drift motion and corresponds to a stabilizing effect. The second term represented by $\omega_\mu\omega_{\eta p}$ corresponds to a large stabilizing effect due to a joint viscous-resistive-pressure effect previously discussed by Lehnert [1]. The resistive-pressure effect simply represents the smoothing and damping effects of resistive diffusion on the plasma density perturbations. The viscous effect is substantially enhanced on account of plasma-neutral gas interaction effects. Note further that the Nernst effect reduces the stabilizing joint viscous-resistive-pressure effect by a factor $3(\gamma-1)/4\gamma$. The third term ω_f^2 represents a destabilizing effect which arises on account of plasma density expansion and compression effects due to the ion-neutral friction drift motion. The last term finally corresponds to a stabilizing effect which arises on account of a joint action of diffusion (due to ion-electron and ion-neutral collisions) across and electron motion along the field lines.

Let us investigate a numerical example by choosing the following data typical for gas blanket boundary layers, i.e. $n=n_n=10^{21} m^{-3}$, $T_e=T_i=T_n=3\times10^4$ °K, $d(\ln n)/dr = -50 m^{-1}$, $d(\ln n_n)/dr = 50 m^{-1}$, $\gamma=5/3$, B=1T, $d(\ln B)/dr = -2$, $k_r=6\times10^2 m^{-1}$, $k_z=6\times10^2 m^{-1}$, $k_\theta>0 m^{-1}$. Thus yielding $\Delta<<0$

Conclusions. Due to the joint action of all effects considered, the present analysis indicates that complete stabilization of localized gravity driven electromagnetic modes can be achieved under rather general conditions in the boundary layers of gas insulated plasmas. Consequently in these regions neutral gas stabilization is an alternative to more conventional type of stabilizing mechanisms associated with minimum-average-B and shear properties of the magnetic field.

This work has been supported by the European Communities under an association contract between Euratom and Sweden.

Reference.

[1] Lehnert, B., Plasma Physics and Controlled Nuclear Fusion Research 1974, IAEA, Vienna II (1975)717.

ELECTRON CYCLOTRON EMISSION FROM THE PLT TOKOMAK PLASMA

V. ARUNASALAM - J.C. HOSEA

PLASMA PHYSICS LABORATORY, PRINCETON UNIVERSITY
PRINCETON, NEW JERSEY 08540 USA

R. CANO

ASSOCIATION EURATOM-CEA SUR LA FUSION
Département de Physique du Plasma et de la Fusion Contrôlée
Centre d'Etudes Nucléaires
Boite Postale n° 6. 92260 FONTENAY-AUX-ROSES (FRANCE)

ABSTRACT - Experimental evidence for black-body emission near the electron cyclotron frequency from a collisionless toroidal plasma is presented. It is suggested that this black-body emission occurs via a mode conversion at the upper hybrid layer. Results of black-body emission near the second harmonic are also presented. The usefulness of this method to measure profiles and temperature fluctuations in a hot toroidal plasma is demonstrated.

Electron temperature profiles and their time evolution in Tokomak devices obtained by measuring the electron cyclotron radiation at the second harmonic have been previously reported [1]. Measurements of the cyclotron emission near the fundamental frequency ω_{ce} have been also reported [2] but these results were widely dominated by reflection from walls surrounding the plasma. On the other hand the lack of a comprehensive theory of the emission around ω_{ce} makes the interpretation of these results very difficult.

In this paper we report simultaneous measurements of the electron cyclotron emission radial profiles of the fundamental and second harmonic carried out in the PLT Tokomak. The experimental arrangement is illustrated in Fig. 1. The emitted radiation is measured in the extraordinary polarization perpendicular to the magnetic field in the direction of the large radius R by two microwave horns placed in the region of high magnetic field. Note that the radiation at the fundamental, in contrast with the second harmonic emission, can propagate out of the plasma only in the direction of increasing magnetic field. Therefore in order to measure only the radiation from the plasma and to avoid the contribution from the reflecting walls the receiving horn must be positioned as shown in Fig. 1. Two superetherodyne receivers have been used, with a local oscillator covering the band 60 - 90 GHz for the ω_{ce} emission and the band 135 - 140 GHz for the $2\omega_{ce}$ emission. Both receivers have the same pass band video amplifiers (F_o = 375 ± 125 MHz).

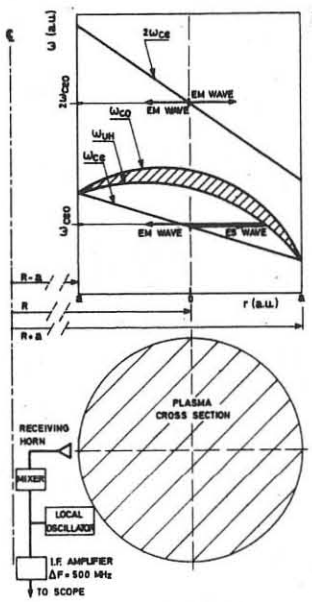

Figure 1 - Experimental set-up and characteristic frequencies profiles : ω_{ce} electron cyclotron, ω_{UH} upper hybrid, ω_{co} upper cut-off.

In Fig. 2 the measured radial profiles of the emitted power at ω_{ce} and $2\omega_{ce}$ are shown. These profiles are obtained by varying the toroidal magnetic field and supposing that the emission is localized in the layer where $\omega_1 = \omega_{ce}$, $\omega_2 = 2\omega_{ce}$ (ω_1 and ω_2 are the frequencies of the two local oscillators).

It is clearly seen from these results and from the systematically observed identical behaviour of the $P_{\omega ce}$ and $P_{2\omega ce}$ as a function of time, that the same power is radiated at ω_{ce} and $2\omega_{ce}$.

For the experimental conditions of Fig. 2 the optically thick layer condition for the second harmonic [1] :

$$\alpha\Delta r = 4\pi^2 \left(\frac{6-\gamma}{6-2\gamma}\right)^2 \gamma \frac{k\,T_e(r)}{2m\,c^2} \frac{R(r)}{\lambda} >> 1$$

where

$$\gamma = \frac{\omega_p^2}{\omega_c^2} \qquad \lambda = \frac{c}{F_o}$$

is easily satisfied, therefore we have $P_{2\omega ce} = k\,T_e \frac{\Delta\omega}{2\pi}$ ($\Delta\omega/2\pi$ is the band of the video amplifier).

The emission at the fundamental shows the same black-body behaviour and this is confirmed by the results shown in Fig. 3 where the $P_{\omega ce}$ profile is compared with the electron temperature profile measured by Thomson Scattering.

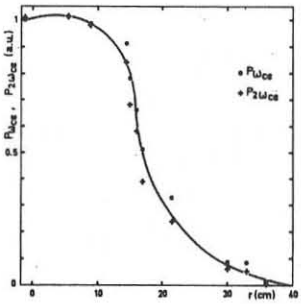

Figure 2 - Measured radiated power vs.radius at ω_{ce}(•) and $2\omega_{ce}$(+).

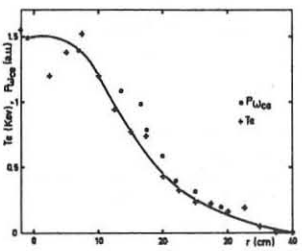

Figure 3 - Power radiated at the ω_{ce} vs.radius (•) and electron temperature measured by Thomson scattering (+), t = 300 ms. I = 350 kA, B = 28 KG, $\bar{n}e = 3.10^{13}$ cm^{-3}.

However according to conventional hot plasma theory for emission at ω_{ce} perpendicular to the magnetic field [3] we find :

$$\alpha\Delta r \simeq \frac{2}{(2\pi)^{1/2}} \frac{\omega_{ce}}{\omega_p} \left(1 - \frac{1}{2}\frac{\omega_p^2}{\omega_{ce}^2}\right) \times$$

$$\times \left(\frac{V_{te}}{c}\right)^3 \frac{R}{\lambda} \sim 10^{-2} << 1$$

This discrepancy can be removed by supposing that perpendicular electrostatic waves thermally excited near the cyclotron layer can propagate towards the upper hybrid layer where they undergo a total mode conversion [4] and finally are emitted outside the plasma in the direction of increasing magnetic field. Considering that transverse Doppler effect is the dominant damping, the condition of black-body emission for perpendicular electrostatic waves is :

$$\alpha\Delta r \simeq \pi^{1/2} (2\pi)^{1/3} \frac{\omega_p^2}{v_{te}} \frac{R}{\omega_{ce}} \times$$

$$\times \left(\frac{\omega_{ce}}{\omega_p} \frac{v_{te}}{c}\right)^{4/3}$$

and with $\bar{n}_e = 3.10^{13}$ cm^{-3}, B = 28 KG, T_e = 1 keV, we have $\alpha\Delta r = 610^3 >> 1$. The weak dependence on the electron temperature suggests that this condition is easily satisfied over most of the plasma cross section in agreement with the results shown in Fig. 3.

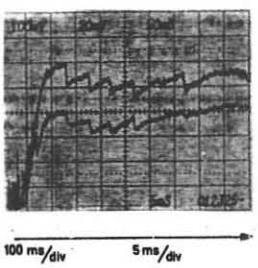

Figure 4 - Sawtooth oscillations of the power radiated at ω_{ce} (lower trace) and $2\omega_{ce}$ (upper trace). The fundamental and second harmonic radiation are localized at r = 0.

The time evolution of the electron temperature and its local fluctuations can be very easily obtained and in Fig. 4 an exemple of the sawtooth temperature oscillations is presented. The emitting layer for both ω_{ce} and $2\omega_{ce}$ is localized at the plasma center (r = 0) and very similar oscillations with $\Delta T_e/T_e \simeq 0{,}1$ can be seen on both signals.

In conclusion the local electron temperature and its time evolution can be readily obtained by the emission measurements at ω_{ce} provided that the receiving horn in positioned as shown in Fig. 1. The optically thick condition for ω_{ce} compared with the corresponding condition for $2\omega_{ce}$ is satisfied over a much wider range of the electron density and temperature values making the emission at ω_{ce} more attractive for the electron temperature measurement.

REFERENCE :

[1] TFR. Group presented by R. Cano, 7Th European Conf. on Controlled Fusion and Plasma Physics, Lausanne Sept. 1975 paper 14 b.

[2] TFR. Group and NPL Submillimeter wave Group presented by A.E. Costley, Ibid paper 14.

[3] Yu. N. Dnestrovskii, D.P. Kostomarov and N.Y. Skrydov Zh. Techn. Fiz. 33, 922 (1963)

[4] I. Fidone and G. Granata Phys. Fluids 16, 1685 (1973)

ELECTRON-CYCLOTRON EMISSION AS A TEMPERATURE DIAGNOSTIC FOR TOKAMAKS

W.R. Rutgers
Association Euratom-FOM, FOM-Instituut voor Plasmafysica,
Rijnhuizen, Jutphaas, The Netherlands

Abstract. Electron-cyclotron emission can be used as a local temperature diagnostic but the interpretation of the measurements is not always simple. Reabsorption and ray refractive effects on the emission at twice the electron-cyclotron frequency are briefly discussed and experimentally verified.

It has been shown[1] that the line profile of cyclotron emission at $2\omega_{ce}$ ($\omega_{ce} = q\,B/m$; the electron-cyclotron frequency) can be used to measure the temporal variation of the electron temperature with good spatial resolution for tokamak discharges under low runaway conditions. For these discharges the optical depth at $2\omega_{ce}$ is much larger than one. Therefore, the specific intensity of radiation is directly proportional to the electron temperature if the electron plasma frequency f_{pe} is considerably smaller than the electron-cyclotron frequency f_{ce} so that effects of plasma dispersion can be neglected.

In this paper measurements of self-absorption in an optically thick line, temperature fluctuations due to internal disruptions in the Princeton Large Torus, as well as measurements of emission under high density conditions ($f_{pe} > f_{ce}$) in the turbulently heated tokamak TORTUR in Jutphaas are presented.

Radiation at $2\omega_{ce}$ from PLT was measured with a three-channel grating polychromator for vertical direction of observation through the centre of the discharge. The measured profile (Fig. 1) is broad, implying that radiation emitted outside the antenna pattern of the detection system is measured after reflection at the vacuum chamber. The direction of observation is important because in the case of a tokamak, radiation at a particular frequency is emitted as well as resonantly absorbed in a vertical plasma layer in which the static magnetic field is constant. For vertical observation cold plasma in front of the light collecting cone can reabsorb radiation from the hotter plasma core if the absorption coefficient is high. The result is a dip in the line profile as measured for $2\omega_c$ (Fig. 1). In fact the plasma centre is completely inaccessible in a plane of constant B for an optically thick plasma due to reabsorption[2] and a space-resolved temperature measurement from cyclotron emission is impossible in this case.
An example of the effect of temperature fluctuation on the emission is shown in Fig. 2. The emission measured at frequencies corresponding to $3\omega_c$ at r = 0, 3, 14 and 18 cm from the axis of the discharge is shown as a function of time when internal disruptions occurred repeatedly. On axis the well-known "sawtooth oscillations" are observed accompanied by an increase in emission outside the instability surface. Here the decay time of the perturbation increases with the radius. These observations show that cyclotron emission can be used in the same way as Bremsstrahlung measurements[3] to study heat transport. The advantage is that, in the case of an optically thick plasma, the emission is proportional to T_e and does not depend on plasma density or effective charge.

Calculations of electron-cyclotron emission are mostly done assuming that the ratio of electron-plasma frequency f_{pe} over electron-cyclotron frequency f_{ce} is smaller than one. Strong modifications of line profiles and total emission can be expected if $f_{pe}/f_{ce} > 1$ (Ref. 4). Therefore, a simple experiment was set up on the turbulent heating experiment TORTUR[5]. Radiation was measured with a Putley detector, a set of wire-mesh filters and a polariser (see Fig. 3). The parameter f_{pe}/f_{ce} was varied by changing the plasma density from 4×10^{19} m^{-3} to 1.4×10^{20} m^{-3}. The total emission and the emission at $2\omega_{ce}$ was measured for the extraordinary mode ($E \perp B$). The temporal behaviour of the emission is consistent with the measured dissipation of energy in a turbulent skin followed by the collapse of this skin and redistribution of energy over the entire cross-section of the discharge[5]. It is known that no propagation at $2\omega_c$ of the extraordinary mode is allowed for $\sqrt{2} < f_p/f_c < \sqrt{3}$ and $f_p/f_c < \sqrt{6}$. When the plasma density is increased, this stopband is indeed found (Fig. 3). Radiation was also measured for constant density and various magnetic fields, because bursts of super-thermal radiation at f_{pe} are also observed occasionally. The level of emission, however, decreases for low B-fields. Therefore cyclotron emission is not overshadowed by this effect. Moreover, the specific intensity is estimated to be 10^{-11} watt m^{-2} sr^{-1} Hz^{-1} for low density, indicating a plasma temperature around 2 keV, which is in agreement with X-ray measurements of T_e (Ref.5). The specific intensity for high densities can be estimated by using the spectral emissivity, as calculated in Ref. 6 for arbitrary density. A correction factor for black-body emission, taking plasma dispersive effects into account, is indicated in Fig. 4 by a broken line. The measurements are in qualitative agreement with this theory but a detailed comparison is difficult because the plasma temperature decreases with increasing density.

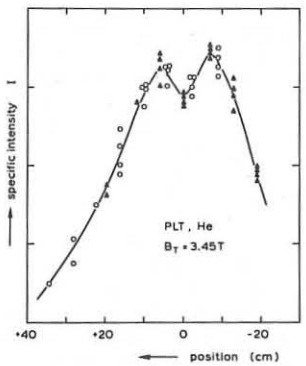

Fig. 1.
Profile of $2\omega_{ce}$ measured with two channels (dots and triangles) of a grating instrument. The line broadening is due to the inhomogeneity in the (static) toroidal magnetic field. Cold plasma in front of the light guide reabsorbs radiation from the hot core where the static B-field, and so $2\omega_c$, has the same value.

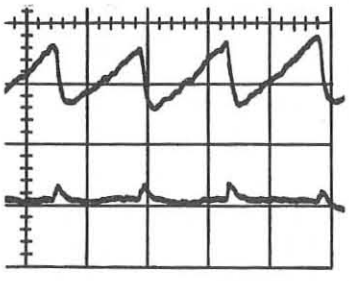

Fig. 2a.
Cyclotron emission versus time for a frequency corresponding to $3\omega_{ce}$ at r = 0 cm (top) and r = 14 cm (bottom). The time-scale is 4 msec/large division. Internal disruptions manifest themselves as sawtooth oscillations on emission from the centre of the discharge. Outside the instability surface an increase in emission is observed.

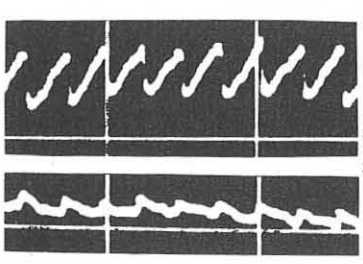

Fig. 2b.
r = 3 cm (top) and r = 18 cm (bottom). The time-scale is 20 msec/division.
Note the much longer decay time for emission at r = 18 cm compared to emission at r = 14 cm.

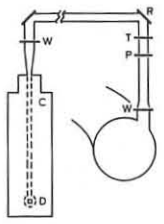

Fig. 3.
W: vacuum window
P: polariser
T: filter 10 ℓ/inch
R: filter 20 ℓ/inch
C: cryostat
D: InSb detector.

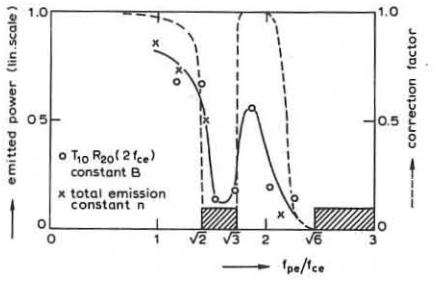

Fig. 4. Plasma emission in the extraordinary mode for various values of f_{pe}/f_{ce}. Circles: emission at $2f_{ce}$ for different densities. Crosses: total emission for different values of the magnetic field. Broken line: see text. Propagation not allowed in the shaded regions.

In conclusion, cyclotron emission measurements can be used as a temperature diagnostic. Complications arising from reflections, reabsorption in outer plasma layers, and plasma dispersion should be avoided by using an absorber opposite the viewing port, looking along the major radius and keeping $f_p/f_c < 1.3$ respectively.

Acnkowledgement. It is a pleasure to mention the hospitality of the Plasma Physics group during my stay at the University of Maryland. Discussions with Drs. D.A. Boyd, F. Stauffer and H.W.H. van Andel were very helpful. This work was performed under the Euratom-FOM association agreement with financial support from ZWO and Euratom.
Part of this work was done at the University of Maryland with financial support from ERDA and NSF.

References.

1. R. Cano, Proc. 7th Eur. Conf. on Contr. Fusion and Plasma Phys., Lausanne (1975), Vol. I, 14b.
2. W.R. Rutgers and D.A. Boyd, submitted to Physics Letters.
3. J.D. Callen and G.L. Jahns, Phys. Rev. Lett. 38 (1977) 491.
4. C.M. Celata, K. Audenaerde and D.A. Boyd, Bull.Am.Phys.Soc. 22(1977) 182.
5. H. de Kluiver et al., this conference.
6. K. Audenaerde, Thesis University of Utrecht (1976).

SPACE POTENTIAL MEASUREMENTS ON EBT

R.L. Hickok, F.M. Bieniosek, P. Colestock, K.A. Connor, & W.C. Jennings
Rensselaer Polytechnic Institute
Troy, New York 12181 U.S.A.
and
R.A. Dandl
Oak Ridge National Laboratory
Oak Ridge, Tennessee 37830 U.S.A.

Abstract: A heavy ion beam probe has been used to measure the space potential profile on EBT. The results indicate an inwardly directed electric field inside the electron rings and an outward directly field on the outside.

Introduction: A heavy ion beam probe diagnostic system has been placed in operation on the ELMO Bumpy Torus (EBT) at Oak Ridge National Laboratory. The ultimate objective of this diagnostic is to provide space and time resolved measurements of n, $\emptyset$, and T_e over the minor cross section of the plasma. Initial effort has concentrated on obtaining a radial profile of the space potential. This paper will provide a brief description of EBT, discuss the characteristics of the diagnostic system and present some initial measurements of the space potential profile.

EBT is a toroidally connected mirror device which uses intense microwave radiation to produce and heat a steady state plasma. There are 24 mirror sectors each having a mirror ratio of approximately 2 to 1. The major radius is 150 cm and the minor radius is 15 cm at the midplane between a pair of mirror coils. Nominal center line magnetic field is 0.5 T. The plasma is formed and heated by 60 kW of radiation at a fequency of 18 GHz and 30 kW at 10.6 GHz.

There are two components to the plasma; a high beta, hot electron annulus in each mirror sector and a less energetic toroidally contained plasma. The high beta electron annuli establish a region where there is a reverse magnetic field gradient which provides stability for the toroidal plasma. There is no conventional rotational transform, but the plasma is confined to toroidal drift surfaces that are determined by the radial pressure gradients and electric field. Typical characteristics for the toroidal plasma are a density of 2×10^{12} and an electron temperature of 200 eV.

Heavy Ion Beam Probing: The principles of heavy ion beam probing are illustrated in Fig. 1. A beam of single charged heavy ions, the primary beam, is directed across the confining magnetic field and through the plasma. Some of the ions undergo ionizing collisions with the plasma electrons to form doubly charged secondary ions. A small detector located outside the plasma looks only at those secondary ions created in a small segment of the primary ion trajectory, thereby providing three dimensional spatial resolution. The observation point can be scanned over the cross section of the plasma by sweeping the injection angle and energy of the primary beam. The intensity of the secondary ion current is a measure of $nf(T_e)$ where $f(T_e)$ is the effective cross section for the ionization reaction. Separate evaluation of n and T_e can be obtained by probing the same point with two ion beams that have different ionizing cross sections, or by observing both the 2^+ and 3^+ secondary ions from a single beam. The energy of the 2^+ secondary ion differs from the injection energy of the primary beam by the space potential at the point where the secondary ion was created. Typically this energy difference can be measured to better than 10^{-4} V_p where eV_p is the energy of the primary beam. Beam probe measurements of n, $\emptyset$, and T_e on other plasma systems have been reported in the literature [1-3].

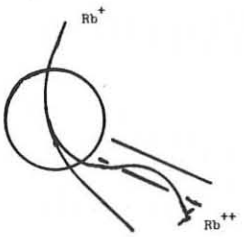

Fig. 1 Heavy Ion Beam Probe Schematic

The beam probe system for EBT is designed to operate with either Rb^+, K^+ or Na^+ primary ion beams. For Rb^+ the energy range is from 7 to 20 keV. Primary beam current is of the order of 10 microamps. This produces a secondary ion current in the 10 nanoamp range for a 5 mm sample length of the primary beam trajectory. The primary beam is chopped at 3 KHz and phase-lock detection is used to improve the signal to noise ratio. The plasma beta in the electron ring region is approximately 0.5 which produces a measurable displacement of the primary trajectories that are tangent to the rings, but negligible distortion of other trajectories. Detailed measurements of the trajectory displacement should provide information about the size and shape of the rings.

Space Potential Measurements: The energy of the secondary ion is compared to the primary beam injection by means of a feedback controlled electrostatic energy analyzer. The beam transmitted by the analyzer is detected with a split plate and the difference signal from the two halves of the detector is fed back to the top of the analyzer through a very high gain amplifier. This holds the beam centered on the split plate detector, and if the system is adjusted such that the beam enters at the design angle, the feedback voltage is directly proportional to the space potential. The analyzer is designed to operate with the beam incident at an angle of 32° with respect to the ground plane. The voltage correction for variation in entrance angle is less than 20 volts for an angular range of ± 4°.

The system is calibrated by reducing the energy sufficiently to bend the primary beam into the analyzer and inserting a precise gain of two amplifier in the feedback chain. It is then slaved to the primary gun voltage so that when it is used for secondary ion detection the feedback signal is proportional to the plasma potential plus any correction due to variation in entrance angle. In operation the analyzer is adjusted to compensate for the 2° difference in entrance angle between the primary and secondary beam. Figure 2 shows the potential profile along the indicated line through the plasma. This line scan, generated by varying the beam energy, was chosen due to the low variation in entrance angle (~ 2°) of secondaries produced along this line. The results show that there is a positive space potential in the ring region with respect to the center of the toroidal plasma. This implies an inwardly directed radial field inside the electron rings and an outwardly directed field outside the rings. The symmetry of the nearly vertical scan is to be expected, but it should not be interpreted as indicating axial symmetry. We are presently carrying out profiles along horizontal scan lines and hope to map the complete cross section in the near future.

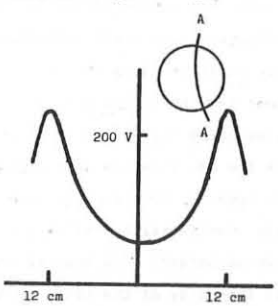

Fig. 2 Space Potential Profile Along the Line A-A. The insert shows the location of this line in the plasma.

References:

1. F. C. Jobes, R. L. Hickok, Nuc. Fusion 10, 195 (1970).
2. J. C. Hosea, F. C. Jobes, R. L. Hickok, and A. N. Dellis, Phys. Rev. Let. 30, 839 (1973).
3. R. E. Reinovsky, J. C. Glowienka, A. E. Seaver, W. C. Jennings, and R. L. Hickok, Trans. Plasma Sci., PS-2,(250) (1974).

MEASUREMENT OF THE POLOIDAL FIELD IN THE PULSATOR TOKAMAK USING A NEUTRAL LI BEAM IN CONJUNCTION WITH THE ZEEMAN EFFECT

K. McCormick and M. Kick
Max-Planck-Institut für Plasmaphysik, D-8046 Garching, FRG

J. Olivain, CEA-CEN
92 Fontenay-aux-Roses, France

Abstract: A technique for measuring the poloidal field in a Tokamak plasma is briefly sketched[1]. The experimental setup on Pulsator is described. To demonstrate the viability of the diagnostic, results for one discharge series are presented and discussed.

The poloidal field $B_p(r)$ causes the orientation of the total magnetic field to assume an angle $\Theta = B_p/B_T$ with respect to the toroidal magnetic field $B_T(r)$. The diagnostic approach used here measures $\Theta(r)$ directly. Since B_T is known, B_p may be calculated.

Referring to Fig.1, a neutral lithium beam of some keV energy is injected into the plasma. The collisionally excited Li resonance line radiation at 6708 Å [2P-2S] is gathered by an f/20 lens from a volume determined by the beam width and imaged field stop size [here, 2x1x1cm^3]. Since the optical system is situated perpendicular to the toroidal field, the line is seen to be split into a Zeeman triplet. The shifted σ components are polarized perpendicular to the local magnetic field direction and have a splitting of $\sim$ 1.1 Å for B_T = 26 kG. The unshifted π component is polarized parallel to the field direction. After passing through the lens the π component is separated from the σ components by a Fabry-Perot of 0.6 Å band width. The orientation of the π component, and therewith the angle Θ, is measured by a polarimeter consisting of a Faraday Rotator (FR) and a Wollaston prism (WP) analyzer. The filtered light is split into two components by the WP, and then detected by two photomultipliers, the output signals of which are fed into a differential amplifier. The servo amplifier, reacting to the difference signal, drives the FR thereby rotating the plane of polarization of the π component until the output of the differential amplifier is nulled. The FR current required to achieve this is proportional to Θ. Thus by monitoring the FR current on an oscilloscope, $\Theta(t)$ is obtained for one radial position. A profile for $\Theta(r,t)$ is built up by scanning the Li^0 beam radially from shot-to-shot.

The ion gun consists of a cathode-anode configuration of the Pierce type. Li ions are provided by the β-Eucryptite[2]-covered cathode. Neutralization takes place in a pulsable Li-vapor cell. The 12o ms pulsed, 6 kV neutral beam used for these measurements has an intensity of the order of magnitude of 1o μA/cm^2, Li^0 equivalent, in the Pulsator torus. Due to the restricted diagnostic accessibility, only the outer 1-9 cm on the plasma radius can be scanned by the beam.

Measurements were made on a 5o kA discharge with $n_{eo} \sim 3 \times 10^{13}$cm^{-3}, B_T = 27 kG and a limiter radius of 11 cm. Fig.2 shows, from the top, the plasma current, the photomultiplier output (in photons/sec 4π ster.) for the cases of the beam voltage on and off and the servo amplifier output (B_p/B_T in mrad.) for three consecutive shots at a radius of 6.5 cm. The PM signal for the beam-off case results from the plasma continuum spectrum. The time constant for the servo amplifier has been adjusted so as to yield an acceptable signal to noise ratio, and this is responsible for the signal rise time at the start of the discharge.

In Fig.3 the experimental results for a series of 36 shots are plotted as a function of radius for t=7o ms. The circles give the mean value and the error bars the largest and smallest values of all data taken at a particular radius. The noise level is about what one would expect for the measured PM signals and time constant, assuming only photon statistics as a noise source. From the experimental points the plasma center is found to lie o.5 cm to the outside so that the plasma radius is lo.5 cm. The safety factor $q = rB_T/RB_p$ at the plasma center is 1.1.

The three curves in Fig.3 are computed for the temperature profile T_e= 8oo eV $[1-(r/11.5)^2]^2$ and the three indicated Z_{eff} profiles. Spitzer resistivity and constant electric field over the radius are assumed. The actual T_e profile, via Thomson scattering, was not measured for this series. The given profile is typical of Pulsator discharges in this density regime. Nevertheless, B_p/B_T is a sensitive function of $T_e(r)$ and since the exact $T_e(r)$ is not known, and because the trapped electron effect has not been included here, these curves are meant to have more of an instructive nature rather than to say anything definitive about $Z_{eff}(r)$. Most importantly, one sees that although the uncertainty in the individual experimental points is large, the points taken together yield a reasonable B_p/B_T profile.

Efforts are now being directed towards producing a more intense neutral beam in order to increase the signal to noise ratio.

References:

[1] J.Fujita and K.McCormick, 6th Eur.Conf., Moscow (1973) 191

[2] J.P.Blewett and E.J.Jones, Phys.Rev. 5o (1936) 464

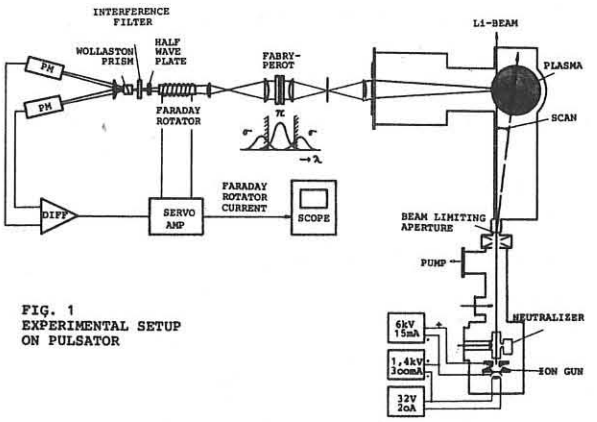

FIG. 1
EXPERIMENTAL SETUP ON PULSATOR

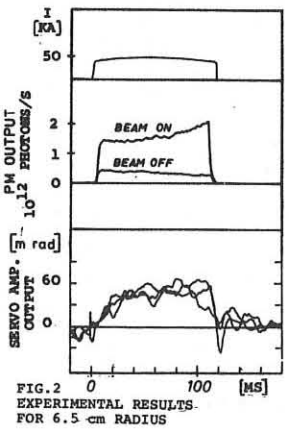

FIG.2 EXPERIMENTAL RESULTS FOR 6.5 cm RADIUS

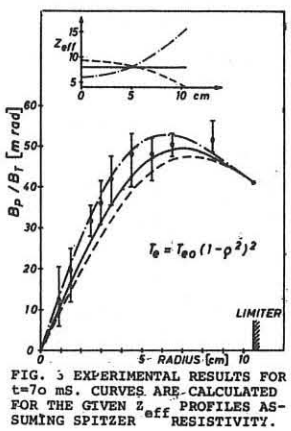

FIG. 3 EXPERIMENTAL RESULTS FOR t=7o mS. CURVES ARE CALCULATED FOR THE GIVEN Z_{eff} PROFILES ASSUMING SPITZER RESISTIVITY.

ION TEMPERATURE DETERMINATION FROM FAST NEUTRAL SPECTRA

Yu.N.Dnestrovskii, S.E.Lysenko
I.V.Kurchatov Institute of Atomic Energy
D.P.Kostomarov
Moscow State University, Moscow, USSR

The problems discussed in this paper deal with the ion temperature determination from fast neutral spectra for thick plasmas $\sigma_{cx}\, na > 1$, where σ_{cx} is the charge-exchange cross-section, n - plasma density, a - plasma radius.

In this case one may see three hardships in explaining the spectra: (1) $N(0) \ll N(a)$ ($N(r)$ - neutral density), (2) central neutral density is determined by recombination, (3) neutral with energies $E \sim 0.1 - 10$ keV undergo several acts of charge-exchange, when moving from the center to the periphery of the plasma column.

The basic equation for the distribution function of neutrals is the following:

$$\vec{v}\nabla f + sf = (s_{cx}N + s_r n)\varphi_i \equiv W(r,v) \qquad (1)$$

where $s = s_{cx} + s_e$, $s_{cx} = \sigma_{cx} v n$, $s_e = \sigma_e v_e n$, $s_r = \sigma_r v_e n$, σ_e and σ_r are the cross-sections of ionization by electrons and photorecombination, φ_i - local Maxwellian ion distribution.

In the diffusion approximation,

$$N = N_1 \operatorname{ch}\lambda(x) + n\sigma_r/\sigma_e, \quad \lambda(x) = \int_0^x \sqrt{\frac{s s_e}{v_1}}\, dx' \qquad (2)$$

At $T_e \sim 1$ keV $\sigma_r / \sigma_e > 10^{-8}$ and recombination is dominant when $\exp(na\sqrt{\sigma_{cx}\sigma_e}) > 10^8 N(a)/n(0)$. For particles leaving plasma parallel to the x-axis we have

$$F = vf(v) = \int_{-a}^{a} W\Phi\, dx \qquad (3)$$

where $\Phi = \exp(\frac{1}{v}\int_a^x s dx')$. Usually the function $F = F(E)$ (where $E = mv^2/2$) is experimentally measured. For "thin" plasma

$$T_i(0) \approx T_i^0 = -1 / \partial \ln F / \partial E$$

If $\mathcal{E} = E/T_i(0) \gg 1$, one may get an asymptotic formula for the integral (3) using saddle-point method. Putting (2) into (3) we obtain

$$F = N_1 I_1 + n(0) I_2 = \exp(-\mathcal{E})\, u(\mathcal{E}) \qquad (4)$$

where

$$I_1 = \left.\frac{s_{cx}\exp(g_1)}{2\pi v_1^3 \sqrt{-g_1''}}\right|_{x = x_1(E)} \qquad I_2 = \left.\frac{2\pi n(1 + s_{cx}/s_e)}{\pi v_1^3 n(0)\sqrt{-g_2''}}\exp(g_2)\right|_{x = x_2(E)} \qquad (5)$$

$$g_1 = g_2 + \sqrt{\frac{m}{2}}\int_0^x \sqrt{s s_e}\, dx', \quad g_2 = -E\tau - \sqrt{\frac{m}{2E}}\int_x^a s(x')dx', \quad \tau = \tau(x) = 1/T_i(x) \qquad (6)$$

The saddle points $x_1(E)$ and $x_2(E)$ can be determined from the following equations:

$$g_1' = \sqrt{\frac{m}{2}}\left(\frac{s}{\sqrt{E}} + \sqrt{s s_e}\,\tau\right) - E\tau' = 0, \quad g_2' = \sqrt{\frac{m}{2}}\frac{s}{\sqrt{E}} - E\tau' = 0 \qquad (7)$$

It is convenient to introduce a correcting factor

$$\Psi = T_i(0)/T_i^0 = 1 - \partial \ln u / \partial \mathcal{E}$$

Let us consider a model problem

$$\left.\begin{aligned} T_i &= T_i(0)\,(1 + \alpha\xi^2)^{-1}, \quad \xi = x/a, \quad n = \text{const} \\ \sigma_{cx} v &= s_{cx} = \text{const}, \quad \sigma_e v_e = s_e = \text{const} = 1/4\, s_{cx} \end{aligned}\right\} \qquad (8)$$

If recombination is not essential, then

$$\Psi = 1 + \frac{1}{2\mathcal{E}}\left(1 - \frac{\mathcal{E}_0}{\mathcal{E}} + \frac{\nu^2\mathcal{E}_0}{\alpha\mathcal{E}^2} - \frac{\nu\mathcal{E}_0}{2\sqrt{5\alpha}\,\mathcal{E}^{3/2}}\right) \qquad (9)$$

If recombination plays the dominant role, then

$$\Psi = 1 + \frac{1}{2\mathcal{E}}\left(1 - \sqrt{\frac{\mathcal{E}_0}{\mathcal{E}}} + \frac{\mathcal{E}_0}{\alpha\mathcal{E}^2}\right)$$

Here $\mathcal{E}_0 = sa(v_1)^{-1}$, $\nu = 1 + \sqrt{\mathcal{E}/5}$. For the T-10 installation at $T_i \approx 0.8$ keV, $n \sim 10^{14}$ cm^{-3}, a = 35 cm, $\sqrt{\mathcal{E}_0} \approx 20$.

The results of the numerical computation of integral (3) are plotted in the Figures given below for the above mentioned parameters when $T_i = T_i(0)(1 - \xi^2)^{1.5}$, $n = n(0)(1 - \xi^2)^{1.5}$.

Neutral density profiles are given in Fig. 1 for two values of plasma density $n(0) = 1$ and 2.10^{14} cm^{-3}. Here and in the other Figures the results of computations without recombination are plotted in dotted lines.

Figures 2 and 3 represent the dependence of Ψ on the energy of neutrals and plasma density. It is evident that when recombination is taken in consideration the correction for the calculation of temperature is much lower. The dependence of the function F on plasma density is plotted in Fig. 4 for fixed energies E = 1.5, 5.5 and 9.5 keV. Central neutral density N(0) curve is also given in that Figure. One can see that for $n > n_{crit} \sim 10^{14}$ cm^{-3} recombination plays the dominant role.

Formulas (5)...(7) make it possible to obtain the information about ion temperature profile from the F(E) spectrum. Let us consider the case when recombination is not essential. Taking the logarithm from (4) and differentiating it, one can get

$$\tau = -\frac{d}{dE}\ln\left(F(E)\frac{\sqrt{E}}{s_{cx}}\right) + \frac{\sqrt{m}}{2\sqrt{2}\,E^{3/2}}\int_x^a s(x')\,dx' \qquad (12)$$

Taking the last equation together with the first one in (7), one can determine two functions $\tau(x)$ and E(x) from the experimentally measured function F(E). The initial conditions in the point x = 0 are the following:

$$\tau'(0) = 0, \quad E(x) \underset{x\to 0}{\to} \infty, \quad \tau(0) = -\lim_{E\to\infty}\frac{d}{dE}\ln\left(F(E)\frac{E}{s_{cx}}\right)$$

The authors thank M.P. Petrov for fruitful discussions.

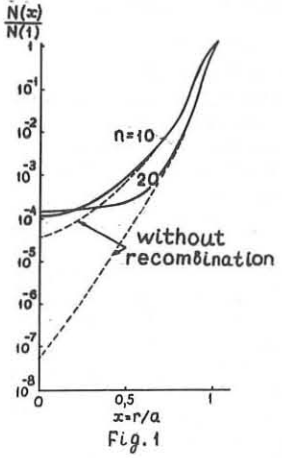

Fig. 1

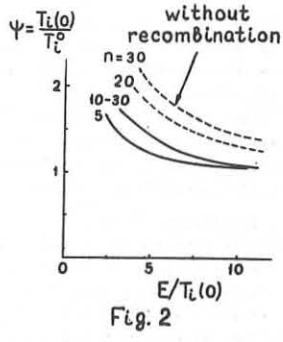

Fig. 2

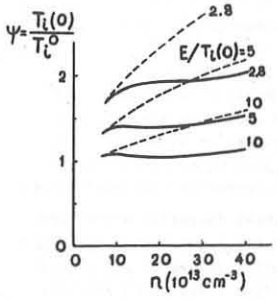

Fig. 3

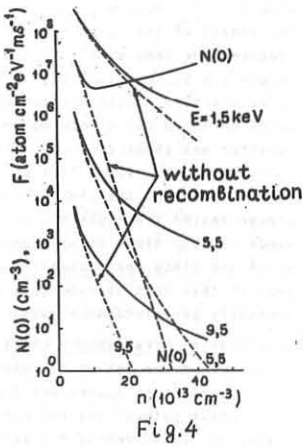

Fig.4

DETECTION OF ATOMIC HYDROGEN BY RESONANCE FLUORESCENCE

P. Bogen and Y.T. Lie
Institut für Plasmaphysik der Kernforschungsanlage Jülich GmbH
Assoziation EURATOM/KFA, D 517 Jülich, Germany

Abstract: An experimental arrangement is described which allows the determination of atomic hydrogen densities down to values of $3\cdot10^9$ cm^{-3} by resonance fluorescence at L_α(1215 Å). Its possible application to measurements in the limiter shadow of a Tokamak is discussed.

Introduction: The knowledge of the neutral hydrogen densities near the walls of Tokamaks is of great importance for the understanding of the energy losses by fast charge exchange neutrals and of the recycling of the hydrogen gas. A measurement of the absolute intensity of a suitable hydrogen line can give the desired information, if the electron density n_e and temperature T_e are known and are sufficiently high. But local hydrogen densities are difficult to derive. An alternative, but technically more involved method, is the resonance fluorescence on the L_α line. This method is practically independent of n_e and T_e (n_e and T_e may be zero) and allows local measurements. Since powerful lasers are not yet available at the desired wavelength of 1215 Å, we have studied the detection limits which can be achieved by resonance fluorescence using a thermal light source.

Theoretical estimates: The number of photons emitted by a light source with a blackbody temperature T per cm^2 surface, per cm wavelength band and per solid angle at the wavelength λ is given by $B_\lambda = (2c/\lambda^4)\left[\exp(hc/\lambda kT)-1\right]^{-1}$, e.g. T=50 000 K, λ=1215 Å, $B_\lambda = 2.8\cdot10^{21}$ photons/cm^{2}s Å sr. In the case of an optically thin absorbing layer of thickness ℓ the amount of light absorbed is given by

$$\ell\int_L \kappa\, d\lambda = \pi e^2\lambda^2 n f \ell / mc^2$$

where κ is the absorption coefficient, f the oscillator strength and n the neutral particle density. For $n\cdot\ell=10^{10}$ cm^{-2} we obtain the value $\ell\int_L \kappa d\lambda = 5\cdot10^{-5}$ Å. Illuminating the scattering volume V with an intensity B_λ using a solid angle $\Delta\Omega_1$, the number of photons scattered into a solid angle $\Delta\Omega_2$ is given by

$$\phi = \frac{1}{4\pi} B_\lambda \int_L \kappa\, d\lambda \cdot V\sigma\cdot\Delta\Omega_1,\ \Delta\Omega_2$$

For an estimate we assume $n=10^{10}$ cm^{-3}, $\Delta\Omega_1=\Delta\Omega_2=10^{-2}$, $V=10^{-2}$ cm^3, $\sigma=10^{-2}$, T=50 000 K, which gives in 1/µs about 100 photons on the photomultiplier and, with 10% quantum yield, 10 photoelectrons, which can easily be detected, if the plasma radiation is not too strong (σ takes account of the losses at the mirrors, windows and the grating). In the above formula, quenching collisions (normally not important) and polarization effects (giving small corrections) are neglected.

Light source: To obtain a low detection limit, the light source should have a high temperature, a large area and a long emission time. A solution might be offered e.g. by a laser produced plasma /1/ or a vacuum sliding spark /2/. Experiments with the latter showed considerable difficulties due to the fact that the plasma ejected from the source damaged the optical parts after a few shots. Therefore we preferred a gas discharge lamp filled with 100 Torr helium where, because of short mean free paths, the damage of the optical parts by the plasma was considerably reduced. The lamp mainly consisted of a quartz tube of 8 cm length and 0.6 cm diameter, the plasma was observed end on through a hole in the electrode. At a current of 40 kA, temperatures up to 70 000 K were measured at the He λ=4686 Å line. The duration was about 2 µs. For the resonance fluorescence on the L_α line, the λ=1215 Å line of the He was used. A special problem is posed by the line reversal due to small amounts of hydrogen inside the light source, especially at the cool ends. Since the L_α lines of hydrogen and deuterium are separated by 0.3 Å and since the deuterium concentration is $1.5\cdot10^{-4}$ times smaller than that of hydrogen, the problem of line reversal can obviously be solved much easier for deuterium than for hydrogen.

Experimental arrangement: Light source, focussing mirror and spectrometer are set up as shown in Fig.1. We used a spectrometer between light source and scattering volume to get a clear distinction between the resonance signals due to L_α and other scattered light. Behind the exit slit of the spectrometer, a LiF window separates the scattering volume from the spectrometer. A number of baffles screens the detector against the stray light produced by the slit and the window, a dump at the end of the scattering chamber absorbs the light beam. Perpendicular to the light beam, the scattered radiation is detected by a solar blind photomultiplier with CsJ photocathode and MgF_2 window. The scattering volume can be filled either with a noble gas or with atomic hydrogen produced from H_2 by an electrodeless ring discharge as indicated in Fig.1 or by a molybdenum wire heated up to 2200 K.

Results: Typical fluorescence signals from atomic deuterium at L_α are shown in Fig.2. The signal at $n=1.5\cdot10^{10}$ cm^{-3} is more than 6 times higher than the false light measured 16 Å away from the line and also 6 times higher than the signal observed in vacuum at L_α. This means, that the detection limit (fluorescence signal = false light signal) is about $n=2.5\cdot10^9$ cm^{-3}. Because the atomic deuterium densities are difficult to measure by other methods, they are derived from a comparison of the fluorescence signals in deuterium with those in krypton (λ=1236 Å), the density of which can easily be determined with a pressure gauge. For equal monitor signals and equal densities, the ratio of the fluorescence signals is $S_D/S_{Kr}=f_D\,\lambda^2_D/f_{Kr}\,\lambda^2_{Kr}=2.2$. The main error in the calibration is presumably caused by line reversal in the light source. A second rough calibration can be derived from the curve of growth of the fluorescence signals in deuterium (Fig.3). Its maximum has to appear at an optical thickness C=1.6 ($C=8.3\cdot10^{-13}\, nf\ell\lambda^2/\Delta_D$ in cgs units, the Doppler width $\Delta_D=7.16\cdot10^{-7}\,\lambda(T/u)^{1/2}$ and u=molecular weight). Since T is not accurately known, this calibration is accurate only within a factor 1.7. Within this error limit, both calibration methods give the same result /3/.

Fluorescence in atomic hydrogen gave a factor of 5 lower signals than in deuterium under otherwise equal conditions, a phenomenon which can easily be understood considering self absorption in the light source.

Conclusions: The detection limit of $3\cdot10^9$ cm^{-3} is sufficiently low to measure the deuterium density in the shadow of the Tokamak limiter where n is estimated to be in the order of several 10^{10} cm^{-3}. The excitation by the light source described above with $\Delta\Omega=10^{-2}$ is equivalent to the excitation by electrons with $n_e=3\cdot10^{12}$ cm^{-3}, T_e=100 eV or $n_e=10^{17}$ cm^{-3}, T_e=1 eV. Therefore the fluorescence radiation should be sufficiently above the noise of the plasma radiation, if tangential observation is possible as it is planned in the TEXTOR apparatus. In this case the illuminating radiation has to pass through a hole of about 1 cm diameter in the liner, which gives only a small perturbation of the plasma wall interaction. The planned arrangement is shown in Fig.4.

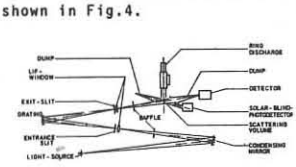

Fig.1 Experimental arrangement

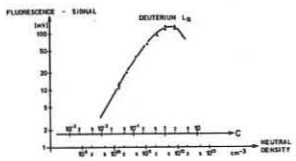

Fig.3 Curve of growth

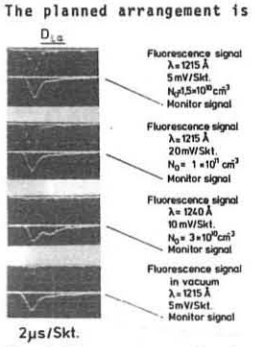

Fig.2 Fluorescence signals

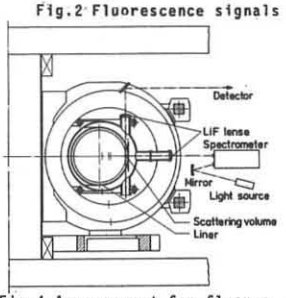

Fig.4 Arrangement for fluorescence measurements in TEXTOR

References:
/1/ Breton, C. and R. Papoular, Plasma Physics 17, 309 (1975)
/2/ Lie, Y.T., Appl. Phys. 2, 297 (1973)
/3/ Bogen, P. and Y.T. Lie, to be published

MODULATIONAL INSTABILITY PRODUCED BY LANGMUIR TURBULENCE IN A MAGNETIC FIELD

R.Pozzoli and D.Ryutov(+)

Laboratorio di Fisica del Plasma - Associazione CNR-EURATOM

Istituto di Fisica, Milano 20133 Italy

Abstract: The modulational instability of broad spectra of Langmuir oscillations, excited by electron beams, in a plasma in a magnetic field, is studied. Criteria of modulational instability are found, which are completely different as compared to the case of no magnetic field.

FORMULATION OF THE PROBLEM We consider the influence of an external magnetic field $\underline{B}$ on the stability of a plasma with a high level of homogenous Langmuir turbulence, with respect to the excitation of low-frequency, long-wavelength perturbations. The existence of the corresponding instability in a plasma with $\underline{B}=0$ was demonstrated in 1964 by Vedenov and Rudakov [1] (see also Ref.2). We restrict ourselves to the case of perturbations with wavenumbers q smaller than the characteristic wavenumber of Langmuir oscillations $\bar{k}$. The case $q \gtrsim \bar{k}$ will be considered separately (for a plasma with $\underline{B}=0$ it has been treated by Nishikawa and Zakharov [3,4]). We shall refer to the case of not too strong magnetic field, when the electron gyrofrequency ω_{ce} is smaller than the electron plasma frequency ω_p. In this case the magnetic field results only in a small correction (as compared to ω_p) to the dispersion relation: (see e.g. Ref.5)

$$\omega = \omega_p + 3\,k^2 v_T^2/2\,\omega_p + \left(\omega_{ce}^2 k_\perp^2/2\,\omega_p k^2\right)\left(1 - \omega_p^2/k^2c^2\right) \qquad (1)$$

where v_T is the electron thermal speed, and $k_\perp$ the component of $\underline{k}$ perpendicular to $\underline{B}$. We consider the case where a broad spectrum of Langmuir turbulence is excited by a beam of electrons with characteristic kinetic energy $\mathcal{E}$ (say, runaway electrons in Tokamaks or beams of relativistic electrons injected into solenoidal systems). Estimating $\bar{k} \simeq \omega_p/c\sqrt{1-m^2c^4/(mc^2+\mathcal{E})^2}$ we observe that in most of the present experiments the magnetic correction in Eq.(1) overbalances the thermal one.

DERIVATION AND ANALYSIS OF THE DISPERSION RELATION The effect of Langmuir oscillations on the low frequency motion of the plasma is due to the ponderomotive force. For one electron it may be written $\underline{f}=-\nabla U$, with $U=(\omega_p/2n)\int N_{\underline{k}}\,d\underline{k}$, where $N_{\underline{k}}$ are the "occupation numbers", related to the spectral energy density of oscillations $W_{\underline{k}}$ by the relation $N_{\underline{k}}=W_{\underline{k}}/\omega_{\underline{k}}$. In the unperturbed state the ponderomotive force is zero. It arises because of the spatial inhomogeneity introduced by the perturbation. The coupling between the perturbation of the occupation numbers $\delta N_{\underline{k}}$ and the density perturbation δn is described by the linearized kinetic equation for the occupation numbers [1,2]: $\frac{\partial \delta N_{\underline{k}}}{\partial t} + \underline{v}_g \cdot \nabla \delta N_{\underline{k}} - \frac{\partial N_{\underline{k}}}{\partial \underline{k}} \cdot \nabla \delta\omega_{\underline{k}} = 0$ where $\underline{v}_g \equiv \frac{\partial \omega}{\partial \underline{k}}$ is the group velocity of Langmuir oscillations and $\delta\omega_{\underline{k}} = \omega_p \delta n/2n$. Considering modulational electrostatic perturbations with frequency $\Omega \ll \omega_{ce}$ and phase velocity $|\Omega/q| \ll v_T$ we treat the electrons as being in Boltzmann equilibrium along the field lines. This results in the relation: $\frac{\delta n}{n} = \frac{e\delta\varphi - \delta U}{T}$ where $\delta\varphi$ is the electrostatic potential of the modulational perturbation. We assume that the ions are cold and can be described by hydrodynamic equations. This leads to the relation: $\frac{1}{n}\left(\frac{\partial^4 \delta n}{\partial t^4} + \omega_{ci}^2 \frac{\partial^2 \delta n}{\partial t^2}\right) = \frac{e}{M}\left[\Delta \frac{\partial^2 \delta\varphi}{\partial t^2} + \omega_{ci}^2 \left(\underline{h}\cdot\nabla\right)^2 \delta\varphi\right]$ where ω_{ci} is the ion gyrofrequency, and $\underline{h}\equiv\underline{B}/B$. Notice that, because of plasma quasineutrality of modulational perturbations we assume $\delta n_i = \delta n_e \equiv \delta n$. From the previous equations we obtain the following dispersion relation:

$$\Omega^2 \frac{1 - \omega_{ci}^2/\Omega^2}{1 - \omega_{ci}^2 \cos^2\theta/\Omega^2} = q^2 \frac{T - T_{eff}}{M}$$

where θ is the angle between $\underline{q}$ and $\underline{B}$, and T_{eff} is defined by the relation $T_{eff} = (\omega_p^2/4n)\int \frac{\underline{q}\cdot\partial N_{\underline{k}}/\partial \underline{k}}{\Omega - \underline{q}\cdot\underline{v}_g} d\underline{k}$ (the integration should be performed according to the Landau rule). Note that T_{eff} is, generally speaking, complex, and depends on both Ω and $\underline{q}$. Since the ions are essentially involved into low-frequency modulational oscillations, we expect that $|\Omega/q| \ll |\underline{v}_g|$. In fact it may be shown, a posteriori, that this relation is verified under very unrestrictive conditions. For this reason we neglect Ω in the denominator of the expression for T_{eff}. With this assumption $T_{eff} = \frac{\omega_p^2}{4n}\int \frac{\underline{\varkappa}\cdot\partial N_{\underline{k}}/\partial \underline{k}}{\underline{\varkappa}\cdot\underline{v}_g} d\underline{k}$ where $\underline{\varkappa} \equiv \underline{q}/q$. Note that now T_{eff} depends only on θ.

We consider here the case of isotropic turbulence (for a detailed investigation of the general case see Ref.6). In this case $N_{\underline{k}} = N(k)$, and $T_{eff} = \frac{\omega_p^2}{4n}\int \kappa^2 \frac{\partial N}{\partial \kappa} I(\kappa)\, d\kappa$ with $I(k) = \int d\sigma \frac{\underline{\varkappa}\cdot\underline{n}}{\underline{\varkappa}\cdot\underline{v}_g}$ where $\underline{n}=\underline{k}/k$, and $d\sigma$ represents the integration over the solid angle in $\underline{k}$-space. Using the Landau rule we can write I in the form: $I = i\pi\int d\sigma\, \underline{\varkappa}\cdot\underline{n}\, \delta\left(\underline{\varkappa}\cdot\underline{v}_g\right) + \mathcal{J}\, d\sigma \frac{\underline{\varkappa}\cdot\underline{n}}{\underline{\varkappa}\cdot\underline{v}_g}$ (2) where $\mathcal{J}$ denotes the principal value of the integral. It is easy to see that the integral with the δ-function in Eq.(2) is zero, and I (and T_{eff}) is real. The stability problem is reduced to the determination of the dependence of T_{eff} on θ, the condition for instability being that for some angle θ $T_{eff} > T$. An estimate for the maximum growth rate of the instability is $\Gamma_{max}(\theta) \sim \bar{k}\sqrt{\frac{T}{M}}\left(\frac{T_{eff}(\theta)}{T} - 1\right)$. The analysis of the integral I is very simple when thermal and relativistic corrections in dispersion relation (1) are neglected. In this case T_{eff} may be written in the form: $T_{eff} = \frac{W}{2n}\frac{\omega_{ce}^2}{\omega_p^2} F(\theta)$, where $W = \int W_{\underline{k}} d\underline{k}$ is the energy density of the Langmuir oscillations, and $F(\theta)$ a well behaved function of θ, which in $\theta=0$ and $\theta=\pi/2$ tends to $-\infty$ and $+\infty$, respectively. Thus, modulational perturbations propagating perpendicularly to the magnetic field tend to be strongly unstable. When relativistic and thermal corrections are taken into account the divergence in $F(\theta)$ is removed, and the analysis of the integral I shows that the most unstable perturbations are in a region around $\theta = \pi/2$. In this region (which turns to be much more larger than the interval $\left|\theta - \frac{\pi}{2}\right| < \sqrt{\frac{m}{M}}$ where our assumptions on the electron motion are not valid) we can estimate $T_{eff} \simeq \frac{W}{n}\frac{\omega_{ce}^2}{\omega_p^2}\frac{1}{\alpha} F(\theta)$ where α is of the order of the introduced corrections and $F(\theta) \sim 1$.

REFERENCES

(+) Permanent address: Institute of Nuclear Physics, Novosibirsk, 630090, USSR

[1] A.A.Vedenov and L.I.Rudakov:Dokl.Acad.Nauk USSR 159,767(1964)

[2] A.A.Vedenov, A.V.Gordeev, L.I.Rudakov:Plasma Phys.9,719(1967)

[3] K.Nishikawa: Jour. Phys. Soc. Japan 24,916,1152(1968)

[4] V.E.Zakharov: Zh. Eksp. Teor. Fiz. 62,1745(1972)

[5] B.N.Breizman and D.D.Ryutov: Nuclear Fusion 14,873(1974)

[6] D.Ryutov and R.Pozzoli: Report FP 77-5 Laboratorio di Fisica del Plasma CNR - Milano (1977) (to be published)

SUPERFINE STRUCTURE OF UHF SPECTRUM OF THE EXPLODING CURRENT CAVITON

N.F. Perepelkin, V.A. Suprunenko, V.I. Petviashvili,*) M.P. Vasil'ev (KPTI AS UkSSR, Kharkov, USSR. *) IAE, Moscow, USSR).

The analysis of numerous plasma experiments shows the sporadic superthermal UHF radiation in the vicinity of plasma frequency $\omega \sim \omega_{pe}$ in current discharges to be the universal characteristic of nonmaxwellian plasma independent of heating technique and a magnetic trap type (stellarators, tokamaks, Z - and θ-pinches). The term "sporadic" radiation is borrowed from astrophysics and it defines the most completely that phenomenon in plasma devices which resembles surprisingly the 1st-type solar radio-emission bursts. A special interest to this type of radiation was shown up in experiments on plasma turbulent heating [1]. In the radiation spectrum a number of intensive harmonics ω_{pe}, $2\omega_{pe}$, ..., decreasing according to the law $\sim\omega^{-2}$, was observed [2]. In the burst $\tau \sim 5 \cdot 10^{-8}$ sec accompanying fast plasma heating in a torus [3] it has been discovered a deep ~100% modulation of $\sim\omega_{pe}$ radiation by frequencies of acoustic range $\sim 2\omega_{pi}$.

A detailed investigation of spatial-time and spectral characteristics of superthermal noises $\sim\omega_{pe}$ and $\sim\omega_{pi}$ in conditions of quasi-stationary current heating of plasma in "Uragan" stellarator [4] led to the conclusion that the noise excitation process had exceptionally explosive threshold character and was probably connected with trapping and accumulation of turbulent noises in local regions of plasma. In these experiments the information on local characteristics of $\sim\omega_{pe}$ and $\sim\omega_{pi}$ oscillation coupling in plasma was obtained by means of probes, as well as by the method of analysing HF - modulation spectrum of UHF -radiation $\sim\omega_{pe}$ observed out of plasma. The mechanism of superthermal emission $\sim\omega_{pe}$ is shown to be connected with nonlinear interection in plasma of two spectra: $\omega \sim \omega_{pe}$ and $\omega \sim \omega_{pi}$; $2\omega_{pi}$. Moreover, the noises $\omega \sim \omega_{pi}$ and $2\omega_{pi}$ were identified as long-wave oscillations with $v_{\parallel} \ll v_{Te}$ excited near low-hybrid-resonance frequencies in inhomogeneous plasma.

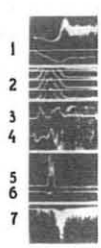

Fig.1

The feature of $\sim\omega_{pe}$ and $\sim\omega_{pi}$ noise excitations in "Uragan" stellarator in pure hydrogen discharges fell into the fact that an intensive flash moment always conformed to a plasma density stripping phase, as well as coincided with a moment of occuring strong local diamagnetic perturbation, which value was $\sim 10^{-2}\frac{H_z^2}{8\pi}$. Fig.1 shows oscillograms for hydrogen discharge (H_z=7.2Koe): 1 - voltage 20mv/cm per div., current - 2 ka/div.; 2 - density $\bar{n}_e$, between lines $\sim 2 \cdot 10^{12} cm^{-3}$; 3 - 2 mm signal interferogram; 4,5,6,7 - probe signals observed from the local area simultaneously ΔH_z, ω_{pe}, γ ($\varepsilon_e \geq$ 10kev) and $2\omega_{pi}$, respectively. (Scanning: 250μsec/div). It has been observed a strong spatial localization of signals ΔH_z, ω_{pe}, ω_{pi}, $2\omega_{pi}$ and γ on the length $\leq$0.5cm on characteristic radii inside the plasma column. The range of signal localization on r and γ depended on value $\frac{I}{H_z}$ and ε_b, so when required it could be withdrawn into the region of combined probe aerials. The conclusion about spatial localization of instability region in plasma has also been drawn from without-contact measurements of UHF noise spectrum. Fig.2 gives the helium plasma spectra, averaged over a great number of discharges, for various magnetic field strengths (1 -4.8; 2 -7.2 and 3 -16.8koe) at constant parameters $\bar{n}_e \sim 4.2 \cdot 10^{12} cm^{-3}$, $T_e \sim$100ev, E=25mv/cm and ε_t=0.58. It is seen that at transition to high magnetic fields $\omega_{ce} > \omega_{pe}$, it takes place a superthermal spectrum shift into the range of wavelengths λ_{pe} conforming to a plasma maximum density in the column centre.

For profound investigation of the generation mechanism of sporadic UHF noises the study of superfine structure of UHF spectrum was performed by two independent methods. In the first (indirect) method the experimental data [4] were used on the fluctuation spectrum of UHF radiation $\omega \sim \omega_{pe}$ which were obtained at square-law detection of noises ω_{pe} in a wide frequency band $\Delta\omega \sim 0.1\omega_{pe}$ for the synthesis, by means of computer, of the similar fluctuation spectrum by selection of spectral components and further square-law transformation of a spectrum-model. In the second method the information was obtained by means of a wide-band pulse UHF analyzer in 5μsec ($\tau \sim$15÷20μsec). Figs.3 and 4 show UHF radiation spectra for the helium plasma, respectively, the spectrum-model and the spectrum at the output of the fast-response analyzer. Notice, that frequency resolution in the analysis in both cases was not worse than 3÷ 6MCps. In the first experiment the superthermal UHF radiation was observed from a periphery plasma region by means of a funnel-shaped antenna on a frequency ω_{pe}=12±0.56Hz (H_z=4.8koe, ε_t=0.58). In the second experiment the radiation was received by a coaxial UHF probe located also in a peripheral plasma region on the radius r=5cm (the radius of an edge undestroyed magnetic surface in the stellarator R_g=6.8cm). The received signal frequency was ω_{pe}=13.1±0.35GHz, the magnetic field H_z=7.5koe, ε_t=0.63. In both cases the maximum plasma density in a column centre was $n_e \approx 3 \cdot 10^{12} cm^{-3}$.

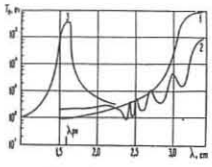

Fig. 2

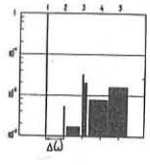

Fig. 3

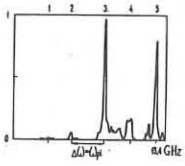

Fig. 4

The spectral analysis results show that both independent methods give practically identical spectra of sporadic UHF emission in the vicinity of electron plasma frequency $\omega \sim \omega_{pe}$ with a characteristic set of coherent lines shifted at a frequency on $\Delta\omega \simeq \omega_{pi} \simeq$105; 150MCps for Z=1;2. In this case it is observed in the spectrum a rather intensive pair of lines displaced on a frequency scale in a characteristic value $2\Delta\omega \simeq 2\omega_{pi}$, where about 80% of plasma UHF radiation energy is concentrated. Q - factor of these lines is high and constitutes $Q \geq 10^3$.

The data of independent measurement of the turbulent noise spectrum in plasma in similar regimes on "Uragan" stellarator" [4], where the sporadic excitation of narrow-band oscillation spectrum $\sim 2\omega_{pi}$ was observed, allow to identify separate lines in spectra presented in Figs3 and 4. Fig.3: 1 - $\omega_{pe}+2\omega_{pi}$; 2 - $\omega_{pe}+3\omega_{pi}$; 3 - $\omega_{pe}+4\omega_{pi}$; 4 - $\omega_{pe}+5\omega_{pi}$; 5 - $\omega_{pe}+6\omega_{pi}$. Fig.4: 1 - ω_{pe}; 2 - $\omega_{pe}+\omega_{pi}$; 3 - $\omega_{pe}+2\omega_{pi}$; 4 - $\omega_{pe}+3\omega_{pi}$; 5 - $\omega_{pe}+4\omega_{pi}$. Thus, the superthermal UHF emission is generated by plasma on fixed frequencies, perhaps the satellites are radiated: $\omega_{pe}+\omega_{pi}$ and $\omega_{pe}+3\omega_{pi}$; or $\omega_{pe}+2\omega_{pi}$ and $\omega_{pe}+4\omega_{pi}$.

It is possible to conclude, while summing up investigation results, that the mechanism of sporadic UHF emission ω_{pe} and the excitation of intensive electromagnetic oscillations in plasma with narrow spectrum $\omega \sim \omega_{pi}$; $2\omega_{pi}$ are solely connected with an explosive process of the release of electromagnetic energy accumulated in resonant plasma cavities-cavitons. We are cannot excluded that it is just the current caviton explosions, that play the main role in transfer phenomena, and also lead to the injection of superthermal electrons and ions into a closed magnetic trap, and these are accelerated to relativistic energies by the quasi-stationary electric field (runaway electrons).

References

1. V.A. Suprunenko et al. Atomnaya Energia (USSR), 1963, 14, 349.
2. E.K. Zavoisky et al. Zh. Eksper. i Teor. Fiz. (USSR), 1971, 60, 1328.
3. N.F. Perepelkin, S.D. Fanchenko. Doklady Ak. Nauk. SSSR, 1969, 189, 288.
4. A.V. Longinov, N.F. Perepelkin, V.A. Suprunenko. Fizika Plasmy. 1976, 2, 626.

ION ACCELERATION IN RESONANCE ABSORPTION EXPERIMENTS

H. Schamel, K. Elsässer
Theoretical Physics I, Ruhr-University Bochum, FRG

Abstract: The importance of density barriers in the generation of fast ions observed in resonance absorption experiments is pointed out. Solving mode-coupling equations numerically, two mechanism are found to be responsible for ion acceleration: i) a transition from a standing to a moving state of the density barriers during a stage called soliton flash, and ii) the enhanced ambipolar fields related with the density barriers.

Experimental observations show the appearance of high energy ions when a plasma is irradiated by a wave. Because the accelerated ions carry an appreciable amount of energy with them, bulk heating of the plasma is reduced. It is therefore desirable to understand the origin of this phenomenon. For this purpose, we solved the mode-coupling equations and explored the physics involved at the resonance layer.

We use an extended version of ZAKHAROV's equations which describe the interaction of Langmuir- and ion waves on the ionic time scale. If E is the collective variable representing the high frequency oscillation, and δn the ion density perturbation, the equations are [1]

$$\left(i\partial_t+\frac{3}{2}\omega_{pe}\lambda_D^2\partial_x^2\right)E=\frac{\omega_{pe}}{2}\left(1-\frac{3}{2}\lambda_D^2\partial_x^2\right)\frac{\delta n}{n_o}E-\frac{\delta\omega}{2}E_{ext}\,e^{-i\delta\omega t} \qquad (1)$$

$$\left(1-\lambda_D^2\partial_x^2\right)\left(\partial_t^2-\nu\omega_{pi}\lambda_D^2\partial_x^2-c_s^2\partial_x^2\right)\frac{\delta n}{n_o}=c_s^2\partial_x^2\left[\frac{|E|^2}{4\pi n_o T_e}+\left(\frac{\delta n}{n_o}\right)^2+\lambda_D^2\partial_x^2\frac{\delta n}{n_o}\right] \qquad (2)$$

In (1) we have included an external electric field oscillating at $\omega_o=\omega_{pe}+\delta\omega$. Due to its presence energy can be exchanged with the system. For $\delta\omega<0$, one is in the regime of the oscillating two stream instability where cavity formation takes place, analogous to what happens at the resonance layer of an inhomogeneous plasma. In the ion equation we have included the full ion dispersion, and also the lowest order ion nonlinearity. In addition to the viscous damping term in (2) we also considered the Landau damping of both waves while solving the equations in the Fourier space. The advantage of such a system against a particle simulation code is that besides the computational efficiency it allows to isolate physical effects and to look for the mechanisms involved. E. g., it turns out that a key role in accelerating ions is played by frequency shifts of the ion waves whose time- and amplitude dependence can easily be investigated.

The numerical findings are as follows: If the external field exceeds a threshold value the system is unstable against the modulational instability. Density cavities are formed in which the high frequency field becomes trapped. It pushes away the electrons by the ponderomotive force (radiation pressure) and, through the ambipolar field, the ions will also be pulled out of the resonance region. Because of mass conservation shoulders will appear on both sides of the cavity. These shoulders are nearly standing in space as long as field trapping takes place. The effective frequency of the ion modes constituting the density perturbation is seen to be nearly zero. At a certain time a strong change in the evolution occurs. The electric field intensity having the shape of a soliton almost completely disappears in a few ion plasma periods, and the ion density perturbation strongly increases. The disappearance of $|E|^2$ is due to the Landau damping of the electron modes being enhanced by the generation of high k - modes, and is also due to an energy exchange with the external field. This stage called soliton-flash (or quasi-collapse[3]) has also been seen in laboratory experiments [2] as well as in particle simulations [3]. The shoulders up to this stage are standing in space and therefore able to reflect and trap ions through the related ambipolar potential. During the flash the ponderomotive force responsible for the downshift of ion wave frequency disappears and the ion modes become ion acoustic-like. As a result the shoulders start moving apart with sound speed, carrying with them the trapped ions. Furthermore these ions are situated near their turning points and experience a strong force due to the gradients of the ambipolar potential. Thus, the ions will move with a larger velocity and leave the region of enhanced density. The shoulders therefore will diffuse as they are moving apart. This effect can clearly be seen in the micro wave absorption experiment of Wong and Stenzel [2] in which 7eV ions ($\approx 35\,T_i$) are found. In this experiment the shoulders are unsymmetric. The shoulder at the lower density side is more pronounced than the opposite one. This is an effect of the density gradient. Accordingly, one would expect a stronger flux of accelerated ions down the density gradient which is indeed observed. Note that the ponderomotive force as a possible acceleration mechanism would predict a symmetric flux of fast ions. Finally we mention that also the particle simulations of Sigov & Khodirev [3] support this idea of ion acceleration.

1) K. Elsässer, H. Schamel, SFB-Report 76-L 2-007 (1976)
2) A. Y. Wong, R. L. Stenzel, Phys. Rev. Lett. 34, 727 (1975), A. Y. Wong, UCLA Preprint PPG-277 (1976)
3) Yu. S. Sigov, Yu. V. Khodirev, Sov. Physics Doklady 21 (1976), 444.

PLASMA PARAMETRIC RESONANCE IN THE NON-MONOCHROMATIC PUMP-WAVE

Yu.M.Aliev, A.A.Chernikov, O.M.Gradov
V.V.Pustovalov, V.P.Silin
P.N.Lebedev Physical Institute, Academy of Sciences of the USSR, Moscow, USSR
V. Stefan
Boris Kidrič Institute of Nuclear Sciences - Vinča, Beograd, Yugoslavia

The effect of a finite-bandwidth pump-wave on the evolution of potential parametric instabilities is considered. It is found that conditions with finite-bandwidth stabilize plasma or facilitate parametric growth of the turbulent noise.

Any real generator of electromagnetic radiation have a finite-bandwidth effect of which on parametric instabilities can be essential [1-3]. In this report we represent some aspects of dynamical finite-bandwidth parametric theory, recently developed by us.

We considered a fully ionized plasma interacting with the pump field

$$\vec{E}(t) = \vec{E_o}(t)\sin(\omega_o t + \phi(t)) \qquad (1)$$

where amplitude $\vec{E_o}(t)$ and phase $\phi(t)$ are assumed to be slow varying compared with carrier frequency ω_o, which is closed to the electron plasma frequency ω_{Le}. First, we considered the case of a set of rectangular impulses with duration τ, repetition period T and peak intensity E_o. Introducing an effective electric field intensity $E^2_{eff} = \frac{\tau}{T} E_o^2$ which characterize time-average power of a generator, we write down the oscillating two-stream instability (OTSI) threshold for rather durable impulses $\gamma_a\tau>>1$ (γ_a - growth rate of OTSI for monochromatic pump-wave),

$$\frac{E^2_{eff,thr}}{4\pi(n_eT_e + n_iT_i)} = \frac{8\tilde{\gamma}}{\omega_o} \qquad (2)$$

where $\tilde{\gamma}$ is a decrement of electron plasma wave. The best conditions for excitation are fulfiled for wave propagating along $\vec{E_o}$ with wave-number k_m satisfying the condition $\Delta\omega_o(k_m) = \omega_o - \omega_{Le}(1 + \frac{3}{2} k_m^2 r_{De}^2) = -\gamma_a$. The expression (2) takes place also in the case of a very short impulses $\gamma_a\tau<<1$, but the extreme wave-number k_m is defined by the condition $\Delta\omega_o(k_m) = -\gamma_a \frac{\tau}{T} + \frac{2\pi n}{T}$, n=0,±1...

The effective threshold of periodical non-decay ($\gamma>>\omega_s$) instability is:

$$\frac{E^2_{eff,thr}}{4\pi n_eT_e} \sim 0{,}78 \frac{\tilde{\gamma}\gamma_s}{\omega_{Le}\omega_s} \qquad (3)$$

and is realized for $\frac{\tau}{T} \sim 0{,}35$. The value (3) is $\frac{\tilde{\gamma}}{\omega_s}$ times less than corresponding expression for instability threshold in the case of monochromatic pump. Let us note that decreasing of the instability threshold takes place also for negative mismatches $\Delta\omega_o + n\pi\frac{\tau}{T} = \omega_s$, n=0,±1 ..., because of excitation of many frequencies in spectral expansion of a pump-wave. The effect of decreasing of the threshold was firstly discovered in [4], for the case of two monochromatic pump-waves. In the case of decay of a pump-wave into Langmuir and ion-acoustic waves such a decrease of the effective field intensity does not occur. So if $T>>\tau$, $|\gamma_s - \tilde{\gamma}|\tau>>1$, $\omega_s\tau>>1$, then

$$\frac{E^2_{eff,thr}}{4\pi n_eT_e} = \frac{16}{\omega_o\omega_s}\left(\tilde{\gamma}\gamma_s + \frac{(\min\gamma_s,\tilde{\gamma})^2\tau}{T}\right) \qquad (4)$$

where ω_s and γ_s are frequency and decrement of ion-acoustic wave.

Let us consider now the case of slowly frequency modulated pump-wave. If the frequency width Δ is defined by periodical frequency modulation

$$\delta\omega(t) = \tilde{\gamma}^2 t \text{ for } |t| < \frac{\Delta}{\tilde{\gamma}^2};\ \delta\omega(t + \frac{2n\Delta}{\tilde{\gamma}^2}) = \delta\omega(t),\ n=0,\pm1.. \qquad (5)$$

then for rather wide spectral width $\Delta>>\gamma_a$ the threshold of OTSI increases by the factor $(\frac{\Delta}{\tilde{\gamma}})^{1/2}$ in comparison with the case of monochromatic pump-wave

$$\frac{E^2_{thr}}{4\pi(n_eT_e+n_iT_i)} = 8\left(\frac{4}{\pi}\frac{\tilde{\gamma}\Delta}{\omega_o^2}\right)^{1/2} \qquad (6)$$

The threshold for the decay instability ($t\to1+s$) with such a pump also increases

$$\frac{E^2_{thr}}{4\pi n_eT_e} = \frac{32}{\pi}\frac{\Delta\cdot\min(\gamma_s,\tilde{\gamma})}{\omega_o\omega_s} \qquad (7)$$

For monotonically time-changing frequency a finite amplification of the coupled wave amplitude takes place [5].

REFERENCES:

1. C.Yamanaka, T.Yamanaka, T.Sasaki, J.Mizui, H.B.Kang. Phys. Rev.Lett. 32, 1038 (1974)
2. C.Yamanaka, T.Yamanaka, H.B.Kang, M.Waki, K.Shimamura. Annual Review, April 1972 - March 1973, p.110. Nagoya University, Institute of Plasma Physics.
3. S.P.Obenschain, N.C.Luhmann,Jr., P.T.Dreiling. Phys. Rev. Lett. 36, 1309 (1976)
4. D.Arnush, K.Nishikawa, et.al. Phys. of Fluids 16, 2270 (1973)
5. V.V.Pustovalov, V.P.Silin, A.A.Chernikov, Quantum Electronics 1977 (in press)

PARAMETRIC EXCITATION IN LOWER HYBRID HEATING OF A TWO-ION SPECIES PLASMA

M.Bornatici+
Associazione EURATOM-CNEN sulla Fusione, Centro Gas Ionizzati, C.P. 65, FRASCATI, Rome, Italy
G.Artico, R.Spigler
Associazione EURATOM-CNR, Centro Studio Gas Ionizzati PADOVA, Italy

Abstract: The parametric excitation of lower-hybrid and Buchsbaum waves in a two-ion species plasma is described by means of the fluid equations. The growth rates are evaluated and the effects of plasma and pump nonuniformities upon the instability thresholds are discussed.

Introduction: The parametric excitation of lower-hybrid and Buchsbaum waves is one of the nonlinear processes which could be important in the heating of the high density region of a multispecies toroidal plasma by RF waves which match the lower-hybrid frequency near the center of the plasma. In a two-ion species plasma in the presence of a uniform magnetic field $\underline{B}=B_o\hat{z}$ and a crossed electric field $\underline{E}=(E_o\cos\omega_o t-\frac{\partial\phi}{\partial x})\hat{x}$ waves propagating in the x-direction can be driven unstable by the coherent relative ion motion induced by the pump field[1,2].

Ion coupling ($k_1\varrho_j\ll 1$): By combining the linearized continuity equation, the x and y-components of the equation of motion, where temperature and collisional effects are neglected, together with the scaled Poisson's equation, i.e., x replaced by $(1+\omega_{pe}^2/\Omega_e^2)^{-1/2}x$, one arrives at the following equation, for a two-ion species plasma,

$$(\frac{\partial^2}{\partial t^2}+\bar{\omega}_{pj}^2+\Omega_j^2)n_j=-\bar{\omega}_{pj}^2 n_{j'}e^{i\mu_{jj'}},\quad (j,j'=1,2;j\neq j') \tag{1}$$

where $n_j=z_j\tilde{n}_j e^{i\mu_j(t)}$, z_j and $\tilde{n}_j$ being the charge number and the density fluctuation of the j-th ion species, respectively,

$$\mu_j=-\frac{k_x e E_o}{\omega_o^2-\Omega_j^2}\frac{z_j}{m_j}\cos\omega_o t, \tag{2}$$

$\mu_{jj'}=\mu_j-\mu_{j'}$; $\bar{\omega}_{pj}^2=(1+\omega_{pe}^2/\Omega_e^2)^{-1}\omega_{pj}^2$. Equations (1) constitute a system of two coupled equations for n_1 and n_2 (here 1 and 2 denote the two-ion species). It appears that the pump field has an effect on the plasma provided that $\mu_1\neq\mu_2$, i.e. $z_1/m_1\neq z_2/m_2$. We consider Eqs.(1) in the weak coupling limit, $|\mu_{jj'}|\ll 1$. For the case in which there are two distinct time scales one can separate Eqs. (1) into a high frequency part, describing the high frequency motion (lower-hybrid wave) and a low frequency part, describing the low frequency motion (Buchsbaum wave). One thus obtains the two coupled equations which describe the propagation across a magnetic field of lower-hybrid and Buchsbaum waves in the presence of an external pump field,

$$(\frac{\partial^2}{\partial t^2}+\omega_{LH}^2)n_{1,LH}=i\bar{\omega}_{p1}^2\mu_{12}n_{1,B}, \tag{3a}$$

$$(\frac{\partial^2}{\partial t^2}+\omega_B^2)n_{1,B}=-i\bar{\omega}_{p2}^2\mu_{12}n_{1,LH}, \tag{3b}$$

with $\omega_{LH}^2\equiv(1+\omega_{pe}^2/\Omega_e^2)^{-1}(\omega_{p1}^2+\omega_{p2}^2)$ the lower-hybrid frequency for a two-ion species plasma: $\omega_B^2=\omega_{p1}^2\Omega_2^2+\omega_{p2}^2\Omega_1^2/(\omega_{p1}^2+\omega_{p2}^2)$ the Buchsbaum or ion-ion hybrid frequency; $\Omega_j^2\ll\bar{\omega}_{pj}^2$.

Thresholds and growth rates: Both decay and purely growing instabilities can result from the ion coupling induced by the pump field. By denoting

$$\Gamma^2\equiv\frac{1}{16}\frac{\bar{\omega}_{p1}^2}{\omega_{LB}}\frac{\bar{\omega}_{p2}^2}{\omega_B}(\frac{k_x V_o}{\omega_o})^2,\quad V_o\equiv\frac{eE_o}{\omega_o}\left|\frac{z_1}{m_1}-\frac{z_2}{m_2}\right|, \tag{4}$$

for the decay instability[3] the minimum threshold, $\left[\Gamma_m^{(d)}\right]^2=\nu_{LH}\nu_B$, and maximum growth rate, $\gamma_o^{(d)}=\Gamma_m(\nu_B+\nu_{LH})\ll\gamma_o^{(d)}\ll\omega_B$), are given by

$$\left(\frac{V_{o,m}}{C_s}\right)^{(d)}=\frac{4}{(k_x\lambda_{de})}(1+\frac{q_1}{q_2}\frac{z_2}{z_1}\frac{m_1}{m_2})^{1/2}(\frac{\Omega_1}{\omega_{pl}})(\frac{\omega_o}{\omega_{LH}})(\frac{\nu_{LH}}{\omega_{LH}}\frac{\nu_B}{\omega_B})^{1/2} \tag{5}$$

$$\frac{\gamma_o^{(d)}}{\omega_o}=\frac{1}{4}\left(1+\frac{q_1}{q_2}\frac{z_2 m_1}{z_1 m_2}\right)^{-1/2}(k_x\lambda_{de})(\frac{\omega_{pl}}{\Omega_1})(\frac{\omega_B}{\omega_o})^{1/2}(\frac{\omega_{LH}}{\omega_o})^{3/2}(\frac{V_o}{C_s}), \tag{6}$$

where $C_s^2=\sum_j\frac{z_j^2 N_j}{N_e}\frac{T_e}{m_j}$; $q_j=\frac{z_j N_j}{N_e}$; ν_{LH} and ν_B are the damping rates of the lower-hybrid and Buchsbaum wave, respectively. For the purely growing instability[3] ($\omega_o<\omega_{LH}$), the minimum threshold is a factor $(\omega_B/2\nu_B)^{1/2}$ higher than the threshold(5), and the maximum growth rate, $\gamma_o^{(a)}=(2\omega_B\Gamma^2)^{1/3}$ ($>\omega_B$), can be written as $\gamma_o^{(a)}=\left[2\omega_B(\gamma_o^{(d)})^2\right]^{1/3}$, where $\gamma_o^{(d)}$ is given by (6) with V_o/C_s such that the threshold for the excitation of the purely growing instability is exceeded.

Numerical evaluation of the instability growth rates: We now consider the specific case of a plasma composed of hydrogen (species 1, hereafter denoted by index H) and a second species, e.g., D^+, He^{+2}, O^{+8}, characterized by $Z_2/A_2=1/2$, with A the atomic mass, so that $\Omega_2=\Omega_H/2$. One then has $\frac{V_o}{C_s}=2.46\times10^{-3}\left[\frac{q_2}{q_H}(1+0.5\frac{q_2}{q_H})\right]^{-1/2}E_o/f_o T_e^{1/2}$ ($\frac{kV}{cm}$, GHz, keV); it follows that $V_o/C_s=4.5\times10^{-3}$, for $q_H=0.8$, $q_2=0.2$, $E_o=3$ kV/cm, $f_o=1$GHz and $T_e=3$ KeV. Threshold (5) turns out to be $(V_{o,m}/C_s)^{(d)}=0.11\,B/(k_x\lambda_{de})f_o(\nu_{LH}/\omega_{LH}\;\nu_B/\omega_B)^{1/2}$, (Tesla, GHz), for $\omega_o=\omega_{LH}$, i.e., $N_H\simeq2\times10^{13}$ cm^{-3}, for $f_o=1$GHz. For collisional damping, $\nu_{LH}/\omega_{LH}\;1.7\times10^{-7}$, $\nu_B/\omega_B\simeq2\times10^{-6}$, so that $(V_{o,m}/Cs)^{(d)}\;10^{-5}$ for $B=5$T, $f_o=1$GHz and $(k_x\lambda_{de})=0.03$, which corresponds to $(k_x\varrho_H)\simeq0.3$ with $T_e=2\,T_H$. Therefore, $V_o/C_s=4.5\times10^{-3}\simeq4.5\times10^{2}(V_{o,m}/C_s)^{(d)}$, i.e., the threshold value of the pump field is about 6.67 V/cm. The growth rate (6), $\gamma_o^{(d)}/\omega_o=24.95\times10^{-3}(f_o/B)^{1/2}V_o/C_s$(GHz, Tesla), yields $\gamma_o^{(d)}/\omega_o=5\times10^{-5}$ for the above parameters. The growth time of the decay instability, $(\gamma_o^{(d)})^{-1}\simeq3\times10^{-6}$ sec, is typically a factor 10^2 shorter than the electron collision time.

The threshold of the purely growing mode is a factor $(\omega_B/2\nu_B)1/2\;5\times10^2$ higher than the threshold of the decay instability so that the case we are considering of a pump field of 3 kV/cm should be marginally stable (the resulting threshold field is in fact about 3.3 kV/cm). We note, however, that the threshold for the excitation of wavelengths shorter than the ion Larmor radius[1,2] is a factor

$$\alpha=\left(\frac{k^2\varrho_1^2\Omega_1^2\omega_{p2}^2+k^2\varrho_2^2\Omega_2^2\omega_{p1}^2}{\Omega_1^2\omega_{p2}^2+\Omega_2^2\omega_{p1}^2}\right)^{1/2},$$

(where $k^2\varrho_j^2\ll1$, with ϱ_j the Larmor radius), smaller than that corresponding to the excitation of wavelengths longer than the ion Larmor radius considered here[1]. For our specific case $\alpha=0.24$, ($T_H=2T_2$, $z_2=2$), and the threshold field for $(k\varrho_j)^2\gg1$ is then about 8×10^2 V/cm.

The density gradient and the finite spatial extent of the pump produce effective thresholds which can be higher than the uniform thresholds. For a local scale length of the density gradient $|dN_j/N_j dx|^{-1}=10$ cm, the finite extent of the pump produces the highest threshold, which can be written as $\gamma_o\gtrsim\gamma_{eff}\equiv k_x|V_x^{(LH)}+V_x^{(B)}|/2$, with $V_x^{(LH)}$ ($V_x^{(B)}$) the x-component of the group velocity of the lower-hybrid (Buchsbaum) wave and $L_x(\gtrsim\frac{2\pi}{k_x})$ the width of the pump in the x-direction. For the case we are considering, $\gamma_{eff}\simeq1.6\times10^6\,\text{sec}^{-1}\simeq5\gamma_o^{(d)}$, ($L_x\simeq1.7$ cm), i.e., the threshold field due to the spatial variation of the pump intensity (the pump wave propagates in well-defined resonance cones) is about 15 kV/cm, for the convective decay instability.

One of the authors (M.B.) whishes to express his gratitude to the Centro Gas Ionizzati, Frascati, for hospitality during part of this work.

References:

(1) E.OTT, J.B. McBRIDE, J.H.ORENS, Phys. Fluids, 16, 270 (1973)
(2) P.K.KAW, Y.C.LEE, Phys. Fluids, 16, 155 (1973).
(3) K.NISHIKAWA, J.Phys.Soc.Jap. 24, 916 (1968).

+ Permanent address: Department of Engineering, University of Pavia.

FINITE FREQUENCY DENSITY MODIFICATIONS BY LOWER-HYBRID CONES[+]

P.K. Shukla*, M.Y. Yu*, and K.H. Spatschek**
* Institut für Theoretische Physik, Ruhr-Universität Bochum, 4630 Bochum, F.R. Germany
** Fachbereich Physik, Univ. Essen, 4300 Essen, F.R. Germany

Abstract: It is analytically shown that the nonlinear interaction of lower-hybrid cones with finite frequency density fluctuations can lead to moving solitary envelopes for the wave electric field.

We consider the propagation of intense lower-hybrid waves, taking into account the nonlinear coupling with finite frequency density perturbations. The physical idea is as follows: In the linear analysis the rf transport reduces to the linear mapping of the source along the characteristic lines which are called lower-hybrid cones. In the nonlinear regime the propagation characteristics is affected by the ponderomotive as well as $\vec{E}\times\vec{B}$ forces. As a result, deviations from the linear cone occur. The nonlinear effects can lead to filamentation of the lower-hybrid field, and the interaction of plasma particles with localized fields affects the transport of the wave energy to the center of the plasma. In particular, Morales and Lee [1] considered the filamentation arising from the coupling of lower-hybrid waves with perturbations in which electrons and ions move adiabatically along the external magnetic field lines, such that both species retain their Maxwellian distributions. The use of adiabatic perturbations is based on the assumption that the generation and evolution of the lower-hybrid filamentation occurs slowly compared to the transit time of the density fluctuations across the width of the wave structure. Such an assumption may be inadequate in real plasmas [2]. Here, we generalize the investigations of Morales and Lee to include finite frequency density perturbations.

From the warm two-fluid equations, one can readily obtain the equation governing the slowly modulated lower-hybrid potential $\phi = \varphi(x,z,t)\exp(-i\omega t) + c.c$, where $\Omega_i \ll \omega \ll \Omega_e$ and $\Omega_j = e_j B_o / m_j c$ is the gyrofrequency of species j. Within a two dimensional model, one [1] finds

$$\partial_t^2 \partial_x \left[1 + \frac{\omega_{pe}^2}{\Omega_e^2}\left(1 + \frac{\tilde{n}}{n_o}\right)\right]\partial_x \phi + \partial_z\left[\partial_t^2 + \omega_{pe}^2\left(1 + \frac{\tilde{n}}{n_o}\right)\right]\partial_z \phi + \partial_t^2\left(a_o \partial_x^4 + c_o \partial_x^2 \partial_z^2 + b_o \partial_z^4\right)\phi + \nabla \omega_{pi}^2\left(1 + \frac{\tilde{n}}{n_o}\right)\cdot \nabla \phi = 0 , \quad (1)$$

where thermal effects have been treated as higher order corrections, and ions are assumed to be unmagnetized. The terms involving $\tilde{n}(x,z,t)$ arise due to the interaction of lower-hybrid cones with the finite frequency density oscillations. We have also defined $a_o = v_e^2 \omega_{pe}^2 / \Omega_e^4 + v_i^2 \omega_{pi}^2 / \omega^4$, $b_o = \sum_j v_j^2 \omega_{pj}^2 / \omega^4$, $c_o = -2 v_e^2 \omega_{pe}^2 / \Omega_e^2 \omega^2 + 2 v_i^2 \omega_{pi}^2 / \omega^4$, $v_j^2 = T_j / m_j$, and $\omega_{pj}^2 = 4\pi n_o e^2 / m_j$. For $\tilde{n} = 0 = a_o = b_o = c_o$, the waves propagate along the characteristic lines $dx/dz = C \equiv (\varepsilon_\perp / |\varepsilon_\parallel|)^{1/2} \ll 1$, where $\varepsilon_\perp = 1 + \omega_{pe}^2 / \Omega_e^2 - \omega_{pi}^2 / \omega^2$, and $\varepsilon_\parallel = 1 - \sum_j \omega_{pj}^2 / \omega^2$.

Applying the usual WKB ansatz, namely $\partial_t \to \partial_t - i\omega$ and $\partial_t \ll \omega$, we obtain from eq. (1)

$$\frac{2i}{\omega}\left[\left(1 + \frac{\omega_{pe}^2}{\Omega_e^2}\right)\partial_x^2 + \partial_z^2\right]\partial_t \varphi + \varepsilon_\perp \partial_x^2 \varphi + \varepsilon_\parallel \partial_z^2 \varphi + a_o \partial_x^4 \varphi + c_o \partial_x^2 \partial_z^2 \varphi + b_o \partial_z^4 \varphi = \alpha \partial_x\left(\frac{\tilde{n}}{n_o}\partial_x \varphi\right) + \beta \partial_z\left(\frac{\tilde{n}}{n_o}\partial_z \varphi\right), \quad (2)$$

where $\alpha = (\omega_{pi}/\omega)^2 - (\omega_{pe}/\Omega_e)^2$, and $\beta = \omega_{pe}^2 / \omega^2$.

Density modifications appear because the large amplitude lower-hybrid wave exerts a low-frequency ponderomotive force on the electrons and ions. The equation for $\tilde{n}$ is given by

$$\partial_t^2(\partial_t^2 + \Omega_i^2)\frac{\tilde{n}}{n_o} - c_s^2\left[\partial_z^2(\partial_t^2 + \Omega_i^2) + \partial_t^2 \partial_x^2\right]\left(\frac{\tilde{n}}{n_o} + \frac{|\nabla\phi|^2}{8\pi n_o T_e}\right) = 0 , \quad (3)$$

where c_s is the sound speed. In deriving (3), the cold plasma dispersion relation for the lower-hybrid wave, namely $\varepsilon_\perp \partial_x^2 \phi - |\varepsilon_\parallel| \partial_z^2 \phi = 0$ has been used. We have also assumed $\omega > \omega_{LH} = \omega_{pi}(1 + \omega_{pe}^2/\Omega_e^2)^{-1/2}$.

Let us introduce the new variables $\xi = x - Cz$, $\zeta = Cz$, and consider solutions in the form $\varphi = \varphi(\xi - Vt, \zeta)$, $\tilde{n} = \tilde{n}(\xi - Vt, \zeta)$. Assuming stationarity in the frame moving with velocity V in the ξ-direction, for $V < (m_e/m_i)^{1/2} C c_s / k\lambda_e$, and $\partial_t \partial_x \ll \Omega_i \partial_z$, where k is the wave vector of the lower-hybrid pump, and λ_e is the electron Debye length, we obtain from (2) and (3)

$$\partial_\rho \psi + \frac{1}{2} i \partial_\xi^2 \psi + \frac{1}{4}\partial_\zeta(|\psi|^2\psi) - \delta \partial_\xi^3 \psi = 0 , \quad (4)$$

where $\psi = -C(\alpha + \beta C^2)^{1/2}\omega^{1/2}\left[8\pi n_o m_i (V^2 - c_s^2 C^2) V P\right]^{-1/2}\partial_\xi \varphi$, $\rho = -(\zeta/|\varepsilon_{\parallel o}|C^2)(2V/\omega)P$, $\delta = (a_o + c_o C^2 + b_o C^4)\omega/2VP$, and $P = 1 + \omega_{pe}^2/\Omega_e^2 + C^2$.

It can be shown [3] that according to eq. (4), a monochromatic wave of amplitude ψ_o becomes convectively unstable if $|\psi_o| > 8\kappa_o$, where κ_o is the effective wave number of the pump. For $\delta = 0$, we obtain the localized solution of eq. (4) by letting $\psi = A\exp(i\theta)$, $\kappa = \partial_\zeta \theta$, $\Omega = -\partial_\rho \theta$. We consider solutions of the form $A = A(\eta)$, $\kappa = \kappa_o + \kappa_1(\eta)$, $\Omega = \Omega_o + \Omega_1(\eta)$, $\eta = \xi - \lambda\rho$, where κ_o, Ω_o, and λ are real constants. We look for solutions which vanish asymptotically at large distances. In the case $2\Omega_o + \kappa_o^2 > 0$, a localized solution [3] for the amplitude is

$$A^2 = \frac{2\Delta^{-2}}{\kappa_o + 2^{1/2}(\Omega_o + \kappa_o^2)^{1/2}\cosh\left[(\eta - \eta_o)/\Delta\right]} , \quad (5)$$

where $\Delta = (\kappa_o^2 + 2\Omega_o)^{-1/2}/2$. Furthermore, the nonlinear phase is determined by $\kappa_1 = (3/8)A^2$, and $\Omega_1 = -\kappa_o^2 - (3/8)\kappa_o A^2$.

In summary, we have shown that the finite frequency perturbations coupled with lower-hybrid waves can yield propagating localized envelopes which can cause transport of rf energy into the plasma beyond the boundary region. Finally, we mention that the role of $\vec{E}\times\vec{B}$ nonlinearity on the soliton profile may cause a damping of the pump wave by the excitation of a sideband. This problem is treated by Kaw et al. [4].

[+] Supported by SFB "Plasmaphysik Bochum/Jülich".

[1] G.J. Morales and Y.C. Lee, Phys. Rev. Lett. 35, 930 (1975)
[2] Y.C. Lee and G.J. Morales, Preprint UCLA PPG 256 (1976)
[3] E. Mjølhus, J. Plasma Phys. 16, 321 (1976)
[4] P.K. Kaw, C.Z. Cheng, and L. Chen, Preprint PPPL 1305 (1976)

VARIATIONAL PRINCIPLE FOR NON-LINEAR STABILITY ANALYSIS

Dirk K. CALLEBAUT and Ahmed H. KHATER*

Physics Department, University of Antwerp (U.I.A.)
Universiteitsplein, 1. B-2610 Wilrijk (Antwerp), Belgium

Abstract: A variational method for mhd stability extending the work of Bernstein[1] to higher orders in the perturbation is given.

Introduction

The variational principle of Bernstein et alui[1] for the study of mhd stability is well known. It may be recalled that it deals with the second order energy variation corresponding to motions of first order in ξ, the perturbation displacement. However in many stability problems this linearized approach is not satisfactory. E.g. it uses infinitesimal perturbations and yields no idea of the domain of validity. A non-linear analysis is desired. A higher order analysis was developped by one of us[2], extending the linearized normal mode analysis. The method is formally rather simple, but the calculation of the coefficients of the higher orders as functions of the various wavenumbers, etc. is very cumbersome. A variational method for higher orders is wanted from:

a) A practical point of view. This requires less calculations than the normal mode analysis: one has only to calculate the sign of the (minimal) change in the potential energy of the system under consideration. Of course, one obtains less information: only the knowledge stable or unstable for a certain range of the linear perturbation ξ or/of ε(see further).

b) A principal point of view. Moreover, this may be a first investigation of a general variational way to study non-linear stability or motion.

Method and calculations.

Consider a (static) equilibrium configuration. All relevant quantities are expanded in series to the fourth order in the linear displacement ξ. The change in the potential energy due to the perturbation is

$$\delta^*W = W - W_o = \Delta_1 W + \Delta_2 W + \Delta_3 W + \Delta_4 W + \ldots \qquad (1)$$

where W_o is the potential energy of the unperturbed system, where $\Delta_1 W = o$ (equilibrium!), where $\Delta_2 W$ is the result of Bernstein et alui[1] and where

$$\Delta_3 W = \frac{1}{2}\int \left[\frac{\Gamma(\gamma+2)}{3\Gamma(\gamma)}\, p_o (\mathrm{div}_o\xi)^3 - \gamma p_o (\mathrm{div}_o\xi)^2 (\xi\,\mathrm{grad}_o\xi - \xi\,\mathrm{div}_o\xi) - 2p_o \left|\frac{\partial \xi_i}{\partial x_{oj}}\right|\right] dv_o + \frac{1}{6}\int \rho_o \xi_i \xi_j \xi_k \frac{\partial^3 \phi_o}{\partial x_{oi}\partial x_{oj}\partial x_{ok}}\, dv_o$$
$$+ \frac{1}{2\mu}\int [(B_o.\Delta B) + B_o^2 \mathrm{div}_o\xi).\{\mathrm{div}_o\xi(\xi.\mathrm{grad}_o\xi + \xi\,\mathrm{div}_o\xi)\}$$
$$- \mathrm{div}_o\xi(\Delta B + B_o\,\mathrm{div}_o\xi)^2 - B_o \left|\frac{\partial \xi_i}{\partial x_{oj}}\right|] \, dv_o - \frac{1}{2}\int \xi_i \Delta_2(\hat{m}_{ij} ds_j) \qquad (2)$$

$$\Delta_4 W = \int [\frac{\gamma p_o}{2}\{(\mathrm{div}_o(\xi.\mathrm{grad}_o\xi - \xi\,\mathrm{div}_o\xi))^2 + 2\mathrm{div}_o\xi \left|\frac{\partial \xi_i}{\partial x_{oj}}\right|\} -$$
$$- \frac{\Gamma(\gamma+2)}{4\Gamma(\gamma)}\, p_o (\mathrm{div}_o\xi)^2 (\mathrm{div}_o(\xi.\mathrm{grad}_o\xi - \xi\,\mathrm{div}_o\xi))$$
$$+ \frac{\Gamma(\gamma+3)}{24\Gamma(\gamma)}\, p_o (\mathrm{div}_o\xi)^4] \, dv_o + \frac{1}{24}\int \rho_o \xi_i \xi_j \xi_k \xi_\ell \frac{\partial^4 \phi_o}{\partial x_{oi}\partial x_{oj}\partial x_{ok}\partial x_{o\ell}} dv_o$$
$$+ \frac{1}{2\mu}\int \{\frac{1}{2}(\Delta B + B_o\,\mathrm{div}_o\xi)^2 . \mathrm{div}_o(\xi \mathrm{div}_o\xi + \xi.\mathrm{grad}_o\xi)$$
$$- 2(B_o.\Delta B + B_o^2 \mathrm{div}_o\xi)\left|\frac{\partial \xi_i}{\partial x_{oj}}\right|\} dv_o - \frac{1}{2}\int \xi_i \Delta_3(\hat{m}_{ij} ds_j) \qquad (3)$$

The third order term is always destabilizing, unless it is zero.

Choosing now the displacement in the form

$$\xi(x,t) = \varepsilon_o e^{\sigma t}\xi(x)$$

as for the first order analysis, one obtains (trivial) expansions in ε_o. Now the method of Callebaut consists in uniting ε_o and $\exp \sigma t$ into one quantity: $\varepsilon = \varepsilon_o \exp \sigma t$ yielding (non-trivial) expansions in ε. E.g.

$$\delta^*W = \varepsilon W_1 + \varepsilon^2 W_2 + \varepsilon^3 W_3 + \varepsilon^4 W_4 + \ldots \qquad (4)$$

Minimizing the functional integral one obtains the Euler equations:

$$E_2 + \varepsilon E_3 + \varepsilon^2 E_4 + \ldots = o \qquad (5)$$

which are a system of partial differential equations. Solving (5) (directly or by iteration) and substituting in (4) and giving values to the parameter ε yields zero-stability lines. Further elaboration and discussion and in particular the application to force-free magnetic fields[3][4] will be presented orally.

References:

(1) I.B. BERNSTEIN, E.A. FRIEMAN, M.D. KRUSKAL and R.N. KULSRUD, Proc. Roy. Soc. London A, 244, 17-46 (1958).

(2) D.K. CALLEBAUT, Simon Stevin, 45, 1-315 (1971).

(3) D.K. CALLEBAUT, report on "Survey of force-free fields", C.E.C.A.M. Workshop (ORSAY-Meudon) 1976, FRANCE.

(4) D.K. CALLEBAUT and A. H. KHATER, report on "Non-linear stability analysis for force-free magnetic fields", C.E.C.A.M. Workshop (ORSAY-Meudon) 1976, FRANCE.

* On leave of absence from the Mathematics Department, Faculty of Science, Assiut University, Assiut, EGYPT.

SELF-CONSISTENT COMPUTATION OF TWO-STREAM EXPLOSIVE INSTABILITY

Z. Sedláček

Institute of Plasma Physics, Czechoslovak Academy of Sciences, Nademlýnská 600, CS 180 69 Prague 9, Czechoslovakia

Abstract: The two-stream explosive instability was investigated numerically with a Hamiltonian model of wave-wave interaction including coupling of the waves to the streams and harmonics generation. An abrupt and almost complete deceleration of the streams accompanied by saturation of the explosive growth and formation of a turbulent state was found.

1. INTRODUCTION

The majority of investigations of explosive instabilities [1-6] are restricted to pursuing the time evolution of the resonance triplet of the interacting waves. Non-linear mechanisms for the explosive growth limitation were proposed [4-6] but the influence of the reaction of the background distribution function evolution and the harmonics generation seem to have been, with few exceptions [7], overlooked. In this contribution, taking the explosive instability of two counter-streaming electron beams with equal densities and equal velocities [3, 6] as a model example, we show by numerical integration of improved coupled-mode equations the dramatic influence of these factors upon the evolution of the explosive instability.

2. HAMILTONIAN DESCRIPTION OF THE WAVE AND STREAM DYNAMICS

The method used was proposed in [9] and tested there on the beam-plasma instability. The basic Hamiltonian is derived from the Fourier transformed microscopic continuum Lagrangian due to Low [10] by an expansion scheme which makes proper distinction between oscillatory and secular variables. Asuming the equilibrium distribution function in the form $F(v) = N_1 \delta(v-V_1) + N_2 \delta(v-V_2)$ one thus obtains:

$$H(\xi_{1,n}, \pi_{1,n}; \xi_{2,n}, \pi_{2,n}) = \sum_{n=-\infty}^{\infty} \left(\frac{1}{2mN_1} \pi_{1,-n} \pi_{1,n} + \frac{1}{2mN_2} \pi_{2,-n} \pi_{2,n} - jnkV_1 \xi_{1,n} \pi_{1,n} - jnkV_2 \xi_{2,n} \pi_{2,n} + \frac{1}{8\pi} e_{-n} e_n \right) \qquad (1)$$

$$e_n = -4\pi q \left[N_1 e^{-jnk\xi_{1,0}} \mathcal{Z}_n(\xi_{1,\alpha}) + N_2 e^{-jnk\xi_{2,0}} \mathcal{Z}_n(\xi_{2,\alpha}) \right]$$

$$\mathcal{Z}_{-n}(\xi_\alpha) = \xi_{-n} + \frac{1}{2!} jnk \sum_{n_1}{}' \sum_{n_2}{}' \delta_{n+n_1+n_2} \xi_{n_1} \xi_{n_2} + \frac{1}{3!} (jnk)^2 \sum_{n_1}{}' \sum_{n_2}{}' \sum_{n_3}{}' \delta_{n+n_1+n_2+n_3} \xi_{n_1} \xi_{n_2} \xi_{n_3} + \dots$$

Here $\xi_{1,n}$, $\pi_{1,n}$; $\xi_{2,n}$, $\pi_{2,n}$ are the Fourier components of the displacement vector and their canonically conjugate momenta for the first and second stream, respectively, $\delta_\alpha = 1$ for $\alpha = 0$ and zero otherwise, and the prime at the sum sign is to denote that terms with $n_i = 0$ are omitted. As seen, the coupling coefficients depend on the variables $\xi_{1,0}$, $\xi_{2,0}$. The equations for the variables $\xi_{1,0}$, $\pi_{1,0}$; $\xi_{2,0}$, $\pi_{2,0}$ describe the evolution of the background distribution function and are, in their turn, dependent on the wave amplitudes, thus providing for the self-consistent description of the waves and streams.

3. COMPUTATIONAL RESULTS

The set of canonical equations generated by the Hamiltonian (1) was solved subject to periodic boundary condition and to the initial conditions corresponding to the resonance triplet (the same as in [3, 6]). Various numbers of space harmonics and orders of wave-wave interaction were tried. In general, each computational run gave a similar overall picture (Fig. 1): an initial explosive stage with coherent wave-wave interaction well described by the idealized theories restricted to the resonance triplet [4-6], followed by a total collapse of the streams, saturation of the wave growth and formation of a turbulent state characterized by stochastic behaviour of all the wave amplitudes and equipartition between the mean kinetic and mean electrostatic energy of turbulent pulsations. Inclusion of higher harmonics and higher-order wave-wave interactions enhances the explosive growth, but does not alter the final state substantially.

4. CONCLUSIONS

It is evident that for the final stage of the explosive instability evolution the enormous alteration of the background distribution function is of dominant importance. The fourth- and higher-order wave-wave interactions alone are not capable of developing the saturated turbulent state. Similar conclusion was drawn by Byers et al. [7] for the case of an explosive instability of cyclotron waves.

5. REFERENCES

[1] B. Coppi et al., Ann. Phys. (N.Y.) 55 (1969), 207.

[2] J. Fukai et al., Phys. Fluids 13 (1970), 3031.

[3] J. Fukai, E.G. Harris, Phys. Fluids 14 (1971), 1748.

[4] V.N. Oraevskii et al., Phys. Rev. Letters 30 (1973), 49; Physica Scripta 7 (1973), 217.

[5] J. Weiland, H. Wilhelmsson, Physica Scripta 7 (1973), 222.

[6] Z. Sedláček, J. Plasma Phys. 15 (1976), 1.

[7] J.A. Byers et al., Phys. Fluids 14 (1971), 826.

[8] S. Hamasaki, N.A. Krall, Phys. Fluids 14 (1971), 1441.

[9] Z. Sedláček, Phys. Letters, in press.

[10] F.E. Low, Proc. Roy. Soc. (London) 248 A (1958), 282.

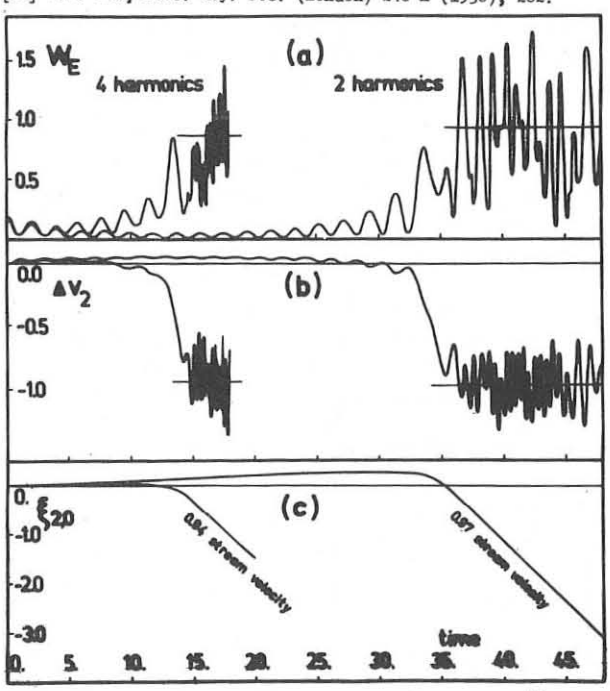

Fig. 1. Plots of (a) the total electrostatic energy W_E (measured by the equilibrium kinetic energy of one stream), (b) variation of the stream velocity ΔV_2 (measured by the equilibrium velocity of the stream), (c) the canonical coordinate $\xi_{2,0}$ - an integral of ΔV_2 (measured by the wavelength $\lambda = 2\pi/k$) to document the total loss of velocity of the streams. The unit of time is ω_{p1}^{-1}, $kV/\omega_{p1} = 1.597$.

STABILITY OF BGK EQUILIBRIA

K.R.Symon*, J.L.Schwarzmeier*
Dept. of Physics, University of Wisconsin, Madison, Wis., U.S.A.
and H.R.Lewis*
Los Alamos Scientific Laboratory, Los Alamos, N.M., U.S.A.

Abstract: An analysis of the stability of a BGK equilibrium solution of the Vlasov equation is presented, as an illustration of a general method of analysis of inhomogeneous equilibria which is particularly suited to numerical computations. Comparisons are made between the results of the analysis and numerical simulations.

The Problem. We consider a one-dimensional electron gas in a fixed ion background of density n_0. We assume a stationary BGK wave solution $f_0(\mathcal{E})$, $\phi_0(x)$, where

$$\mathcal{E} = \tfrac{1}{2} m v^2 - e\phi_0(x), \quad \phi_0(x+a) = \phi_0(x). \tag{1}$$

The linearized Vlasov-Poisson equations for a small perturbation f, ϕ in density and electrostatic potential are

$$\frac{\partial f}{\partial t} + v\frac{\partial f}{\partial x} + \frac{e}{m}\frac{\partial \phi_0}{\partial x}\frac{\partial f}{\partial v} = -\frac{e}{m}\frac{\partial f_0}{\partial v}\frac{\partial \phi}{\partial x}, \quad \frac{\partial^2 \phi}{\partial x^2} = 4\pi e\int f dv. \tag{2}$$

It is convenient to transform to a modified perturbed distribution function g as follows:

$$f = P\phi + g, \quad P = -ef_0' = -e\frac{\partial f_0}{\partial \mathcal{E}}. \tag{3}$$

Equation (3) is a special case of a general class of useful transformations in which P can be any suitably chosen operator. We substitute Eq.(3) into Eqs.(2) to obtain

$$\frac{\partial g}{\partial t} + \mathcal{L} g = e f_0' \frac{\partial \phi}{\partial t}, \quad \Lambda\phi = 4\pi e\int g dv, \tag{4}$$

where $\mathcal{L}, \Lambda$ are the Liouville and Debye operators:

$$\mathcal{L} = v\frac{\partial}{\partial x} + \frac{e}{m}\frac{\partial \phi_0}{\partial x}\frac{\partial}{\partial v}, \tag{5}$$

$$\Lambda = \frac{\partial^2}{\partial x^2} - k_D^2(x), \quad k_D^2(x) = -4\pi e^2\int f_0'(\mathcal{E}) dv. \tag{6}$$

Note that k_D is the reciprocal Debye length. The algebraic merit of this transformation is that it eliminates $\partial\phi/\partial x$ from the Vlasov equation. The physical merit is that the Poisson equation now contains a term which may make the eigenfunctions of Λ resemble the x-dependence of the eigenfunctions of $\mathcal{L}$.

The Solution. We introduce eigenfunctions of the operators $\Lambda, \mathcal{L}$:

$$\Lambda\eta_n(x) = \lambda_n \eta_n(x), \tag{7}$$

$$\mathcal{L}\left[\delta(\mathcal{E}-\mathcal{E}')\, e^{ir\Omega(\mathcal{E}')\tau(x,\mathcal{E})}\right] = ir\Omega(\mathcal{E}')\delta(\mathcal{E}-\mathcal{E}')\, e^{ir\Omega(\mathcal{E}')\tau(x,\mathcal{E})}, \tag{8}$$

where $\Omega(\mathcal{E})$ is the frequency of the particle orbit with energy $\mathcal{E}$, r is any integer, and $\tau(x,\mathcal{E})$ is the time required for a particle on the orbit of energy $\mathcal{E}$ to go from some reference point to the point x. There are ordinarily several orbits at each energy; integrals over $\mathcal{E}$ are then understood to include sums over each such orbit. All eigenfunctions can be chosen to have the Floquet form:

$$\eta_n(x) = e^{ikx} h(x), \quad h(x+a) = h(x). \tag{9}$$

The entire problem now becomes diagonal in the index k. We assume a fixed choice of k; in the example below, $k = \pi/a$. We expand the perturbations in these eigenfunctions:

$$g(x,v,t) = \Sigma_r \gamma_r(\mathcal{E},t)\, e^{ir\Omega(\mathcal{E})\tau(x,\mathcal{E})}, \tag{10}$$

$$\phi(x,t) = \Sigma_n \alpha_n(t)\eta_n(x). \tag{11}$$

We Laplace transform the resulting equations for the coefficients γ_r, α_n, solve the Vlasov equation for the transformed coefficients $\tilde{\gamma}_r$, and substitute in the field equation to obtain:

$$\Sigma_{n'} D_{nn'}(\omega)\tilde{\alpha}_{n'} = \mathcal{I}_n(\omega), \tag{12}$$

where ω is the Laplace transform frequency variable, $\mathcal{I}_n(\omega)$ depends upon the initial conditions, and the dispersion matrix is

$$D_{nn'}(\omega) = \lambda_n \delta_{nn'} + 4\pi e^2 \Sigma_r \int d\mathcal{E}\, \frac{\omega f_0'(\mathcal{E}) K_{nr}^*(\mathcal{E}) K_{n'r}(\mathcal{E})}{\omega - r\Omega(\mathcal{E})}, \tag{13}$$

where

$$K_{nr}(\mathcal{E}) = \int d\tau\, e^{-ir\Omega(\mathcal{E})\tau}\eta_n[x(\tau,\mathcal{E})]. \tag{14}$$

The Dispersion Matrix. The matrix $D(\omega)$ has the interesting and useful property

$$[D_{nn'}(\omega)]^* = D_{n'n}(\omega^*). \tag{15}$$

A matrix with this property may be called a hermitian function. When Eq.(12) is solved for $\tilde{\alpha}_n$, and the Laplace transform inverted, the solution may be expressed as a superposition of van Kampen modes located along the cut in the real ω-axis associated with the matrix $D(\omega)$, plus a sum of discrete normal modes at complex frequencies ω which are roots of the dispersion relation

$$det\,[D_{nn'}(\omega)] = 0. \tag{16}$$

The coefficients of the eigenfunctions $\eta_n(x)$ for any normal mode form an eigenvector corresponding to a null eigenvalue of the matrix $D(\omega)$ evaluated at the normal mode frequency.

Numerical Methods. The above analysis is particularly suited to the numerical determination of the frequencies, growth rates, and perturbed potentials and distribution functions for the normal modes. We discretize the energy spectrum of the orbits, choosing a finite number of energies suitable for describing the perturbation. Integrals over energy become sums. We also choose a small number of eigenfunctions $\eta_n(x)$. The transformation (3) results in an operator Λ whose eigenfunctions match rather well the low frequency normal modes. Thus a single eigenfunction $\eta_1(x)$ leads to fairly good results, and three lead to quite accurate results, as we shall see below.

Simulation results. The above analysis was applied to a particular case for which results from numerical simulations were available for BGK equilibrium and for the unstable normal mode. The equilibrium potential is shown by the solid, approximately sinusoidal curve in the figure below. Also shown is the form of the perturbed potential associated with the unstable mode, and the corresponding eigenfunction (dashed curve) of the operator Λ for this case. If the perturbed potential is expanded in the first three eigenfunctions of Λ, the result is indistinguishable from the simulation result. In the table below, we show the theoretical and simulation results for the growth rate (in units of ω_p^{-1}) using a matrix $D(\omega)$ based upon one or three eigenfunctions of Λ, and for the coefficients of the three eigenfunctions in the expansion of the perturbed potential.

	Theory	Simulation
Growth rate (1X1)	3.03	3.10±.04
Growth rate (3X3)	3.07	3.10±.04
Coeff. of η_1	0.99894	0.99861
Coeff. of η_2	0.03765	0.04115
Coeff. of η_3	0.02662	0.03215

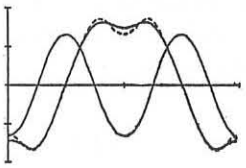

*Supported by U.S. Energy Research and Development Administration.

QUASI-LINEAR EQUATIONS FOR THE TWO-MODE MODEL.

W. Malfliet
U.I.A. University of Antwerp, Dept. of Physics,
Universiteitsplein 1 B-2610 Wilrijk (Belgium)

Abstract : The usual approximation to investigate the perturbations in the kinetic theory of plasma consists of the one-mode ansatz. To obtain a more rigorous description we introduce a two-mode model which has several interesting features as illustrated for the quasi-linear equations.

1. Introduction : The one-mode analysis is currently used in the kinetic theory of plasma in order to facilitate the calculations. This seems to be a serious restriction, not only from the mathematical point of view, because the required reality condition immediately imposes the property $\omega_R(\vec{k})=-\omega_R(-\vec{k})$ for the real frequencies. Moreover there exists often more solutions of the dispersion relation in such cases than for instance one mode with positive phase velocity.

As an example we examine the usual quasi-linear analysis of the Vlasov-Poisson system.

2. Analysis : The dielectric function in the Vlasov theory is defined by

$$D(\vec{k},p) = 1 - \frac{4\pi e^2}{mk^2} \int_C \frac{\vec{k}.\frac{\delta F_o}{\delta \vec{v}}}{(p+i\vec{k}.\vec{v})}\, d\vec{v} = 0 \quad , \qquad (1)$$

if the longitudinal electrostatic fluctuations vary like $\exp(i\vec{k}.\vec{r} - pt)$ with $p = -i\omega_R(\vec{k}) - \gamma(\vec{k})$. With the aid of $u = \vec{k}.\vec{v}/k$ and $\int F_o(\vec{v})d^2v_\perp = F_o(u)$ eq. (1) is transformed into

$$D(\vec{k},p) = 1 - \frac{4\pi e^2}{mk^2} \int_C \frac{k}{(p+iku)} \frac{\delta F_o(u)}{\delta u}\, du \qquad (2)$$

Similarly the dielectric function for the $(-\vec{k})$-modes, which are also present, reads

$$D(-\vec{k},p) = 1 - \frac{4\pi e^2}{mk^2} \int_C \frac{k}{(p+iku)} \frac{\delta F_o(-u)}{\delta u}\, du \qquad (3)$$

It is easily observed that $D(\vec{k},p) = D(-\vec{k},p)$ for symmetric distribution functions. This means that the frequencies must be the same irrespective of the $\vec{k}$-sign !

In the limit of long wavelengths the frequencies are found from eq. (2) to be :

$$(\omega_R(\vec{k}) - kv_m)^2 = \omega_p^2 (1+3(k/k_D)^2+\ldots) \qquad (4)$$

and

$$\gamma(\vec{k}) = \frac{\pi}{2k^2} (\omega_R(\vec{k}) - kv_m)^3 \frac{\delta F_o(u)}{\delta u}\bigg|_{u=\frac{\omega_R(\vec{k})}{k}} \qquad (5)$$

with $|\gamma/\omega| \ll 1$, $|\vec{k}| = k$ and $v_m = \int uF_o(u)du$ which characterizes the asymmetry of the distribution function.

For the $(-\vec{k})$-modes we have from eq. (3)

$$(\omega_R(-\vec{k}) + kv_m)^2 = \omega_p^2(1 + 3(k/k_D)^2+\ldots) \qquad (6)$$

and

$$\gamma(-\vec{k}) = \frac{\pi}{2k^2} (\omega_R(-\vec{k}) + kv_m)^3 \frac{\delta F_o(-u)}{\delta u}\bigg|_{u=\frac{\omega_R(-\vec{k})}{k}} \qquad (7)$$

We immediately infer that there are two modes $\omega_R(\vec{k})$ and $-\omega_R(\vec{k})$ which must satisfy the relations $\omega_R(\vec{k}) = -\omega_R(-\vec{k})$ and $\gamma(\vec{k}) = \gamma(-\vec{k})$, if $v_m \neq 0$. In the other case ($v_m = 0$) there exist two possible relations. First the just mentioned ones, (odd property) and secondly we have two modes for which $\omega_R(-\vec{k}) = \omega_R(\vec{k})$ and again $\gamma(\vec{k}) = \gamma(-\vec{k})$ holds. Now the quasi-linear equations can be derived in both cases.

a) $\omega_R(\vec{k}) = -\omega_R(-\vec{k})$. In particular the diffusion coefficient may be written as :

$$D^{\alpha\beta}(\vec{v}) = \frac{e^2}{m^2} \int d\vec{k}\gamma(\vec{k})k_\alpha k_\beta \left[\frac{Q^{(1)}(\vec{k})}{(\vec{k}.\vec{v}-\omega_R(\vec{k}))^2+\gamma^2(\vec{k})} + \right.$$

$$\left. + \frac{Q^{(2)}(\vec{k})}{(\vec{k}.\vec{v}+\omega_R(\vec{k}))^2+\gamma^2(\vec{k})} \right] \qquad (8)$$

where $Q^{(i)}(\vec{k})$ $(=Q^{(i)}(-\vec{k});i=1,2)$ represents the spectral function of the potential waves moving to the right (i=1) (positive phase velocities) and to the left (i=2,negative phase velocities). The total spectral energy is defined as $Q(\vec{k}) = \sum_i Q^{(i)}(\vec{k})$.

b) $\omega_R(\vec{k}) = \omega_R(-\vec{k})$. In this case we have :

$$D^{\alpha\beta}(\vec{v}) = \frac{e^2}{m^2} \int d\vec{k}\gamma(\vec{k})k_\alpha k_\beta \left[\frac{P^{(1)}(\vec{k})}{(\vec{k}.\vec{v}-\omega_R(\vec{k}))^2+\gamma^2(\vec{k})} + \right.$$

$$\left. + \frac{P^{(2)}(\vec{k})}{(\vec{k}.\vec{v}+\omega_R(\vec{k}))^2+\gamma^2(\vec{k})} \right] \qquad (9)$$

The spectral functions $P^{(i)}(\vec{k})$ have now the property $P^{(i)}(\vec{k}) = P^{(j)}(-\vec{k})$ $(i,j=1,2;\ i\neq j)$. Hence waves moving to the right and to the left appear in both terms of eq. (9).

The usual conservation laws still hold in both cases and the different approximations for the diffusion coefficient may be used as well.

More practical examples can be considered. The two-stream instability problem for instance will show very easily this behaviour of the different modes.

Lower Hybrid Heating in a Mirror Plasma

H.Derfler, O.Gehre, F.Leuterer, H.M.Mayer, M.Tutter

Max-Planck-Institut für Plasmaphysik
D-8046 Garching, Fed.Republic of Germany
EURATOM-Association

Abstract: We examine a rf plasma produced in a mirror machine. The density obtained corresponds to the lower hybrid density. We observe resonance cone propagation, parametric decay and harmonic excitation.

The mirror machine "Liwerex" has a length of 2.8 m, a center magnetic field of 6000 Gauß, and a mirror ratio of 1.8. The plasma is produced in the center of the device by 30 kW rf power at $f_o \approx 106$ MHz in 2 msec pulses, which are applied coaxially to a ring between two limiters, as shown in Fig.1. Preionization is done by short, negative 500 V pulses fed to two Penning plates at the end of the mirror. We used deuterium at a pressure of 1 to $4 \cdot 10^{-4}$ Torr. At pressures $< 2 \cdot 10^{-4}$ Torr we obtain a maximum density of $6 \cdot 10^{11}\,cm^{-3}$, which agrees with the lower hybrid density. At higher pressures we can exceed this value; the diamagnetic signal, however, decreases with increasing pressure. Fig.2 shows the phase shift of a microwave interferometer and the diamagnetic signal as functions of the applied rf power. The diamagnetic signal increases proportionally, while the density saturates. From the diamagnetic signal $T_i \approx 90$ eV was evaluated, and synchrotron radiation measurements

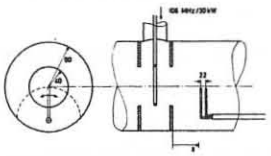

Fig.1

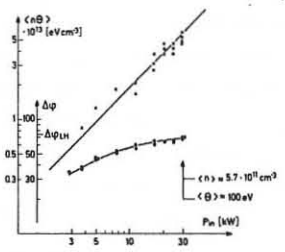

Fig.2

at $2\,f_{ce}$ yielded $T_e \approx 2$ eV. The value of T_i was confirmed by charge exchange measurements.

With an axially movable and tunable double coax probe we determined radial profiles of the axial electric field. In Fig.3 top we see that the profil taken at f_o shows strong maxima at radial positions near the limiter radius. With increasing distance from the coupler these maxima occur at the same radial position, but get smeared out. We believe that this is due to a resonance cone[1] propagating with a very small cone angle, because $f_o \approx f_{LH}$ in this case. Indeed, interferometric measurements confirmed the forward character of this field in axial direction and the backward wave character in radial direction. The maxima decrease by about 10 dB in a distance of 30 cm. The frequency spectrum around f_o is asymmetric and exhibits sidebands at $\Delta f \approx n \cdot f_{ci}$ at the low frequency side. Corresponding lines near $f \approx n \cdot f_{ci}$ are observed in the low frequency spectrum, which suggests parametric decay. Radial profiles at the frequency of the first sideband as well as at the corresponding low frequency line are also shown in Fig.3 and show an even more pronounced

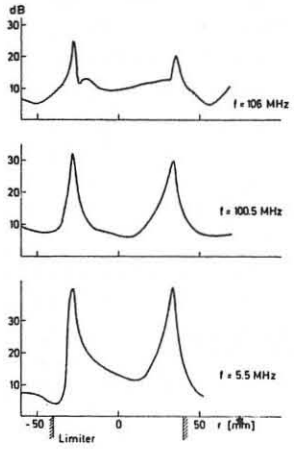

Fig.3

localization at the position of the pump frequency maximum as observed earlier by[2]. The sideband and decay line maxima are, however, more than 20 dB weaker than the pump wave maximum. With increasing rf power the line character of the spectra disappears in increasing background noise. At constant power and increasing neutral gas pressure the lines disappear nearly in the same way as does the diamagnetic signal.

In addition to this parametric pump decay we observe a very strong generation of harmonics of the pump frequency (up to the 17th). The intensity of successive harmonics decreases by only 4 dB. From this we may estimate, that the power in the harmonics is about 1/4 to 1/2 of the power in the pump wave. The harmonics also propagate along resonance cones, which because of their higher frequency penetrate deeper into the plasma, as shown in Fig.4 for the 5th harmonic. At higher harmonics the maxima can be seen to join on the axis and then diverging again with increasing distance from the coupler.

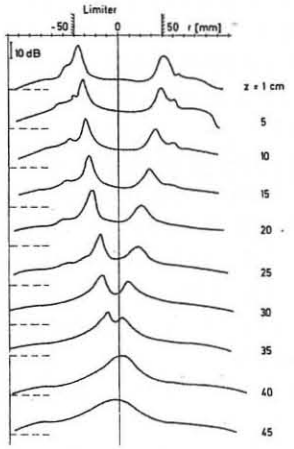

Fig.4

In Fig.5 we compare the measured cone angle for each harmonic with theoretical curves for various densities. These have been obtained from the resonance cone equation

$$\operatorname{tg}\theta_c = \sqrt{-\frac{\varepsilon_\perp}{\varepsilon_\parallel}}$$

assuming homogeneous density profile. The first harmonics also show parametric sidebands, which themselves propagate along resonance cones corresponding to their frequencies.

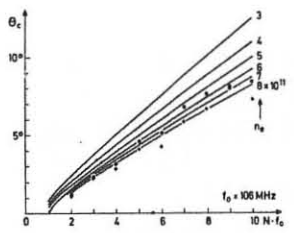

Fig.5

References

1) R.K.Fisher, R.Gould, Phys.Rev.Lett. 22, 1093 (1969)
2) P.Javel, G.Müller, U.Weber, R.R.Weynants, IPP 2/229 (1976)

ABOUT LOW HYBRID HEATING IN TOKAMAKS

S.L. Musher, A.M. Rubenchik, B.I. Sturman

Institute of automation and electrometry
Siberian Branch of USSR Academy of Sciences, Novosibirsk, USSR

We calculated the absorption energy distribution via parametric instabilities for tokamak TM-3.

1. In a usual scheme of low hybrid heating energy must release mainly in the center of plasma at the expense of the transformation of an electromagnetic wave into plasma one [1-2]. But recent experiments on large units [3] showed that a greater part of HF power absorbes in plasma periphery. This absorption is explained most likely by the development of parametric instabilities [3-5].

Anomalous dissipation caused by collective processes allows, as opposed to the usual scheme, to optimize heating characteristics without binding it rigidly to the existance of transformation point. In the present work we will show that it is possible to achieve rather uniform plasma heating by choosing frequency, slowing-down of electromagnetic wave and type of excited oscillations.

2. Let us consider isothermal $T_e \sim T_i$ plasma with the density changing smoothly across the magnetic field. Choose its direction for z axis, and let x axis be in the direction of the density gradient. Let electromagnetic wave propogates along the x, its energy $\mathcal{E}$ changes in conformity with the equation

$$\frac{\partial}{\partial x} v_{gr} \mathcal{E} = -\Gamma \mathcal{E} - Q \qquad (1)$$

The energy flow into plasma attributed to parametric instabilities was found in [6].*) With the fulfilment of a rather mild condition $\omega_p^2 > \omega\omega_H$ and rather high exceedings over a threshold $E > E_{th}$

$$Q = 0.1 \frac{\omega_p^4}{\omega\omega_H^3} \frac{E_x^2}{8\pi nT} \frac{E_x^2}{8\pi} \qquad (2)$$

Threshold field E th is defined by collisions or by the inhomogeneity of plasma and pumping. Density and temperature profiles we chosen close to those observed in tokamaks

$$n = n_0\left(1.1 - \frac{x^2}{a^2}\right); \qquad T = T_0\left(1.1 - \frac{x^2}{a^2}\right)^{\alpha} \qquad (3)$$

where a is a small radius of torus.

In the frequency range under consideration there are two types of electromagnetic waves, i.e. fast and slow ones. Until recently plasma heating was mainly related to S-wave for which it is easier to fulfil transformation conditions and the opaqueness area is narrower [2].

3. For S-wave $v_{gr} \simeq c\frac{\omega}{\omega_p n_z}$; $\mathcal{E} = \frac{E_x^2}{8\pi}$; $\Gamma = \nu_{ei}$. In concrete calculations plasma parameters were used corresponding to tokamak TM-3 - $T_0 = 900$ eV; $n_0 = 5\cdot10^{13}$, $\omega_H = 7\cdot10^{11}$. The value of the incident power $P(-a) = \mathcal{E}(-a) v_{gr}(a)$ changed in the limits from $\approx w/cm^2$, which corresponds to the parameters of HF generators commonly used, to 100 kw/cm^2. Representative results of the calculations, when $n_z = 1{,}5$, are given in Figs. 1. From these calculations it followes that selecting frequency and power of pumping it is possible to obtain rather uniform plasma heating. The situation is extremely critical to the change of the heating parameters however. The part of energy absorbed in the center decreased 3 times as the power increased twice, about 2 times as the frequency decreased from $2{,}5\omega_i$ to $1{,}5\,\omega_i$, and 2,5 times as α (see (3)) increased from 1,5 to 2 times (see Fig. 1).

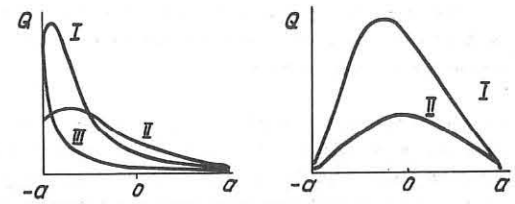

Spatial distribution of the absorbed energy.
Fig.1. $P(-a) = 3$ kw/cm^2. Curve I corresponds $\omega = 1.5\,\omega_i$, $P(a)/P(-a) = 0.13$. Curve II - $\omega = 2.5\omega_i$, $P(a)/P(-a) = 0.29$. Curve III - $\omega = 1.5\omega_i$, $\alpha = 2$.
Fig.2. The heating by a fast wave. $P(-a) = 15$ kw/cm^2. Curve I corresponds $\omega = \omega_i$, Curve II - $\omega = 2\,\omega_i$.

It should be noted that in all calculations presented a considerable part of energy is absorbed at the edge of the interval, $x \simeq -a$. This fact indicates that energy absorption in the region of limiters, $x < -a$, which was not taken into account can be rather substantial.

With other heating parameters the energy distribution over a section can be obtained with the help of the following similitude relationships (see (1) - (2)) $\frac{n^2 n_z^2 P_0 a}{T H^2} = const$.

4. Plasma heating by a fast wave has become the subject of study only in very recent time [8]. For a fast wave $v_{gr} \simeq c\frac{\omega\omega_H}{\omega_p^2} n_z$

$$\mathcal{E} = \frac{E_x^2}{8\pi} n_z^2 \quad ; \quad \Gamma = 2\nu_{ei}\frac{\omega_p^2}{\omega_H^2} \qquad (4)$$

Accordingly the similitude relationship is of the form:
$n^3 P_0 a / (T H^4 n_z^4) = const$

In the plasma periphery v_{gr}^f exceeds considerably v_{gr}^s, but in the center they are of the same order. Therefore the wave energy and thus anomalous absorption in the periphery for the F-wave considerably reduce when the power of pumping are the same and the area of the energy absorption shifts towards the center $Q \sim n^3 p^2/T$, see Fig. 2.

Extremely substantial appears to be strong dependence of the energy absorption by the F-wave on n_z, as it is seen from (1) (4) $Q \sim n_z^{-6}$. Equations (1),(3) illustrate that for the F-wave collisional damping results in the heating of the central plasma areas as well. With the dependence on n_z so strong taking into account the toroidality is quite essential [8] $n_z = n_z^0 (A-1)/(A - r/a)$.

The absence of absorption of the F-wave energy in the periphery allows to combine a collective method of plasma heating with that based on linear transformation. In conclusion it may be said that a relatively long absorption length of F-wave makes in promising for heating in large-scale devices.

*) The coefficient in (2) is taken from work [7], where the numerical simulation of the parametric instability was carried out.

References

1. T.N. Stix, Theory of Plasma waves N.Y. 1962.
2. V.E. Golant, A.D. Pilya, Sup. Fiz. Nauk, 104, 413, 1971.
3. V.V. Alikaev et al. I.T.P 45.523.1975. V.E. Golant et al. Nuclear Fusion 1975 Suppl. W.M. Hooke, Bull.Am.Phys.Soc." 20.1313.1975.
4. S.L.Musher, A.M. Rubenchik, B.I. Sturman. Pis'ma Zh.Exsp. Teor. Fiz. 25, N8, 1977.
5. A.M. Rubenchik, Pis'ma Zh. Tech.Fiz. 2, 21, 1976.
6. B.I. Sturman, JETP 71, 613, 1976.
7. R.L. Berger, L. Chen. PPPL MATT 1169, 1976.
8. A.V. Longinov, K.N. Stepanov, Pis'ma Zh. Exsp. Teor. Fiz. 24, 457, 1976.

THE WAVE EXCITATION IN A PLASMA AT A HELICAL RESONANCE HF HEATING

R.A.Demirkhanov, A.G.Kirov, S.Y.Ilyinsky, V.V.Onishenko, A.V.Sukachov, and D.A.Voytenko

Sukhumi Institute of Physics and Technology of the State Committee on Utilization of Atomic Energy, Sukhumi, USSR

The main experimental dependences and an approximated theoretical model of the plasma resonance HF heating in a toroidal trap when $B_0/(4\pi\rho_i)^{1/2} \simeq \tilde{\omega}/\tilde{k}_\parallel$ (I) (where $\tilde{\omega}$ is the HF field angular frequency, and $\tilde{k}_\parallel$ is the wave number along the torus $\tilde{k}_\parallel = 2\pi R/n$) had been reported at the recent conference /I/. The theory /2/ in case of the condition $B_0/(4\pi\rho_i)^{1/2} \simeq \frac{1}{\sqrt{2}}\tilde{\omega}/\tilde{k}_\parallel$ (2) met, predicts the "helical resonance" - the excitation of helical HF MHD oscillations in a plasma at $\omega \ll \omega_{Bi}$. These oscillations may be represented in the first approximation, as consisting of two types of waves: magnetic acoustical and Alfven ones. The phenomenon observed is treated as a constrained resonance HF field excitation of stable helical modes of Kruskal-Shafranov type with $\gamma = 0$. It follows from the theory that the field distribution in the plasma must be:

$$\tilde{H}_\vartheta = \frac{4\pi}{c} j_{0z}^{ext} \frac{1}{z_n} \left\{ -\left[\frac{1}{h_0^2} + \frac{2}{|m|q^2}\left(1-\frac{1}{q^2}\right)\right] e^{\frac{x-x_r}{\Delta s}} + \left(1-\frac{1}{q^2}\right)^2 \left(\frac{x}{x_r}\right)^{|m|-1} \right\} \quad (3)$$

where z_n is the resonance denominator. The first addend is a skinning quasi-Alfven wave and the second one - a fast magnetic - acoustical wave.

At $B_0/(4\pi\rho_i)^{1/2} \simeq \tilde{\omega}/\tilde{k}_\parallel$ (4), a "pure" Alfven resonance is realizable when a volume Alfven wave with $\lambda_r < r_p$ is excited in the plasma (r_p is the plasma radius). In case of a nonuniform dencity distribution over the radius there can be a singular point (3) within the column and there can occur the Alfven wave excitation, amplification and effective dissipation /4/. Both resonances greatly differing in their physical nature, slightly differ in their resonance field value (B_0), especially if we consider the real nonuniform density distributions. Therefore, the macroscopic empirical dependences presented in /I/ do not allow to make a single-meaning conclusion necessary for thermonuclear predictions between these two mechanisms of the HF field excitation and complification in the plasma volume. In both cases, the dissipation mechanisms of HF energies should be different.

In R-02 device described in /I/ we have carried out a number of measurements on the HF field distribution within the plasma in the resonance region by means of miniature multicoil magnetic probes. The spectral composition of the oscillations has been measured by a spectral analyzer. The present paper gives also the results of neutron emission measurements in the resonance regime operating with deuterium, these measurements complete the assessments of ion heating in the resonance obtained as a result of diamagnetic and spectroscopic measurements.

The measurements have been carried out in the region of the resonance peak, B_0=IIkGs/I/ at $n_e \simeq 2{,}5 \cdot 10^{13}\,cm^{-3}$. A rotation helical magnetic quadrupole field with m_0=2, n_0=6, f=I,2 MHz, $\bar{J}_c \leq 400A$ has been used as an exciting HF field. The quasi-stationary current in the plasma $\bar{J}_p \leq IkA$, the stellarator rotational angle being $i_0 \simeq 0{,}5\pi$. Helium and deuterium served as operating gases. Probe and diamagnetic signal measurements have been accompanied by microwave measurements of the density and the quasi-stationary current in the plasma and the current in the HF winding. It should be noted that the HF field was turned on from the very beginning for stabilization aims. The plasma density increased and reached its resonance value for given B_0 in the region of 300-400 μs after the discharge onset. This led to the fact that the plasma average density in the discharge process had passed successively the value corresponding to the "quasi-Alfven resonance" (3), and afterwards it went through the value corresponding to the "helical resonance" (2). When the average density approached to some critical value of $\bar{n}_{res}$ meeting Expression (I), the HF power began to be strongly absorbed, and there appeared the voltage drop in the circuit and the diamagnetic signal growth. The diamagnetic signal grows up to its peak value for I00-I50 μs. The probe measurements showed that during this period a considerable growth of the HF field level took place in the plasma. Afterwards, all of the parameters reach stationary values. Fig.I shows the HF field distribution in the plasma at the moment of the peak value reached for diamagnetism. It can be seen that nearly for the half of the radius, the HF field increases 3-4 times in comparison with the vacuum HF field intensity in the same point but without the plasma and at the same currents in the HF winding. It should be immediately noted that on removing the magnetic probe tubings out of the HF field intensity and the diamagnetic signal in the plasma began to increase. This indicates that the real gains are higher at the resonance, than cited. The total pattern of the HF field distribution and the sign characteristic change, in the first approximation, well coincides with Expr.(5), if δ_s = Icm, which corresponds to the discharge electron conductivity within the accuracy of the factor of two. The initial pressure can be chosen based on the average density value: $\bar{n}_e \leq \bar{n}_{res}$. In such a case we observe some amplification the HF field, its spatial maximum being shifted to the plasma surface while the discharge develops, i.e., we observe the density increase. The above dynamics coincide with the motion of the local "Alfven resonance" point (3), with increasing the peak value of the density nonuniform profile in time. However, there is no marked heating of the plasma in such conditions. Unfortunately, we are short of the experimental date identifying this regime with the "Alfven resonance" exactly.

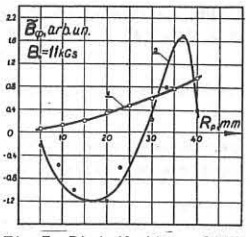

Fig.I. Distribution of HF field amplitudes in the plasma at the fixed point of time

Fig.2 shows the HF field intensity at the second negative peak (Fig.I) of the plasma specific energy and the HF circuit current (for the constant voltage at the HF generator) as functions of the intensity of B_0 field during the discharge stationary stage, when $\bar{n}_e = \bar{n}_{res}$. Here, a well-defined correlation between the excitation, the HF field resonance and the

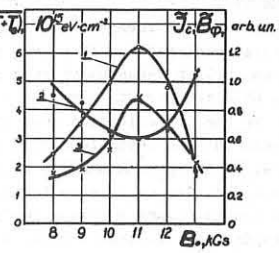

Fig.2. I) plasma specific energy; 2) winding current, $\bar{J}_c$; 3) field value in the plasma.

Fig.3. I,2) sequence of the small radius points from the centre to the periphery; 3) vacuum field on the plasma surface; 4) diamagnetic signal.

plasma heating is also seen. The current drop in the HF circuit indicates the resonance absorption of the HF power. Fig.3 shows the diamagnetic signal and the HF field intensity in the plasma at resonance as functions of the current $\bar{J}_c$. The analysis of these dependences indicates that at first there occurs the HF field excitation and amplification in the plasma, and after the field attains some threshold magnitude the plasma energy begins to increase fast. This fact coincides with the results of /I/ and indicates a nonlinear type of the HF energy mechanism dissipation /2/. This hypothesis is partially confirmed by measuring the spectra of magnetic probe signals, the probes being located in the plasma. The spectrum analyzer proved that the HF field frequency harmonics: $\frac{\omega}{\pi}$, $\frac{3}{\pi}\omega$, 2ω excite which constituted a marked part of the plasma diamagnetism growth and the stationary stage when energy removal from the plasma was sustained by the HF energy dissipation.

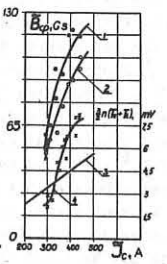

The following conclusions can be drawn: I) in the resonance heating regime the HF field excitation and its factor of five gain (at least) take place over the whole plasma volume; 2) the distribution type of fields in the plasma indicates that this resonance is most close to the "helical resonance" as judged by its pattern; 3) some experimental data indicate the parametric effects appeared in the resonance, these effects may be responsible for the HF energy dissipation /2/.

The ion temperature evaluated on the basis of the neutron emission amounts to $T_i \simeq 3 \cdot 10^2$ ev (deuterium, B_0=IIkGs, $n = 3 \cdot 10^{13}\,cm^{-3}$) which well agrees with the diamagnetic and spectroscopic measurement results /I/.

REFERENCES

I. R.A.Demirkhanov et al., 7-th Europ.Conf. on Contr.Fus. and Plasma Phys., Loussane, I975.

2. А.Г.Елфимов и др. Препринт СФТИ-2, Сухуми, I976.

3. A.Hasegava, L.Chen, Phys.Fluids, I7, p.I399, I974.

DYNAMICAL STABILIZATION OF MHD CURRENT INSTABILITIES IN A TOROIDAL SYSTEM WITH RESONANT EXCITATION OF HELICAL HF WAVES IN A PLASMA

R.A.Demickhanov, A.G.Kirov, S.I.Ilyinsky, N.I.Malikh and V.V.Onishenko

Sukhumi Institute of Physics and Technology of the State Committee on Utilization of Atomic Energy, Sukhumi, USSR

Dynamic stabilization of MHD instabilities in order to get $q \simeq I$ is one of the means of optimization the thermonuclear reactor based on tokamak. The dynamical HF stabilization effect of MHD current instabilities, including the disruptive instability, has been demonstrated in the experiment described in /I/. In those experiments the HF field has been skinned at the plasma column boundary and plasma parameters have not been large ones, $T_e < 100$ eV. Although the stabilization effect is distinctly exhibited and plasma macroscopic oscillations were completely removed the HF field pressure required to stabilize has been relatively large, $\tilde{B}_f^2/\bar{B}_z^2 = 0{,}5$, while it was considerably less than the plasma pressure, $\beta_f \gg I$. The skin HF stabilization drawbacks are such that: I) the skinning process can result in the density gradient sharpening and diffusion loss increase and 2) with such a method of stabilization there is no direct effect on volume modes which develop in the centre of the plasma column and can play a decisive role in developing the disruptive instability, according to the recent investigation /2/.

In our experiments in R-02 /3/ it has been found that a resonant interaction of a helical HF field with a magnetized plasma column takes plase when $B_0(4\pi\rho_i)^{-1/2} = \lambda f$ (I) where λ is the HF field period along the torus and f is its frequency. In /4/ the HF excitation and amplification in a magnetized plasma in such conditions have been indicated and a theoretical model of the phenomenon has been offered. In case of a helical resonance /I/, we have performed comparable investigations of the plasma column macroscopic MHD instability within and outside the resonance region in order to determine the effect of the HF wave volume excitation in a plasma on the dynamical stabilization conditions.

The experiments have been carried out in R-02 device which is $\ell = 2$ stellarator with a longitudinal current in the plasma /3/. A stabilizing HF field is presented by a rotating helical quadrupole with m=2, n=6 and f=I,2 MHz. The toroidal magnetic field intensities are $B_0 = 5 \div 14$ kGs, plasma densities: $1 \div 7 \cdot 10^{13}$ cm^{-3} and helium and hydrogen were used as operating gases. The stellarator rotational angle is $\iota_a < \pi$.

Without the HF field the discharge is macroscopically unstable; especially strong instabilities develop at $q_x \leq 1.4$. With the HF field the discharge regime essentially changes. At small magnetic fields, $B_0 = 5 \div 8$ kGs and large densities, $n_e \simeq 5\text{-}7 \cdot 10^{13}$ cm^{-3} when $B_0(4\pi\rho_i)^{-1/2} \ll \lambda f$ and the HF field is skinned some critical value of the HF field intensity exists which meets the ratio: $\tilde{B}_f/B_f \simeq 0{,}65$ /2/ and when it is slightly exceeded ($\sim 5 \div 10$ %) the discharge transforms into a stable state in a threshold manner, the plasma conductivity essentially increasing at the same time. The measurements of this stabilizing current threshold value in a HF circuit, $\tilde{I}_c$, at various magnitudes of a quasistationary current in the plasma, allowed us to determine the stability region in these conditions (Fig.I). The stabilizing HF field threshold value well coincides with the results of experiments in R-O device/5/ and the predictions of the dynamical stabilization theory for skinning HF fields /6/: $\tilde{B}_f/\bar{B}_f \geq \left\{ m\left[\max(m_0, m) - 1\right]\right\}^{-1/2}$ (3). Qualitatively, the discharge transformation into a stable state on meeting the condition $B_0/(4\pi\rho_i)^{1/2} \simeq \lambda f$ remains unchanged, i.e., at a given quasistationary current in the plasma there exists the HF current critical value in the circuit and when it is exceeded the discharge transforms into a macroscopically stable state in a threshold manner. However, this critical value becomes considerably lower than (2) and is equal to $\tilde{B}_f/\bar{B}_f \geq 0{,}2$, where $\tilde{B}_f$ is the field generated by the HF currents, $\tilde{I}_c$, in a HF windings, at the plasma boundary omitting the HF fields generated by the HF currents in the plasma itself. The corresponding stability region in Fig.I is limited by Curve 2 from above. The variation of the discharge main characteristics, the plasma current and density measured by a microwave interferometer with $\lambda = 2{,}3$ mm, is shown in Fig.2 and 3, respectively, with the transition through the stability threshold. In these figures the HF current stabilizing value in the windings for Traces 2 is only I0 % higher than for Traces I.

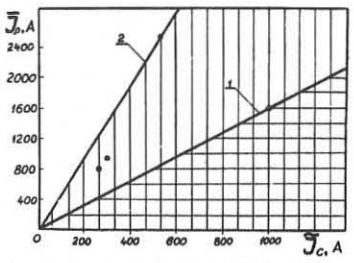

Fig.I. Current plasma stability regions for dynamical stabilization.
I-Nonresonance regime.
2-Resonance regime (stability region is shaded).

As it follows from the measurements presented in another paper contributed to this conference, in case of a helical resonance in the plasma, a considerable amplification of the HF field takes place (3÷5 times). The stability condition (3) approximately holds if one accepts the field within the plasma as B_f. This fact indicates that in the present case the inner HF field exerts a stabilizing effect.

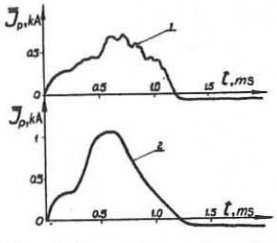

Fig.2. Current variation in plasma at transition through the stability threshold.

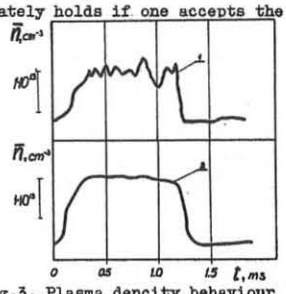

Fig.3. Plasma dencity behaviour at transition through the stability threshod.

The analysis of the experimental data allows to make the following conclusions.

I. In the conditions of the helical resonance, the HF currents in the circuit necessary for stabilization and, thus, the value of the active power absorbed in the HF circuit, can be essentially reduced (the power being less approximately by an order of magnitude);

2. In case of the helical resonance, inner volume modes can be stabilized in principle;

3. In a thermonuclear reactor, it is possible to combine the functions of additional heating and sustaining the MHD stability at small q in the same high-frequency system at $\omega < \omega_{Hi}$.

REFERENCES

I. R.A.Demirkhanov et al., "6-th European conference on Controlled Fusion and Plasma Physics", vol. I, p.I69, Moscow, I973.

2. С.В.Мирнов, И.Б.Семенов. Препринт ИАЭ-2723, Москва, I976.

3. R.A.Demirkhanov et al., "7th European Conference on controlled Fusion and Plasma Physics", Loussana, I975.

4. R.A.Demirkhanov et al., "6-th Intern. Conf. on Plasma Phys. and Contr.Nucl. Fusion Research", Berchtesgaden, FRG, I976.

5. Р.А.Демирханов, А.Г.Киров и др. "Письма в ЖЭТФ", I7, 397, I973.

6. В.П.Сидоров, Т.Р.Солдатенков "Ядерный синтез", I2, 73,I972.

DYNAMICAL FEEDBACK CONTROL OF THE CURRENT PLASMA COLUMN POSITION AND STABILITY IN TOROIDAL SYSTEMS

R.A.Demirkhanov, A.G.Kirov, G.I.Astapenko, L.F.Rouchko, E.M.Lomakin, A.V.Sukachov, V.B.Maiburov

Sukhumi Institute of Physics and Technology of the State Comittee on Utilization of Atomic Energy, Sukhumi, USSR

ABSTRACT: The experimental results on feedback control of the major radius and vertical direction plasma column equilibrium in R-OI device and feedback stabilization of MHD kink instability in R-O device are presented.

Laboratories in several countries develop the thermonuclear reactor projects based on tokamak. There arises a problem of optimizing plasma and reactor parameters and impoving its technological and economical aspects without altering the principal design of tokamak. We suppose that the most considerable effect can be achieved by introducing plasma dynamical control systems: I) by improving the equilibrium control quality over the major radius and vertical direction, especially during initial stage of discharge and additional heating stage; 2) by dynamical stabilization of MHD instabilities in order to get $q \sim I$.

As the estimations show, on lowering the safety factor q, we can essentially limit the reactor size and cost, the constant magnetic field intensity requirement, etc.

The principal possibility of the equilibrium dynamical control by feedback in the discharge stationary stage has been demonstrated on TO-I /I/. Dynamic stabilization of MHD and disruptive instabilities by HF fields in toroidal systems with the current at small q's has been demonstrated in our experiments on R-O and RT-4 devices /2/. The effects of flute instability feedback stabilization in mirror machine has been shown in /3/. The theory /4/ predicts the possibility of suppressing MHD current instabilities by feedback while the experimental data analysis suggests that surface kink MHD modes are responsible for exciting disruptive instability /5/.

The present paper gives the experimental results of plasma column equilibration and stability dynamic control by feedback. The results show the possibility of considerable improvement of current toroidal discharges by dynamic control methods.

Experiments of major radius and vertical direction plasma column equilibration control by means of magnetic fields have been carried out in R-OI tokamak (R=45cm, a =3,7cm) at B_o=IOkG, $p \sim I.IO^{-4}$torr, J_p =I÷5kA. The fast control system (0 - 200 kHz) is designed according to the impedance principle /I/; it controls the column position during all stages of the discharge, including the initial stage.

The main goal of the experimentsis to study the behaviour of the discharge parameters (J_p, $B_\perp$, β_J, σ) as a function of the major radius control system gain $K_\perp = \frac{B_\perp \text{ contr.}}{B_\perp \text{ perturb.}}$, from $K_\perp \lesssim 0{,}5$ up to $K_\perp = 5$; $K_\perp$ = I,6 corresponds to the ideal casing. The system controlling the column vertical position has the constant gain K_r = 3, which corresponds to the ideal casing too. The control system introduced results in complete elimination of the column displacement in the vertical direction at $K_r \geqslant 2$ and in considerable improvement of the discharge parameters. Further increase in K_r up to 7 does not effect the discharge.

The major radius plasma column equilibrium experimental results at various K are shown in Fig. I:

I) $K_\perp \lesssim 0{,}5$ (sections of control windings are closed);
2) $K_\perp$ = I;
3) $K_\perp$ = 2;
4) $K_\perp$ = 3 ÷ 4.

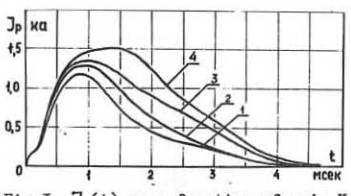

Fig.I. $J_p(t)$ as a function of gain $K_\perp$.

It is seen that at closed sections of control windings, the discharge current decreases fastly after reaching maximum in a time of I msec, which coincides with the time constant of windings. On changing the gain from $K_\perp$ = I to $K_\perp$ = 3, the discharge current increases approximately by a factor of I,5, the current duration at the level of 0,5 increases by a factor of 2 and the loop voltage decreases from IO÷I5 v to 3÷5 v. On further increase of the gain up to 4 ÷ 5, there is no improvement of discharge parameters. The measurements of plasma conductivity accomplished at $K_\perp \sim 4$, $J_p \sim 2{,}5$ kA and $B_o \sim$ IO kG, gave $\sigma \sim 5.IO^{15}$ CGSE which corresponds to plasma temperature of 60 eV.

The controlling field value, $B_\perp$, being somewhat high in comparison with the required value $B = \frac{J_p}{cR}\left(\ln\frac{8R}{a} + \beta_J + \frac{l_i - 2}{2}\right)$ indicates that we can reach $\beta_J > I$ at $K_\perp \simeq 3$.

Thus, the experiments with a fast control system of plasma equilibrium indicate the considerable improvement of the discharge parameters by including a rigid control of the major radius from the initial stage of the discharge and by including the automatic control in the vertical direction too.

The experiments on the stabilization of the kink instability have been performed on R-O device /2/. In order to accomplish these experiments there has been developed a sixchannel feedback system including three pairs of helical windings with m=I,2,3; n=I, amplifiers with phase correction and current power output amplifiers. Each pair of helical winding consists of "sine" and "cosine" windings, which are shifted at angle $\pi/2$ relative to each other along the major azimuth. Amplifiers with phase correction have the summator which summarizes signals from "sine" and "cosine" windings of various weights. It allows to introduce a spatial phase shift. The output amplifiers permit to obtain I5 A of loading current in the frequence range from I00 kHz to I,5 MHz. In the experiments identifying kink instability modes ranges of q-values have been determined at which kink instability with m=I,2,3; n=I occurs. The data obtained are well agreed with the theoretical conclusion, however, it has been found that the main unstable mode development, for example, m=2, is accompanied by the excitation of intense m=I; 3 modes. This can be partially explained by the magnetic axis displacement over the major radius in R-O.

In order to exert an active effect on plasma , m=2 mode has been chosen. Without feedback, the plasma current increases up to the values corresponding to the safety factor $q \simeq 2$; there occurs Shafranov-Kruskal kink instability which restricts further increase of the plasma current.

With feedback the plasma parameters improve essentially when amplifiers phase characteristics and spatial phase shifts have been chosen correctly. There has been a considerable increase of plasma conductivity and plasma current magnitude and duration; the operation at $q \simeq$ I,5 has been provided (Fig.2). At the gain of control system equal to the conducting casing close to the plasma, the optimal spatial phase shift is $\Delta\varphi \simeq 70°$ (Fig. 3).

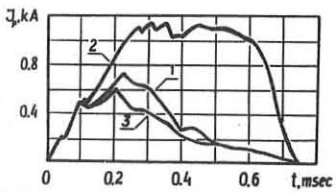

Fig.2. $J_p(t)$ dependence:
I) without feedback;
2) with feedback, $\Delta\varphi \simeq 70°$;
3) with feedback, $\Delta\varphi \simeq 230°$.

However, the analysis of the results obtained shows that at this stage of experiments a complete suppression of kink instability cannot be provided. This may be explained by the fact that (as it follows from the analysis of the dispersion relation for kink modes with feedback) at given frequency characteristics of amplifiers, we can only reduce the kink instability growth rate, because the feedback system frequency range is restricted by low frequencies.

Thus, the experiments show that the feedback stabilization system can considerably influence the current discharde parameters in toroidal systems. In such cases the currents in control windings are $J_{contr} < IO^{-2} J_p$, where J_p is the plasma current.

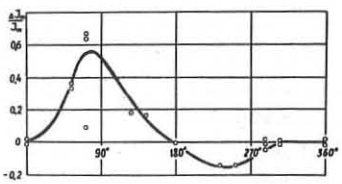

Fig.3. The current amplitude change vs spatial phase shift $\Delta\varphi$.

REFERENCES

I. L.I.Artemenkov et al. 6 Europ.Conf.on Contr.Fus. and Plasma Phys., I, p.153Moscow, I973. В.Ф.Губарев, Ю.И.Самойленко, ЖТФ, 44, 4, I974.
2. R.A.Demirkhanov et al., 6-th Europ. Conf. on Contr. Fus. and Plasma Phys., I, p.I69, Moscow, I973.
3. V.A.Zhil'tsov et al., 5-th Int. Conf. on Plasma Phys. and Contr. Nucl. Fus. Res., I, p.355, Tokyo, I974.
4. Б.В.Арсенин, Атомная энергия, 33, 2, I972.
5. С.В.Мирнов, И.Б.Семенов, Препринт ИАЭ-2723, Москва, I976.

Shear Alfven Wave Heating Experiment in the Heliotron D

K.Uo, T.Obiki, A.Sasaki, T.Mutoh, S.Kinoshita and A.Iiyoshi
Plasma Physics Laboratory
Kyoto University, Uji, JAPAN

Abstract: The plasma heating in the Heliotron D device is successfully performed using the Shear Alfven wave. The cause of the quick electron temperature decay during the rf pulse is investigated.

A method of plasma heating which make use of the shear Alfven wave has been proposed by Hasegawa and Chen (1). Experimental results of the shear Alfven wave heating have also been reported in refs. (2), (3), (4) and (5), and they showed the significant heating of the plasma. However, it has been reported that during the rf pulse the electron temperature quickly reduced after the temperature reached the maximum value. In this paper, some preliminary results of these phenomena are reported.

Heliotron D device is used in this heating experiment. The details of the experimental arrangement was described in ref (2), (4) and (6). A helium plasma was produced by an Ohmic discharge and a plasma current, I_{OH}, is 5 ~ 15 kA with a toroidal magnetic field strength of 2 ~ 3 kG. The ion temperature, T_i = 20 ~ 50 eV averaged on a chord including the center was measured by Doppler broadening of the He II 4686 Å line, the plasma density n_e of 3×10^{12} ~ 2×10^{13} cm^{-3} by a 4 mm microwave interferometer, and the electron temperature at the plasma column center, T_e = 30 ~ 300 eV by the Thomson scattering of a laser light. The positions of the measuring apparatus for the temperatures are located approximately at the opposite side of the rf antenna along the torus. The toroidal length of the antenna section is 1.45 m which corresponds to the wave length of 2.9 m and a toroidal mode number n = 2.

Examples of the time variation of the plasma parameters with and without the rf pulse are shown for three different plasma parameters in Fig.1. The upper curves show the variations of the electron temperature and the lower curves that of the ion temperature. The electron temperature is almost doubled at the maximum in each case and the ion temperature increased about 15 ~ 20 eV. The electron temperature rises quickly at the beginning of the rf pulse and it decreases also quickly, during the rf pulse, down to the level without the rf pulse. The plasma current does not change significantly during the rf pulse and no large amplitude fluctuations are observed during and after the rf pulse. The plasma density measured by the microwave interferometer shows a gradual increase during the rf pulse, its rise time is longer than that of the electron temperature.

The rapid decrease of the electron temperature seems to be caused by an rf breakdown in the vicinity of the rf antenna due to the electrostatic field of the applied rf power. We have taken time integrated photographs of the plasma at the rf antenna section. Figure 2 shows examples with and without the rf pulse. It can be seen that the light intensity at the plasma region and in the vicinity of the rf coil is increased when the rf power is applied. The occurrence of the rf breakdown is also confirmed by the spectroscopic measurement. Figure 3 shows a time variation of C III line intensities at the rf section and at the opposite side of the torus. It is also shown that the impurity line intensity is larger at the rf section at the beginning of the rf pulse than at the opposit side. This implies the impurity concentration is increased by the breakdown. These facts suggest that the electron energy is lost at the rate of the energy confinement time of Joule heating (100 ~ 200 μs) as shown in Fig.1 if the rf power input to the plasma is prevented by the breakdown.

In conclusion, although the experiment is at the preliminary stage, the rf breakdown at the rf antenna section seems to cause the quick decay of the electron temperature. However, this phenomena is not essential for this heating scheme since the breakdown is avoidable with use of an electrostatic shield.

References

(1) A.Hasegawa and L.Chen, Phys. Rev. Lett., 35 (1975) 370.
(2) A.Iiyoshi, T.Obiki, M.Sato, A.Sasaki, T.Mutoh, S.Adachi, K.Uo, Proceedings of the third International Meeting of Theoretical and Experimental Aspects of Heating of Toroidal Plasmas, Grenoble, vol.2 (1976) 305.
(3) K.Uo, A.Iiyoshi, T.Obiki, S.Morimoto, A.Sasaki, K.Kondo, O.Motojima, S.Yoshioka, I.Ohtake, M.Nakasuga, M.Sato, K.Hanatani and T.Mutoh, IAEA-CN-35-D4, Berchtesgaden, 1976.
(4) T.Obiki, T.Mutoh, S.Adachi, A.Sasaki, A.Iiyoshi and K.Uo, to be published.
(5) S.N.Golovato, J.L.Shohet and J.A.Tataronis, Phys. Rev. Lett., 37 (1976) 1272.
(6) K.Uo, S.Morimoto, S.Konoshima, M.Koyama and A.Iiyoshi, Phys. Rev. Lett., 31 (1973) 986.

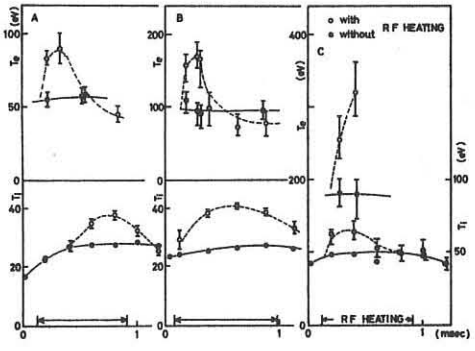

Fig.1 Time variations of T_e, T_i, with and without rf pulse. (plasma current = 12 ~ 15 kA, magnetic field = 2.9 kG, electron density = A) 1.0×10^{13} cm^{-3}, B) C) 0.6×10^{13} cm^{-3}, rf input power = A) B) 300 kW, C) 500 kW)

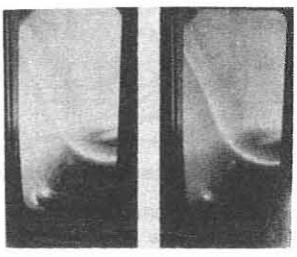

WITH RF WITHOUT RF

Fig.2 Time integrated photographs with and without rf pulse at the rf coil section.

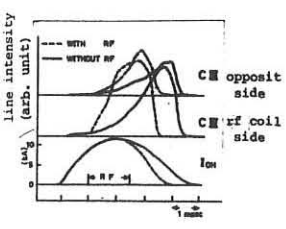

Fig.3 Time variation of C III intensities at the rf coil section and the opposit side of the torus.

MAGNETOACOUSTIC RESONANCE HEATING OF A PLASMA BOUNDED BY PARTIALLY IONIZED LAYERS

M. Bureš and E. Tennfors
Association EURATOM-NE
Royal Institute of Technology, S-10044 Stockholm 70, Sweden

Abstract. A partially ionized boundary region surrounding a RF-heated plasma may absorb a considerable fraction of the power unless a resonance is used to enhance the RF field in the plasma.

1. Introduction. Full-scale fusion reactors are likely to operate in the impermeable plasma density regime [1], with a lowly ionized gas blanket surrounding the plasma core. Radio-frequency fields in the boundary regions produce currents and dissipation, influencing the heating efficiendy and the plasma--gas-blanket balance. In the internal ring device F IV B we have used the lowest magneto-acoustic resonance at about 1 MHz to sustain an impermeable plasma [2,3]. The resonance was also studied by the excitation of eigenoscillations in a rotating plasma [4]. The damping of the oscillations and the variation of the resonance frequency indicates that absorption in the boundary region and the influence of the plasma-gas-blanket balance on the boundary conditions are important. To estimate these effects, we use a simple cylindrical model and compare the results with experiments in F IV B.

2. The cylindrical model. We consider a homogeneous fully ionized plasma column of radius r_o surrounded by a homogeneous partially ionized shell with the inner and outer boundary radii r_o and r_w respectively. The steady magnetic field $\underline{B}_o$ is axial and homogeneous. The absorption in the fully ionized region is assumed to be due to resistivity, while ion-neutral collisions are more important in the outer shell. Obtained profiles of the oscillating field quantities are published elsewhere [5].

Fig.1 shows the frequency dependence of the fraction g(ω) of the total power that is absorbed in the fully ionized region. Three cases with different plasma radius are shown. The other parameters are: B_o=0.25 T, r_w=0.1m, T=10^5K(plasma)and 8×10^3K (shell), $n_i=10^{21}m^{-3}$ (plasma)and $2\times10^{20}m^{-3}$ (shell),and $n_n=8\times10^{20}m^{-3}$ in the shell. It is obvious,that most of the power is absorbed in the blanket except at the resonance peaks for the case with a thin layer. We also observe how the resonances shift as the plasma-gas-blanket boundary r_o moves.

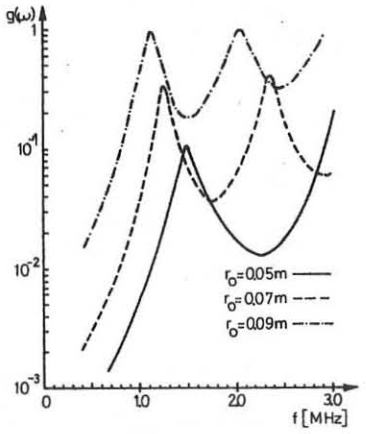

Fig.1.The fraction of the total power absorbed in the fully ionized region.

3. Experiments. A rotating impermeable hydrogen plasma with ion density $10^{21}m^{-3}$ in a magnetif field of 0.37 T is created in the internal ring device F IV B by crossed field technique [2].

After an initial phase the velocity of rotation decreases until the heating power reaches the minimum level [2,3]. Then, a transition to a lowly ionized state takes place. A radio--frequency field is applied by a coil around the plasma. The RF-power P_{rf} delivered to the coil is measured by a fast analog multiplier, and the azimuthal induced current J_φ by a Rogowski coil. The radial low-frequency current and voltage associated with the rotation indicate the input power P_r due to rotation. Fig.1 shows the power input by rotation, P_r, by RF, P_{rf}, and the amplitude of the azimuthal current J_φ as functions of time. The current indicates a resonance both during acceleration and deceleration of the rotation. The total RF power P_{rf} on the other hand seems to be higher after the resonance, which suggests that the resonance in the present case decreases the RF field in the blanket. However, even at the resonance, the fields and the dissipation may have a considerable effect.

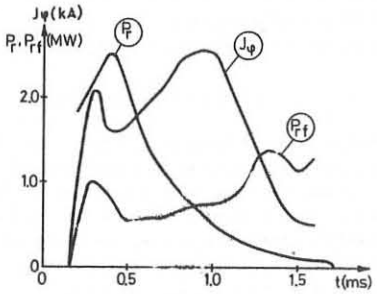

Fig.2, Heating power and azimuthal current during a discharge.

Fig.3 shows the ratio of the induced current to the current J_1 in the antenna coil, all points measured at the resonance. For high induced fields, J_φ does not increase linearly with J_1. This may be due to heating of the boundary region, which may alter the resonance conditions and increase the dissipation in the blanket. At high fields, ionization may also be important, but that is not included in our simple model.

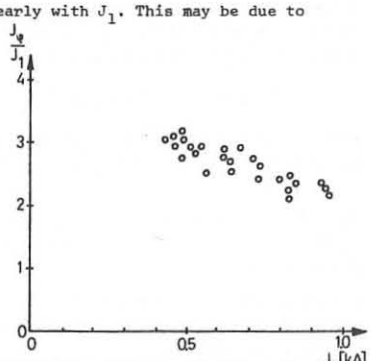

Fig.3. The ratio of induced current to antenna current at resonance.

4. Conclusions. For frequencies in the region of the frequency of ion-neutral collisions, the absorption in a partially ionized boundary layer may be considerable, unless a resonance enhances the fields in the plasma region. This absorption may provide a means to control the plasma-gas--blanket balance, but decreases the efficiency of plasma heating. At the resonance the induced current seems to saturate at about 3kA. Further studies are needed to see how serious this limitation is.

Acknowledgements.We thank Prof. B.Lehnert and the fusion research group at the Royal Inst, of Technology.This work has been supported by the European Communities under an association contract between Euratom and Sweden.

[1] LEHNERT,B.,Nucl,Fusion 13(1973)781.
[2] LEHNERT,B.,BERGSTRÖM,J.,BUREŠ,M.,TENNFORS,E.,and WILNER,B., Plasma Physics and Controlled Fusion Research(Proc.4th Int, Conf.Madison,1970)1,IAEA,Vienna(1971)59.
[3] LEHNERT,B.,BERGSTRÖM,J.,BUREŠ,M.,HOLMBERG,S.,and TENNFORS,E., Physica Scripta 9(1974)109-118.
[4] BUREŠ,M.,TENNFORS,E.,and THORSTENSEN,B.,6th Europ.Conf.on Controlled Fusion and Plasma Physics I(1973)575.
[5] BUREŠ,M.,TENNFORS,E.,Roy.Inst.of Techn.Stockholm, TRITA-EPP-76-20(1976).

TOROIDAL DRIFT MAGNETIC PUMPING

E. CANOBBIO

ASSOCIATION EURATOM-CEA
Département de Physique du Plasma et de la Fusion Contrôlée
Service IGn - Centre d'Etudes Nucléaires
85 X - 38041 GRENOBLE CEDEX

ABSTRACT : A set of azimuthal coils which carry properly dephased rf-currents in the KHz frequency range can be used to heat toroidal plasmas by perpendicular Landau damping of subsonic Alfvén waves /1/. The heating mechanism and the rf-field structure are discussed in some detail.

THE HEATING SCHEME. In any toroidal plasma there is a thin almost cylindrical vertical shell where the $\vec{B}$-lines of force lie essentially parallel to the equatorial plane. (Throughout the paper the (R, ϕ, Z) coordinates based on the vertical axis of symmetry will be used). There the particle guiding centers drift with unidirectional vertical velocity

$$v_Z = v_{\perp Z} \simeq (v_{//}^2 + v_g^2/2)/R\omega_c > v_{//}\, B_Z/B \qquad (1)$$

where $\vec{v}_g$ is the gyrovelocity and $\omega_c = eB/mc$. Superposed to velocity (1) there is, of course, the magnetization drift-c.rot($mv_g^2\vec{B}/2B$) /2/ which ensures that the mass flow along Z vanishes. As shown in Ref. /1/, condition (1) can be exploited to produce substantial perpendicular Landau-damping of axisymmetric Alfvén waves provided they have a vertical component of the electric field, $E_{1Z}(R)\cdot\exp i(kZ-\omega t)$ which travels along Z with phase velocity of the order of $V \equiv v_{ti}^2/R\omega_{ci}$ ($v_{ti}^2 = 2\,T_i/m_i$) - the drift velocity of the thermal ions in the toroidal field. More specifically :

1 - The optimum frequency for Toroidal Drift Magnetic Pumping (TDMP) is $\omega = \alpha kV$ or, assuming $k = \pi/b$ (here b is the vertical minor radius of the plasma) $f_{(KHz)} \simeq \alpha\, T_{i(keV)}/b_{(m)} R_{(m)} B_{(T)}$ where $\alpha = \alpha(T_e/T_i)$ with $\alpha \simeq 3.4$ if $T_e = T_i$ and $\alpha \simeq 4.3$ if $T_e = 2\,T_i$.

2 - Frequency ω has to exceed ν_{coll} for the energy exchanges of the resonant ions (whether trapped or passing) which have $v_{//}^2 + v_g^2/2 = \alpha v_{ti}^2$, so that $v^2 \simeq 3\alpha v_{ti}^2/2$. For a deuterium plasma, this condition reads

$$25(\alpha T_{i(keV)})^{5/2} >> b_{(m)}\, R_{(m)}\, B_{(T)}\, n_{(10^{13}cm^{-3})} \qquad (2)$$

where n is the ion density. The relatively high α-values make it possible to fulfill (2) even if the plasma is quite collisional with respect to diffusion.

3 - The TTMP shell defined by (1) has an average radial width $2|\Delta R| = 2\alpha^{3/4} b \cdot \rho_\theta/R$ where ρ_θ is the poloidal ion Larmor radius at the edge of the plasma current.

4 - In terms of $\xi(R)\exp i(kZ-\omega t)$, the Fourier transform of the radial component of the MHD-displacement vector $\vec{\xi}$, the mean power density absorbed within the TDMP shell is

$$P = (3nT_i/2)\; kV|\xi/R|^2 . F(\alpha\,;\, T_e/T_i) \qquad (3)$$

where, as an example, $F(3.4\,;\,1) \simeq 47.3$ and $F(4.3\,;\,2) \simeq 144$. These large numerical factors help to compensate for the fact that absorption is restricted to the TDMP shell. This is due to two effects : first, the resonance surface in velocity space, $v_{//}^2 + v_g^2/2 = \text{const.}$, is much closer to the equidensity surfaces, $v^2 \simeq \text{const.}$, than in the usual cases where the resonance surface is $v_{//} = \text{const.}$; second, the rate of change of the kinetic energy of the particles, $d\varepsilon/dt = e\,\vec{v}.\vec{E}_1 + \mu\partial B_1/\partial t \simeq e v_z E_{1Z}$, depends on the sum of the curvature and the grad B drifts rather than on the betatron term as in compressional TTMP.

Eq. (3) has been obtained by assuming that the unperturbed velocity distribution function is a uniform maxwellian and that in the TDMP shell $E_{Z1}(R)$ is essentially a symmetric function of $(R-\bar{R}(Z))$, where $\bar{R}(Z)$ is the radial distance of the shell middle-point at distance Z from the equatorial plane. Such a field configuration can always be produced by properly distributing the rf-currents among various azimuthal coils. Then $v_R \partial f_1/\partial R \neq 0$, and we may write the linearized Vlasov as $i(kv_Z-\omega)f_1 + (d\varepsilon/dt)df_M/d\varepsilon = 0$ (the term $(d\vec{v}/dt)_0 . \partial f_1/\partial \vec{v}$ is negligible because of (1)).

SINGLE PARTICLE MOTION. Contrary to TTMP, also the energy of the gyromotion is increased by the TDMP field since $|dB/dt|_1 \simeq \vec{v}_1 \cdot \text{grad } B = cE_{1Z}/R \neq 0$ (as shown later B_1 is negligible). However $(v_g/v)^2$ decreases when $d\varepsilon/dt > 0$. This is not at variance with the preferential increasing of $v_{\perp Z}$ due to E_{1Z}.

The particle kinetic energy can only increase if the rf-field destroys at least one of the 3 adiabatic invariants which are associated with the 3 velocity components $\vec{v}_g$, $\vec{v}_{//}$, and $\vec{v}_\perp$ /3/. The magnetic moment is obviously constant. The longitudinal invariant $J_{//}$ is not conserved because $k_{//}^{-1} \simeq B/kB_Z \simeq qR/kr$ ($q = rB_\phi/RB_\theta$) is comparable with the connection length. Since, however, $\omega/k_{//} << v_{ti}$, $J_{//}$-changes are of no profit to power absorption. TDMP can be said to rely entirely upon changes of $J_\perp$, the third invariant. Notice that in axisymmetric systems the exact invariant $P_\phi = mRv_\phi + eRA_\phi/c$ corresponds to $J_{//} = \text{const}$ if $\vec{B} = \vec{B}_\phi$, and to $J_\perp = \text{const}$ if $\vec{B}$ is purely poloidal. Otherwise $P_\phi = P_\phi(J_{//}, J_\perp)$ and both invariants may well change.

RF-FIELD STRUCTURE. By proper choice of the rf-coils it is in principle always possible to produce non-rigid MHD displacements which have the required structure within the TDMP shell and are compatible with the presence of solid limiters (e.g. radial rail-limiters). However, a quantitative picture of the wave structure is arduous, essentially because the symmetry of the TDMP shell is intrinsically different from the natural symmetry of the MHD-wave pattern in toroidal geometry.

Quantitative predictions can obviously be made in the one dimensional case of a vertical cylindrical plasma shell confined radially between R_1 and R_2, with pressure $p = p(R)$ and $\vec{B} = \vec{B}_\phi(R) + \vec{B}_Z(R)$ where $\vec{B}_Z$ corresponds to the poloidal field of a toroidal plasma ($\int_{R_1}^{R_2} dRRB_Z = 0$). The whole set of the linearized ideal MHD-equations reduces to a single Euler equation $(f\xi')' - g\xi = 0$ /4/ where the prime indicates d/dR. Since the TDMP frequencies are well below the MHD-frequencies we may limit our attention to the "marginal stability" limit ($\omega^2 = 0$) :

$$f = RB_Z^2/4\pi\,; \qquad g = 2p' + (k^2R^2 + 1)f/R^2 .$$

Thus ξ is independent of B_ϕ. The EM-fields are

$$\vec{E}_1 = \{((\xi' - \xi/R)\omega B_\phi/ck \;\; ; \;\; -i\xi\omega B_Z/c \;\; ; \;\; i\xi\omega B_\phi/c\} \qquad (4)$$

$$\vec{B}_1 = \{ikB_Z\xi \;\; ; \;\; -(RB_\phi)'\xi/R \;\; ; \;\; -(RB_Z\xi)'/R\}$$

This shows that $B_{1\phi} = 0$, as anticipated. f and g vanish at the magnetic axis ($R = R_0$) where p' and $B_Z \to 0$. Apart from the case of unusually steep p-profiles, and if we consider plasmas with $8\pi p \simeq O(B_Z^2)$ and TDMP fields with $k \simeq \pi(R_2 - R_1)^{-1}$, then $g \simeq k^2 f$. As a result, for a large class of equilibrium profiles, ξ behaves essentially as a Bessel function of an imaginary argument which depends on kR. The amplitudes are found in terms of the external fields (B_{1R}, B_{1Z}, $E_{1\phi}$) by using the jump conditions $\langle p_1 + \vec{B}_1 . \vec{B}_0/4\pi \rangle = 0$ and $\langle \vec{n} . \vec{B} \rangle = 0$ at the plasma edge where $\vec{n}$ is the unit normal. If the rf-coils are located outside the liner (some of them could then be those producing the equilibrium vertical $\vec{B}$-field) the rf-current intensity has to be high enough to overcome field attenuation which is mainly due to ohmic losses in the walls. With JET-like parameters ($T_i = B = R = 3$; $b = 1.3$; $b/a = 1.6$ - a is the horizontal minor radius of the plasma) a global heating time $\simeq 0.3$ s requires $|\xi/a| \simeq 5.5\; 10^{-2}$. This is a reasonably low value as far as magnetic surface deformations and MHD stability limits are concerned. However, it certainly requires fairly high voltages in externally located coils. At the price of some additional complexity, the situation could be improved if the rf-coils are fed in such a way /5/ as to produce helical fields which match the MHD-singular surface $q = 1$ (if it exists in the plasma) because then local field amplification can occur /6/.

REFERENCES.

/1/ - E. CANOBBIO, IAEA Berchtesgaden Conference 1976.

/2/ - C. LONGMIRE, Elementary Plasma Physics, Interscience Publishers, 1963.

/3/ - B. LEHNERT, Dynamics of Charged Particles, North-Holland Publ. Co. Amsterdam 1964.

/4/ - W.A. NEWCOMB, Ann. Phys. (N.Y) 10 (1960) 232 ; J.P. GOEDBLOED, Physica 53 (1971) 501.

/5/ - F. KOECHLIN and A. SAMAIN, Phys. Rev. Lett. 26 (1971) 490.

/6/ - E. CANOBBIO, These Proceedings.

RESONANT MHD-PUMPING AT ARBITRARILY LOW FREQUENCY

E. CANOBBIO

ASSOCIATION EURATOM-CEA
Département de Physique du Plasma et de la Fusion Contrôlée
Service IGn - Centre d'Etudes Nucléaires
85 X - 38041 GRENOBLE CEDEX

ABSTRACT : Helical rf-fields with appropriate wave numbers can be used to exploit for heating purposes the existence within the plasma of the MHD-singular surfaces where $\vec{k}.\vec{B}_0 = 0$. In this way the TTMP heating rate can exceed the non-resonant value by a factor of order $1/\beta$ and the working frequency $\omega \simeq (\vec{k}.\vec{B}_0/B_0)v_{ti}$ can in principle be choosen arbitrarily low (but preferentially $\omega \gtrsim \nu_{coll}$).

INTRODUCTION. RF -launching structures designed to produce nonvanishing poloidal wave numbers $K_\theta \equiv m/r$ in addition to toroidal wave numbers $K_\phi \equiv n/R$, have been considered for ICRH /1/, TTMP /2/,/3/, Alfvèn-Wave Heating /4 - 7/ , and for Toroidal Drift Magnetic Pumping /8/. In the Proto-Cleo experiment /7/ the inequality

$$|\vec{k}.\vec{v}_A| \equiv |\vec{k}.\vec{B}_0(4\pi\rho)^{-1/2}| \equiv |m\, B_\theta/r + nB_\phi/R|(4\pi\rho)^{-1/2} < \omega_{ci} \qquad (1)$$

($\omega_{ci} = eB_0/m_i c$) was satisfied in spite of the fact that $|m\, v_{A\theta}/r|$ and $|nv_{A\phi}/R|$ were both larger than ω_{ci}.

In the TTMP litterature there is no mention of the analogous possibility of lowering the working frequency by exploiting the existence of the MHD singular surfaces within the plasma. The TTMP frequency is $\omega \simeq nv_{ti}/R$ in the compressional version ($v_{ti}^2 = 2T_i/m_i$), $\omega \simeq v_{ti}/R$ in the torsional version of Ref. /2/ and $\omega \simeq v_{ti}/qR$ ($q \equiv rB_\phi/R\, B_\theta$) in the axisymmetric $|m| = 2$ version /3/ producing surface heating. This oversight is surprising in view of the obvious interest of using frequencies which are so low that the rf-coils can either be put outside the liner (if $\omega/2\pi \lesssim 10$KHz) or be protected by stainless steel if they have to be in face of the plasma ($\omega/2\pi \simeq$ a few 10 KHz).

WORKING FREQUENCY. The correct expression of the optimum TTMP frequency is

$$\omega = (\vec{k}.\vec{B}_0/B_0)\, v_{ti}\, F(T_e/T_i, m, n) \qquad (2)$$

where F is a factor of order unity /2/, /3/, /9/. Power deposition is still substantial at $\omega \pm \Delta\omega$ with $\Delta\omega \lesssim \omega/2$.

Eq. (2) implies that in the neighbourhoods of the singular surfaces $r = r_s$ where $\vec{k}.\vec{B}_0 = 0$ (or $q = -m/n$) plasma heating may be produced at arbitrarily low ω. Since in most of the performant Tokamaks q(0) is slightly below unity, the singular surfaces $q(r) = 1$ is imbedded in the flat central region of the plasma : therefore $n = -m = \pm 1$ are the most interesting combinations. They are produced either by a pair of helical windings (ideally represented by a sheet current $\vec{j}^*.\delta(r-r_c)$ with $j_\phi^*/j_\theta^* = -R/r_c$) or, more conveniently, by the pair of horizontal coils proposed in /2/. In the absence of surface $q = 1$, surface $q = 2$ can be considered. The rf-coils should be designed so as to avoid the production of intense higher-(m, n) harmonics which would satisfy condition $\vec{k}.\vec{B}_0 \to 0$ at the plasma edge, with adverse effects on confinement. Notice, incidentally, that in the Stellarators, where $|B_\theta/r|$ increase with r, such peripheric resonances may well have been excited in the TTMP and Alfvèn-wave experiments, where pumpout occurred during heating /10/, /7/.

RF-FIELD STRUCTURE. As is well known from stability theory in cylindrical geometry /11/,/12/, the whole set of the linear ideal MHD-Eqs. reduces to a single Euler Eq. $(f\xi')' - g\xi = 0$, where ξ is the radial component of the displacement vector $\vec{\xi} = \vec{\xi}(r).\exp i(m\theta + kz - \omega t)$, and the prime indicates d/dr. Since in a low-β plasma, the TTMP frequencies (2) are very small compared with the MHD frequencies (1), we may limit our attention to the "marginal stability" limit $\omega^2 = 0$. Assuming, moreover, $k^2r^2 \ll m^2$, which is appropriate to the Tokamak scaling, we have

$$f = (\vec{k}.\vec{B}_0)^2\, r^3/m^2 \quad ; \quad g = f(m^2 + k^2r^2 - 1)/r^2 + \\ + \{8\pi p' + (\vec{k}.\vec{B}_0)(kB_z - mB_\theta/r)2r/m^2\}\, k^2r^2/m^2 . \qquad (3)$$

In the neighbourhoods of a singular surface $r = r_s$, if $x \equiv r - r_s$, we may write $f = \alpha x^2$, $g = \beta + \gamma x + \delta x^2$ and find the solutions to Eq. (3) in terms of hypergeometric functions /11/, which behave like $\xi_1 = x^{\nu_1}$ and $\xi_2 = x^{\nu_2}$ (if $x \to 0$) with

$$2\,\nu_{1,2} = -1 \pm \{1 + 32\pi\, p'/r\, B_z^2\, [(\ln (B_\theta/r\, B_z))']^2\}^{1/2} \qquad (4)$$

The sign of the expression under the square root is positive when Suydam's criterion is satisfied : then one of the solutions is infinite at r_s.

The radial width of the resonance zones is governed by the position of the roots of the quadratic equation $g(\frac{nq(r)}{m}) = 0$/12/, which in our problem play the role of two cut-offs. If $m^2 = 1$, the resonance zone is quite broad

$$3\, nq(r_{1,2}) = 1 \pm 2\,(1 - 6\pi rp'/B_\theta^2)^{1/2} \qquad (5)$$

If $|m| \geq 2$

$$\Delta q \equiv q(r_2) - q(r_1) \simeq 2\, kr/n \simeq 2|mB_\theta/nB_z| \qquad (6)$$

The largest field components in these zones are $B_{1//} = \vec{B}_1.\vec{B}_0/B_0 \simeq B_\theta^2\, \xi'/B$, $E_{1r} \simeq -\xi'\omega r\, B_z/mc$, and the electrostatic field $\vec{E}_{les} = (\mathrm{grad}\, n_1)T_e/en_0$ which ensures charge neutrality /2/, /3/, /9/. In contrast with the stability case, these fields are not eigenmodes : they are driven by the external rf-currents.

POWER ABSORPTION. The large rate of change of the kinetic energy of each particle in the resonant zones, $e\vec{v}.\vec{E}_1 + \mu\partial B_1/\partial t$ ($\vec{v}$ is the guiding-center velocity and μ the constant magnetic moment), results in a very important TTMP heating of the plasma ions (primarily along $\vec{B}_0$) if condition $\omega = v_{//}\, \vec{k}.\vec{B}_0/B_0$ is satisfied by $v_{//} = O(v_{ti})$ on a substantial fraction of the zones defined by Eqs. (5) and (6). Since $\Delta k_{//} \equiv \Delta(\vec{k}.\vec{B}_0/B_0) \simeq \Delta q(n/qR)$, in order to have $\omega = \alpha v_{ti}/qR$ with $\alpha \ll 1$, from $\Delta k_{//}/k_{//} \simeq \Delta q(n/\alpha)$ we conclude that TTMP occurs on a fraction of order α of the $m^2 = 1$ resonance zone, and on the entire $|m| \geq 2$ - resonance zones it $\alpha \gtrsim 2\, m\, B_\theta/B_z$.

Of course Eq. (4) implies that our ideal model breaks before a singular surface is reached. A reasonable estimate of the average enhancement factor for the rf-energy density in zones (5) and (6), is $\simeq (v_A/v_{ti})^2 \simeq 1/\beta$. This implies that a large fraction of the reactive power $\int_V dV\omega(B_1^2 + E_1^2)/8\pi$ (V is the plasma volume) could be dissipated. However, just as in the case of resonances at higher frequency (Alfvèn and hybrid) it is then hard to predict how much heating will be due to Landau processes, to linear mode conversion or to non-linear (e.g. parametric) effects /4/. We also notice that if ω is choosen as low as $v_{ti}^2\, m/rR\,\omega_{ci}$ - the "transit frequency" in the vertical drift motion - at the singular surfaces the condition $\omega = \vec{k}.\vec{v} \to \vec{k}_\perp.\vec{v}_\perp$ can be fulfilled by the vertical drift velocity in the toroidal field /8/.

REFERENCES.

/1/ - OVCHINNIKOV, S.S. et al., Madison IAEA Conference 1971, english transl. : Nuclear Fusion Supplement 1972, p. 347.
/2/ - KOECHLIN, F and SAMAIN, A. Phys. Rev. Lett. 26 (1971) 490.
/3/ - KOECHLIN, F and SAMAIN, A. Plasma Phys. 14 (1972) 349.
/4/ - HASEGAWA, A and CHEN Liu, Phys. Rev. Lett. 32 (1974) 454 ; Phys. Fluids 19 (1976) 1924.
/5/ - TATARONIS, J.A and GROSSMANN W. Nuclear Fusion 16 (1976) 667.
/6/ - IIYOSHI, A., et al., Heating of Toroidal Plasmas, Grenoble 1976, Vol. 2 p. 305.
/7/ - GOLOVATO, S.N., SHOHET, J.L., and TATARONIS, J.A., Phys. Rev. Lett. 37 (1976) 1272.
/8/ - CANOBBIO, E., Berchtesgaden IAEA Conference 1976.
/9/ - CANOBBIO, E., "Plasma Physics and Controlled Nuclear Fusion Research" 1971, Vol. III p. 491.
/10/ - MILLAR, W., Report CLM-R 144 (1975) ; PACHER, H.D. et al., Bull. Am. Phys. Soc. 18 (1973) 1353 ; CANOBBIO, E. Varenna Symposium Sept. 1976.
/11/ - NEWCOMB, W.A., Ann. Phys. (N.Y.) 10 (1960) 232 ; HAIN, K. and LÜST, R., Z. Naturforsch 13a (1958) 936 ; GOEDBLOED, J.P., Phys. Fluids 16 (1973) 1927.
/12/ - SHAFRANOV, V.D., Soviet Phys. Tech. Phys. 15 (1970) 175.

ELECTRON LANDAU DAMPING OF LOWER HYBRID WAVES FROM A FINITE LENGTH ANTENNA

M. BRAMBILLA

ASSOCIATION EURATOM-CEA
Département de Physique du Plasma et de la Fusion Contrôlée
Service TGn - Centre d'Etudes Nucléaires
85 X - 38041 GRENOBLE CEDEX

ABSTRACT : Launching and propagation of Lower Hybrid Waves to heat large plasmas by Electron Landau Damping is discussed. Conditions on the appropriate frequency and on the antenna location in the plasma density profile are derived.

1 - For simplicity we use a plane model, with the antenna located at x = 0, and the plasma surface at $x = x_p \geq 0$. The static magnetic field is along z, and the density gradient along x. To excite the slow wave inside the plasma, the antenna electric field should be mainly E_z :

$$E_z^a(z,t) = e^{-i\omega t} \int dk_{//}\, \varepsilon^a(k_{//})\, e^{ik_{//}z}$$

(E_z^a should be the selfconsistent field ; for example if the launching structure is a waveguide array - the Grill - E_z^a should include the reflected wave in each guide, as well as the higher order evanescent modes locally excited at the waveguide mouths /1/). In terms of $\varepsilon^a(k_{//})$ the power flux through any plane x = const in front of the antenna (of length h in the y direction) can be written

$$\phi = \frac{\hbar\omega}{8} \int_{k_{//}^2 > k_0^2} \frac{|\varepsilon_a(k_{//})|^2}{\kappa_\perp} \,\mathrm{Im}\, Y_s \, dk_{//} \qquad (1)$$

where $k_0 = \omega/c$, $\kappa_\perp = \sqrt{k_{//}^2 - k_0^2}$, and $(\mathrm{Im}\, Y_s)/\kappa_\perp$ is the resistive part of the surface admittance of the plasma,

$$Y_s = \frac{Z_s^{-1}}{|\mathrm{Ch}(\kappa x_p) + Z_s^{-1}\mathrm{Sh}(\kappa x_p)|^2}, \qquad Z_s = -i\frac{\kappa c}{\omega}\left(\frac{E_z}{B_y}\right)_{x=x_p} \qquad (2)$$

(waves with $k_{//}^2 < k_0^2$ do not contribute to ϕ since they are evanescent beyond the cut-off $\omega_{pe}^2 = \omega^2$; moreover $\mathrm{Im}\, Y_s = 0$ for $n_{//}^2 < n_{//crit}^2 = (1 - \omega^2/\Omega_{ci}\Omega_{ce})^{-1}$ in the absence of surface absorption since accessibility is not satisfied). For $x_p \neq 0$, evanescence of waves with $k_{//}^2 > k_0^2$ in vacuum makes Y_s exponentially small. We conclude that the antenna should not be screened from the tenuous plasma existing in the shadow of the limiter, in particular when relatively large value of $n_{//}^2$ are required, as appropriate for ELD.

2 - The detailed solution for the field in the plasma, required to evaluate Z_s, has been given elsewhere /1/. We assume a linear density profile

$$\frac{\omega_{pe}^2}{\omega^2} = \alpha^2 + \frac{x - x_p}{L_n} \qquad (3)$$

If $\alpha^2 < 1$ one finds for $n_{//}^2 > n_{//crit}^2$

$$Z_s = \frac{1}{(\alpha^2-1)^{1/2}} \frac{e^{-\pi i/3} I_{-1/3}(\xi) + I_{1/3}(\xi)}{I_{-2/3}(\xi) + e^{-\pi i/3} I_{2/3}(\xi)} \qquad (4)$$

where $\xi = (2/3)\,\kappa_\perp L_n (1-\alpha^2)^{3/2}$. In this case a low density layer $\omega_{pe}^2 < \omega^2$ in which waves are evanescent exists close to the antenna, so that waves with large $n_{//}^2$ are strongly suppressed from the power spectrum, as shown by the exponential decrease of $\mathrm{Im}\, Z_s^{-1}$ as soon as $\xi > 1$. Of course, an antenna designed to excite $n_{//}$ values in this range will also be badly mismatched,a fact confirmed numerically using the code described in Ref . /1/. If $\alpha^2 > 1$ on the other hand, waves with $n_{//}^2 > n_{//crit}^2$ propagate freely to the damping region, and one finds

$$Z_s = \frac{1}{(\alpha^2-1)^{1/2}} \frac{e^{-\pi i/3} J_{-1/3}(\eta) - J_{1/3}(\eta)}{J_{-2/3}(\eta) + e^{-\pi i/3} J_{2/3}(\eta)} \qquad (5)$$

where $\eta = (2/3)\,\kappa_\perp L_n (\alpha^2-1)^{3/2}$. For large $n_{//}^2$, $Z_s^{-1} \sim i(\alpha^2-1)^{+1/2}$. However, since $\mathrm{Re}\, Z_s \to 0$ for large η, matching would again be poor and reflection almost total for an antenna designed to excite values of $n_{//}$ such that $\eta \gg 1$.

The best situation, both for coupling and for ELD, occurs when the plasma density near the antenne is close to the cut-off density, so that $\alpha^2 \sim 1$. More precisely, provided $\kappa_\perp L_n |\alpha^2-1|^{3/2} \ll 1$ for the values of $n_{//}$ excited by the antenna, both Eqs. (4) and (5) reduce to

$$Z_s = e^{-\pi i/3} \frac{\Gamma(\frac{1}{3})}{\Gamma(\frac{2}{3})} \left(\frac{\kappa_\perp L_n}{3}\right)^{1/3} \qquad (6)$$

In this case coupling is good over a broad range of L_n /1/, and the power in the large $n_{//}$ region of the spectrum is only moderately reduced by the factor $\ln Z_s^{-1}/\kappa_\perp$ in Eq. (1).

The experimental results on coupling of LH waves with 2 and 4 waveguides on H1 /2/ and ATC /3/ at Princeton are in excellent agreement with the theory developed for the Grill /1/ provided Eq. (6) is used for Z_s, while neither of Eqs. (4) and (5) gives fitting results. This apparently indicates that a low density plasma with $\omega_{pe}^2 \sim \omega^2$ indeed exists close to the Grill aperture. It is important that this situation be maintained also in larger devices to achieve good matching, in particular for ELD.

3 - Knowledge of the power spectrum allows to evaluate the electron power absorption per unit volume. In a torus of radius R at a distance $r = x_p - x$ from the axis,

$$P_{ELD} = \frac{\omega^2 h}{16\pi^2 c r R} \int_{k_{//}^2 > k_0^2} \frac{|\varepsilon_a(k_{//})|^2}{\kappa_\perp} \,\mathrm{Im}\, Y_s \cdot \gamma \cdot e^{-2k_0 \int \gamma dx} dk_{//} \qquad (7)$$

where γ is the inverse absorption length for ELD. It should be noted however that the usually quoted expression for γ,

$$\gamma = \sqrt{\pi}\frac{\omega_{pe}}{\omega} \frac{x_e^3 e^{-x_e^2}}{(1 + \frac{\omega_{pe}^2}{\Omega_{ce}^2} - \frac{\omega_{pi}^2}{\omega^2})^{1/2}} \qquad (8)$$

where $x_e = \omega/k_{//}v_{the}$, fails when the wave approaches the Linear Turning Point /4/ where the slow wave transforms linearly into a hot plasma electrostatic wave, which can be effectively absorbed by ion cyclotron damping. Since waves with large $n_{//}^2$ encounter the LTP at lower density, this process tends to compete with ELD by depleting the large $n_{//}$ portion of the spectrum. To logarithmic accuracy eq. (8) leads to the condition

$$n_{//}\sqrt{T_e} \geq 5 - 7$$

(T_e in keV) for efficient ELD. On the other hand the condition to avoid LTP depletion is

$$n_{//}\sqrt{T_i} < 9\,\frac{\omega^2}{\omega_{pi}^2}\left(1 + \frac{\omega_{pe}^2}{\Omega_{ce}^2} - \frac{\omega_{pi}^2}{\omega^2}\right)$$

Clearly, apart from the uninteresting case $T_e \gg T_i$, these two conditions are compatible only if ω is sufficiently larger than the resonant lower hybrid frequency in the centre of the plasma (a factor of 1.5 to 2 is usually found to be sufficient). Of course this brings the frequency within the domain in which parametric instabilities are also more likely.

AKNOWLEDGMENT. We are indebted to W.M. HOOKE, S. BERNABEI and R.W. MOTLEY for discussions about their experimental results.

REFERENCES.

/1/ - M. BRAMBILLA, Nucl. Fusion 16, 47, 1976 and Internat. School of Plasma Physics, Varenna 1976, to be published.

/2/ - S. BERNABEI, M. HEALD, W.M. HOOKE, F.L. PAOLONI, Phys. Rev. Letters 34, 866, 1975 ; S. BERNABEI et al., PPL report 1288, September 1976.

/3/ - W.M. HOOKE, S. BERNABEI, private communication.

/4/ - T.H. STIX, Phys. Rev. Letters 15, 878, 1965.

$p - B^{11}$ FUSION SYSTEMS

D R Sweetman and J G Cordey

Culham Laboratory, Abingdon, Oxon. OX14 3DB, U.K.
(Euratom/UKAEA Fusion Association)

ABSTRACT: The optimum way to run a magnetically contained $p - B^{11}$ fuelled reactor is as a driven hot ion system. The gain factor, Q, is calculated for this case including relativistic corrections to the ion-electron transfer rates and the effect of α-particle poisoning. A Q of 1.1 is obtained but the poisoning and the synchrotron radiation can reduce this substantially.

1. MODEL: Several authors have considered the $p + B^{11} \rightarrow 3\alpha + 8.7$ MeV reaction for essentially neutron free power production[1]. In the most recent of these assessment, Moreau[1] considers magnetic confinement systems but dismisses them because of the unlikelihood of achieving the self-sustaining ignition condition due to the excessive power loss by bremsstrahlung and synchrotron radiation. Beam-plasma (TCT) systems are unprofitable for the same reasons. These systems are however not the optimum way to use a fuel such as $p - B^{11}$ and in this paper we consider the alternative driven hot-ion (HIT) scheme[2] which is particularly well adapted to such high temperature operation. The power balance model we have taken is shown in Fig.1. Ions are assumed to be injected at ≈ MeV energy and quickly equilibrate with the ion bath at temperature T_i. The electrons reach a temperature T_e about half that of the ions: they are heated predominantly by heat transfer from the ions (P_{ie}) and cooled by bremsstrahlung (P_b), by synchrotron radiation (P_s) and by any other losses (P_e). The thermonuclear power (P_N) is generated as α-particles which quickly transfer their energy to the ion and electron baths. For the cases under consideration about 90% of the energy goes to the ions.

The "Q value" defined as P_N/P_{inj} where P_{inj} is the injected power, has been evaluated by solving the power balance equations for the system. T_i is fixed at the optimum value and the electron power balance equation is solved iteratively to give T_e.

At the temperatures of interest (T_e = 100-200 keV) the electrons are near relativistic. For the condition $T_e \leq m_o c^2$, we find the classical Spitzer ion-electron transfer rate must be divided by $1 - 0.3\ kT_e/m_o c^2$. The bremsstrahlung loss was evaluated using the recipe given by Maxon[3] which treats both the electron-ion and the electron-electron contributions relativistically.

An important further problem not considered by other workers is that of the α-particle contamination in these high burn-up systems. In all of the present work we have included the dilution effect of the α-particles; to estimate the power loss problem we have taken two limiting cases, (i) the ions and their associated electrons are extracted at zero temperature; and (ii) the ions and their associated electrons are extracted with mean energy of $\frac{3}{2}\ kT_i$ and $\frac{3}{2}\ kT_e$ respectively.

2. Q WITHOUT SYNCHROTRON RADIATION: In this case Q is independent of the absolute value of the density. The choice of T_i depends critically on the variation of $\overline{\sigma v}$ with temperature. There is some variation in the basic cross-section data and the integration over the Maxwellian involves using data from more than one source. The best available data is the most recent data from Tombrello[4] supplemented with that of Segel et al.[4] at energies of > 1.4 MeV. For this case Q maximises with T_i near 300 keV which we have taken as standard.

Variation of the mixture ratio n_B/n_p shows a maximum in Q for $n_B/n_p \approx 0.17$ relatively independent of other parameters: this has again been taken as standard. Under these conditions the maximum Q is achieved when the lifetime of the α-particles is set to zero and the energy loss associated with the ions and any electron losses additional to bremsstrahlung are set to zero. Under these conditions Q = 1.13. Increasing the α lifetime to that required for them to thermalise (ie. $n_p \tau_\alpha \approx 10^{14}\ cm^{-3}\ sec$) reduces Q to 1.08. Adding additional loss via the electron channel, expressed as an energy confinment time τ_E, reduces Q further as is illustrated in Fig.2. This figure also illustrates the sensitivity to $\overline{\sigma v}$, the dashed curve showing the effect of increasing $\overline{\sigma v}$ by × 2.5; ignition is achieved for $n_e \tau_E > 3{\cdot}5.10^{15}\ cm^{-3}\ sec$.

Fig.3 shows the effect on Q of (a) increasing the α containment time beyond that required for thermalisation, (b) introducing an associated energy loss as discussed above, (c) making various assumptions as to the proton and boron loss rates. On the pessimistic assumption that all the ions must be extracted at the same rate, there is an optimum $n_p \tau_i$ of $2.10^{15}\ cm^{-3}\ sec$ for which Q is only 0.31.

3. Q WITH SYNCHROTRON RADIATION: In this case the calculation becomes system-dependent. For present purposes we have calculated the synchrotron radiation using the Trubnikov formalism which evaluates the black-body radiation up to the transparency limit. This gives for the present parameter range a power loss which scales as $B^{3.6}\beta^{0.6}(a/\xi)^{-0.44}T_e^{\approx 2.7}$ where a is the plasma radius and ξ the wall absorbtivity. Relativistic corrections enhance this further.[5] Since the thermonuclear power scales as $B^4\beta^2$, the effect of synchrotron radiation is only weakly B dependent; it does however depend on the profile of B assumed. Fig.4 shows the scaling of Q with β for two limiting assumptions as to the effective B in the plasma: the upper limits assumed $B = (1-\beta)^{\frac{1}{4}}B_o$ and the lower limits assume $B = B_o$ where B_o is the vacuum magnetic field (= 50 kG in Fig.4).

4. CONCLUSIONS: The driven hot-ion system is optimum for the $p - B^{11}$ fuel. With the best available values of the cross-section, the Q value obtained if the α-particles are extracted at zero energy and $\beta \approx 1$ is only 1.1. The assumption that all ions must be extracted at the same rate and at $\frac{3}{2}\ kT_i$ mean energy reduces Q even further. To avoid degradation of Q due to synchrotron radiation β must be high.

It should be pointed out that Q is very sensitive to the value of the cross-section about which there is some uncertainty. For example the $\overline{\sigma v}$ given by Fowler et al.[6] and used by Dawson[1] gives a maximum Q of 5.9 at T_i = 200 keV. A Q of ≥ 5 would be required to give a plausibly economic system.

REFERENCES
[1] eg. D C Moreau, Nucl. Fus. 17 13 (1977); J M Dawson, B.A.P.S. Paper 8 E-14 (Nov.1976); T Weaver et al. UCRL 74352.
[2] D R Sweetman, Symp. on Plasma Heating, Varenna, 1976; J G Cordey, F A Haas, Berchtesgaden Conf. Paper B12-1 (1976).
[3] S Maxon, Phys. Rev. A 5 1630 (1972).
[4] T Tombrello, private communication; Segel et al. Phys. Rev. 139 818 (1965).
[5] B A Trubnikov, 2nd Geneva Conf. 31, 93 (1958); T C Chu, UCRL-77167 (1975).
[6] W A Fowler et al., Ann. Rev. of Astron.& Astro. 13 69 (1975).

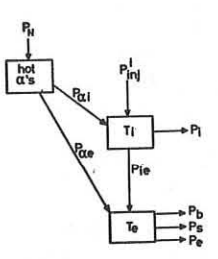

Fig.1

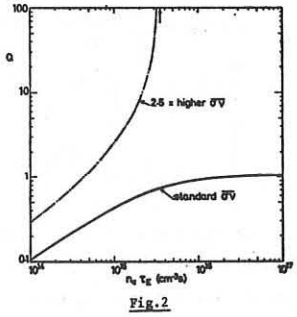

Fig.2

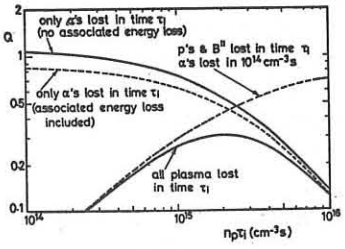

Fig.3

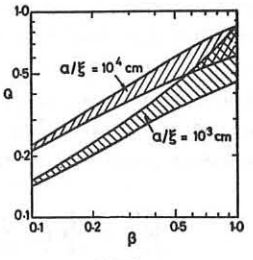

Fig.4

HEAT AND PARTICLE TRANSPORT TO A WALL OF A TOKAMAK REACTOR

N.N.Vasilyev, A.V.Nedospasov, V.G.Petrov, M.Z.Tokar
Institute of High Temperatures of the USSR Academy of Sciences
Moscow, USSR

Abstract: The interaction of plasma with the neutrals that are generated in surface recombination is under consideration. The artificial turbulence in the near wall region is assumed. It is shown that the turbulent blanket can be an alternative to a divertor by helium removal and reactor wall safeguard from sputtering.

In a tokamak reactor the desirable thermal outflux from plasma should reach the values 0,4-1 MW/m^2. In this case the wall is subjected to a bombardment with particles with energy strongly exeeding the sputtering threshold of the wall. In ref. /1/ a method for defence of the first wall has been discussed. It represents an artificial plasma turbulisation in the vicinity of the wall to secure the required thermal fluxes at low plasma temperature. In the present report it is assumed that Bohm diffusion is created in a near wall region by any method.

Electrons and ions diffuse to the cooled wall, termalisate and recombinate there. As a result of desorbing an influx of cold neutral atoms is generated. The neutral density is supposed to be small and therefore the neutral mutual collisions can be neglected. The elementary processes taken into the account for neutrals are as follows: the ionisation and the exitation by electrons and the charge exchange with ions. As the chanrge exchange and ionisation probabilities are similar, a considerable part of neutrals returns to the wall. Some neutrals can leave the camera through wall holes and then may be absorbed in cryopanels, for instance. Thus the withdrawal of unburned fuel as well as helium generated may be provided. This enables a steady reactor operation. It is turned out that the summary holes area should be small. The neutral behaviour is described with one-dimensional kinetic equation. The boundary condition is represented by the distribution function of the atoms desorbed from the wall f_c (x=0). The equation may be written in the following integral form:

$$f_a = f_c \exp\left\{-\int_0^x \frac{[K_i+K]\,n}{v_x}\,dx'\right\} + f_+ + f_-$$

$$f_+ = \int_0^x \frac{K n_a}{v_x} f_i \exp\left\{\int_x^{x'} \frac{[K_i+K]n}{v_x}\,dx''\right\}dx', \quad v_x>0 \qquad (1)$$

$$f_- = \int_\infty^x \frac{K n_a}{v_x} f_i \exp\left\{\int_x^{x'} \frac{[K_i+K]n}{v_x}\,dx''\right\}dx', \quad v_x<0$$

Here k=const and k_i are the charge exchange and ionisation constants respectively, f_i is the ion distribution function. From (1) the integral equations for the atom density n_a and the mean energy $\mathcal{E}_a$ are obtained. The magnitude of the cold atoms influx is found from the steady-state conditions. Plasma is described in hydrodynamics manner, magnetic field being equal to 50 kG. Lines of force are supporsed to be parallel to the wall surface. The balance equations of the isothermal plasma are the following

$$\frac{d\Gamma}{dx} = \frac{d}{dx}\left(D\frac{dn}{dx}\right) = K_i n n_a \qquad (2)$$

$$\frac{dQ}{dx} = \left[-\left(I_i K_i + I_e K_e\right) + \left(\mathcal{E}_a - \frac{3}{2}T\right) + \mathcal{E}_a K_i\right] n n_a \qquad (3)$$

Here I_e and K_e are exiting energy and the exiting constant of the atoms respectively. $Q = \varkappa \frac{dT}{dx} + (3T + I_i)\Gamma$ is the total thermal flux.

The boundary conditions at the wall are defined by the fact that the heat transfer at x = 0 depends on the particle flux and the thermal conductivity flux is reduced here to zero. Demensions of the considered region are chosen sufficiently large (0,2 m), thus on the inner side of the region the neutral flux is small. The plasma density, the outflux and the thermal outflux on the inner side are supposed of the values that are expected in the future reactor e.g. n_1 = 10^{20} m^{-3}, Γ_1 = $2\cdot10^{20}$ m^{-2} sec^{-1} Q_1 = 1 MW/m^2 respectively. The plasma outflux is assumed to exceed significantly burning out. Such a situation may be secured by a turbulence due to trapped particle instability. It provides a small helium fraction in a reaction region /2/.

The equations system has been solved numerically. It is turned out that the neutrals transfer 30 per cent of the energy outflux. The charge exchanged neutral outflux exeeds fifty times Γ_1 . The mean energy profile of plasma (1) and that of the charge exchanged atoms (2) are presented in the figure 1. Plasma and the charge exchanged atom density profiles are presented in the figure 2.

For the case of molibdenium total sputtering of the wall has been obtained with value being equal to S=1.5·10^{18}m^{-2} sec^{-1}. The impurity density at the wall is estimated from the balance of the inlet and outlet particles $\frac{n_z \bar{v}_z}{4} = S$, it is equal to $n_z \sim 6\cdot10^{15}$ m^{-3}. Due to the turbulent diffusion the impurity density profile has to be flat. At lower thermal fluxes the near wall plasma temperature along with the sputtering would be significantly smaller.

References

1. A.V.Nedospasov, 7-th Europ.Conf. on Controlled Fusion and Plasma Physics, Laussanne, 1975, p.129.
2. B.Badger, et al. "UWMAK-III, A Noncircular Tokamak Power Reactor Design", University of Wisconsin Nuclear Engineering Dept. report UWFOM-150 (1976).

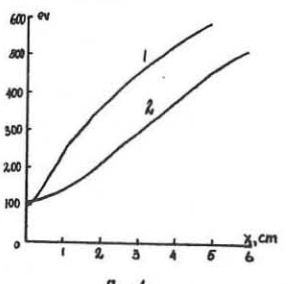

Fig. 1.

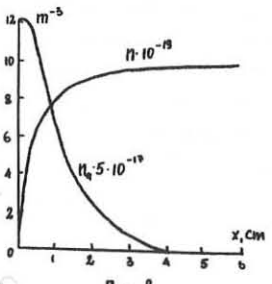

Fig. 2.

PLASMA ENERGY BALANCE WITH TURBULENT TRANSPORT COEFFICIENTS FOR TOKAMAK REACTOR

V.K.Kolesnikov, V.G.Petrov, V.D. Khait

Institute of High Temperatures of the USSR Academy of Sciences
Moscow, USSR

Abstract: A global plasma energy balance model is investigated. The anomalous transport coefficients due to trapped-particle mode are employed. The existence of the steady state conditions with temperature below 20 kev is demonstrated. The operation mode providing the maximum specific power is found, the thermal outflux being set as a parameter.

The present optimistic situation in the fusion investigations gives rise to analyses of a future tokamak reactor operation. Some analyses have been already fulfilled /1-3/. They have discovered several problems to be solved. In particular it became clear that the energy and particles transport mechanisms existing in the present tokamaks i.e. neoclassical and pseudoclassical regimes will cause too high plasma temperatures in large reactors. Under these mechanisms helium removal is a very difficult problem. Since plasma pressure is limited by the equilibrium conditions, high temperatures lead to low plasma densities resulting in a small specific power generated that is not acceptable from the power generation point. The optimum temperature is 10-20 kev and it can not be provided in large reactors with neoclassical transport. The reduction of the temperature is not effective by means of input high Z impurities since a presence of impurities results in a significant decrease of a fuel density /2/. The modern theoretical concept /4/, however, show a possibility of trapped particle mode at temperatures higher than those, that may be achieved in existing devices. The anomalous transport coefficient due to this mode is strongly dependent on the electron temperature ($T_e^{3/2}$). Just this fact allows to hope temperature stabilising at the sufficiently low level. The existing theory, however, is the approximate one and it is impossible to specify the numerical coefficients because of the lack of the experimental data. Thus, probably, it is of no sense to investigate the energy balance of turbulent plasma on the base of two-dimensional and even one-dimensional equations /5/. A global model based on equations averaged over a bulk seems to be more adequate to the present standart of an anomalous transport knowledge. In the present work the average equations of ion and electron energy balance as well as α-particles balance have been solved together the transport being anomalous due to trapped particles mode. The fuel losses due to a diffusion and burning are supposed to be repraced by the fuel ice that is thrown in. The torus section is supposed to be round, all variables are prescribed to depend especially on the current radius r. For obtaining the average equations under these conditions it is necessary to specify density and temperature profiles. These profiles are chosen on the base of the symmetry conditions at a torus axis as well as the finitness of the energy and particles outfluxes at the wall. Of course, these conditions can not define the profiles in the single way. This uncertainty, in fact, means the vagueness in choosing a numerical factor for the fluxes expressions, which in turn also are not exactly known. The values of a fuel concentration at the axis and at the wall can be set on the base of boundary conditions. In this case densities and temperatures are: $n = n_1 + (n_0 - n_1)\left(1 - \frac{r^2}{a^2}\right)^{6/13}$, $T = T_0\left(1 - \frac{r^2}{a^2}\right)^{6/13}$. It gives us the opportunity for some reactor optimisation. The values $\beta_\theta = \frac{\langle n(T_e + T_i)\rangle 8\pi}{H_\theta^2}$ and the thermal flux q_0 are being set. As it is known these values are limited. The dimensions and the reactor power are searched under the condition of the maximum generated power. Let's note that a total power (W) is calculated with the regard for the neutron energy as well as for the blanket reaction energy, i.e. 21 MEV for an every fusion reaction. The optimisation problem is based on the fact that under condition $T_e = T_i$ the specific fusion power is proportional to $\beta_\theta^2 F(T)$, where the function F(T) has the maximum at certain T=T*. The meaning T* depends on a temperature profile and for the chosen profile T* $\approx$ 17 kev. For the chosen concentration profile the problem is in the definition of the values n_1 and n_0, which make the temperature equal to T*. In the presented table there are shown the steady state reactor parameters at H = 50 kG, $\beta_0 = 2,5$, $q = \frac{aH_\theta}{RH_\theta} = 2,5$ for three different energy outfluxes.

References

1. Ю.Н.Днестровский, Д.П. Костомаров, в сборнике "Вычислительные методы в физике плазмы, стр. 483, Москва, "Мир", 1974.
2. A Fusion Power Plant, ed. by R.G.Mills, Princeton University Plasma Physics Laboratory, Princeton, New Jersey, 1974.
3. UWMAK-III, A noncircular Tokamak Power Reactor Design, Nuclear Engineering Dept. Report UWFDM-150 (University of Wisconsin) Madison, Wisconsin, 1976.
4. Kadomtsev B.B., Pogutse O.P., Nucl.Fusion, 1971, 11, No.1, 67.
5. Kesner J., Conn W., Nucl. Fusion, 1976, 16, No.3, 397.

R, m	9,63	I2,6	I5.7
a, m	3,2I	4,2I	5,23
W, GW	3,65	8,4	I6,2
n_1, $10^{19} m^{-3}$	8,5	7,32	6,I5
n_0, $10^{19} m^{-3}$	II,8	I2,2	I2,5
n_{as}, $10^{19} m^{-3}$	0,I4	0,I2	0,I04
T_{oe}, kev	I9,6	I9,8	I9,9
T_{oi}, kev	I7,0	I7,0	I7,0
Energy outflux, $\frac{MW}{m^2}$	3,00	4,00	5,00
Bremsstrahlung $\frac{KW}{m^2}$	36,9	48,5	59,3
Plasma energy outflux $\frac{KW}{m^2}$	463	622	775
Plasma losses g/sec	0,I	0,4	I,I7
Helium outflux 10^{-3} g/sec	7,20	I6,60	32,0

NUCLEAR HYBRID PLANT WITH LASER FUSION REACTOR

R.R.Grigoriantz*, A.V.Kalinin*, O.S.Popel*, E.M.Shelkov*, E.E.Shpilrain*, O.N.Krokhin**, V.B.Rozanov**, G.V.Sklizkov**

* Institute of High Temperature, USSR Academy of Sciences

** P.N.Lebedev Physical Institute, USSR Academy of Sciences

For a long time fusion energetics using purely thermonuclear plants was considered as an alternative to nuclear energetics based on fission reactors or as an independent direction in the future energetics. It was only recently that it has been realized that this approach doesn't make use of the advantages of both fields of energetics to the full.

It now appears that fusion energetics (at least the fusion plants of the first generation) is to be a subsystem of the large systems of nuclear energetics, and it is to be closely bound with this system by a common development strategy, technology, fuel cycles and so on.

In a sense, D-t reactors can be considered as generators of neutrons which can be used to realize fission reactors in the nuclear fuel.

Such a hybrid scheme which combines fusion reactors as neutron sources and fission reactors as neutron consumers have certain advantages over purely thermonuclear reactors and fission reactors. Note the main of these advantages.

In the hybrid scheme the requirements for D-T reactor are considerably reduced. In this case it is not necessary to reach high energy breeding coefficient of fusion reaction, which is especially important for fusion reactors with a high value of self needs.

In the case of a laser initiated reactor, the requirement for the value of laser beam energy and for the laser efficiency are sharply reduced. Simultaneouly, a manufacture of D-T targets is simplified, and also a fraction of the laser system cost in the total expenditure is reduced.

As compared with the fission reactor, a hybrid reactor can do without an expensive process of the nuclear fuel enrichment because an external neutron source makes it possible to use unenriched natural or depleted uranium.

The reactor core can be subcritical with the neutron breeding ratui less than unity, which excludes the risk of a breakdown (nuclear explosion), and consequently a breakdown protection is not required.

The present paper summarizes the main results of the project of a nuclear hybrid plant with a laser thermonuclear reactor. The project has been developed at the Institute of High Temperatures and P.N.Lebedev Physical Institute of the USSR Academy of Sciences. The hybrid reactor with thermal power about 2500 MW is a cylindrical explosion chamber of the radius R = 1.5 m and height H = 3 m surrounded with a blanket. The protection of the first explosion chamber wall is to be provided with a thin liquid lithium layer (wetted wall). The blanket consists of two zones: a zone of the fission fueld (the core) and a zone of tritium regeneration. The tritium regeneration ratio is equal to unity. The core is a set of cassettes cooled with helium.

It is supposed that HF laser sistem of total energy 5.10^5 J and total efficiency 3% can be made for thermonuclear microexplosion initiation with energy gain of 40. Laser heat is not utilised in the energy cycle. The fission blanket is to be initially charged with natural or even depleted uranium. The initial core energy breeding ratio is equal to 4. Thus, the initial total breeding ratio $K_f = K_{fus} \cdot K_{fis} = 160$. As plutonium is produced in the core, the K_{fis} increases. The maintaining of the constant reactor thermal power is to be realized with a reduction of microexplosion frequency.

The regime of the reactor exploitation is energetic. Electric energy is produced with helium gas turbines as well as with steam turbines of the second loop.

The initial efficiency of the plant is equal to 24 percent, within three years of the plant operation the efficiency should be increased up to 40 percent. Specific capital costs of generating energy are to be amounted to 250 roubles per kilowatt.

A fraction of the laser system cost in the total expenditures is equal to about 8 percent. Notice that for a purely laser fusion reactor this value is equal to 40 percent, for the same accepted costs of one joule of the laser beam energy.

The reactor cost , however, has increased very considerably (up to 50 percent of the total plant cost). This is a result of a more complicated design of the reactor. In the pure reactor the moderated neutron energy is released in the liquid helium. In the hybrid reactor the energy is released by pulses (pulse duration being 10^{-7} sec) in the solid-state uranium carbide. The heating time determines small size of fuel particles, and in the long run it complicates the blanket design. Measures are taken to provide for the leaking cassete removal during the reactor operation.

Specific calculated costs have been rated according to methology of determination of the power project esonomic efficiency accepted in this country. They have been found in the range from 0.95 copeck per kilowatt hour and to 0.8 copeck per kilowatt hour for the values of energy breeding ratio equaled 160 and 4000, respectively.

The hybrid laser plants can be competitive with the best modern plants.

ANOMALOUS ALPHA PARTICLE TRANSPORT IN FUSION PLASMA*

D. J. Sigmar
Oak Ridge National Laboratory, Oak Ridge, Tennessee, USA
(on leave of absence from MIT)

H. C. Chan
Massachusetts Institute of Technology, Cambridge, Mass, USA

[Due to the strong localization of the fusion born α-particles in velocity and configuration space and their coupling to Alfven waves in the background plasma the relaxation of α-s is anomalous (non-Coulombic). In a finite system, the enhanced electromagnetic fluctuations can produce rapid spatial losses of up to 50% of the α-population and energy. In turn, these losses tend to prevent the α-velocity distribution from attaining a stable collisional equilibrium, thus maintaining a steady state turbulence level. A self-consistent numerical quasilinear calculation is performed for the most dominant mode, showing the evolution of the α-distribution yielding the anomalous loss rates.]

α-particles are born with a velocity distribution function $f_\alpha \sim \delta(E - E_\alpha)$ where $E_\alpha = 3.5$ MeV and a spatial distribution $n_\alpha = \langle\sigma_f v\rangle n_d^2 t$, where $\langle\sigma_f v\rangle \propto T^{-2/3} \exp[-20/T^{1/3}]$ is strongly peaked in the hot reactor core, as is the square of the deuteron density n_d. Due to the ordering, $v_{thi} < c_A < v_\alpha < v_{the}$, this free energy can be released via Alfven-wave-instabilities. (Here, the subscripts stand for ion, Alfven, alpha and electron velocity). Since the first papers by Kolesnichenko and Korablev [1] on "thermonuclear instabilities" in 1967, a large number of such linear instabilities have been found, reviewed recently by Lominadze [2].

In an infinite medium one expects these instabilities to exist transiently until the combination of turbulent and collisional spreading of the α-distribution produces a stable shape $\frac{\partial f_\alpha}{\partial E} < 0$. Practical toroidal reactor designs however are far removed from this condition and the particle confinement time τ_p will therefore be finite and if anomalous diffusion is strong enough to produce the inequality $\tau_p < \tau_s$ (where τ_s is the collisional slowing down time of a fast α-particle), the stable shape $\frac{\partial f_\alpha}{\partial E} < 0$ will not be attainable.

In this paper we will quantitatively pursue such a case for the linear instability recently discovered by Kaladze, Mikhailovskii [3].

In Ref. [3], shear Alfvén wave $\omega = K_\parallel C_A = p \cdot \omega_{b\alpha}$ is resonating with the bounce motion of magnetically trapped α-particles (where $p = 1, 2, \ldots$ is an integer and $\omega_{b\alpha}$ is the α-banana bounce frequency.) The mode is destabilized by $\partial f_\alpha/\partial E > 0$, its growth rate being maximized for radial wavelengths of the order of a banana width of the energetic α-particles: $K_r \delta r_b \sim 0(1)$, and $K_\theta \ll K_r$ (where K_θ is the poloidal wave vector). The growth due to the unstable α-distribution is opposed by damping on the electrons, [5] yielding a threshold α-density for instability

$$\frac{n_\alpha}{n_\alpha} \geq (k_r\rho_\alpha)^2 (k_r\rho_i)^2 \frac{C_A}{v_{the}} \epsilon^{-1/2} \sim 10^{-5}$$

where ρ denotes the gyroradius and $\epsilon = r/R$ the inverse aspect ratio of the Tokamak. Such low values of threshold density can be exceeded in times shorter than τ_s (when $\partial f_\alpha/\partial E < 0$ would be obtained in the absence of turbulence). We study the time evolution of the α-distribution obeying

$$\frac{\partial f_\alpha}{\partial t} = \frac{\partial}{\partial E} D_E \frac{\partial f_\alpha}{\partial E} - \frac{D_x}{d_{1/2}^2} f_\alpha + C(f_\alpha) + S_f, \qquad (1)$$

where $S_f = \langle\sigma_f v\rangle n_d^2 \delta(v - v_\alpha)/4\pi v_\alpha^2$, C is the Coulomb operator, and the quasilinear diffusion coefficients are given by

$$D_E = \sum_{p,k} \frac{e^2}{m^2} |E_{rk}|^2 \frac{p^2\omega_b^2}{4k_r^2} J_p^2 \left(\frac{2k_r v_D}{\omega_b}\kappa\right) \delta(\omega - p\omega_b)$$

$$D_x = \sum_{p,k} \frac{c^2}{2B^2} |E_{\theta k}|^2 J_p^2 \delta(\omega - p\omega_b),$$

with $\kappa = 4(p\omega_b - \omega)/p\omega_b$ as defined in Ref. [3]. The magnetic moment is conserved in this low frequency instability. For simplicity, the spatial diffusion term $\frac{\partial}{\partial x} D_x \frac{\partial f_\alpha}{\partial x}$ has been approximated as shown in Eq. (1), where $d_{1/2}$ is taken to be the time dependent self consistent half width of the α-density profile, obtained from the simultaneous solution of

$$\frac{\partial n_\alpha}{\partial t} - \frac{\partial}{\partial x} \overline{D}_x \frac{\partial n_\alpha}{\partial x} = \langle\sigma_f v\rangle n_d^2 \qquad (2)$$

(The bar over $\overline{D}x$ denotes a velocity average.) The boundary condition for Eq. (2) is $n_\alpha(a,t) = 0$ with a the minor plasma radius.

Before we give quantitative results it is useful to estimate analytically under which time asymptotic conditions the distribution function will be prevented to arrive at the stable shape $\partial f_\alpha/\partial E < 0$. Integrating (1) with respect to energy,

$$0 = D_E \frac{\partial f_\alpha}{\partial E} - d_{1/2}^{-2} \int dE\, D_x f_\alpha + \frac{1}{\tau_s} \int dE\, \hat{C}(f_\alpha) \ldots \qquad (3)$$

where we have explicitly displayed the collisional slowing down time. Thus, $\partial f_\alpha/\partial E$ will remain positive if, roughly, $\overline{D}_x/d_{1/2}^2 > \tau_s^{-1}$ where the left side equals the inverse particle confinement time τ_p. With $\overline{D}_x \sim \gamma/K_\parallel^2 \sim \gamma\, \delta r_b^2 = (\frac{\gamma}{\omega}) p\omega_{b\alpha}\, \delta r_b^2$, (4a) becomes

$$\tau_s > (p\omega_{b\alpha})^{-1} \left(\frac{\omega}{\gamma}\right) \frac{d_{1/2}^2}{\delta r_b^2} \qquad (4)$$

It now becomes apparent from the turbulence condition (4) why the nonlinear form of the Kaladze-Mikhailovskii-mode treated here constitutes a nonnegligible anomalous transport mechanism. Typically, with $\tau_s \gtrsim 500$ msec, $2\pi/\omega_{b\alpha} \sim 5 \times 10^{-3}$ msec, $\omega/\gamma \sim 10^3$, and $d_{1/2} \sim \frac{a}{2}$, nominally $\delta r_b/a \leq \frac{1}{20}$ is required for stabilization, a very stringent requirement on size or plasma current (and therefore field strength).

Since (4b) was derived heuristically, we conclude with an exact numerical evaluation of α-particle losses from Eqs. (1) and (2). For example, for the reference case B = 30 KG, T(0) = 20 keV, $n_e = 10^{14}$ cm^{-3}, a = 125 cm, a/R = 1/4, q = 3 we find that after one collisional slowing down time f_α shows a strong depletion of (resonant) particles between $1.7 \leq E \leq 3.5$ MeV, an anomalous broadening of the α-density profile width from 35 cm to 70 cm, and a loss of $\gtrsim$ 50% of all trapped α-particles and their energy. These losses roughly increase with q^2 and T^2 and decrease with B, where q is the safety factor, T the plasma temperature and B the magnetic field.

*Research sponsored by the Energy Research and Development Administration under contract with Union Carbide Corporation.

[1] Y. I. Kolesnichenko, V. N. Oraevskii, Atomanya Energiya 23, 289 (1967); L. V. Korablev, Sov. Phys. JETP 26, 922 (1968).
[2] D. G. Lominadze, A. B. Mikhailovskii, W. M. Tang, Sov. J. Plas. Phys. 2, 286 (1976). See references quoted in Ref. 4, below.
[3] T. D. Kaladze, A. B. Mikhailovskii; Kurchatov Institute Report IAE 2679 (1976).
[4] A. B. Mikhailovskii, Sov. Phys. JETP 41, 890 (1976).
[5] V. S. Belikov et al., Sov. Phys. JETP 39, 828 (1974).

PRELIMINARY CONSIDERATIONS REGARDING THE EFFECT OF α-PARTICLES ON A REFUELLING-PELLET

C.T. Chang

Association Euratom-Research Establishment Risø

DK-4000 Roskilde, Denmark

Abstract: The plasma of a fusion reactor is not an effective stopping medium for the 3.52 MeV α-particles. Expected range and energy deposition in a solid deuterium pellet are examined.

The injection of a solid D_2 (or DT) pellet has long been suggested as a possible means of refuelling a fusion reactor. Recently, questions were raised regarding the possible role that might be played by the 3.52 MeV α-particles produced by the D-T reaction. In this note, some preliminary computational results will be presented first, possible directions for future exploration will then be indicated.

Slowing down process: Through Coulomb collisions with the reactor plasma ions and electrons, the speed of the α-particles will be attenuated and acquire some spread in the velocity space. According to Cordey[1] the stationary distribution function, f(v), after neglecting the high velocity tail part is given approximately by

$$f(v) = \frac{3 n_\alpha}{4\pi\left[\ln\left[1+(V_0/V_c)^3\right]\right]} \frac{V^2}{V^3+V_c^3} \qquad (V<V_0)$$

For $\langle V_e\rangle > V_0 > \langle V_i\rangle$ (1)

where $\langle v_e\rangle$ and $\langle v_i\rangle$ are the average thermal speed of plasma electrons and ions respectively, v_0 is the initial speed of the α-particles, and

$$V_c = 0.974\left(\frac{m_e}{M_\alpha}\right)^{1/3}\langle V_e\rangle \qquad (1a)$$

For a fusion reactor with $kT_e = kT_i = 20$ kev and $n_e = 2\times10^{14}$ cm^{-3}, $\langle v_i\rangle = 1.6\times10^8$, $\langle v_e\rangle = 9.5\times10^9$ cm/sec and $v_c = 6\times10^8$ cm/sec. For the 3.52 MeV α-particle, $v_0 = 1.3\times10^9$ cm/sec, accordingly, the average energy and speed of the α-particles at the end of the slowing-down process are respectively,

$$\langle E_\alpha\rangle_s = 2.19 \text{ MeV}, \qquad \langle V_\alpha\rangle_s = 0.61\ V_0$$

Taking a burn factor $f_b = 3.5\%$, the corresponding energy and particle flux are

$$\langle F_\alpha\rangle_s = 0.81\times10^9 \text{ Watt/cm}^2, \qquad \langle N_\alpha\rangle_s = 2.77\times10^{21} \text{ cm}^{-2}\text{sec}^{-1}$$

(As a comparison, the corresponding figures for the plasma electrons are $F_e = 2.56\times10^9$ watt/cm^2 and $N_e = 4.75\times10^{23}$ $cm^{-2}sec^{-1}$)

To estimate the distance required for the α-particles to reach the stationary state the stopping power formula might be consulted. According to Stix[2], this can be written approximately as

$$\frac{dE}{dx} = \frac{2\pi Z_\alpha^2 e^4}{E}\left(\frac{M_\alpha}{m_e}\right) n_e \ln\Lambda\left[\left(\frac{m_e}{M_D}\right) + \frac{4}{3\sqrt{\pi}}\left(\frac{m_e}{M_\alpha}\right)^{3/4}\left(\frac{E}{kT_e}\right)^{3/2}\right] \qquad (2)$$

For $\langle V_e\rangle > V_0 > \langle V_i\rangle$

Treating $\ln\Lambda$ as a constant, the required distance, D, for the slowing down of α-particles from E_0(3.52 MeV) to $\langle E_\alpha\rangle$(2.19 MeV) can be obtained by integrating eq. (2) analytically. After inserting the previously mentioned plasma parameters, we obtain $D \simeq 1.8\times10^8$ cm. The corresponding required time will be $\tau \simeq 0.08$ sec. Similarly, the time required for slowing down the α-particles to an average energy comparable to the thermal energy of the plasma electrons or ions, will be $\tau_{s\alpha} \simeq 0.2$ sec. Comparing τ with the envisaged pellet penetration time of $t_p \simeq 10^{-4}$ sec (when no appreciable drag is experienced by the pellet), we might expect that the pellet will be subject to the direct bombardment of approximately 3×10^{21} α-particles per sq. cm per sec at an energy about 3 MeV.

The interaction of such high energy α-particles on the pellet can be divided into two stages; (a) direct impact phase, (b) further slowing down of α-particles in the cold (?) and dense ablated plasma. The interaction mechanism of the second stage clearly depends much on the state of the ablated plasma formed around the pellet after the impact of α-particles (∿ 3 MeV) and plasma electrons and ions near the reactor wall, a few remarks concerning the expected events occurring in the direct impact phase, therefore, might be worthwhile.

Expected impact phenomena of the 3 MeV α-particles: From the tabulated values of Northcliffe and Schilling[3], we expect the range in solid D_2 for 3 MeV α-particles to be around 0.06 mm, thus for a 5 mm pellet, the energy of the α-particles will be deposited in a thin shell. According to Lindhard et al[4], for incident ions at high energy, the energy deposited in the atomic motion tends to a limiting value and is inversely proportional to the electronic stopping number, k. Extrapolating the calculated data of Sigmund et al[5], we expect that only 1/1000 of the total energy carried by the α-particles will be deposited to the atoms, most of the energy will be spent in causing excitation and ionization of the bound electrons. This amount of energy eventually will end up as a temperature rising of the pellet. Its influence on the thermal and mechanical properties of solid deuterium (or DT compound) in term of the ablation rate of the pellet is a subject of future exploration.

Acknowledgment: The author wishes to acknowledge helpful discussions with H. Sørensen and J. Schou regarding the impact of energetic α-particles in solid deuterium.

References:

1) J.G. Cordey, E.P. Gorbunov, J. Hugill, J.W.M. Paul, J. Sheffield, E. Speth, P.E. Scott, V.I. Treshin, Nuclear Fusion 15, (1975) 441, and J.G. Cordey; private communication.

2) T.H. Stix, Plasma Physics 14, (1972) 367.

3) L.C. Northcliffe and R.F. Schilling, Nuclear Data Tables A7, (1970) 233.

4) J. Lindhard, V. Nielsen, M. Scharff, and P.V. Thomsen, Mat. Fys. Medd. Dan. Vid. Selsk. 33, No. 10 (1963).

5) P. Sigmund, M.T. Matthies, and D.L. Phillips, Radiation Effects 11, (1971) 39.

PARAMETERS OF A FIELD-REVERSED MIRROR REACTOR*

R. S. Devoto, G. A. Carlson, W. C. Condit, J. D. Hanson
Lawrence Livermore Laboratory, University of California
Livermore, California 94550, U.S.A.

Abstract: Computations have been made of the parameters of a neutral-beam driven, field-reversed mirror reactor as a function of beam injection energy. Q values of 4-5 and a fusion power of 10-50 MW per cell are found at beam energies of 200-500 keV. Cost estimates indicate a direct capital cost of < \$1000/kW$_e$ for multicell versions of the reactor.

Recent experiments in the 2XIIB mirror device have yielded peak β values of 1.5-1.8 at high beam currents.[1] This result, coupled with the finding of apparently stable reversed-field layers a few gyroradii in thickness in a theta pinch,[2] have inspired experiments in 2XIIB aimed at attaining field reversal by off-axis aiming of the neutral beams. Simultaneously, we have computed the probable parameters for an eventual reactor application.

Our calculations proceed from the assumptions that the reversed-field plasma has a minor radius a of only a few ion gyroradii and that the density profile must be diffuse (we take a parabolic or cubic dependence on minor radius). The assumed shape is shown in Fig. 1; the ratio of major radius R and length L to minor radius are parameters; we assume R/a = 2 and L/R = 3.0. We would expect the possible length to be limited by tearing instabilities, although very long field-reversed layers have been observed.[3]

Using the above density profile and assuming constant ion and electron energies we can formulate zero-dimensional fluid equations for the central density n_e, and the mean electron and ion energies, $\bar{E}_e$ and $\bar{E}_i$,

$$\frac{\partial n_e}{\partial t} = 0 = \dot{n}_0 - \frac{n_e}{\tau_p}$$

$$\frac{\partial (n_e \bar{E}_e)}{\partial t} = 0 = \dot{Q}_{ie} - \frac{n_e \bar{E}_e}{\tau_{Ee}} - \frac{5}{3}\frac{n_e \bar{E}_e}{\tau_p} - \dot{Q}_s - \dot{Q}_B$$

$$\frac{\partial (n_e \bar{E}_i)}{\partial t} = 0 = \dot{n}_0 E_{IN} - \frac{n_e \bar{E}_i}{\tau_{Ei}} - \frac{5}{3}\frac{n_e \bar{E}_i}{\tau_p} - \dot{Q}_{ie}$$

$\dot{n}_0$ is the rate of increase of central density due to beam deposition, τ_{Ee} and τ_{Ei} are electron and ion heat conduction times, τ_p is the particle confinement time, $\dot{Q}_{ie}$ is the usual term for ion-electron energy transfer for Maxwellian species, and $\dot{Q}_s$ and $\dot{Q}_B$ are synchrotron and bremsstrahlung radiation terms. The total plasma pressure is related to the applied magnetic field B_0 by $p_\perp = \beta B_0^2/2\mu_0$. $\dot{n}_0$ or, equivalently, the absorbed beam current, is adjusted to correspond to a cubic (or parabolic) profile. Estimates suggest that if $M = \int_{\ell=a}^{\ell=0} n \langle\sigma\rangle d\ell = 1.75$, a cubic profile will be attained. A different value of M changes the central density, the effect on mean energies being weak. Tangential injection (perpendicular to the plane of Fig. 1) is assumed.

A variety of assumptions about the confinement times are possible. It seems likely that ion heat conduction will be classical, so we have taken $\tau_{Ei} = (a/\rho_i)^2 \tau_{ii}$, where ρ_i is the ion gyroradius. Note that if the ions are mirror confined outside the field-reversed region, the ion energy could be nearly constant, yielding a very large τ_{Ei}. For τ_{Ee} we have taken 1/5 of the classical value $(a/\rho_e)^2 \tau_{ei}$. Various possibilities for τ_p have been examined. For the small sizes necessitated by the required plasma dimensions of a few gyroradii, the basic time governing τ_p must be no worse than approximately $(a/\rho_i)^2 \tau_{ii}$ for a viable reactor. If it is somewhat better, approaching a classical confinement time $(a/\rho_e)^2 \tau_{ei}$, reactor parameters look even better. For a "reference" case we take $\tau_p = f(j, L/a)(a/\rho_i)^2 \tau_{ii}$, where f is a factor derived from the 1-D density equation and depends on the assumed profile as well as on the ratio of length to minor radius. One parameter remains to be specified, the ratio of minor radius to ion gyroradius, ($S \equiv a/\rho_i$). Since only layers of a few gyroradii appear stable, we take S = 5.

Results of the calculations for this typical case appear in Figs. 2-3, plotted against the injection energy. Typically, the mean ion energy is 1/3 the injection energy, and the electron energy 1/2 the ion energy, except at high $\bar{E}_e$ where radiation losses cool the electrons below this value. Attractive values of Q, the ratio of total fusion power to beam input power, are found at 300 keV injection energy. For this case, the applied B field of 60 kG is within the range for present-day superconductors. The total fusion power P_F can be controlled somewhat by the ratio L/R. For the present choice of L/R = 3.0, P_F = 30 MW is computed. This is a very small power for projected reactors; to increase the total output of a fusion plant one could also line up a series of field-reversed cells.[4]

Figure 4 shows the estimated direct capital cost of a multicell (10 or more) field-reversed mirror reactor as a function of injection energy. The optimum injection energy is about 300 keV. A single cell field-reversed mirror reactor will have a higher \$/kWe cost because of end effects (blanket and shield end caps, etc.) and the dominance of the reactor containment building.

References

(1) F. H. Coensgen et. al., in Proceedings, 6th International Conf. on Plasma Physics and Controlled Fusion, IAEA, 1976.
(2) A. G. Eskov et. al., in Seventh European Conf. on Controlled Fusion and Plasma Physics (1975), Vol. I, p. 55.
(3) A. Eberhagen and W. Grossman, Z. Phys. 248, 130 (1971).
(4) W. C. Condit et. al., The Technology of Controlled Nuclear Fusion, CONF 760935-P1 (1976), Vol. I, p. 107.

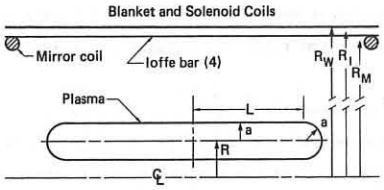

Fig. 1. Geometry of field-reversed plasma cell.

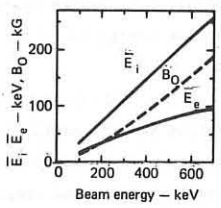

Fig. 2. Mean ion and electron energies and magnetic field vs. injection energy.

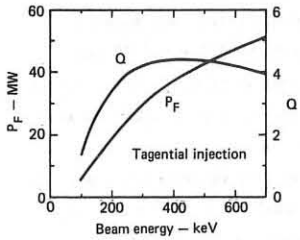

Fig. 3. Total fusion power and Q vs. injection energy for S = 5, R/a = 2, L/R = 3.

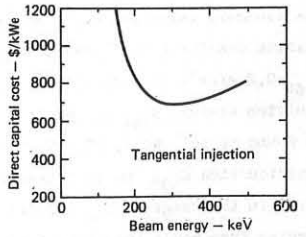

Fig. 4. Dependence of capital cost of multicell reactor on injection energy.

*Work performed under the auspices of the U.S. Energy Research and Development Administration under contract No. W-7405-Eng-48.

ON PROPAGATION OF BURNING IN A WALL-LIMITED THERMONUCLEAR FUEL WITH VARIABLE DENSITY

Chernukha V.V., Fedulov M.V.

1. To obtain a commercially profitable pulsed fusion reactor requires the ratio (K_ε) of fusion energy to energy input (E_{in}) deposited in the target by the ignition system to be sufficient for high cycle efficiency and the energy yield, according to [1], should be fairly large. In spherical targets [2] usually under consideration an increase in K_ε with E_{in} is small. So to consider the targets is of interest in which compression of the main fraction of fuel determined by the condition of burn propagation from the ignition zone rather than the ignition condition as is the case with spherical targets.

The target of corved body surrounded by inertial walls will be considered below, in which maximum fuel density occurs in the ignition zone neighbouring the plane of symmetry and reduces to the periphere [1] (Fig.1). We do not intend to touch upon the process of target compression and ignition zone heating ($Z \leqslant Z_{ign}$), assuming that at a certain moment taken as the initial time the compression has already been completed and the ignition zone heated up to reguired temperature.

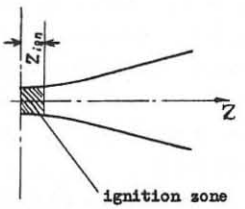

Fig.1.Schematic diagram of target.

A quasi-one-dimensional approach has been used for calculations, i.e. all hydrodynamic values and relative ion concentrations are assumed to be dependent on Z only. However, in every cross - section of the target an additional density variation due to radial espansion as well as leakage take place.

The speed of the interface between fuel and walls was calculated via that of the matter behind a strong shock wave front at a pressure equal to that in the fuel. We did not allow for the influence of wall heating by α -particles and radiation. Radial heat leakage calculations were provided as in [4]. The radiant energy both from fuel and walls was thought to be entirely lost.

2. As density decreases along the target axis the cross-section radius should increase; it was taken that $r \simeq kZ$ far from the plane of symmetry and with allowance for the quasi-one-dimensional approach the proportionality constant k was limited to 0,5. The computer calculations have shown the burn propagation to be steady-state if ρz exceeds the boundary value $\sim 0{,}7$ g/cm^2. The representative behaviour of this burning propagation near the boundary value can be illustrated by the case where a maximum density (ρ_s) was choseb to be 100 g/cm^3 [2] and $\rho_s Z_{ign} = 0{,}2$ g/cm^2. In case of instantaneous deposition the required ignition energy, E_{ign} (accounting for a half of ignition zone) is found to be 60 kj ($T_e = T_i \simeq 17$ kev). An increase in ignition time τ_{ign} up to 1 nsec results in reducing power which in the range of $\tau_{ign} \simeq 0{,}1 \div 1$ nsec is $\sim 10^{15}$ W. As the burning fron moves away from the plane of symmetry the energy loss ratios become stable: heat conduction losses and those associated with α -particle escape account for every 20-25 percent of the total α -particle energy; the summary radiation and radial expansion losses are not in excess of 10%. Thus about a half of the α -particle energy is spent for heating of new fuel portions. Note, that this heating starts with absorption of the energy of α -particles decelerating in cold fuel. Heat conduction and shock compression contribute somewhat later with the fuel being compressed by a factor of 1,5-2 [3].

If a target is large enough the main energy input depends on a shaped fuel compression. Using the calculation results which give the burn up factor of 10÷15% and assuming the compression to be cold, one can obtain a dependence of K_ε on the minimum target density ρ_1 ($> 0{,}2$ g/cm^3):

$$K_\varepsilon \simeq 10^5 \xi \rho_1^{-2/3} \qquad (1)$$

where ξ is the fuel compression efficiency.

3. If deuterium with small additions of tritium and/or helium-3 is used instead of D-T fifty-fifty fuel unstable isotopes can be totally bred at the appropriate initial concentration ratios ($\lesssim 0{,}5\%$ T and $\lesssim 6\%$ He-3) Here the optimum temperature values become shifted to the range of 40-60 kev and the critical values ρz increase by 10÷15.

In case of pure D-fuel the optimum burning temperature is 80-100 kev, and ρz increases by a factor of 30.

4. In conclusion it should be noted that the target considered is of a certain interest for application in CTR. The main technological problems in its realization should be likely connected with providing shaped compression and ignition energy deposition for a relatively short period of time without spherical symmetry.

References

1. Velikhov E.P., Golubev V.S., Chernukha V.V. "Fusion reactor design problems". VIENNA, 1974, 235-239.
2. Mason R.J., Morse R.L. Ph.Fluids 18, 814, 1975.
3. Настоящий А.Ф., Шевченко Л.П., Атомная энергия, 32, № 6, 1972.
4. Настоящий А.Ф. Атомная энергия, 32, №1, 1972.
5. Chu M.S. Ph.Fluids 15, N3, 1972.
6. Asano N. et al. J.of the Phys.Soc.of Japan 41, N5, 1976.

1) The process of burn propagation in an immovable wall-limited fuel (with constant density) taking heatconduction to walls into account has been considered in [3].

2) This density is maximum permissible for the quasi-one-dimensional approach as at larger ρ_s the density values for the walls and fuel become close (the walls were supposed to be iron).

3) A low factor of compression has been obtained also in [5], though α -particle transfer was not taken into consideration (in this connection see ref [6]).

ELECTRON AND ION HEATING BY NEUTRAL INJECTION IN DITE TOKAMAK

R.D. Gill, K.B. Axon, R.S. Hemsworth, J. Hugill, P.J. Lomas,
J.W.M. Paul, R. Prentice, P.E. Stott and D.D.R. Summers
Culham Laboratory, Abingdon, Oxon, OX14 3DB, UK
(Euratom/UKAEA Fusion Association)

Abstract: Neutral injection heating experiments are reported in which we have observed ion temperature rises of 52% and central electron temperature rises of 75%.

The DITE tokamak (R = 117 cm, a = 27 cm, B_ϕ = 9 - 27 kG and I_G = 50 - 200 kA) has been used to study the heating effects of neutral injection on both the electrons and ions. The two neutral beam sources deliver a combined power of 200 kW in the direction of the plasma current and along a line tangent to a major radius R = 105 cm. The ion sources produce roughly equal fluxes of H neutrals with energies E_o, $E_o/2$ and $E_o/3$ where $E_o \leq 30$ keV.

This injection system has been previously [1] used to study the ion heating at I_G = 150 kA and it was found that the ion temperature, T_i, measured by charge-exchange, approximately doubled. A detailed analysis of these results has subsequently been carried out. Deposition and Fokker-Planck computer programs have been used to describe the transfer of power from the neutral beams to the plasma ions and an ion energy balance program [2] was used to determine the radial power transfer. The effects of electron-ion heating, charge-exchange, particle diffusion and neo-classical thermal conduction were considered and good agreement has been attained between experiment and theory. A typical analysis is shown in Fig. 1, where the radial power balance is plotted as a function of the minor radius. The dominant heat loss in the plasma centre is due to thermal conduction, but as $T_i > T_e$ collisional transfer to the electrons is also significant.

We have now carried out a further series of experiments to investigate the degree of ion heating under a number of different conditions. In injection experiments designed to study ion heating it is desirable to inject into a plasma with a high electron temperature and this was achieved in DITE by the addition of 2% of Neon to the discharge [3], producing the plasma conditions listed in the table. At I_G = 150 kA, the time variation of T_i was measured for co-directional injection with a neutral power, P = 190 kW (see Fig. 2). A striking increase in T_i can be seen compared with the P = 0 curve and a peak value of 670 eV was attained. The other plasma parameters such as n_e, T_e and Z_{eff} were substantially unchanged during injection. At I_G = 190 kA the variation in T_i was investigated as a function of the injected power. The results in Fig. 2 show that T_i is linearly dependent upon P.

The main features of the results taken at different values of I_G and B_ϕ are: (a) little heating is achieved when the injection direction is counter to the gas current direction; (b) the amount of heating in the co-direction gradually increases to a maximum at I_G = 150 kA and falls thereafter. The lack of heating in the counter direction is probably due to pitch angle scattering of the injected particles, by impurities, into the loss cone. The increase in co-injection heating as a function of I_G may be understood as a consequence of the increased neutral injection power transferred to the ions at higher gas currents. As I_G increases the parameters n_e and T_e both increase while the neutral density, n_o, decreases. The high values of n_o at low I_G causes substantial neutral injection power losses by charge-exchange while lower values of T_e cause a larger fraction of the incident power to transfer to the electrons at the expense of the ions. The fall in the amount of ion heating at I_G = 190 kA is not yet understood.

In another series of experiments, we investigated the effects of injection into discharges in which the torus walls had been gettered with titanium [4]. These discharges were all characterised by a value of Z_{eff} close to unity and a low ohmic input power of ≈ 300 kW. Hydrogen gas was admitted continuously to give a gradually rising electron density as shown in Fig. 3. The injectors delivered 200 kW of neutral power in the co-direction. The heating effects of these beams can be clearly seen in Fig. 3 where substantial increases occur in both T_i and the central value of T_e. It can also be seen that the time dependence of the temperature rise is in reasonable agreement with the injection period (t = 40 to 100 msec). Ruby laser temperature and density profiles were also measured before, during and after the injection period. Before injection the profiles had a pronounced hollow character [3], and the profiles taken at t = 80 ms are shown in Fig. 4. The total energy content of the electron component of the plasma, W, can be calculated from these profiles and this shows that $\Delta W/W$ = 24%. The ion temperature also shows a large rise of $\Delta T_i/T_i$ = 52%.

One of the main difficulties in the interpretation of this experiment is the fear that the injection process may change the energy balance in the plasma by the introduction of impurities and thus increase the electron temperature [3]. The measured loop volts and ohmic power input are observed to decrease slightly during injection and this would argue against increased impurity levels. Stronger evidence was obtained from measurements of the soft X-ray emission from the plasma.

Without injection, the X-ray spectra, from an Si(Li) detector, showed that the X-ray anomaly factor was about unity, as expected for a plasma with $Z_{eff} \approx 1$. This anomaly factor is very sensitive to changes in the impurity level and can easily change by orders of magnitude on the introduction of small amounts of impurity. We observed the time dependence of the intensity of X-rays with $E_x > 700$ eV and found that it rose by a factor of 3 during injection, returning to its previous level after injection. The expected rise in this intensity deduced from the laser measurements of $T_e(r)$ was a factor of 2.7. This is consistent with an unchanged anomaly factor during injection and provides strong evidence that impurities are not being introduced by the injection.

Calculation of the expected rise in T_e requires a thorough evaluation of the different processes contributing to the energy balance in both hollow and non-hollow discharges. The calculation of the ion temperature increase requires a detailed treatment of the electron-ion heating and this is also in progress. However, rough estimates show that 72 kW of the injected power should go to the electrons and heat them by 24% if the energy containment time is unchanged.

It is a pleasure to acknowledge the assistance given by the DITE engineering and operating teams and the Neutral Injection Group.

References

[1] Paul, J.W.M., et al, Proc. of 6th Conference on Plasma Physics and Controlled Nuclear Fusion Research, Berchtesgaden (1976) Paper CN-35/A17.
[2] Stott, P.E., Plasma Physics, 18 (1976) 251.
[3] Hugill, J., et al, this conference.
[4] Stott, P.E., et al, this conference.

TABLE

B_ϕ (T)	I_G (kA)	n_e*10^{13} (cm-3)	T_e (eV)	T_i (eV)	Z_{eff}	ΔT_i Co	ΔT_i Counter
0.9	40	0.6	320	150	7.3	27	-16
1.3	100	1.35	490	330	5.5	66	23
2.0	150	2.1	845	440	6.8	220	18
2.7	190	2.5	1000	540	7.6	100	

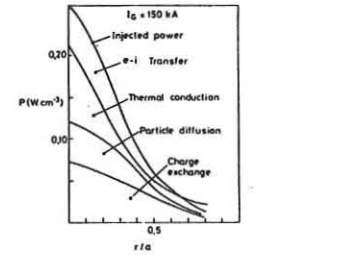

Figure 1

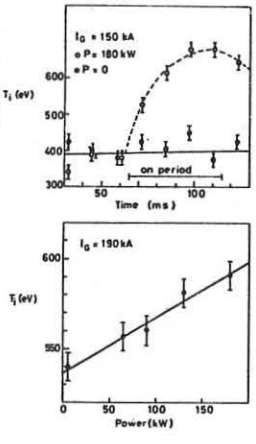

Figure 2

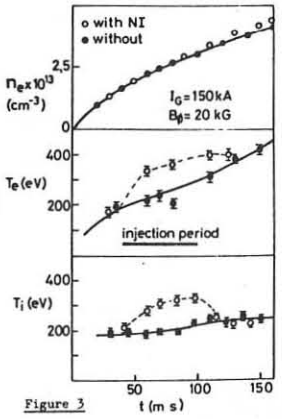

Figure 3

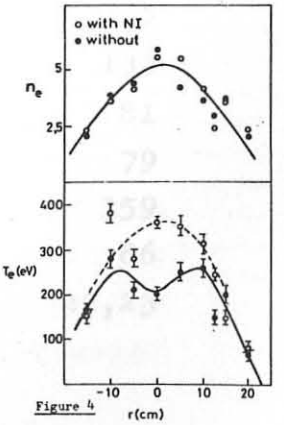

Figure 4

AUTHOR INDEX

I.

J.

K.

L.

M.

N.

O.

P.

Q.

R.

P.

Q.

R.

Y.

Z.

Tisk: ČVTS - DŮM TECHNIKY PRAHA